SOVIET PHYSICS

JETP

A translation of the Zhurnal Éksperimental'noĭ i Teoreticheskoĭ Fiziki.

Vol. 14, No. 6, pp 1209-1457 - (Russ. orig. Vol. 41, No. 6, pp 1699-2046, December, 1961) June, 1962

QUANTUM GALVANOMAGNETIC EFFECTS IN n-InAs

Kh. I. AMIRKHANOV, R. I. BASHIROV, and Yu. É. ZAKIEV

Dagestan Branch, Academy of Sciences, U.S.S.R.

Submitted to JETP editor February 5, 1961; resubmitted July 25, 1961

J. Exptl. Theoret. Phys. (U.S.S.R.) 41, 1699-1703 (December, 1961)

The Hall effect and the electrical resistance of n-InAs were investigated in strong pulsed magnetic fields at 20—360°K. Quantization of the carrier motion in the magnetic fields produced an infinite rise in the resistance. At liquid hydrogen temperatures a carrier-density effect was observed.

THERE are several theories of galvanomagnetic effects in semiconductors in very strong magnetic fields.[1-5] However, these theories lead to contradictory results.[2,3] The available experimental data are insufficient to check the theories; furthermore, disagreement between one of the theories[3] and experiment has been reported.[6,7] New data are obviously needed in the region of strong fields. The present paper describes investigations of the Hall effect and magnetoresistance of n-InAs at 20—360°K in pulsed magnetic fields. To the authors' knowledge this is the first such study on n-InAs.

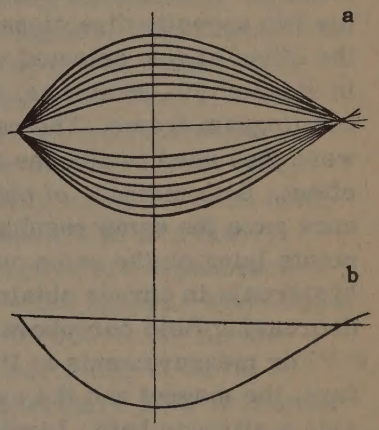

FIG. 1. a) Oscillograms of magnetoresistance; b) oscillogram of magnetic field.

EXPERIMENTAL METHOD

Pulsed magnetic fields were produced by discharging a capacitor bank through a solenoid made of beryllium bronze. The bank had a capacitance of 1200 μf and was charged to 3 kv. The apparatus produced fields of 450 kgauss in a working volume of 0.4 cm^3. In this volume the field was uniform to within 3%. The field intensity was measured with an integrating circuit.[8] The field-intensity oscillogram is given in Fig. 1. The samples were rectangular parallelepipeds of dimensions from 5 × 0.5 × 0.5 mm to 8.0 × 0.5 × 0.5 mm, and were cut from a homogeneous ingot. The homogeneity was verified by measuring the electrical resistance and the Hall effect. Current leads and potential probes were soldered to the samples using pure tin. The potential probe contacts were ohmic and their areas did not exceed 0.12 mm^2. To avoid surface effects the samples were etched.[9]

A check of the influence of the sample shape showed that the magnetoresistance in a quantizing magnetic field is independent of the length-to-width ratio provided that this ratio is greater than 10 (Fig. 2). The Hall potential difference was measured across transverse potential probes placed symmetrically in the middle of the sample. The magnetoresistance was measured using the potential probes as well as the sample ends. No edge effects were observed in the quantizing field. Experiments using steady magnetic fields showed that edge effects were strong in weak fields, but

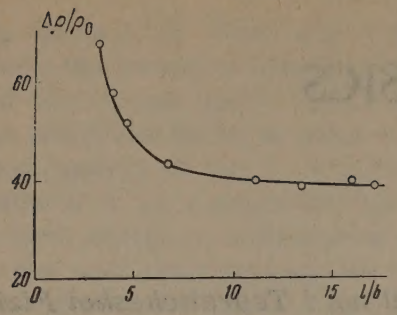

FIG. 2. The dependence of magnetoresistance on the parameter l/b for sample G1; l is the length of the sample and b is its width. H = 350 kgauss, T = 77°K.

in fields capable of quantization (H ≥ 25 kgauss at 77°K) the magnetoresistance measured using the potential probes was indistinguishable from that across the ends of the sample.

The results obtained in weak pulsed magnetic fields were checked by measurements in steady fields of 26 kgauss. The measured potential differences were recorded with an OK-17M oscillograph. Induction effects were cancelled out with a coil placed in the field with the sample.

The dependence of each effect (the Hall effect or magnetoresistance) on the field was determined using the two outer oscillograms (Fig. 1) obtained for two opposite directions of current. Records of the effect at five selected values of the field, taken in steps of 50—80 kgauss, were made on the same oscillogram frame. The peak oscillogram values were then used to plot the field dependence of the effect. Both methods of obtaining the field dependence gave the same results, with all experimental points lying on the same curve. The absence of hysteresis in curves obtained with increasing and decreasing field corroborated the results.

For measurements at liquid-nitrogen temperature, the magnet and the sample were placed inside a nitrogen bath. Liquid hydrogen was poured into a special Dewar which contained a holder and the sample. This Dewar was placed in the working volume of the magnet. The sample temperature was measured with a copper-constantan thermocouple. The sample temperature was unaffected by passage of currents of density up to 120 amp/cm^2. The current density actually used in the measurements did not exceed 15 amp/cm^2. In a field of 450 kgauss at 20°K the electric field intensity in pure samples reached 8 v/cm but there were no departures from Ohm's law.

RESULTS

Eight samples were cut from an ingot with an impurity carrier density $n \approx 3 \times 10^{16}$ cm^{-3}. Four

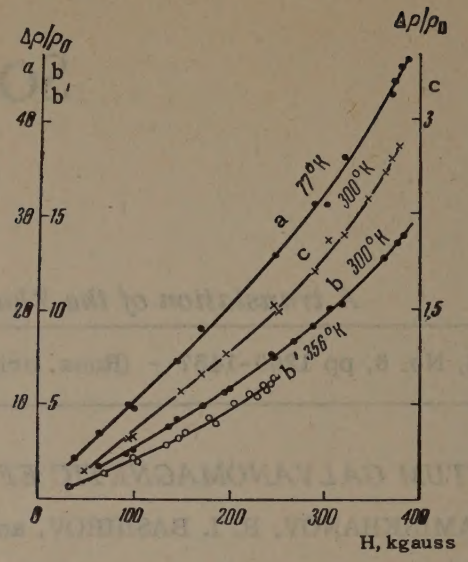

FIG. 3. The dependence of magnetoresistance on the magnetic field intensity for two samples of InAs: G1 (curves a, b, and b') and M-13 (curve c).

more samples were obtained from a less pure ingot with $n \approx 2 \times 10^{18}$ cm^{-3}. Figures 3 and 4 give the Hall coefficient R and the magnetoresistance $\Delta\rho/\rho_0$ in a transverse magnetic field, for two typical samples: G1 with a conductivity of 175 ohm^{-1} cm^{-1}, R = 200 cm^3/coul at 77°K, and M-13 with a conductivity of 2870 ohm^{-1} cm^{-1}, R = 3 cm^3/coul at 77°K.

If the effective carrier mass in n-InAs is taken to be $m^* = 0.03m_0$, where m_0 is the free-electron mass, then at H > 10^5 gauss the cyclotron resonance frequency is $\hbar\omega_0 > 5.8$ kT at 77°K and $\hbar\omega_0 > 22$ kT at 20°K.

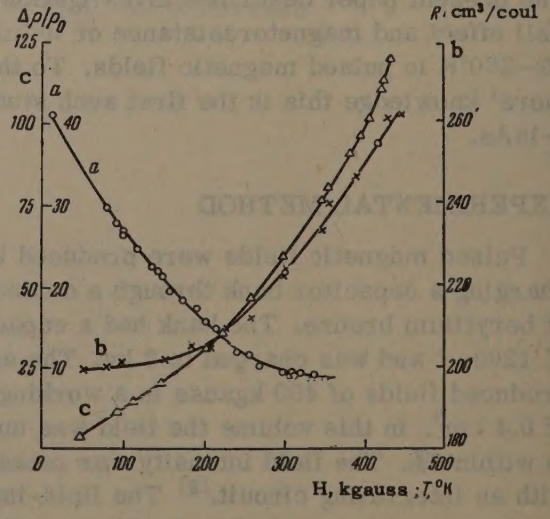

FIG. 4. Sample G1: a) the dependence of magnetoresistance on temperature (H = 252 kgauss); b) the dependence of the Hall coefficient on the magnetic field intensity (T = 20°K); c) the dependence of magnetoresistance on the magnetic field intensity (T = 20°K).

The Hall coefficient of sample G1 was independent of the magnetic field intensity up to 400 kgauss both at 300 and at 77°K. At 20°K the value of R was also practically constant in fields of up to 160 kgauss. Above 160 kgauss, R began to rise and increased by a factor of 1.4 when 450 kgauss was applied. An increase of the Hall coefficient with the magnetic field intensity was reported earlier for n-InSb[10,11] and for p-Ge.[12] An interesting feature in the case of InAs is that sample G1 was degenerate at 20°K and its reduced chemical potential in the absence of a magnetic field was $\mu^* = \mu_0/kT = 8.1$, taking the effective electron mass as $0.03m_0$.[13] The conduction band and impurity levels overlapped in the absence of a magnetic field. With increase of the magnetic field intensity the overlap was removed and above 160 kgauss the activation energy of impurities became positive and greater than the mean energy of conduction electrons. Consequently the equilibrium carrier density decreased above 160 kgauss.

In the strongly degenerate InAs sample M-13 the Hall coefficient was not affected by magnetic fields at 20°K because the conduction-band and impurity-level overlap was considerable.

Our investigations of the Hall effect showed that InAs can be used to construct probes for measuring the intensities of strong magnetic fields.

Figures 3 and 4 show that at 77°K magnetoresistance $\Delta\rho/\rho_0$ rose in sample G1 as $H^{1.20}$; in the seven other samples similar to G1 the exponent of H ranged from 1.13 to 1.20. Sample G1 was degenerate at 77°K with $\mu_0^* = 2.1$. According to the theory of Adams and Holstein,[3] there should be a strong dependence of $\Delta\rho/\rho_0$ on H in the case of degeneracy: $\Delta\rho/\rho_0 \propto H^5T$ if carriers are scattered on acoustical vibrations of the lattice, and $\Delta\rho/\rho_0 \propto H^{3/2}T^0$ in the case of pure Rutherford scattering. Measurements of the Nernst-Ettingshausen effect and values of $R\sigma$ at 20—300°K showed that carrier scattering in sample G1 was of mixed phonon-ion type. The weak dependence of $\Delta\rho/\rho_0$ on H at 20—77°K can be accounted for in terms of the Adams-Holstein theory[3] if it is assumed that a strong magnetic field removes degeneracy.[2,5] The assumption was confirmed by the fact that the criterion of degeneracy in the presence of a magnetic field,[2] $\frac{4}{9}(\mu_0/\hbar\omega_0)^2\mu_0 \gg kT$, was not satisfied in sample G1 at 77°K in a field of 10^5 gauss: $\frac{4}{9}(\mu_0/\hbar\omega_0)^2\mu_0 \approx \frac{1}{10}$ kT.

Classical statistics predicts $\Delta\rho/\rho_0 \propto H^2T^{-1/2}$ for acoustical scattering and $\Delta\rho/\rho_0 \propto H^0T^{-3/2}$ for scattering of carriers on impurity ions.[3] Combination of the two types of scattering can produce the dependence of $\Delta\rho/\rho_0$ on H which was actually observed at 77°K.

At 20°K the magnetoresistance rose almost linearly with the magnetic field intensity up to 160 kgauss: $\Delta\rho/\rho_0 \propto H^{1.1}$; above 160 kgauss it was found that $\Delta\rho/\rho_0 \propto H^{1.74}$. The more rapid rise of magnetoresistance above 160 kgauss was due to reduction of the carrier density. Klinger and Voronyuk[5] showed that reduction of the equilibrium carrier density in a magnetic field makes the dependence of $\Delta\rho/\rho_0$ on H more pronounced. Above 160 kgauss it was found that $R \propto H^{0.6}$; the exponent in the dependence of $\Delta\rho/\rho_0$ on H also increased by 0.6 on transition from below 160 kgauss to stronger fields.

With increase of temperature, carrier scattering on acoustical lattice vibrations becomes more intense and scattering on impurity ions becomes important. In accordance with this prediction it was found that in the quantum region, $\Delta\rho/\rho_0 \propto H^{1.45}$ at 300°K while $\Delta\rho/\rho_0 \propto H^{1.55}$ at 360°K; the quantum region at these two temperatures lies above 240 kgauss.

The magnetoresistance of the less pure sample M-13 was an order of magnitude smaller than that of sample G1. Consequently the quantum region in M-13 began above 300 kgauss. Degeneracy was not removed by fields of up to 400 kgauss. The observed dependence $\Delta\rho/\rho_0 \propto H^{1.50}$ at $H > 350$ kgauss was less marked than the theoretical dependence[3] predicted for the degenerate case. The magnetic field intensity may have been insufficient to produce agreement with this theory.

Figure 3 gives the temperature dependence of magnetoresistance at H = 252 kgauss. When temperature was lowered from 300 to 186°K, the magnetoresistance rose according to $\Delta\rho/\rho_0 \propto T^{-1.30}$. Further reduction of temperature to 77°K showed $\Delta\rho/\rho_0 \propto T^{-0.72}$ Between 77 and 20°K it was found that $\Delta\rho/\rho_0 \propto T^{0.50}$. Below 160 kgauss the rise of $\Delta\rho/\rho_0$ on cooling from 77 to 20°K was negligible.

The longitudinal magnetoresistance, $\Delta\rho_{\parallel}/\rho_0$ was too small to be measured: in sample G1 it could not have been greater than 0.2.

[1] P. N. Argyres, Phys. Rev. 109, 1115 (1958); P. N. Argyres and E. N. Adams, Phys. Rev. 104, 900 (1956).

[2] P. N. Argyres, J. Phys. Chem. Solids 8, 124 (1959).

[3] E. N. Adams, and T. D. Holstein, J. Phys. Chem. Solids 10, 254 (1959).

[4] V. L. Gurevich and Yu. A. Firsov, JETP 40, 199 (1961), Soviet Phys. JETP 13, 137 (1961).

[5] M. I. Klinger and P. I. Voronyuk, JETP 33, 77 (1957), Soviet Phys. JETP 6, 59 (1958).

[6] É. A. Zavadskii and I. G. Fakidov, FMM 10, 495 (1960).

[7] V. R. Karasik, DAN SSSR 130, 521 (1960), Soviet Phys. Doklady 5, 100 (1960).

[8] Furth, Levine, and Waniek, Rev. Sci. Instr. 28, 949 (1957).

[9] J. R. Dixon and D.P. Enright, J. Appl. Phys. 30, 733 (1959).

[10] H. P. R. Frederikse and W. R. Hosler, Phys. Rev. 108, 1136 (1957).

[11] R. J. Sladek, J. Phys. Chem. Solids 5, 157 (1958).

[12] V. R. Karasik and G. B. Kurganov, FTT 2, 2594 (1960), Soviet Phys. Solid State 2, 2313 (1961).

[13] Zwerdling, Keyes, Foner, Kolm, and Lax, Phys. Rev. 104, 1805 (1956).

Translated by A. Tybulewicz
286

FORBIDDEN E TRANSITIONS IN Tb^{159} *AND* Yb^{173}

G. A. VARTAPETYAN, Z. A. PETROSYAN, and A. G. KHUDAVERDYAN

Physics Institute, Academy of Sciences, Armenian S.S.R.

Submitted to JETP editor May 5, 1961

J. Exptl. Theoret. Phys. (U.S.S.R.) 41, 1704-1709

Two half-lives are measured: $T_{1/2} = (1.7 \pm 0.7) \times 10^{-10}$ sec for the 364-kev level of Tb^{159} and $T_{1/2} = (1.2 \pm 0.7) \times 10^{-10}$ sec for the 351-kev level of Yb^{173}. The E1 transition probabilities are calculated and compared with the values derived from the Nilsson model. It is concluded that, just as in the case of Hf^{177}, E1 transitions occur in both nuclei with probabilities differing widely from the theoretical values.

THE probability ratio of the 208- and 321-kev E1 transitions in Hf^{177} disagrees strongly with the Alaga formula.[1] However, it has been shown that the probability of the 208-kev transition is close to the value calculated from the Nilsson model, whereas disagreement by a factor of about 400 results for the 321-kev transition.[2] It is interesting to consider whether this occurs for all E1 transitions of deformed nuclei, to which the Alaga formula cannot be applied.

Table I shows disagreement with the Alaga formula for E1 transitions forbidden by the asymptotic selection rules in Tb^{155}, Tb^{157}, Tb^{159}, Yb^{173}, and Lu^{175}.[3] In the present work we measured the absolute probabilities of E1 transitions in Tb^{159} and Yb^{173}.

THE Tb^{159} NUCLEUS

The decay of Gd^{159} has been studied in[4], where the character and intensity ratio of γ transitions were calculated. An upper limit $T_{1/2} \leq 5 \times 10^{-10}$ sec was obtained for the half-life of the 364-kev level. Mtzger and Todd,[5] using the resonance scattering method, obtained $\tau = (2 \pm 0.3) \times 10^{-10}$ sec for the mean life of this level, whereas in the present work we have used delayed β-γ coincidences. The 364-kev photons were detected with a NaI(Tl) crystal, while β radiation was detected with an anthracene crystal. We used FÉU-33 photomultipliers and a "fast-slow" coincidence circuit with 6×10^{-9} sec resolving time.[6]

The time distribution of delayed coincidences was compared with an instantaneous resolution curve for a Ru^{103} source used under the same conditions (Fig. 1). The centers of gravity of the two curves are separated by $\tau = (2.5 \pm 1) \times 10^{-10}$ sec; this indicates $T_{1/2} = (1.7 \pm 0.7) \times 10^{-10}$ sec for the half-life of the 364-kev level.

Three γ quanta with energies 225, 307, and 364 kev are emitted from the 364-kev level. The conversion coefficient of 364-kev radiation[4,5] indicates an E1 transition. Malik et al[7] assign an E2 + M1 character to this transition. Nathan and Popov[8] used Coulomb excitation of Tb^{159} to investigate the 364-kev level, and calculated the reduced electric transition probability B(E2). The latter authors showed that E1 and E2 transitions cannot be distinguished. Taking their value for B(E2), $T_{1/2} \approx 10^{-9}$ sec is obtained for the 364-kev level.

However, the results obtained by Coulomb excitation and delayed coincidences agree in general.[9] We can therefore conclude that the given transition is more likely to be of E1 character.

Toth and Nielsen[10] have recently studied the 327- and 227-kev levels of Tb^{157} and Tb^{155}, respectively, from which E1 quanta are emitted. The intensity ratios for these nuclei are given in

Table I. Ratios of reduced E1 transition probabilities

Nucleus	Transition energy, kev	Experimental ratio	Theoretical ratio (strong interactions)
Tb^{155}	227; 161	1 : 0.007	1 : 0.43
Tb^{157}	327; 265; 183	1 : 0.0075 : 0.105	1 : 0.43 : 0.07
Tb^{159}	364; 307; 225	1 : 0.013 : 0.12	1 : 0.43 : 0.07
Yb^{173}	351; 272; 171	1 : 57 : 39	1 : 0.3 : 0.037
Lu^{175}	396; 282; 145	1 : 1.4 : 1	1 : 0.125 : 0.0125
Hf^{177}	321; 208	1 : 100	1 : 0.125

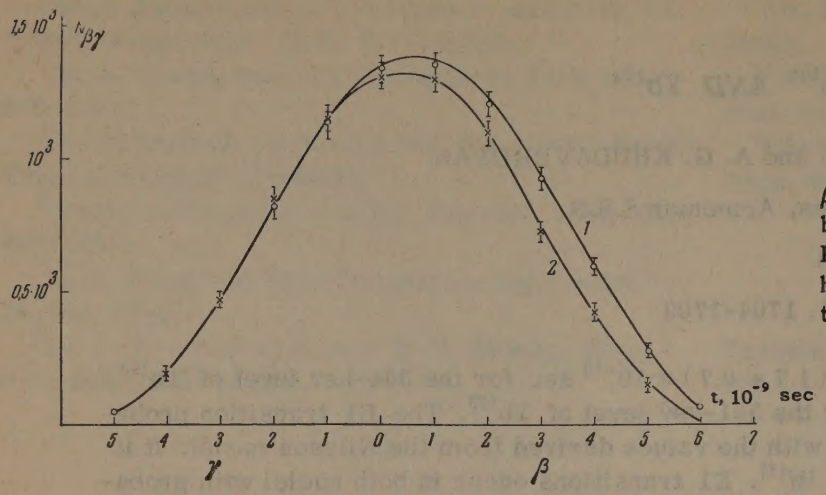

FIG. 1. Delayed-coincidence curves. 1 – Gd^{159}, $\beta-\gamma_{364}$; 2 – Ru^{103}, $\beta-\gamma_{364}$ (selecting pulses produced by Compton electrons recoiling from 495-kev γ rays). Pulse delays are represented to the left of zero on the horizontal axis for the γ counter, and to the right for the β counter.

Table II

Nucleus	Transition energy, kev	Ratio of calculated (from Weisskopf formula) to experimental M2 transition probability*	Nucleus	Transition energy, kev	Ratio of calculated (from Weisskopf formula) to experimental M2 transition probability*
Tb^{159}	225	0,8	Lu^{175}	396	1.3
Tm^{169}	63	0.35—3.5		282	2
Yb^{173}	351	0.8	Hf^{177}	208	1.1
	171	0.55	Lu^{177}	147	0.8

*For transitions where the E1/M2 ratio in the E1 + M2 mixture is known.

Table I. The Tb^{159} nucleus is very similar to Tb^{157} and Tb^{155} [10]; this furnishes an additional argument in favor of assigning E1 character to the 364-kev transition.[4,5] Using the results given in [4] for the intensity ratio and conversion coefficients of 364-kev E1 radiation and 225-kev E1 + M2 radiation in Tb^{159}, we computed the following transition probabilities:

$$P_{364}(E1) = 4\cdot10^{9}\,\text{sec}^{-1}, \qquad P_{225}(E1) = 1.2\cdot10^{8}\,\text{sec}^{-1}.$$

As in the case of the M2 radiation in mixed E1 + M2 transitions observed in rare earth elements, we find that the transition probability of a 225-kev M2 transition is in good agreement with the value calculated from the Weisskopf formula (Table II).

The conversion coefficient for the 307-kev transition has not been measured. We obtain the percentage of M2 in the 307-kev transition by assuming that the Alaga formula holds for unforbidden M2 transitions [1,6]. The result E1/M2 = 2.7 gives $P_{307}(E1) = 3\times10^{7}\ \text{sec}^{-1}$.

By comparing these E1 transition probabilities with values computed from the Nilsson formula,[2] we obtain the different degrees of forbiddenness:

$$f_{N364} = 10, \qquad f_{N225} = 6, \qquad f_{N307} = 300.$$

THE Yb^{173} NUCLEUS

Lu^{173} decay has been studied by two groups of investigators,[11,12] who obtained the γ-ray ratios and conversion coefficients. By using these values and assuming that the Alaga and Weisskopf formulas are applicable to unforbidden M2 transitions (Table II) we arrive at an order of magnitude for the half-life of the 351-kev level. It must be noted that the conversion coefficients for the 171-, 272-, and 351-kev transitions and the intensity of the 351-kev transition obtained by Bichard et al[12] differ from the results given in [11]. Taking the results given in [12], we find that the ratio $B_{272}(M2)/B_{351}(M2)$ is 225 times larger than the theoretical result, whereas M2 transitions are allowed. These results therefore appear to be incorrect. From the M2 percentage in 351- and 171-kev radiation and the intensity ratios in [11] we obtain $T_{1/2} \approx 7\times10^{-10}$ sec for the half-life of the 351-kev level.

MEASUREMENT OF THE HALF-LIFE OF THE 351-kev LEVEL

The Lu^{173} nucleus is converted by electron capture to Yb^{173} in a 351-kev excited state, from which it goes to the ground state mainly by the cascade emission of 272- and 79-kev γ rays. The half-life of the 351-kev level can be measured by using x_{capt}-γ_{272} delayed coincidences. For the purpose of detecting 50-kev x rays and 272-kev γ rays we used two NaI(Tl) crystals; the resolving time of the system was 9×10^{-9} sec. The channel registering capture x rays also registered x rays from a 79-kev conversion transition. We

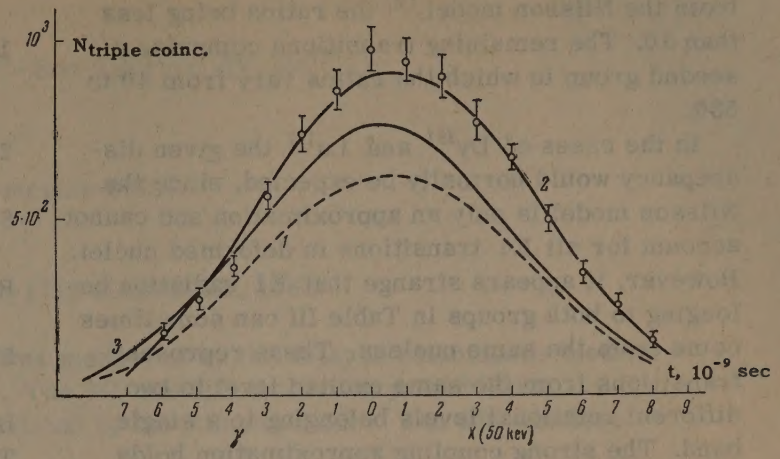

FIG. 2. Delayed-coincidence curves. 1 – Lu^{173}, $x_{conv} + x_{capt} - \gamma_{272}$; 2 – Lu^{173}, $x_{capt} - \gamma_{272}$ (computed curve and experimental points); 3 – Na^{22}, $\gamma_{50} - \gamma_{272}$ (with registration in both instances of pulses equivalent to those produced by Compton electrons recoiling from 510-kev γ rays).

thus obtained a combined $x_{capt} + \gamma_{conv} - \gamma_{272}$ coincidence curve (curve 1 in Fig. 2).

The pure x_{capt}-γ_{272} curve can be derived either by subtracting the x_{conv}-γ_{272} curve from curve 1, or by measuring x_{capt}-γ_{79} triple coincidences.

The x_{conv}-γ_{272} curve can be computed from knowledge of the conversion coefficient for the 79-kev transition, the 79-kev level lifetime,[13] and the K/L capture ratio for the transition to the 351-kev level.[11] Curve 2 is calculated by subtracting the x_{conv}-γ_{272} curve from curve 1. Figure 2 shows the experimental results for triple coincidences, which fit well the computed curve 2. Curve 3 is the instantaneous resolution curve for Na^{22}. The separation of the centers of gravity of curves 2 and 3 gives the mean lifetime $\tau = (6 \pm 1) \times 10^{-10}$ sec and half-life $T_{1/2} = (4.2 \pm 0.7) \times 10^{-10}$ sec. The latter agrees well with the result $(4.7 \pm 0.3) \times 10^{-10}$ sec given in [14].

The measured half-life of the 351-kev level is of the same order as that computed from data in [11], while assuming that the Alaga and Weisskopf formulas are valid for allowed M2 transitions.

The following probabilities were calculated for 351-, 272-, and 171-kev E1 transitions:

$$P_{351}(E1) = 4.7 \cdot 10^7 \text{ sec}^{-1}, \quad P_{272}(E1) = 1.35 \cdot 10^9 \text{ sec}^{-1},$$

$$P_{171}(E1) = 1.65 \cdot 10^8 \text{ sec}^{-1}.$$

By comparing these results with the analogous values calculated by means of the Nilsson functions,[2] we obtain the corresponding degrees of forbiddenness f_N:

$$f_{N351} = 530, \quad f_{N272} = 2.5, \quad f_{N171} = 0.7.$$

Table II gives the ratio between the M2 transition probabilities for Yb^{173} calculated from Weisskopf's formula and the experimental values (when the M2/E1 ratio is known from [11]).

DISCUSSION OF RESULTS

Table III gives information regarding the E1 transition probabilities obtained by us together with other known analogous probabilities of transitions in rare earth elements.[15,16] For one group of these E1 transitions the experimental probabilities agree with the theoretical values derived

Table III

Nucleus	Transition energy, kev	Ratio of computed (from Nilsson formula) to experimental E1 transition probability		Nucleus	Transition energy, kev	Ratio of computed (from Nilsson formula) to experimental E1 transition probability	
		First group	Second group			First group	Second group
Eu^{153}	98	⩽5		Dy^{161}	25.8	1.2	
Gd^{155}	86	2.3			75		40
	106	2.5		Tm^{169}	63	0.6	
Tb^{155}	227	?			272	2.5	
	161		?	Yb^{173}	171	0.7	
	327	?			351		530
Tb^{157}	183	?			282	10	
	265		?	Lu^{175}	145	1.35	
	364	10			396		100
Tb^{159}	225	6		Hf^{177}	208	0.6	
	307		300		321		400
				Lu^{177}	147		250

from the Nilsson model,[2] the ratios being less than 10. The remaining transitions comprise a second group in which the ratios vary from 40 to 530.

In the cases of Dy^{161} and Lu^{177} the given discrepancy would normally be expected, since the Nilsson model is only an approximation and cannot account for all E1 transitions in deformed nuclei. However, it appears strange that E1 radiation belonging to both groups in Table III can sometimes come from the same nucleus. These represent transitions from the same excited level to two different rotational levels belonging to a single band. The strong coupling approximation holds for these nuclei, so that the Alaga formula is applicable.

It would be interesting to consider whether the rotation-single-particle or rotation-vibration interactions observed in Tb^{159}, Lu^{175}, and Hf^{177} (which have little effect on energy levels or on the probabilities of unforbidden γ transitions) can appreciably change the probabilities of forbidden E1 transitions.

In conclusion we wish to thank A. I. Alikhanyan for his interest.

[1] G. A. Vartapetyan, JETP **38**, 1916 (1960), Soviet Phys. JETP **11**, 1378 (1960).

[2] S. G. Nilsson, Kgl. Danske Videnskab. Selskab, Mat.-fys. Medd. **29**, No. 16 (1955).

[3] H. Vartapetian, Compt. rend. **244**, 65 (1957).

[4] Nielsen, Nielsen, and Skilbried, Nuclear Phys. **7**, 561 (1958).

[5] F. R. Metzger and W. B. Todd, Nuclear Phys. **13**, 177 (1959).

[6] H. Vartapetian, Ann. phys. **3**, 569 (1958).

[7] Malik, Nath, and Mandeville, Phys. Rev. **112**, 262 (1958).

[8] O. Nathan and V. I. Popov, Nuclear Phys. **21**, 631 (1960).

[9] Alder, Bohr, Huus, Mottelson, and Winther, Revs. Modern Phys. **28**, 432 (1956).

[10] K. Toth and O. B. Nielsen, Nuclear Phys. **22**, 57 (1961).

[11] Dzhelepov, Preobrazhenskii, and Serzhenko, Izv. AN SSSR Ser. Fiz. **22**, 795 (1958), Columbia Tech. Transl. p. 789.

[12] Bichard, Mihelich, and Harmatz, Phys. Rev. **116**, 720 (1959).

[13] Berlovich, Bonits, and Nikitin, Izv. AN SSSR Ser. Fiz. **25**, 218 (1961), Columbia Tech. Transl. p. 210.

[14] Berlovich, Bonits, and Gusev, Report at Eleventh Conference on Nuclear Spectroscopy, Riga, 1961.

[15] B. R. Mottelson and S. G. Nilsson, Kgl. Danske Videnskab. Selskab, Mat.-fys. Medd. **1**, No. 8, 1959.

[16] B. S. Dzhelepov and L. K. Peker, Skhemy raspada radioaktivnykh yader (Decay Schemes of Radioactive Nuclei), AN SSSR, 1958.

Translated by I. Emin
287

THE LIFETIME AND NATURE OF THE 686-*kev LEVEL IN* Re^{187}

G. A. VARTAPETYAN

Physics Institute, Academy of Sciences, Armenian S.S.R.

Submitted to JETP editor May 16, 1961

J. Exptl. Theoret. Phys. (U.S.S.R.) 41, 1710-1712 (December, 1961)

The half-life of the 686-kev level in Re^{187} was measured by the delayed coincidence method and found to be $T_{1/2} = (2 \pm 0.7) \times 10^{-10}$ sec. The E1 and E2 transition probabilities are compared with the corresponding ones calculated by the Nilsson model. The 686-kev level is not necessarily a vibrational level.

THE level scheme of Re^{187} has been studied by many authors.[1,2] Nonetheless the nature of the 686 and 511 kev levels is not clearly understood. Gallagher, Edwards, and Manning,[1] who compared the distribution of these levels with computations based on the Nilsson model conclude that both levels are vibrational. If so, these are the first vibrational levels to be discovered in odd nuclei.

Since the energy predictions of the Nilsson model are rather approximate, we shall consider in this paper the transition probabilities of the 686- and 511-kev levels of the Re^{187} nucleus and the 646-kev level of the Re^{185} nucleus.

The ground state of Re^{185} and Re^{187} has a spin $5/2$ and, according to Mottelson and Nilsson,[3] corresponds to the Nilsson state [402], No. 27. By analogy with the 646-kev level in the Re^{185} nucleus[3,4], one can assume that the 511-kev level with spin $1/2$ is the state [400]. It is easy to see that E2 transitions from both the 511 and 686 kev levels are permitted by the asymptotic selection rules.[3] Nilsson's wave functions[3] were used to compute the E2 transition probabilities B(E2). These were found to agree with those given by the Weisskopf formula. The measured B(E2) values for these two transitions obtained by the Coulomb excitation method were 4 to 6 times larger than the theoretical ones.[4]

As for the 686-kev level with spin $5/2$, it corresponds to Nilsson's state [532 $5/2$], No. 36. Under these conditions a 480 kev E2 transition is hindered.[3] Computation of the probability $P_{\gamma E2}$ of this transition by the Nilsson method yields a degree of hindrance 10 times what it is according to the Weisskopf formula. Such hindered E2 transitions have been found in deformed Ta^{181} and Np^{237} nuclei.[3]

In the case of these nuclei the experimental values for the degree of hindrance (according to the Weisskopf formula) vary within a range of 20 to 400. Taking $P_{\gamma E2} = 2.5 \times 10^8$ sec^{-1}, we obtain for the half-life of the 686-kev level the value $T_{1/2} = 1.2 \times 10^{-9}$ sec (where we have also taken into consideration the data in[1,2] for the γ-ray intensity ratios).

This period was measured experimentally by the method of delayed $\beta - \gamma_{480}$ and $\beta - \gamma_{686}$ coincidences. The β-particles were detected with an anthracene counter and the photons with a NaI(Tl) crystal. The resolving time of the "fast-slow coincidence" circuit[5] was 6×10^{-9} sec. The delayed coincidence curves were compared with instantaneous resolution curves for Co^{60}. In both cases the centers of gravity of the curves were shifted by an amount $\Delta = (3 \pm 1) \times 10^{-10}$ sec. Hence, the half-life of the 686-kev level is $T_{1/2} = (2 \pm 0.7) \times 10^{-10}$ sec, and the ratio of the experimental and theoretical (Nilsson's) probabilities $P_{\gamma E2}$ is 6.

Thus, our result indicates a larger value for the probability of the E2(480 kev) transition than does the Nilsson model. Results of a similar nature were also obtained for E2 transitions with energies of 646 and 511 kev in Re^{185} and Re^{187} nuclei respectively.

At this point it should be noted that for hindered E2 transitions in Ta^{181} and Np^{237} nuclei where Nilsson's description is assumed to be accurate, the experimental values for B(E2) also exceed Nilsson's theoretical values.[6] Therefore, the divergence observed in the case of Re^{187} for the hindered E2(480 kev) transition is no particular reason to assume that the 686-kev level is not a Nilsson state. The excess of the transition probabilities over those predicted by the Nilsson and Weisskopf formulae in the cases of Re^{185} and Re^{187} nuclei can be explained by the fact that for these nuclei the strong coupling approximation is not quite accurate.

Nucleus	Transition energy in kev	Ratio of the E2 transition probability to probability computed by the Weisskopf formula	Nucleus	Transition energy in kev	Ratio of the E2 transition probability to probability computed by the Weisskopf formula
$_{75}Re^{185}$	646	4.5 (permitted)	$_{79}Au^{197}$	78	28
Re^{187}	480	0.7 (hindered)		279	27
	511	6 (permitted)		550	25
$_{77}Ir^{191}$	82.6	15	$_{81}Tl^{203}$	279	10
	356	47		689	7
Ir^{193}	73	25	Tl^{205}	205	5
	368	20	$_{82}Pb^{207}$	569	1.5

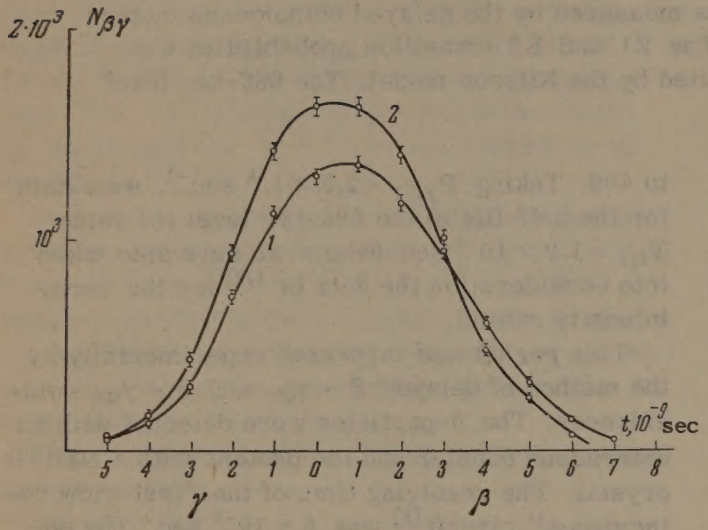

Delayed coincidence curves: 1) W^{187} nucleus, $\beta-\gamma_{480}$ coincidence, 2) Co^{60} nucleus, $\beta-\gamma_{480}$ coincidence (Compton electrons from 1.17- and 1.33-Mev γ quanta). (The numbers on the abscissa to the left of zero correspond to the delay of the pulse from the γ counter, and to the right of zero to the β-counter delay.)

These slightly deformed nuclei may represent an analogy with the transition zone nuclei[7] listed in the table. The examined levels are single-particle levels with collective effects that increase the probability of E2 transitions.

Assuming that the 686 kev level is the [532 5/2] state in Nilsson's nomenclature, we can compute the E1 transition probabilities for the 686 and 552 kev radiations. The transition probabilities given here for these two γ-radiations are in good agreement with the values computed by the Alaga formula. It must be said of this type of transition and generally of E1 transitions in deformed nuclei[8] that their experimental probabilities are either equal to the theoretical values based on the Nilsson model or about ten times smaller. Indeed, according to Nilsson $P_{\gamma E1}(686) = 2.3 \times 10^{10}$ sec^{-1}, which is about 10 times the experimental value for $P_{\gamma E_1}$.

Moreover, the relatively low energy of these levels tends to indicate that they are not of a vibrational nature. Nathan and Popov[4] think that they observed vibrational levels in odd Tb^{159} and Ho^{165} nuclei whose transition probabilities were of the same order as those computed by the Weisskopf formula. It is worth noting that these levels have lower energies than the vibration energies computed on the basis of the vibration rotation interactions observed in the indicated nuclei.[9]

Thus, we cannot assert (unlike Gallagher, Edwards, and Manning[1]) that the 686- and 511-kev levels in the Re^{187} nucleus are vibrational. Our result tends rather to indicate that the 686-kev level is a single-particle state. To reach a more definite conclusion we would need to know the theoretical values based on the intermediate coupling hypothesis, both for transitions from vibrational levels in odd nuclei (to determine whether they are close to the values obtained by the Weisskopf formula) and for the 480 kev transition of the Re^{187} nucleus.

I take this opportunity to express my appreciation to A. I. Alikhanyan for his interest in this paper.

[1] Gallagher, Edwards, and Manning, Nucl. Phys. 19, 18 (1960).

[2] M. Vergnes, Ann. Physique 5, 11 (1960).

[3] B. R. Mottelson and S. G. Nilsson, Mat.-Fys. Skr. Dan. Vid. Selsk. 1, No. 8 (1959).

[4] O. Nathan and V. I. Popov, Nucl. Phys. 21, 631 (1960).

[5] H. Vartapetian, Ann. de Physique 3, 569 (1958).

[6] Yu. N. Gnedin, Izv. AN SSSR, Ser. Fiz. 25, 83 (1961), Columbia Tech. Transl. p. 82.

[7] Alder, Bohr, Huus, Mottelson, and Winther, Revs. Modern Phys. 28, 432, 1956.

[8] Vartapetyan, Petrosyan, and Khudaverdyan, JETP 41, 1704 (1961), this issue p. 1213.

[9] R. K. Sheline, Revs. Modern Phys. 32, 1 (1960).

Translated by A. Skumanich
288

ELASTIC SCATTERING OF 247-Mev GAMMA RAYS ON HYDROGEN

P. S. BARANOV, L. I. SLOVOKHOTOV, G. A. SOKOL, and L. N. SHTARKOV

P. N. Lebedev Physics Institute, Academy of Sciences, U.S.S.R.

Submitted to JETP editor June 9, 1961

J. Exptl. Theoret. Phys. (U.S.S.R.) 41, 1713-1721 (December, 1961)

The angular distribution of 247 ± 10 Mev gamma rays produced in the synchrotron of the Lebedev Physics Institute, which were scattered elastically on hydrogen, has been investigated. Differential cross sections were obtained for c.m. scattering angles of 148, 132, 108, 93, 70, and 55°. The experimental results are compared with calculations based on one-dimensional dispersion relations with an additional contribution from a single-meson intermediate state taken into account.

1. INTRODUCTION

THE elastic scattering of a γ quantum by a proton (the Compton effect) is an elementary process whose investigation can in principle supply information regarding the structure of the proton. At the present time we unfortunately have no satisfactory meson theory of the proton Compton effect at γ-ray energies above the meson photoproduction threshold. Some endeavors to construct a theory of the Compton effect based on different variants of meson theory or even using a phenomenological approach have produced no positive results.

The attempts to develop a theory of the Compton effect on the basis of dispersion relations are more promising.[1-4] However, difficulties are encountered when the contribution of the high-energy region and the effect of the nonphysical region are taken into account.[5]

It has been noted[6] that when constructing a theory of the Compton effect one must take into account the relation between γ-ray scattering and the two-photon decay of the π^0 meson. It is then possible in principle to determine from experimental data the mean life of the π^0 meson (a fundamental property).[7]

At the present time very meager experimental information is available regarding the elastic scattering of γ rays on hydrogen at energies above the meson photoproduction threshold. In the only experimental investigation[8] the dependence of the differential cross section on γ-ray energy was measured in the 120 — 280 Mev range for 90° and 130° c.m. scattering angles. The present work is a detailed investigation of the angular distribution of elastically scattered γ rays of about 250 Mev.

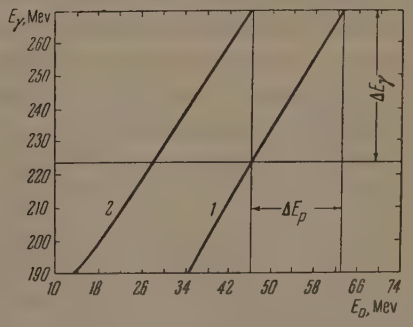

FIG. 1. Kinematic relation between proton energy and γ-ray energy at a fixed angle of proton recoil ($\theta_p = 36°$). 1 — for Compton effect; 2 — for π^0 photoproduction.

2. FORMULATION OF THE EXPERIMENT

Method of identifying the process. The principal difficulty encountered in the experimental investigation of the proton Compton effect,

$$\gamma + p \to p' + \gamma' \qquad (1)$$

is its extremely small cross section ($\sigma_{tot} \sim 2 \times 10^{-31}$ cm^2). At energies below the meson photoproduction threshold we can confine ourselves to registering only the scattered γ ray, without observing the recoil proton.[9]

Above the meson photoproduction threshold the difficulties are augmented considerably by the photoproduction of neutral mesons and their subsequent decay to two γ quanta:

$$\begin{array}{l} \gamma + p \to p' + \pi^0, \\ \qquad\qquad \downarrow \\ \qquad\qquad \gamma_1 + \gamma_2 \end{array} \qquad (2)$$

with a cross section that is two orders of magnitude larger than the cross section for process (1). For these reasons, the experimental investigation

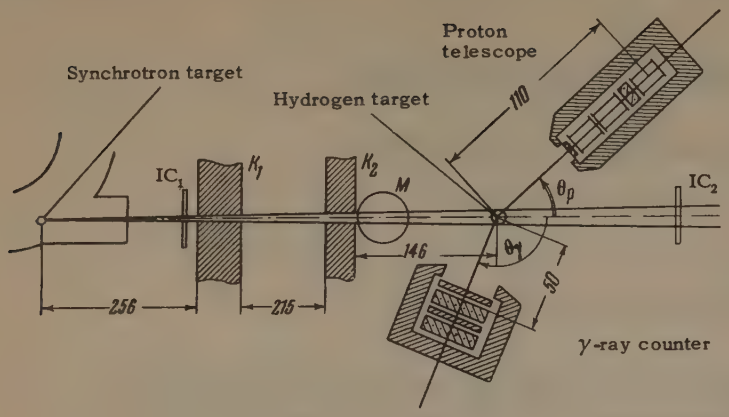

FIG. 2. Experimental geometry (with notation explained in the text).

of elastic γ-ray scattering on hydrogen in the given energy region depends primarily on identifying process (1) against the background of process (2).

In the present work process (1) was identified by registering coincidences between scattered γ rays and recoil protons. The registration of a recoil proton and the determination of its energy for a fixed γ-ray energy provide the basis for distinguishing between processes (1) and (2).

Figure 1 shows the kinematic relation between the recoil-proton energy in reactions (1) and (2) and the incident γ-ray energy for a fixed proton-recoil angle. It is apparent that in a certain γ-ray energy range, $\Delta E_\gamma = E_1 - E_2$, the energy of protons from reaction (1) exceeds that from (2). Since the bremsstrahlung spectrum is continuous, the described method of discrimination can be used only at the end of the spectrum, where $E_1 = E_{\gamma\,max}$. The scattered γ ray must be registered in addition to the proton in order to distinguish process (1) from the reaction

$$\gamma + p \rightarrow n + \pi^+, \qquad (3)$$

since the proton telescope sometimes registers charged mesons. The distinction of reaction (1) from reaction (3) is based on the difference between the neutron and γ-ray directions associated with a given angle of charged-particle flight. This difference in the correlated angles is used to exclude the background reaction

$$\gamma + d \rightarrow n + p, \qquad (4)$$

which can occur in the 0.02% natural admixture of deuterium contained in liquid hydrogen.

An upper estimate of the background process associated with electron production in the hydrogen target, and with the subsequent electron-proton scattering, has shown that this process contributes $\lesssim 0.2\%$ and can be neglected for all the registration angles used in our work.

The background from the walls of the hydrogen target was also sharply reduced by registering proton-γ coincidences.

Experimental geometry (Fig. 2). The bremsstrahlung beam from the synchrotron of the Physics Institute, operated at 260 Mev maximum energy, passed through two lead collimators K_1 and K_2 before entering the liquid hydrogen target. The γ-ray pulse duration was $\sim 3000\,\mu$sec, corresponding to variation of the maximum bremsstrahlung energy from 244 to 260 Mev. The beam was monitored by two thin-walled ionization chambers IC_1 and IC_2, one placed ahead of collimator K_1, and the other positioned behind the hydrogen target.

Proton telescope. Protons were registered by a telescope consisting of three proportional counters and one scintillation counter placed ahead of either the first or last proportional counter. The proportional counters were glass cylinders of 60-mm diameter and 200-mm length, each with its axial wire parallel to the flight paths of the registered particles. Pieces of 250-micron aluminum foil were cemented to the ends of the counters. The counters were filled with argon and 1% CO_2 at 500 mm Hg. A collimated Po^{210} α-particle source was placed within each proportional counter for the purposes of energy calibration of the counter and a sensitivity check of the setup during operation. The proportional counters in the proton telescope served to determine the energy range of registered protons and to distinguish protons from charged particles of smaller mass ($e^\pm$, $\pi^\pm$). The minimum proton energy was fixed by the total amount of matter ahead of the third telescope counter, while the maximum proton energy was set by the electronic threshold in the amplifying circuit connected to the third counter.

The scintillation counter in the proton telescope consisted of a plastic scintillator (p-terphenyl in polystyrene) 60 mm in diameter and 5.5 mm thick

for measurements at 16, 24, 36, and 44°, or 0.3 mm thick for measurements at 56° and 64°, a Plexiglas light pipe, and a FÉU-33 photomultiplier. In the work involving coincidences with γ-ray counter pulses the use of a scintillation counter in the proton telescope resulted in a sharp reduction of the random correlation background, and provided for supplementary discrimination of process (1) from the background process (3) based on the time of flight of particles in these reactions. The angle resolution of the proton telescope was $\pm 1.5°$.

Gamma-ray counter. The γ-ray counter consisted of two liquid scintillators (p-terphenyl in phenylcyclohexane) in Plexiglas containers of 150-mm diameter and 30-mm thickness, used in conjunction with FÉU-33 photomultipliers. A lead converter 8 mm thick was placed before each scintillator. Pulses from the two photomultipliers were summed and sent into coincidences with pulses from the scintillation counter in the proton telescope. The angle resolution of the γ-ray counter was $\pm 9°$; its efficiency was found experimentally to be $\sim 80\%$ by comparing the proton-γ coincidence count from reaction (2) with the count of protons alone. Details of the technique and the energy dependence found for γ-ray registration efficiency are described in [10].

Hydrogen target. Our liquid hydrogen target has been described in [11]. The irradiated target volume was a thin-walled brass cylinder of 15-mg/cm^2 wall thickness, 50-mm diameter and 100-mm length. The γ-ray beam had the same diameter as the cylinder. Vacuum pipes were used for γ-ray beam entrance and exit. The first section of the entrance vacuum pipe was located between the poles of a 2000-gauss electromagnet M 20 cm long (Fig. 2). In order to reduce the amount of matter in the proton path, the target vacuum cylinder was equipped with windows covered by 250-micron aluminum foil. The construction and thermal regime of the hydrogen target insured continuity of the measurements during a prolonged period, with liquid hydrogen added at intervals of ~ 50 hours.

Electronics. Figure 3 is a block diagram of the electronic circuit. Pulses from the proportional counters P_1, P_2, and P_3 were amplified and fed through threshold circuits and gates to slow coincidence circuits I, II, and III having the resolving time $\tau = 2 \times 10^{-6}$ sec. Proton-γ coincidences were registered by a fast coincidence circuit with 4×10^{-9} sec resolving time (gated by the scintillation counters), from which pulses were fed to the coincidence circuit III.

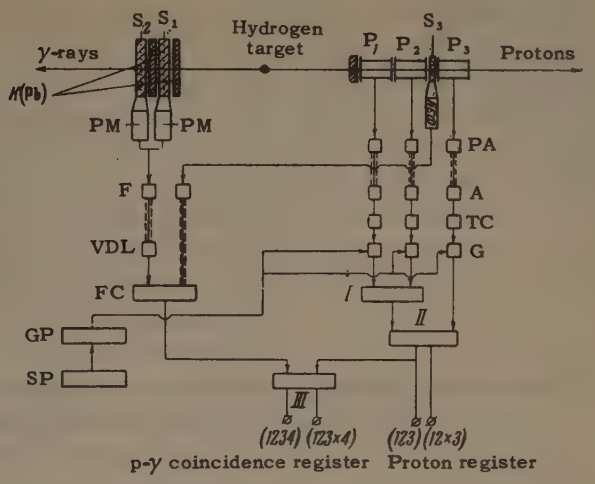

FIG. 3. Block diagram of electronic circuit. P – proportional counters; S – scintillation counters; I, II, III – "slow" coincidence circuits; PA – preamplifiers; A – amplifiers; TC – threshold circuits; G – gates; K – lead converters; F – pulse former; VDL – variable delay line; FC – "fast" coincidence circuit; GP – gating pulse; SP – master pulse from synchrotron.

The entire apparatus was adjusted by registering the photoproduction of π^0 mesons on protons [reaction (2)]. The operation of all electronic units was charted, the dependence of the p-γ coincidences on delay time in one of the fast-coincidence channels was determined, and the resolution times of all coincidence circuits were selected.

In adjusting for the registration of process (1) we took into account the different proton flight times in reactions (1) and (2).

Formulation of experiment and measurement procedure. Our experiments were designed to determine the angular distribution of γ rays, with a given energy, scattered elastically on protons. The kinematic conditions for distinguishing reactions (1) and (2) permitted measurements over a γ-ray range $\Delta E_\gamma \sim 20$ Mev for the maximum bremsstrahlung energy $E_{\gamma max} = 260$ Mev.

The measuring procedure consisted in the alternate registration of yields from reaction (1) at the angles $\theta_p = 16, 24, 36, 44, 56$, and 64°, and of the yield from reaction (2) at $\theta_p = 16°$. The transition to registration of process (2) was accomplished by changing both the energy adjustment of the proton telescope and the angle of the γ-ray counter. For the sake of reliability and convenience in treating the data, the yield of reaction (2) was measured as far as possible in the same γ-ray energy range as for reaction (1).

The measuring procedure gave the yield ratio of processes (1) and (2) for a given γ-ray energy, so that the cross section for (1) could be calculated

θ_p, deg	θ_γ, deg	θ^*_γ, deg	$\bar{\theta}_p$ (l.s.) deg	$\Delta\bar{\theta}_p$ (l.s.), deg	$\bar{\theta}_\gamma$ (c.m.s.) deg	$\bar{E}_\gamma$, Mev	$\Delta\bar{E}_\gamma$, Mev	Yield ratio ($\times 10^4$) of reactions (1) and (2)	$\frac{d\sigma}{d\Omega}/\left(\frac{e^2}{Mc^2}\right)^2$, cm²/sr (c.m.s.)
16	140	104	15.5	±1.65	148.0	247.7	± 5	140±12	4.17±0.35
24	121	94	23.5	±1.70	132.2	247.8	± 5	110±9.0	3.33±0.28
36	94	140	35.0	±1.70	108.8	247.2	± 5	74±8.0	3.09±0.33
44	78	—	42.5	±1.70	93.1	245.2	± 6	25.7±2.7	2.08±0.24
56	56	94	54.5	±2.0	70.3	237.0	±15	9.43±1.37	1.60±0.20
64	42	76	62.0	±2.0	54.8	232.6	±15	8.07±1.07	1.34±0.18

dependence of differential cross sections given in [8]. Figure 4 shows the resulting angular distribution.

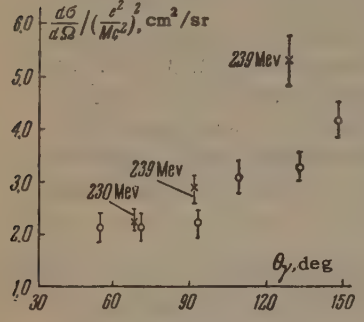

FIG. 4. Angular distribution (c.m.) of γ rays scattered elastically on hydrogen, converted to 247 Mev (lab. system). o – present work; x – from [8].

Comparison with other experimental results. The literature contains only one experimental investigation[8] of the Compton effect at energies above the photomeson threshold. In that work the energy dependence of the cross section at c.m. γ-ray angles 90° and 129° was measured for E_γ = 239 Mev. The differential cross section for the Compton effect is also given at θ_γ = 70° (c.m.) for E_γ = 230 Mev. Our angular distribution can thus be compared with only three points in [8]. Figure 4 shows that both experiments reveal the same tendency toward growth of the cross section for $\theta_\gamma > 90°$, with greater increases in [8].

Comparison with theory. Among the theoretical studies of the Compton effect at energies above the photomeson threshold the work based on dispersion relations is of current interest. Dispersion relations for the proton Compton effect were first derived by Bogolyubov and Shirkov.[1] Numerical results have been given by several investigators.[2,3,7] Our results can be compared directly with those of Akiba and Sato (abbreviated hereafter as AS)[3] and of Jacob and Mathews (abbreviated as JM).[7] The results given in [2] pertain to lower γ-ray energies.*

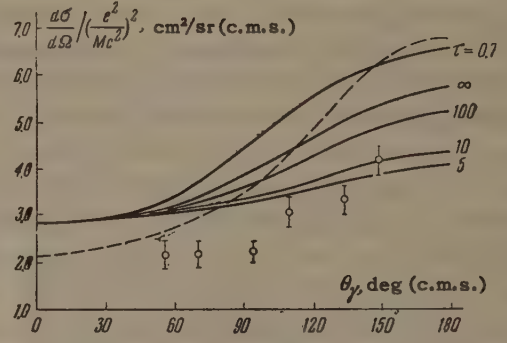

FIG. 5. Comparison of our results, converted to E_γ = 247 Mev (lab. system), with theoretical results of Akiba and Sato [3] (dashed curve) and of Jacob and Mathews [7] (continuous curves). The numerals at the ends of the curves are values of τ in the unit 10^{-18} sec.

Figure 5 shows the data of AS interpolated by us for 247-Mev γ rays, and the data of JM converted by us to the same energy for different values of the mean π^0 life. Both investigations suffer from some uncertainty in the calculation of the dispersion integrals, associated with the existence of a nonphysical region and with the high-energy contribution (5). At 247 Mev the inaccuracy associated with the nonphysical region can appear at c.m. angles $\theta_\gamma > 70°$.[1] In addition to the basic diagrams of the process the JM article takes into account the Low diagram[6] relating γ-ray scattering to two-photon π^0 decay. The Low amplitude makes no contribution to the differential cross section at $\theta_\gamma = 0°$ and increases monotonically with the angle.

The JM result corresponding to zero contribution from the Low amplitude (the curve for $\tau = \infty$) should be close to the AS result. Figure 5 shows large disagreement between the two theoretical studies, and thus indicates the incompleteness of the existing theory.

The comparison of the AS and JM results with our experimental findings in Fig. 5 shows that our absolute values lie somewhat closer to the AS curve at small angles, but fall considerably below that curve at large angles. We could expect that an additional contribution from the Low amplitude

*Note added in proof (November 17, 1961). After the present article had been sent to press L. I. Lapidus and Chou Kuang-chao published (Preprint D-740 of the Joint Institute for Nuclear Research) numerical calculations for the Compton effect, extended to 300-Mev rays. These results are not compared with ours in the present article.

when a cross section for (2) was known.

The measurements at each angle θ_p for reaction (1) were checked by varying the γ-ray counter angle.

Measurements were also obtained with an empty target for a few thicknesses of the absorbers ahead of the proton telescope, in order to determine the compensating effect of hydrogen in the target. The p-γ coincidence count in the checking measurements and in the empty target run practically agreed and comprised about 10% of the count from reaction (1). Since the yield from (1) was very small, amounting to from 10 to 3 pulses per hour, a long period was required for the accumulation of sufficient data. In order to obviate all types of errors associated with variation of the synchrotron operating mode the measurements were performed in a number of runs, each of which included several angles θ_p. The sensitivity of the proton telescope was measured regularly at the beginning and end of each run. All measurements were monitored by thin-walled ionization chambers, whose absolute sensitivity was determined with a thin-walled graphite chamber.

Special attention was devoted to the stability of the energy limit $E_{\gamma max}$ and to the shape of the lengthened γ-ray pulse. Continuous visual monitoring was employed for this purpose.

3. RESULTS

Treatment of experimental data. The data obtained in each run of measurements on reaction (1) were subjected to separate statistical analysis, and the average yield per unit radiation dose was computed. This yield was then converted for 100% γ-ray counter efficiency, taking the energy dependence of the efficiency into account.[10] All experimental runs were also combined statistically for each angle, with weighting according to the total radiation dose in each run.

The measurements for the "background" process (the yield at the varied angle θ_γ^*) were treated similarly, and were subtracted from the corresponding values for reaction (1). The measured yields were used to compute the ratio between the differential cross sections for reactions (1) and (2), averaged over the registered energy and angle intervals. In our calculations we used Schiff's bremsstrahlung spectrum, averaged over the energies of the electrons impinging on the synchrotron target.

The table gives the weighted mean angles $\bar{\theta}$ and energies E and the corresponding half-widths $\Delta\bar{\theta}_p$ and $\Delta\bar{E}_\gamma$ calculated by means of the angular and energy resolution functions. Specific calculations of the resolution functions were performed by successive numerical integration taking account of the relation between variables. Integration limits were determined by the combined geometry of the proton telescope and target, the registered energy range of the proton telescope, and the kinetics of the process. The geometry of the γ-ray counter did not affect the calculation of the resolution functions.

Corrections for multiple proton scattering in the absorbers were computed for the mean proton energy in the registered interval, using Sternheimer's results.[12]

The last column of the table gives the absolute differential cross sections for reaction (1) in the c.m. system. These were obtained by using the cross section for reaction (2) in the lab. system, $\frac{d\sigma}{d\Omega}(16°) = (26.6 \pm 2.7) \times 10^{-30}$ cm^2/sr, obtained from the literature.[13]

Our absolute value of the cross section for (2) derived from the bremsstrahlung flux agreed with the foregoing value within statistical error limits.

Accuracy of results. Because of our procedures in the measurements and handling of the data, inaccuracy of the differential cross sections was determined mainly by the statistical inaccuracy ($\pm$ 10%) of the measured yields. For the differential cross section ratio the inaccuracy of other quantities in the calculation is unimportant because of mutual cancellation. This does not apply to the inaccuracy, not exceeding $\pm$ 5%, in determining the solid angle of the γ-ray counter. The accuracy of the absolute cross section for reaction (1) was found to be about $\pm$ 15%. This was determined by the indicated errors of the cross section ratio and by the $\pm$ 10% inaccuracy of the cross section for reaction (2).

The foregoing inaccuracy estimates are valid for all angles, except in the cases of γ rays scattered at 56° and 74° in the c.m. system. For these two angles a $\pm$ 3% error in determining the maximum bremsstrahlung energy can lead to a $\pm$ 25% error in the cross section.

4. DISCUSSION

Angular distribution. The table shows that the differential cross sections measured in the present work pertain in most instances to γ-ray energies close to 247 Mev. For the purpose of analyzing the angular distribution all results were converted to the single energy value 247 Mev, using the energy

in the AS calculations with the sign given by JM for the interference term would bring about agreement with experiment for all angles.

Figure 5 shows that the JM theoretical results disagree with our experimental absolute values for all the given lifetimes τ.

Lapidus and Chou Kuang-chao[14] have recently pointed out that the relative sign of the pole diagram used by JM is incorrect. A correction of the sign of the pole term should increase the discrepancy between the JM theory and our data. It should be mentioned in this connection that the agreement between the JM theory and experiment concerning the energy dependence of the cross section appears to be accidental.

The theoretical curves given in Fig. 5 were obtained using numerical calculations of the dispersion integrals. As already noted, these results may be incorrect, especially for large angles.

The experimental data can be compared with the theoretical angular distribution in a form unassociated with numerical calculations of dispersion integrals. Following JM, we fitted our data for the angular distribution to the formula

$$\frac{d\sigma}{d\Omega} = A\frac{(1-y)^3}{(y-y_0)^2} + \frac{B+Cy+Dy^2}{y-y_0}, \qquad (5)$$

where the parameter A is associated with the π^0 lifetime. The π^0 lifetime derived on the basis of this approximation was four orders of magnitude smaller than that obtained in experiments on K^+-meson decay[15] and from the Primakoff effect.[16] This discrepancy between the values of the π^0 lifetime obtained in [15] and [16], on the one hand, and from the use of Eq. (5) as an approximate equation for our data, on the other, indicates that the JM theoretical treatment is inaccurate.

It should be noted that a theoretical study by Nelipa and Fil'kov,[17] using double dispersion relations, also yields a form of angular distribution different from that of JM.

Further improvement of the theory, especially an improvement of the approximation formula, will apparently permit a more detailed comparison of the theory with our experimental results, and will determine the π^0 lifetime more accurately from the angular distribution of γ rays scattered elastically on hydrogen.

The authors wish to thank Professor P. A. Cerenkov, Professor V. I. Gol'danskiĭ, Doctor of Physical and Mathematical Sciences, A. M. Baldin, and the synchrotron crew of the Physics Institute.

[1] N. N. Bogolyubov and D. V. Shirkov, DAN SSSR 113, 529 (1957), Soviet Phys.-Doklady 2.

[2] L. I. Lapidus and Chou Kuang-chao, JETP 39, 1056 (1960), Soviet Phys. JETP 12, 735 (1961).

[3] T. Akiba and I. Sato, Progr. Theoret. Phys. (Kyoto) 19, 93 (1958).

[4] J. Mathews, Ph.D. Thesis, California Institute of Technology, 1957.

[5] A. M. Baldin, JETP 39, 1151 (1960), Soviet Phys. JETP 12, 800 (1961).

[6] F. E. Low, Proc. 1958 Annual Intern. Conf. on High Energy Physics, p. 98.

[7] M. Jacob and J. Mathews, Phys. Rev. 117, 854 (1960).

[8] Bernardini, Hanson, Odian, Yamagata, Auerbach, and Filosofo, Nuovo cimento 18, 1203 (1960).

[9] Gol'danskiĭ, Karpukhin, Kutsenko, and Pavlovskaya, JETP 38, 1695 (1960), Soviet Phys. JETP 11, 1223 (1960).

[10] Baranov, Slovokhotov, Sokol, and Shtarkov, Pribory i tekhnika éksperimenta (Instruments and Experimental Techniques) No. 3, 63 (1961).

[11] L. I. Slovokhotov, Preprint, Phys. Inst. AN, 1960.

[12] R. M. Sternheimer, Rev. Sci. Instr. 25, 1070 (1954).

[13] Vasil'kov, Govorkov, and Gol'danskiĭ, JETP 37, 11 (1959), Soviet Phys. JETP 10, 7 (1960).

[14] L. I. Lapidus and Chou Kuang-chao, JETP 41, 294 (1961), Soviet Phys. JETP 14, 210 (1962).

[15] Blackie, Engler, and Mulvey, Phys. Rev. Letters 5, 384 (1960).

[16] Tollestrup, Berman, Gomez, and Ruderman, Proc. 1960 Annual Intern. Conf. on High Energy Physics at Rochester, Interscience Publishers, New York, 1960, p. 27.

[17] N. F. Nelipa and L. V. Fil'kov, Preprint, Phys. Inst. Acad. Sci., A-2, 1961.

Translated by I. Emin
289

THE CHANGE IN THE CONCENTRATION OF CURRENT CARRIERS IN BISMUTH DUE TO ADMIXTURES OF SELENIUM

N. E. ALEKSEEVSKII and T. I. KOSTINA

Institute for Physics Problems, Academy of Sciences, U.S.S.R.

Submitted to JETP editor June 10, 1961

J. Exptl. Theoret. Phys. (U.S.S.R.) 41, 1722-1724 (December, 1961)

The galvanomagnetic properties of bismuth containing admixtures of selenium have been investigated. From the values of the Hall constant in high fields it was established that one selenium atom changes the electron concentration in bismuth by $3 \times 10^{-2} \pm 10\%$ electrons per atom.

BASED on the results of investigations of the de Haas-van Alphen effect,[1,2] cyclotron resonance,[3] the anomalous skin effect,[4] and of its galvanomagnetic properties,[5] bismuth can be classified as a metal with a closed Fermi surface. For this group of metals the asymptotic behavior of the resistance tensor in a magnetic field is determined by the relation between the number of electrons n_1 and of holes n_2. Owing to the small number of carriers (10^{-5} electrons per atom) small admixtures of other elements to bismuth exert a great influence on its magnetic and electrical properties, and as we have shown,[6] bismuth can be taken out of one group of metals (with $n_1 = n_2$) to another (with $n_1 \neq n_2$) by a relatively small number of admixtures. It seemed of interest to make a detailed study of the effect of small admixtures on the galvanomagnetic properties of bismuth and to estimate the change in the carrier concentration produced by the admixtures.

The initial bismuth of 99.998 purity ($r_{300°K}/r_{4.2°K} = 30$) was purified by zone refinement. After 20 — 30-fold recrystallization the ratio $r_{300°K}/r_{4.2°K}$ reached 260. Radioactive selenium was introduced as the impurity, and its concentration was monitored by the specimen's γ-ray intensity. Specimens with 0.5×10^{-4} and 3.05×10^{-4} selenium were studied. Single crystal specimens in the form of 2 — 2.5 mm diameter rods, 30 mm long, were prepared by Kapitza's method.[7] In all the investigations the trigonal axis of the specimens coincided with the specimen axis.

Figure 1a shows the dependence of $\Delta r_{HT}/r_{0T} = \{r_H(T) - r_0(T)\}/r_0(T)$ on the field for specimens Bi-1 (pure bismuth with $r_{300°K}/r_{4.2°K} = 260$) and Bi-2 (selenium admixture 0.5×10^{-4}, $r_{300°K}/r_{4.2°K} = 62$). While specimen Bi-1 shows the characteristic quadratic dependence of $\Delta r/r$ on field with the quantum oscillations, already observed by Shubnikov,[8] superimposed on it, the resistance of Bi-2 tends to saturation in the same effective fields ($H_{eff} = H_0 r_{300°K}/r_{4.2°K}$)*. As is well known,[9] if the number of electrons is not equal to the number of holes ($n_1 \neq n_2$), then in large fields the resistance tends to saturation, the value of which depends on the temperature, on the purity of the metal and on the direction of the magnetic field relative to the crystallographic axes, while the Hall "constant" tends to the constant value $R = 1/ec\,(n_1 - n_2)$.

Figure 2 shows the dependence of the Hall constant R on field for specimens Bi-2 (0.5×10^{-4} selenium) and Bi-3 (selenium admixture 3.05×10^{-4}). It can be seen that the Hall constant R tends to saturation for both specimens, but we did not observe any appreciable reduction in the anisotropy of R with respect to the direction of the magnetic field relative to the crystallographic axes. Having determined the values of n_1 and n_2 from the Hall constant for both specimens, the change in carrier concentration, produced by one atom of admixture, can be evaluated from their difference. If it is assumed that the Fermi surface for the holes changes little for these concentrations, then one atom of selenium produces a change of $3 \times 10^{-2} \pm 10\%$ electrons per atom in the electron concentration.[6]

*We should point out that a second quadratic dependence, $\Delta r/r = f(H)$,[9] should be observed for metals with an equal number of electrons and holes ($n_1 = n_2$) in sufficiently great magnetic fields. Figure 1b shows the ratio $\Delta r/r$ for Bi-1 as a function of H^2. Two regions of a quadratic dependence of $\Delta r/r$ on field are clearly seen.

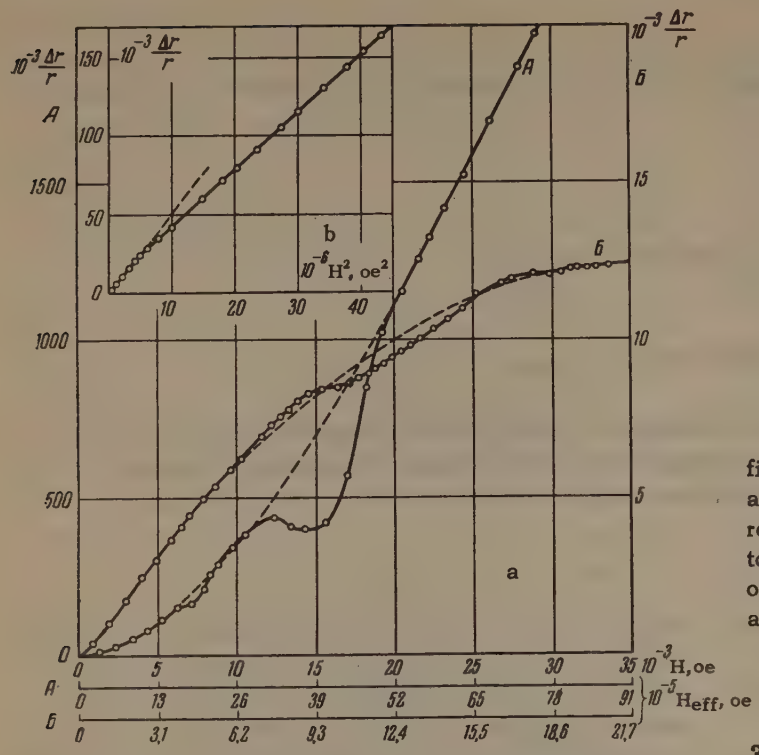

FIG. 1. a – The dependence of $\Delta r/r$ on the intensity of the magnetic field; T = 4.2°K, current parallel to the trigonal crystal axis, field parallel to the binary axis: curve A – for specimen Bi-1, curve B – for Bi-2; b – the dependence of $\Delta r/r$ on H^2 for specimen Bi-1 in the range of magnetic fields from 0 to 6.6 koe.

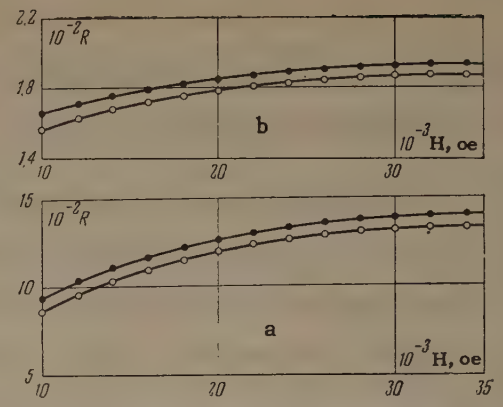

FIG. 2. The dependence of the Hall constant on magnetic field strength (T = 4.2°K): a – for specimen Bi-2 (0.5×10^{-4} Se) and b – for specimen Bi-3 (3.05×10^{-4} Se). Full circles – current parallel to the trigonal axis of the specimen, field parallel to the binary axis; open circles – current parallel to the trigonal axis of the specimen, field perpendicular to the binary axis.

The initial bismuth specimens and the bismuth with the admixtures were prepared at our request in the Rare Metal Institute by R. A. Dul'kina, for which we express our sincere gratitude.

[1] D. Shoenberg, Phil. Trans. Roy. Soc. **A245**, 1 (1952).

[2] N. B. Brandt, JETP **38**, 1355 (1960), Soviet Phys. JETP **11**, 975 (1960).

[3] Galt, Yager, Merritt, and Cetlin, Phys. Rev. **114**, 1396 (1959).

[4] G. E. Smith, Phys. Rev. **115**, 1561 (1959).

[5] N. E. Alekseevskiĭ and Yu. P. Gaĭdukov, JETP **36**, 449 (1959), Soviet Phys. JETP **9**, 311 (1959).

[6] Alekseevskiĭ, Brandt, and Kostina, Izv. AN SSSR Ser. Fiz. **21**, 790 (1957), Columbia Tech. Transl. p 792.

[7] P. L. Kapitza, Proc. Roy. Soc. **A119**, 358 (1928).

[8] L. Schubnikow and W. J. de Haas, Leiden Comm. **19**, No. 207a (1930).

[9] Lifshitz, Azbel', and Kaganov, JETP **31**, 63 (1956), Soviet Phys. JETP **4**, 41 (1957).

Translated by R. Berman
290

ALPHA DECAY OF Pu^{239}

B. S. DZHELEPOV, R. B. IVANOV, and V. G. NEDOVESOV

Radium Institute, Academy of Sciences, U.S.S.R.

Submitted to JETP editor June 12, 1961

J. Exptl. Theoret. Phys. (U.S.S.R.) 41, 1725-1728 (December, 1961)

The α spectrum of Pu^{239} was measured with a double focusing magnetic α spectrograph. Besides the well known α transitions, some new transitions to the excited levels of the U^{235} nucleus (104, 198, 224 and 299 kev) have been detected. A possible interpretation of the U^{235} levels is discussed. A Pu^{239} decay scheme is presented.

We undertook an investigation of the α spectrum of Pu^{239} using a double focusing α spectrometer.[1] Plutonium sources prepared by sputtering in vacuum were used for the measurements. Several exposures were made under the conditions indicated in Table I. In experiments 1—4 the magnetic field was adjusted to make the focusing conditions optimal for different portions of the spectrum.

All the exposures were made at constant instrument aperture, which amounted to 0.21% of 4π for the central point of the source.

Figure 1 shows the α spectrum of Pu^{239} obtained in exposures 1, 4, and 5; the measurement results are listed in Table II. In addition to the known α lines[2-4] we observed α transitions to the 104-, 198-, and 299-kev levels (α_4, α_8, and α_{11} in Table II). In [3,5] are given data on the existence of an α transition to the 234-kev levels; in this region of the spectrum we see the lines α_9 and α_{10}, corresponding to transitions to the 224-kev level and possibly to the 243-kev level. It must be noted that the analysis of the data obtained on low-intensity transitions is considerably hindered by the fact that the spectral lines have long "tails" on the low-energy side.

The transition α_5 is probably connected with the α decay of Pu^{240} (transition to the 4^+ level of the daughter nucleus U^{236}), contained as an impurity in our source; the line α_{12} can be attributed to the presence of a U^{233} impurity.

It is known[6,7] that the ground state of U^{235} has spin and parity $7/2^-$ (the [743] level in the Nilsson scheme[8] for deformed nuclei). However, the excitation energy of the first single-particle state of U^{235} is less than 1 kev. In the α decay of Pu^{239} the transition to this level with characteristic $1/2^+$ [631] is facilitated. On the basis of the α decay of Pu^{239} and the spectrum of the conversion electrons[2,3,5] it has been shown that the levels 13, 51, 84, and 150 kev are members of a rotation band with characteristic $K = 1/2^+$, and their spins and parities are respectively $3/2^+$, $5/2^+$, $7/2^+$, and $9/2^+$.

Table I

No. of experiment	Source dimensions, mm^2	$E(r_0)$,* Mev	Line half-width, kev	Duration of exposure, hours
1	0.5 × 10	5.150	8	1
2	0.5 × 10	5.138	10	98
3	0.5 × 10	5.040	10	120
4	0.5 × 10	4.980	10	150
5	2.0 × 15	4.850	20	85

*$E(r_0)$ – energy of the α particles moving in the given field on a circular orbit with radius $r_0 = 335$ mm (the focusing conditions are optimal for particles with this energy).

Calculation based on the formula for the energy spectrum of the rotational band with $K = 1/2^+$ yields energies of 200 and 302 kev for the $11/2^+$ and $13/2^+$ levels. One must therefore assume that the lines α_8 and α_{11} which we have observed are due to the decay of Pu^{239} to the levels $11/2^+$ and $13/2^+$ of the rotational band of a state with spin and parity $1/2^+$ ($K = 1/2^+$).

Coulomb excitation of the U^{235} nucleus[9] disclosed levels at 46 and 104 kev, which are members of the rotational band of the ground state of the nucleus ($K = 7/2^-$) with spins $9/2$ and $11/2$. The α spectrum shows clearly an α line corresponding to the transition to the 104-kev level. If we assume that this is indeed an α transition to the $11/2^-$ level of the band with $K = 7/2^-$, then there should exist two other transitions, to the ground state and to the 46-kev level. These, however, are practically impossible to observe, since the former coincides in energy with the transition to the $1/2^+$ level, and although the latter differs by 5 kev from the transition to the 51-kev level, its intensity is tens of times smaller, making its observation very difficult.

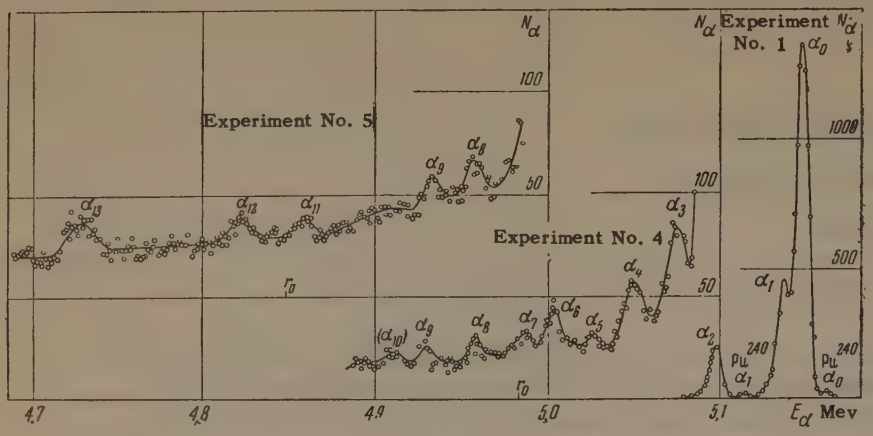

FIG. 1. The spectrum of Pu^{239} obtained in exposures 1, 4, and 5.

Table II

No. of line	Energy of level, kev	Transition intensity, %	Hindrance coefficient
α_0	1	72	1.7
α_1	13	17	6.1
α_2	51	11	5.7
α_3	84	0.038	950
α_4	104	0.030	1030
α_5	Transition of Pu^{240} to the 4^+ level of U^{236}.		
α_6	150	0.018	800
α_7	170	0.008	1290
α_8	198	0.008	860
α_9	224	0.008	580
α_{10}	243?	~0.003	~1200
α_{11}	299	0.004	360
α_{12}	U^{233} impurity (ground-state transition)		
α_{13}	424	0.007	30

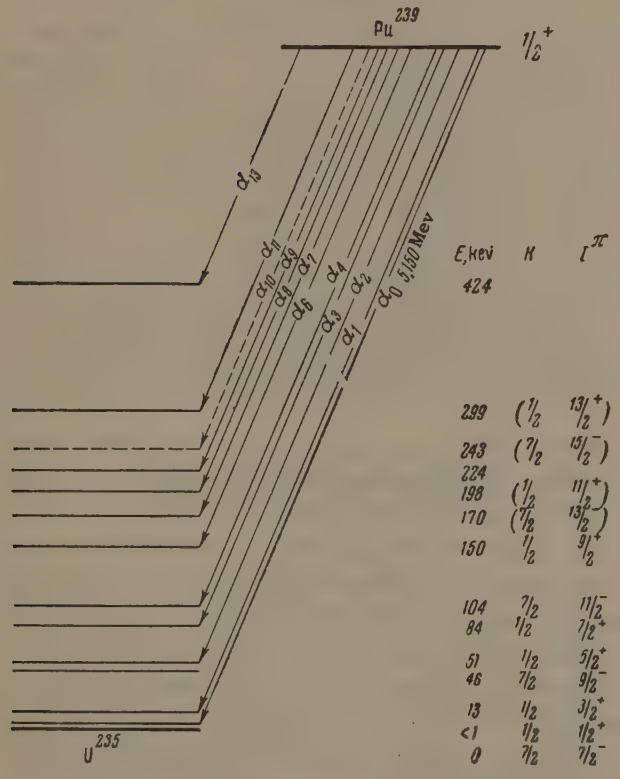

FIG. 2. Proposed decay scheme of Pu^{239}.

If our assumption concerning the nature of the 104-kev level is correct, the next members of this rotational band should be the 170- and 243-kev levels with spin and parity $13/2^-$ and $15/2^-$. The 170-kev level was observed earlier and the parity of this state was shown[5] to be negative. According to our data, the 243-kev level apparently also exists, although without complete reliability. The intensity ratios of the 104-, 170-, and 243-kev α transitions do not contradict the assumption that they belong to a single rotational band, but a serious objection to such an identification of the α_4, α_7, and α_{10} transitions is the excessive difference in the spins of the initial $(1/2^+)$ and final $(15/2^-)$ states of nuclei for the 243-kev level.

Naturally, a final solution of this problem can be obtained only if more complete and more accurate data are obtained on the α decay and on the spectrum of the conversion electrons, the latter being very complicated. The proposed decay scheme is shown in Fig. 2.

The authors are grateful to L. L. Gol'din and G. I. Novikova for graciously furnishing the plutonium source for our measurements. The authors are also grateful to V. A. Belyakov and V. N. Delaev for help in the measurements.

[1] Dzhelepov, Ivanov, Nedovesov, and Chumin, Izv. AN SSSR, ser. Fiz. **23**, 782 (1959), Columbia Technical Translations p. 780.

[2] Novikova, Kondrat'ev, Sobolev, and Gol'din, JETP **32**, 1018 (1957), Soviet Phys. JETP **5**, 832 (1957).

[3] G. I. Novikova, Dissertation, Institute of Theoretical and Experimental Physics, Academy of Sciences U.S.S.R. 1957.

[4] F. Asaro and I. Perlman, Phys. Rev. **88**, 828 (1952).

[5] Tret'yakov, Grishuk, and Gol'din, JETP **34**, 811 (1958), Soviet Phys. JETP **7**, 560 (1958).

[6] Strominger, Hollander, and Seaborg, Table of Isotopes, UCRL 1928 (1958).

[7] B. S. Dzhelepov and L. K. Peker, Skhemy raspada radioaktivnykh izotopov (Decay Schemes of Radioactive Isotopes) AN SSSR, 1958.

[8] B. R. Mottelson and S. G. Nilsson, Math. Fys. Skr. Dan. Vid. Selsk. **1**, No. 8 (1959).

[9] J. O. Newton, Nucl. Phys. **3**, 345 (1957); **5**, 218 (1958).

Translated by J. G. Adashko
291

A NEW ISOTOPE Er^{159}

A. A. ABDURAZAKOV, F. M. ABDURAZAKOVA, K. Ya. GROMOV, and G. Ya. UMAROV

Joint Institute for Nuclear Research; Tashkent Polytechnic Institute

Submitted to JETP editor June 20, 1961

J. Exptl. Theoret. Phys. (U.S.S.R.) 41, 1729-1732 (December, 1961)

The conversion-electron spectrum from the decay of neutron-deficient erbium isotopes was measured with a constant magnetic field β spectrograph. A new erbium isotope of mass number 159 ($T_{1/2} \sim 1$ hr) has been discovered. Some new γ transitions which arise in the decay chain $Er^{159} \rightarrow Ho^{159} \rightarrow Dy^{159}$ have been detected. A decay scheme for this chain is proposed.

THE spectrum of the conversion electrons produced in the decay of the neutron-deficient erbium isotopes was measured with a constant magnetic field β spectrograph.[1] The neutron-deficient erbium isotopes were obtained by the bombardment of tantalum with 660-Mev protons from the synchrocyclotron of the Joint Institute for Nuclear Research.

In a previous article[2] we discussed the data on the conversion electrons produced in the decay of erbium isotopes with a half-life greater than two hours. In the present experiment we studied the conversion-electron lines whose intensity decayed, according to our estimates, with a half-life $T_{1/2} < 2$ hr. We estimated the half-life from the decay in intensity (darkening) of the conversion lines on photographic film from successive exposures in the β spectrograph.

The target was bombarded for two hours. The exposure of the first film was usually begun 3 — 4 hr after the end of the bombardment and 30 — 40 min after separation of the erbium. The table lists the conversion-electron lines which we ascribe to isotopes with $T_{1/2} < 2$ hr.

Gromov and Dneprovskiĭ[3] observed conversion-electron lines of energy 118.9, 123.5, 255.8, 301.0 and 307.4 kev during the study of the conversion-electron spectrum of an erbium fraction. The half-life of these lines, according to [3], is 50 ± 10 min. These lines are, of course, identical to lines No. 6, 7, 15, and 16 observed by us. We suggest that all the lines listed in the table are produced in a decay chain which starts with a previously unknown erbium isotope with a half-life of about one hour. The mass number of the new isotope can be determined on the basis of the following known experimental facts.

1. The mass numbers 165, 161, 160, and 158

Conversion-electron Lines of the Chain

$$_{68}Er^{159} \xrightarrow[K]{\sim 1\ hr} {}_{67}Ho^{159} \xrightarrow[K]{33\ min} {}_{66}Dy^{159}$$

No.	H_ρ	E_e, kev	Identification of lines	$h\nu$, kev	Z*	Basis of identification
1	753.6	47,7	L_1 —56.8	56.8±0,1	(66)	Decay scheme
2	928.2	70,8	L_1 —79.9	79,9±0.1	(66)	Decay scheme
3	1185	111,3	—	—	—	—
4	1189	112,1	—	—	—	—
5	1196	113.1	—	—	—	—
6	1231	119.3	K —173,2	173,2±0,2	(66)	Decay scheme
7	1256	123,7	K —177.5	177,5±0,2	(66)	[7]
8	1400	150,3	K —205,9	205.9±0,3	67	(K, L_{II},L_{III})
9	1630	196.0	K —249.8	249,8±0,3	66	(K, L)
10	1635	197,0	$L_1 + L_{II}$ —205,9			
11	1639	197.9	L_{III} —206,0			
12	1646	199,4	K —253.2	253,2±0.3	66	(K, L)
13	1838	240,5	L_1 —249.6			
14	1855	244.2	L_1 —253,3			
15	1907	255,6	K —309,4	309.4±0,4	66	(K, L)
16	2103	300,4	L_1 —309,5			

*Charge of nucleus in which transition occurs.

are apparently excluded, since the half-lives of these erbium isotopes are considerably greater than two hours.

2. Dalkhsuren et al[4] studied the Er^{163} spectrum and observed γ rays of energy ~300, 430 and 1100 kev. According to their data, the intensity of these γ rays is no greater than 0.2% per decay. No γ rays with energy less than 300 kev were observed. On the other hand, we observed a number of conversion lines (lines Nos. 1 — 12) which, no doubt, are associated with γ transitions from energies below 300 kev. It is also obvious that we cannot observe conversion lines of γ transitions with energy 300 kev and greater and a γ-ray intensity less than 0.2% per decay. These arguments enable us to exclude the mass number 163.

3. We can definitely eliminate the mass numbers 157, 156, and 155, since in the decay of erbium isotopes with such mass numbers we should have observed the well-known intense γ transitions of the daughter isotopes 326.6-kev Dy^{157},[5] 138.0-kev Ho^{159},[6] and 227.0-kev Dy^{155}.[5] Despite a careful search, the conversion lines associated with these transitions were not observed.

4. Toth[7] observed the radioactive Ho^{159} isotope with a half-life of 33 min. He studied the Ho^{159} γ spectrum with a scintillation γ spectrometer and observed γ rays of energy 125, 180, 250, and 305 kev. Conversion lines Nos. 9, 12, 13, 14, 15, and 16 can be identified as K and L lines of the 249.8, 253.2, 309.4 kev γ transitions. The difference in energy of the K and L lines was determined with sufficient accuracy to establish that these transitions take place in the dysprosium nucleus. It is obvious that the energies of these three transitions coincide, within the limits of experimental accuracy, with the 250- and 305-kev γ-ray peaks observed by Toth. The conversion-electron lines Nos. 2 — 7 must include lines (K or L) associated with the 125- and 180-kev γ lines, but we do not have any reliable arguments for the identification of these lines. Hence the comparison of the data of Toth with our results leads to the conclusion that the lines listed in the table arise in the decay chain

$$Er^{159} \xrightarrow[K]{\sim 1\ hr} Ho^{159} \xrightarrow[K]{33\ min} Dy^{159}.$$

According to the data in the table, we can also identify the 205.9-kev transition. The difference in energy between the K, L_{II}, and L_{III} lines shows that this transition occurs in the holmium nucleus, i.e., it arises in the decay $Er^{159} \rightarrow Ho^{159}$.

On the basis of the data we can make some comments on the decay scheme $Er^{159} \rightarrow Ho^{159} \rightarrow Dy^{159}$. The quantum characteristics of $_{66}Dy^{159}_{93}$ should be determined by the 93rd neutron. Consideration of the Nilsson diagram indicates that the 93rd neutron should be in the $3/2^-$ [521] state. The data in the literature on the Dy^{159} decay does not contradict the assumption that the ground state has a spin $3/2^-$. In this connection, to construct the Ho^{159} decay scheme we should, first of all, seek the rotational band level of the Dy^{159} ground state. The energy of the first rotational band level of the $3/2^-$ [521] state is 55 kev in $_{64}Gd^{157}_{93}$ and 60 kev in $_{64}Gd^{155}_{91}$. We can expect that the energy of the first rotational level of Dy^{159} is close to this value. Among the lines in the table is one at 47.7 kev, which can be identified as the L_1 line of the 56.8-kev γ transition. We assume that this transition determines the energy of the Dy^{159} first rotational state $5/2\ 3/2^-$ [521]. The energy of the second rotational level in the first approximation can then be estimated from the formula $E = A[I(I+1) - I_0(I_0+1)]$. The parameter A is calculated from the value of the energy level with spin $5/2$. It turns out that the energy of the level with spin $7/2$ should be about 136 kev. If it is assumed that the 70.8-kev line is the L_1 line of the 79.9-kev transition and that this transition takes place between Dy^{159} rotational band levels with spins $7/2$ and $5/2$, then the energy of the level with spin $7/2$ turns out to be 136.7 kev. Energy considerations also permit us to introduce a 309.7-kev level. Three transitions with energies 309.4, 253.2, and (if we identify the 119.3-kev line as a K line) 173.1 kev go from this level. The proposed scheme is shown in the figure.

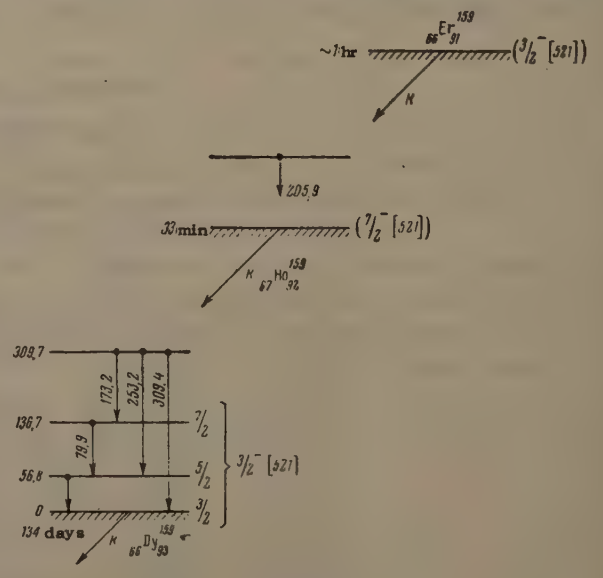

Proposed decay scheme for the decay $Er^{159} \xrightarrow[K]{\sim 1\ hr} Ho^{159} \xrightarrow[K]{33\ min} Dy^{159}$.

The authors express their sincere gratitude to B. S. Dzhelepov for his interest in this work and to V. A. Khalkin and Wang Fu-Chün for preparing the erbium samples.

[1] Abdurazakov, Abdurazakova, Gromov, Dzhelepov, and Umarov, Izv. AN Uzb. SSR (Bull. Acad. Sci. Uzbek S.S.R.) **5**, 53 (1961).

[2] Abdurazakov, Gromov, Dzhelepov, and Khalkin, Izv. AN SSSR, Ser. Fiz. **25**, 1096 (1961), Columbia Tech. Transl., in press.

[3] K. Ya. Gromov and I. S. Dneprovskiĭ, ibid. **25**, 1105 (1961).

[4] Dalkhsuren, Gvozdeva, Kuznetsova, Levenberg, Norseev, Pokrovskiĭ, and Yutlandov, Materialy tret'ego soveshchaniya po neĭtronodefitsitnym izotopam (Proc. Third Conf. on Neutron-Deficient Isotopes), Dubna, 1961.

[5] Abdurazakov, Gromov, Dzhelepov, and Umarov, Izv. AN SSSR, Ser. Fiz. **24**, 1126 (1960), Columbia Tech. Transl. p. 1130.

[6] E. P. Grigor'ev and B. S. Dzhelepov, DAN SSSR **135**, 564 (1960), Soviet Phys.-Doklady 5, 1243 (1961).

[7] K. S. Toth, Inorg. and Nucl. Chem. 7, 1 (1958).

Translated by E. Marquit
292

INVESTIGATION OF RADIOACTIVE DECAY OF Np^{237}

S. A. BARANOV, V. M. KULAKOV, P. S. SAMOĬLOV, A. G. ZELENKOV, and Yu. F. RODIONOV

Received by JETP editor June 21, 1961

J. Exptl. Theoret. Phys. (U.S.S.R.) 41, 1733-1739 (December, 1961)

Results of an investigation of the radioactive decay of Np^{237} are presented. More than 20 fine-structure monoenergetic α groups have been established by analyzing the α spectrum of Np^{237}. Most of the groups have been detected for the first time. On the basis of the experimental data obtained with the help of a β and γ spectrometer it has been possible to detect twelve γ transitions in the Pa^{233} nucleus. An energy level scheme for the Pa^{233} nucleus is constructed on the basis of the data obtained.

1. INTRODUCTION

THE radioactive isotope Np^{237}, discovered by Wahl and Seaborg [1] in the early Forties, is transformed via α decay into the β-radioactive isotope Pa^{233}. The half-life of Np^{237} is 2.2×10^6 years. The low specific activity of this isotope has hitherto made difficult precise research of the fine structure of the α radiation and of the electron spectrum. Some information on the radiation produced in the decay of this nucleus and on the levels of the daughter nucleus Pa^{233} is contained in several papers.[2-10]

We undertook a more precise study of the radioactive decay of Np^{237}, using apparatus of considerable efficiency and good resolution.

2. APPARATUS AND PREPARATION OF RADIOACTIVE SOURCES

We used in our research magnetic α and β spectrometers with double focusing of the charged-particle beam in an angle $\pi\sqrt{2}$, and also spectrometric proportional counters, a scintillation spectrometer, and other devices. The α, β, and γ spectrometers were described in our earlier articles.[11-13] We shall therefore discuss briefly only the preparation of the radioactive sources.

The sources for the α, β, and γ spectrometric measurements were prepared on the same day when the neptunium was thoroughly rid of extraneous impurities by triple chemical purification. The source for the α spectrometer was obtained by evaporating the 4 $\mu g/cm^2$ of neptunium on a glass base in vacuum. The source area was 10 $\times$ 100 mm. For β-spectrometer measurements we used three sources of much greater surface density; the size of the strongest source was 1×4 cm. It must be noted that the solution used to prepare the sources was also monitored by an ionization chamber with a grid and by a scintillation γ spectrometer, to check on the possible presence of other α- and β-active isotopes. Within the accuracy of instruments of this type we could observe no other α-active impurities.

3. FINE STRUCTURE OF α RADIATION OF Np^{237}

To obtain detailed information on the α structure of Np^{237} with the aid of an α spectrograph it is necessary to use a source of relatively large effective area and apparatus of high resolution. In our experiments the effective source area was 1—3 cm^2 and the minimum apparatus line width was 4.4 kev. To investigate a relatively wider region of the spectrum (~500 kev) and to carry out control experiments, several exposures with total duration of 300 hours were necessary. The energy calibration of the instrument was described by us earlier.[14] The standard line employed was the known group of other particles from Np^{237} with energy 4787.0 kev.[7]

The results of the investigation of the fine structure of the α radiation from Np^{237} are shown in Fig. 1 and in Table I.

As can be seen from Fig. 1, the α spectrum of Np^{237} is very complicated and contains more than 20 monoenergetic α lines. Some groups of α particles are exceedingly close in energy, the spacing not exceeding 2—5 kev in many cases. The conclusion that several α groups exist is therefore based on analysis of the shapes and half-widths of the α lines. Thus, for example, a comparison of the α_5 line (see the spectrum in the upper part of Fig. 1) with the groups $\alpha_{0,1,2}$, $\alpha_{6,7}$, $\alpha_{13,14}$ etc clearly indicates that the latter have a complicated composition. To confirm the data obtained we made three control experiments, which established

Table I. Fine Structure of α spectrum of Np^{237}

α_i	E_α, kev	J, %	Hindrance coefficient	E_{lev}, kev	α_i	E_α, kev	J, %	Hindrance coefficient	E_{lev}, kev
α_0	4872.3	0,441	2200	0	α_{11}?	4698.2	0.067	920	177.1
α_1?	4869.8	0,925	1000	~2—3	α_{12}	4693.4	0,178	320	182.0
α_2	4861.8	0.242	3400	~10.6	α_{13}	4663.0	1.605*	20	212.0
α_3	4816.3	1.487	270	57,0	α_{14}	4658.1	0.573*	56	217.3
α_4	4802.3	1.565	210	71,2	α_{15}	4638.4	4.617**	5	238.6
α_5	4787.0	51,42	5	86,3	α_{16}	4597.16	0,063	180	279.5
α_6	4769.8	19,38	10	104.2	α_{17}	4593.9	0,085	130	283.2
α_7	4764.7	16.82	10	109.5	α_{18}	4580.0	0.024	360	297.3
α_8	4740.3	0.019	6400	~134.3	α_{19}	4572.7	0.054	140	304.8
α_9?	4711.3	0.126	610	163.8	α_{20}	4513.5	0.01	120	~365
α_{10}	4707.3	0.293	250	167.9	α?	~4385.0	0.02	30	~496

*$J_{13} + J_{14} + J_Z = 2.178$.
**Sum of three lines $\alpha_X + \alpha_y + \alpha_{15}$ (see Fig. 1).

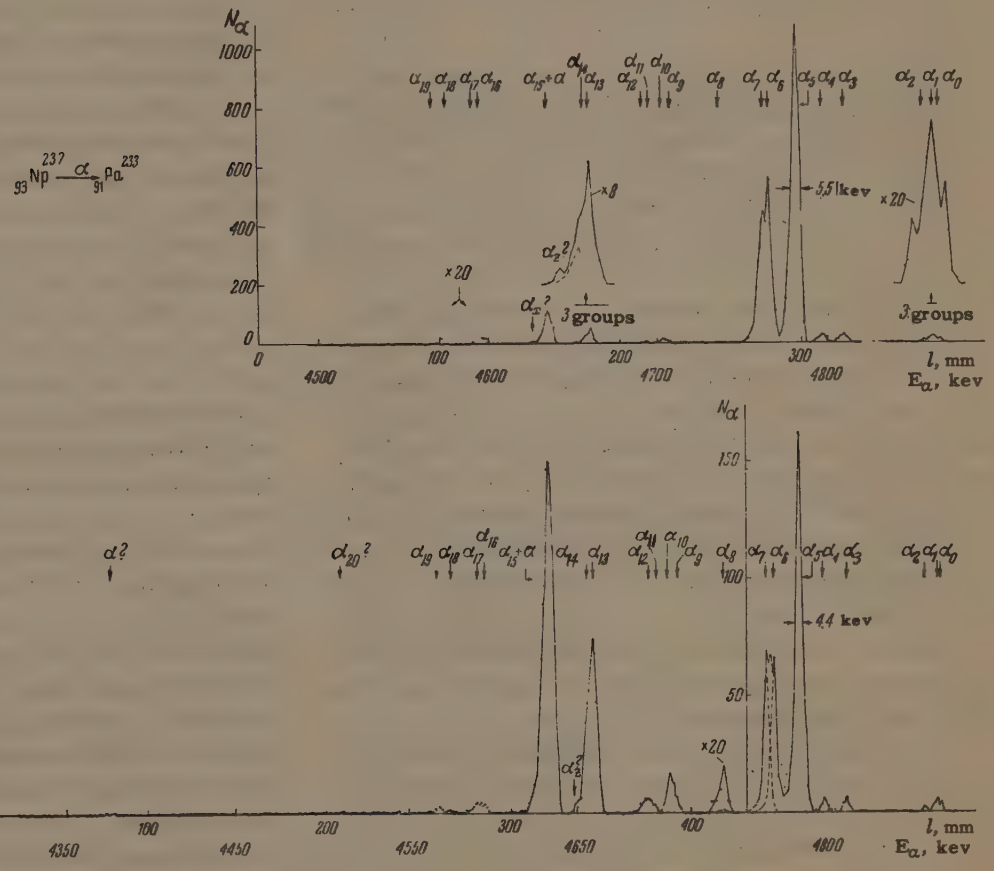

FIG. 1. Apparatus spectrum of the fine structure of α radiation of Np^{237}.

the reproducibility of the initial results. The lower half of Fig. 1 is part of the spectrum, obtained in one of the control experiments.

In the next experiment we investigated the portion of the α spectrum of Np^{237} in the energy range ~4350—4750 kev (see Fig. 1), using a wider and more intense source. The resolution of the α spectrograph was somewhat worse in this experiment than in the preceding ones. The purpose of the experiment was to confirm the series of α lines (α_9—α_{12}, α_{16}—α_{19}) with large statistical accuracy, and also to detect new ones with intensity ~0.01%.

An analysis of the plotted α spectrum has confirmed with great certainty the existence of the complex groups just mentioned, and also disclosed some other α lines (see Fig. 1).

It must be noted that the accuracy with which the energies of most individual components in the complicated groups were determined did not exceed 2 kev. It is also obvious that the intensities of these components (except α_6 and α_7) cannot

be estimated accurately. Consequently the intensities listed in Table I for these lines are not exact. This inaccuracy is due primarily to the arbitrariness entailed in the graphic resolution of a complex group into individual components.

4. MEASUREMENT OF THE ELECTRON AND γ SPECTRA

The electron and γ spectra were investigated in order to detect new γ transitions in Pa^{233} and to determine the class of multipolarity of some of the more intense γ transitions. Measurements of the electron and γ spectra were made directly after radiochemical elimination from the Np^{237} of the daughter Pa^{233}, and therefore the activity of the Pa^{233} was small and did not affect the measurement results.

The β spectrometer used to investigate the electron spectrum permitted the use of sources with relatively large effective areas ($S_{max} = 4$ cm^2). However, the slight specific activity of Np^{237} ($T_{1/2} = 2.2 \times 10^6$ years) did not make it possible to obtain a source of required intensity with small surface density.

The low activity and the large thickness of the sources did not allow us to plot the electron spectrum with high degree of resolution. The spectra obtained in three different experiments, however, were identical and enabled us to separate reliably the conversion lines characterizing the γ transitions in Pa^{233}. In the analysis of the electron spectrum we took into account the measured γ spectrum, and also the data on the investigation of the α radiation of Np^{237}.

Table II summarizes some of the data on the γ transitions, obtained from the analysis of the electron and γ spectra for Pa^{233}.

The determination of the multipolarity of most γ transitions in Pa^{233} is impossible because of the low intensity and insufficient resolution of the conversion-electron lines. A comparison of the data obtained with a proportional counter, a β spectrometer, and a γ spectrometer enabled us to establish the multipolarity only for the 29 kev (E1), 57 kev (E2), and 86 kev (E1) γ transitions. The results obtained do not contradict the data of Magnusson et al.[7]

It is mentioned in the literature[15] that an anomalously high internal-conversion coefficient was obtained for 86-kev γ rays. The possible existence of an 84-kev γ transition can apparently change this anomaly.

Table II. Energy (kev) of γ transitions in Pa^{233}

β spectrometer	Proportional counter	γ spectrometer	Multipolarity
29.6	29,6	30	*E*1
55.0?	—	—	*E*2?
56.8	57–58	57–60	*E*2
84.5?, 85.9	84—90	—	*E*1
105.0	~104	106	—
108.4	~108		
133.5	—	130–145	—
144.5	—		
?	—	~160?	—
207	—	—	—
240	—	~250	—

5. ENERGY LEVELS OF Pa^{233}

The most complete among the energy level schemes listed in the literature[7,16-18] for Pa^{233} is found in the book by Mottelson and Nilsson[18]. This scheme is based on the data of an unpublished paper by Asaro, Perlman, and Stephens devoted to a study of the α decay of Np^{237} (see also [19]), and the known Nilsson diagrams. Our new data make it possible to supplement this scheme.

An analysis of the experimental data enables us to state that the Pa^{233} nucleus has more than 20 energy levels in a relatively narrow energy interval (0—400 kev). So large a number of levels indicates that this nucleus has several rotational bands with different values of K (spin projection on the symmetry axis of the nucleus). Of course, one cannot exclude the existence of levels belonging to bands with different K but having the same spins and parities. An "interaction of rotational levels"[20], corresponding to different states of the nucleus K [N, n_z, λ], K' [N', n'_z, λ'] etc, should therefore take place in this nucleus. This may violate O. Bohr's interval rule for rotational bands and, in accordance with[21], probably causes a considerable increase (or decrease) in the intensities of some α transitions.

The data given above were used to construct the energy level scheme for Pa^{233} shown in Fig. 2. On the left side of this figure is the Nilsson diagram; the vertical dashed line on the diagram corresponds to $\delta = 0.24$, a value customarily used for Pa^{233}.[18] If we ascribe to the ground state of this nucleus an orbit $1/2^-$ [530] (see[18,22]), then, in accordance with this diagram, the final levels $5/2^+$ [642], $5/2^-$ [523], $3/2^-$ [521], and $7/2^+$ [633] should be observed. As indicated by Mottelson and Nilsson[18], the existence of a "hole" level, with characteristics $3/2^+$ [651] is likewise not excluded, from the point of view of the Nilsson diagram.

The ground state of Pa^{233} has a spin $3/2$[23] and

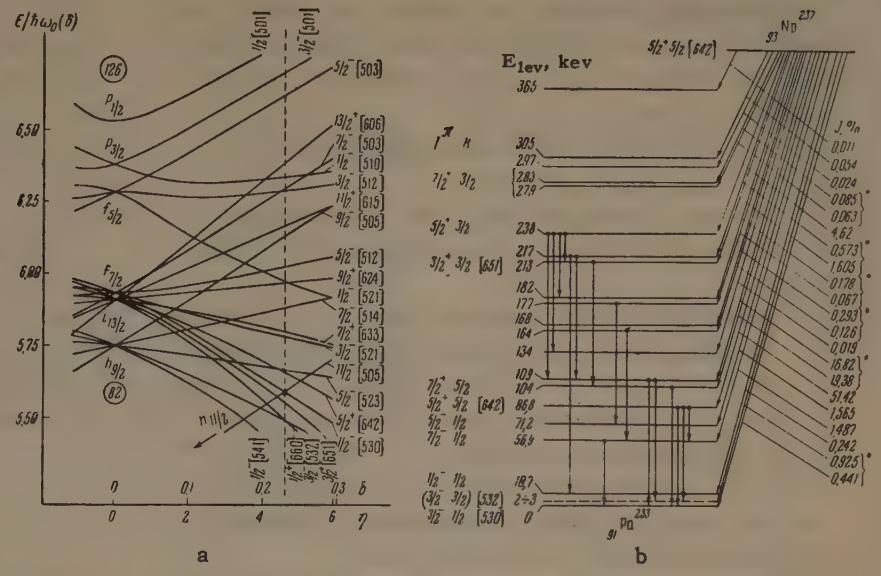

FIG. 2. Energy-level scheme of the Pa^{233} nucleus; a—Nilsson diagram for odd Z, b—experimentally obtained level scheme of Pa^{233}. Levels due to α_x, α_y, and α_z transitions are not indicated.

negative parity.[24] The levels with energies 51 and 71 kev[18,22] and the ~11-kev level observed in our experiments apparently belong to the main rotational band ($^3/_2^-$ $^1/_2$ [530]) with a spin sequence $^3/_2^-$, $^1/_2^-$, $^7/_2^-$, $^5/_2^-$, etc. It must be noted that although there is no doubt of the existence of the α_2 group, nonetheless the energy of the level (E_{lev} ≈ 11 kev) has not been determined with sufficient accuracy.

The next levels of this rotational band, with characteristics $^{11}/_2^-$ and $^9/_2^-$, can apparently be the 164- and 177-kev levels, respectively, but there is no rigorous proof of the correctness of this statement.

The favored transition α_5 actually gives grounds for assuming[18,22] that the single-particle 87-kev level can be assigned an orbit $^5/_2^+$ $^5/_2$ [642], so long as the ground state of Np^{237} is $^5/_2^+$ $^5/_2$ [642]. The members of this rotational bands are apparently the levels at 87 kev ($^5/_2^+$ $^5/_2$ [642]), 104 kev ($^7/_2^+$), 168 kev ($^9/_2^+$), and 249 kev ($^{11}/_2^+$). However, the assumption that the last two levels belong to the indicated rotational band is hardly correct, in view of the indicated interaction. It is not excluded that the third member of the rotational band referred to here is a level with energy 109 kev, since the intensity of the α_7 group, which goes to this level, is high.

As indicated above, the existence of a 'hole' level with characteristics $^3/_2^+$ [651] is expected from the point of view of the Nilsson diagram. The 213-kev level apparently confirms this assumption. It is possible that one of the lines of the complex groups ($\alpha_{15} + \alpha_y$ and $\alpha_{16} + \alpha_{17}$) determines accordingly the positions of the next levels ($^5/_2^+$ and $^7/_2^+$) of the new rotational band.

Analysis of the complex line group (α_0, α_1, α_2) (see Fig. 1) apparently indicates that there exists still another level with energy 2—3 kev. Naturally, the lines α_0 and α_1 are not sufficiently well separated and a certain arbitrariness in the interpretation of the experimental results can therefore not be excluded. We do not insist that this level exists. If it does, however, we must ascribe to it either an orbit $^5/_2^-$ $^5/_2$ [523] or $^3/_2^-$ $^3/_2$ [532].

The interpretation we presented for most Pa^{233} levels is quite arbitary. We cannot pretend that the proposed level scheme of this nucleus is complete or final.

It is our duty to thank S. N. Belen'kii, K. I. Merkulova, A. A. Arutyunov, Yu. I. Dmitriev, and Yu. I. Filenko (a student of the Moscow Engineering Physics Institute) for help with the measurements, and also to G. I. Khlebnikov for radiochemical elimination of decay products and extraneous impurities from the Np^{237}.

[1] A. C. Wahl and G. T. Seaborg, Phys. Rev. **73**, 940 (1948).

[2] J. Mack, Revs. Modern Phys. **22**, 64 (1950).

[3] D. Dunlavey, and G. Seaborg, Phys. Rev. **87**, 165 (1952).

[4] D. Engelkemeir, and L. Magnusson, Phys. Rev. **94**, 1395 (1954).

[5] Bleaney, Llewellyn, Pryce, and Hall, Phil. Mag. **45**, 992 (1954).

[6] D. Strominger, and J. Rasmussen, Phys. Rev. **100**, 844 (1955).

[7] Magnusson, Engelkemeir, Friedman, Porter, and Wagner, Phys. Rev. **100**, 1237 (1955).

[8] R. Thorne, Nature **178**, 484 (1956).

[9] Dobbs, Roberts, and Parker, Bull. Am. Phys. Soc. **1**, 207 (1956).

[10] Kondrat'ev, Novikova, Vorob'ev, and Gol'din, Izv. AN SSSR, ser. fiz. **20**, 875 (1956), Columbia Tech. Transl. p. 795.

[11] Baranov, Zelenkov, Shchepkin, Beruchko, and Malov, Atomnaya énergiya **7**, 262 (1959); Izv. AN SSSR ser. fiz. **23**, 1402 (1959), Columbia Tech. Transl. p. 1389.

[12] P. S. Samoilov, PTÉ (Instrum. and Exptl. Techniques) No. 6, 33 (1959).

[13] Baranov, Rodionov, Shishkin, and Chistyakov, JETP **34**, 1367 (1958), Soviet Phys. JETP **7**, 946 (1958).

[14] Baranov, Zelenkov, and Kulakov, Izv. AN SSSR ser. fiz. **24**, 1035 (1960), Columbia Tech. Transl. p. 1045.

[15] Asaro, Stephens, Hollander, and Perlman, Phys. Rev. Lett. **2**, 442 (1960).

[16] B. S. Dzhelepov and L. K. Peker, Skhemy raspada radioaktivnykh yader (Decay Schemes of Radioactive Nuclei), AN SSSR, 1958.

[17] D. Strominger and J. M. Hollander, UCRL-8289, Berkley, California (1958).

[18] B. Mottelson, and S. Nilsson, Mat-Fys. Scr. Dan. Vid. Selsk. **1**, 8 (1959).

[19] I. Perlman, and J. O. Rasmussen, Handbuch d. Physik **42**, 109 (1957).

[20] A. Kerman, Mat-Fys. Medd. Kyldaske Vid. Selsk. **30**, 15 (1955).

[21] O. Prior. Ark. Fysik. **16**, 15 (1959).

[22] Stephens, Asaro, and Perlman, Phys. Rev. **113**, 212 (1959).

[23] J. Hubbs and J. Winicur, Bull. Am. Phys. Soc. **11**, 319 (1958).

[24] Hamilton, Hollander, and Petterson, UCRL 9438, Berkley, California (1960).

Translated by J. G. Adashko
293

ENERGY LEVELS OF U^{232}

S. A. BARANOV, P. S. SAMOĬLOV, Yu. F. RODIONOV, S. N. BELEN'KII, and S. V. PIROZHKOV

Submitted to JETP editor June 21, 1961

J. Exptl. Theoret. Phys. (U.S.S.R.) 41, 1740-1747 (December, 1961)

Radioactive decay of Pa^{232} was studied with a double-focusing magnetic β-spectrometer and a scintillation γ-spectrometer. An energy level scheme for the U^{232} nucleus is derived by analyzing the β spectrum, conversion-electron spectrum, and γ-ray spectrum. The scheme agrees with the level schemes of other even-even deformed nuclei. The existence of E0 transitions between the levels $0_2^+ \rightarrow 0_1^+$ and $2_2^+ \rightarrow 2_1^+$ is established. The experimental data are compared with the predictions of the Bohr-Mottelson theory and the theory of nonaxial deformed even-even nuclei developed by Davydov, Filippov, Rostovskii, and Chaban.

INTRODUCTION

A study of the levels of deformed even-even nuclei is of interest from the point of view of checking the theories that have recently been used to describe these levels. The prevalent notions are that a developed band of rotational levels ($I = 0^+, 2^+, 4^+$), connected with the collective motion of the nucleons in the nucleus, exists near the ground state of these nuclei, with octupole oscillation bands ($I = 1^-, 3^-$) and β and γ vibrational nuclear levels located above the rotational band. These notions are confirmed by the experimental data obtained in investigations of radioactive decay of the nuclei (see, for example,[1]).

The experimental data hitherto obtained on the levels of U^{232} have been contradictory[2] and did not fit the framework of the above scheme. We have continued our investigation of the decay of Pa^{232} in order to construct a more complete level scheme for U^{232}.

1. PREPARATION OF SOURCE AND EXPERIMENTAL PROCEDURE

The Pa^{232} was obtained by bombarding Pa^{231} with slow neutrons. The bombarded substance was a mixture of 0.5 mg protactinium oxide and 15 mg magnesium oxide. The initial Pa^{231} sample had practically no extraneous α and β active impurities, as checked by high-transmission spectrometers. After the irradiation, the mixture of oxides was dissolved in an 8N solution of hydrochloric acid with addition of a few drops of hydrogen fluoride. After the mixture was completely dissolved, 5 mg of aluminum chloride was added to bind the fluorine ions. The resultant solution was passed through a column with Dowex-1 x-8 anion-exchange resin, on which the protactinium was gathered. After passing the entire solution, the compound was washed out to eliminate the extraneous activity of the hydrochloric acid. The protactinium was then selectively washed out of the resin with a mixture of 8N HCl + 0.1 N HF. The cleaning operation was then repeated. The result was 5 ml of pure solution of protactinium, which was evaporated in a platinum crucible to 0.5 ml. The sources for the β and γ spectrometric measurements were prepared of this solution.

To investigate the electron spectrum, the Pa^{232} specimens were made by evaporating the solution on a thin organic film, on which a semi-transparent strip of Aquadag was deposited beforehand. The sources for the β spectrometer had dimensions ranging from 1×30 to 5×40 mm.

The window of the electron counter had dimensions corresponding to those of the source and was covered with a celluloid film, which transmitted all electrons with energies above 2 kev.

The electron and γ spectra were measured with the apparatus described in our earlier papers.[3,4]

2. EXPERIMENTAL RESULTS

The electron spectrum produced in the β decay of Pa^{232} is shown in Figs. 1—3, while the γ spectrum is shown in Fig. 4. Conversion-electron lines are interpreted in Table I.

The electron spectrum in the energy range from 1 to 110 kev was measured with a source measuring 1×30 mm. In addition to the conversion lines of the known 47.5- and 109-kev γ transitions, the spectrum shows the electron lines 45, 9, 16, and 19, which are respectively interpreted

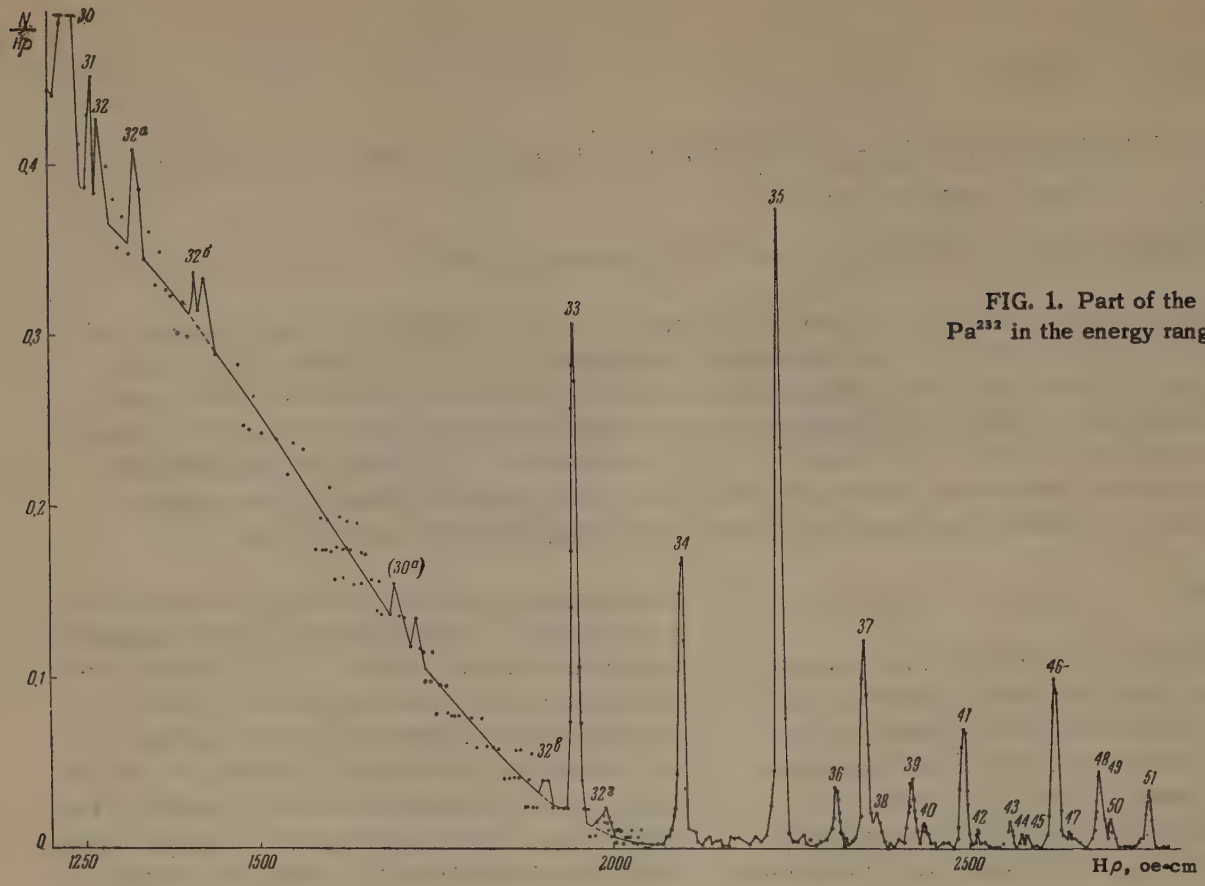

FIG. 1. Part of the electron spectrum of Pa^{232} in the energy range from 1 to 120 kev.

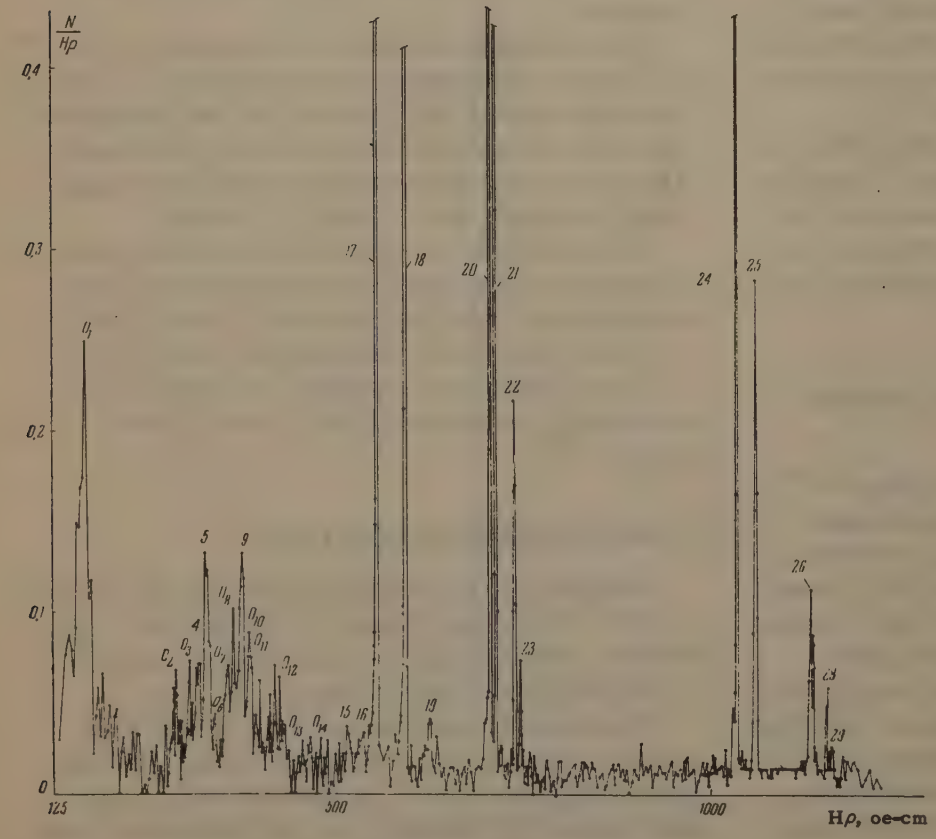

FIG. 2. Part of electron spectrum of Pa^{232} in the energy range from 120 to 500 kev.

Table I

Number of electron line in spectrum	Observed electron energy, kev	Interpretation	γ-transition energy, kev	Intensity, relative units
4	8.3	L_I	30	10
5	9	L_{II}	29.9	27
9	12.5	L_{III}	29.7	26
16	25.2	$M_{II, III}$	≈30	7
		Average:	29.9	
17	26.5	L_{II}	47.5	330
18	30.33	L_{III}	47.5	275
20	42.5	M_{II}	47.6	91
21	43.4	M_{III}	47.7	73
22	46.3	N_I	47.6	54
23	47.2	O	47.4	14
		Average:	47.55	
24	88.2	L_{II}	108.8	75
25	91.6	L_{III}	108.8	46
26	103.9	M_{II}	109.0	19
27	104.5	M_{III}	108.8	13
28	106.8	N	108.8	
29	108.2	O	108.6	
		Average:	108.8	
19	32	K	147.6	6
31	126.6	$L_{I, II}$	147	≈2
32	130	L_{III}	147	≈2
32a	140	M	≈147	≈2
		Average:	147	
30	121	K	236.6	≈8
30a	215	L	236	≈1.5
		Average:	≈236	
32b	163	K	≈280	
32b	267	L	≈280	
32c	274	M	≈280	
		Average:	≈280	
33	266.9	K	382.5	8.3
37	361.8	$L_{I, II}$	382.8	3.7
38	365.7	L_{III}	382.8	0.7
39	378	M	≈383	1.3
40	382	N	≈383	0.6
		Average:	382.8	
34	301.2	K	416.8	5.2
41	396.0	$L_{I, II}$	416.9	2.2
42	399.8	L_{III}	417	0.2
43	411.2	M	416.7	0.4
44	415.2	N	116.7	0.15
45	417.0	O	417	0.13
		Average:	416.8	
35	334.3	K	449.9	10
46	429.3	$L_{I, II}$	450	2.7
47	432.6	L_{III}	449.8	0.35
48	444	M	449.5	(1.1)
50	448.2	N	449.6	0.2
		Average:	449.9	
36	351	K	466.6	1
(49)	444.6	L	≈466.4	(0.35)
		Average:	466.5	
51	463.7	K	579.2	1
53	558.4	$L_{I, II}$	579.4	0.5
54	562.5	L_{III}	579.7	
56	574.7	M	579.8	0.5
57	577.5	N	≈579	
		Average:	579.5	
55	567.5	K	683	1
58	661.5	$L_{I, II}$	682.5	0.17
59	665.2	L_{III}	682.4	
		Average:	682.6	
60	700.8	K	816.4	0.9
65	794.5	L	816.3	0.5
66	812	M	≈817	
		Average:	816.6	
61	702	K	817.6	0.9
		Average:	817.6	
62	747.5	K	863	1.5*
67	841	L	863	0.6**
		Average:	863	
63	750	K	866	
68	845	L	866	
		Average:	866	
64	876.8	K	892.5	1.1
72	870.7	L	892.4	0.35
73	887.0	M	~892	0.16
		Average:	892.3	
69	848	K	963.5	12.6
74	945.7	L	963.7	0.4
75	960	M	964	0.15
		Average:	963.7	
76	1035	K	1150	0.2

* $\Sigma(K\ 863 + K\ 866)$.
** $\Sigma(L\ 863 + L\ 866)$.

as L_I, L_{II}, L_{III}, M_{II} and M_{III} conversion lines of the 30-kev γ transition and the K line of the 147-kev γ transition. The spectrum shows a large number of Auger-electron lines, O_1—O_{14}, which are not interpreted in this paper.

The electron spectrum from 110 kev to 1 Mev was measured with a 3 × 35 mm source of activity 15 times greater than that of the preceding source. Multipole measurements and checks of the period of fall-off of the conversion-electron line intensities have established that lines 34, 41, 42, and 43 belong to the 416.8-kev γ transition, while line 36 corresponds to the 466.5-kev γ transition in U^{232}. Ong Ping Hok and Sizoo,[2] who worked with a mixture of Pa^{230}, Pa^{232}, and Pa^{233}, were apparently in error in assuming that the 416.8- and 466.5-kev γ transitions belonged to Pa^{233} and Pa^{230} respectively. They observed in the same

FIG. 3. Part of electron spectrum of Pa^{232} in the energy range from 500 to 980 kev.

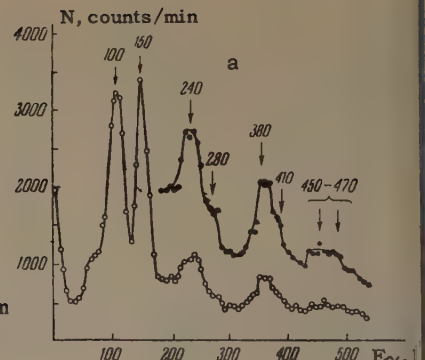

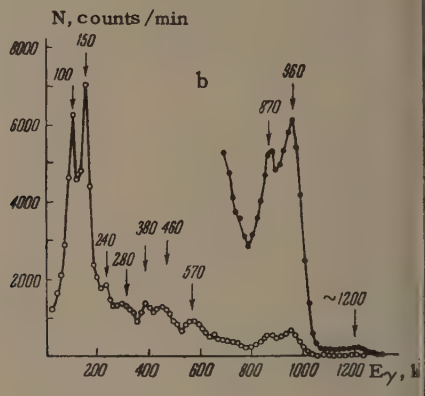

FIG. 4. γ-ray spectrum of Pa^{232} measured with scintillation γ spectrometer.

energy region intense conversion lines which they ascribed to a 517-kev γ transition in U^{232}. We observed no 517-kev γ transition in our measurements.

In addition to the indicated conversion lines, we observed the lines 30, 32b, 32c, and 32d, assigned to the 236- and 280-kev γ transitions. The very weak conversion line No. 78 (see Table I) is assigned to the 1150-kev γ transition.

The existence of the newly-observed γ transitions with energies 147, 236, 280, and 1150 kev is confirmed by measurement of the spectrum of the γ rays produced in the decay of Pa^{232} (Fig. 4). The γ-ray spectra were measured with a scintillation γ spectrometer with resolution 8—9% for Cs^{137} (E_γ = 667 kev) when a 30 × 20 mm NaI(Tl) crystal is used.

Analysis of the β spectrum of Pa^{232} with the aid of a Fermi-Kurie plot[5] has shown that this spectrum consists of at least four partial spectra (see Table II). We note that the low-energy partial β spectrum (E_{max} = 260 kev, J = 51%) is

Table II

Component	E_{max}, kev	Intensity, %	$\log_{10} ft$
I	260 ± 30	51	5.7
II	330 ± 30	34	6.1
III	640 ± 50	6	7.9
IV	1220 ± 100	9	8.6

apparently the sum of two or three components with end-point energies less than 260 kev.

3. DISCUSSION OF RESULTS

By comparing the experimental and theoretical values of the relative conversion coefficients on the K and L subshells, we established the multipolarity class for several γ transitions in U^{232} (Table III). However, our experimental data do not yield an unambiguous level scheme for U^{232}. We can therefore make only the following assumptions concerning the series of levels of this nucleus (see also [8,9]).

The levels with energies 0, 47.5, 108.8, and ~ 321 kev are members of the main rotational band. Their energies, spins, and parities are in good agreement, like in all other even-even nuclei, with the predictions of the theory of O. Bohr and B. Mottelson [10] and also with earlier data by others. [2,8]

Unfortunately, no such definite conclusion can be drawn concerning the remaining levels of this nucleus. This can be illustrated by the following example. The recently published short communication by Bjornholm, Knutsen, and Nielsen, [11] devoted to the rotational and vibrational levels of U^{232}, points to the existence of a 564-kev γ transition in this nucleus. We did not observe this γ transition in our measurements. We therefore cannot regard it as established that the 564-kev level is due to octupole oscillations of the nucleus and that its characteristics K, I, and π are 0 and 1^- as indicated in [11].

Let us consider the existence of β and γ vibrational levels in U^{232}. The conversion lines of the 816.4- and 817.5-kev γ transitions could not be separated. But the shape of their summary line indicates that this is a complex electron line (Fig. 3). The γ-ray spectrum shows no 817-kev line. It is established from this spectrum that the contribution of the 960- and 870-kev γ lines to a possible 817-kev line cannot be more than 10%. Consequently, the internal-conversion coefficients of the 816.4- and 817.5-kev γ transitions exceed the internal conversion coefficient of the 866- and 863-kev γ transitions by more than tenfold. This indicates that if the 816.4- and 817.5-kev γ transitions are not pure E0 transitions, they at least contain a large admixture of E0 transition. Thus, we can assume that the 816.4-kev level has spin and parity 0^+, while the characteristic of the 863-kev level is 2^+, i.e., they apparently form a band of β-vibrational levels. In accordance with the observed class E2 of γ transitions with energies 833 and 30 kev, we assign spin and parity 2^+ to the 893-kev level, which may be a γ-vibrational one. We were unable to draw from our data any conclusions concerning the character of the remaining levels.

Let us see how the values of the energies and spins of the identified levels agree with the predictions of the existing theories.

Table III

γ-transition energy, kev	K/L				$(L_I+L_{II})/L_{III}$				M_{II}/M_{III}		Multipolarity of γ-transition
	Experiment	Theory* for			Experiment	Theory* for			Experiment	Theory**	
		$E1$	$E2$	$M1$		E_1	E_2	M_3			
30					1.42						$M1+E2$
47.5					1.2±0.05		1.2		1.3 ± 0.1	1.2	$E2$
108.8					1.6±0.05		1.6		1.5 ± 0.2	1.5	$E2$
147	1.5	0.5	0.12								$E1$
236	6	5	0.5								$E1$
(280)?											
383	1.8	5	1.5	4.9	5.3	8.4	4	200			$M1+E2$
416.8	2.2	5.1	1.5	5	10	9	4.5	200			$M1+E2$
450	3.3	5.2	2	5	8	10	5.5	220			$M1+E2$
466.5	(4)	5.3	2.1	5.1		12	6.5	230			$(E1)$
580	2										?
683	5										$(E1)$
816.4	3.5										$E0$
817.5											$E0\,(+E2)$
863	2.5	~6	~3								$(E2)$
866											$(E2)$
893	3.8	~6	~3								$E2$
963	6.8	6	4	6							$(E1)$?

*The theoretical values of the coefficient of internal conversion on the K and L subshells were taken from Sliv and Band [6].

**The theoretical values of the coefficient of internal conversion on the M subshells were taken from Rose [7].

The lower band of rotational levels is well described both by the theory of O. Bohr and Mottelson for axial deformed nuclei, and by the theory developed in the adiabatic approximation by Davydov and Filippov [12] for non-axial deformed nuclei. The theory of non-axial nuclei was further developed to account for the connection between the rotation of nuclei with β oscillations, [13] which, depending on the values of the non-axiality and non-adiabaticity parameters γ and μ and on the position of the 2_1^+ and 2_2^+ levels makes it possible to establish the values of other levels of even-even deformed nuclei. For U^{232}, in terms of the indicated theory, we have $\mu = 0.212$ and $\gamma = 8.8°$.

Using the Mallmann tables obtained on the basis of the Davydov and Chaban formulas, [13] we can establish the following level-energy ratios: $E(6_1^+)$: $E(2_1^+) = 6.75$ and $E(0_2^+)$: $E(2_1^+) = 19.6$. The first value coincides with the experimental one, while the second differs from the experimental one (~ 17.1) by 15%. The energy determined for the β-vibrational level 0^+ is thus in satisfactory agreement with the predictions of the theory. [13]

In conclusion, we are grateful to G. V. Shishkin, A. A. Arutyunov, and Yu. A. Dmitriev for help in the measurement of the electron spectra.

[1] J. Perlman, Proc. Intern. Conf. on Nucl. Structure, Kingston, Canada, 1960, p. 547.

[2] Ong Ping Hok and J. G. Sizoo, Physica **20**, 77 (1954).

[3] Baranov, Rodionov, Shishkin, and Chistyakov, JETP **34**, 1367 (1958), Soviet Phys. JETP **7**, 946 (1958).

[4] P. S. Samoĭlov, PTÉ (Instrum. and Meas. Techniques) No. 6, 33 (1959).

[5] B. S. Dzhelepov and L. N. Zyryanova, Vliyanie elektricheskogo polya atoma na β-raspad (Effect of Atom's Electric Field on Beta Decay), AN SSSR, 1956.

[6] L. A. Sliv and I. M. Band, Tablitsy k.v.k. γ-izlucheniya (Tables of Gamma Radiation Internal Conversion Coefficients), Parts I and II, AN SSSR,

[7] M. E. Rose, Internal Conversion Coefficients, Amsterdam (1958).

[8] B. S. Dzhelepov and L. K. Peker, Skhemy raspada radioaktivnykh izotopov (Decay Schemes of Radioactive Isotopes), AN SSSR, 1959.

[9] C. J. Gallagher, Jr. and T. D. Thomas, Nucl. Phys. **14**, 1 (1959).

[10] A. Bohr and B. Mottelson, Mat-fys. Medd. Dan. Vid. Selsk. **27**, 16 (1953).

[11] Bjornholm, Knutsen, and Nielsen, Bull. Am. Phys. Soc. **6**, 239 (1961).

[12] A. S. Davydov and G. F. Filippov, JETP **35**, 440 (1958), Soviet Phys. JETP **8**, 303 (1959).

[13] A. S. Davydov and A. A. Chaban, Nucl. Phys. **20**, 499 (1960).

Translated by J. G. Adashko
294

PROTON-PROTON SCATTERING AT 8.5 Bev

DO IN SEB, L. F. KIRILLOVA, P. K. MARKOV, L. G. POPOVA, I. N. SILIN, É. N. TSYGANOV, M. G. SHAFRANOVA, B. A. SHAKHBAZYAN, and A. A. YULDASHEV*

Joint Institute for Nuclear Research

Submitted to JETP editor June 21, 1960

J. Exptl. Theoret. Phys. (U.S.S.R.) 41, 1748-1756 (December, 1961)

Elastic pp scattering at 8.5 Bev was studied with the aid of emulsion pellicles exposed perpendicularly to the primary proton beam. Altogether 480 elastic scattering events have been found. The total elastic scattering cross section is (8.74 ± 0.40) mb. The differential cross section is investigated in the c.m.s. angular interval from 1.5° to 20.5°. The experimental data are not in agreement with the simple model in which the real part of the phase shifts and the dependence of the interaction cross section on the spin state are neglected. The total pp interaction cross section computed from the experimental data under these assumptions exceeds the experimental value by more than three standard deviations of the error. It can be said that the real part of the scattering amplitude does not exceed half of the imaginary part. The rms pp interaction range is found to be 1.15 ± 0.05 f.

1. EXPERIMENTAL ARRANGEMENT, ANALYSIS OF EVENTS AND RESULTS

SOME of our data on proton-proton elastic scattering at 8.5 Bev have been published earlier.[1] We now present results based on improved statistics.

Two emulsion stacks (hereafter referred to as stacks Nos. 1 and 2) were used in the experiment. Stack No. 1 consisted of 400 NIKFI-BR emulsion pellicles 10 × 10 × 2 cm exposed to the 8.5-Bev internal proton beam of the proton synchrotron of the Joint Institute for Nuclear Research. The beam entered the stack perpendicularly to the plane of the emulsion. The emulsion contained $(2.90 \pm 0.06) \times 10^{22}$ hydrogen atoms per cm^3.

The emulsion was scanned under magnifications of × 630 and × 450 over an area 3 × 3 cm in the central region of the pellicle. The mean beam-proton density in this area was $(2.01 \pm 0.05) \times 10^5$ particles/cm^2. The total volume of emulsion scanned was 8.03 cm^3.

In order to determine the efficiency for finding the events and to increase the reliability of the results, the volume was scanned twice. From the two-prong stars found we selected stars whose external appearance resembled pp elastic scattering. Upon examination, part of them could be rejected as obviously not conforming with the criteria for pp elastic scattering (events classified as "not-to-be-measured"), the remaining part was measured carefully. The events in the latter group ("to-be-measured") were used to determine the scanning efficiency in the c.m.s. angular interval 0 — 12.5°. The efficiency for finding events in the region 0 — 2.5° was investigated very carefully. Events which proved not to be elastic scattering were segregated according to the angular intervals as a function of the "recoil-proton" range.

In order to improve the statistical accuracy in the determination of the scanning efficiency in the angular interval 12.5 — 20.5°, we also used the events of the "not-to-be-measured" type for which the scanning efficiency did not differ from elastic scattering. These events were also sepa-

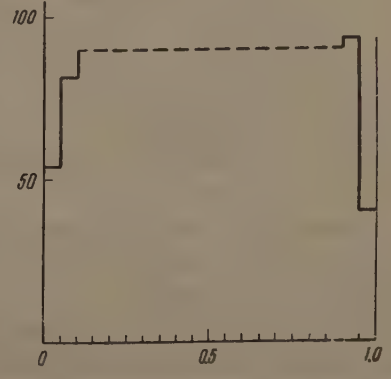

FIG. 1. Depth distribution of the recorded two-prong elastic-like stars. The abscissa axis represents the distance from the glass in fractions of the total pellicle thickness, the ordinate axis gives the number of events.

*Physico-technical Institute, Acad. Sci. Uzbek S.S.R.

Table I

$\theta_{c.m.s.}$, deg	Scanning efficiency		Differential cross sections, mb/sr		
	Stack 1	Stack 2	Stack 1	Stack 2	Combined data
1.5 — 2.5	0.916 ± 0.030	1.000 — 0.000	153.6 ± 33	142^{+49}_{-41}	149 ± 27
2.5 — 4.5	0.970 ± 0.008	0.918 ± 0.046	124.0 ± 15	103^{+32}_{-26}	120 ± 13
4.5 — 6.5	0.968 ± 0.010	0.914 ± 0.035	93.0 ± 11	92^{+21}_{-15}	93 ± 9.6
6.5 — 8.5	0.945 ± 0.015	0.868 ± 0.049	63.3 ± 7.7	51^{+13}_{-10}	59.5 ± 6.3
8.5 — 10.5	0.845 ± 0.036	—	35.9 ± 5.5	—	35.9 ± 5.5
10.5 — 12.5	0.890 ± 0.040	—	13.3 ± 2.9	—	13.3 ± 2.9
12.5 — 14.5	0.700 ± 0.055	—	6.5 ± 2.1	—	6.5 ± 2.1
14.5 — 16.5		—	4.0 ± 1.5	—	4.0 ± 1.5
16.5 — 18.5		—	1.0 ± 0.7	—	1.0 ± 0.7
18.5 — 20.5		—	0.5 ± 0.5	—	0.5 ± 0.5

rated into angular intervals as a function of the range of the slow proton or its ionization found from gap measurements.

If N_1 is the number of events of a given type found in one scanning and N_2 is the number of events of the same type found in the second scanning, while N_{12} is the number of events which were found in the first scanning that were also found in the second scanning, then, if the scanning efficiency is constant for the entire volume, the efficiency of the first, second, and double scannings are

$$\varepsilon_1 = N_{12}/N_2, \quad \varepsilon_2 = N_{12}/N_1,$$
$$\varepsilon = [1 - (1 - \varepsilon_1)(1 - \varepsilon_2)],$$

respectively. The statistical error in the determination of the scanning efficiency is given by the expressions*[2]:

$$(\overline{(\Delta\varepsilon_1)^2})^{1/2} = (\varepsilon_1(1-\varepsilon_1)/N_2)^{1/2}, \quad (\overline{(\Delta\varepsilon_2)^2})^{1/2} = (\varepsilon_2(1-\varepsilon_2)/N_1)^{1/2},$$
$$(\overline{(\Delta\varepsilon)^2})^{1/2} = N_{12}\left\{\left(\frac{1-\varepsilon_1}{N_1}\right)^3 + \left(\frac{1-\varepsilon_2}{N_2}\right)^3 + \left(\frac{1-\varepsilon_1}{N_1} + \frac{1-\varepsilon_2}{N_2}\right)^2\left(\frac{1-\varepsilon_1\varepsilon_2}{N_{12}}\right) - 2\left(\frac{1-\varepsilon_1}{N_1} + \frac{1-\varepsilon_2}{N_2}\right)\left[\left(\frac{1-\varepsilon_1}{N_1}\right)^2 + \left(\frac{1-\varepsilon_2}{N_2}\right)^2\right]\right\}^{1/2}.$$

If the conditions given above are not fulfilled, the calculated value of the efficiency is overestimated. However, if the scanning efficiency is high (90 — 97%), this systematic error cannot be appreciable. Upon examination of the events it was important to discard events situated at distances less than 20 μ from the free surface and from the glass in unprocessed emulsion, since such events were missed very frequently (Fig. 1).

The calculated scanning efficiency for stack No. 1 is shown in Fig. 2 and in Table I as a function of the scattering angle.

To separate cases of elastic scattering on a free proton we used the same criteria given earlier in [1]. The range of the recoil proton was measured with an error not exceeding 5%. The angle of emission of the recoil proton was measured to an accuracy of 1.5 — 2°. The scattering angle of the primary proton was measured by means of the method described earlier in [1] to an accuracy of 3 — 4′. Such an accuracy of measurement made it possible to reduce the contribution from background to (0.55 ± 0.15)% (method of estimation of background is described in [1]).

Altogether, 354 cases (including 145 cases reported earlier[1]) satisfying the elastic scattering criteria within the limits of three standard deviations were found. The measured differential cross sections are shown in Table I.

In order to improve the statistics in the region of small scattering angles we used the water-soaked stack No. 2.[3] The stack was exposed to an 8.2-Bev internal proton beam in the proton synchrotron of the Joint Institute for Nuclear Research also perpendicularly to the plane of the emulsion pellicles. The beam density at the time of exposure was 1.8×10^5 protons/cm^2. The emulsion was also scanned twice with an immersion

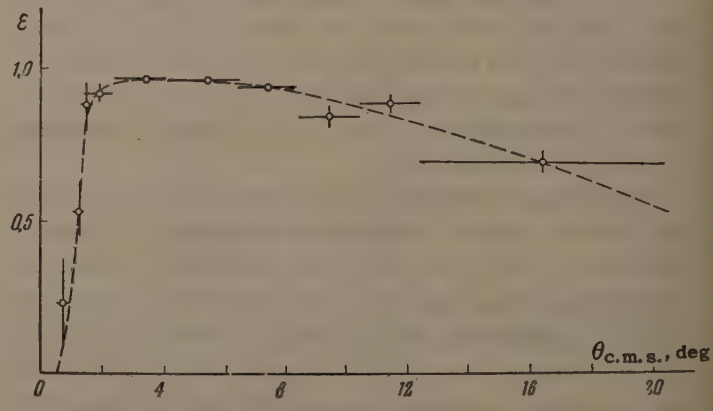

FIG. 2. Variation of the scanning efficiency for pp elastic scattering for a double scanning as a function of the c.m.s. scattering angle.

*In[2] and[10] it was shown that the formulas for $\Delta\varepsilon_1$ and $\Delta\varepsilon_2$ in[11] are not valid. In[2], moreover, it was shown that the formula for $\Delta\varepsilon$ in[11] is also not valid.

objective under a magnification × 630. The events were analyzed in the manner described previously in [1].

To determine the angle of emission of the scattered proton θ, we carried out, as a rule, the "coarse" measurements described in [1]. The standard deviation of the beam divergence was 5′. The mean thickness of the pellicles was 1100 μ. In this case the accuracy of the measurement of θ was about 6′. Events with range $R \lesssim 200\,\mu$, doubtful cases, and 12 cases of different range for establishing the range—energy curve were measured accurately [1] on a base of 3300 μ. The contribution from background events to the number of separated cases is (1.0 — 1.3)%. The scanning efficiency was determined from cases of scattering and elastic-like events of the "to-be-measured" type with the recoil-proton ranges lying in the same interval. The efficiencies are also shown in Table I.

The water-soaked emulsion contained $(5.40 \pm 0.13) \times 10^{22}$ hydrogen nuclei per cm^3. The use of the water-soaked stack made it possible to increase the speed for finding elastic scattering events in the small-angle region two- to three-fold. We found in this stack 126 cases of elastic scattering, of which 107 were in the angular interval 1.5 — 8.5 (c.m.s.). To determine the differential cross section we introduced a correction for the loss of cases at the glass and free surface of the emulsion. The data for stack No. 2 are shown in Table I along with the combined data for stacks Nos. 1 and 2.

The elastic scattering cross section turned out to be 8.74 ± 0.40 mb.

2. DISCUSSION OF RESULTS

We have shown earlier that the measured values of the differential cross sections at small angles greatly exceed the differential cross sections at 0° calculated from the optical theorem under the assumption of a spin-independent interaction. The total cross section for pp interactions σ_{tot} was taken there as 30 mb. Subsequently, it was found that the total cross section considerably exceeded this value; [4,5] the mean value from the two measurements is $\sigma_{tot} = 41.5 \pm 1.0$ mb. According to our data, the differential cross section at 2° is 149 ± 27 mb/sr, while the optical theorem leads to the value 111 ± 5 mb/sr.

As was stressed earlier, [1] the discrepancy between the experimental data on the differential cross sections in the small-angle region and the value calculated from the spin-independent model of a purely absorbing proton can be explained only by the existence of a real part in the scattering amplitude or a difference in the total pp interaction cross section in the singlet and triplet states, or both factors simultaneously. The study of the interference between Coulomb and nuclear scattering can clarify this matter. If the amplitude of the nuclear scattering has a real part comparable to the imaginary part, then we should observe interference between the nuclear and Coulomb scattering, depending on the sign of the real part. Conversely, if the real part of the scattering amplitude is small, then the increase in the differential cross section close to the angle zero to a value greater than that given by the optical theorem can be explained only by the dependence of the cross section on the spin states.

To study these possibilities we carried out calculations according to the following schemes.

A. We considered a complex potential [6] varying with the distance by a Gaussian law. It was assumed for simplicity that the interactions involving the proton spins σ_1 and σ_2 can be due either to spin-orbital or spin-spin forces (tensor forces are not considered). We assumed that at large energies E the quasi-classical approximation is valid (in our case the wagelength $\lambda\!\!\!^{-}$ is 0.99 × 10^{-14} cm, which is much smaller than the proton radius) and we calculated the nuclear phase shift from the formula

$$\delta_l = -\frac{E}{\hbar^2 c^2 k} \int_{(l+1/2)/k}^{\infty} \frac{V(r, \sigma_1, \sigma_2)\, dr}{\sqrt{r^2 - k^{-2}(l+1/2)^2}}.$$

The Coulomb phase-shift calculations followed the method given by Stapp, Ypsilantis, and Metropolis. [7]

From the well-known expression for the M matrix of identical particles with spin ½ and with allowance for the Coulomb interaction, we calculated, by the method of least squares, the best fit for the differential cross sections and the corresponding parameters for the potential. In a number of variants we also used the experimentally determined total cross sections for pp interactions. At the same time, we calculated the total and inelastic pp cross sections from the identical-particle formulas.

Silin and Shakhbazyan showed [6]* that the spin-orbit interaction, at least in the generally adopted form, cannot cause a strong difference in the

*As a result of errors made in the calculation and in the program for the calculation of model 5 in [6] the conclusion in [6] that only one variant can occur when the real part of the potential has a plus sign and the singlet state predominates over the triplet state is not valid.

Table II*

Calculation A		Calculation B	
Given parameters	Results of calculation	Given parameters	Results of calculation
σ_{tot} not fixed $\varkappa \equiv 1$ $u \equiv 0$	$\sqrt{\overline{r^2}} = (1.19 \pm 0.04) \cdot 10^{-13}$ cm $w = 53.1 \pm 5.2$ Mev $\sigma_{tot} = 48.3 \pm 1.8$ mb $\chi^2 = 3.87$	σ_{tot} not fixed $\varkappa \equiv 1$ $A \equiv 0$	$\sqrt{\overline{r^2}} = (1.15 \pm 0.04) \cdot 10^{-13}$ cm $B = (0,554 \pm 0.056) \cdot 10^{14}$ cm^{-1} $\sigma_{tot} = 47.6 \pm 1.6$ mb
$\varkappa \equiv 1$ $u_{initial} > 0$	$\sqrt{\overline{r^2}} = (1.22 \pm 0,05) \cdot 10^{-13}$ cm $u = 32,5 \pm 3$ Mev $w = 34,6 \pm 5,6$ Mev $\chi^2 = 7.6$	$\varkappa \equiv 0,8$ $A_{initial} > 0$	$\sqrt{\overline{r^2}} = (1.15 \pm 0.04) \cdot 10^{-13}$ cm $A = (0.348 \pm 0.049) \cdot 10^{14}$ cm^{-1} $B = (0.623 \pm 0.092) \cdot 10^{14}$ cm^{-1} $\chi^2 = 5,76$
$\varkappa \equiv 1$ $u_{initial} < 0$	$\sqrt{\overline{r^2}} = (1,15 \pm 0,04) \cdot 10^{-13}$ cm $u = -26,1 \pm 4,2$ Mev $w = 46.3 \pm 6,7$ Mev $\chi^2 = 6.06$	$\varkappa \equiv 1$ $A_{initial} < 0$	$\sqrt{\overline{r^2}} = (1.23 \pm 0.04) \cdot 10^{-13}$ cm $A = (-0.350 \pm 0.029) \cdot 10^{14}$ cm^{-1} $B = (0.398 \pm 0,062) \cdot 10^{14}$ cm^{-1} $\chi^2 = 6,96$
$\varkappa_{initial} < 1$ $u_{initial} > 0$	$\varkappa = 0,24 \pm 0,11$ $\sqrt{\overline{r^2}} = (1,11 \pm 0.10) \cdot 10^{-13}$ cm $u = 41,5 \pm 71,8$ Mev $w = 138,8 \pm 89,0$ Mev $\chi^2 = 6.29$	$\varkappa_{initial} < 1$ $A_{initial} > 0$	$\varkappa = 0,28 \pm 0,18$ $\sqrt{\overline{r^2}} = (1.14 \pm 0,11) \cdot 10^{-13}$ cm $A = (0,490 \pm 0,560) \cdot 10^{14}$ cm^{-1} $B = (1.36 \pm 1,09) \cdot 10^{14}$ cm^{-1} $\chi^2 = 5,85$
$\varkappa_{initial} < 1$ $u_{initial} < 0$	$\varkappa = 0.29 \pm 0,28$ $\sqrt{\overline{r^2}} = (1,11 \pm 0.08) \cdot 10^{-13}$ cm $u = -48,7 \pm 19,5$ Mev $w = 108.6 \pm 98$ Mev $\chi^2 = 5,85$	$\varkappa_{initial} < 1$ $A_{initial} < 0$	$\varkappa = 0.34 \pm 0.29$ $\sqrt{\overline{r^2}} = (1.12 \pm 0,07) \cdot 10^{-13}$ cm $A = (-0,401 \pm 0.33) \cdot 10^{14}$ cm^{-1} $B = (1,25 \pm 0,99) \cdot 10^{14}$ cm^{-1} $\chi^2 = 5.85$
$\varkappa_{initial} < 1$ $u \equiv 0$	$\varkappa = 0.25 \pm 0,07$ $\sqrt{\overline{r^2}} = (1,09 \pm 0,04) \cdot 10^{-13}$ cm $w = 144.8 \pm 28.8$ Mev $\chi^2 = 6.15$		
$\varkappa_{initial} > 1$ $u \equiv 0$	$\varkappa = 16,5 \pm 67,8$ $\sqrt{\overline{r^2}} = (1,13 \pm 0,06) \cdot 10^{-13}$ cm $w = 4,3 \pm 18,0$ Mev $\chi^2 = 6.55$		

*Everywhere except for the first row we took $\sigma_{tot} = 41.5 \pm 1.0$ mb.

scattering cross sections of the singlet and triplet states at high energies. We therefore considered a complex potential of form

$$V(r, \sigma_1, \sigma_2) = -\{(u_1 + iw_1) + (-1)^{S+1}(u_2 + iw_2)(\overline{\sigma_1\sigma_2})\} \exp\{-\gamma^2 r^2\},$$

where S is the total spin of the system of two protons, $(\overline{\sigma_1\sigma_2})$ are the eigenvalues of the operator $(\sigma_1\sigma_2)$, and the parameter γ is connected with the rms radius of the interaction by the relation

$$(\overline{r^2})^{1/2} = \sqrt{3/2}/\gamma.$$

The following elements of the scattering matrix are different from zero: M_{SS}, $M_{1,1} \equiv M_{-1-1} \equiv M_{00} = M_t$. If the equality of the particle masses are taken into account, we obtain a factor 2 in the expressions for the total cross sections. For simplicity, we determined the parameters of the singlet potential and the value of the ratio of the triplet to the singlet potential, which is assumed to be the same for the real and imaginary parts, i.e., we used the expressions

$$V_S = -(u + iw)\, e^{-\gamma^2 r^2}, \qquad V_t = \varkappa V_S.$$

The transition from u, w, κ to the quantities u_1, w_1, u_2, w_2 is given by the relations

$$u_1 = \tfrac{1}{2} u(1 - \varkappa), \quad w_1 = \tfrac{1}{2} w(1 - \varkappa),$$
$$u_2 = \tfrac{1}{2} u(3\varkappa - 1), \quad w_2 = \tfrac{1}{2} w(3\varkappa - 1).$$

B. We used the optical model in which we considered the dependence of the complex refractive index on the spin states. The Coulomb interaction was taken into account by the method of Bethe.[8] Here, however, the nuclear scattering amplitude was not written in the Born approximation, but in the quasi-classical approximation and was different for the singlet and triplet states. In order to limit ourselves to the least number of parameters, we also used a simplified dependence of the complex refractive index on the spin states. The refractive indices for the singlet s and triplet t states were taken with a Gaussian dependence on the distance:

$$K_s = (A + iB)\, e^{-r^2/a^2}, \qquad K_t = \varkappa K_s.$$

The quantity a is connected with the rms radius of interaction by the relation $(\overline{r^2})^{1/2} = \sqrt{3/2}\, a$.

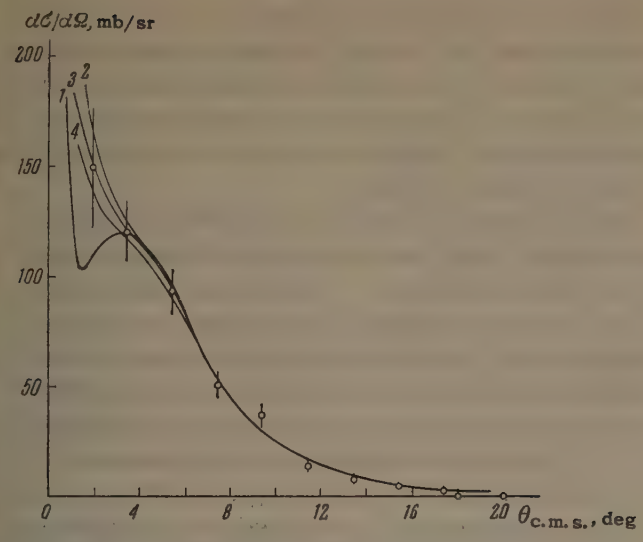

FIG. 3. Experimentally measured differential cross sections and the best fits calculated for variants: 1) $\varkappa = 1$, $u > 0$; 2) $\varkappa = 1$, $u < 0$; 3) $\varkappa = 1$, $u = 0$; 4) $\varkappa = 0.24$, $u > 0$.

The nuclear and electromagnetic form factors were taken to be the same. It should be noted that, under the conditions of applicability of the optical model, the amplitudes for identical and nonidentical particles reduce to the same expression. We used in the calculation the experimental value of the total cross section and the method of least squares for the calculation of the model parameters.

To characterize the deviation of the calculated curve from the experimental points in both schemes of calculation, we used the quantity χ^2, whose mean value is $\overline{\chi^2} = n - m$, where n is the number of experimental points, and m is the number of unfixed parameters of the model.

The errors in the determination of the parameters calculated from the error matrix by a linearization method are not valid if the function is already strongly nonlinear in these parameters within the limits of error (of course, if the errors are small, the linearity condition can be used). Hence we employed the quantity χ^2 to estimate the errors. If the selected function is linear with respect to the parameters, then if one of the parameters is changed from its value at the minimum by one standard deviation and if all the remaining parameters are minimized, χ^2 increases to unity; for a change by two standard deviations, χ^2 increases to 4, etc. In the general case, such an estimate can be invalid; however, it can frequently be used in the nonlinear case, too, since here the linearity condition is not a necessary one. A sufficient condition is the possibility of obtaining a good approximation of the second derivatives of the selected function with respect to its parameters in terms of the first derivatives. This condition is also necessary for good convergence of the linearization method used in our case.

The results of the calculations by the two schemes of calculation are shown in Table II. In the most general case when none of the four parameters are fixed, solutions exist for $u > 0$ ($A > 0$) and $u < 0$ ($A < 0$) for both $\kappa < 1$ and $\kappa > 1$. In the latter case the parameters cannot be estimated with any reasonable accuracy and therefore this solution is not shown. The variant with $\kappa = 0$ (the absence of triplet states) is rejected by the χ^2 criterion, since $\chi^2 = 59.5$ with $\overline{\chi^2} = 8$.

It follows from the calculations that within the framework of the models employed, proton-proton scattering cannot be described without spin and a real part of the potential. Indeed, if σ_{tot} is not fixed in the initial data, then its subsequent calculation from the parameters for the best-fit curve leads to a calculated value greater than the experimental one, the difference $\sigma_{tot\,calc} - \sigma_{tot\,exptl}$ is approximately three full standard deviations. In this case the differential cross sections for purely nuclear scattering at 0° are 151 ± 11 and 146 ± 9 mb/sr, respectively, for calculations A and B.

The variants $\kappa = 1$ and $\kappa < 1$ for $u < 0$ ($A < 0$) do not differ from each other according to the χ^2 criterion; the values of χ^2 in these variants differ by less than unity. In the variants $\kappa = 1$ and $\kappa < 1$ for $u > 0$ ($A > 0$) the values of χ^2 differ by the quantity ~ 1.3. Hence, if we initially assume that the true value of κ lies in the region $0 < \kappa < 1$, then in the case $u > 0$ ($A > 0$), we obtain

$$\varkappa = 0.24^{+0.76}_{-0.11}.$$

With good statistics it should, perhaps, be possible to distinguish this case from the case $\kappa = 1$, $u > 0$ ($A > 0$). However, with our statistical accuracy this difference lies within the limits of one standard deviation, which is illustrated in Fig. 3 (see curves 1 and 4).

The calculation shows that the experimental results can also be explained without the assumption of the existence of a real part of the potential ($u = 0$). As seen from Table II, if it is assumed that $\kappa < 1$, then we obtain $\kappa = 0.25 \pm 0.07$, and for $\kappa > 1$ the best value is $\kappa = 16.5$, but with a large error.

We also carried out an analysis based on the assumptions made by Grishin et al[9]. Here it was assumed that the real part of the scattering amplitude and its dependence on the spin can be neglected if the scattering amplitude is considered not to change sign in the angular intervals $0 - 90°$ and the identity of the particles is neglected. With

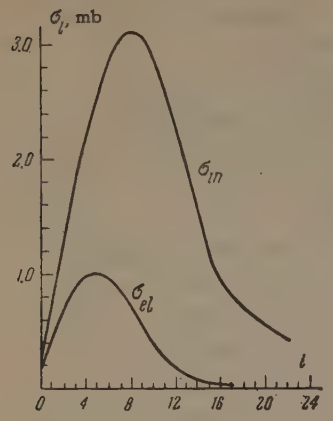

FIG. 4. Partial cross sections for pp elastic σ_{el} and inelastic σ_{in} interactions obtained under the assumptions formulated by Grishin et al.[9]

such an approach we calculated from the experimental data the values $\beta_l = \exp(2i\delta_l)$, where δ_l is the phase shift.

From the unitarity conditions we have $0 \leq \beta_l \leq 1$. We calculated the values of β_l for all values of l up to $l_{max} = 22$. The smallest value should be obtained for β_0. The calculated value was $\beta_0 = +0.27$ and in this sense such a view of the obtained experimental data does not contradict the unitarity condition, although such an approach is not in agreement with the results of the foregoing calculations. This is due to the fact that β_0 is determined with a large error, since the basic contribution to β_0 comes from scattering at large angles. It thus follows that the unitarity criterion can only be used in the case of much greater accuracy.

The pp total interaction cross section is found to be $\sigma_{tot} = 47.3$ mb, which is in agreement with the foregoing calculations. In view of the smallness of the contribution of the first phases, the uncertainty in the total cross section is small.

The partial cross sections for elastic and inelastic interactions obtained in the calculation are shown in Fig. 4. It is seen that the maximum of the partial contributions is observed at $l = 5$ for the elastic interaction and at $l = 8$ for the inelastic interaction. As has already been indicated, the basic contribution to the first phase shifts comes from large-angle scatterings, which were not measured by us, and thus the errors in the calculated first phase shifts are large. However, for β_7, for example, the errors are less than 15%.

3. CONCLUSIONS

1. The rms pp interaction range is independent of all the models discussed above and turns out to be $(1.15 \pm 0.05) \times 10^{-13}$ cm.

2. A difference of three standard deviations is observed between the experimental data and the results of the calculations if it is assumed that the scattering amplitude does not depend on the proton spins and does not contain a real part. An attempt was made to explain this disparity by the existence of a spin-spin interaction and the presence of a real part in the scattering amplitude. If the scattering amplitude does not depend on the spins, then the real part of the scattering amplitude does not exceed 0.5 of the imaginary part and takes on its maximum value.

If it is assumed that the scattering amplitude has no real part, there must be a difference between the interactions in the singlet and triplet states. If it is assumed that the interaction in the singlet state predominates over the interaction in the triplet state ($\kappa < 1$), then $\kappa = 0.25 \pm 0.07$. If the reverse occurs ($\kappa > 1$), then the best value is $\kappa = 16.5$ and as κ approaches unity the value of χ^2 increases and passes through the value 1 when $\kappa = 6.5$. The statistics obtained in this experiment do not permit us to establish which is the cause of the observed discrepancy—the real part of the scattering amplitude or the spin-spin interaction.

In conclusion, the authors express their sincere gratitude to V. I. Veksler for his constant interest and to K. D. Tolstov for assistance in this work.

[1] Lyubimov, Markov, Tsyganov, Cheng, and Shafranova, JETP 37, 910 (1959), Soviet Phys. JETP 10, 651 (1960); Markov, Tsyganov, Shafranova, and Shakhbazyan, JETP 38, 1471 (1960), Soviet Phys. JETP 11, 1063 (1960).

[2] M. I. Podgoretskiĭ and E. N. Tsyganov, Preprint, Joint Institute for Nuclear Research (in press).

[3] Do, Kriventsova, Lyubomilov, and Shafranova, Materialy III Mezhd. konf. po yadern. fotografii, (Proceedings of Third International Conf. on Nuclear Photography), Moscow, 1960.

[4] von Dardel, Frisch, Mermod, Milburn, Piroué, Vivargent, Weber, and Winter, Phys. Rev. Lett. 5, 333 (1960).

[5] Ashmore, Cocconi, Diddens, and Wetherell, Phys. Rev. Lett. 5, 576 (1960).

[6] I. N. Silin and B. A. Shakhbazyan, Preprint D-616, Joint Institute for Nuclear Research, Dubna, 1960.

[7] Stapp, Ypsilantis, and Metropolis, Phys. Rev. 105, 302 (1957).

[8] H. Bethe, Ann. Phys. 3, 190 (1958).

[9] Grishin, Saitov, and Chuvilo, JETP 34, 1221 (1958), Soviet Phys. JETP 7, 844 (1958); Blokhintsev, Barashenkov, and Grishin, JETP 35, 311 (1958), Soviet Phys. JETP 8, 215 (1959).

[10] K. D. Tolstov, Preprint, Joint Institute for Nuclear Research (in press).

[11] Lim, Laby, and Hopper, Nuovo cimento, Suppl. 15, 382 (1960).

Translated by E. Marquit
295

INVESTIGATION OF THE C^{12} (α, 4α) REACTION

S. S. VASIL'EV, V. V. KOMAROV, and A. M. POPOVA

Submitted to JETP editor June 27, 1961

J. Exptl. Theoret. Phys. (U.S.S.R.) **41**, 1757-1760 (December, 1961)

The disintegration of the C^{12} nucleus induced by 23-Mev α particles into three α particles is investigated. Space and energy distributions of the decay products as well as excitation energies of the possible intermediate nuclei C^{12*} and Be^8 are presented. It is established that the basic reaction mechanism is the decay of the O^{16} nucleus into four α particles with a resonance interaction between the final-state α particles.

THE disintegration of the C^{12} nucleus into three α particles induced by 23-Mev α particles can proceed by various mechanisms through various energetically possible channels. The present study attempted to analyze the relative probability of these different mechanisms by methods adopted in our preceding investigations of light nuclear decays.[1-4]

Alpha particles were accelerated in the 120-centimeter cyclotron of the Research Institute for Nuclear Physics of the Moscow State University. Extracted from the cyclotron chamber through a system of quadrupole lenses and a deflecting magnet into the experimental room, they entered a chamber containing photographic plates (in a special cassette) inclined at an angle of 6° to the incident beam. Exposures of tenths of a second were used. Stars formed in the emulsion by the incident 23 ± 1-Mev α particles and by α particles from disintegrations were observed in NIKFI photographic plates (types Ya-2, T-1, T-3, and D, from 50 to 400 μ thick). The decay of C^{12} nuclei in the emulsion was observed, and from the resultant stars the energy and emission angle of all α particles produced in the reaction as well as the energy of the incident α particles could be computed. All data were transformed into the center-of-mass (c.m.) system. About 100 stars resulting from the disintegration of C^{12} nuclei induced by 23 ± 1-Mev α particles were found among the stars analyzed.

The following mechanisms for the α-particle induced decay of a C^{12} nucleus into three α particles are possible:

$$C^{12} + \alpha \to O^{16*} \to C^{12*} + \alpha \to Be^8 + 2\alpha \to 4\alpha, \quad (1)$$

$$C^{12} + \alpha \to O^{16*} \to C^{12*} + \alpha \to 4\alpha, \quad (2)$$

$$C^{12} + \alpha \to O^{16*} \to Be^8 + Be^8 \to 4\alpha, \quad (3)$$

$$C^{12} + \alpha \to O^{16*} \to Be^8 + 2\alpha \to 4\alpha, \quad (4)$$

$$C^{12} + \alpha \to O^{16*} \to 4\alpha, \quad (5)$$

$$C^{12} + \alpha \to C^{12*} + \alpha \to Be^8 + 2\alpha \to 4\alpha, \quad (6)$$

$$C^{12} + \alpha \to C^{12*} + \alpha \to 4\alpha. \quad (7)$$

The first five mechanisms involve decay through the compound system O^{16}. The last two involve the decay of the C^{12} nucleus into three α particles as the result of a direct interaction between the incident α particle and the nucleus.

In order to determine the probabilities of these mechanisms, the distributions of excitation energy of the intermediate nuclei C^{12} and Be^8, as well as the α-particle angular and energy distributions, were investigated. It was noted when processing the stars that certain of them contained pairs of α particles with very small angular divergence. This fact suggested the possibility that a Be^8 nucleus in the ground state was involved in the reaction. To test this hypothesis, the energy distribution of all possible values of excitation energy for the Be^8 nucleus was plotted as calculated from the energies of and angles between the α particles. Since four α particles are produced in each event, it was necessary to consider six possible values of Be^8 excitation energy [$E_{excit}(Be^8)$] for each star.

The $E_{excit}(Be^8)$ distribution obtained is shown in Fig. 1a. It must be kept in mind that out of six $E_{excit}(Be^8)$ values for each decay event two can have a physical sense, since two intermediate Be^8 nuclei can be produced at a time. If the intermediate Be^8 nucleus takes part in the decay of C^{12} into three α particles, maxima corresponding to known levels of the Be^8 nucleus must appear against the background of a continuous distribution of $E_{excit}(Be^8)$ values. As can be seen from Fig. 1a, the ground and 2.9-Mev levels of Be^8 do appear in the distribution, and there is also an indication that the well-known broad level in the 8—14-Mev interval is involved in the decay.

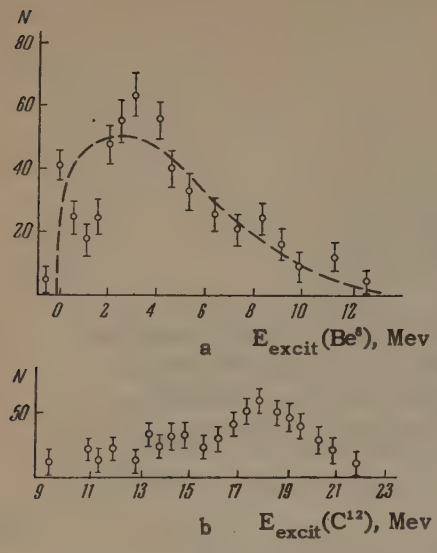

FIG. 1. Excitation energy of possible intermediate nuclei from $C^{12}(\alpha, 4\alpha)$ reaction induced by 23±1-Mev α particles: a – Be^8 nucleus, b – C^{12} nucleus.

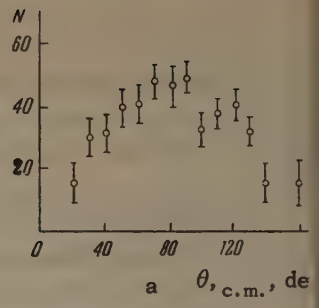

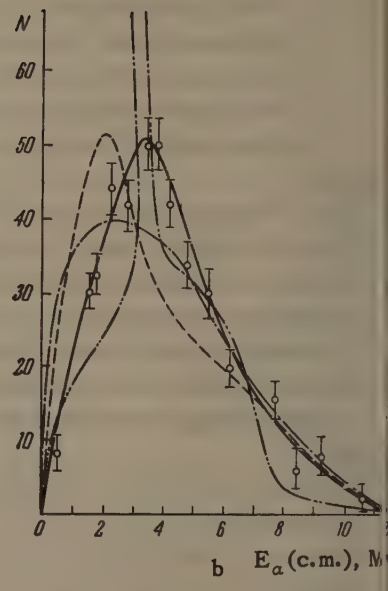

FIG. 2. Distribution (c.m.) of α particles from the reaction $C^{12}(\alpha, 4\alpha)$ induced by 23±1-Mev α particles: a – angular distribution, b – energy distribution.

In order to examine the possibility that the C^{12} nucleus decayed into three α particles through channels (1) and (2), excitation energies of the C^{12} nucleus were computed from the energy of the three α particles resulting from the decay of the intermediate nucleus C^{12}. Since it was impossible to determine which three of the four α particles produced in the reaction could have resulted from the decay of the C^{12} nucleus, its excitation energies were calculated from all possible combinations of three from the four α particles. Thus, if the reaction proceeded via mechanisms (1) or (2), the true values of $E_{excit}(C^{12})$ had to be weighted by $\frac{1}{4}$.

The distribution of $E_{excit}(C^{12})$ values is presented in Fig. 1b, from which it is evident that maxima corresponding to known C^{12} nuclear levels are not observed. If the intermediate nucleus C^{12} had actually been involved in the decay, its 9.6-Mev level with zero isotopic spin should have appeared as a maximum against the background of false $E_{excit}(C^{12})$ values (Fig. 1b). This level stands out far enough from neighboring levels and, as has been shown by the authors in a study of the decay of the C^{12} nucleus induced by 10–19-Mev neutrons,[5] this level can appear when the C^{12} nucleus decays.

Therefore, mechanisms (1) and (2) may be considered as not very probable for the given decay. Moreover, if the C^{12} nucleus decayed into three α particles by mechanism (2), that is, the intermediate Be^8 nucleus was not involved in the decay, the $E_{excit}(Be^8)$ distribution (Fig. 1a) should have been described by a curve calculated for mechanism (2) by a method used earlier.[2] This curve is plotted in dashes on Fig. 1a. Its disagreement with the experimental data is sufficient testimony to the improbability of the reaction having occurred via mechanism (2).

The angular distribution of α particles from the reaction is presented in Fig. 2a. As is visible from the graph, this distribution is symmetrical with respect to 90° within the limits of statistical accuracy, which indicates the absence of a direct interaction mechanism in the decay. This conclusion is confirmed by the absence of a high-energy "tail" in the energy distribution of the α particle (Fig. 2b).

We examine next mechanisms (3), (4), and (5), which have to do with the decay of the compound system O^{16*} into two, three, or four particles respectively. The probability of these mechanisms occurring can be determined by investigating the energy distributions of the α particles produced in the reaction. If the reaction proceeds via a direct decay of the compound system O^{16*} into four independent particles, the energy distribution of the α particles must obey the following relation

$$F(E_\alpha) = E_\alpha^{1/2}(E_{max} - \mu E_\alpha)^{1/2},$$

where E_α is the α-particle energy, E_{max} is the maximum α-particle energy, and μ is the mass coefficient. The curve plotted from this formula is presented in Fig. 2b by the dot-dashed line (one dot). No agreement with experiment is observed.

If the compound system O^{16*} decays into two Be^8 nuclei which then decay into two α particles

each, it is possible to construct a distribution of α particles from the Be^8 decay in the center-of-mass system of all the products formed. In doing so we must consider the fact that both Be^8 nuclei may be produced in the first excited state, or one may be in the ground state and the second in the first excited state. A curve that takes into account the probability of Be^8 nuclear levels appearing is plotted in a dot-dashed line (two dots) in Fig. 2b.

The case of two Be^8 nuclei being formed in the ground state was not considered in the calculations. If the O^{16*} system decays into two Be^8 nuclei in the ground state, the star formed by the α-particle tracks in the emulsion will have the characteristic form of two pairs of grouped tracks. After transforming into the center-of-mass system, it becomes possible to separate out such stars. There were none of them among the stars we observed. A comparison of the two-dot dot-dashed curve with experimental results shows that mechanism (3) is improbable.

The probability of mechanism (4) occurring can be investigated by comparing the experimental energy distributions of α particles with the curve calculated assuming a three-particle decay of the O^{16*} system into two α particles and a Be^8 nucleus in the ground or first excited state (taking into account the probability of appearance of the Be^8 nuclear states). The theoretical curve is plotted in dashes in Fig. 2b. In this case the agreement with experimental data was likewise not good.

Let us examine one other possible way for light nuclei to decay into several particles which has not been considered in earlier studies, namely, the simultaneous decay of the compound system into particles which interact in the final state. In this case we will have the decay of O^{16*} into four α particles resonantly scattering on the levels of the Be^8 nucleus. The solid line in Fig. 2b represents the curve calculated using this hypothesis by the method given in [4]. As can be seen from the graph, the experimental data are in good agreement with this calculation.

We may thus conclude that the decay of the C^{12} nucleus into three α particles induced by α particles proceeds with high probability through the direct decay of the compound system into α particles which interact in the final state. The intermediate nucleus Be^8 appears in this decay as the result of the resonance interaction of the final-state α particles from the simultaneous decay of the compound system O^{16*}. From this it is clear why, when the Be^8 excitation energy distribution (Fig. 1a) indicated a large probability that this unstable nucleus should appear, the disintegration actually proceeded with low probability by mechanisms (1), (3), (4) and (6), which involve states of the intermediate Be^8 nucleus.

[1] V. V. Komarov and A. M. Popova, JETP **38**, 253 (1960), Soviet Phys. JETP **11**, 184 (1960).

[2] Vasil'ev, Komarov, and Popova, Izv. AN SSSR, Ser. Fiz. **24**, 1149 (1960), Columbia Tech. Transl. p. 1151.

[3] Vasil'ev, Komarov, and Popova, Izv. AN SSSR, Ser. Fiz. **25**, 1117 (1961), Columbia Tech. Transl. in press.

[4] Vasil'ev, Komarov, and Popova, Report at second All-Union Conference on Nuclear Reactions at Low and Medium Energies, Moscow, 1960.

[5] Vasil'ev, Komarov, and Popova, JETP **33**, 1321 (1957), Soviet Phys. JETP **6**, 1016 (1958).

Translated by Mrs. J. D. Ullman
296

LEVELS OF THE Si^{30} *NUCLEUS FROM THE* $Si^{29}(d, p)Si^{30}$ *REACTION*

K. I. ZHEREBTSOVA, V. F. LITVIN, LIU CHAO-YUNE, and Yu. A. NEMILOV

Radium Institute, Academy of Sciences, U.S.S.R.

Submitted to JETP editor June 30, 1961

J. Exptl. Theoret. Phys. (U.S.S.R.) **41**, 1761-1762 (December, 1961)

New data on the 8.149- and 8.571-Mev levels of the Si^{30} nucleus are obtained by measuring on a multispectrograph the energy and angular distributions of protons emitted in the (d, p) reaction.

SOME new data on the levels of the Si^{30} nucleus were obtained during study of the $Si^{29}(d, p)$ stripping reaction on a multi-angle magnetic analyzer, the multispectrograph.[1,2] The bombarding deuteron energy was 6.58 Mev. The 0.5-mg/cm^2 target was composed of 34.9% Si^{28}, 63.7% Si^{29}, and 1.4% Si^{30}.

Figure 1 presents the proton energy spectrum measured at an emission angle $\theta = 20°$.

Because of the insufficient abundance of the isotope Si^{29} in the target, data which we obtained earlier for the $Si^{28}(d, p)Si^{29}$ reaction[3] as well as the results of Browne and Radzyminski's study of Si^{30} nuclear levels[4] were used to identify the proton groups.

A number of Si^{30} nuclear levels discovered by Browne and Radzyminski[4] were confirmed by us.

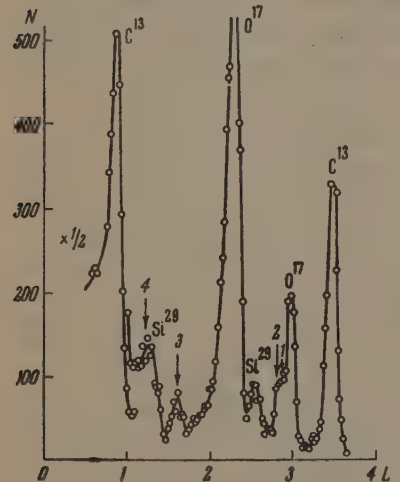

FIG. 1. Energy spectrum of protons emitted at $\theta = 20°$ (N is the number of proton tracks in the microscope field of vision; L is the coordinate along the photographic plate). Proton groups 1, 2, 3, and 4 correspond to Si^{30} states with excitation energies $E_1 = 6.630$, $E_2 = 6.734$, $E_3 = 8.149$, and $E_4 = 8.571$ Mev (E values are taken from [4]).

Because of the complexity of the proton energy spectrum (presence in the target of C^{12}, O^{16}, and Si^{28} contamination), some of the proton groups from the $Si^{29}(d, p)Si^{30}$ reaction could not be obtained at all angles; angular distributions have as yet been obtained for only two groups, which correspond to the Si^{30} levels at excitation energies of 8.149 and 8.571 Mev. These are given in Fig. 2.

A comparison of experimental and theoretical[5] angular distributions yielded values for the orbital angular momentum transferred to the final nucleus by the neutron, as well as for final-state spins and parities, which are presented in the table.

The presence in the target of a considerable admixture of Si^{28} allowed us to compare the probabilities of neutron "sticking" in the p-state of Si^{29} and Si^{30} nuclei, since both proton groups were obtained in the same experiment.

The last column of the table gives the neutron "sticking" probability Λ_n,[5] taking as unity the

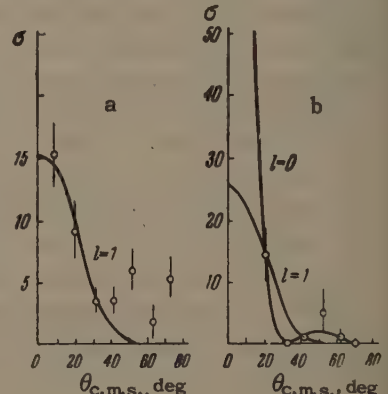

FIG. 2. Angular distributions of proton groups corresponding to various levels of the Si^{30} nucleus: a) group 3, $E_3 = 8.149$ Mev; b) group 4, $E_4 = 8.571$ Mev. The solid curves are calculated from the formula of Bhatia et al.[5]

Final nucleus	Excitation energy, Mev	l_n	Possible values, I, π	Shell model configuration	Λ_n
Si^{29}	4.93	1	$^3/_2^-$	$2P_{3/2}$	1
Si^{30}	8.149		$0^-, 1^-, 2^-$	$(2S_{1/2})^1 (2P_{3/2})^1$ or $(2S_{1/2})^1 (2P_{1/2})^1$	0.43±0.20
Si^{30}	8.571	1 or 0			

magnitude of Λ_n for the $2P_{3/2}$ state of the Si^{29} nucleus.

Study of the (d, p) reaction on isotopically enriched silicon will be continued.

[1] Yu. A. Memilov and V. F. Litvin, Pribory i tekhnika eksperimenta (Instruments and Exptl. Techniques) No. 2, 32 (1960).

[2] V. F. Litvin, Trudy RIAN (Trans. Radium Inst. Acad. Sci. U.S.S.R.) 9, 141 (1959).

[3] Alekseev, Zherebtsova, Litvin, and Nemilov, JETP 39, 1508 (1960), Soviet Phys. JETP 12, 1049 (1961).

[4] C. P. Browne and J. T. Radzyminski, Nucl. Phys. 19, 164 (1960).

[5] Bhatia, Huang, Huby, and Newns, Phil. Mag. 43, 485 (1952).

Translated by Mrs. J. D Ullman
297

THE ELECTRICAL PROPERTIES OF THIN NICKEL FILMS AT LOW TEMPERATURES

O. S. GALKINA, L. A. CHERNIKOVA, CHANG KAI-TA, and E. I. KONDORSKII

Moscow State University

Submitted to JETP editor July 1, 1961

J. Exptl. Theoret. Phys. (U.S.S.R.) **41**, 1763-1766 (December, 1961)

The electrical properties of thin nickel films of very high purity, obtained by thermal evaporation in a vacuum inside a vessel kept in a helium bath during the deposition, have been investigated. Films with thicknesses from 30 A and upwards had a residual resistivity and Hall e.m.f. of the order of magnitude close to that of bulk nickel specimens.

A considerable number of papers have been devoted to the study of ferromagnetic films. However, the features of the magnetic properties of films obtained in a vacuum of the order of 10^{-5}—10^{-6} mm Hg, found by several authors[1,2] are, as shown by the later investigations of Neugebauer,[3] related to a considerable extent to the effect of contamination by the residual gas on deposition and to the oxidation of the film on bringing it into the atmosphere. In particular, it was shown in Neugebauer's work that the saturation magnetization of thin nickel films, deposited in a vacuum of 10^{-9} mm Hg is independent of thickness down to a thickness of about 30 A.

The present investigation was carried out with the aim of finding out to what extent the electrical and galvanomagnetic properties of films with thicknesses down to 30 A, deposited in a vessel immersed in a liquid helium bath, differ from the corresponding properties of bulk specimens.

The films were obtained by thermal evaporation of nickel. Figure 1 shows the general appearance of the evaporation apparatus. A tungsten wire serves as evaporator. After the preparation of the evaporator (cleaning, degassing and preconditioning in a vacuum of 10^{-7} mm Hg) the substrate was sealed into the vessel and a second degassing of the whole apparatus was carried out in the same vacuum. A beaker, optically polished to 0.1 interference fringe, was used as substrate. Four platinum leads were sealed into the ends of the beaker. Current and Hall contacts were deposited onto the substrate by cathode sputtering. During deposition of a film the apparatus was in a helium bath. The residual gasses, other than helium, were thus frozen out. The pressure in the apparatus before evaporation started, calculated from the amount of helium in the atmosphere, was of the order of 10^{-13} mm Hg. The amount of metal deposited was controlled by measuring the electrical resistance during the process of deposition.

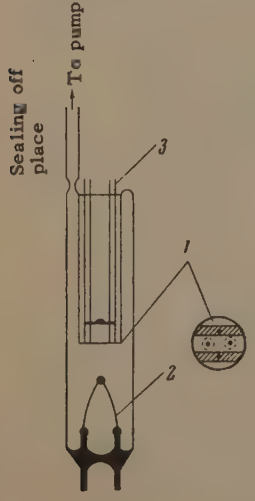

FIG. 1. Apparatus for deposition of the films: 1—substrate with deposited platinum contacts, 2—evaporator, 3—platinum electrodes.

The temperature dependence of the electrical resistance was studied for films of thickness from 1300 down to 30 A at temperatures from 2 to 300°K. In the temperature range 4.2 to 40°K the temperature was measured with a constantan resistance thermometer, and above 40°K by a copper-constantan thermocouple. The thickness of the films was determined by an interferrometric method, using a universal monochromator of the UM-2 type*.

Figure 2 shows curves indicating the change of electrical resistance of the films studied, on heating newly condensed films from 4.2 to 300°K and on cooling to the original temperature (4.2°K) after holding at 300°K. Further heating produces no further changes in the form of curves 3 and 4. Calculation showed that the specific electrical resistivity for films of all the thicknesses mentioned above is close to the specific resistivity of bulk nickel. Destruction of the vacuum (taking the films into the air after keeping them for three months in the vessel) led to a rapid and sharp increase in

*The authors are grateful to Yu. Durasova for measuring the film thickness.

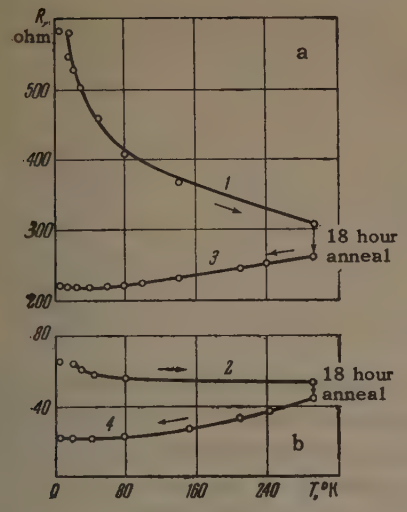

FIG. 2. a – the change of electrical resistivity of a freshly deposited film on heating from 4.2°K to room temperature: b – the change of electrical resistivity of a film on cooling it from room temperature to 4.2°K after holding at room temperature for 18 hours: curve 1 – for d = 50 A, curve 2 – for d = 135 A, curve 3 – for d = 50 A, curve 4 – for d = 135 A.

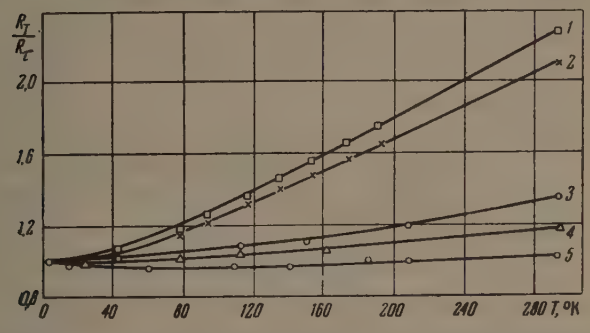

FIG. 3. The dependence of R_T/R_τ on temperature for films of different thickness: curve 1 – d = 1300 A; curve 2 – d = 835 A; curve 3 – d = 135 A; curve 4 – d = 75 A; curve 5 – d = 30 A.

electrical resistance: the resistance of thick films increased 1.5—2 fold, and of thin films several tens of times.

Figure 3 shows curves of the dependence of R_T/R_τ on temperature for heated films of various thicknesses. Here R_T is the resistance of a film at temperature T and R_τ is the resistance at helium temperature. The thinner the film the smaller is the relative change of resistance on increasing the temperature. For films of thickness 1300 A the value of $R_\tau/R_0 = 0.4$, where R_0 is the resistance at room temperature. For a 30 A thick film $R_\tau/R_0 = 0.95$. In addition, the curves show that the boundary of the residual resistance region is shifted to higher temperatures for thin films.

Figure 4 shows curves of the dependence of the specific resistivity on film thickness for temperatures of 300 and 4.2°K. It can be seen that the resistivity at 300°K of films with thicknesses from 1300 to 300 or 400 A is independent of thickness and does not increase significantly with decreasing thickness for thin films of thickness from 300 to 30 A. An increase of resistivity with decreasing thickness is already observed at 4.2°K for films of thickness less than 900 A. The resistivity decreases 2—2.5 fold on going from room temperature to helium temperature for thick films

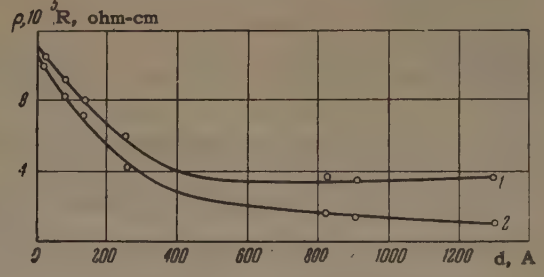

FIG. 4. The dependence of electrical resistivity on film thickness for temperatures: curve 1 – 300°K and curve 2 – 4.2°K.

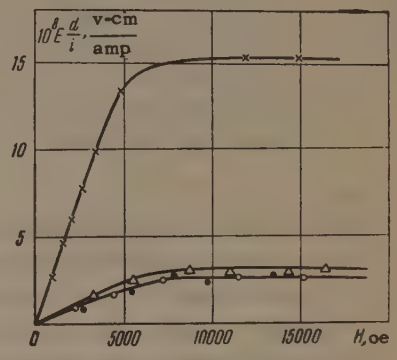

FIG. 5. The dependence of the Hall field for films of different thickness on the strength of the applied magnetic field: × – d = 50 A, Δ – d = 835 A, ○ – d = 1000 A, ● – d = 1300 A.

(d > 1000 A) and decreases by only 4—5% for thin films (d < 100 A).

We also studied the Hall effect in the films we obtained. The dependence of the Hall field on the magnetic field H, perpendicular to the plane of the film, is shown in the curves of Fig. 5. The Hall field was measured at room temperature. It corresponds approximately to the bulk specimen value for thicknesses of 1300 – 835 A, but increases on going to 50-A films, evidently connected with the increase in resistivity of such a film.

Preliminary calculations show that the behavior of the resistivity and its temperature dependence for thin films less than 300—400 A thick, must be related to the fact that the electron mean free path in these films becomes comparable with the film thickness.

In conclusion the authors express their deep thanks to A. I. Shal'nikov for valuable advice and great help in the carrying out of this work.

[1] Colombani, Coureaux, and Huet, Colloque international de Magnetisme, July, 1958, Centre National de la recherche Scientifique, Paris, 1959, p. 239.

[2] N. I. Ginzburg and A. M. Polyakov, ZhTF 28, 1029 (1958), Soviet Phys. Tech. Phys. 3, 957 (1958).

[3] C. A. Neugebauer, Structure and Properties of Thin Films, ed. Neugebauer, Newkirk and Vermilyea, New York 1959, p. 358.

Translated by R. Berman
298

ISOMER SHIFTS FOR THE 23.8-kev GAMMA TRANSITION IN Sn^{119}

V. S. SHPINEL', V. A. BRYUKHANOV, and N. N. DELYAGIN

Nuclear Physics Institute, Moscow State University

Submitted to JETP editor July 1, 1961

J. Exptl. Theoret. Phys. (U.S.S.R.) 41, 1767-1770 (December, 1961)

By measuring the resonance absorption of the γ quanta by nuclei in crystals, we have determined the isomer shifts for the 23.8-kev transition of Sn^{119} in several compounds of tin. We discuss a possible qualitative interpretation of the shifts; according to this interpretation, when the Sn^{119} nucleus is excited there is an increase in the effective radius of the proton distribution in the nucleus and the proton core of Sn^{119} in the excited state does not have spherical symmetry.

THE method of resonance absorption of γ quanta can be used to measure small changes in the energy of nuclear γ transitions and, in particular, the magnitudes of the isomer shifts [1] which result from the interaction with the atomic electrons of the nuclear charge in the ground and excited states. We have previously noted [2] the presence of such shifts for the 23.8-kev γ transition in Sn^{119}. Recently a detailed investigation of such shifts for the 14.4-kev γ transition in Fe^{57} has been made by de Benedetti, Lang, and Ingalls [3] and by Walker, Wertheim, and Jaccarino.[4]

In the present work we have measured the isomer shift for the 23.8-kev γ transition of Sn^{119} in various tin compounds. The measuring technique and apparatus are the same as those we used earlier.[5,6] The measurements were made with a source of Sn^{119m} in the form of SnO_2; in this source there is no quadrupole splitting of the emission line and the effect of recoilless emission of γ quanta is large at room temperature. The source was kept at room temperature in all measurements, while the absorbers of various crystalline compounds of tin were at liquid nitrogen temperature or at room temperature. Some of the results have been published previously;[2,5] for some of the substances previously measured, improved data are given in the present paper.

Typical resonance absorption spectra are shown in Figs. 1 and 2. In Fig. 1 we give the resonance absorption spectrum for SnF_2, in which the absorption line is split into two components as a result of quadrupole interaction of the excited Sn^{119} nucleus with the electric field gradient in the crystal. The value of the isomer shift δ was determined relative to the energy of the γ transition in a SnO_2 crystal at room temperature (i.e., the

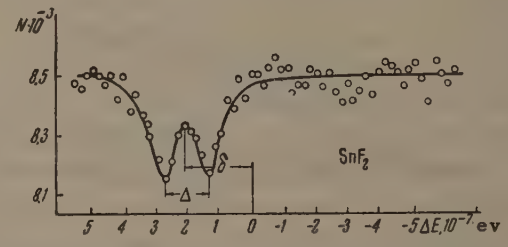

FIG. 1. Resonance absorption spectrum for SnF_2 polycrystal at liquid nitrogen temperature ($\Delta E = E_0 v/c$, where $E_0 = 23.8$ kev, v is the velocity of the absorber and c the velocity of light; N is the total number of pulses counted).

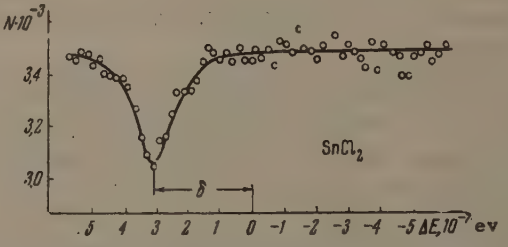

FIG. 2. Resonance absorption spectrum for $SnCl_2$ polycrystal at liquid nitrogen temperature (notation the same as in Fig. 1).

emission line of the source). Figure 2 shows the absorption spectrum for a $SnCl_2$ crystal, in which there is no quadrupole splitting. Similar resonance absorption spectra were taken for eleven tin compounds with the absorbers at liquid nitrogen temperature. The results of the measurements are shown in the table. For some of the compounds the isomer shift was also measured with the absorber at room temperature. Within the limits of error, the isomer shift was the same as at liquid nitrogen temperature*; the exception was $SnNb_3$,

*The existence of a temperature dependence of the isomer shift for the β-Sn crystal [7] which we reported earlier has not been confirmed by the later measurements.

Isomer shifts* of the 23.8-kev γ transition of Sn^{119}

Chemical compound	Isomer shift, 10^{-8} ev	Chemical compound	Isomer shift, 10^{-8} ev
SnO_2	$\leqslant 1$	SnO	22,0±1,5
$SnCl_4 \cdot 5H_2O$	2,2±1,0	$SnCl_2$	30.6±3,0
SnI_4	13.0±2,0	$SnBr_2$	1,6±0,7
SnS_2	8,5±2,0	β-Sn	22,0±2,0
$(NH_4)_2 \cdot SnCl_6$	3,3±1,5	$SnNb_3$	18.0+1,5
SnF_2	23,5±3,0		

*Shifts measured at liquid-nitrogen temperature relative to γ-transition energy in SnO_2 crystal at room temperature.

for which the relative change in energy was of the order of 1.5×10^{-12} for a change in temperature from liquid nitrogen to room temperature.

In addition to the previously observed cases of the β-Sn and SnO crystals,[5,8] quadrupole splitting of the absorption line was found only in SnF_2 (Fig. 1). For this crystal the magnitude of the splitting Δ was $(15.5 \pm 2.5) \times 10^{-8}$ ev and (as for the SnO crystal) was not strongly temperature dependent (unlike the case of β-Sn[7]).

From the data in the table we see that the isomer shifts for the 23.8-kev γ transition of Sn^{119} do not show such clear regularities as one finds for the 14.4-kev transition in Fe^{57}. It appears that the magnitude of the shift is affected not only by the valence of the tin atom in the particular compound but also by the chemical activity (electronegativity) of the other atoms, and by the crystal lattice structure. The latter is confirmed, for example, by the existence of an isomer shift between the two tin modifications β-Sn and α-Sn,[9] which are identical chemically but have different crystal structures.

We may note, however, that as a rule divalent tin compounds have a larger isomer shift than do tetravalent compounds. In the outer shell of the tin atom there are two p electrons, which give a much smaller contribution to the isomer shift than do the s electrons. We can assume that for divalent compounds of tin it is just these two p electrons that participate in the chemical bond; the valence electrons of the next shell (the two s electrons) only enter into the chemical binding for the tetravalent compounds, and this results in a marked change in the isomer shift. According to this interpretation one would conclude that the density of the s-electron wave function in the region of the nucleus is less in tetravalent compounds than in divalent compounds. The isomer shift is proportional to the product of the change in the square of the effective charge radius of the nucleus and the change in the square of the electron wave function at the nucleus for the two different compounds. Comparing the isomer shifts for di- and tetravalent compounds of tin, we can write

$$E_{II} - E_{IV} \sim (R_e^2 - R_0^2)\,[\,|\psi(0)|_{II}^2 - |\psi(0)|_{IV}^2],$$

where R_e and R_0 are the effective charge radii for the Sn^{119} nucleus in the excited and ground states, $\psi(0)$ is the electron wave function (mainly from s electrons) at the nucleus. The left side of this equality is positive; the term in square brackets on the right is also positive (according to the interpretation given above). Consequently $R_e^2 > R_0^2$, i.e., when the Sn^{119} is excited the effective radius of the charge distribution increases. The excitation of the Sn^{119} nucleus may be regarded as the excitation of the odd neutron (or of a group of neutrons). Nevertheless, the proton-magic core of the Sn^{119} nucleus does not remain inert in such an excitation, as is convincingly shown by the change in the radius of the charge distribution in the nucleus when it changes to the excited state. The presence of quadrupole interaction shows that the proton-magic core of the Sn^{119} nucleus does not have a spherically symmetric shape (at least in the excited state). These facts can be understood if we assume that the outer neutrons exert a polarizing force on the proton core of the nucleus, causing it to deform and changing the effective radius when there is an excitation.

A more detailed (quantitative) interpretation of the observed isomer shifts cannot be given, since the electronic wave functions are not known for the tin atom; the interpretation is complicated by the possible influence on the isomer shift of the crystal structures of the tin compounds.

[1] O. C. Kistner and A. W. Sunyar, Phys. Rev. Letters **4**, 412 (1960).

[2] Bryukhanov, Delyagin, Zvenglinskii, and Shpinel', JETP **40**, 713 (1961), Soviet Phys. JETP **13**, 499 (1961).

[3] DeBenedetti, Lang and Ingalls, Phys. Rev. Letters **6**, 60 (1961).

[4] Walker, Wetheim and Jaccarino, Phys. Rev. Letters **6**, 98 (1961).

[5] Delyagin, Shpinel' and Bryukhanov, JETP **41**, 1347 (1961), Soviet Phys. JETP **14**, 959 (1962).

[6] Bryukhanov, Delyagin, Zvenglinskii and Sergeev, Prib. i Tekh. Éksp., in press.

[7] Shpinel', Bryukhanov and Delyagin, JETP **40**, 1525 (1961), Soviet Phys. JETP **13**, 1068 (1961).

[8] Delyagin, Shpinel', Bryukhanov, and Zvenglinskii, JETP **39**, 220 (1960), Soviet Phys. JETP **12**, 159 (1961).

[9] Boyle, Bunbury and Edwards, Proc. Phys. Soc. (London) **77**, 1062 (1961).

Translated by M. Hamermesh
299

PARAMAGNETIC RESONANCE IN SOLUTIONS OF Cr^{3+} *SALTS*

N. F. USACHEVA

Physico-Technical Institute, Kazan' Branch, Academy of Sciences, U.S.S.R.

Submitted to JETP editor July 1, 1961

J. Exptl. Theoret. Phys. (U.S.S.R.) 41, 1771-1772 (December, 1961)

The influence of additions of $Al(NO_3)_3$ to aqueous solutions of $Cr(NO_3)_3$ on the EPR (electron paramagnetic resonance) spectrum of the latter is studied. The EPR line width is found to be independent of the macroscopic viscosity of the solution.

PREVIOUS measurements of the temperature dependence of the line width ΔH of paramagnetic resonance in violet-colored aqueous solutions of the nitrate of trivalent chromium [1] showed that this dependence could not be explained by the theory of paramagnetic relaxation presented by McConnell.[2] However changes in ΔH in solutions over a wide temperature range can always be ascribed not only to a direct dependence of the relaxation time on temperature, but also to a change in the initial splitting of the spin sublevels with temperature. This is made more probable by the fact that cases are known among solid chromium salts in which the trigonal field constant D changes gradually with temperature over a wide range of the latter.[3] Therefore it was of interest to look into the dependence of the EPR line width in solutions of chromium salts on the viscosity at constant temperature. In doing this we strove to create changes in the viscosity of the solution without any disturbance to the immediate surroundings of a Cr^{3+} ion. It is to be noted that measurements of ΔH as a function of viscosity have hitherto been made only on solutions of Mn^{2+} salts.[4,5]

We prepared two series of aqueous solutions. Samples of the first series contained 0.6 mole/liter of $Cr(NO_3)_3$ and varying concentrations of $Al(NO_3)_3$ (from 0 to 2.5 mole/liter). The second series consisted of samples containing 0.01 mole/liter of $Cr(NO_3)_3$ and the same concentrations of $Al(NO_3)_3$ as in the first series. The coefficient of viscosity η of each sample was measured with an Ostwald viscosimeter at 295°K. The EPR measurements were carried out at the same temperature in a PÉ-1301 double-modulation radiospectrometer at 9346 Mc/sec. The line width was measured as the separation between the maximum and minimum of the first derivative of the absorption curve. The results obtained agree with the earlier data, within the limits of accuracy of the measurement (± 10%). Thus, for 0.6 mole/liter $Cr(NO_3)_3$ in water δH = 130 oe, which corresponds accurately to Kozyrev's data,[4] if it is assumed that the shape of the absorption line in $Cr(NO_3)_3$ solutions is Lorentzian.

It is certain that the predominant type of chromium ions in the violet aqueous nitrate solutions is $[Cr(H_2O)_6]^{3+}$. Since we added the nitrate of another trivalent ion, Al^{3+}, in order to increase the viscosity, we had grounds for believing that the concentration of Cr^{3+} ions, holding in the first sphere not only water but also acid residues, will not increase here by any substantial amount. This found some confirmation in the measurements of the optical absorption spectrum of the solutions, made with an SF-2M spectrophotometer. It turned out that in the given series the location and intensity of the two observed absorption bands (the centers of which are at $\lambda_1 = 0.412\mu$ and $\lambda_2 = 0.580\mu$) do not depend on the Al^{3+} ion concentration in the solution. At the same time, in going from the violet aqueous solutions of chromium nitrate to the green aqueous solutions of chromium chloride $[Cr(H_2O)_4Cl_2]Cl$, a shift of the centers of both absorption bands toward longer wavelengths is observed. This shift equals 0.020μ and lies outside the limits of error of the experiment.

The results of our EPR measurements are presented in the figure. It can be seen from it that the more concentrated solution exhibits a slight widening of the EPR line with the increase in viscosity as the Al^{3+} concentration is made greater. For an almost ninefold increase in viscosity, the line width increases correspondingly only 1.6 times. On the other hand, for the 0.01 mole/liter $Cr(NO_3)_3$ solutions (Curve 1) the line width remains unchanged for a ninefold increase in viscosity, within the limits of error. It is natural to attribute the weak dependence of δH on η observed in the 0.6 mole/liter $Cr(NO_3)_3$ solu-

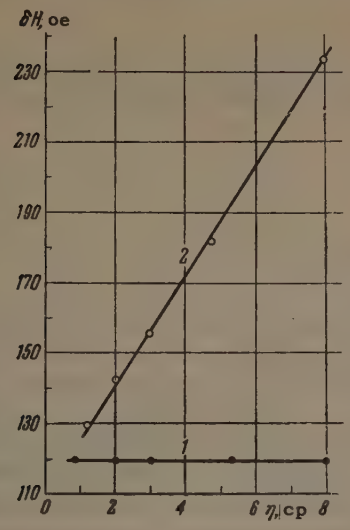

tions (Curve 2) to the contribution to the width brought about by the magnetic dipole interaction between the $[Cr(H_2O)_6]^{3+}$ ions. This contribution is practically nil at a concentration of 0.01 mole/liter Cr^{3+}, where the line width is evidently completely determined by the spin-lattice relaxation. According to any of the theories on paramagnetic relaxation in liquid solutions,[2,6,7] the independence of the spin-lattice relaxation time of the macroscopic viscosity η is rather unexpected. This independence can apparently be explained only by assuming that the correlation time τ_c is not connected with the macroscopic viscosity of the solution as a whole, but with the microscopic viscosity on the boundary between the paramagnetic complex and the solvent. This microviscosity apparently changes little with the ionic concentration, as was first proposed by Tishkov[8] in an analysis of the data on paramagnetic relaxation in parallel fields in solutions of Mn^{2+} salts. Our measurements, having been made by a different method and on a different ion, confirm this hypothesis.

In conclusion the author wishes to thank B. M. Kozyrev and N. S. Garif'yanov for guidance and assistance with the work, and R. R. Shagidullin for the optical measurements accomplished for the present work.

[1] Avvakumov, Garif'yanov, Kozyrev, and Tishkov, JETP 37, 1564 (1959), Soviet Phys. JETP 10, 1110 (1960).

[2] H. M. McConnell, J. Chem Phys. 25, 709 (1956).

[3] S. A. Al'tshuler and B. M. Kozyrev, Élektronnyi paramagnitnyi rezonans (Electron Paramagnetic Resonance), Fizmatgiz, 1961, p. 109.

[4] B. M. Kozyrev, Doctoral Dissertation, FIAN 1957

[5] Tinkham, Weinstein, and Kip, Phys. Rev. 84, 848 (1951).

[6] S. A. Al'tshuler and K. A. Valiev, JETP 35, 947 (1958), Soviet Phys. JETP 8, 661 (1959).

[7] I. V. Aleksandrov and G. M. Zhidomirov, JETP 40, 1720 (1961), Soviet Phys. JETP 13, 1211 (196).

[8] P. G. Tishkov, Dissertation, Kazan' State Univ., 1961.

Translated by L. M. Matarrese
300

DIRECT MEASUREMENT OF THE MOMENTUM OF CONDUCTION ELECTRONS IN A METAL

M. S. KHAĬKIN

Institute for Physics Problems, Academy of Sciences, U.S.S.R.

Submitted to JETP editor July 11, 1961

J. Exptl. Theoret. Phys. (U.S.S.R.) 41, 1773-1779 (December, 1961)

A method for "cutting-off" cyclotron resonances is described which can be employed for direct measurement of the Fermi momentum of conduction electrons in a metal. Results of experiments on tin single crystals are presented and discussed. The electron momentum in one of the Fermi surface sections has been measured with an accuracy of ~2.5% in the range of angles ±26° from the [100] axis in the (010) plane.

A study of the phenomenon of cyclotron resonance is a direct and most reliable method for measuring the effective masses of conduction electrons.[1-5] However, this phenomenon can also be used to study several other characteristics of the electrons in a metal. Kaner and Azbel',[6] for example, note the possibility in principle of measuring the Fermi momentum of electrons. An experimental method for the direct measurement of the momentum of conduction electrons is described in the present paper, and the results of the first experiments carried out by this method are presented.

THEORY

Let us consider the motion of an electron along the largest closed orbit which can still be contained within a metal plate of thickness D_z situated in a constant magnetic field H_y (Fig. 1a). We integrate the x component of the equation of motion of the electron $\dot{\mathbf{p}} = (e/c)[\mathbf{v} \times \mathbf{H}]$ with respect to time, over the limits of half a period of revolution:

$$\int_0^{T/2} \dot{p}_x dt = -\frac{e}{c} H_y \int_0^{T/2} v_z dt.$$

We take $p_x = -p_{-x}$ (Fig. 1b), since the Fermi surface has central symmetry. As a result we find

$$|p_x| = H_y D_z e/2c. \qquad (1)$$

This formula gives the extremal value of the momentum component p_x of electrons belonging to a certain section of the Fermi surface, if it is known for what field H_y the diameter of their orbits becomes equal to D_z. The latter condition can be determined by observing cyclotron resonance on the electrons of the given group. If resonances of order 1 to n (at field H_n) are observed, but the n + 1 order resonance, which can be seen for a thicker plate, is missing for a given plate, then $H_n > H_y > H_{n+1}$ and the value of H_y can be determined with higher relative accuracy the higher the order n, i.e. the thicker the plate.

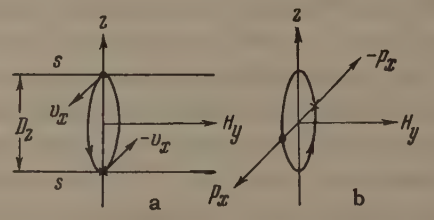

FIG. 1. The trajectory of an electron in spatial coordinates (a) and in momentum coordinates (b). Corresponding points of the trajectory are indicated by the same symbols. s is the intersection of the surfaces of the metal plate with the plane of the drawing.

For reduction of experimental data, it is convenient to express p_x in terms of n, using the formula for the field H_y at cyclotron resonance:[1]

$$H_n = m^*\omega c/ne, \qquad (2)$$

where m* is the effective mass of the electrons and ω the frequency of the high-frequency measuring field. Substituting H_n into (1) in place of H_y, we obtain

$$p_x = m^*\omega D_z/2n. \qquad (3)$$

We should regard n as the magnitude of the measuring field H_y^{-1} at which "cutting-off" of the electron orbits takes place, not necessarily having an integer value, as distinct from the meaning of n in (2).

The considerations presented indicate the means

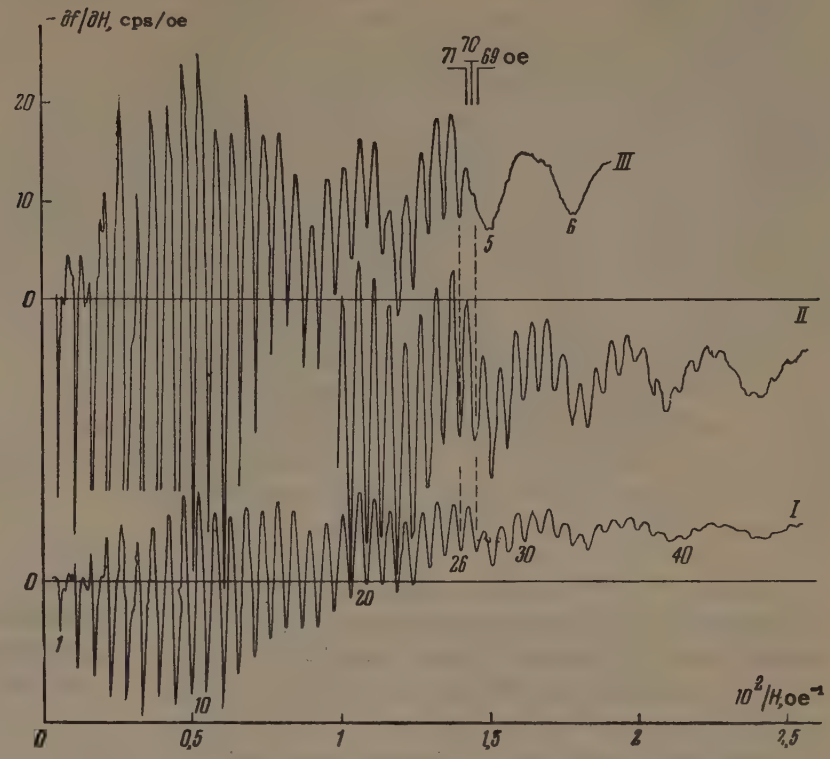

FIG. 2. Trace of cyclotron resonances on tin single crystals of thickness 2 mm (curves I and II) and of thickness 0.982 mm (curve III). It can be seen that in curve III resonances of order 27 and higher are missing. The orders of the resonances are shown under curves I and III; the traces of some deep resonances on curve III are cut off.

of a direct experimental measurement of the Fermi momentum of electrons in a metal.*

EXPERIMENT

The experimental investigations were carried out by the frequency modulation method[7] on single crystals of extremely pure tin, characterized by the resistance ratio $\rho_{20°C}/\rho_{3.75°K} = 1.4 \times 10^5$ (specimen No. 6 of[8]); at 3.75°K the electron mean free path is ~1 mm. The single crystals were in the form of 18 mm diameter disks of different thickness and were grown from the melt in demountable polished quartz molds; their natural surfaces received no further treatment. The plane surfaces of the disks had the (010) orientation; the disks were placed in a strip resonator[7] so that the high-frequency currents flowed in the [100] direction.

The results of experiments at a temperature of 3.75°K with the constant magnetic field directed along the [001] axis are shown in Fig. 2, which records the derivative of the frequency of the measuring oscillator with respect to the field; this quantity is proportional to the logarithmic derivative of the reactive part of the surface impedance of the specimen with respect to the field.[7] Curve I was obtained with a 2 mm thick specimen, curve II is a repeat trace of part of curve I with greater amplification. The minima of the curves are the cyclotron resonances; their order numbers are shown under curve I. The effective mass of the investigated group of electrons, belonging to the section of the Fermi surface by the (001) plane, was calculated from the period of the resonances and found to be $m^*_{(001)} = (0.558 \pm 0.005)\, m_e$. Resonances of longer period are also clearly visible, corresponding to a mass $m^* = 0.101\, m_e$ (detailed measurements of the effective masses of electrons in tin are given elsewhere[4]).

Curve III was obtained with a specimen of thickness $D_z(4°K) = 0.982 \pm 0.003$ mm. In this case only 26 resonances are observed; the resonance of order $n = 27$ is already missing—this means that the diameter of the corresponding electron orbit is greater than the thickness of the specimen. For weaker fields only resonances for electrons of smaller effective mass are seen on curve III ($n = 5, 6, \ldots$). The clearly visible phenomenon of "cutting-off" the electron orbit by the surface of the metal is also observed on a specimen of thickness 0.4 mm in the region of the most intense resonances ($n = 10$—11).

The value of n_0 corresponding to the magnetic field strength at which the electron orbit cut-off takes place can be determined from curve III in the following way. The resonance $n = 26$ is clearly visible; the next maximum of the curve, corre-

*Analogous measurements on semiconductors should evidently also be possible in principle. However, in that case, in view of the existence of only first order resonance, one would have to determine the conditions for "cutting-off" the orbits both by changing the constant magnetic field and the frequency of the measuring field, which greatly complicates the experiment.

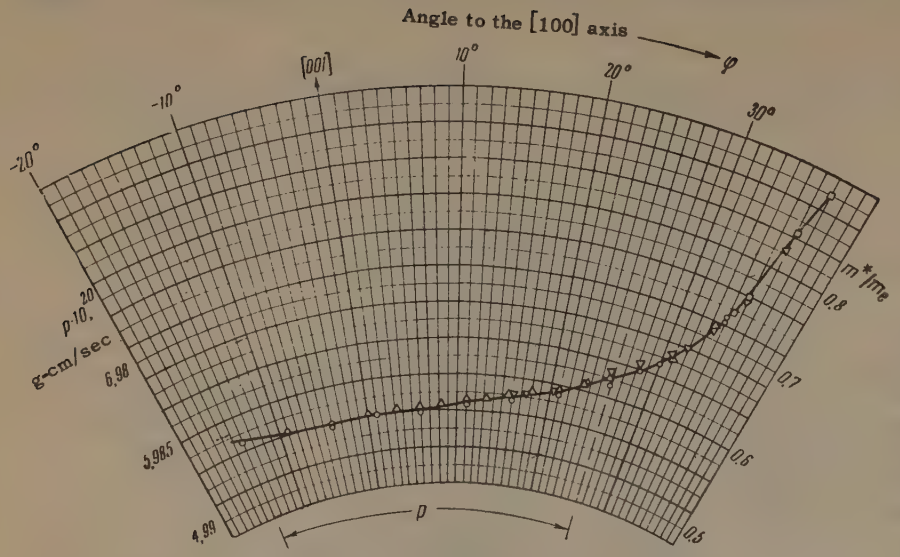

FIG. 3. The dependence of the electron momentum p [Eq. (4)] and of the effective mass m^*/m_e [Eq. (2)] on the direction φ in a tin crystal. The angle φ represents: 1) the direction of the vector p relative to the [100] axis in the (010) plane within the limits 0–26°; 2) the direction of the normal to the section, giving the mass m^*/m_e, relative to the [001] axis in the (010) plane. Different symbols refer to different experiments.

sponding to n = 26.5, is also observed. Resonance 27 is missing - its position is marked by the dashed line (the magnetic field strength is shown above curve III for convenience). We can thus take $n_0 = 26.75 \pm 0.25$. Substituting n_0 into (3), with $\omega = 5.967 \times 10^{10}$ cps, we find the momentum of the electrons belonging to the point on the section of the Fermi surface by the (001) plane determined by the [100] direction:

$$p_{[100]} = (5{,}57 \pm 0{,}15) \cdot 10^{-20} \text{ g-cm/sec}. \quad (4)$$

We can also calculate the mean Fermi velocity of the electrons belonging to the (001) section from the experimental data given:

$$v_{(001)} = \omega D_z / 2n = (1.10 \pm 0{,}01) \cdot 10^8 \text{ cm/sec}. \quad (5)$$

If the curvature of the Fermi surface changes little on circuiting along this section (which is evidently the case, as will be explained below), then the value of the electron velocity at each point of the surface must differ little from the mean value found.

The crystallographic orientation of the studied section of the Fermi surface is determined by the direction of the constant magnetic field. The dependence of the effective mass [4,5] and momentum of the electrons on direction can be obtained by carrying out experiments with rotation of the field at different angles from the [001] axis in the (010) plane of the specimen. The results of such experiments are shown in Fig. 3. The accuracy in measuring the absolute values of the masses is about ±1% and of the momentum ±2.5%; the accuracy in measuring their relative variations in one experiment on rotating the field is several times better.

It turned out that the cutting-off of the electron orbits studied in these experiments took place at a value of n_0 that remained constant, within the accuracy of measurement, over the ±26° rotation of the field. According to (3) this indicates that for electrons of the given group the momentum is proportional to the effective mass:

$$p = (9{,}98 \pm 0{,}15) \cdot 10^{-20} m^*/m_e \text{ g-cm/sec}. \quad (6)$$

For larger angles of field rotation, resonances of sufficiently high order for observing cut-off are no longer obtained, but measurements of the effective mass can be carried out up to ~37°.

DISCUSSION

Part of the section of the Fermi surface by the (010) plane and by the (100) plane equivalent to it can be constructed from the obtained dependence of electron momentum on the direction. The section of the first Brillouin zone for tin is given in Fig. 4; the lengths of the segments are shown in units of $2\pi/a$, where a = 5.796 A at 4°K (a/c = 1.8470). The experimental points represent the values of the wave vector in units of $2\pi/a$, calculated from the measured momentum values (Fig. 3). The full line shows the part of the section of the Fermi surface constructed from the experimental points and supplemented from symmetry considerations. The continuation of this section, shown by the dashed line (the angles have been smoothed out arbitrarily), takes account qualitatively of the increase in the electron effective mass with rotation of the field. It lies within 37° to the [100] axis, beyond which cyclotron resonance and, consequently, closed electron orbits cease to be observed in this section.

A comparison of these data with the results of a study of the Fermi surface of tin by the de Haas-van Alphen effect [9] leads to the following conclusions.

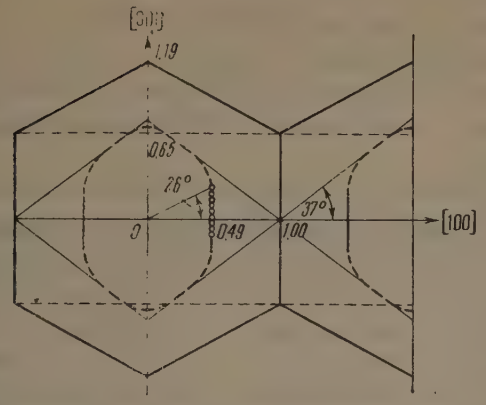

FIG. 4. Sections of the Fermi surface constructed from the experimental results. The hexagon shown by the thick line represents the section of the first Brillouin zone by the (010) plane.

The section of the Fermi surface found pertains evidently to the open hole surface of the fourth zone,[9] represented in Fig. 5. With the magnetic field parallel to the [001] axis, the electrons describe the orbit ζ; Gold and Priestley[9] estimated the corresponding effective mass from the temperature dependence of the de Haas-van Alphen effect at 0.70 m_e, and calculated it by Harrison's method,[10] which gave 0.38 m_e. The value $m^* = 0.558\ m_e$ obtained by the method of cyclotron resonance is certainly more reliable.

The electrons go over to inclined orbits as the direction of the magnetic field is changed, and one of these, ζ' is shown in Fig. 5; the angle $\sim 37°$, within which cyclotron resonance is observed, practically coincides with the angle $\sim 32°$ in which the G-oscillations[9] are observed.

The diameter of the ζ orbit in the [100] direction is $1.02(2\pi/a)$, as can be seen from Fig. 4. If it is assumed that the ζ orbit is circular, its area is $0.82(2\pi/a)^2$, while the area calculated from the period of the G-oscillations is $0.93(2\pi/a)^2$. The difference between these values does not exceed the possible errors, and the shape of the ζ orbit must, evidently, be really close to a circle.

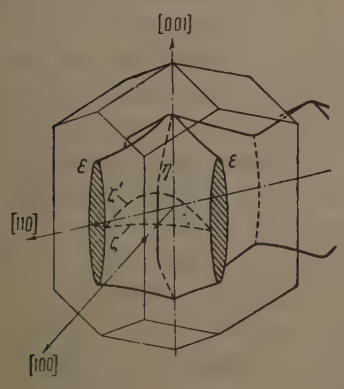

FIG. 5. The hole Fermi surface of the fourth Brillouin zone referred to the first zone of tin.[9] The section η is constructed from the results of the present work. The shaded sections ε must, evidently, be lower and considerably broader in the (001) plane.

Taking into account this fact, and also the appearance of the section of the Fermi surface, shown in Fig. 4, it can be deduced that the shape of the part of the Fermi surface on which the orbits ζ and ζ' occur (Fig. 5) is close to the surface of a right cylinder. The increase in the effective mass of the electrons on rotating the field (Fig. 3) also confirms this, indicating a decrease in curvature and an increase in the area of the electron orbits on going from ζ to ζ'. This conclusion contradicts somewhat the weak dependence of the period of the G-oscillations on field direction, noted by Gold and Priestley.[9] However, this disagreement is probably due to the low accuracy of measuring the period of the G-oscillations, as can be judged from the scatter of the experimental points in Figs. 1 and 2 of[9].

A comparison of the results of the present work with the conclusions of Alekseevskii et al[11] cannot be so detailed, since the method used there only made it possible to consider some topological features of the Fermi surface. It should be stated that there are no contradictions with the later communication of Alekseevskii and Gaĭdukov.[12]

The order of magnitude calculation of the electron momentum $p_{[100]} \approx 2 \times 10^{-20}$ g-cm/sec., made by Galkin, Kaner, and Korolyuk[13] does not differ from the results of the present work or from that which should have been expected, since the orders of magnitudes of the velocity and effective mass of the electrons are known. Comparison of numerical values is, evidently, meaningless in view of the uncertainties of the data of Galkin et al[13]. We only note that in a later work of Korolyuk[14] the momentum for the plane (100) containing the direction [010], equivalent to [100] is calculated as $p \approx 5 \times 10^{-20}$ g-cm/sec., which practically coincides with the result of the present work. Olsen[15] obtained a somewhat smaller absolute value for the electron momentum in the [100] direction, namely $(4.5 - 4.8) \times 10^{-20}$, but the form of the directional dependence of the momentum quoted by him agrees with that found here.

CONCLUSIONS

The present work is the first attempt at an experimental measurement of the momentum of electrons in a metal and a study of its Fermi surface by the new method of "cutting-off" the electron orbits in cyclotron resonance. The results obtained are evidence of the great possibilities of the method.

The only serious drawback to its wide application is the necessity of observing high order cyclotron resonances, which requires, above all, the use of single crystals of very high quality, prepared from extremely pure metals (naturally, the method of measuring the surface impedance of the specimens must also be sufficiently good).

Even when these requirements are satisfied, however, high order resonances are by no means observed for all the electron groups. But if one is content to lower the accuracy of the results, cutting-off of the cyclotron resonances of less high order can be observed on specimens of smaller thickness. In these cases the observation of the cutting-off of the orbit for cyclotron resonance in a magnetic field inclined relative to the plane of the specimen, as a function of the angle of inclination of the field, can be a useful method for the accurate measurement of the diameter of the orbit (for cyclotron resonance in the central sections of the Fermi surface).

The author is grateful to P. L. Kapitza for his interest in the work, to R. T. Mina for help with the preparation of the specimens and to G. S. Chernyshev and V. A. Yudin for technical assistance.

[1] M. Ya. Azbel' and É. A. Kaner, JETP **32**, 896 (1957), Soviet Phys. JETP **5**, 730 (1957); É. A. Kaner and M. Ya. Azbel', JETP **33**, 1461 (1957), Soviet Phys. JETP **6**, 1126 (1958).

[2] M. S. Khaĭkin, JETP **37**, 1473 (1959), Soviet Phys. JETP **10**, 1044 (1960).

[3] M. S. Khaĭkin, JETP **39**, 513 (1960), Soviet Phys. JETP **12**, 359 (1961).

[4] M. S. Khaĭkin, JETP **42**, No 1 (1962).

[5] M. S. Khaĭkin and R. T. Mina, JETP **42**, No 1 (1962).

[6] É. A. Kaner, DAN SSSR **119**, 471 (1958), Soviet Phys. Doklady **3**, 314 (1958); M. Ya. Azbel', JETP **39**, 400 (1960), Soviet Phys. JETP **12**, 283 (1961).

[7] M. S. Khaĭkin, Prib. i Tekhn. Éksper. (Instrum. and Exp. Techniques) No. 3, 95 (1961).

[8] V. B. Zernov and Yu. V. Sharvin, JETP **36**, 1038 (1959), Soviet Phys. JETP **9**, 737 (1959).

[9] A. V. Gold and M. G. Priestley, Phil. Mag. **5**, 1089 (1960).

[10] W. A. Harrison, Phys. Rev. **118**, 1190 (1960).

[11] Alekseevskii, Gaĭdukov, Lifshitz, and Peschanskii, JETP **39**, 1201 (1960), Soviet Phys. JETP **12**, 837 (1961).

[12] N. E. Alekseevskii and Yu. P. Gaĭdukov, JETP **41**, 1079 (1961); Soviet Phys. JETP **14**, 770 (1962).

[13] Galkin, Kaner and Korolyuk, JETP **39**, 1517 (1960), Soviet Phys. JETP **12**, 1055 (1961).

[14] A. P. Korolyuk, Thesis, Kharkov State University, 1961.

[15] T. Olsen, Proc. Int. Conf. on the Fermi Surface, ed. W. A. Harrison and M. B. Webb, p. 237, New York, 1960.

Translated by R. Berman
301

INVESTIGATION OF THE ALPHA RADIOACTIVITY OF NATURAL PLATINUM

K. A. PETRZHAK and M. I. YAKUNIN

Radium Institute, Academy of Sciences, U.S.S.R.

Submitted to JETP editor July 17, 1961

J. Exptl. Theoret. Phys. (U.S.S.R.) 41, 1780-1782 (December, 1961)

The α radiation of platinum of natural isotopic composition was studied with a grid ionization chamber. More precise values for the α-particle energies and half-life of the isotope Pt^{190} were obtained. A conjecture was made as to the existence of some new α lines in the spectrum.

THE α activity of natural platinum was detected for the first time by Porschen and Riezler using photographic plates,[1,2] and was ascribed to the isotope Pt^{190}. Kohman predicted the α activity of this isotope earlier.[3] A half-life T of about 10^{12} years and an α-particle energy $E = 3.3 \pm 0.2$ Mev were found for Pt^{190}. Macfarlane and Kohman,[4] studying platinum enriched in Pt^{190} as well as natural platinum with a large proportional counter, determined the values $T = (6.9 \pm 0.5) \times 10^{11}$ years and $E = 3.11 \pm 0.03$ Mev.

Our investigation of the α activity of platinum was carried out with a cylindrical pulse ionization chamber containing a grid as well as auxiliary equipment, which permitted α particles to be analyzed from the ionization and orientation of their tracks. Taking into account corrections for wall and end effects, the greatest chamber collecting power was $2900 \times 2\pi$ cm^2-sr. The platinum used was a natural isotopic mixture containing up to 0.11% of the usual impurities, 321 ± 5 mg being deposited on the effective surface of the chamber cathode by cathode sputtering. A layer of samarium up to 1 μg/cm^2 thick covering the platinum, as well as natural uranium, periodically employed, served as reference sources. All the equipment was calibrated and monitored by a generator of pulses of precise height.

When analyzing the α spectra (to be more accurate, the pulse-height distributions), calculated corrections were introduced for the shifting of the peaks. The largest corrections were those associated with energy loss by the α particles in the platinum layer (25—27 kev) and with the effect due to the positive ions (~3 kev for samarium; 4—7 kev for platinum, within the limits of the chosen energy interval; 15 and 22 kev for U^{238} and U^{234} respectively). The remaining corrections, including those associated with electron collection time and the effect of recoil nuclei, were smaller.

The pulse heights were compared with the energies of α particles from the reference sources, taking into account the corrections mentioned above and also the unresolved fine-structure components in the α-particle spectra of the uranium isotopes. The pulse height turned out to be proportional to the energy of the α particles. According to the empirical formula we derived for the α-particle energies ($E = 0.226V + \Delta$, where E is the α-particle energy in Mev, V is the pulse height in relative units, and Δ is the total calculated correction in Mev), the Sm^{147} α particles had an energy of 2.225 Mev, which is close to the recently obtained value of 2.223 + 0.002 Mev,[4] and the main groups of U^{238}, U^{235} and U^{234} α particles had energies of 4.19, 4.39, and 4.77 Mev respectively, that is, close to the known values. This shows the applicability of the given formula to our energy evaluations, and indicates that the ionization is proportional to α-particle energies when α particles with such energies are slowed down in argon containing 5% methane (the gas mixture used in the chamber).

The α spectra obtained by us are presented in the figure. The main peak in the right-hand section, which corresponds to Pt^{190}, yielded an α-particle energy of 3.17 ± 0.02 Mev and a half-life of $(4.7 \pm 1.7) \times 10^{11}$ years. The errors here are somewhat higher than the calculated errors: for the first value because of the indeterminacy of data on the energy of Sm^{147} α particles, and for the second because of the complexity of the spectra obtained. Certain peaks observed in the spectrum could not have resulted from background fluctuations or interference, since the pulses coming from both anode and cathode were analyzed jointly. The possibility is not excluded that certain of these peaks are related to Pt^{190}, but it is impossible to make definite assumptions. We can only note that the α particle groups detected are in no way con-

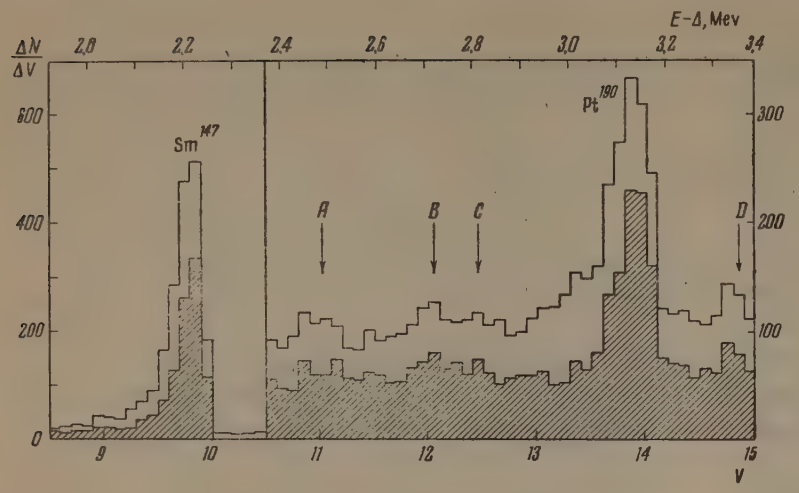

Pulse-height distribution of α particles emitted from the layer of platinum (321 mg/2900 cm^2) and samarium (~1.8 mg/1900 cm^2) within a solid angle of 2π (outside contour) and 1.1π (crosshatched area). The right-hand section was obtained during 126 hours of observation, the left-hand during 4.6 hours; V is the pulse height.

nected with the well-known energy levels of the Os^{186} nucleus (137 and 764 kev). It is possible to relate group A (corresponding to an energy of ~2.50 Mev) or a part of this group to the probability of detecting α particles from Sm^{146}; the value E = 2.55 ± 0.05 Mev is known[5] from this isotope artificially obtained). Group B (E = 2.75 Mev) and the apparently associated weak group C (E ≈ 2.85 Mev) are observed, but poor statistics and the relatively large background prevent the confirmation of their presence here. We are inclined to assign group B to the isotope Pt^{192}, for which only the lower limit of the half-life, or 10^{14} years, is estimated. We note that Porschen and Riezler,[2] who observed several tracks on photographic plates corresponding to α particles with an energy of ~2.6 Mev, attributed them to Pt^{192}. Macfarlane and Kohman[4] could not detect Pt^{192} α particles, since there was low resolution (width at half maximum of ~0.5 Mev) in the spectrum from the natural platinum. In the present study the resolution in the platinum spectrum was ~80—90 kev. Additional research is necessary to clarify the nature of group D (E ~ 3.40 Mev).

[1] W. Porschen and W. Riezler, Z. Naturforsch. **9a**, 701 (1954).

[2] W. Porschen and W. Riezler, Z. Naturforsch. **11a**, 143 (1956).

[3] T. P. Kohman, Phys. Rev. **73**, 16 (1948).

[4] R. B. Macfarlane and T. P. Kohman, Phys. Rev. **121**, 1758 (1961).

[5] D. C. Dunlavey and G. T. Seaborg, Phys. Rev. **92**, 206 (1953).

Translated by Mrs. J. D. Ullman
302

DETERMINATION OF THE SIGN OF THE LOCAL MAGNETIC FIELD AT GOLD NUCLEI DISSOLVED IN IRON AND NICKEL

B. N. SAMOĬLOV, V. V. SKLYAREVSKII, and V. D. GOROBCHENKO

Submitted to JETP editor July 17, 1961

J. Exptl. Theoret. Phys. (U.S.S.R.) 41, 1783-1786 (December, 1961)

The sign of the local magnetic field at the gold nucleus has been determined by measuring the asymmetry of the β radiation from Au^{198} polarized in dilute solutions of gold in iron and nickel. The most probable values for the fields are $H_n = -1.0 \times 10^6$ oe in iron and $H_n = -1.8 \times 10^5$ oe in nickel.

MEASUREMENTS have been made of the asymmetry of the β radiation from Au^{198} nuclei, polarized in dilute solutions of gold in iron and nickel, in order to determine the sign of the local magnetic field at the dissolved gold nuclei. The study of the anisotropy of the γ radiation of Au^{198}, oriented in an Fe-Au alloy, could give only[1] the absolute value of the local field H_n, since the angular distribution of the γ radiation from oriented nuclei depends only on even powers of the product $\mu_n H_n$ (where μ_n is the magnetic moment of the nucleus). The direction can be found from measurements of the asymmetry of the β radiation from oriented nuclei.[2]

The angular distribution of the β electrons emitted by oriented nuclei can be written in the form

$$N(\theta) = S_n\left[1 + \sum_k (f_k/f_{km})\, B_k P_k(\cos\theta)\right], \qquad (1)$$

where S_n is a factor determined by the spectrum shape for an n-th forbidden β transition; the f_k are parameters describing the degree of orientation of the nuclei, and f_{km} their maximum possible values; the B_k are parameters which contain the dependence of the β ray distribution on the nuclear matrix elements, and $P_k(\cos\theta)$ are Legendre polynomials.

The overwhelming majority of Au^{198} nuclei decay according to the scheme $2^-(\beta)2^+$, which corresponds to a first-forbidden β transition. The electron spectrum has an end point $W_0 = 2.9\ mc^2$ (where m is the electron mass and c is the velocity of light) and has an allowed shape. In the case of a first-forbidden transition, the summation in (1) goes over k = 1, 2, 3; i.e., the electron angular distribution is determined by the orientation parameters f_1, f_2 and f_3. At not too low temperatures, f_3 is negligibly small and the term with k = 3 can be dropped. Using the approximate expressions for B_1 and B_2, which were found by M. Morita and R. Morita[3] for the case of $\alpha Z/2\rho \gg W_0$ and $(\alpha Z)^2 \ll 1$,* (where ρ is the nuclear radius in units of the Compton wavelength $\hbar/mc$, and α is the fine structure constant), and also making use of the fact that the electron spectrum has an allowed shape, one can show that the approximate expression

$$N(\theta) \approx S_1\left[1 - \frac{1/3 + 2\sqrt{2/3}\,\lambda/\mu}{1 + (\lambda/\mu)^2}\,\frac{p}{W}\,\frac{f_1}{f_{1m}}\,P_1(\cos\theta)\right] \qquad (2)$$

gives the angular distribution correctly. Here $p = \sqrt{W^2 - 1}$ is the momentum of the electron, and λ and μ are parameters which are linear combinations of the nuclear matrix elements, in the notation of M. and R. Morita.

The asymmetry of the β radiation can be characterized by the value of the quantity

$$\varepsilon_\beta = [N(0) - N(\pi)]/N_0, \qquad (3)$$

where $N(\theta)$ is the β counting rate at an angle θ relative to the direction of the magnetizing field on the sample, and N_0 is the isotropic counting rate in the absence of orientation. Substituting the values of $N(0)$ and $N(\pi)$ from (2) into (3) and using the approximate equation $f_1/f_{1m} \approx \mu_n H_n/2kT$, we find for ϵ_β the expression

$$\varepsilon_\beta \approx -\frac{1/3 + 2\sqrt{2/3}\,\lambda/\mu}{1 + (\lambda/\mu)^2}\,\frac{p}{W}\,\frac{\mu_n H_n}{k}\,\frac{1}{T}. \qquad (4)$$

This expression was used for determining the intensity of the local magnetic field H_n, since all the other parameters appearing on the right side of the equation are determined independently. The

*The latter inequality is satisfied only approximately, but this does not affect the form of (2) and manifests itself only in the definition of the parameters λ and μ in terms of the matrix elements.

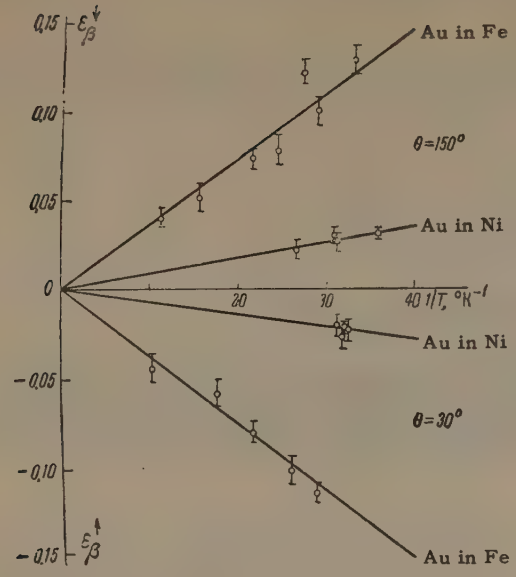

FIG. 1. Temperature dependence of asymmetry of β radiation from Au^{198} dissolved in iron and in nickel; $\varepsilon_\beta^\uparrow = [N(30°) - N_0]/N_0$; $\varepsilon_\beta^\downarrow = [N(150°) - N_0]/N_0$, $\varepsilon_\beta = \varepsilon_\beta^\uparrow - \varepsilon_\beta^\downarrow$.

ratio λ/μ can be found from the results of Steffen,[4] who studied the β-γ angular correlation. The average value of $\overline{p/W}$ over the portion of the electron spectrum recorded by us was taken to be 0.78; and the nuclear moment was set at μ_n = +0.5 n.m. No direct measurements of the sign of the magnetic moment of Au^{198} have been made, but according to the shell model it is very probably positive. The values of ϵ_β and 1/T were determined separately in the experiments.

The apparatus and experimental method were the same as in our previous work.[2] The samples contained ~0.3 w % of gold for the iron alloy ~1 w % for the nickel alloy. After activation with thermal neutrons the samples were annealed for 2—3 hours at ~1000°C. Figure 1 shows the results of several series of experiments with the Fe-Au alloy and of one series with Ni-Au. Each point was determined from the change in intensity of the β radiation when the sample was artificially heated to the temperature of the helium bath. We see that the points lie well on a straight line, which corresponds to a dependence of ϵ_β only on 1/T, i.e., only on f_1. After making corrections for the fact that the direction of polarization and the direction of the β radiation which is recorded are not the same, and for the fraction of scattered electrons in the recorded radiation* (this was done in supplementary experiments), we found from the slopes of the lines the following values for ϵ_β:

*Corrections were made only for back-scattering of electrons from the material of the cold pipe. No corrections were made for electrons scattered from the walls of the apparatus.

$$\varepsilon_\beta = -(8.9 \pm 0.3) \cdot 10^{-3} T^{-1}$$

for gold dissolved in iron, and

$$\varepsilon_\beta = -(1.6 \pm 0.1) \cdot 10^{-3} T^{-1}$$

for gold in nickel.

Substituting these values in (4), we can find the dependence of the local field on the parameter λ/μ. For gold in iron,

$$H_n = (6.2 \pm 0.2) \frac{1 + (\lambda/\mu)^2}{1/3 + 2\sqrt{2/3}\lambda/\mu} \cdot 10^5 \text{ oe};$$

for gold in nickel

$$H_n = (1.1 \pm 0.07) \frac{1 + (\lambda/\mu)^2}{1/3 + 2\sqrt{2/3}\lambda/\mu} \cdot 10^5 \text{ oe}.$$

The dependence is shown graphically in Fig. 2.

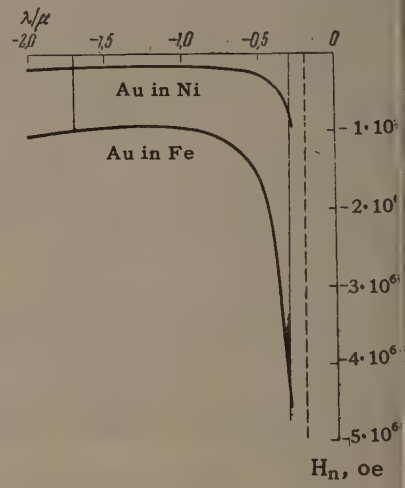

FIG. 2. Dependence on the parameter λ/μ of the local magnetic field at gold nuclei dissolved in iron and nickel. The most probable value is $\lambda/\mu = -1$.

From Steffen's work we can get only the approximate value $\lambda/\mu = -1 \pm 0.7$. But as we see from the curve, despite the large uncertainty in the determination of λ/μ, the local field intensity in iron is apparently close to the value $H_n \approx -1.0 \times 10^6$ oe, which agrees in absolute value with our previous results.[1] The local field in nickel is 5.6 times smaller and is equal to $H_n \approx -1.8 \times 10^5$ oe.* Thus in both iron and nickel the direction of the local field at the gold nuclei is opposite to the domain field.

At present only one mechanism has been proposed which leads to a negative sign for the local magnetic field. This is the contact field of the electrons of the inner s shells. This mechanism assumes that there is a partial polarization of the

*The degree of quadrupolarization of the gold nuclei is approximately 30 times smaller in nickel than in iron. This may explain the negative result of the attempt to detect the field at the nuclei of gold in nickel from the anisotropy of the γ radiation.[5] Probably insufficient sensitivity is the reason why Roberts et al. give a zero value for the field at gold nuclei in nickel, as found by them from an investigation of the Mössbauer effect.[6]

inner shells by the exchange and dipole interaction with the unfilled shell of the paramagnetic ion. The assumption of such a mechanism for the origin of the local field is equivalent to assuming an uncompensated shell for the impurity atom. Also not completely excluded is the possibility of explaining the negative sign of the local field as the result of contact interaction with the polarized conduction electrons of the alloy, assuming that their polarization has the opposite sign. However such an assumption is not in agreement with the conclusions of Kondorskii.[8]

The authors sincerely thank E. K. Zavoĭskii, L. V. Groshev, Ya. A. Smorodinskii, D. P. Grechukhin, D. F. Zaretskii, Yu. M. Kagan and L. D. Puzikov for valuable discussions, O. A. Chilashvili for help with the measurements, V. N. Agureev, N. V. Razzhivin and I. B. Filippov for help in preparing the equipment and carrying out the experiments, and also N. E. Yukovich, V. A. Drozdov and V. D. Sheffer for preparing the liquid helium.

[1] Samoĭlov, Sklyarevskii, and Stepanov, JETP **38**, 359 (1960), Soviet Phys. JETP **11**, 261 (1960).

[2] Samoĭlov, Sklyarevskii, Gorobchenko, and Stepanov, JETP **40**, 1871 (1961), Soviet Phys. JETP **13**, 1314 (1961).

[3] M. Morita and R. S. Morita, Phys. Rev. **109**, 2048 (1958).

[4] R. M. Steffen, Phys. Rev. **118**, 763 (1960).

[5] Samoĭlov, Sklyarevskii and Stepanov, Proceedings VII th Conf. Low Temp. Physics, Toronto, 1960; Univ. of Toronto Press, 1961, p. 171.

[6] L. D. Roberts and J. O. Thomson, Bull. Am. Phys. Soc. **6**, 230 (1961).

[7] D. A. Goodings and V. Heine, Phys. Rev. Letters **5**, 370 (1960). A. J. Freeman and R. E. Watson, Phys. Rev. Letters **5**, 498 (1960).

[8] E. Kondorskii, JETP **40**, 381 (1961), Soviet Phys. JETP **13**, 260 (1961).

Translated by M. Hamermesh
303

INVESTIGATION OF THE $\pi^- + n \to \pi^- + n + m\pi^0$ *REACTION WITH A 2.8-Bev/c* π^- *– MESON BEAM*

Yu. D. BAYUKOV, G. A. LEKSIN, and Ya. Ya. SHALAMOV

Institute of Theoretical and Experimental Physics, Academy of Sciences, U.S.S.R.

Submitted to JETP editor July 18, 1961

J. Exptl. Theoret. Phys. (U.S.S.R.) 41, 1787-1792 (December, 1961)

Production of mesons in the reaction $\pi^- + n \to \pi^- + n + m\pi^0$ is investigated with a freon bubble chamber. The momentum of the incident meson is 2.8 Bev/c. The results obtained are compared with the statistical theory and the peripheral interaction model.

At present there is very little information about the reaction

$$\pi^- + n \to \pi^- + n + m\pi^0, \qquad m = 1, 2, \qquad (1)$$

and about the isotopically symmetrical reaction

$$\pi^+ + p \to \pi^+ + p + m\pi^0.$$

A study of these reactions supplements the information on inelastic interaction between pions and nucleons at high energies, and in particular on the applicability of the statistical theory and also the model of peripheral collision between the incoming meson and a meson in the "jacket" of the nucleon.

1. EXPERIMENTAL PROCEDURE

To obtain data on reaction (1), we examined stereo photographs obtained with a 17-liter freon bubble chamber [1] 50 cm long. The π^--meson beam had a momentum 2.8 ± 0.3 Bev/c. The bubble chamber operated without a magnetic field. The main feature that made this procedure feasible was the relatively high efficiency of registering the γ quanta produced in the decay of the π^0 mesons.

In scanning the stereo photographs we selected the single-prong stars accompanied by electron-positron conversion pairs, directed towards the interaction point. It was assumed that the chosen single-prong stars are produced via reaction (1) when the incoming mesons interact with the quasi-free neutrons of the nuclei contained in the freon. Since the screening coefficient of the nucleon in the nucleus is not known for reaction (1), no absolute cross sections were determined.

Altogether 221 events were registered. In addition, we registered two single-prong stars in which the conversion pairs were accompanied by "forks" of two pions, produced in K^0 meson decay. The efficiency of registering reactions with production of neutral strange particles has been estimated previously [2] to be ~0.4. Consequently the contribution of such reactions to the investigated process can be estimated at $\lesssim 3\%$ and is disregarded.

2. ANGULAR DISTRIBUTIONS OF γ QUANTA AND π^- MESONS

The angular distribution of the registered γ quanta accompanying the single-prong stars is shown by the dashed line of Fig. 1. The abscissas are the cosines of the angle of emission of the γ quantum in the c.m.s. of the incoming meson and nucleon, while the ordinates are the numbers of the γ quanta. The circles denote the angular distribution of the γ quanta with account of the γ

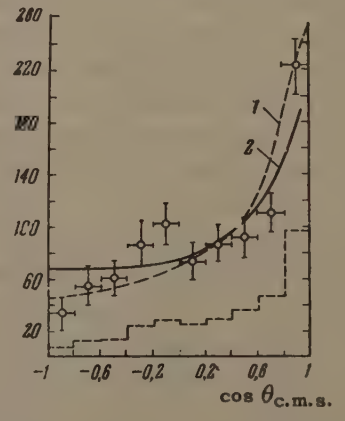

FIG. 1. Angular distribution of γ quanta in the c.m.s. of the incoming meson and nucleon. Dashed histogram—distribution of registered γ quanta without account of efficiency. The circles represent the same distribution with account of the γ counting efficiency in the chamber. Curves 1 and 2—calculated angular distributions assuming 50% (curve 1) and 30% (curve 2) contribution from peripheral collisions.

counting efficiency for the chamber. The errors are statistical.

The counting efficiency ε was determined for each γ quantum producing a pair directed towards the single-prong star. For this purpose we measured the distance L along the direction of γ-quantum motion from the point of interaction to the boundaries of that region of the chamber, where the conversion pair, if produced, would be registered in the scanning. The counting efficiency of a γ quantum leaving a given point in a given direction is $\varepsilon = 1 - \exp(-L/L_k)$, where $L_k = 30$ cm is the known conversion length for the freon mixture in the bubble chamber.

As can be seen from Fig. 1, the angular distribution of the γ quanta in the πN c.m.s. is anisotropic and asymmetrical. The ratio of the number of γ quanta emitted forward and backward in the πN c.m.s. is 1.76 ± 0.30. It is possible that this ratio is underestimated compared with the data for the free nucleon, since it is known that the γ-quantum angular distribution for all the stars (including those accompanied by development of a nuclear cascade) is relatively large in γ quanta emitted backward.

Figure 2 shows the angular distribution of the π^- mesons in the laboratory system (l.s.). The same figure shows for comparison the angular distribution of the γ quanta in the l.s. Both distributions are normalized to the same area. It is seen that within the limits of statistical errors the angular distributions of the γ quanta and of the π^- mesons are the same. Figure 3 shows the angular distribution of the π^- mesons for two groups of mesons: with momentum > 300 Mev/c (solid curve) and with momentum < 300 Mev/c (dashed curve). The choice of 300 Mev/c is based on the experimental feasibility of determining the momentum in the chamber. The momenta of the π^- mesons were estimated from the ionization, multiple scattering, and also from the range if the π^- meson stopped in the chamber. The abscissas in Fig. 3 are the cosines of the l.s. π^--meson emission angle. The two distributions are likewise normalized to the same area. The experimental data indicate that the anisotropy increases with increasing π^--meson energy.

The angular distributions of the γ quanta in the πN c.m.s., as affected by the l.s. π^--meson emission angle, π^- meson momentum, and the number of counted γ quanta all agree, within the limits of statistical errors. A tendency can be observed, however, towards increasing anistropy in the γ-quantum distribution with decreasing number of γ quanta directed towards the point of interaction (Fig. 4). Thus, the anisotropy for γ quanta from

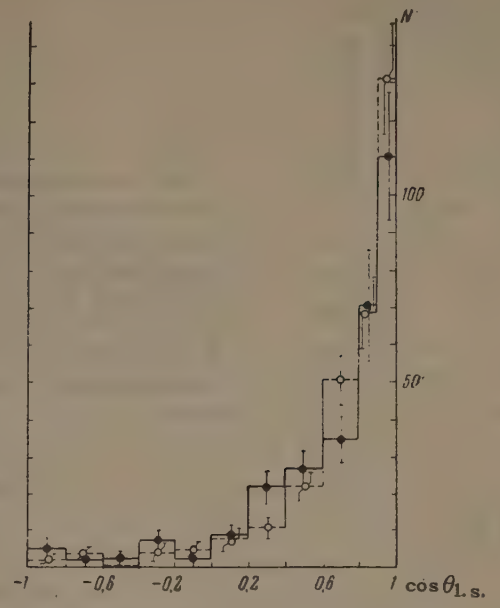

FIG. 2. Angular distributions of γ quanta and π^- mesons in the l.s., normalized to equal area. Solid curves – π^- mesons, dashed curves – γ quanta.

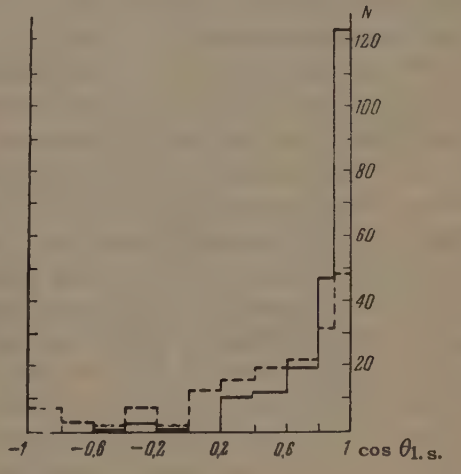

FIG. 3. Angular distributions of π^- mesons in the l.s. as affected by the π^--meson momentum p_{π^-}; solid curves – p_{π^-} > 300 Mev/c, dashed – p_{π^-} < 300 Mev/c.

stars with a single registered γ quantum (histogram 1 of Fig. 4) is 1.7 ± 0.4, that for two registered γ quanta (histogram 2 of Fig. 4) is 1.7 ± 0.5, while that for three to five γ quanta (histogram 3, Fig. 4) is 1.5 ± 0.7.

We can also note that the anisotropy of the angular distribution of γ quanta from stars with π^--meson emission angle > 41° in the l.s. (1.85 ± 0.47) exceeds that for < 41° in the l.s. (1.68 ± 0.39).

3. MULTIPLICITY OF π^0-MESON PRODUCTION

Table I lists the distribution of the single-prong stars relative to the number of electron-positron conversion pairs directed towards the point of in-

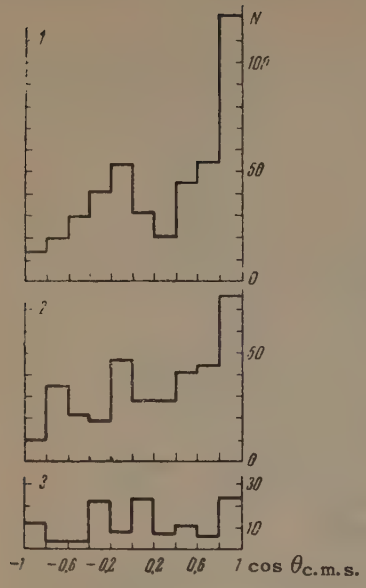

FIG. 4. Angular distributions of γ quanta in the πN c.m.s. as affected by the number of registered γ quanta emitted from stars: 1 – stars with single γ quantum; 2 – stars with two γ quanta; 3 – stars with 3, 4, and 5 γ quanta.

teraction, and also as a function of the l.s. π^--meson emission angle. In Table I, and further in the text, N_1—number of single-prong stars with one registered electron-positron conversion pair directed towards the point of interaction, N_2—the same with two pairs, etc, N_0—the total number of single-prong stars with pairs, and N—total number of registered conversion pairs. The last line of Table I lists the values of N_1—N_5, N_0, and N for all π^--meson emission angles. The values obtained are determined by the multiplicity of π^0-meson production in reaction (1) and by the average conversion γ counting efficiency in the chamber.

The average γ counting efficiency was calculated from the formula

$$\bar{\varepsilon} = \left(\bar{n}/\sum_k \varepsilon_k^{-1}\right)^{-1},$$

where n—number of registered electron-positron pairs. It was shown that within the limits of statistical errors the average γ counting efficiency does not vary with the π^--meson emission angle. Nor do changes occur in the counting efficiency of γ quanta accompanying single-prong stars with 1, 2, etc. counted conversion γ quanta, i.e., the counting efficiency can be assumed constant for all the single-prong stars. We can therefore calculate the average counting efficiency of the γ quanta produced in reaction (1) for the entire chamber, independently of the π^--meson emission angle. The value obtained was 0.34 ± 0.02.

Starting from this value and the values of N_4 and N_5, and also from the fact that not a single event was registered with six electron-positron pairs, we can estimate the contribution of the cases with production of three π^0 mesons. The relative contribution to reaction (1) from processes involving the production of one and two π^0 mesons can be based on the ratios N_1/N_0, N_2/N_0, N_3/N_0, N/N_0. Knowing the contribution of the reactions with m = 1, 2, 3, we can readily determine the average multiplicity of π^0-meson production, which was found to be 1.47 ± 0.15. The error includes here the uncertainties in the contributions of the channels of reaction (1) with different m (see the last line of Table II).

Figure 5 shows the dependence of the average multiplicity (ordinates) on the π^--meson emission angle (abscissas), calculated by the method indi-

Table I

π^- meson emission angles	Number of registered single-prong stars						Total number of pairs, N
	N_1	N_2	N_3	N_4	N_5	N_0	
0— 15°	31	14	1	—	—	46	62
15— 30°	33	15	1	1	—	50	70
30— 60°	43	21	3	1	—	68	98
60— 90°	25	10	3	—	1	39	59
90—180°	10	6	1	1	—	18	29
0—180°	142	66	9	3	1	221	318

Table II. Multiplicity of π^0 Production in the Reaction $n + \pi^- \rightarrow n + \pi^- + m\pi^0$ for $E_{\pi^-} = 2.8$ Bev

	Percentage of cases with different m			Average multiplicity, $\bar{m}$
	$m=1$	$m=2$	$m=3$	
Statistical theory with account of the isobar (data of[3])	55	37	8	1.53
Experimental data	~63±5	~27±5	~10±5	1.47±0.15

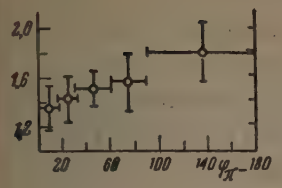

FIG. 5. Dependence of multiplicity of π^0-meson production on the l.s. π^--meson emission angle.

cated above for five angle ranges. There is a tendency for the multiplicity to increase with increasing π^--meson emission angle. The multiplicity of production of π^0 mesons in reaction (1) depends only on the π^-meson momentum, being 1.33 ± 0.15 for a meson with momentum > 300 Mev/c and 1.71 ± 0.12 when the momentum is < 300 Mev/c. The errors are statistical.

4. DISCUSSION OF THE RESULTS

Table II shows comparisons of the average multiplicity and of the percentage ratio of different channels of reactions (1) with the statistical theory. The calculation was made by Maksimenko[3] using statistical theory with the isobar taken into account. The agreement between calculation and experiment is satisfactory. However, the statistical theory cannot explain the noted dependence of the multiplicity on the π^--meson emission angle and on the momentum, nor the observed angular distributions of the γ quanta and π^- mesons.

We note that the γ-quantum angular distributions given in Figs. 1, 2, and 4 coincide with the angular distributions of the π^0 mesons from reaction (1) if the π^0-meson spectrum is sufficiently hard, as is apparently the case of 2.8-Bev π^- mesons. At any rate, the angular distribution of the π^0 mesons is not broader than the given γ-quantum distributions.

The observed anisotropy in the angular distribution of the neutral and charged mesons in the πN c.m.s. can be explained by assuming, as is frequently done in the literature, the existence of peripheral $\pi\pi$ collisions along with the central πN collisions. If at the same time the angular distribution of the π mesons produced by the central collision is assumed to be isotropic in the πN c.m.s. (in accord with the statistical theory), and the distribution of the π mesons from the peripheral collisions is assumed to be isotropic in the $\pi\pi$ c.m.s., then the fraction of peripheral collisions is determined by the results obtained. To reconcile an anisotropy value 1.76 ± 0.30 we must assume $\gtrsim 30\%$ peripheral collisions (curve 2 of Fig. 1). The angular distribution of the γ quanta is in good agreement with the assumed 50% contribution of the peripheral collisions (curve 1 of Fig. 1). It is easy to understand why the concept of an interaction between the incoming meson and the weakly bound meson in the "jacket" of the nucleon explains qualitatively the similarity in the angular distributions of the π^0 and π^- mesons (Fig. 2) and the dependence of the multiplicity on the π^--meson emission angle (Fig. 5).

The results of the present investigation do not contradict the assumed validity of the statistical theory (with account of the isobar, and possibly with account of the π-meson interaction in the final state) when a large number of mesons (> 2 or 3) is produced. The angular distribution of the π^0 mesons apparently becomes more isotropic with increasing multiplicity (Fig. 4).

These conclusions are in good qualitative agreement with those reached in investigations of the production of > 1-Bev mesons in πN interactions other than the reaction (1). Thus, to explain the angular distribution of charged pions produced in π^-p collisions at 4.5 Bev, Walker[4] considered first direct knock-out of pions from the nucleon. His data indicate an isotropic pion distribution in the pion c.m.s. From the value ~7 mb, given by Walker[4] for the cross section of inelastic πN collision via the $\pi\pi$ channel, we can estimate the fraction of the peripheral collisions to be about 30%. The notion of central and peripheral collisions was developed by V. S. Barashenkov many times. In his work[5], based on the data of Belyakov et al[6] concerning the production of charged 7-Bev mesons in emulsion, Barashenkov estimates the fraction of the peripheral collisions to be 50—60%. Grote et al[7], in an investigation quite similar to[6], deduced the presence of $\pi\pi$ interaction from an analysis of the target mass.[8] The contribution of peripheral collisions to scattering is also proposed by Shalamov and Shebanov[9] to explain the angular distribution of π^0 mesons produced in the reaction $\pi^- + p \rightarrow n + m\pi^0$ at 2.8 Bev.

The foregoing investigations and many other experiments[10,11] indicate that the statistical theory is applicable to an evaluation of the mean multiplicity of production of mesons and of the angular and momentum distributions of the secondary particles in processes having large multiplicity.

In conclusion, we are grateful to Yu. S. Krestnikov and V. A. Shabanov for supplying the films, N. S. Khropov, M. U. Khodakova, V. A. Krutilina, Z. I. Pal'mina, and Yu. S. Petrykin for help in the measurements, and also N. G. Birger for numerous discussions.

[1] Blinov, Lomanov, Meshkovskii, Shalamov, and Shebanov, PTÉ (Instrum. and Meas. Techn.) No 1, 35 (1958).

[2] Bayukov, Leksin, and Shalamov, JETP **41**, 1025 (1961), Soviet Phys. JETP **14**, 728 (1962).

[3] V. M. Maksimenko, Dissertation, Phys. Inst. Acad. Sci, 1960.

[4] W. D. Walker, Phys. Rev. **108**, 852 (1957).

[5] V. S. Barashenkov, Preprint, Joint. Inst. Nuc. Res. R-540, 1960.

[6] Belyakov, Wang, et al, JETP **39**, 937 (1960), Soviet Phys. JETP **12**, 650 (1961).

[7] Grote, Krecker, Kundy, Lanius, Manske, and Meier, Nucl. Phys. **24**, 300 (1960).

[8] N. G. Birger and Yu. A. Smorodin, JETP **37**, 1355 (1959), Soviet Phys. JETP **10**, 964 (1960).

[9] Ya. Ya. Shalamov, and V. A. Shebanov, JETP **39**, 1232 (1960), Soviet Phys. JETP **12**, 859 (1961).

[10] G. Maenchen and W. Fowler, et al, Phys. Rev. **108**, 850 (1957).

[11] R. C. Whitten, and M. M. Block. Phys. Rev. **111**, 1676 (1958).

Translated by J. G. Adashko
304

PHOTOPRODUCTION OF π^0 MESONS ON DEUTERIUM AT 170–210 Mev

A. S. BELOUSOV, S. V. RUSAKOV, E. I. TAMM, and L. S. TATARINSKAYA

P. N. Lebedev Physics Institute, Academy of Sciences, U.S.S.R.

Submitted to JETP editor July 20, 1961

J. Exptl. Theoret. Phys. (U.S.S.R.) 41, 1793-1803 (December, 1961)

The ratio of the π^0-meson photoproduction cross sections on deuterium and hydrogen was measured for energies in the range of 170–210 Mev. The measurements were carried out for meson emission angles of 44, 84, and 124° in the laboratory system. The experimental data are compared with the momentum approximation theory.

INTRODUCTION

A relatively large number of published experimental results [1-4] on the photoproduction of π^0 mesons on deuterium were obtained at bremsstrahlung energies > 200 Mev. Only one experiment [5] was carried out near the photoproduction threshold. However, the π^0-meson photoproduction on hydrogen at these energies has been studied rather extensively.

The energy range near the photoproduction threshold is of special interest, since the transitions into final S and P states of the meson-nucleon system are mainly involved. This greatly facilitates the interpretation of experimental results. In fact, disregarding for the time being the dependence of the corresponding transition operator T on the spin and polarization, we can write

$$T = f(E_1;\ M_1(1/2);\ M_1(3/2);\ E_2),$$

where E_1 and E_2 are the amplitudes of the electrical dipole and quadrupole transitions respectively, and $M_1(1/2)$ and $M_1(3/2)$ are the amplitudes of the magnetic dipole transitions into the state with total angular momentum of $1/2$ and $3/2$ respectively.

Baldin and Govorkov [6] have shown that the amplitudes E_2 and $M_1(1/2)$ near the photoproduction threshold can be neglected. Therefore, the main contribution to the process under consideration is due to the transition to the $3/2$–$3/2$ state and, in the energy range of interest, we have

$$T = f(E_1;\ M_1^3(3/2)).$$

The above considerations facilitate the comparison between the experimental results and the momentum approximation theory. A test of the applicability of that theory to the processes under consideration is interesting for its own sake.

Thus, we can expect that the study of the reactions

$$\gamma + d \begin{cases} \nearrow \pi^0 + d \\ \searrow \pi^0 + p + n \end{cases} \qquad \text{(I)}$$

in the energy range near the threshold and the comparison of their parameters with the known parameters of the process

$$\gamma + p \to \pi^0 + p \qquad \text{(II)}$$

will yield information on the photoproduction of π^0 mesons on the neutron.

For an analysis of the process (I), it is necessary to know the relative contribution of both reactions at various primary-photon energies, and also the angular distributions.

The simplest method of comparing the processes (I) and (II) is the measurement of the ratio of their differential cross sections under identical conditions.

APPARATUS

The experiments were made with the synchrotron of the Lebedev Physics Institute of the U.S.S.R. Academy of Sciences. A diagram of the setup is shown in Fig. 1. Liquid deuterium and hydrogen placed in a vacuum target (VGM-1) developed in the photon-meson laboratory of the Physics Institute of the Academy [7] were used in the experiments. The working volume of the target, using the chosen method of collimation, was 53 cm^3. The collimation system and the filtering magnet ensured the removal of electrons from the bremsstrahlung beam.

The method employed in the experiment, that of π^0-meson detection using one of the decay γ rays, has poor angular definition (details below), but permits us to obtain the results relatively rapidly

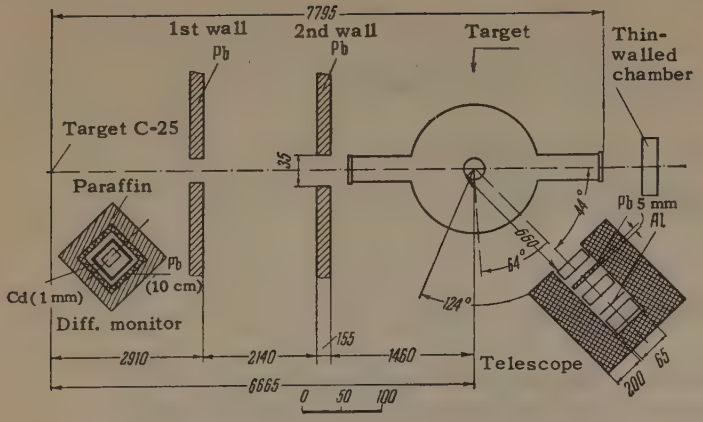

FIG. 1. Diagram of the experimental setup (geometry in the hall).

with good statistical accuracy. In experiments carried out in order to determine the most interesting range of angles and energies for further detailed investigations, such a method of π^0-meson detection is definitely acceptable. The decay γ rays were detected by a scintillation telescope consisting of three counters employing liquid scintillators and FÉU-33 photomultipliers.

The block diagram of the electronic apparatus is shown in Fig. 2. The pulses from counters 2 and 3 were fed to a fast coincidence circuit.[8] This branch of the telescope circuit forms the coincidence channel. The output pulses from counters 1 and 3 were fed to a similar coincidence circuit, and then into an anticoincidence circuit. In the coincidence channel, the pulses passed through a distributed amplifier (with gain $k = 30$) and a discriminator, and were then fed to an anticoincidence system. The pulses of the anticoincidence channel were fed to the second input of this system passing through a discriminator and a generator producing standard square pulses of 2×10^{-7} sec duration. The resolving times of the fast coincidence circuit and of the anticoincidence circuit were $\tau = (5-6) \times 10^{-9}$ sec and $\tau = 2 \times 10^{-7}$ sec, respectively.

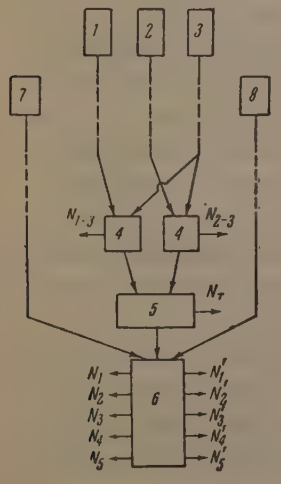

FIG. 2. Block diagram of the electronic apparatus: 1, 2, 3 – photomultipliers and output stages, 4 – coincidence circuits, 5 – anticoincidence circuits, 6 – time analyzer, 7 – trigger of the time analyzer, 8 – differential monitor, N_1–N_5 – outputs of analyzer recording the effect, N_1'–N_5' – outputs of analyzer recording the pulses from the differential monitor, N_T – telescope count.

The electronic circuit of the telescope is such that the anticoincidence system produces, in addition to the output signal fed to the time analyzer, another fast signal with a rise time of (1–2) $\times 10^{-8}$ sec. This enabled us, where necessary, to analyze the coincidences of the telescope pulses with a signal of a single counter or an analogous telescope, obtaining a resolution better than 10^{-8} sec.

The pulse from the telescope output was fed to a time analyzer similar to the one described in [9]. In the analyzer, the signals were fed to channels, each of which corresponded to a definite range of maximum energies in the bremsstrahlung radiation spectrum from the synchrotron. The time analyzer was triggered by pulses produced in a special circuit at the moment the magnetic field of the synchrotron reached a given value. Such a method enabled us to fix the required energy range of each analyzing channel.

The effect was measured for each of the three selected angles in five channels with maximum energy equal to 178, 186, 194, 202, and 210 Mev. The time spread of the bremsstrahlung pulse from the synchrotron ensured the measurement of the upper limit of the spectrum from 160 to 220 Mev. Thus, it was possible to avoid the errors due to instability of the energy at the limits of the pulse duration. Simultaneously with the recording of the effect in the corresponding branch of the analyzer, pulses of a differential monitor (see below) were recorded in five channels of the analyzer. A special test system operating with a Co^{60} source was used for a regular check of the sensitivity of the electronics.

PRINCIPAL CHARACTERISTICS

In order to calculate the yield of reactions (I) and (II), it is first necessary to know the efficiency of the telescope for γ rays. This efficiency was measured in a series of experiments using monoenergetic electrons in which the detection probability of an electron with a given energy, produced by a photon in the i-th layer of a lead converter, was measured. The efficiency η of the γ-ray telescope determined in such a way is shown in Fig. 3. With good accuracy, it can be written in the form

$$\eta = \begin{cases} 0.0052-0.12 & E_\gamma \leqslant 110 \text{ Mev} \\ 0.42 & E_\gamma > 110 \text{ Mev} \end{cases} \quad (1)$$

Such an efficiency is in good agreement with the known efficiencies of analogous γ-ray telescopes described in the literature.

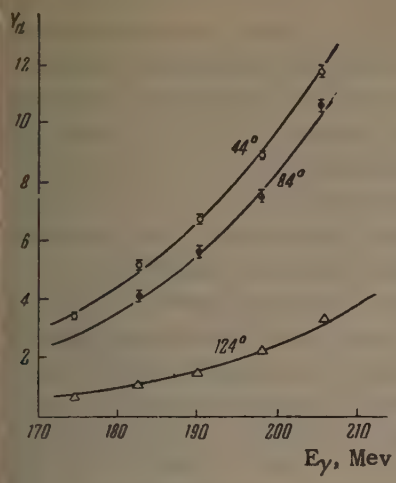

FIG. 3. Energy dependence of the γ-ray yield in the decay of π^0 mesons from deuterium (per 100 counts of the monitor).

In addition to the telescope efficiency, it is necessary to take the following facts into consideration:

1. Spurious counts due to the detection of photons propagating out from the target within the solid angle $\Delta\Omega$ of the telescope and producing a pair in the lead shielding.

2. Spurious counts due to the fact that the efficiency of the anticoincidence circuit is different from unity, since there exists a certain trigger threshold of the generator of standard pulses (see block diagram) which, at its input, receives the diffuse amplitude spectrum of the pulses after the coincidence circuit.

3. Missing counts due to the conversion of protons in the walls of the target and in the absorber before reaching the lead converter of the telescope.

These corrections, calculated as a result of a series of special experiments in which the position of converters and the operating conditions of the telescope were varied, are not greater than 10%.

Let us now consider the problem of monitoring the bremsstrahlung beam. It was mentioned above that, simultaneously with the detection of the telescope pulses in the corresponding channels of the analyzer, the pulses of a monitor counter were recorded. The analyzer channel width was chosen to be 8 Mev, which corresponds to a time of about 200 μsec. (For different channels, the time did not differ by more than 5%.) The effect recorded in each analyzer channel referred to a definite number of counts of the differential monitor.[9]

Corrections were made to account for the sensitivity of the differential monitor to the induced activity and neutron background, and also for the variation of the monitor counting rate with maximum energy of the bremsstrahlung spectrum. In order to reduce the role of these corrections, the differential monitor was used only for determining the relative intensity distribution in the channels. According to this distribution, the total count of a thin-wall monitor chamber was divided among the channels. The absolute calibration of the thin-wall ionization chamber was carried out using a thick graphite chamber and using the induced activity from the $C^{12}(\gamma, n)C^{11}$ reaction in a plate placed in the bremsstrahlung beam. The latter method was used for a regular check of the calibration. Both methods used in different series of measurements agreed to within 5 to 10%.

Having thus determined the counting response of a thin-wall chamber in Mev for the given value of the upper energy of the bremsstrahlung spectrum I^i (Mev/count), we can easily show that the number of photons per count of the thin-wall chamber with energies between the photoproduction threshold and to the maximum energy in the i-th channel (w^i_{max}) is given by the relation

$$n^i_\gamma = I^i \int_{w_t}^{w^i_{max}} f_{sp}(w, w^i_{max})\, dw \Big/ \int_{w_t}^{w^i_{av}} w f(w, w^i_{av})\, dw, \qquad (2)$$

where w_t is the energy corresponding to the photoproduction threshold, w^i_{av} is the mean value of the maximum energy in the bremsstrahlung spectrum for the i-th channel, and $f_{sp}(w, w^i_{max})$ is the energy spectrum of photons taking into account the spread of the beam from an electron with energy w^i_{max} incident upon the synchrotron target.

The integrals in Eq. (2) were calculated graphically for all channels taking the beam spread into account and using the tables of Penfold and Less.[10] The difference in the π^0-meson photoproduction thresholds on hydrogen and deuterium was taken into account in the calculations.

MEASUREMENTS

The energy dependence of the γ-ray yield from the decay of π^0 mesons produced on hydrogen and deuterium was measured for the angles of 44, 84, and 124° in the laboratory system (l.s.). The 170—210 Mev and 160—220 Mev energy ranges for an angle of 84° were investigated. A comparison of the experimental conditions at various angles of the principal γ-ray telescope was checked by a test telescope, whose position did not change throughout the experiment. The measurements were carried out alternatively with hydrogen, deuterium, and an empty target. The energy dependence of the yield decay γ rays from π^0 meson decay from deuterium is given in Fig. 3.

Using this data, we have determined the cross section for the emission of decay γ rays in the

l.s. by the photon difference method. In order to check the efficiency of the array, the monitoring, and the other parameters entering into the cross section, the results obtained with hydrogen were used to calculate the coefficients A, B, and C in the expression $d\sigma/d\Omega = A + B \cos\theta + C \cos^2\theta$. For the same purpose, we have determined the energy dependence of the total cross section of the process. Both results are in agreement with previously known values,[11-13] within the limits of statistical errors. This provides the basis for using the results of the experiment for further analysis.

The chance coincidence background was determined during the measurements by introducing a time delay in one of the coincidence channels. When working at an angle of 44° in the range of small energies, it was smaller than 2—3%. However, the background from the empty target was considerable, and varied from 30% in the first channel to 15% in the last one. The relatively large statistical errors are due to this fact.

The energy width of the analyzer channels was periodically reset, and, for a long period of time, the variation in the width of separate channels was less than 5%. The graph characterizing the energy resolution of the analyzer channel has a tail at small energies. It was, however, shown that the number of protons due to such a characteristic of the curve is negligibly small.

A certain contribution to the measured effect may be due to γ rays from the Compton effect on nucleons. However, in the narrow range of energies at which the experiment was carried out, the cross section for this process is small (of the order of 10^{-32} cm^2/sr)[14] and varies little with the energy of the primary beam. In connection with the above, the use of the photon difference method practically removes the contribution of the Compton effect to the final result. In addition, in control experiments on channels set for energies lower than the photoproduction threshold there were practically no counts.

Throughout the present article, only statistical errors are indicated.

DISCUSSION OF THE RESULTS

The analysis of the experimental data and their comparison with theory was carried out along two lines. First, using the value of the ratio of the cross sections of processes (I) and (II) obtained by the momentum approximation theory, the ratio of the decay photon yield was calculated. Second, the angular and energy dependences of the cross sections of process (I) were used to calculate the corresponding distributions of the decay photons. The experimental results were compared with the distributions obtained in such a way. To calculate the distributions, it is necessary to know the angular resolution of the array.

It can be shown (see the Appendix) that the angular resolution function, or the probability that a neutral pion emitted in the photoproduction at an angle θ_π is detected by a γ-ray telescope placed at an angle θ_γ (the angles are reckoned with respect to the direction of the bremsstrahlung beam) is given by the equation

$$W(\theta_\pi, \beta_\pi, \theta_\gamma) = \frac{\sin\theta_\pi}{\pi} \int_0^\pi \frac{(1-\beta_\pi^2)\,\eta(E_\gamma)\,d\varphi}{[1-\beta_\pi(\cos\theta_\pi\cos\theta_\gamma + \sin\theta_\pi\sin\theta_\gamma\cos\varphi]} \quad (3)$$

where $\eta(E_\gamma)$ is the γ-ray telescope efficiency and β_π is the π^0-meson velocity. The remaining symbols θ_π, θ_γ, and φ are defined in Fig. 8 (see below). Since the angular resolution functions for given values of θ_π and θ_γ depend on the π^0-meson velocity, they should be calculated separately for each of the three investigated processes (photoproduction on hydrogen and elastic and inelastic photoproduction on deuterium).

For the photoproduction of mesons on hydrogen and the elastic photoprocess on deuterium, a unique kinematic relation exists between θ_π, β_π, and the energy for the primary photon κ. For the inelastic process, where, in the final state, three particles are produced, such a relation does not exist. Moreover, at a given angle θ_π, mesons will be emitted with a certain velocity distribution which is determined by the binding energy of the nucleons in deuterium and the interaction of nucleons in the final state. These distributions have a maximum in the range of velocities determined by the single-nucleon kinematics, and can be constructed by using the formulae and tables of[15]. Thus, for the inelastic process, it is possible to determine the range of variation of β_π for a given angle θ_π, and then to calculate the angular resolution for the limiting values of β_π.

The angular resolution function was calculated by numerical integration of Eq. (3) for the three investigated processes. Typical functions of angular resolution for $\theta_\gamma = 84°$ are shown in Fig. 4. For inelastic photoproduction on deuterium, the graphs corresponding to the limiting values of β_π are slightly different, and the average value of the angular resolution function was used for the process.

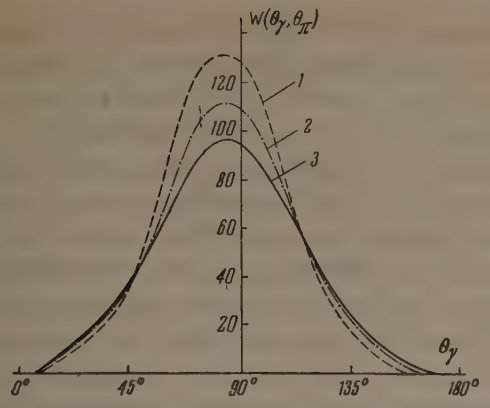

FIG. 4. Angular resolution function of the arrangement for $E_\gamma = 210$ Mev and the angle $\theta_\pi = 84°$. Curve 1—for the elastic photoproduction of π^0 on deuterium, 2—for π^0 photoproduction on hydrogen, 3—for inelastic π^0 photoproduction on deuterium accompanied by the emission of π^0 mesons with minimum energy.

Using the momentum approximation, we write the photoproduction cross section for π^0 mesons on deuterium [16] in the form

$$d\sigma = \left(\frac{1}{2\pi}\right)^2 \frac{k^3\, d\Omega dp}{k^2/E + (k^2 - \varkappa k)/2M} \langle M \rangle^2_{f_0}, \qquad (4)$$

where $\mathbf{k}$ is the meson momentum, $\mathbf{p}$ the relative momentum of nucleons in the deuteron, κ the momentum of the primary photon, E the meson energy, M the nucleon mass, and $\langle M \rangle^2_{f_0}$—square of the photoproduction matrix element. In order to obtain cross sections that can be compared with the experimental results, it is necessary to integrate Eq. (4) over the relative momentum of nucleons $\mathbf{p}$ within the limits from 0 to p_{max}. For this purpose, we have to know all the parameters determining the matrix element and the wave function of the final state of the nucleons. This can be avoided using the so-called completeness theorem approximation. [16,17] In this approximation, the differential cross section of the process (I) can be written as

$$(d\sigma/d\Omega)_d^{compl.} = A_p^2 + A_n^2 + 2\mathrm{Re}\, A_p A_n^* F(2q). \qquad (5)$$

where A_p and A_n are the π^0-meson photoproduction amplitudes on protons and neutrons respectively, $F(2q)$ is the form factor of the deuteron given by the expression

$$\int e^{-2i\mathbf{qr}} \varphi_d(\mathbf{r})\, d\mathbf{r} = F(2q), \qquad (6)$$

where $\mathbf{q} = (\boldsymbol{\kappa} - \mathbf{k})/2$, $\mathbf{r}$ is the relative nucleon coordinate, and $\varphi_d(\mathbf{r})$ is the total function of the ground state of the deuteron.

The cross section of the elastic process in this case will have the form

$$(d\sigma/d\Omega)_d^{el} = A_p^2\, F^2(q) + A_n^2 F^2(q) + 2\mathrm{Re}\, A_p A_n^* F^2(q). \qquad (7)$$

In this notation, the photoproduction cross section of π^0 mesons on hydrogen is

$$(d\sigma/d\Omega)_p = A_p^2. \qquad (8)$$

If we assume that $A_p = A_n$, then we have

$$\left(\frac{d\sigma}{d\Omega}\right)_d^{compl.} \Big/ \left(\frac{d\sigma}{d\Omega}\right)_p = 2\,[1 + F(2q)], \qquad (9)$$

$$\left(\frac{d\sigma}{d\Omega}\right)_d^{el} \Big/ \left(\frac{d\sigma}{d\Omega}\right)_p = 4F^2(q). \qquad (10)$$

The functions $F(q)$ and $F(2q)$ can easily be calculated if we accept any wave function of the ground state of the deuteron. It is found that, for a relatively large class of wave functions and taking into account both S and D waves, the form factor F and its dependence on q differ relatively little.

In the range of small angles θ_π, the form factor of the deuteron tends to unity when the primary photon energies tend to the threshold value for photoproduction, i.e., when q tends to zero. The total cross section for the photoproduction of π^0 mesons on deuterons is then equal to the elastic cross section [see Eqs. (9) and (10)], and the ratio of the cross sections of the processes (I) and (II) should be equal to four.

Using the Hulthén wave function of the ground state of the deuteron, and using Eqs. (6), (9), and (10), we have calculated the energy dependence of the ratio of the cross sections of the processes (I) and (II) for three angles. The results obtained in this way are in agreement with the experimental results shown in Fig. 5.

It can be seen that, for all investigated angles of emission of π^0 mesons, the ratio of the total

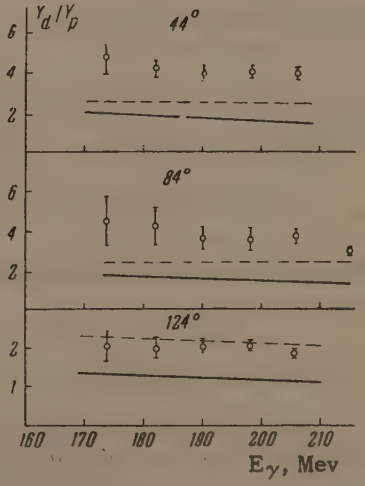

FIG. 5. Ratio of the integral yields of π^0 mesons from deuterium and hydrogen for the angles 44, 84, and 124°. Solid line—calculated ratio of the cross section of elastic processes on deuterium to the cross section on hydrogen, dashed line—calculated ratio of the total cross sections of photoproduction on deuterium and hydrogen.

and elastic cross section of process (I) to the cross section of process (II) depends very little on energy. These results are well confirmed by the experiment. However, the experimentally obtained value of this ratio for 44 and 84° is considerably greater than the theoretical value, and already in this range of angles and energies, is equal to about four. At 124° the experimental point coincides with good accuracy with the theoretical curve corresponding to the ratio of the total cross sections. For this angle, within the limits of the whole investigated energy range, the form factor F(q) is small, and the elastic photoproduction of π^0 mesons on deuterons is suppressed.

Thus, the comparison made shows that, at 170—210 Mev energies of primary photons at l.s. angles θ_π smaller than 90°, the cross section of the elastic photoproduction of π^0 mesons on deuterium is considerably greater than the value expected from the momentum approximation theory.

For a more detailed comparison of the experiment with the momentum approximation, we have used the results of Lebedev and Baldin.[14] In this reference, the cross sections of the elastic and inelastic processes in reaction (I) are obtained taking the interaction of nucleons in the final state into account. The calculations are free from the above-mentioned assumptions, but the S-wave photoproduction is not taken into account. The differential cross sections of both branches of reaction (I) in the l.s. are given by the equation

$$\left(\frac{d\sigma}{d\Omega}\right)_d^{\text{el}} = \left(\frac{1}{2\pi}\right)\frac{4}{3}(7-5\cos^2\theta_\pi)\,|M_1(^3/_2)|^2 k_s^2 \times \frac{|F((\varkappa^2+k_s^2-2\varkappa k_s\cos\theta_\pi)/2)|^2}{|k_s/\sqrt{1+k_s^2}+(k_s-\varkappa\cos\theta_\pi)/2M|}, \quad (11)$$

where $(2\pi)^4\,|M_1(^3/_2)|^2 = (0.6\pm0.1)\times10^{-4}k^2$, and k_s is the root of the equation

$$\cos\theta_\pi = \frac{(\varkappa^2-k^2)-4M(\varkappa-\sqrt{1+k^2})}{2\varkappa k}.$$

The remaining symbols have been explained above. Furthermore,

$$\left(\frac{d\sigma}{d\Omega}\right)_d^{\text{inel}} = \frac{1}{2\pi}\frac{\alpha M}{2}\{(7-5\cos^2\theta_\pi)\,[F^t(p_s,q_s) + E^t(p_s,q_s)] + (1-\cos^2\theta_\pi)\,[F^s(p_s,q_s) - E^s(p_s,q_s)]\}\,p_s\,|M_1(^3/_2)|^2; \quad (12)$$

where

$$q_s = |\varkappa-\mathbf{k}|/2,$$

$$p_s = \{M[\varkappa-\varepsilon-\sqrt{1+k^2} - (\varkappa^2+k^2-2\varkappa k\cos\theta_\pi)/4M]\}^{1/2}.$$

The functions $E^{t,s}$ and $F^{t,s}$ have been tabulated in[15], ε is the binding energy of nucleons in the deuteron, and $\alpha = \sqrt{M\varepsilon}$. Equation (12) was integrated over k by a numerical method.

The angular dependence of the photon yield in π^0-meson decay was determined using the corresponding angular resolution function for each of the channels of reaction (I). The calculations carried out for primary photon energies of 174 and 206 Mev are compared with the experimental data in Fig. 6. The theoretical curves are normalized to the experimental point corresponding to $\theta_\pi = 124°$ and primary photon energy of 174 Mev.

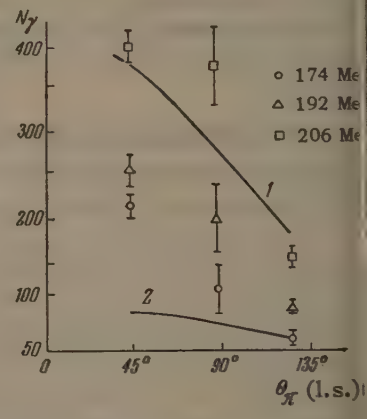

FIG. 6. Angular dependence of the production cross section of decay γ rays from π^0 mesons on deuterium. Curve 1 – calculated for E_γ = 206 Mev, curve 2 – for E_γ = 176 Mev. The calculated curves are normalized at the point E_γ = 206 Mev, θ_γ = 124°.

The character of the angular dependence of the cross section for the energy of 206 Mev is in satisfactory agreement with the experiment. It can be seen that, at these energies, the contribution of the elastic cross section is already small.

For 192 and 174 Mev, the experimentally obtained angular dependence of the cross section has a considerably steeper forward peaking than that which follows from the theory.

Thus, both methods of comparing the results of the experiment with the momentum approximation indicate the existence of a discrepancy in the region where the contribution of the elastic process of π^0 meson photoproduction on deuterium is considerable. Further experiments in the range of small energies and small angles θ_π are necessary for a more detailed analysis.

In addition to the above-described method of analyzing the results, experimental data were used to determine the ratio of differential cross sections of the processes (I) and (II) for the energy ranges from the reaction threshold to 178 Mev, and from 178 to 210 Mev. The results are shown in the table and in Fig. 7 where, for the angle of 84°, they are compared with earlier ratios of the differential cross sections.[1,4,5] It can be seen that the results of the present experiment are in good agreement with the conclusions of André.[5] All the known data show that, in the energy range

Differential Ratios of the yield of π^0 Mesons from Deuterium and Hydrogen

$\theta_{l.s.}$, deg.	E_γ	
	$E_n = 178$ Mev	178–210 Mev
44	4,8±0,8	3,7±0,3
84	4,5±1,3	3,5±0,6
124	1,95±0,2	1,7±0,1

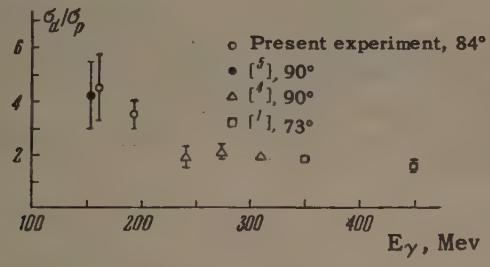

FIG. 7. Differential ratio of the cross sections for the photoproduction of π^0 mesons on deuterium and hydrogen according to the data of different authors.

of about 200 Mev, the ratio of the cross sections σ_d/σ_p increases sharply.

The experiments are at present being continued in order to measure the ratio of the cross sections of processes (I) and (II) at an angle $\theta_p \approx 0°$ in the range from the reaction threshold to 240 Mev. The π^0 mesons are, in that case, detected from the two decay photons.

In conclusion, the authors take the opportunity to express their gratitude to P. N. Shareĭko for designing the electronic apparatus and taking part in the measurements, to A. M. Baldin and A. I. Lebedev for valuable discussion, and also to the members of the synchrotron team.

APPENDIX

ANGULAR DISTRIBUTION FUNCTION OF A γ-RAY TELESCOPE

Let κ be the momentum of the primary photon, and k and p_γ the momenta of the π^0 meson and of the decay photon respectively moving in the direction of the telescope. The definition of the angles θ_γ, θ_π, θ_x, and φ is clear from Fig. 8.

If $d\sigma/\sigma\Omega$ is the angular distribution of π^0 mesons in the l.s., then the number of mesons propagating at an angle θ_π within a unit solid angle is

$$n_{\pi^0} = K\,(d\sigma/d\Omega)\sin\theta_\pi\,d\theta_\pi\,d\varphi; \qquad (A.1)$$

where K is a factor depending on the number of nuclei in the target and the primary photon flux.

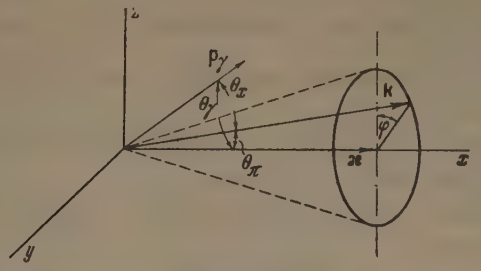

FIG. 8

The probability of the decay of a π^0 meson with velocity β_π into two photons so that one of them is emitted at an angle θ_x to the direction of motion of the π^0 meson in the l.s. can be written as

$$P(\theta_x\,\beta_\pi) = (1-\beta_\pi^2)/2\pi\,(1-\beta_\pi\cos\theta_x)^2. \qquad (A.2)$$

The number of photons propagating in the direction of the telescope and due to the decay of $n\pi^0$ mesons Eq. (A.1), will then be given by

$$n_\gamma = \frac{K}{2\pi}\frac{d\sigma}{d\Omega}\sin\theta_\pi\,d\theta_\pi\,d\varphi\,\frac{1-\beta_\pi^2}{(1-\beta_\pi\cos\theta_x)^2}. \qquad (A.3)$$

The decay photons from mesons propagating on the generator of the cone with an opening angle θ_π (the angle θ_x is variable) will also propagate in the same direction. In order to take these γ rays into account, it is necessary to integrate Eq. (A.3) over the angle φ. Moreover, as can easily be shown

$$\cos\theta_x = \cos\theta_\pi\cos\theta_\gamma + \sin\theta_\pi\sin\theta_\gamma\cos\varphi. \qquad (A.4)$$

Finally, it is necessary to take into consideration the contribution of the decay photons from π^0 mesons emitted at different angles. For this purpose, it is necessary to integrate Eq. (A.3) also over θ_π.

Taking the detection efficiency of the γ-ray telescope into account, we shall obtain the number of the decay photons detected per unit time by the telescope set at an angle θ_γ to the direction of the bremsstrahlung beam (the solid angle of the telescope enters through the factor K):

$$N_\gamma(\theta_\gamma) = \int_0^\pi\int_0^{2\pi}\frac{K}{2\pi}\frac{d\sigma}{d\Omega}\sin\theta_\pi\,\frac{\eta(E_\gamma)(1-\beta_\pi^2)}{(1-\beta_\pi\cos\theta_x)^2}\,d\varphi\,d\theta_\pi. \qquad (A.5)$$

η is given by Eq. (1), and

$$E_\gamma = \mu_0 c^2/2\gamma\,(1-\beta_\pi\cos\theta_x),$$

where $\mu_0 c^2$ is the meson rest mass and $\gamma = (1-\beta_\pi^2)^{-1/2}$. Introducing the angular resolution function of the telescope (see text) $W(\theta_\pi, \beta_\pi)$, we obtain

$$N_\gamma(\theta_\gamma) = \int_0^\pi \frac{d\sigma}{d\Omega}\,W(\theta_\pi\beta_\pi)\,d\theta_\pi,$$

where, taking Eq. (A.4) into account, $W(\theta_\pi, \beta_\pi)$

written in the form (5) is determined by Eq. (A.5).

[1] Keck, Tollestrup, and Bingham, Phys. Rev. **103**, 1549 (1956).

[2] Belousov, Kutsenko, and Tamm, Dokl. Akad. Nauk SSSR **102**, 921 (1955).

[3] Wolfe, Silverman, and DeWire, Phys. Rev. **99**, 268 (1955).

[4] G. Cocconi and A. Silverman, Phys. Rev. **88**, 1230 (1952).

[5] C. C. Andre, University of California Radiation Laboratory, Report 2425, 1953.

[6] A. M. Baldin and B. B. Govorkov, Nuclear Phys. **13**, 193 (1959).

[7] L. I. Slovokhotov, Report, Physics Institute of the Academy of Sciences, 1961.

[8] A. A. Rudenko, Pribory i Tekhn. Éksperimenta (Instruments and Exptl. Techniques) No. 6, 60 (1958).

[9] Vasil'kov, Govorkov, and Kutsenko, ibid. No. 2, 23 (1960).

[10] A. S. Penfold and J. E. Less, Analysis of Photo Cross Sections, University of Illinois, 1958.

[11] R. G. Vasil'kov and B. B. Govorkov, JETP **37**, 317 (1959), Soviet Phys. JETP **10**, 224 (1960).

[12] L. J. Koester and F. E. Mills, Phys. Rev. **105**, 1900 (1957).

[13] R. G. Vasil'kov and B. B. Govorkov, JETP **37**, 317 (1959), Soviet Phys. JETP **10**, 224 (1960).

[14] L. S. Hyman, Ph. D. Thesis, Massachussetts Institute of Technology, 1959.

[15] A. I. Lebedev and A. M. Baldin, Report, Physics Institute of the Academy of Sciences, 1961.

[16] A. M. Baldin, Dissertation, Physics Institute of the Academy of Sciences, 1953.

[17] G. F. Chew and H. W. Lewis, Phys. Rev. **84**, 779 (1951).

Translated by H. Kasha
305

OBSERVATION OF THE REACTION $\mu^- + He^3 \rightarrow H^3 + \nu$

O. A. ZAĬMIDOROGA, M. M. KULYUKIN, B. PONTECORVO, R. M. SULYAEV, A. I. FILIPPOV, V. M. TSUPKO-SITNIKOV and Yu. A. SHCHERBAKOV

Joint Institute for Nuclear Research

Submitted to JETP editor July 25, 1961

J. Exptl. Theoret. Phys. (U.S.S.R.) 41, 1804-1808 (December, 1961)

A diffusion chamber filled with He^3 was used to observe the $\mu^- + He^3 \rightarrow H^3 + \nu$ reaction. The upper limit of the mass of the neutral particle emitted in muon capture by nucleons ($m_\nu < 6$ Mev) was determined by measuring the recoil energy of H^3. According to preliminary data, the probability of this reaction is $(1.30 \pm 0.40) \times 10^3$ sec^{-1} and agrees with the theoretical value predicted by the universal theory of weak interactions.

ONE of the most studied among the weak interactions of nonstrange particles is the capture of a muon by a nucleon. The study of the not yet observed capture of a μ^- meson by a free proton is of great interest. However, the interpretation of the experimental results will be complicated by various molecular effects.[1] In experiments on the capture of muons in complex nuclei, it is the total probability of the various processes which has generally been measured.[2] The only definite process studied in detail is the process of the absorption of a muon by the C^{12} nucleus with the formation of B^{12}.[3,4] But even in this case, the interpretation of the experimental results is made more difficult by insufficiently accurate knowledge of the nuclear wave functions and by a number of other factors. Also, the results of the measurements made by different authors do not agree with each other at the present time.

Interest in the experimental study of the capture reaction of slow μ^- mesons in He^3 with formation of tritium and a neutrino in the final state

$$\mu^- + He^3 \rightarrow H^3 + \nu \qquad (1)$$

is due to the fact that the theoretical calculations [5,6] of the probability of this reaction, based on the known value of ft for the β decay of tritium, have high accuracy. Measurement of the probability of the process (1) makes it possible to determine the effective muon-nucleon interaction constant and thus to confirm the validity of the universal theory of weak interactions.[7]

In addition, determination of the energy of the tritium formed in process (1) makes it possible to estimate by a direct method the upper limit of the mass of the neutral particle emitted in the muon capture, and to prove, by the same method, the existence of the process [8]

$$\mu^- + p \rightarrow n + \nu, \qquad (2)$$

which, although it is generally accepted, has not yet been observed with complete reliability either for free protons or in complex nuclei.*

The first results of a study of the reaction (1) are described below.

Because He^3 is a rare isotope, we first contemplated using a mixture of hydrogen and helium for the study of muon capture in He^3, relying on an effective interception of the muons from the state of meso-hydrogen, similar to the well-known interception of muons by deuterium and other nuclei. However, as experiments carried out by us with a diffusion chamber filled with a mixture of hydrogen and helium have shown (as well as the theoretical estimates of S. S. Gershteĭn) an effective interception of muons by the helium does not occur, even at a helium concentration of 15 per cent. Therefore, we used pure He^3 in the subsequent experiments.

In the experiments, a diffusion chamber was used which was filled with He^3 at a pressure of 20 atm. The purity of the gas used was better than 99.999 per cent. The impurity of tritium amounted to about 10^{-15}. The vapor pressure of the methyl alcohol in the sensitive layer of the chamber was less than 50 mm Hg. The chamber was placed in a magnetic field of 6000 oe and was also inserted in the extracted 217-Mev/c meson beam of the synchrocyclotron of the Joint Institute for Nuclear Research. The slowing of the mesons and the separation of the mesons from pions was accomplished by a copper filter located near the chamber. Spe-

*The most direct measurement of the energy carried by the neutral particle in the process of muon capture by the nucleus, was made by Fry;[9] nevertheless, his data do not permit a reliable estimate of the mass of the neutral particle.

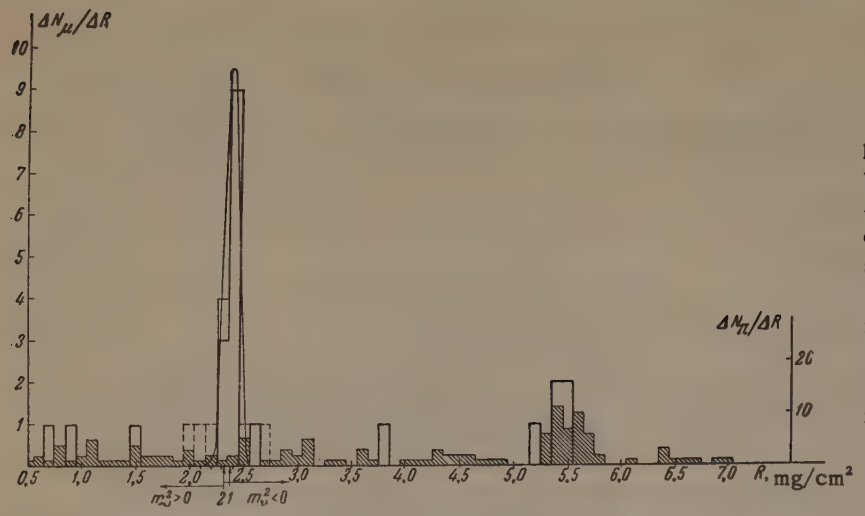

FIG. 1. Spectrum of the range of particles stopped in the sensitive layer of the chamber; the spectrum is connected with the stopping of mesons. $\Delta N_\mu/\Delta R$ is the number of cases per range interval obtained in a "muon exposure;" $\Delta N_\pi/\Delta R$ is the same factor, obtained in "pion exposure." The arrow 1 marks the experimental range of tritium in reaction (1); the arrow 2 – the expected range of tritium in reaction (1), computed from the range-energy relation [10] under the assumption that the mass of the neutrino is equal to zero.

cial precautions were taken to shield the chamber from thermal neutrons which produce the reaction

$$n + He^3 \rightarrow p + H^3, \qquad (3)$$

with a large cross section, creating a large background and a large ion content in the chamber.

To date, about 6000 photographs of the stopping of mesons in He^3 have been obtained in "muon exposure," i.e., in exposures in which the thickness of the filter corresponds to a maximum number of muons present in the chamber. The identification of the reaction (1) was based on the fact that the nucleus of tritium emerges with a sharply defined energy (1.897 Mev) and consequently has a definite range. Single-pronged stars produced by the stopped mesons were analyzed. Figure 1 shows the spectrum of path lengths of the secondary charged particles stopped in the sensitive layer of the chamber ("muon histogram"). The six cases shown with dashed lines in this drawing were identified with less reliability because of poor visibility condition or because the track of the stopped meson was short. To clear up the problem of the background which can be produced by the stopped pions present as an impurity in the "muon exposure," some 1200 pion stars were analyzed. These were obtained in a separate experiment ("pion exposure"), in which the thickness of the filter was chosen so as to obtain a maximum of pion stops in the chamber. The histogram of the paths of products of the pion stars which stop in the sensitive layer of the chamber is shown in the same drawing by shaded rectangles ("pion histogram"). The latter histogram is "normalized" to the area of the "muon histogram" in the region of paths from 5.00 to 6.00 mg/cm^2, where events of radiative capture of π^- mesons in He^3 should generally occur:

$$\pi^- + He^3 \rightarrow H^3 + \gamma.$$

From the number of stars obtained in the observed range interval it follows that the impurity of pions stopped in the chamber in the "muon exposure" amounted to ~2 per cent. This estimate agrees with the independent determination of the pion impurity made from the total number of stars in a chamber filled with He^4.

The results obtained indicate that the stars recorded in the "muon exposure," in the entire range interval considered, were chiefly produced by pions, with the exception of the region around 2.40 mg/cm^2, where a monoenergetic group of particles formed by stopped muons is apparently observed. An estimate of the absolute scatter of the values of the range was carried out on the basis of the measurement of a large number of total ranges of the proton and tritium formed in He^3 by thermal neutrons in the reaction (3). The number of such events on each frame was about 20. The mean square error of the range in these measurements was found to be equal to 0.06 mg/cm^2. The error curve with this half-width is also plotted in Fig. 1 for illustration of the scale of the range spread of the monoenergetic particles measured.

It is seen that the group of particles with range of about 2.40 mg/cm^2 can actually be regarded as monoenergetic. The energy of these particles agrees with the expected value of the energy of H^3 in process (1). This means that in the capture of the muon in He^3 there is a transition in which only one neutral particle should be emitted. In this case, its mass is very small and is compatible with a value equal to zero (see below), while its spin must be half integral. It can be assumed that 14 cases of μ^- meson capture in He^3 with formation of tritium and a neutrino in the final state were observed by us. A typical photograph of process (1) is shown in Fig. 2. The mean value of the range of the tritium, determined from the 14 cases, amounts to 2.37 ± 0.02 mg/cm^2.

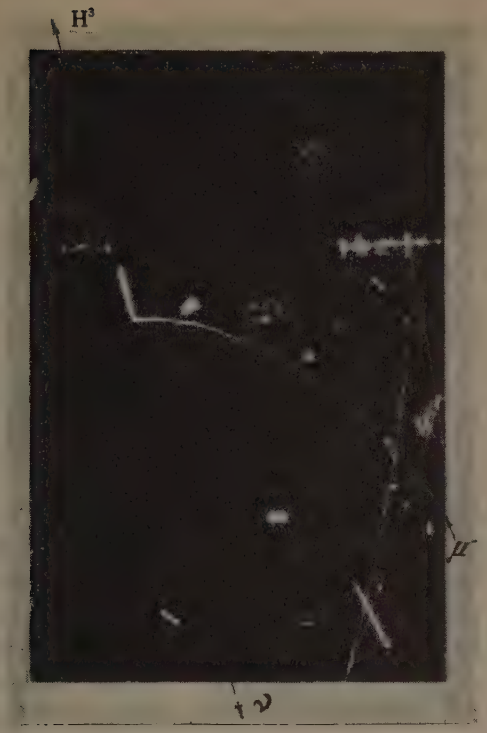

FIG. 2. Typical photograph of the reaction $\mu^- + He^3 \rightarrow H^3 + \nu$. The short traces visible on the photograph are generated by thermal neutrons in the reaction $n + He^3 \rightarrow H^3 + p$ ($R_{H^3} + R_p = 0.86$ mg/cm²).

Using this value of the range and experimental data on the ionization losses of the energy of protons in helium,[10] one can determine the upper limit of the mass of the neutral particle emitted in the process of muon capture by the nucleons. In this case it is shown that its mass is less than 6 Mev, with a probability of 99 per cent. The masses of the charged particles taking part in the process (1) were taken to be the following: $m_{He^3} = 2808.22$ Mev, $m_{H^3} = 2808.75$ Mev, $m_\mu = 105.65$ Mev. It should be remarked that the estimate carried out includes only the statistical errors in the determination of the range of tritium and does not take into account possible systematic errors which can undoubtedly take place, in particular, in the transition from range to energy. Therefore, a more definite conclusion would be that it was not possible for us to observe the finite mass of the muon neutrino emitted in the reaction (1); the scale of uncertainty in the mass of the neutrino, as analysis of the various inaccuracies shows, amounts to ~8 Mev.

The probability of reaction (1), Λ, can be determined in practice as the ratio of the number of cases of this reaction to the total number of muon stoppings in He^3, multiplied by the known probability of μ-e decay. The observed number of cases of (1) and the number of muon stoppings satisfying the accepted sampling criteria (5196) were corrected with account of the effectiveness of the scanning. The effectiveness of the recording of the tritium was determined from analysis of the spectrum of visible lengths of tracks of charged particles in pion stars, and amounted to (88 ± 4) per cent. The effectiveness of the scanning was determined from the results of independent repetition of scanning of part of the material, and was shown to be equal to 94 per cent.

Taking the value 2.21×10^{-6} sec for the lifetime of the muon, we obtain a value of Λ equal to $(1.30 \pm 0.40) \times 10^3$ sec^{-1}. This result should be compared with the theoretical value of $(1.54 \pm 0.08) \times 10^3$ sec^{-1}, obtained by Wolfenstein[6] on the basis of the universal theory of weak interactions, and is clearly the most accurate of the theoretical values of Λ.

The reliability of the agreement of the result that was obtained with the theory is small because of its large statistical error; therefore, at the present time, work is being carried on by us on the improvement of the statistical accuracy of the results. It can be noted, however, that the accuracy with which the universal interaction theory is tested in the experiment described above (~30 percent) is comparable with the accuracy of the test of this theory[6] by experiments on the study of a pure Gamow-Teller transition in the reaction $\mu^- + C^{12} \rightarrow B^{12} + \nu$. The result obtained by us gives the first rough information on the value of the vector constant of μ-nucleon interaction, the sign of which, as is well known,[11] is opposite to the sign of the axial-vector constant.

If we assume that the hyperfine states of the He^3 mesoatoms are statistically populated (there are strong theoretical arguments in favor of this [12]), then the probability of the reaction (1) determines the value of $3G_G^2 + G_F^2$, where G_G and G_F are the Gamow-Teller and Fermi effective coupling constants. For our purpose, one can express them approximately in terms of the axial-vector $g_A^{(\mu)}$ and the vector $g_V^{(\mu)}$ constants:

$$G_F = g_V^{(\mu)}, \qquad G_G \approx g_A^{(\mu)}.$$

Combining the most accurate value of the probability of the reaction $\mu^- + C^{12} \rightarrow B^{12} + \nu$, equal to $(6.31 \pm 0.24) \times 10^3$ sec^{-1} [4] with the value of the probability of the process $\mu^- + He^3 \rightarrow H^3 + \nu$, we get the result that $|g_V^\mu| < 2\,|g_A^\mu|$, with a probability of 90 per cent.

The authors express their deep gratitude to P. L. Kapitza, V. P. Peshkov, V. M. Kuznetsov and A. I. Filimonov for invaluable help in carrying out purification of He^3 from tritium at the Insti-

tute for Physical Problems of the U.S.S.R. Academy of Sciences, and S. S. Gershteĭn for numerous useful discussions. We are grateful to V. P. Dzhelepov and L. I. Lapidus for interest in the work, and also to G. M. Aleksandrov, V. V. Kuznetsov, V. I. Orekhov, V. F. Poenko, A. G. Potekhin, D. B. Pontecorvo and I. V. Falomkin for help in the preparation of the apparatus and participation in the measurements.

[1] S. S. Gershteĭn and Ya. B. Zel'dovich, Usp. Fiz. Nauk 71, 581 (1960), Soviet Phys. Uspekhi 3, 593 (1961); S. Weinberg, Phys. Rev. Lett. 4, 575 (1960).

[2] J. C. Sens, Phys. Rev. 113, 679 (1959).

[3] Burgman, Fisher, Leontic, Lundby, Mennier, Stroot, and Teja, Phys. Rev. Lett. 1, 469 (1958); Harrison, Argo, Kruse, and McGuire, Phys. Rev. 114, 626 (1959); Fetkovich, Fields, and McIlweir, Phys. Rev. 118, 319 (1960).

[4] Maier, Bloch, Edelstein, and Siegel, Phys. Rev. Lett. 6, 417 (1961).

[5] A. Fujii and H. Primakoff, Nuovo cimento 10, 327 (1958); Chu, Chou and Peng, Acta Phys. Sinica 16, 61 (1960); B. L. Ioffe, JETP 37, 159 (1959), Soviet Phys. JETP 10, 113 (1960); C. Wentz, Nucl. Phys. 16, 59 (1960).

[6] L. Wolfenstein, Proc. of the 1960 Ann. Int. Conf. on High Energy Phys. of Rochester, Univ. of Rochester, 1960, p. 529; Bull. Amer. Phys. Soc. 6, 33 (1961).

[7] E. C. G. Sudarshan and R. E. Marshak, Proc. of the Padua-Venice Conf. on mesons and newly discovered particles, 1957; R. P. Feynman and M. Gell-Mann, Phys. Rev. 109, 903 (1958).

[8] B. Pontecorvo, Phys. Rev. 72, 246 (1947).

[9] W. F. Fry, Phys. Rev. 90, 999 (1953).

[10] S. K. Allison and S. D. Warshaw, Revs. Modern Phys. 25, 779 (1953).

[11] V. L. Telegdi, Proc. of the 1959 Kiev and of the 1960 Rochester Ann. International Conf. on High Energy Physics. Egorov, Zhuravlev, Ignatenko, Kuptsov, Li and Petrashku, JETP 41, 684 (1961); Soviet Phys. JETP 14, 494 (1962).

[12] A. P. Bukhvostov and I. N. Shmushkevich, JETP 41, 1895 (1961), Soviet Phys. JETP 14, 1347 (1962).

Translated by R. T. Beyer
306

SUPERCONDUCTING SOLENOIDS FOR STRONG MAGNETIC FIELDS USING Nb_3Sn

N. E. ALEKSEEVSKII and N. N. MIKHAĬLOV

Institute for Physics Problems, Academy of Sciences, U.S.S.R.

Submitted to JETP editor July 25, 1961

J. Exptl. Theoret. Phys. (U.S.S.R.) **41**, 1809-1810 (December, 1961)

Data are presented on superconducting solenoids constructed of Nb_3Sn, and the critical current vs. external magnetic field curve for this superconducting compound is discussed.

THE superconducting intermetallic compound Nb_3Sn having a critical temperature $T_c = 18.06°K$ was discovered some time ago,[1] but only at the beginning of the present year was it established that, although the magnetic field begins to penetrate this material at a relatively low value of the field intensity, the resistance nevertheless remains zero up to 100 koe, while the current density in the sample can reach 10^5 amp/cm^2.[2-4] These data indicate a real possibility for construction of solenoids from this superconductor to generate strong fields.

Practical use of this compound, unfortunately, is impeded by its extreme brittleness. Kunzler et al[2] have described the use of a superconductor based on Nb_3Sn, prepared by filling a tube of niobium with a mixture of powdered Nb and Sn, drawing this combination through a die to a diameter of ~0.4 mm, and then sintering the powder within the capillary thus formed at ~1000°C.

We have developed several alternate techniques for preparing mechanically durable superconducting wires and ribbons using Nb_3Sn, consisting of an inner core of niobium and a relatively thin surface layer of the intermetallic compound. Small short-circuited solenoids containing from 20 to 112 turns were made from compound wire of this type, 0.3 mm in diameter, and the dependence of the field H_x within the coils upon the external field H_0 was investigated. If one uses the values of the residual fields of the solenoids to compute the currents flowing through them, one can obtain the field dependence of the critical current at 4.2°K shown in Fig. 1. In this graph the points corresponding to a field of ~30 koe were obtained from experiments on the destruction of superconductivity in a single wire 0.3 mm in diameter by a current in a constant field, while the point at ~80 koe was obtained from the destruction of superconductivity in a single wire of the same sort in a pulsed coil.

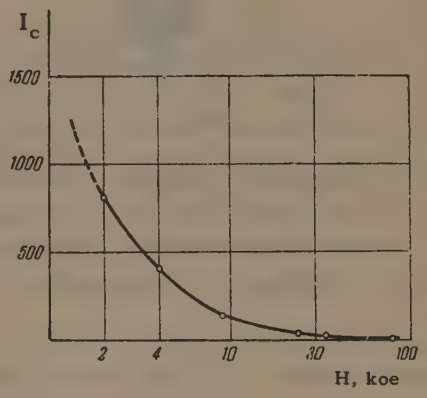

FIG. 1

It is evident that the curve thus obtained is similar to that representing the external magnetic field dependence of the critical current in a binary superconducting alloy (see [5]), and is characterized by an extremely high critical current for zero external field ($I_c \approx 1800$ amp), which corresponds to a critical current-induced field at the surface of the superconductor of ~24 koe. This value is quite close to that of H_{c1}, which may be obtained for Nb_3Sn from measurements of the magnetic moment* (see [6]).

Another feature of this relation is the very slow decrease in critical current with field for strong fields.

The high value for the frozen-in field of the short-circuited solenoid can be illustrated by the photograph in Fig. 2, which shows the helium Dewar containing the coil. Several quite heavy iron bolts are supported freely against the outer surface of the Dewar under the influence of the scattered field (the axis of the coil is horizontal, the number of turns n = 900, and the external dimensions of the coil are d = 18 mm, l = 20 mm). The field within the coil in this experiment

*H_{c1} represents the first critical field of the alloy, corresponding to a change in the induction in the sample as the external field is increased.

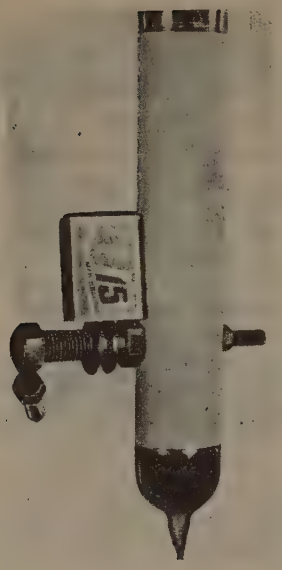

FIG. 2

amounted to ~15 koe. It should be mentioned that this value for the field is not the limiting one for this coil, and was determined by the parameters of the magnet used to excite the magnetic field in the coil.

In addition to short-circuited coils, we have also constructed small externally-supplied coils. With these, we used as lead-in conductors superconducting busbars prepared by a method analogous to that proposed by Kunzler, et al,[2] with the exception that copper tubing was used in place of niobium.

[1] Matthias, Geballe, Geller, and Corenzwit, Phys. Rev. 95, 1435 (1954).

[2] Kunzler, Buchler, Hsu, and Wernick, Phys. Rev. Lett. 6, 89 (1961).

[3] Arp, Kropschot, Wilson, Love, and Phelan, Phys. Rev. Lett. 6, 452 (1961).

[4] Betterton, Boom, Kneip, Worsham, and Roos, Phys. Rev. Lett. 6, 532 (1961).

[5] N. E. Alekseevskii, JETP 8, 1098 (1938).

[6] Bozorth, Williams, and Davis, Phys. Rev. Lett. 5, 148 (1960).

Translated by S. D. Elliott
307

INVESTIGATION OF THE ENERGY DEPENDENCE OF THE CROSS SECTION FOR PHOTOPRODUCTION OF π^+ MESONS ON HYDROGEN NEAR THRESHOLD

M. I. ADAMOVICH, É. G. GORZHEVSKAYA, V. G. LARIONOVA, N. M. PANOVA, V. M. POPOVA, S. P. KHARLAMOV, and F. R. YAGUDINA

P. N. Lebedev Physics Institute, Academy of Sciences, U.S.S.R.

Submitted to JETP editor July 31, 1961

J. Exptl. Theoret. Phys. (U.S.S.R.) 41, 1811-1817 (December, 1961)

The differential cross sections for photoproduction of positive pions on hydrogen have been measured in the photon energy range from 167 to 212 Mev. The measurements are carried out at an angle $\theta = \cos^{-1}(k\omega - 0.93)/kq$ (the angle for which the contribution of the nonphysical region to the dispersion integrals is zero). The results are in good agreement with the dispersion theory. A detailed analysis is made of the experimental results together with the data on the angular distribution.

INTRODUCTION

PHOTOPRODUCTION of π^+ mesons on hydrogen is one of the fundamental reactions of meson physics. Particular interest is attached to the region near the energy threshold of pion production.

Photoproduction of mesons on hydrogen was investigated in many laboratories, but only recently were experimental data obtained on the angular distribution of the mesons in a wide range of angles, for photon energies of 185[1], 230[2], 260, and 290 Mev[3]. All these experimental data, together with data on π^0 mesons,[4], were compared with the results of dispersion theory. The comparison has shown that experiment does not agree with theory as well as expected. For angles close to 180°, the experimental points lie below the theoretical ones, the deviation reaching several standard errors at certain energies. At low angles the discrepancy is less, but the point always lies somewhat above the theoretical curve.

As emphasized by Baldin[5], the reason for this may be that the theoretical cross sections depend on the contributions that the nonphysical region and the regions with very high energies make to the dispersion integral. Baldin also noticed that, unlike the scattering of pions on nucleons, where the contribution of the nonphysical region is small only when the angles are very small, in the case of photoproduction of pions on nucleons the contribution from the nonphysical region is equal to zero along a curve satisfying the relation

$$k\omega - kq\cos\theta = k_t = 0{,}93, \qquad (1)$$

where k — photon momentum, k_t — threshold value of the photon momentum, q, ω — the momentum and total energy of the pion (here and throughout $\hbar = c = \mu = 1$, where μ is the pion mass) and θ — angle of meson emission. All the quantities are in the center-of-mass system (c.m.s.).

An investigation of the experimental data on the photoproduction of π^0 mesons at angles satisfying relation (1) has shown that experiment agrees well with theory.[5] No such check was made on the theory for the photoproduction of charged mesons, owing to the lack of experimental data. We have therefore undertaken to measure the energy dependence of the cross section of the photoproduction of π^+ mesons on hydrogen at angles θ satisfying relation (1). The dependence of the angle θ on the photon energy E_γ in the laboratory system (l.s.), defined by this relationship, is shown in Fig. 1. The figure also shows plots of $k\omega - kq \times \cos\theta = 0.7$ and $k\omega - kq\cos\theta = 1.6$. Within the region bounded by these curves, the experimental data on the photoproduction of π^0 mesons agree with the theory within 10 or 15%.[5] It is seen from the figure that at photon energies near threshold (165 — 220 Mev) the measurements must be made in the interval 50 — 60° (c.m.s.), corresponding to 40 — 50° in the l.s.

EXPERIMENT

We measured the differential cross section of photoproduction of π^+ mesons in the photon energy

interval from 167 to 212 Mev, at 42.5° (l.s.) to the photon beam. This corresponds to the c.m.s. angles indicated in Fig. 1 by the dashed line. As can be seen from the figure, Eq. (1) is rigorously satisfied for 195 Mev photons, while the value of $k\omega - kq\cos\theta$ for the boundary values of 167 and 212 Mev is respectively 0.88 and 0.99, which differs little from the value 0.93 in Eq. (1).

A photon beam from the synchrotron of the Physics Institute of the Academy of Sciences, with maximum energy 250 Mev, was guided by a system of collimators and a clearing magnet to a hydrogen target, comprising a vertical brass cylinder of 50 mm diameter and 17 μ wall thickness. The cylinder was in the center of a vacuum chamber of 519 mm diameter. Outside the vacuum chamber was placed, on a special holder, a detector comprised of a stack of 50 NIKFI type BK-400 pellicles measuring 5 × 10 cm. The stack was placed between two emulsion blocks 2 cm thick and was so secured that the mesons entered the stack from the end. A diagram of the experimental setup is shown in Fig. 2.

The pellicles, processed in the usual manner, were scanned under MBI-1 microscopes with magnifications 300 and 210. All π-μ decays were registered, as well as (for additional control) the terminations of the muon and pion tracks near the stopping points. To determine the background of the π^+ mesons produced in the target walls, we also registered the π^- mesons terminating in a star with one or more prongs. By tracing the

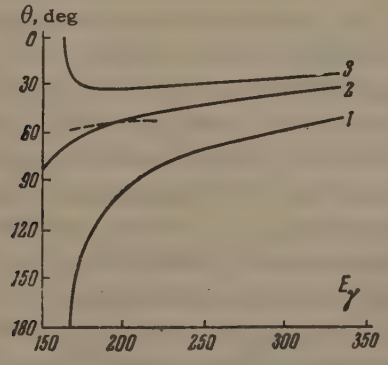

FIG. 1. Curves 1 and 3 are plots of $k\omega - kq\cos\theta = 0.7$ and $k\omega - kq\cos\theta = 1.6$. Curve 2 is the dependence of the angle of zero contribution of the nonphysical region to the dispersion integrals on the photon energy E_γ.

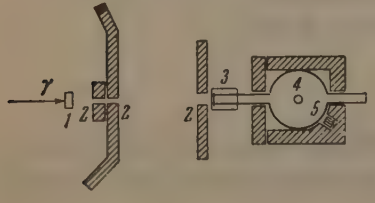

FIG. 2. Diagram of experimental setup: 1 – monitor, 2 – collimators, 3 – clearing magnet, 4 – target, 5 – pellicle stack.

Table I. Distribution of number of π^+ mesons over the photon energy intervals

E_γ interval, Mev	Number of π^+ mesons	E_γ interval, Mev	Number of π^+ mesons
164.7—169.5	403	192.0—196.6	299
169.5—173.9	329	196.6—201.3	261
173.9—178.6	357	201.3—205.7	261
178.6—183.0	319	205.7—210.2	259
183.0—187.4	287	210.2—214.8	228
187.4—192.0	319		

tracks in neighboring pellicles we were able to identify reliably each event and to eliminate the random background, and also to increase the counting efficiency. Altogether 3322 π-μ decay events and 64 π^- mesons were observed in a 340 cm^2 area.

The energy of the π^+ mesons was determined from the position of the π-μ decay in the plate. Table I lists the distribution of the number of π^+ mesons over the energy intervals. In determining the meson energy we took account of the losses in the liquid hydrogen and in the target walls. These range from 1 to 0.1 Mev, depending on the meson energy. The correction for the scattering of the meson in the emulsion did not exceed 0.1 Mev.

In the determination of the cross section, we calculated the nuclear interaction between the mesons and emulsion for each energy interval, which resulted in a correction ranging from 0 to 12.7%, and the decay in flight, which gave a correction ranging from 4.2 to 6.9%. The background due to mesons from the target walls was on the average 2%. The intensity of the photon beam was measured with a thick-wall graphite chamber. The solid angle ranged from 2.5×10^{-3} to 3.3×10^{-3} sr, depending on the interval.

The cross sections obtained are shown in Fig. 3. The errors indicated are statistical. The absolute values of the cross sections were normalized in accordance with the data of the Illinois group.[1,6]

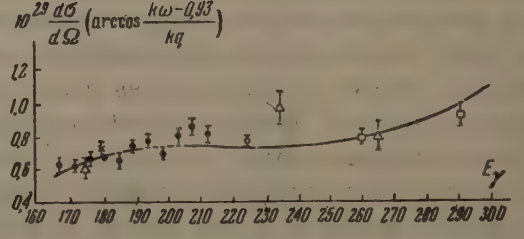

FIG. 3. Dependence of the differential cross section at an angle $\theta = \cos^{-1}(k\omega - 0.93)/kq$ on the photon energy: ● – our data, ○ – data of[2], □ – data of[3], × and Δ – data of[6].

DISCUSSION OF RESULTS

Figure 3 shows the dependence of the cross sections obtained for the photoproduction of π^+ mesons at angles $\theta = \cos^{-1}(k\omega - 0.93)/kq$ on the photon energy, and also experimental data obtained by others.[2,3,6] The solid curve is calculated by dispersion theory, with the imaginary part of the resonant amplitude taken from the experimental data (see [5]). As can be seen from the figure, the experimental data are in good agreement with the theoretical curve.

To permit a more detailed comparison of experiment with theory and to obtain the threshold value of the square of the π^+ -meson photoproduction matrix element, these data were reduced by the least squares method to determine the dependence of $\chi^{-1}d\sigma/d\Omega$ on the meson momentum, where $\chi = (q/k) \times (1 + \omega/M)^{-2}$ and M is the nucleon mass. The dependence of the square of the photoproduction matrix element $\chi^{-1}d\sigma/d\Omega$ on the square of the meson momentum q^2, calculated from dispersion theory, is represented by the solid line of Fig. 4. Generally speaking, this dependence is given by

$$\chi^{-1}d\sigma/d\Omega = A + Bq + Cq^2 + Dq^3 + \ldots \qquad (2)$$

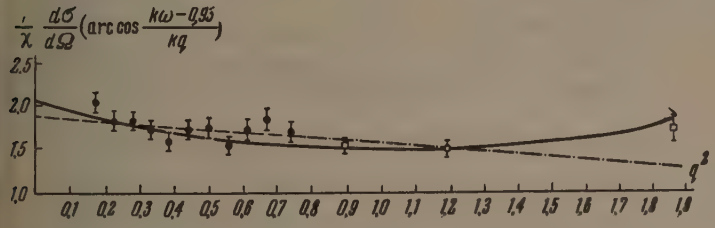

FIG. 4. Dependence of the square of the photoproduction matrix element on the square of the meson momentum.

However, for angles satisfying the relation $k\omega - kq\cos\theta = \text{const}$, this dependence simplifies to

$$\chi^{-1}d\sigma/d\Omega = a_0 + a_1q^2 + a_2q^4 + \ldots \qquad (3)$$

The coefficients a_0, a_1, a_2, etc. were determined from the experimental data by the least squares method. The expression

$$S = \sum_{i=1}^{n} p_i \left[\frac{1}{\chi_i}\frac{d\sigma_i}{d\Omega} - (a_0 + a_1q_i^2 + a_2q_i^4 + \ldots)\right]^2, \qquad (4)$$

where p_i is the weight of the i-th measurement of $\chi^{-1}d\sigma/d\Omega$, was minimized.

As a result of this analysis we obtained the following expressions

$$\frac{1}{\chi}\frac{d\sigma}{d\Omega}\left[10^{-29}\frac{\text{cm}^2}{\text{sr}}\right] = (1{,}90 \pm 0{,}15) - (0{,}34 \pm 0{,}22)\,q^2, \qquad (5)$$

$$\frac{1}{\chi}\frac{d\sigma}{d\Omega}\left[10^{-29}\frac{\text{cm}^2}{\text{sr}}\right] = (2.39 \pm 0.21) - (2.87 \pm 0.93)\,q^2 + (2{,}80 \pm 1{,}0)\,q^4, \qquad (6)$$

with almost identical Gauss criteria $S/(n - m) \approx 0.01$, where n is the number of experimental points and m is the number of parameters.

These expressions were obtained from our experimental values of q^2 in the interval from 0.17 to 0.74. In this region, both expressions describe the experimental results sufficiently well. In order to find the preferred expression, we extrapolated to the region of values $q^2 > 0.74$.

Figure 4 shows $\chi^{-1}d\sigma/d\Omega$ as a function of q^2. The dashed line shown is a plot $\chi^{-1}d\sigma/d\Omega$ vs. q^2 as obtained from (5). The extrapolation of this curve to $q^2 > 0.74$ is shown by the dash-dot line. The figure shows that the experimental data practically coincide with the theoretical values. The data of Malmberg and Robinson[2] for $q^2 = 0.89$ and of Knapp et al[3] for $q^2 = 1.18$ and 1.84 are also in good agreement with (5), and, as can be readily shown, completely disagree with (6).

For a more detailed comparison let us examine the experimental and theoretical expansions of the square of the matrix element in powers of q. It proved more convenient to represent the theoretical data in the form of an expansion

$$\left(\omega - \frac{1}{2M}\right)^3 \frac{1}{\chi}\frac{d\sigma}{d\Omega} = A_0 + A_1q^2 + A_2q^4 + \ldots \qquad (7)$$

in even powers of q. The coefficients of this expansion are listed in Table II. As can be seen from the table, the coefficients A_0 and A_1 agree very well with theory. The coefficients A_2 and A_3 are subject to large errors and it is premature to compare them with theory. Furthermore, their contribution to the square of the matrix element is small in the investigated region. The third line of Table II shows the theoretical value of the coefficients, calculated under the assumption that the dispersion integrals are equal to zero.

Thus, an investigation of the energy dependence of the cross section at an angle $\theta = \cos^{-1}(k\omega - 0.93)/kq$ yields for the square of the matrix element at the pion photoproduction threshold a value $a_0 = (1.90 \pm 0.15) \times 10^{-29}$ cm^2/sr, which agrees well with the theoretical value $a_0 = 2.04 \times 10^{-29}$ cm^2/sr. It must be emphasized that the threshold value was obtained by extrapolating the experimental data on the basis of the dispersion theory. Our theoretical premises are free of the uncertainties connected with the possible influence of the nonphysical region. In addition, the contribution of the region of high energies along the

Table II. Coefficients of the expansion of (7) in even powers of q (in units of 10^{-29} cm^2/sr)

	A_0	A_1	A_2	A_3	A_4
Experiment	1,50±0.11	2,18±0,26	0.33±0.28	—0.23±0.08	0.14±0,01
Theory, with account of the dispersion integrals	1.62	1,92	0.14	—0.69	0.10
Theory without account of the dispersion integrals	1.62	1,96	0,35	—0.18	—0.02

curve (1) is a constant. This clarifies greatly the fundamental parameters of pion physics at low energies.

Indeed, if we use the obtained threshold value a_0, the theoretical ratio $\sigma^-/\sigma^+ = 1.28$, and the difference in the pion-nucleon scattering s-phases $|\alpha_3 - \alpha_1|/q = 0.245 \pm 0.007$,[7] we obtain the following ratio of the probabilities of scattering with charge exchange and radiation capture of negative pions in hydrogen (the Panofsky ratio):

$$P = \sigma(\pi^- + p \to n + \pi^0)/\sigma(\pi^- + p \to n + \gamma) = 1{,}57 \pm 0.11.$$

The weighted mean obtained from many measurements of the directly-measured Panofsky ratio[8-13] is P = 1.54 ± 0.015. However, good agreement of the two results does not mean complete agreement with theory, for possible deviations from the theoretical amplitude may influence the threshold parameters. This is illustrated by the following example.

Using P = 1.54 ± 0.015, $|\alpha_3 - \alpha_1|/q = 0.245 \pm 0.007$, and our threshold value of the square of the matrix element for positive pions $(1.90 \pm 0.15) \times 10^{-29}$, we obtain $\sigma^-/\sigma^+ = 1.34 \pm 0.11$. The theoretical value of σ^-/σ^+ with an account of the γ-3π interaction is [14]

$$R = \frac{\sigma^-}{\sigma^+} = \frac{\{1 + \mu/2M + \mu(\mu_p + \mu_n)/2M + \lambda_1 g^{-1}[1/4(\mu_p - \mu_n) + 1/2\xi]\}^2}{\{1 - \mu/2M - \mu(\mu_p + \mu_n)/2M - \lambda_1 g^{-1}[1/4(\mu_p - \mu_n) + 1/2\xi]\}^2}, \quad (8)$$

where the coupling constant is $g^2/4\pi = 15$, μ_p and μ_n are the anomalous magnetic moments of the proton and neutron respectively, ξ is the probability of dissociation of the nucleon, and λ_1 is the effective coupling constant of the γ-3π interaction. If $\sigma^-/\sigma^+ = 1.35$, then λ_1 is positive and lies between $\lambda_1 = 0.26$ when $\xi = 0$ and $\lambda_1 = 0.17$ when $\xi = 1$. The positive sign of λ_1 agrees with the fact that the γ-3π interaction is responsible for the isoscalar part of the electromagnetic form factor of the nucleon.[14] Thus, further study of the threshold parameters can yield interesting information on the influence of pion-pion interaction.

Unfortunately, the experimental data obtained do not enable us to calculate the photoproduction amplitudes and to compare them with theory. This is due both to the insufficient accuracy of the experimental data and to the complexity of the equations for the amplitudes. We have attempted to determine the amplitudes from our experiments, using the angular distribution of the pions at a photon energy 185 Mev.[1]

According to the theory, the differential cross section of pion photoproduction has the following dependence on the photoproduction amplitudes

$$d\sigma/d\Omega = (q/k)\{|F_1|^2 + |F_2|^2 - 2\mathrm{Re}\, F_1^* F_2 \cos\theta + \tfrac{1}{2}\sin^2\theta[|F_3|^2 + |F_4|^2 + 2\mathrm{Re}\, F_2^* F_3 + 2\mathrm{Re}\, F_1^* F_4 + 2\mathrm{Re}\, F_3^* F_4 \cos\theta]\}, \quad (9)$$

where we have for the region near threshold

$$F_1 = \sqrt{2}F_{10} - \sqrt{2}F_{11}\cos\theta, \qquad F_2 = \sqrt{2}F_{20},$$
$$F_3 = \sqrt{2}F_{30} + \sqrt{2}F_{31}/(1 - \beta\cos\theta),$$
$$F_4 = \sqrt{2}F_{41}/(1 - \beta\cos\theta);$$

β — velocity of the pion. It follows from these formulas that if we have experimental data for 0 and 180° we can determine the amplitude F_{10} and the sum of the amplitudes $F_{11} + F_{20}$.

Using our data[1] for 15° and 165° in the c.m.s., we obtain the following two sets of solutions for 185 Mev photon energy

$$(F_{10})_1 = (1{,}81 \pm 0{,}034)\cdot 10^{-2},$$
$$(F_{11} + F_{20})_1 = -(0{,}105 \pm 0{,}034)\cdot 10^{-2},$$
$$(F_{10})_2 = -(1{,}81 \pm 0{,}034)\cdot 10^{-2},$$
$$(F_{11} + F_{20})_2 = (0{,}105 \pm 0{,}034)\cdot 10^{-2}.$$

In addition to the indicated errors, we must also take into account an uncertainty on the order of 5% due to the presence of the term with $\sin^2\theta$. Theo-

retically, $F_{10} = 1.92 \times 10^{-2}$ and $(F_{11} + F_{20}) = 0.110 \times 10^{-2}$. The value of F_{10}, determined from the coefficient a_0 in the expansion of $\chi^{-1}d\sigma/d\Omega$ in powers of q, is $\pm(1.85 \pm 0.074) \times 10^{-2}$. If we confine ourselves only to positive F_{10}, we find that the sign of $F_{11} + F_{20}$ is the opposite of the theoretical value. An analogous conclusion follows also from the analysis of other experimental angular distribution data.[3,4,6]

Figure 5 shows the dependence of the coefficient B_0 of $\cos\theta$ in the angular distribution of the photomesons. The coefficient B_0 was calculated from the formula

$$B_0 = 2\beta[\beta(B+D) + A + C + E]/(1-3\beta^2), \quad (10)$$

where A, B, C, D, and E are the coefficients in the expansion

$$(1-\beta\cos\theta)^2 d\sigma/d\Omega = A + B\cos\theta + C\cos^2\theta + D\cos^3\theta + E\cos^4\theta,$$

obtained by reducing the experimental data by the method of least squares.[15] At photon energies $E_\gamma < 230$ Mev, we have $B_0 \sim -4F_{10}(F_{11} + F_{20})$.

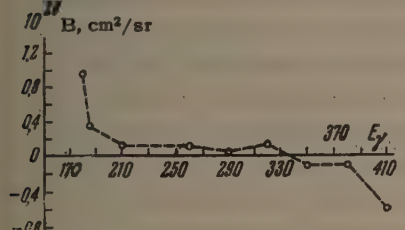

FIG. 5. Dependence of the coefficient B_0 on the photon energy E_γ.

As can be seen from the plot, B_0 is positive up to $E_\gamma = 330$ Mev, passes through zero at 330 Mev, and becomes negative when $E_\gamma > 330$ Mev. The positive value of B_0 at low energies indicates that the sum $F_{11} + F_{20}$ is a negative quantity. As was already mentioned, the theoretical value of this quantity remains positive. To be sure, it must be noted that the coefficient B_0 is subject to a very large statistical error (which reaches 200% in some cases). Disregarding the errors, so interesting a conclusion should stimulate an exhaustive study of the angular distributions of π^+ mesons near threshold ($E_\gamma < 230$ Mev).

More accurate experiments near threshold will permit in the future a more detailed comparison between experiment and theory and hence determine the pion photoproduction amplitudes.

In conclusion the authors are grateful to Prof. P. A. Cerenkov for interest in the work, to A. M. Baldin and A. I. Lebedev for valuable hints in the discussion of the results. The authors are also grateful to the entire synchrotron crew and particularly to Engineer A. A. Svetlov.

[1] Adamovich, Gorzhevskaya, Larionova, Panova, Popova, Kharlamov, and Yagudina, Tenth Rochester Conference, 1961.

[2] J. H. Malmberg and C. S. Robinson, Phys. Rev. 109, 158 (1958).

[3] Knapp, Kenney, and Perez-Mendez, Phys. Rev. 114, 605 (1959).

[4] A. M. Baldin and B. B. Govorkov, DAN SSSR 127, 993 (1959), Soviet Phys. Doklady 4, 851 (1960).

[5] A. M. Baldin, JETP 39, 1151 (1960), Soviet Phys. JETP 12, 800 (1961).

[6] Beneventano, Bernardini, Carlson-Lee, Stoppini, and Tau, Nuovo cimento 4, 323 (1956).

[7] J. Hamilton and W. S. Woolcock, Phys. Rev. 118, 291 (1960).

[8] Cassels, Fidecaro, Wetherell, and Wormald, Proc. Phys. Soc. A70, 405 (1957).

[9] Kuehner, Morrison, and Tornabene, Proc. Phys. Soc. 73, 545 (1959).

[10] E. L. Koller and A. M. Sachs, Phys. Rev. 116, 760 (1959).

[11] N. P. Samios, Phys. Rev. Lett. 4, 470 (1960).

[12] Derrick, Fetkovich, Fields, and Deahl, Phys. Rev. Lett. 5, 230 (1960).

[13] Dunaitsev, Pantuev, Prokoshkin, Tang, and Khachaturyan, Proc. 1960 Ann. Intern. conf. on High Energy Physics at Rochester, Publ. Univ. Rochester, 1961, p. 181.

[14] Kawaguchi, Miyamoto, and Fujii, Nuovo cimento 20, 408 (1961).

[15] M. J. Moravcsik, Phys. Rev. 107, 600 (1957).

Translated by J. G. Adashko
308

NEUTRINO PRODUCTION IN THE ATMOSPHERE

G. T. ZATSEPIN and V. A. KUZ'MIN

P. N. Lebedev Physics Institute, Academy of Sciences, U.S.S.R.

Submitted to JETP editor March 8, 1961

J. Exptl. Theoret. Phys. (U.S.S.R.) 41, 1818-1827 (December, 1961)

The energy spectra and angular distribution of neutrinos produced in the atmosphere in the $\pi \to \mu + \nu$ and $\mu \to e + \nu + \bar{\nu}$ decays are calculated taking the μ-meson energy losses at neutrino energies $\varepsilon = 10^9 - 3 \times 10^{11}$ ev into account. It is shown that the neutrino flux from the $\mu \to e + \nu + \bar{\nu}$ decay is comparable with that from the $\pi \to \mu + \nu$ decay. μ-meson energy losses only weakly affect neutrino production. K mesons produce neutrinos more efficiently than do π mesons. An experimental arrangement for detecting high-energy cosmic ray neutrinos is proposed.

1. INTRODUCTION

CONSIDERABLY increased attention has recently been given to possible experiments on the detection of neutrinos in cosmic rays.[1-5] This interest is due primarily to the possible investigation of weak interactions at high energies, and to the possibility of finding an explanation to a number of basic theoretical questions (the behavior of the weak interaction cross section with increasing energy,[4-6] the existence of an intermediate vector meson responsible for weak interactions, the existence of two pairs of neutral leptons: muonic and electronic,[7,6] etc.). On the other hand, cosmic-ray neutrino experiments open a new approach to a number of astrophysical problems.

The main object of the investigation in the underground cosmic-ray neutrino experiment as proposed by Markov, and in a modified form by us,[8] are the neutrino-nucleon reactions of the type

$$\nu + N \to N' + \mu,$$
$$\nu + N \to N' + \mu + n\pi \qquad (1)$$

(where N denotes a baryon). This is so because the cross sections of these processes are considerably larger than the cross sections of lepton-lepton interactions[6,9,4] and because of the remarkable interaction properties of the μ meson.[4,5] The character of the energy dependence of the interaction cross section of neutrinos with nucleons may vary with the transferred momentum corresponding to the nucleon size $\hbar/M_N c$. The study of interactions at neutrino energies $\varepsilon \gtrsim 1$ Bev is therefore of special interest.

The neutrino flux in cosmic rays consists basically of two components of different origin. One comprises the truly cosmic neutrinos, i.e., those coming to earth from outer space, of galactic or metagalactic origin. The other component comprises the neutrinos produced by cosmic rays in the atmosphere of the earth. If we make the natural assumption that the "intrinsic" high-energy neutrinos are due to cosmic rays only, then their intensity should be of the same order of magnitude as the intensity of photons of corresponding energies incident upon the earth from outer space (if we neglect the proton absorption processes). Up to now, photons have not been found in the primary cosmic radiation, and the upper limit of the acceptable flux obtained by the Bristol group[10] amounts to 10^{-3} of the cosmic-ray particle intensity. The possible flux of photons and neutrinos calculated from commonly accepted astro-physical values turns out to be two orders of magnitude lower.[3] As has been shown by our calculations, the flux of atmospheric high-energy neutrinos amounts to $\sim 10^{-1}$ of the intensity of primary cosmic rays, i.e., three orders of magnitude greater than the expected flux of intrinsic cosmic neutrinos. Therefore, if we do not take various far-reaching hypotheses[11] into consideration, we can suppose that in the experiment on cosmic-ray neutrinos we shall have to deal with neutrinos of atmospheric origin.

The atmospheric neutrinos are convenient for experiments devoted to the study of high-energy weak interactions, since their energy spectrum and angular distributions in the atmosphere can be calculated very exactly. This permits us to calculate the spectrum and angular distribution of the detected products of neutrino reactions with matter in the apparatus for each variant of the theory. Any deviations can be observed and interpreted. The low intensity, which imposes difficult requirements

upon the experiment is, however, a drawback.

The estimate of the flux of atmospheric neutrinos from the $\pi \to \mu + \nu$ decay was carried out by Markov and Zheleznykh.[5] Exact calculations of the neutrino spectrum have not been carried out so far. We have calculated the spectrum of neutrinos from the $\pi \to \mu + \nu$ and $\mu \to e + \nu + \bar{\nu}$ decays, taking into account the energy losses of μ mesons and the angular distributions of neutrino flux in the atmosphere. The calculation carried out gives higher neutrino fluxes than the earlier estimates, and therefore supports the optimistic conclusions of Markov and Zheleznykh[4,5] on the feasibility of the experiments with high-energy cosmic-ray neutrinos.

2. NEUTRINOS FROM PION DECAY

Pions produced in the collisions of primary radiation with air nuclei produce both μ mesons and neutrinos in their decay. The energy spectrum of such neutrinos can easily be calculated from the π-meson spectrum, and, in the case where the μ mesons are produced only by π mesons, is determined without ambiguity by the well-known μ-meson spectrum.

Let us consider the one-dimensional problem, assuming that all secondary particles conserve the direction of the primary ones. The path x of the particles is measured in mass units and is calculated from the top of the atmosphere. Let $P^{\pi}(x, E, \theta)$ be the π-meson spectrum at the depth x at a zenith angle θ. The function of the neutrino source is then given by the expression

$$G_{\pi}^{\nu}(x, \varepsilon, \theta) = \int_{E_{min}(\varepsilon)}^{E_{max}(\varepsilon)} [l_{\pi}(E)\, \rho(x, \theta)]^{-1} P^{\pi}(x, E, \theta)\, D_{\pi\nu}(E, \varepsilon)\, dE, \quad (2)$$

where ε is the neutrino energy, $l_{\pi}(E)$ is the linear decay mean free path of a π meson with energy E, $\rho(x, \theta)$ is the air density, and $D_{\pi\nu}(E, \varepsilon)d\varepsilon$ is the spectrum of neutrinos originating from the decay of π mesons with energy E in the laboratory system (l.s.). The values E_{min} and E_{max} and the function $D_{\pi\nu}(E, \varepsilon)$ are found from the kinematics of the $\pi \to \mu + \nu$ decay:

$$E_{min} = \varepsilon (1 - m^2/M^2)^{-1}, \quad E_{max} = \infty,$$

$$D_{\pi\nu}(E, \varepsilon)\, d\varepsilon = d\varepsilon\, [E (1 - m^2/M^2)]^{-1} \text{ for } (M/E)^2 \ll 1,$$

where m and M are the masses of the μ and π mesons, respectively.

The spectrum $P^{\pi}(x, E, \theta)$ and the function $G_{\pi}^{\nu}(x, \varepsilon, \theta)$ are calculated as described in the previous article.[12] By integrating the function $G_{\pi}^{\nu}(x, \varepsilon, \theta)$ over the depth x, we find the neutrino spectrum:

$$P_{\pi}^{\nu}(x, \varepsilon, \theta) = (1 - e^{-x})\, F^{\nu}(\varepsilon, \theta) \approx \frac{I_{\pi} A_{\pi\nu} \varepsilon^{-(\gamma+1)}}{1 + 3.28\, \varepsilon / E_{\pi}(\theta)} (1 - e^{-x}),$$

$$F^{\nu}(\varepsilon, \theta) = \frac{I_{\pi}}{1 - m^2/M^2} \int_{\varepsilon (1 - m^2/M^2)^{-1}}^{\infty} \frac{E^{-(\gamma+2)}\, dE}{1 + E/E_{\pi}(\theta)},$$

$$A_{\pi\nu} = \frac{1}{1+\gamma} \left(1 - \frac{m^2}{M^2}\right)^{\gamma}, \quad (3)$$

where x is expressed in the units of λ (interaction mean free path of π mesons), I_{π} is the intensity of π-meson production at E = 1 (energy expressed in Bev), γ is the exponent of the integral production spectrum of the π mesons, and $E_{\pi}(\theta)$ is the critical π-meson energy for which the decay probability of a π meson at the depth x = 1 is equal to the probability of nuclear interaction. The quantity $E_{\pi}(\theta)$ was calculated earlier.[12] To simplify the calculations, we have assumed $\lambda = \lambda_n$, where λ_n is the absorption mean free path in the atmosphere of the π-meson producing component; according to experimental data, $\lambda_n = 120$ g/cm^2.

At sea level, ($x \gg 1$), the vertical-flux spectrum can be approximated by the function (in units of $cm^{-2} sec^{-1} sr^{-1} Bev^{-1}$)

$$I\, P_{\pi}^{\nu}(\varepsilon, 0)\, d\varepsilon = \begin{cases} 1.85 \cdot 10^{-2} (0.08 + \varepsilon)^{-2.80}\, d\varepsilon, & 1 \leqslant \varepsilon \leqslant 10 \\ 6.65 \cdot 10^{-2} (1.1 + \varepsilon)^{-3.22}\, d\varepsilon, & 10 \leqslant \varepsilon \leqslant 300 \end{cases}. \quad I \quad (4)$$

The total neutrino flux with energy >1 Bev is equal to $P_{\pi}^{\nu}(>1.0) = 8.9 \times 10^{-3}\, cm^{-2} sec^{-1} sr^{-1}$. In the article of Zheleznykh and Markov,[4] this flux was found to be $4 \times 10^{-3}\, cm^{-2} sec^{-1} sr^{-1}$. Equation (3) permits us to calculate the angular distributions in the atmosphere of the neutrinos from the $\pi \to \mu + \nu$ decay.

3. NEUTRINOS ORIGINATING IN MUON DECAY

Muons also contribute to the flux of atmospheric neutrinos. Owing to the large path traversed by μ mesons in the atmosphere, and the large energy fraction transferred in their decay to the neutrinos, muons, in spite of their long lifetime, produce a neutrino flux comparable to that from the $\pi \to \mu + \nu$ decay. The spectrum of neutrinos and antineutrinos from the $\mu^{\pm}$ meson decay is found by integrating the neutrino source function $G_{\mu}^{\nu}(x, \varepsilon, \theta)$ for the $\mu \to e + \nu + \bar{\nu}$ decay over x.

The function $G_{\mu}^{\nu}(x, \varepsilon, \theta)$ is constructed similarly to the function (2), provided the μ-meson spectrum $P^{\mu}(x, E, \theta)$ is known:

$$G_\mu^\nu(x, \varepsilon, \theta) = \int_{E_{min}(\varepsilon)}^{E_{max}(\varepsilon)} [l_\mu(E)\,\rho(x,\theta)]^{-1} P^\mu(x, E, \theta)\, R_{\mu\nu}(E, \varepsilon)\, dE, \quad (5)$$

$$R_{\mu\nu}(E, \varepsilon,) = R_{\mu\nu}^{(-)}(E, \varepsilon) + R_{\mu\nu}^{(+)}(E, \varepsilon), \quad (6)$$

where $l_\mu(E)$ is the decay mean free path of μ mesons with energy E; $R_{\mu\nu}^{(-)}(E, \varepsilon)d\varepsilon$ and $R_{\mu\nu}^{(+)}(E, \varepsilon)d\varepsilon$ are the neutrino spectra from the decay of μ^- and μ^+ mesons with energy E, respectively, in the l.s.

From the decay kinematics, we find the values of $E_{min}(\varepsilon)$ and $E_{max}(\varepsilon)$:

$$E_{min} = \varepsilon, \qquad E_{max} = \infty \quad \text{for } (m/E)^2 \ll 1.$$

The spectra $R_{\mu\nu}^{(-)}(E, \varepsilon)$ and $R_{\mu\nu}^{(+)}(E, \varepsilon)$ are calculated in the Appendix [Eqs. (18) and (19)]. For antineutrinos we have $R_{\mu\bar\nu}^{(-)} = R_{\mu\nu}^{(+)}$ and $R_{\mu\bar\nu}^{(+)} = R_{\mu\nu}^{(-)}$.

The expression for the spectrum $P_\mu^\nu(x, \varepsilon, \theta)$ can be conveniently written in the form:

$$P_\mu^\nu(x, \varepsilon, \theta) = \int_\varepsilon^\infty P_d^\mu(x, E, \theta)\, R_{\mu\nu}(E, \varepsilon)\, dE, \quad (7)$$

where

$$P_d^\mu(x, E, \theta) = \int_0^x [l_\mu(E)\,\rho(t, \theta)]^{-1} P^\mu(t, E, \theta)\, dt \quad (8)$$

represents the total number of μ mesons which decayed while moving in the atmosphere at a zenith angle θ between the top of the atmosphere and the level x, and which had an energy E at the moment of decay.

A general expression for the μ-meson spectrum $P^\mu(x, E, \theta)$ was obtained by us earlier [12] taking the decay and the energy loss of μ mesons in a spherical atmosphere into account. For the neutrino spectrum at energies $\varepsilon \lesssim 10^{11}$ ev, the expression simplifies somewhat since we can restrict ourselves to ionization losses only (see Fig. 1). $P^\mu(x, E, \theta)$ is then of the form

$$P^\mu(x, E, \theta) = I_\pi A_{\pi\mu} E^{-(\gamma+1)} \int_0^x e^{\mu - t}\left[1 + \frac{\beta}{E}(x - t)\right]^{-(\gamma+1)} \times \left\{1 + \frac{1{,}22E}{E_\pi(\theta)}\left[1 + \frac{\beta}{E}(x - t)\right]\right\}^{-1} dt, \quad (9)$$

where

$$A_{\pi\mu} = \frac{1 - (m/M)^{2(\gamma+1)}}{(1+\gamma)(1 - m^2/M^2)}, \qquad \mu = \frac{mc}{\tau_{0\mu}} \int_x^t \frac{dz}{\rho(z, \theta)\,[E + \beta(x - z)]}, \quad (9a)$$

and β is the ionization energy loss of the μ mesons per unit path. For angles $0.1 < \cos\theta \leq 1$, the atmosphere can, with sufficient accuracy, be regarded as flat, so that $\rho(x, \theta) = h_0^{-1} x \cos\theta$ (h_0 is the height of the homogeneous atmosphere) and

$$e^\mu = (t/x)^\delta [1 + (\beta/E)(x - t)]^{-\delta},$$

$$\delta = mch_0/\tau_{0\mu}[E + \beta x]\cos\theta = h_0/l_\mu(E + \beta x)\cos\theta. \quad (9b)$$

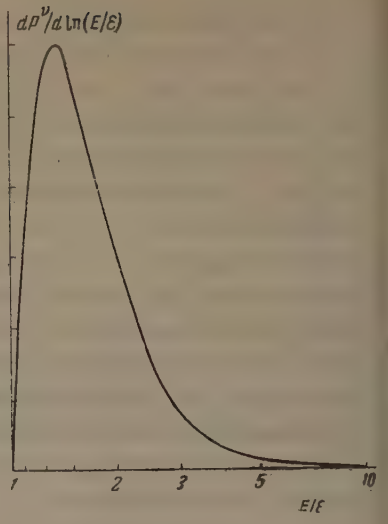

FIG. 1. Contribution of μ mesons of different energies to the flux of neutrinos with energy ε.

Substituting (9) and (8) and integrating numerically, we obtained the function $P_d^\mu(x, E, \theta)$. Using relation (7), we then found the spectrum and the angular distribution in the atmosphere of neutrinos from the $\mu \to e + \nu + \bar\nu$ decay, taking the energy loss of the μ mesons into account.

If we neglect the μ-meson energy loss, i.e., if we set $\beta = 0$, then ($x \gg 1$)

$$P_d^\mu(x, E, \theta) = \{1 - \exp[-L(x, x_{eff}, \theta)/l_\mu(E)] \times \Gamma(1 + \delta)\}\, F_1^\mu(E, \theta), \quad (10)$$

where $L(x, x_{eff}, \theta)$ is the effective linear path traversed by the μ mesons in a spherical atmosphere from the point of production to sea level. The values of $L(x, x_{eff}, \theta)$ for various θ and the function F_1^μ have been found earlier.[12] $\Gamma(z)$ is the gamma function.

Substituting (10) into (7) we find $P_\mu^\nu(x, \varepsilon, \theta)$. The calculated spectrum is found to differ little from the neutrino spectrum calculated with account of the energy loss of the μ mesons. The losses lead to a neutrino flux decrease that is small and varies little with energy. The role of the losses determined by the factor $1 - P^\nu/P^\nu$ (without loss) varies from ~25% for neutrino energy $\varepsilon = 1$ Bev to ~12% for $\varepsilon = 100$ Bev.

Since anyway the role of the losses varies little with increasing zenith angle θ, the angular distributions calculated with and without account of the energy loss differ little. The angular distribution in the atmosphere of neutrinos from the $\pi \to \mu + \nu$ and $\mu \to e + \nu + \bar\nu$ decays is shown in Fig. 2.

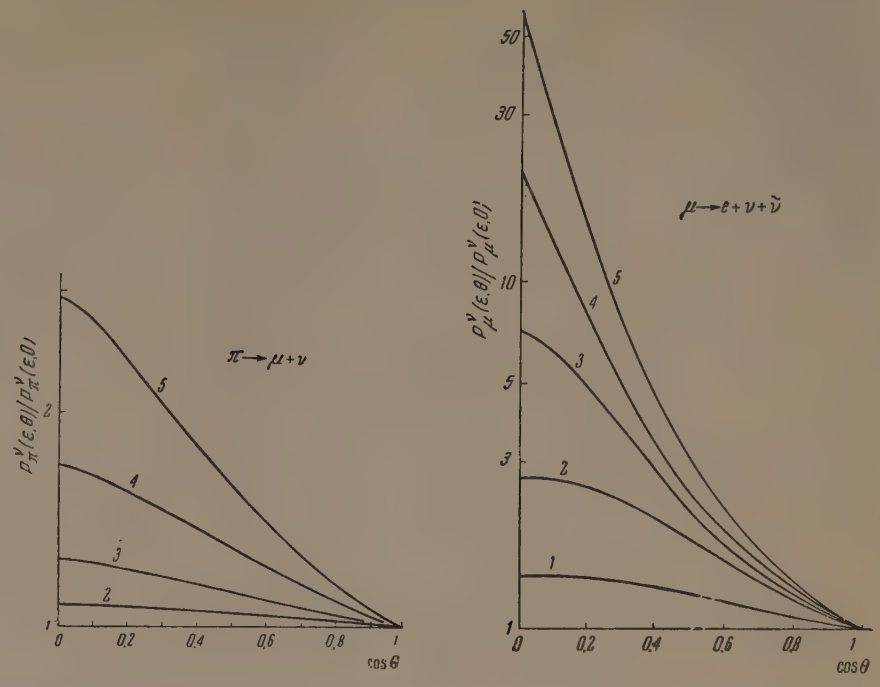

FIG. 2. Distributions of neutrinos of different energies in the atmosphere for the two production mechanisms: curve 1 – $\varepsilon = 1 \times 10^9$ ev, curve 2 – $\varepsilon = 3 \times 10^9$ ev, curve 3 – $\varepsilon = 1 \times 10^{10}$ ev, curve 4 – $\varepsilon = 3 \times 10^{10}$ ev, curve 5 – $\varepsilon = 1 \times 10^{11}$ ev.

The neutrino spectrum from the μ-meson decay, with account of the μ-meson energy loss in the vertical flux at sea level is approximated by the function (in units of $cm^{-2}\,sec^{-1}\,sr^{-1}\,Bev^{-1}$)

$$P_\mu^\nu(\varepsilon, 0)\,d\varepsilon = \begin{cases} 7{,}65\cdot10^{-2}\,(0{,}37+\varepsilon)^{-3{,}75}\,d\varepsilon, & 1 \leqslant \varepsilon \leqslant 10 \\ 1{,}48\,(3{,}5+\varepsilon)^{-4.51}\,d\varepsilon, & 10 \leqslant \varepsilon \leqslant 100 \end{cases} \quad (11)$$

(we do not differentiate here between muonic and electronic neutrinos). The total neutrino flux with energy greater than 1 Bev is equal to

$$P_\mu^\nu(>1.0) = 1.17\cdot10^{-2}\ cm^{-2}\,sec^{-1}\,sr^{-1}.$$

The total spectrum of the neutrinos from the decay of π and μ mesons $P^\nu = P_\pi^\nu + P_\mu^\nu$ in the vertical flux is approximated by the function (in the same units)

$$P^\nu(\varepsilon, 0)\,d\varepsilon = \begin{cases} 6{,}0\cdot10^{-2}\,(0.15+\varepsilon)^{-3{,}15}\,d\varepsilon, & 1 \leqslant \varepsilon \leqslant 10 \\ 0{,}12\,(0{,}9+\varepsilon)^{-3{,}34}\,d\varepsilon, & 10 \leqslant \varepsilon \leqslant 300. \end{cases} \quad (12)$$

The total flux of neutrinos with energy greater than 1 Bev is then

$$P^\nu(>1.0) = 2.06\cdot10^{-2}\ cm^{-2}\,sec^{-1}\,sr^{-1}.$$

The spectra of electronic ν_e and muonic ν_μ neutrinos are given by the relations

$$P_{\nu_e} = P_\mu^\nu/2, \qquad P_{\nu_\mu} = P_\pi^\nu + P_\mu^\nu/2.$$

The energy spectra of neutrinos in the vertical and horizontal flux are shown in Fig. 3. The angular distribution in the atmosphere of the total neutrino flux from the $\pi \to \mu + \nu$ and $\mu \to e + \nu + \bar{\nu}$ decays is shown in Fig. 4.

So far we have always had the total flux of neutrinos and antineutrinos in mind when speaking about neutrinos. Moreover, it was not necessary to take the positive excess of π and μ mesons in the atmosphere into account, and $P^\pi(x, E, \theta)$ and $P^\mu(x, E, \theta)$ denoted the total intensity of mesons of both signs. In order to calculate the partial intensity of ν and $\bar{\nu}$, it is necessary to define $P^\pi(x, E, \theta)$ and $P^\mu(x, E, \theta)$ as the spectrum of mesons of one sign. To calculate the spectrum of electronic or muonic neutrinos and antineutrinos from the $\mu \to e + \nu + \bar{\nu}$ decay, it is also necessary to use the function $R_{\mu\nu}^{(+)}$ of the form (19) or $R_{\mu\nu}^{(-)}$ from Eq. (18) instead of $R_{\mu\nu}$ from Eq. (6). Thus, say for electronic neutrinos, the expression (7) will now have the form

$$P_{\nu_e}(x, \varepsilon, \theta) = \int_0^\infty P_d^{\mu(+)}(x, E, \theta)\ R_{\mu\nu}^{(+)}(E, \varepsilon)\,dE. \quad (13)$$

Using this expression, let us estimate the spectrum of electronic neutrinos and antineutrinos $k_\nu(\kappa)$ and $k_{\bar{\nu}}(\kappa)$ determined by the relations

$$P_\nu(\varepsilon) = k_\nu(\varkappa)\,P_d^{\mu(+)}(\varepsilon), \quad P_{\bar{\nu}}(\varepsilon) = k_{\bar{\nu}}(\varkappa)\,P_d^{\mu(-)}(\varepsilon),$$

where κ is the exponent of the integral spectrum of decaying $\mu^+(\mu^-)$ mesons. For simplicity, let us write

$$P_d^{\mu(+)}(E) = P_d^{\mu(-)}(E) = AE^{-(\varkappa+1)}.$$

Substituting $R_{\mu\nu}^{(+)}$ from Eq. (19) and $R_{\mu\nu}^{(-)}$ from Eq. (18) into (13) for ν_e and $\bar{\nu}_e$ respectively, we find

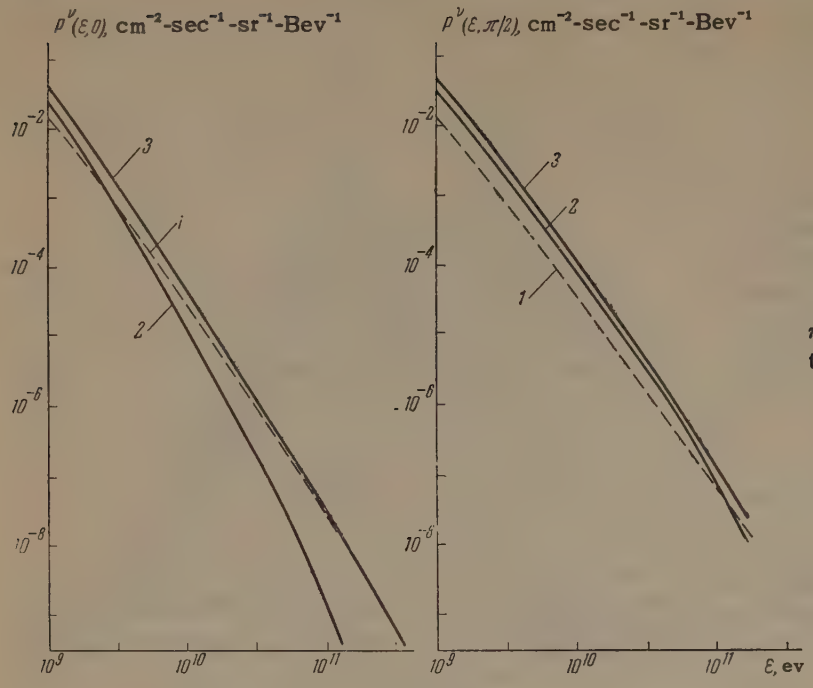

FIG. 3. Different energy spectra of neutrinos from $\pi \to \mu + \nu$ (curve 1) and $\mu \to e + \nu + \bar{\nu}$ (curve 2) and the total spectrum (curve 3) for the angle $\theta = 0$ and $\theta = \pi/2$.

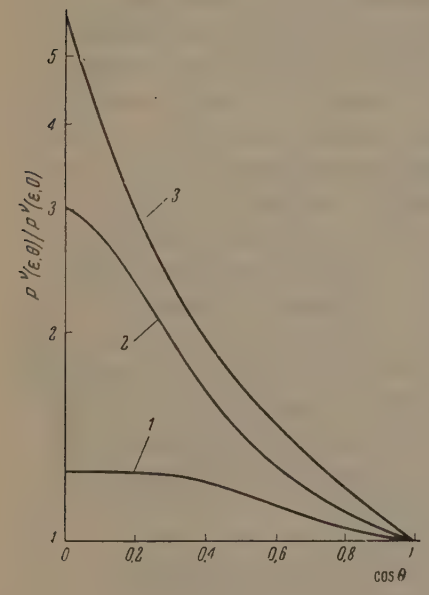

FIG. 4. Angular distribution in the atmosphere of the total neutrino flux from the $\pi \to \mu + \nu$ and $\mu \to e + \nu + \bar{\nu}$ decays at neutrino energies 1 – $\varepsilon = 1 \times 10^{9}$ ev, curve 2 – $\varepsilon = 1 \times 10^{10}$ ev, curve 3 – 1×10^{11} ev. The curves are normalized to the intensity of the vertical flux.

$$k_{\nu}(\varkappa) = \frac{5}{3}\frac{1}{\varkappa+1} - \frac{3}{\varkappa+3} + \frac{4}{3}\frac{1}{\varkappa+4},$$

$$k_{\bar{\nu}}(\varkappa) = 2\left(\frac{1}{\varkappa+1} - \frac{3}{\varkappa+3} + \frac{2}{\varkappa+4}\right).$$

For $\kappa = 2$, the ratio $k_{\nu}/k_{\bar{\nu}}$ amounts to $4/3$. This means that, replacing the quantity $R_{\mu\nu}$ in Eq. (7) by, say $2R^{(-)}_{\mu\nu}$, the flux of neutrinos and antineutrinos (electric and muonic) will increase by 2/1.75 times, i.e., by 14%.

It should be noted that we have neglected the polarization of cosmic-ray μ mesons. Taking the polarization into account increases the neutrino intensity from μ-meson decay by ~5%.

4. NORMALIZATION OF THE NEUTRINO SPECTRA

The neutrino spectra from the π and μ meson decay were normalized to experimental spectra of the μ mesons at sea level.[13,14] For this, we have calculated the spectrum of the μ mesons at sea level taking into account the decay and energy loss of the μ mesons according to Eqs. (9) and (9b) for different values of γ and I_{π}.

For $I_{\pi} = 0.159$ cm^{-2}sec^{-1}sr^{-1}Bev^{-1} and for $\gamma = 1.62$, the calculated spectrum of the μ mesons agrees with the experimental results within the errors of the experiment in the 10^{9}–10^{12} ev energy range. It should be noted that the values of I_{π} and γ chosen are close to those obtained by Paine, Davison, and Greisen;[13] $I_{\pi} = 0.156$ cm^{-2}sec^{-1}sr^{-1} Bev^{-1}, $\gamma = 1.64$.

5. DISCUSSION OF RESULTS

The above calculations show that the $\pi \to \mu + \nu$ $\mu \to e + \nu + \bar{\nu}$ decays produce comparable neutrino fluxes. Account of the energy loss by the μ mesons causes little change in the intensity of the neutrino flux from the $\mu \to e + \nu + \bar{\nu}$ decay. The neutrino fluxes in the atmosphere are anisotropically distributed, and the degree of anisotropy $P^{\nu}(\varepsilon, \pi/2)/P^{\nu}(\varepsilon, 0)$ increases with increasing neutrino energy, tending to about 10 for the $\pi \to \mu + \nu$ decay[12] and to 10 $L(x, x_{eff}, \pi/2)/L(x, x_{eff}, 0)$ ~300 for the $\mu \to e + \nu + \bar{\nu}$ decay for $\varepsilon \gg 10^{12}$ ev. For the neutrino energies under consideration,

$\varepsilon = 10^9 - 10^{11}$ ev, the angular distributions of the total neutrino flux from the $\pi \to \mu + \nu$ and $\mu \to e + \nu + \bar{\nu}$ decay are close to the distributions of the neutrino flux from the π-meson decay. Since the neutrinos of energies under consideration traverse the whole earth without absorption (the absorption cross section $\sigma \ll \sigma_{critical} \sim 10^{-34}$ cm^2/nucleon), the angular distribution of neutrino fluxes from the lower hemisphere are identical to the distributions from the upper hemisphere at every point on the earth's surface:

$$P^{\nu}(\varepsilon, \theta) = P^{\nu}(\varepsilon, \pi - \theta).$$

We have assumed in the calculations that all secondary particles conserve the direction of motion of the primary ones. Such an assumption is acceptable since, at low neutrino energies $\varepsilon \sim 1$ Bev, their fluxes (both from π- and μ-meson decays) are distributed in the atmosphere quasi-isotropically, and at high energies, $\varepsilon \gtrsim 10$ Bev, the angle of emission of particles in the l.s. is small.

It should be noted that the results of calculations of the neutrino spectrum are practically independent of the arbitrarily chosen value λ for normalization of the spectra according to the experimental data on the μ-meson spectrum. In fact, the function $f(x, E, \theta) = P^{\pi}(x, E, \theta)/L_{\pi}(E)\rho(x, \theta)$ determines the number of π mesons with energy E which decay per unit path length at the depth x. Since the parameters I_{π} and γ determining the function $f(x, E, \theta)$ are chosen for a match between the calculated and observed μ-meson spectrum, $f(x, E, \theta)$ is fixed and independent of the choice of λ. The neutrino spectra are therefore calculated very accurately, even though the auxiliary function $P^{\pi}(x, E, \theta)$, when substituting λ for λ', is determined with a relative error of the order $\lambda/\lambda'(1 + E_{\pi}/E)$.

The inaccuracy in calculating the neutrino spectrum is thus mainly due to the indeterminacy of the contribution of K mesons to the neutrino flux. K mesons produce neutrinos more efficiently than π mesons since the energy distribution between the neutrino and the μ meson is more favorable for the neutrino ($E_{\nu}/E_{\mu} \approx 0.91$ for the $K \to \mu + \nu$ and 0.30 for the $\pi \to \mu + \nu$ decay), and because of the shorter lifetime and the higher mass of the K mesons. Thus, if the fluxes of the μ mesons with energies ~1 Bev from the $K \to \mu + \nu$ and $\pi \to \mu + \nu$ decays are equal, the neutrino flux of the same energies from K mesons will be roughly six times greater than from π mesons. A neutrino with an energy of ~100 Bev is produced by K mesons roughly 11 times more efficiently. This means that there is a ten percent contribution of K mesons to the μ-meson flux of ~100 Bev energy, so that the neutrino flux of corresponding energies increased by a factor of two. Unfortunately, the experimental data available so far do not permit us to determine the contribution of K mesons to the neutrino flux. The accuracy of the data is such that it permits a contribution of the order of several tens percent to the neutrino flux of K mesons even in the energy range of ~1 Bev, not considering higher energies. At any rate, it is clear that, by assuming the π mesons to be the only source of the μ mesons, we do not overestimate the neutrino flux.

The results obtained show that the total vertical flux of neutrinos with energy greater than 1 Bev from the π and μ meson decays in the atmosphere is five times greater than the estimate of Zheleznykh and Markov,[4] which took only the $\pi \to \mu + \nu$ decay into account. This fact, and an account of the increase of the flux for inclined directions, increases the possibility of detecting μ mesons from reaction (1).

It is necessary to mention here the experimental setup for the detection of events of the type (1). We assume that to observe μ mesons produced by neutrinos [in particular in reactions of type (1)] it is not practical to construct arrays with fixed reaction volume.[3,4] As has been shown by Zheleznykh and Markov, in fixed-volume arrays of reasonable dimensions the main part of the μ mesons come from the outside, i.e., are spurious. It is, therefore, necessary to use an array that detects μ mesons produced only below it and is based on the measurement of the delay in the signals produced by μ mesons traversing three rows of scintillators.

The proposed array is schematically shown in Fig. 5. Here 1, 2, and 3 denote mosaic layers of scintillation counters placed at a sufficient distance from each other, by means of which we can fix the trajectory of the μ meson traversing the array and measure the relative delay times; this enables us to separate the mesons arriving from the lower hemisphere. Absorber a, whose total

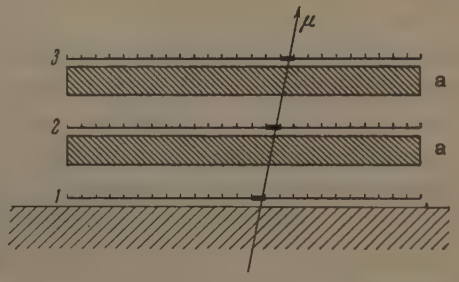

FIG. 5. Array for the detection of events of type (1) produced by neutrinos from the lower hemisphere (explanation in text).

thickness determines the threshold energy of μ-meson detection, is placed between the scintillators. Such an array permits us to determine the statistics of events (1) for different threshold energies and the angular distributions of the detected μ mesons. Both results are sensitive to the behavior of the effective cross section of μ-meson production as a function of neutrino energy, and thus to the particular theoretical assumptions made. The existence of an intermediate meson may, in addition, be observed by the detection of μ meson pairs.

APPENDIX

SPECTRA OF THE PARTICLES FROM THE $\mu \to e + \nu + \bar{\nu}$ DECAY

Formulas are given below for the spectra of neutrinos and antineutrinos in the $\mu^- \to e^- + \nu + \bar{\nu}$ decay for the V-A variant of the four-fermion interaction.* The energy spectrum of the neutrinos from the $\mu^- \to e^- + \nu + \bar{\nu}$ decay in the coordinate system in which the μ meson is at rest (c.m.s.) calculated neglecting the electron mass is

$$N_\nu(x)\,dx = 2x^2(3-2x)\,dx, \tag{14}$$

where $x = E_\nu/E_m$, E_ν is the neutrino energy, and $E_m = m/2$ is the maximum neutrino c.m.s. energy. Because of the symmetry of the matrix element with respect to the permutation of the momenta of the neutrino and of the electron, the neutrino spectrum [14] coincides naturally with the electron spectrum.[15]

The spectrum of antineutrinos in the c.m.s. is given by the formula

$$N_{\bar\nu}(x)\,dx = 12x^2(1-x)\,dx, \tag{15}$$

where $x = E_{\bar\nu}/E_m$. The mean energies carried away by neutrinos and antineutrinos equal 0.35 and 0.30 m respectively.

In the l.s., the spectra ν and $\bar\nu$ are of the form (assuming an unpolarized μ-meson beam)

$$N_{\nu L}(y)\,dy = \begin{cases} \dfrac{16}{(1-\beta^2)^3}\left[3(1-\beta^2) - \dfrac{4}{3}(3+\beta^2)\,y\right] y^2\,dy, & 0 \leqslant y \leqslant \dfrac{1-\beta}{2} \\ \dfrac{1}{\beta}\left\{\dfrac{5}{3} + \dfrac{4}{(1+\beta)^3}\left[\dfrac{8}{3}y - 3(1+\beta)\right] y^2\right\} dy, & \dfrac{1-\beta}{2} \leqslant y \leqslant \dfrac{1+\beta}{2}, \end{cases} \tag{16}$$

$$N_{\bar\nu L}(y)\,dy = \begin{cases} \dfrac{32}{(1-\beta^2)^3}[3(1-\beta^2) - 2(3+\beta^2)\,y]\,y^2 dy, & 0 \leqslant y \leqslant \dfrac{1-\beta}{2} \\ \dfrac{2}{\beta}\left\{1 + \dfrac{4}{(1+\beta)^3}[4y - 3(1+\beta)]\,y^2\right\} dy, & \dfrac{1-\beta}{2} \leqslant y \leqslant \dfrac{1+\beta}{2}, \end{cases} \tag{17}$$

where β is the velocity of the μ meson in units of the light velocity, $y = \varepsilon/E$, ε is the energy of the neutrino (antineutrino), and E is the energy of the μ meson in the l.s.

In the limit $\beta \to 0$, the spectra (16) and (17) transform (as they should) into (14) and (15). In practice, $\beta \approx 1$, $(m/E)^2 \ll 1$, and they become $(0 \leq y \leq 1)$

$$N_{\nu L}(y)\,dy \equiv R^{(-)}_{\mu\nu}(E, \varepsilon)\,d\varepsilon = \left(\tfrac{5}{3} - 3y^2 + \tfrac{4}{3}y^3\right) dy, \tag{18}$$

$$N_{\bar\nu L}(y)\,dy \equiv R^{(+)}_{\mu\nu}(E, \varepsilon)\,d\varepsilon = 2(1 - 3y^2 + 2y^3)\,dy. \tag{19}$$

[1] M. A. Markov, Proc. 1960 Ann. Intern. Conf. on High Energy Physics at Rochester, Univ. of Rochester, 1961.

[2] F. Reines, Ann. Rev. Nuclear Sci., ed. by Segrè, Friedlander, and Meyerhoff, 10, 1960, p. 1.

[3] K. Greisen, Ann. Rev. Nuclear Sci., ed. by Segrè, Friedlander, and Meyerhof, 10, 1960, p. 1.

[4] I. M. Zheleznykh and M. A. Markov, Preprint, Joint Inst. Nuc. Res., 1960.

[5] M. A. Markov and I. M. Zheleznykh, Nuclear Phys., in press.

[6] M. A. Markov, preprint, Joint Inst. Nuc. Res. 1960.

[7] B. Pontecorvo, JETP 37, 1751 (1959), Soviet Phys. JETP 10, 1236 (1960).

[8] Zheleznykh, Zatsepin, Kuz'min, and Markov, Proceedings of the Cosmic Ray Meeting, Borzhomi-Erevan, 1961.

[9] Y. Yamaguchi, Progr. Theoret. Phys. (Kyoto) 23, 1117 (1960).

[10] Duthie, Fowler, Kaddoura, Perkins, Pinkau, and Wolter, Preprint, 1961.

[11] B. Pontecorvo and Ya. Smorodinskii, Preprint, Joint Inst. Nuc. Res., D-668, 1961.

[12] G. T. Zatsepin and V. A. Kuz'min, JETP 39, 1677 (1960), Soviet Phys. JETP 12, 1171 (1960).

[13] Paine, Davison, and Greisen, Proc. Cosmic Ray Conf. IUPAP, Moscow, 1959, vol. 1, p. 293

[14] Ashton, Brooke, Gardener, Hayman, Jones, Kisdnasamy, Lloyd, Taylor, West, and Wolfendale, Nature 185, 364 (1960).

[15] T. D. Lee and C. N. Yang, Phys. Rev. 105, 1671 (1957).

*These formulas have been obtained by Yu. S. Kopysov and V. A. Kuz'min.

Translated by H. Kasha
309

SLOW ELECTRONS IN POLAR CRYSTALS

A. V. TULUB

Leningrad State University

Submitted to JETP editor March 23, 1961

J. Exptl. Theoret. Phys. (U.S.S.R.) 41, 1828-1838 (December, 1961)

We have considered the interaction between a non-relativistic particle and a scalar field and have applied the theory to the polaron problem. We use a Lee, Low, and Pines canonical transformation to obtain from the Hamiltonian of the system an effective Hamiltonian; we solve the corresponding Heisenberg equations of motion. The energy is obtained from a variational principle for arbitrary values of the coupling constant. We consider, moreover, the scattering of polarons by phonons as a resonance scattering process; we evaluate the value of the resonance momentum in the strong coupling region. The strong dependence on the coupling constant g which is characteristic for the resonance momentum leads to an upper limit of g^2 of about 8 or 9.

THE electrons in polar crystals create around themselves a localized polarization of the ionic lattice, which accompanies the electrons when they are transferred to the conduction band. If the dimensions of this polarization are sufficiently large, one can, according to Pekar, [1] consider the crystal in the continuous-medium approximation, taking the periodic field of the lattice into account by introducing an effective electron mass m. The latter appears as a basic, unknown parameter in the whole theory, and ultimately determines the magnitude of the coupling constant g for the electron-phonon interaction. This constant is, as a rule, insufficiently small to justify the usual perturbation theory, at least of the first perturbation-theory approximation.

The simplest and most reliable method for determining the effective mass consists in studying the mobilities of the current carriers, which at the present time are already known experimentally for a number of polar crystals. To solve this problem we need know the mobility as a function of the coupling constant for a wide range of coupling constants. For most polar crystals the intermediate coupling range is apparently of most interest; this range is at the same time the most complicated one from a theoretical point of view and the one for which there are in the literature greatly contradictory calculations. [2,3] When solving the problem of the mobility it is natural to start from two extreme approximations in the polaron theory, the weak and strong coupling approximations, with the aim of a subsequent extrapolation of the mobility values found in these regions to the intermediate coupling region.

The scattering of optical phonons by a polaron is a typical problem in resonance scattering; [2,3] when evaluating the scattering amplitude it is convenient to start from Low's well-known method; [4] to apply this method we need know the explicit form of the eigenfunctionals of the polaron in the initial and final states in a form sufficiently convenient for the calculation. In this connection, we develop in the first part of this paper a new method for solving the polaron problem.

A study of the mobility is also of interest because it provides an opportunity to establish the limits of applicability of the whole polaron theory as a physical problem, since the condition for the existence of scattering of polarons by optical phonons is at the same time also the condition that limits the maximum possible coupling-constant values permitted in the theory. Indeed, when the coupling constant increases, the effective dimensions of the polaron decrease, and at the same time the wavelength of the vibrations of the crystalline lattice, which are responsible for the scattering, also decreases. The latter, moreover, cannot be less than a quantity of the order of the dimensions of the elementary cell, so that not all a priori chosen coupling constants are permissible in a real physical problem. Even if we make the most extreme assumption that the whole of the polaron mobility is connected with the scattering by the shortest waves existing in the crystal, it turns out that the maximum coupling constant corresponding to this scattering is approximately equal to $g^2_{max} \approx 8$ to 9.

These values lie at the border of applicability of the strong-coupling formulae; the situation is

thus just the opposite of the one assumed to occur in the first papers on polaron theory: it seems unlikely that there are polar crystals with strong coupling and at the same time with anomalously large effective polaron mass characteristic of strong coupling. A proof of this statement will be given in the second part of this paper, in which we consider the scattering theory in the strong-coupling region.

1. STATEMENT OF THE PROBLEM AND BASIC EQUATIONS

The polaron energy operator can be written in the second-quantization representation in the form

$$H = -\frac{\hbar^2\nabla^2}{2m} + \sum_k \hbar\omega_k^0 a_k^+ a_k + \sum_k V_k (a_k e^{i\mathbf{kr}} + a_k^+ e^{-i\mathbf{kr}}), \quad (1.1)$$

where a_k and a_k^+ are the phonon field operators, m the effective mass, and ω_k^0 the frequency of the longitudinal optical phonons; the function V_k is of the form

$$V_k = \frac{\hbar\omega_k^0}{k} g \left(\frac{4\pi}{uL^3}\right)^{1/2}, \quad u = \sqrt{\frac{2m\omega_k^0}{\hbar}}, \quad (1.2)$$

where g is the coupling constant,

$$g^2 = \frac{e^2}{2\hbar\omega_k^0} u \left(\frac{1}{n^2} - \frac{1}{\varepsilon}\right), \quad (1.3)$$

ϵ is the static dielectric constant, and n the refractive index for light.

For polar crystals a typical situation is one where ϵ, n, and ω_k^0 are known sufficiently accurately and the only unknown quantity is the effective mass m, which at the same time determines the value of g:

$$g^2 = g_0^2 (m/m_0)^{1/2}, \quad (1.4)$$

where g_0^2 is the value of the coupling constant for the case where the effective mass is equal to the electron mass in vacuo, m_0.

It is well known that we can eliminate the electron coordinates from (1.2) by using the canonical transformation

$$S = \exp\left\{\frac{i}{\hbar}\left(\mathbf{P} - \sum_k \hbar\mathbf{k} a_k^+ a_k\right)\mathbf{r}\right\}, \quad (1.5)$$

where $\mathbf{P}$ is the total momentum of the system.

Having transformed the energy operator using (1.5), we follow Lee, Low, and Pines [5] and subject it to one more canonical transformation:

$$U = \exp\left\{\sum_k f_k (a_k - a_k^+)\right\}, \quad (1.6)$$

where f_k is a function of k and $(\mathbf{k}\cdot\mathbf{P})$. We can write the operator obtained after the transformations (1.5) and (1.6) in the form

$$H = H_0 + H_1, \quad (1.7)$$

where we take for the effective Hamiltonian H_0 [6] the expression

$$H_0 = \frac{\mathbf{P}^2}{2m} + 2\sum_k V_k f_k + \sum_k \left(\hbar\omega_k^0 - \frac{\hbar\mathbf{kP}}{m}\right) f_k^2 + \frac{1}{2m}\left(\sum_k \mathbf{k} f_k^2\right)^2 + \mathcal{H}_0, \quad (1.8)$$

$$\mathcal{H}_0 = \sum_k \hbar\omega_k(\mathbf{P})\, a_k^+ a_k + \frac{1}{2m}\sum_{k,k'} \mathbf{k}\mathbf{k}' f_k f_{k'} (a_k a_{k'} + a_k^+ a_{k'}^+ + a_k^+ a_{k'} + a_{k'}^+ a_k), \quad (1.9)$$

while the operator H_1 is of the form

$$H_1 = \sum_k (V_k + f_k \cdot \hbar\omega_k(\mathbf{P}))(a_k + a_k^+) + \sum_{k,k'} \frac{\mathbf{k}\mathbf{k}'}{m} f_{k'} (a_k^+ a_k a_{k'} + a_k^+ a_{k'}^+ a_k) + \frac{1}{2m}\sum_{k,k'} \mathbf{k}\mathbf{k}' a_k^+ a_{k'}^+ a_k a_{k'}; \quad (1.10)$$

$$\hbar\omega_k(\mathbf{P}) \equiv \hbar\omega_k^0 - \frac{\hbar\mathbf{k}}{m}\mathbf{P} + \frac{\hbar^2 k^2}{2m} + \frac{\hbar}{m}\sum_{k'} \hbar\mathbf{k}' f_{k'}^2. \quad (1.11)$$

The operator $\mathcal{H}_0$ is a quadratic expression in the phonon absorption and annihilation operators and can be diagonalized in the usual way. If we denote by ν_k the frequencies of the normal vibrations we can write the required polaron self-energ ΔE in the form*

$$\Delta E = \frac{1}{2}\sum_k (\nu_k - \omega_k) = -\frac{1}{8\pi i}\int_C \frac{ds}{\sqrt{s}} \ln \Delta(s), \quad (1.12)$$

where we have denoted by $\Delta(s)$ the quantity

$$\Delta(s) = \prod_k (s - \nu_k^2) \Big/ \prod_k (s - \omega_k^2), \quad (1.13)$$

and the integration contour C is in the complex s-plane (Fig. 1). One can show that

$$\Delta(s) = \prod_{i=1}^{3} D^{(i)}(s), \quad (1.14)$$

$$D^{(i)}(s) = 1 - \frac{2}{(2\pi)^3}\int \frac{k_i^2 f_k^2 \omega_k}{s - \omega_k^2}\, d\mathbf{k}. \quad (1.15)$$

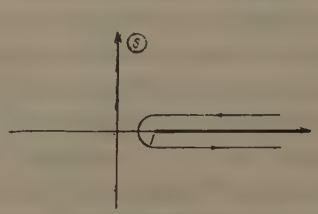

FIG. 1

*In the following we put $\hbar = 1$, and in Secs. 1 and 2 also $\omega_k^0 = 1$.

From (1.12) and (1.14) we get for the particular case where $\mathbf{P} = 0$, for instance, an expression for the energy of the ground state of the operator H_0:

$$E = -\frac{3}{8\pi i}\int_C \frac{ds}{\sqrt{s}} \ln D(s) + 2\sum_k V_k f_k + \sum_k f_k^2, \quad (1.16)$$

where according to (1.15)

$$D(s) = 1 - \frac{2}{3(2\pi)^3}\int \frac{k^2 f_k^2 \omega_k}{s - \omega_k^2} dk. \quad (1.17)$$

If we moreover denote by α_k the physical-particle operators in terms of which $\mathcal{H}_0$ is a diagonal operator, we can show that [7]

$$[a_k, a_{k'}^+] = [\alpha_k, \alpha_{k'}^+] = \delta_{kk'}, \qquad [H_0, \alpha_k^+] = \omega_k \alpha_k^+ \quad (1.18)$$

and that the mathematical expectation of H_1 with respect to the eigenfunctions Λ of the operator H_0 is equal to zero. The operators a_k are linear combinations of the operators α_k of the physical particles*

$$a_k = (M_+)_{kk'}\alpha_{k'} + (M_-^*)_{kk'}\alpha_{k'}^+, \quad a_k^+ = (M_+^*)_{kk'}\alpha_{k'}^+ + (M_-)_{kk'}\alpha_{k'}, \quad (1.19)$$

where the matrices M_+ and M_- are of the form

$$(M_\pm)_{kk'} = \tfrac{1}{2}(\omega_k\omega_{k'})^{-1/2}(\omega_k \pm \omega_{k'})(k|\Omega_+|k'),$$
$$(k|\Omega_\pm|k') = \delta(k-k') + \mathbf{k}\mathbf{k}' f_k f_{k'} \frac{2(\omega_k\omega_{k'})^{1/2}}{(\omega_{k'}^2 - \omega_k^2 \pm is) D_\pm(\omega_k^2)}. \quad (1.20)$$

The ground state functional Λ_0 satisfies the equation $\alpha_k\Lambda_0 = 0$, and from this it follows that Λ_0 is of the form

$$\Lambda_0 = \text{const}\cdot\exp\left\{\frac{1}{2}\iint a_k^+ A_{kk'} a_{k'}^+ dk\, dk'\right\}\Phi_0;$$
$$A^* = M_-M_+^{-1}, \quad a_k\Phi_0 = 0. \quad (1.21)$$

The polaron state eigenfunction can thus be approximately written in the form

$$\Psi_0 = \exp\left\{i\left(\mathbf{P} - \sum_k \mathbf{k} a_k^+ a_k\right)\mathbf{r}\right\}\exp\left\{\sum_k f_k(a_k - a_k^+)\right\}\cdot\Lambda_0. \quad (1.22)$$

We now determine the form of the function f_k from the condition that the energy (1.16) be a minimum. Setting the functional derivative of E with respect to f_k equal to zero we get for f_k the integral equation

$$f_k = -V_k/(1 + k^2/2\mu), \quad (1.23)$$

$$\mu^{-1} = \frac{\omega_k}{2\pi i}\int_C \frac{ds}{\sqrt{s}} \frac{1}{(s - \omega_k^2) D(s)}. \quad (1.24)$$

The method of solving the problem by perturbation theory is evident. It consists in expanding in (1.24) the function $D^{-1}(s)$ in a power series and integrating afterwards over s. We give here the expressions obtained in that way for the self-energy and for the polaron effective mass:

$$E = -g^2 - 1.26(g^2/10)^2 - 1.875(g^2/10)^3,$$
$$m^* = 1 + g^2/6 + 2.24(g^2/10)^2. \quad (1.25)$$

The result (1.25) for E is somewhat better than the one from the path integral method. [8] The operator gives a contribution only to the term in g^6.

*We sum (integrate) over repeated indices.

2. THE STRONG-COUPLING REGION

We turn now to the main problem, the strong-coupling approximation. To elucidate the character of the solution in that region we turn to the analytical properties of the function D(s). To do this we write the function D(s) in the form

$$D(s) = D(1) + \frac{s-1}{3\pi^2}\int_0^\infty \frac{k^4 f_k^2 \omega_k dk}{(\omega_k^2 - 1)(\omega_k^2 - s)}, \quad (2.1)$$

where D(1) is the value of D(s) at s = 1:

$$D(1) = 1 + Q \equiv 1 + \frac{1}{3\pi^2}\int_0^\infty \frac{k^4 f_k^2 \omega_k}{\omega_k^2 - 1} dk. \quad (2.2)$$

As a function of the complex variable s, D(s) possesses the following properties: 1) D(s) has a cut along the real axis from s = 1 to ∞ and has not other singularities; 2) $D^*(s) = D(s^*)$; 3) as $s \to \infty$, sD(s) increases at least as s. Because of these properties we can write for $[(s-1)D(s)]^{-1}$

$$\frac{1}{(s-1)D(s)} = \frac{1}{2\pi i}\int_{C+\rho} \frac{ds'}{(s'-s)(s'-1)D(s')}, \quad (2.3)$$

where $C + \rho$ is the contour of Fig. 2.

It follows from (2.3) that $D^{-1}(s)$ satisfies the integral equation

$$\frac{1}{D(s)} = \frac{1}{1+Q} + \frac{s-1}{3\pi^2}\int_0^\infty \frac{k^4 f_k^2 \omega_k dk}{(s - \omega_k^2)(\omega_k^2 - 1)|D(\omega_k^2)|^2}. \quad (2.4)$$

Integrating by parts we can write Eq. (1.12) for ΔE in the form

$$\Delta E = \frac{1}{2\pi^2}\int_0^\infty dk k^4 f_k^2 \omega_k \frac{1}{2\pi i}\int_C \frac{\sqrt{s}}{(s - \omega_k^2)^2}\frac{1}{D(s)} ds,$$

and using this and (2.4) we get

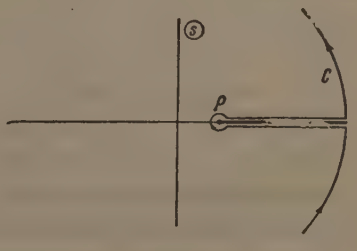

FIG. 2

$$\Delta E = \frac{1}{2\pi^2}\int_0^\infty \frac{k^4 f_k^2 dk}{2(1+Q)} + \frac{1}{12\pi^4}\iint_0^\infty \frac{k^4 f_k^2 p^4 f_p^2 \omega_p \{\omega_k\omega_p + \omega_k(\omega_k+\omega_p)+1\}}{(\omega_k+\omega_p)^2(\omega_p^2-1)\,|\,D(\omega_p^2)\,|^2}\,dpdk. \quad (2.5)$$

Using (2.4) we can write Eq. (1.24) for μ^{-1} in the form

$$\mu^{-1} = \frac{1}{1+Q} + \frac{1}{3\pi^2}\int_0^\infty \frac{p^4 f_p^2(\omega_k\omega_p+1)\,dp}{(\omega_p^2-1)(\omega_k+\omega_p)\,|\,D(\omega_p^2)\,|^2}. \quad (2.6)$$

The constant Q introduced in Eq. (2.2) above is connected with the renormalization of the charge in the following way. Had we written the expression for the energy operator $\mathcal{H}_0$ in the form

$$\mathcal{H}_0 = \sum_k \omega_k a_k^+ a_k + \lambda\Big(\sum_k \mathbf{k} f_k (a_k + a_k^+)\Big)^2,$$

the renormalized coupling constant $\bar{\lambda}$ would be determined, as in ordinary pair meson theory,[9] from the relation

$$\bar{\lambda} = \lambda/(1+\lambda Q). \quad (2.7)$$

Equation (2.6) is in the general case very complicated and its exact solution almost impossible. We therefore evaluate the energy by a direct variational principle, and put the function f_k equal to

$$f_k = -V_k \exp(-k^2/2a^2), \quad (2.8)$$

where a is a parameter to be varied, and where one can easily check that for strong coupling $a^2 \gg 1$. Substituting (2.8) into (1.17) we find for the real and imaginary parts of D(s) the expressions

$$\mathrm{Re}D(\omega_k^2) = 1+\lambda v(y), \qquad \mathrm{Im}D(\omega_k^2) = k^3 f_k^2/6\pi;$$

$$v(y) = 1 - ye^{-y^2}\int_0^y e^{t^2}dt - \xi e^{\xi^2}\int_\xi^\infty e^{-t^2}dt;$$

$$\lambda = 4g^2 a/3\sqrt{2\pi}, \qquad y = k/a, \qquad \xi = \sqrt{y^2+4/a^2}. \quad (2.9)$$

In the strong coupling region $\xi \to y$, and the expression for the energy E can, if we use (1.16) and (2.5), be written in the form

$$E = \tfrac{3}{16}a^2\Big[1+q\Big(\frac{1}{\lambda}\Big)\Big] - \frac{g^2 a}{\sqrt{\pi}}\Big(2-\frac{1}{\sqrt{2}}\Big); \quad (2.11)$$

$$q\Big(\frac{1}{\lambda}\Big) = \frac{2}{\sqrt{\pi}}\int_0^\infty \frac{e^{-y^2}(1-\Omega(y))\,dy}{(1/\lambda + v(y))^2 + \pi y^2 e^{-2y^2}/4},$$

$$\Omega(y) = 2y^2\Big\{(1+2y^2)\,ye^{y^2}\int_y^\infty e^{-t^2}dt - y^2\Big\}. \quad (2.12)$$

In the strong coupling region we put $1/\lambda \to 0$. As a result of numerical integration we obtained for q(0) the value q(0) = 5.75,* and from this we get by varying E with respect to a

$$E = -0.105 g^4. \quad (2.13)$$

This energy value is very close to the well-known result $E = -0.106\ g^4$.[8,10] The effective Hamiltonian H_0 chosen earlier thus already contains in it the usual strong coupling approximation.

An electron in the conduction band causes polarization of the ionic lattice. This polarization is characterized by the density of the continuously distributed charge $\rho(|\mathbf{r}-\mathbf{r_e}|)$, which can be evaluated from the usual equations ($\zeta = |\mathbf{r}-\mathbf{r_e}|$)

$$4\pi\rho(\zeta) = -\nabla^2\varphi(\zeta), \quad (2.14)$$

$$\varphi(\zeta) = -\frac{1}{e}\Big(\Psi(r_e), \sum_k V_k(a_k e^{i\mathbf{kr}} + a_k^+ e^{-i\mathbf{kr}})\,\Psi(r_e)\Big). \quad (2.15)$$

Substituting into (2.15) the functionals (1.22) found earlier we get, using the fact that $(\Lambda_0, a\Lambda_0) = 0$, the following expression for ρ:

$$\rho(\zeta) = -e^2\Big(\frac{1}{n^2}-\frac{1}{\varepsilon}\Big)\frac{a^3}{(2\pi)^{3/2}}e^{-\zeta^2 a^2/2}. \quad (2.16)$$

The total induced charge e′ is equal to

$$e' = -e\Big(\frac{1}{n^2}-\frac{1}{\varepsilon}\Big). \quad (2.17)$$

If we define arbitrarily the polaron radius r_p as the radius of the sphere inside of which there is half of the induced charge (2.17), we get for r_p the expression†

$$r_p = \frac{2.18}{a}\Big(\frac{\hbar}{2m\omega}\Big)^{1/2}. \quad (2.18)$$

3. POLARON SCATTERING. THE MAXIMUM VALUE OF THE COUPLING CONSTANT

One must construct the theory of scattering of polarons by optical lattice vibrations as a resonance scattering theory, as was shown convincingly by Schultz.[3] In the weak-coupling region the theory leads to the same results for the mobility as the usual consideration, that is, it leads to the equations of Fröhlich, Mott, and Davydov and Shmushkevich.[11]

To calculate the scattering amplitude we use Low's well-known method.[4] According to Low

*It is of interest to note that as $\lambda \to \infty$ the integrand in (2.12) has a steep maximum at $y^4 = 3\lambda/4$; however, if we take into account that the domain of integration over y is in fact limited and if we use the values $g^2 \approx 10$ considered in the following, this singularity does not arise.

†We must note that the integration in all formulae is over the dimensionless parameter $k(\hbar/m\omega)^{1/2}$. We have written Eq. (2.18) for clarity in the original system of units [see (1.2) and (1.3)].

we can write the required matrix element of the scattering matrix S in the form ($\hbar = 1$)

$$\langle \mathbf{P}, \mathbf{k} | S - 1 | \mathbf{P}_0, \mathbf{k}_0 \rangle = -2\pi i \delta(E - E_0) R; \quad (3.1)$$

$$R = V_{k_0} V_k \int dv \{(\Psi, e^{-i\mathbf{kr}} (H - E - \omega^0 - i\varepsilon)^{-1} e^{i\mathbf{k}_0\mathbf{r}} \Psi_0) + (\Psi, e^{i\mathbf{k}_0\mathbf{r}} (H - E + \omega^0 - i\varepsilon)^{-1} e^{-i\mathbf{kr}} \Psi_0)\}. \quad (3.2)$$

The initial momenta of the polaron and of the phonon are respectively denoted by $\mathbf{P}_0$ and $\mathbf{k}_0$, and the final momenta by $\mathbf{P}$ and $\mathbf{k}$; $E = P^2/2m^*$ is the polaron energy, and Ψ_0 and Ψ are the wave functionals (1.22) of the initial and final polaron states.

In the following we consider the low temperature region where $P^2/2m^* < \omega^0$. The only term responsible for scattering will in this case be the first term in (3.2) which can be evaluated as follows. We push consecutively the operators $\exp\{i(\mathbf{P}_0 + \mathbf{k}_0 - \Sigma_k \mathbf{k} a_k^+ a_k)\mathbf{r}\}$ and $\exp\{\Sigma_k f_k (a_k - a_k^+)\}$ through $(H - E - \omega^0 - i\epsilon)^{-1}$ from the right to the left and integrate the expression obtained in this way over the volume dv. We get as a result

$$\langle \mathbf{P}, \mathbf{k} | S - 1 | \mathbf{P}_0, \mathbf{k}_0 \rangle = -i(2\pi)^4 \delta(E - E_0) \delta(\mathbf{P}_0 + \mathbf{k}_0 - \mathbf{P} - \mathbf{k}) M. \quad (3.3)$$

Here

$$M = V_k V_{k_0} (\Lambda_0, (H_0' + H_I' - \omega^0 - i\varepsilon)^{-1} \Lambda_0),$$

$$H_0' = H_0 + \mathbf{Pk}/\mu + k_0^2/2m,$$

$$H_I' = H_I - \frac{1}{m} \sum_k \mathbf{k}\mathbf{k}_0 a_k^+ a_k - \frac{1}{m} \sum_k \mathbf{k}\mathbf{k}_0 f_k (a_k + a_k^+);$$

$$\mu \equiv m(1 - \eta)^{-1}, \quad \eta \mathbf{P} \equiv \sum_k \mathbf{k} f_k^2; \quad (3.4)$$

H_0 and H_1 are given by (1.9) and (1.10).

To evaluate (3.3) we follow Low and Pines [2] and introduce a functional Ω:

$$c\Omega = (H_0' + H_I' - E - \omega^0 - i\varepsilon)^{-1} \Lambda_0, \quad (3.5)$$

$$c = (k_0^2/2m + \mathbf{P}_0\mathbf{k}_0/\mu - \omega^0 - i\varepsilon)^{-1}, \quad (3.6)$$

which satisfies the integral equation

$$\Omega = \Lambda_0 - (H_0' - E - \omega^0 - i\varepsilon)^{-1} H_I' \Omega. \quad (3.7)$$

We write Ω in the form

$$\Omega = u\Lambda_0 + \sum_k v_k a_k^+ \Lambda_0 + \sum_{k,k'} W_{kk'} a_k^+ a_{k'}^+ \Lambda_0 + \ldots \quad (3.8)$$

In the single-phonon approximation, $\Omega = u\Lambda_0 + \Sigma_k v_k a_k^+ \Lambda_0$, we get for the coefficients u and v_k the following set of equations:

$$u = 1 - c \sum_k v_k \varphi_k, \quad (3.9a)$$

$$\delta E_k v_k = -u\varphi_k - u \sum_{k'} A_{kk'} \varphi_{k'} - \frac{u}{m} \sum_{k'} \mathbf{k}\mathbf{k}' f_{k'} A_{kk'} - \frac{1}{m} \sum_{k'} \mathbf{k}\mathbf{k}' f_k f_{k'} v_{k'} - \frac{1}{m} \sum_{k'k''} A_{kk'} f_{k'} \mathbf{k}'\mathbf{k}'' f_{k''} v_{k''}, \quad (3.9b)$$

where

$$\delta E_k = (\mathbf{k}_0 - \mathbf{k})^2/2m + \mu^{-1}\mathbf{P}_0(\mathbf{k}_0 - \mathbf{k}) - i\varepsilon,$$

$$\varphi_k = -\mathbf{k}\mathbf{k}_0 f_k/m + V_k + f_k\omega_k = -\mathbf{k}\mathbf{k}_0 f_k/m + \Phi_k. \quad (3.10)$$

If we recognize that (1.20) and (1.21) imply that the matrix $A_{kk'}$ can be written as $A_{kk'} = (\mathbf{k}\cdot\mathbf{k}')Q(k, k')$, the solution of these equations can be written in the form

$$cu = \left\{ \frac{k_0^2}{2m} \frac{1 - I - K + 2U}{1 + I + K} - \omega^0 (N + T + 1) \right\}^{-1};$$

$$U = 2L + M + (L + S)(L + M), \quad (3.11)$$

$$I = \sum_k \frac{(\mathbf{k}\mathbf{k}_0)^2 f_k^2}{m k_0^2 \delta E_k}, \quad K = \sum_k \frac{(\mathbf{k}\mathbf{k}_0)^2 f_k T_k}{m k_0^2 \delta E_k}, \quad L = \sum_k \frac{\mathbf{k}\mathbf{k}_0 f_k \Phi_k}{k_0^2 \delta E_k},$$

$$M = \sum_k \frac{\mathbf{k}\mathbf{k}_0 \Phi_k T_k}{k_0^2 \delta E_k}, \quad S = \sum_k \frac{\mathbf{k}\mathbf{k}_0 k^2 f_k T_k}{m k_0^2 \delta E_k}, \quad T = \frac{1}{\omega^0} \sum_k \frac{k^2 f_k \Phi_k}{m \delta E_k},$$

$$N = \frac{1}{\omega^0} \sum_k \frac{\Phi_k^2}{\delta E_k}, \quad T_k \equiv \sum_{k'} \frac{(\mathbf{k}\mathbf{k}')^2}{k'^2} Q(k, k'). \quad (3.12)$$

After integrating over the final momenta P and k and over the initial momentum $\mathbf{k}_0$ we get for the probability w for scattering per unit time the following expression

$$w = \frac{1}{\tau} = \frac{m^* P_0}{8\pi^4} \int |V_{k_0}|^4 |cu(k_0)|^2 e^{-\omega_0/kT} dk_0. \quad (3.13)$$

The factor $\exp(-\omega^0/kT)$ gives the number of phonons per unit volume at low T as a function of the temperature T. The function $|cu(k_0)|^2$ is of the form

$$|cu(k_0)|^2 = 1/(A^2 + P_0^2 B^2) \quad (3.14)$$

and as $P_0 \to 0$ the integrand in (3.13) has thus the form

$$\lim_{P_0 \to 0} \frac{P_0}{A^2 + P_0^2 B^2} = \frac{\pi}{B} \delta(A),$$

that is, the scattering cross section is determined by the magnitude of the resonance momentum $A(\mathbf{k}_r) = 0$. When $g^2 \approx 1$, Eq. (3.13) becomes Low and Pines' well-known formula. [2]

When the coupling constant increases the magnitude of the resonance momentum will increase also, and in the strong coupling case the integrals (3.12) can thus be evaluated in the limit of large k_0. In that region the quantities L, M, S, and T

are of order g^{-4} compared to the main terms I and N, and the integral K turns out on an estimate to be approximately an order of magnitude smaller than I. In the strong coupling region we get for the resonance momentum, after evaluating the integrals I and N in (3.11), the expression

$$\frac{k_r}{\sqrt{2m\omega^0}} = a\left(\frac{g^2 a}{6\sqrt{2\pi}}\right)^{1/2}\left(1+\frac{27}{8}\frac{\sqrt{2\pi}}{g^2 a}+O(g^{-6})\right). \quad (3.15)$$

We now consider the contribution from the two-phonon terms to the scattering amplitude. If we retain in the expansion (3.8) the terms $\Sigma_{kk'}W_{kk'}a_k^+a_{k'}^+\Lambda_0$ the equation for the coefficients $W_{kk'}$ becomes

$$\left\{\omega^0+\frac{(\mathbf{k}+\mathbf{k}'-\mathbf{k}_0)^2}{2m}\right\}W_{kk'} = -\frac{u}{2m}\{(\mathbf{k}+\mathbf{k}')\mathbf{k}_0-(\mathbf{k}\mathbf{k}')\}A_{kk'}$$
$$-\frac{\mathbf{k}\mathbf{k}'}{2m}(v_k f_{k'}+v_{k'}f_k)-\frac{1}{2}(v_k\varphi_{k'}+v_{k'}\varphi_k)$$
$$+ \text{ integral terms.} \quad (3.16)$$

The left-hand side of (3.16) contains the parameter k_0 squared, and the right-hand side only to the first power. If we take this into account, the correction terms in $W_{kk'}$ in Eq. (3.9b) for v_k will be of the order $k_0^{-1} \sim g^{-4}$ as compared with the terms written down in (3.9b). In the strong coupling region the two-phonon terms thus make a small contribution to the scattering amplitude.

Let us dwell on the problem of the maximum values of the coupling constant g of the electron-phonon interaction. The maximum value of the phonon quasi-momentum is $k_{max} = 2\pi/a^0$, where a^0 is the lattice constant. Since the right-hand side of Eq. (3.15) increases as g^4 in the strong coupling region, we can find such values of g that the scattering cannot take place at all, for when the coupling constant increases the lattice vibrations with the very shortest wavelengths become responsible for the scattering.

The maximum momentum corresponds to a wavelength $\lambda = a^0$. In that wave all ions in the lattice are at the nodes of the wave; it hardly makes sense therefore to speak of scattering by this wave, which is in actual fact a fictitious one. Even if we make the extreme assumption that all of the mobility of the polarons is caused only by the scattering by a single wave with $k = \pi/a^0$, which is already connected with a displacement of the ions, this assumption will lead to a rather severe limitation on the coupling constant. These values were evaluated using (3.15) and are listed in the table.

For most polar crystals the values of g^2_{max} are thus of the order of 8 or 9. These values actually reduce to zero the region where the strong coupling can be applied, i.e., weak or intermediate coupling must occur in real crystals. The most important consequence following from this is the relatively small magnitude of the polaron effective mass. Indeed, even if we make the extreme non-physical assumption that all of the mobility is connected with the scattering by the shortest wavelength in the crystal, we get an appreciable error in the result obtained from the asymptotic formula for the polaron effective mass, $m^*/m = 0.020\,g^8$ [8] for $g^2 \approx 8$ to 9 (in contradistinction to the energy):[3] for instance, if $g^2 \leq 8$, the effective mass must be less than 30 m.

The restrictions on the permissible coupling-constant values follow, of course, also from the condition that the polaron dimensions must not be less than the lattice constant. This criterion leads, however, to values of g^2 larger than the ones in the table and, moreover, this criterion is not so well defined as the one we just considered which is based upon scattering theory.

Let us consider some other observations about the theory. In all preceding calculations we assumed that the upper limit of integration could be taken to be infinite. In the weak or intermediate coupling regions this assumption is undoubtedly correct since the integrands decrease steeply with increasing k, but in the strong coupling region this problem requires a more detailed consideration. We already mentioned that the integration

Crystal	a^0, Å	$\hbar\omega\cdot10^2$, ev	$\frac{2\pi}{a^0}\left(\frac{2\hbar}{2m\omega^0}\right)^{-1/2}$	g_0^2	g^2_{max}
LiF	4.02	8.37	10.6	5.2	7,7
NaF	4,62	5.68	11.2	6.3	8.6
NaCl	5,63	3.21	12.1	5.5	8,4
NaBr	5.96	2.51	12.8	5.0	8.3
NaJ	6.46	2.19	12.8	4.8	8.1
KCl	6.28	2.61	12.1	5.8	8.6
KBr	6.58	2.01	13.1	5.7	8,8
KJ	7.05	1.65	13.5	4.9	8.4
RbCl	6.54	2.21	12.6	6.4	9.1
RbBr	6.85	1.60	14.2	6.7	9.7
RbJ	7,33	1.33	14.5	5.8	9.2
AgCl	5.54	2,41	14.2	3.9	7.8

over k means an integration over the dimensionless parameter $k(\hbar/m\omega^0)^{1/2}$. It is clear from the table that we can on an average put $k_{max}(\hbar/2m_0\omega^0)^{1/2} \approx 12$, and we then get for the typical case when $g_0^2 = 5$

$$x_{max} = k_{max}(\hbar/m\omega^0)^{1/2} \approx 60\sqrt{2}/g^2.$$

When evaluating the integrals in (2.12) and (2.13) we made the change of variable $y = x/a$ and set the upper limit of integration for $g^2 \approx 9$ at about $y = 3.66$. The numerical integration in (2.12) was taken up to 3.5, beyond which the integrand was vanishingly small. One can thus assume that the numerical value for the energy given here is basically correct.

Considering the strong coupling region further, we must show the extent to which the operator H_1 is a perturbation with respect to H_0. If we use perturbation theory to evaluate the contribution from H_1 to the energy, we can, owing to the fast decrease of the function f_k at large k, make the numerical contribution from H_1 small in the range of g^2 values considered above. At any rate, taking the operator H_1 into account leads to a decrease in the energy, as compared with (2.13), and to a smaller polaron radius. The values of g^2_{max} given in the table are therefore still undoubtedly overestimates.

It follows from all this that strong coupling turns out to be in fact incompatible with the scattering of polarons by optical lattice vibrations. Taking dispersion into account has no important influence whatever on this result since the large k region makes a small contribution to the numerical values of the integrals I and N. As far as the already well-known experimental data are concerned, they indicate either the use of weak (PbS, PbSe) or intermediate coupling (AgCl, AgBr).[12] The latter crystals are of most interest since the numerical values of the mobility enable us in that case to estimate in the most direct manner the magnitude of the polaron effect; we shall consider these problems later.

In conclusion I express my deep gratitude to Academician V. A. Fock for a number of valuable hints and also to Professor H. Lehmann and W. Zimmermann for their interest in this paper and to Professor G. Höhler for drawing my attention to Schultz's paper.[3] I am grateful to Professor L. É. Gurevich and V. I. Perel' for an interesting discussion.

[1] S. I. Pekar, Issledovanie po elektronnoĭ teorii kristallov (Study of the Electron Theory of Crystals), Gostekhizdat, 1951, German translation Akademie Verlag 1954.

[2] F. E. Low and D. Pines, Phys. Rev. **98**, 414 (1955).

[3] T. D. Schultz, Phys. Rev. **116**, 526 (1959); H. Osaka, Progr. Theoret. Phys. (Kyoto) **25**, 517 (1961).

[4] F. E. Low, Phys. Rev. **97**, 1392 (1955).

[5] Lee, Low, and Pines, Phys. Rev. **90**, 297 (1953).

[6] E. P. Gross, Phys. Rev. **100**, 1571 (1955).

[7] A. V. Tulub, Vestnik LGU (Leningrad State Univ.) **22**, 104 (1960).

[8] R. P. Feynman, Phys. Rev. **97**, 660 (1955).

[9] A. Klein and B. H. McCormick, Phys. Rev. **98**, 1428 (1955).

[10] V. M. Buĭmistrov and S. I. Pekar, JETP **32**, 1193 (1957), Soviet Phys. JETP **5**, 970 (1957); G. Höhler, Z. Physik **146**, 372 (1956).

[11] H. Fröhlich and N. F. Mott, Proc. Roy. Soc. (London) **A171**, 496 (1939); B. I. Davydov and I. M. Shmushkevich, UFN **24**, 21 (1940).

[12] K. Kobayashi and F. C. Brown, Phys. Rev. **113**, 507 (1959); Burnham, Brown, and Knox, Phys. Rev. **119**, 1560 (1960).

Translated by D. ter Haar
310

COVARIANT DERIVATION OF THE WEIZSÄCKER-WILLIAMS FORMULA

V. N. GRIBOV, V. A. KOLKUNOV, L. B. OKUN', and V. M. SHEKHTER

Submitted to JETP editor April 28, 1961

J. Exptl. Theoret. Phys. (U.S.S.R.) 41, 1839-1841 (December, 1961)

We present a simple and manifestly covariant derivation of the Weizsäcker-Williams formula.

RECENTLY in a whole series of papers, starting with that of Chew and Low,[1] the contribution of pole diagrams to the cross sections for various processes has been calculated. Pomeranchuk and Shmushkevich [2] have pointed out that the cross section for inelastic processes occurring in a Coulomb field and calculated in the pole approximation using the "Coulomb photon" coincides with the well-known Weizsäcker-Williams formula (WW).[3] In calculating the invariant pole matrix element, Pomeranchuk and Shmushkevich,[2] in the spirit of the original quasi-classical derivation of Weizsäcker and Williams, used quantities measured in the rest system of the incident particles. In this note we give an explicitly covariant derivation of the WW formula.*

Let us calculate the cross section for the process shown in Fig. 1. Here k and p are the momenta of the colliding charged particles (for example, an electron and a proton), $k^2 = \mu^2$, $p^2 = m^2$; p′ and k′ are the momenta of the particles created, $p'^2 = p^2 = m^2$; q is the momentum of the virtual photon. We want to express the cross section associated with this graph in terms of the cross section for the photoprocess with a real photon q ($q^2 = 0$, $e_\mu q_\mu = 0$) shown in Fig. 2.

The cross section of the photoprocess for a photon of given polarization, integrated over the momenta of the created particles and summed over their polarizations, can be written in the form

$$\sigma_p^e = -e_\mu e_\nu T^0_{\mu\nu}. \tag{1}$$

For an unpolarized photon

$$\sigma_p = \tfrac{1}{2}\delta_{\mu\nu}T^0_{\mu\nu} = \tfrac{1}{2}T^0_{\mu\mu}. \tag{2}$$

In the expression for the cross section corresponding to the diagram of Fig. 1, after integration over the momenta of the particles k′ and summation over polarizations, there appears the tensor $T_{\mu\nu}$ depending on the vectors k and q, such that

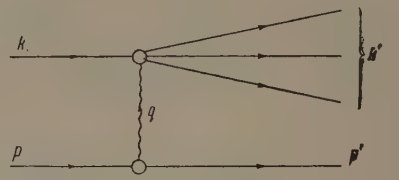

FIG. 1

FIG. 2

$$T^0_{\mu\nu} = T_{\mu\nu}|_{q^2=0}. \tag{3}$$

The most general expression for the tensor $T_{\mu\nu}$ which satisfies the condition of gauge invariance

$$q_\mu T_{\mu\nu} = 0, \qquad q_\nu T_{\mu\nu} = 0, \tag{4}$$

has the form

$$T_{\mu\nu} = a\left(\frac{q^2}{kq}k_\mu k_\nu + kq\cdot\delta_{\mu\nu} - k_\mu q_\nu - k_\nu q_\mu\right) + b\,(q^2\delta_{\mu\nu} - q_\mu q_\nu). \tag{5}$$

The invariant functions a and b depend on k^2, q^2 and kq. Since the amplitude for the photoprocess has no singularity at $q^2 = 0$, this is also true for the functions a and b.* Substituting (5) in (2) we get

$$\sigma_p = a\,(kq). \tag{6}$$

The cross section for the process shown in Fig. 1, expressed in terms of the tensor $T_{\mu\nu}$, is equal to

$$d\sigma_{ww} = -\left[\frac{kq}{\sqrt{(kp)^2 - k^2p^2}}\right] \times e^2Z^2\frac{1}{q^4}(2p-q)_\mu(2p-q)_\nu T_{\mu\nu}\frac{dp'}{(2\pi)^3\,2E'}. \tag{7}$$

*Arguments similar to our are contained in part in the work of Dalitz and Yennie[4] concerning the creation of pions in electron-proton collisions. See their paper for references to earlier work on the Weizsäcker-Williams method.

*The functions a and b for the Compton scattering of pseudophotons were found by A. Badalyan.[5]

The factor in square brackets is the ratio of the invariant fluxes for the reactions $k+q=k'$ and $k+p=k'+p'$. The expression $Ze(2p-q)$ is the photon vertex part for the spinless nucleus p. Changing to the variables q^2, $\omega^2=(k+q)^2$ and φ (where φ is the angle between p' and k' in the laboratory system) we easily find

$$dp'/2E'=d\omega^2\,d(-q^2)\,d\varphi/8\sqrt{(kp)^2-k^2p^2}. \tag{8}$$

Integrating (7) over the azimuthal angle φ, substituting in (5) and using the fact that $2pq=q^2$, we get the invariant formula

$$d\sigma_{WW}=\frac{Z^2\alpha}{2\pi}\frac{(kp)^2(kq)}{(kp)^2-k^2p^2}\left\{a\left[1+\frac{(kq)^2p^2}{(kp)^2q^2}-\frac{(kq)}{(kp)}\right]\right.$$

$$\left.+b\left[p^2-\frac{q^2}{4}\right]\frac{(kq)}{(pk)^2}\right\}\frac{d\omega^2}{(kq)}\frac{dq^2}{q^2}. \tag{9}$$

Using (6), we have

$$d\sigma_{WW}=\frac{Z^2\alpha}{\pi}\sigma_p\left(1-\frac{k^2p^2}{(kp)^2}\right)^{-1}\left\{\left[1+\frac{(kq)^2p^2}{(kp)^2q^2}-\frac{(kq)}{(kp)}\right]\right.$$

$$\left.+\frac{b}{a}\frac{(p^2-q^2/4)(kq)}{(pk)^2}\right\}\frac{dq^2}{q^2}\frac{d\omega^2}{2kq}. \tag{10}$$

For large electron energies ($kp\gg kq$, $(kp)^2\gg k^2p^2$), this formula simplifies:

$$\sigma_{WW}=\frac{Z^2\alpha}{\pi}\sigma_p\left(1+\frac{(kq)^2p^2}{(kp)^2q^2}\right)\frac{dq^2}{q^2}\frac{d\omega^2}{\omega^2-q^2-k^2} \tag{11}$$

and coincides with the result of WW. As for the last term in (10), for the case of large electron energy it is small, since $p^2(kq)^2/(pk)^2q^2\ll 1$, and $q^2/kq\ll 1$. This term is missing from the original result of WW, but appears in that of Pomeranchuk and Shmushkevich.[2] In the terminology of WW,[3] it apparently corresponds to the small contribution from the photoprocess due to longitudinal "pseudophotons."

In conclusion, we note in a recent paper of Badalyan and Smorodinskii,[6] what appears to be an incorrect assertion that they have given a new derivation of the Weizsäcker-Williams formula and that the relation found by them enables one to get the cross section for photoproduction, for a given polarization of the photon, from the differential cross section for electric production. Actually the derivation which they present is just the usual classical calculation of the spectrum of pseudophotons, since the expression for the energy-momentum tensor does not depend on the choice of gauge. It is therefore natural that the expression obtained by them does not contain the term which was found in [2] and is contained in formula (10). The expression given in [6] for the polarization vector of the pseudophoton is correct only to the extent that one can neglect this term. The correct expression is obtained if the vector $P\equiv 2p-q$, which enters for the lower vertex of the diagram in Fig. 1, is represented in the form

$$P_\mu=Ae_\mu+\frac{(Pk)}{(kq)^2-k^2q^2}[(kq)\,q_\mu-q^2k_\mu].$$

Here $(eq)=(ek)=0$. The vector e_μ is spacelike, and if we normalize it so that $e=-1$, it will be the polarization vector of the pseudophoton, while

$$A^2=\frac{(Pk)^2}{(kq)^2-k^2q^2}\left[-q^2-\frac{P^2[(kq)^2-k^2q^2]}{(Pk)^2}\right].$$

The spectrum of pseudophotons is proportional to A^2. The second term in the expression for P_μ gives the additional term which was mentioned above.

The authors thank I. Yu. Kobzarev, I. Ya. Pomeranchuk, and I. M. Shmushkevich for valuable discussions.

[1] G. F. Chew and F. E. Low, Phys. Rev. 113, 1640 (1959).

[2] I. Ya. Pomeranchuk and I. M. Shmushkevich, Nuclear Phys. 23, 452 (1961).

[3] K. F. Weizsäcker, Z. Physik 88, 612 (1934). E. J. Williams, Phys. Rev. 45, 729 (1934). Kgl. Danske Videnskab. Selskab, Mat.-fys. Medd. 13, #4, 1935. A. I. Akhiezer and V. B. Berestetskii, Kvantovaya Elektrodinamika (Quantum Electrodynamics) second edition, Fizmatgiz, 1959, p. 376.

[4] R. Dalitz and D. Yennie, Phys. Rev. 105, 1598 (1957).

[5] A. Badalyan, JETP 41, 1315 (1961), Soviet Phys. JETP 14, 935 (1962).

[6] A. Badalyan and Ya. A. Smorodinskii, JETP 40, 1231 (1961), Soviet Phys. JETP 13, 865 (1961).

Translated by M. Hamermesh
311

EFFECT OF COULOMB AND NUCLEAR INTERACTIONS ON DEUTERON STRIPPING REACTIONS

V. G. SUKHAREVSKII and I. B. TEPLOV

Nuclear Physics Institute, Moscow State University

Submitted to JETP editor May 4, 1961

J. Exptl. Theoret. Phys. (U.S.S.R.) 41, 1842-1844 (December, 1961)

The differential cross section for the $Si^{30}(d, p)Si^{31}$ reaction is calculated taking into account Coulomb and nuclear interactions. Including these interactions has little effect on the ratio of the cross sections at the maxima of the angular distributions for different states of the final nucleus ($l = 0$ and $l = 2$).

It is known that the absolute value of the cross section for a stripping reaction of the type (d, p) and (d, n) is much more sensitive to the Coulomb and nuclear interactions of the particles participating in the reaction than are their angular distributions. To study the influence of these interactions we have computed the differential cross section for stripping with distorted deuteron and proton waves, for the reaction $Si^{30}(d, p)Si^{31}$ which was investigated in [1]. The interactions in the initial and final states were accounted for using the formula found in the paper of Tobocman and Kalos.[2] The values of the radial Coulomb functions were taken from tables computed on the "Strela" digital computer of Moscow State University.[3]

The computation was carried out for the $Si^{30}(d, p)Si^{31}$ reaction with formation of the final nucleus in the ground state ($l_n = 2$, Q = 4.36 Mev) and the first excited state ($l_n = 0$, Q = 3.61 Mev) for deuterons with an energy of 4.25 Mev. The radial integrals entering into the computational formulas were found by numerical integration. The maximum values of the orbital angular momenta of the deuteron and proton were taken to be 6 and 8, respectively. The integration was carried out to the value kr = 8 (where k is the wave number of the captured neutron). The errors due to the neglect of higher orbital angular momenta and large values of kr did not exceed a few percent.

The computed angular distributions are shown in the figure for three cases: 1) Coulomb and nuclear interaction not included; the angular distribution coincides with Butler's results ($R = 6.5 \times 10^{-13}$ cm); 2) only the Coulomb interaction is included; 3) includes the Coulomb interaction plus the nuclear scattering of the protons by a hard sphere of radius 5.5×10^{-13} cm and scattering of the deuterons by a hard sphere of radius 6.5×10^{-13} cm.

As expected, for the case of $l = 2$, including the Coulomb interaction shifts the principal maximum, which was at 45° for the Born approximation, toward larger angles. This shift is about 15°. Putting in the nuclear interaction gives a shift of the maximum in the opposite direction by 20°. Just as in the work of Tobocman and Kalos,[2] the characteristic features of the computed distributions are: a) only a slight difference from the Butler theory at small angles and b) nonzero cross section at the minima.

Inclusion of Coulomb and nuclear corrections results in a considerable reduction in the absolute cross section for the reaction. Although the computations of the absolute cross section are qualitative, they nevertheless give much more reliable values for the cross sections than do the plane-wave computations of the Butler theory. For easy visualization, the differential cross sections for all three variants of the interaction are shown on the figure with the same value at the principal maximum; their actual relative amplitudes are given by the normalization factor N, using the relation

$$\sigma(\vartheta) = N\sigma_0(\vartheta), \qquad (1)$$

where $\sigma_0(\theta)$ is the differential cross section computed from the Butler theory. The computed values of N are presented in the table, in which we also give the results of Tobocman and Kalos [2] for the $F^{19}(d, p)F^{20}$ reaction with formation of the final nucleus in the ground ($l = 2$, Q = 4.37 Mev) and excited ($l = 0$, Q = 0.88 Mev) states.

The main conclusion from the results given in the table is that when one includes Coulomb

Reaction	E_d, Mev (lab)	E_d/B (cms)	$l=0$			$l=2$		
			N_c	$N_{c+n.s.}$	$N_{c+n.a.}$	N_c	$N_{c+n.s.}$	$N_{c+n.a.}$
$F^{19}(d, p)F^{20}$	14,3	5.3	0.74	0.16	0.38	0.47	0.21	0.23
$F^{19}(d, p)F^{20}$	3,6	1.3	0.16	0.13	0.08	0.20	0.07	0.15
$Si^{30}(d, p)Si^{31}$	4.25	1.1	0.27	0.008	—	0.03	0.004	—

N_c is the correction for Coulomb interaction, $N_{c+n.}$ the correction for Coulomb and nuclear interaction; n.s. denotes hard-sphere scattering of protons for the fluorine reaction and hard-sphere scattering of protons and deuterons for the silicon interaction; n.a. means absorption of protons with $l \leqslant l_1$, where $l_1 = \hbar^{-1} r[2m_p(E_d + Q - Ze^2/r)]^{1/2}$; E_d is the deuteron energy and B is the height of the Coulomb barrier.

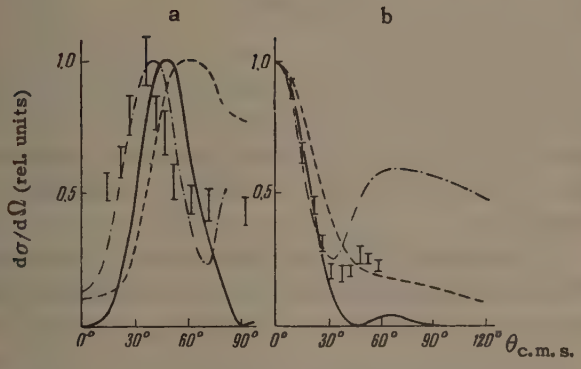

Angular distribution of protons, computed for three interaction variants, for the reaction Si^{30} (d, p) Si^{31} with formation of the Si^{31} nucleus a) in the ground state, $l = 2$; b) in the first excited state (0.76 Mev), $l = 0$. The experimental points are from data of[1], the solid line is the Butler theory; the dashed line includes Coulomb interaction; the dot-dashed curve includes both Coulomb and nuclear interactions.

and nuclear interactions the ratio of the corrections $N_{l=0} / N_{l=2}$ for formation of the final nucleus in different states is relatively close to unity and varies from 0.5 to 2, depending on the value of the parameter E_d/B and the character of the nuclear interaction which is included.

The fact that the ratio of the corrections for different values of the orbital angular momentum transfer l is close to unity is important, since it allows us in analyzing the structure of different states of the final nucleus to use the reduced widths computed from the Butler theory.

Because of the incompleteness of the theory, the absolute values of the corrections N and, consequently, the absolute values of the reduced widths are correct only to order of magnitude. One can give a convenient criterion for the applicability of such corrections to the stripping cross section. Since the value of the dimensionless reduced width θ^2 in stripping reactions must not exceed unity, the value of θ^2 computed including the corrections must satisfy the relation

$$\theta^2 = \theta_0^2/N \leqslant 1, \qquad (2)$$

where θ_0^2 is the dimensionless reduced width computed from the simple Butler theory. Then we must satisfy the condition

$$N \geqslant \theta_0^2. \qquad (3)$$

This simple criterion shows that the correction N for Coulomb and nuclear interaction which appears in the relation (1) must not be less than the dimensionless reduced width θ_0^2 computed from the Butler theory omitting the perturbing interactions.

[1] V. G. Sukharevskii, JETP 36, 52 (1959), Soviet Phys. JETP 9, 37 (1959).

[2] W. Tobocman and M. H. Kalos, Phys. Rev. 97, 132 (1955).

[3] Luk'yanov, Teplov and Akimova. Tablitsy kulonovskikh volnovykh funktsii (Tables of Coulomb Wave Functions) Computer Center, AN SSSR, 1961.

Translated by M. Hamermesh
314

HYDRODYNAMICS OF A NONISOTHERMAL PLASMA

E. E. LOVETSKII and A. A. RUKHADZE

P. N. Lebedev Physics Institute, Academy of Sciences, U.S.S.R.

Submitted to JETP editor May 19, 1961

J. Exptl. Theoret. Phys. (U.S.S.R.) **41**, 1845-1849 (December, 1961)

The single-fluid magnetohydrodynamic equations with particle collisions taken into account are obtained for a nonisothermal plasma. The effect of particle collisions on the spectrum of magnetohydrodynamic and magnetic-sound plasma waves is investigated.

1. Klimontovich and Silin [1] (cf. also [2] and [3], Secs. 15 and 24) have carried out a single-fluid magnetohydrodynamic analysis of a nonisothermal plasma in which particle collisions were neglected. The possibility of carrying out this hydrodynamic analysis rests on the fact that weakly damped magnetohydrodynamic and magnetic-sound waves can propagate in a nonisothermal plasma in which $T_e \gg T_i$. These waves are damped by Cerenkov absorption and cyclotron absorption in the plasma. When particle collisions are taken into account, however, the dispersion relation for the weakly damped waves, which is obtained when particle collisions are neglected can be changed markedly, even when the collision integral in the kinetic equation is a relatively small term. Specifically, it will be shown below that under certain conditions the damping factor for the plasma waves is determined by the particle collisions while the wave frequencies are essentially unaffected by collisions.

In the high-frequency region, where the thermal motion of the plasma particles can be neglected, the important collisions are electron-ion collisions (cf. [3], Secs. 16 and 23). Here we consider a nonisothermal plasma in the frequency region ω (or the region of the characteristic time of the problem $1/\omega$) defined by the condition

$$kv_i \ll \omega \ll kv_e, \tag{A}$$

where v_e and v_i are the thermal velocities of the electrons and ions, while k is the wave vector (the characteristic dimension of the problem is $1/k$); the ion-ion collisions predominate under these conditions. Electron-electron and electron-ion collisions can be neglected. Below we derive the magnetohydrodynamic equations for a nonisothermal rarefied plasma with ion-ion collisions taken into account. We assume that (A) and the following conditions are satisfied:

$$\omega \ll \Omega_i \ll \omega_{Li}, \tag{B}$$

where $\Omega_i = e_iB_0/Mc$ is the ion Larmor frequency and $\omega_{Li} = \sqrt{4\pi e_i^2 N_i/M}$ is the ion Langmuir frequency.

2. If particle collisions are neglected the complete system of magnetohydrodynamic equations for a single-fluid nonisothermal plasma is

$$\partial \mathbf{B}/\partial t = \mathrm{rot}\,[\mathbf{vB}], \quad \mathrm{div}\,\mathbf{B} = 0, \tag{1}*$$

$$\partial \rho/\partial t + \mathrm{div}\,\rho\mathbf{v} = 0, \tag{2}$$

$$\frac{\partial \mathbf{v}}{\partial t} + \left(\mathbf{v}\frac{\partial}{\partial \mathbf{r}}\right)\mathbf{v} = -\frac{v_s^2}{\rho}\frac{\partial \rho}{\partial \mathbf{r}} + \frac{1}{4\pi\rho}[\mathrm{rot}\,\mathbf{B}, \mathbf{B}] + \frac{1}{\rho_0}\mathbf{F}_1^{\mathrm{dis}}, \tag{3}$$

where $v_s = \sqrt{|e_i/e|\kappa T_e/M}$ is the velocity of sound while $\mathbf{F}_1^{\mathrm{dis}}$ represents the dissipative forces due to Cerenkov absorption and cyclotron absorption of the plasma waves. In contrast with the nondissipative terms, the dissipative term in the magnetohydrodynamic equations is obtained in an approximation linear in the function that describes the deviation of the particle distribution from the equilibrium (Maxwellian distribution); $\mathbf{F}_1^{\mathrm{dis}}$ is given by the expression [1]

$$F_{1i}^{\mathrm{dis}} = \frac{\rho_0 v_s^2}{B_0^2}\left\{\left[B_{0i}\left(\mathbf{B}_0\frac{\partial}{\partial \mathbf{r}}\right) + \left[\mathbf{B}_0\left[\mathbf{B}_0\frac{\partial}{\partial \mathbf{r}}\right]\right]_i\right]\frac{1}{B_0^2}\left(\mathbf{B}_0\frac{\partial}{\partial \mathbf{r}}\right)B_{0j} - \left[\mathbf{B}_0\left[\mathbf{B}_0\frac{\partial}{\partial \mathbf{r}}\right]\right]_i\frac{\partial}{\partial r_j}\right\}\int d\mathbf{r}'\,Q_1(\mathbf{r}-\mathbf{r}')\,v_j(\mathbf{r}', t), \tag{4}$$

where

$$Q_1(\mathbf{r}) = \frac{1}{(2\pi)^3}\sqrt{\frac{\pi}{2}\frac{m}{\kappa T_e}}\int d\mathbf{k}e^{i\mathbf{kr}}\frac{B_0}{|\mathbf{kB}_0|}.$$

Account of plasma particle collisions in the equation of motion (3) and in the expression for $\mathbf{F}_1^{\mathrm{dis}}$, gives rise to a dissipative force $\mathbf{F}_2^{\mathrm{dis}}$ due to ion-ion collisions. To obtain an expression for $\mathbf{F}_2^{\mathrm{dis}}$ we recall the derivation of Eq. (3). Mul-

*rot = curl, [vB] = v × B

tiplying the ion kinetic equation by $\mathbf{p}$ and integrating over the momenta we have

$$\frac{\partial \rho v_i}{\partial t} = -\frac{\partial}{\partial r_j}\Pi_{ij}(\mathbf{r}, t) + \rho\frac{e_i}{M}\left\{E_i + \frac{1}{c}[\mathbf{vB}]_i\right\}, \quad (5)$$

where $\Pi_{ij}(\mathbf{r}, t)$ is the momentum flow tensor:

$$\Pi_{ij}(\mathbf{r}, t) = \int d\mathbf{p} p_i v_j f^{(i)}(\mathbf{p}, \mathbf{r}, t). \quad (6)$$

The thermal motion of the ions in a nonisothermal plasma can be neglected if (A) is satisfied; hence, as a first approximation, the momentum flow tensor can be written in the form

$$\rho v_i v_j. \quad (7)$$

Substituting this expression in (5) and eliminating the electric field $\mathbf{E}$ (this is done by taking account of the motion of the electrons in the plasma) we obtain the equation of motion (3).

When ion-ion collisions are introduced, Eq. (7), which represents the nondissipative part of the momentum flow tensor, must be supplemented by the dissipative part of $\Pi_{ij}(\mathbf{r}, t)$. We limit ourselves to the approximation linear in the deviation of the distribution function from the equilibrium (Maxwellian) function. Solving the ion kinetic equation by successive approximations in the collision integral and expressing the dissipative part of $\Pi_{ij}(\mathbf{r}, t)$ in terms of the hydrodynamic quantities we can write the equation of motion of the plasma in the form

$$\frac{\partial \mathbf{v}}{\partial t} + \left(\mathbf{v}\frac{\partial}{\partial \mathbf{r}}\right)\mathbf{v} = -\frac{v_s^2}{\rho}\frac{\partial \rho}{\partial \mathbf{r}} + \frac{1}{4\pi\rho}[\mathrm{rot}\,\mathbf{B}, \mathbf{B}] + \frac{1}{\rho_0}(\mathbf{F}_1^{\mathrm{dis}} + \mathbf{F}_2^{\mathrm{dis}}), \quad (8)$$

where the dissipative force $\mathbf{F}_2^{\mathrm{dis}}$, due to ion-ion collisions, is given by

$$\frac{\partial^2 F_{2i}^{\mathrm{dis}}}{\partial t^2} = -\frac{\sqrt{2}}{5}\rho_0 \nu_{ii} v_i^2\left[3\frac{B_{0i}(\mathbf{B}_0\partial/\partial \mathbf{r})}{B_0^2} - \frac{\partial}{\partial r_i}\right] \times \left[3\frac{B_{0j}(\mathbf{B}_0\partial/\partial \mathbf{r})}{B_0^2} - \frac{\partial}{\partial r_j}\right] v_j(\mathbf{r}, t). \quad (9)$$

Here,

$$\nu_{ii} = \frac{4}{3}\sqrt{2\pi/M}e_i^4 N_i L\,(\varkappa T_i)^{-3/2}$$

is the effective ion-ion collision frequency (L is the Coulomb logarithm), $v_i^2 = \varkappa T_i/M$, while $v_A^2 = B_0^2/4\pi\rho_0$ is the Alfvén velocity.

Equations (1), (2), and (8) form the complete system of magnetohydrodynamic equations for a single-fluid nonisothermal plasma with ion-ion collisions taken into account.

When the gradients are parallel to the fixed magnetic field $\mathbf{B}_0$ (i.e., when $\mathbf{k}\cdot\mathbf{B}_0/B_0 = k$) Eqs. (1), (2), and (8) become the ordinary hydrodynamics equations for a nonisothermal plasma (i.e., with no fixed magnetic field). Obviously the continuity equation (2) retains its form under these conditions; using the equation of motion (8) we then find

$$\frac{\partial \mathbf{v}}{\partial t} + \left(\mathbf{v}\frac{\partial}{\partial \mathbf{r}}\right)\mathbf{v} = -\frac{v_s^2}{\rho}\frac{\partial \rho}{\partial \mathbf{r}} + \mathbf{F}_2^{\mathrm{dis}} + \frac{v_s^2}{(2\pi)^2}\sqrt{\frac{\pi}{2}\frac{m}{\varkappa T_e}}\frac{\partial}{\partial \mathbf{r}}\int d\mathbf{r}'\frac{1}{(\mathbf{r}-\mathbf{r}')^2}\mathrm{div}\,\mathbf{v}(\mathbf{r}', t), \quad (10)$$

where

$$\frac{\partial^2 \mathbf{F}_2^{\mathrm{dis}}}{\partial t^2} = -\frac{4\sqrt{2}}{5}\rho_0 \nu_{ii} v_i^2\,\mathrm{grad}\,\mathrm{div}\,\mathbf{v}(\mathbf{r}, t). \quad (11)$$

We note that the dissipative term in (8) and (10), $\mathbf{F}_2^{\mathrm{dis}}$, which is due to ion-ion collisions, is a spatially localized quantity and takes account of ion inertia; this is in contrast with the other dissipative term $\mathbf{F}_1^{\mathrm{dis}}$, due to Cerenkov and cyclotron absorption. This last feature is a consequence of the time dependence of $\mathbf{F}_2^{\mathrm{dis}}$ [cf. (9) and (11)].

3. We now consider the effect of ion-ion collisions on the spectrum of magnetohydrodynamic and magnetic-sound plasma waves. In the approximation used here the magnetohydrodynamic waves for which $\mathbf{v}$ is perpendicular to $\mathbf{k}$ and $\mathbf{B}_0$ are not damped. This result follows because we have neglected terms of order ω/Ω_i in deriving the expressions for the dissipative forces $\mathbf{F}_1^{\mathrm{dis}}$ and $\mathbf{F}_2^{\mathrm{dis}}$. The magnetohydrodynamic dispersion relation is [2,3]

$$\omega^2 = k^2 v_A^2 \cos^2\vartheta, \quad (12)$$

where ϑ is the angle between $\mathbf{k}$ and $\mathbf{B}_0$.

The dispersion relation for the magnetic-sound waves for which $\mathbf{v}$ lies in the plane of $\mathbf{k}$ and $\mathbf{B}_0$ is

$$\omega_\pm^2 = \tfrac{1}{2}k^2\{v_A^2 + v_s^2 \pm [(v_A^2 + v_s^2)^2 - 4v_A^2 v_s^2\cos^2\vartheta]^{1/2}\},$$

$$\gamma_\pm = \frac{kv_s}{2|\cos\vartheta|}\sqrt{\frac{\pi}{8}\left|\frac{e_i}{e}\right|\frac{m}{M}} \times\left\{1 \pm \frac{\cos 2\vartheta\,[(v_s/v_A)^2\cos 2\vartheta - 1]}{[1 + (v_s/v_A)^4 - 2(v_s/v_A)^2\cos 2\vartheta]^{1/2}}\right\} + \frac{2\sqrt{2}}{5}\nu_{ii}\left(\frac{v_i}{v_s}\right)^2 \times\left\{\frac{1}{2} + \frac{9}{8}\left(\frac{v_s}{v_A}\right)^2\sin^2\vartheta \mp \frac{1}{8}\left[1 + \left(\frac{v_s}{v_A}\right)^4 - 2\left(\frac{v_s}{v_A}\right)^2\cos 2\vartheta\right]^{-1/2} \times\left[\left(1 - \left(\frac{v_s}{v_A}\right)^2\cos 2\vartheta\right)\left(4 + 3\left(\frac{v_s}{v_A}\right)^2\sin^2\vartheta\right) + 2\sin^2\vartheta\left(2 + 3\left(\frac{v_s}{v_A}\right)^2(1 + \cos^2\vartheta)\right)\right]\right\}. \quad (13)$$

For waves that propagate along the fixed magnetic field ($\vartheta = 0$) we have

$$\omega_+^2 = k^2 v_A^2, \quad \gamma_+ = 0, \quad \omega_-^2 = k^2 v_s^2,$$

$$\gamma_- = \sqrt{\frac{\pi}{8}\left|\frac{e_i}{e}\right|\frac{m}{M}}\, kv_s + \frac{2\sqrt{2}}{5}\nu_{ii}\left(\frac{v_i}{v_s}\right)^2. \qquad (14)$$

We note that ω_- and γ_- give the frequency and damping factor for the ordinary hydrodynamic waves, i.e., waves that propagate in the absence of an external magnetic field.

It follows from (13) and (14) that the collision contribution to the damping factor is independent of the magnitude of the wave vector. Thus, in the approximation used here particle collisions do not act to disperse a wave packet in any direction in space (do not affect the shape of the packet) and only cause an exponential damping in time. Hence the spreading of a wave packet is due completely to the Cerenkov absorption and is a linear function of time, as shown in [1]. The spreading rate is

$$\sqrt{(\pi/8)\,|e_i/e|\,(m/M)}\; v_s.$$

Equations (13) and (14) show that the collision absorption becomes greater than the Cerenkov absorption when

$$\frac{1}{k} = \lambda > l_i \frac{5\sqrt{\pi}}{8}\sqrt{\left|\frac{e_i}{e}\right|\frac{m}{M}}\left(\left|\frac{e_i}{e}\right|\frac{T_e}{T_i}\right)^{3/2},$$

where $l_i = v_i/\nu_{ii}$ is the ion mean free path. In the other limiting case, where

$$\lambda \ll l_i \sqrt{\left|\frac{e_i}{e}\right|\frac{m}{M}}\left(\left|\frac{e_i}{e}\right|\frac{T_e}{T_i}\right)^{3/2}, \qquad (15)$$

the particle collisions in the plasma can be neglected. Thus, Eq. (15) determines the limits of applicability of the hydrodynamic analysis of Klimontovich and Silin. [1]

The appearance of a parameter with the dimensions of length l_i in the equations of motion (8) and (11) gives us some basis for postulating the existence of stationary shock waves of finite width in the hydrodynamics of a nonisothermal plasma with ion-ion collisions taken into account. However, a simple analysis of Eqs. (2) and (11) for the one-dimensional case shows that there can be no stationary shock wave with a finite front width in the approximation used here.

4. The dispersion relations (12) and (13) can also be obtained by solving the electromagnetic dispersion equation:

$$|\, k^2\delta_{ij} - k_i k_j - \omega^2 c^{-2}\,\varepsilon_{ij}\,(\omega, \mathbf{k})\,| = 0. \qquad (16)$$

The dielectric tensor is computed in the usual way, by solving the kinetic equations for the electrons and ions with ion-ion collisions taken into account and introducing the conditions in (A) and (B). As a result we obtain

$$\varepsilon_{ij}(\omega, \mathbf{k}) = \begin{pmatrix} \varepsilon_{11} & 0 & 0 \\ 0 & \varepsilon_{22} & \varepsilon_{23} \\ 0 & \varepsilon_{32} & \varepsilon_{33} \end{pmatrix}, \qquad (17)$$

where*

$$\varepsilon_{11} = \omega_{Li}^2 / \Omega_i^2,$$

$$\varepsilon_{22} = \frac{\omega_{Li}^2}{\Omega_i^2} + i\sqrt{2\pi}\,\frac{\omega_{Li}^2 v_s^2 k \sin^2\vartheta}{\omega\Omega_i^2 v_s\,|\cos\vartheta|}\sqrt{\left|\frac{e_i}{e}\right|\frac{m}{M}} + i\frac{\sqrt{2}}{5}\frac{\omega_{Li}^2\nu_{ii}v_i^2k^2\sin^2\vartheta}{\omega^3\Omega_i^2},$$

$$\varepsilon_{33} = -\frac{\omega_{Li}^2}{\omega^2} + \frac{\omega_{Li}^2}{v_s^2k^2\cos^2\vartheta}\left(1 + i\sqrt{\frac{\pi}{2}\left|\frac{e_i}{e}\right|\frac{m}{M}}\,\frac{\omega}{kv_s\,|\cos\vartheta|}\right) + i\frac{4\sqrt{2}}{5}\frac{\omega_{Li}^2\nu_{ii}v_i^2k^2\cos^2\vartheta}{\omega^5},$$

$$\varepsilon_{23} = -\varepsilon_{32} = -i\frac{\omega_{Li}^2}{\omega\Omega_i}\operatorname{tg}\vartheta\left(1 + i\sqrt{\frac{\pi}{2}\left|\frac{e_i}{e}\right|\frac{M}{m}}\,\frac{\omega}{kv_s\,|\cos\vartheta|} - \frac{2\sqrt{2}}{5}\frac{\omega_{Li}^2\nu_{ii}v_i^2k^2\sin\vartheta\cos\vartheta}{\omega^4\Omega_i}\right).$$

If there is no fixed magnetic field the acoustic wave spectrum (14) corresponds to the longitudinal electromagnetic plasma wave spectrum

$$\varepsilon^l(\omega, k) = 0, \qquad (18)$$

where

$$\varepsilon^l(\omega, k) = \frac{\omega_{Li}^2}{k^2v_s^2} - \frac{\omega_{Li}^2}{\omega^2} + i\left(\sqrt{\frac{\pi}{2}\left|\frac{e_i}{e}\right|\frac{m}{M}}\,\frac{\omega\omega_{Li}^2}{k^3v_s^3} + \frac{4\sqrt{2}}{5}\frac{\omega_{Li}^2\nu_{ii}k^2v_i^2}{\omega^5}\right). \qquad (19)$$

5. In conclusion we point out the limits of applicability of the magnetohydrodynamic equations obtained above for a nonisothermal plasma with ion-ion collisions taken into account. As we have indicated, in solving the ion kinetic equation one usually makes use of an expansion in powers of the collision integral. An estimate of the successive terms in the expansion shows that the expansion parameter is the small quantity

$$\frac{\lambda}{l_i}\left(\left|\frac{e}{e_i}\right|\frac{T_i}{T_e}\right)^{3/2} \ll 1. \qquad (20)$$

It is evident that (20) is more general than (15).

The authors are indebted to V. P. Silin for discussion.

[1] Yu. L. Klimontovich and V. P. Silin, JETP **40**, 1213 (1961), Soviet Phys. JETP **13**, 852 (1961).

[2] K. N. Stepanov, Ukr. fiz. Zhurn. (Ukrainian Physics Journal) **4**, 5 (1959).

[3] V. P. Silin and A. A. Rukhadze, Electromagnitnye svoĭstva plazmy i plazmopodobynykh sred (Electromagnetic Properties of Plasma and Plasma-Like Media), Atomizdat, 1961.

Translated by H. Lashinsky
313

*tg = tan.

COMMENT ON THE PROBLEM OF THREE PARTICLES WITH POINT INTERACTIONS

R. A. MINLOS and L. D. FADDEEV

Moscow State University

Submitted to JETP editor June 3, 1961

J. Exptl. Theoret. Phys. (U.S.S.R.) 41, 1850-1851 (December, 1961)

An integral equation for the wave function of three particles with point interactions is considered. It is shown that the discrete spectrum of the equation is infinite and extends to $-\infty$.

SKORNYAKOV and Ter-Martirosyan[1] have obtained an integral equation for the determination of the wave function of a system of three particles interacting via point-like potentials. In the simplest case of scalar identical particles this equation has the form

$$\left(\alpha+i\sqrt{z-\tfrac{3}{4}\mathbf{k}^2}\right)\varphi(\mathbf{k})+\frac{1}{\pi^2}\int\frac{\varphi(\mathbf{k}')\,d\mathbf{k}'}{\mathbf{k}^2+\mathbf{k}\mathbf{k}'+\mathbf{k}'^2-z}=0. \quad (1)$$

However, as was first noted by Danilov,[2] the corresponding homogeneous equation has a solution for arbitrary z, so that Eq. (1) does not uniquely determine the required solution.

The asymptotic form of any solution $\varphi(\mathbf{k}, z)$ is

$$\varphi(\mathbf{k}, z)=A(z)\frac{\sin s_0\ln|\mathbf{k}|}{\mathbf{k}^2}+B(z)\frac{\cos s_0\ln|\mathbf{k}|}{\mathbf{k}^2}+o\left(\frac{1}{\mathbf{k}^2}\right), \quad (2)$$

where s_0 is some number (see below), and the ratio $A(z)/B(z)$ can be arbitrary. Starting from the orthogonality conditions for the eigenfunctions, Danilov arrives at the following recipe: Take those solutions of Eq. (1) for which

$$A(z)=\beta B(z), \quad (3)$$

where β is a fixed parameter independent of z. Danilov proposes to express this constant β in terms of the energy of the bound state of all three particles, E_0, assuming vaguely that only one bound state with energy $E(\beta)$ exists for this choice of the solution. The parameter β is determined by the condition $E(\beta)=E_0$.

We shall show in the present paper that the homogeneous equation corresponding to Eq. (1), together with condition (3), has a solution for an infinite set of negative values z_n, which extends to $-\infty$. In other words, the model of Ter-Martirosyan and Skornyakov, in the more precise form proposed by Danilov, has an infinite number of bound states, and there is no ground state.

For the proof we restrict ourselves to the spherically symmetric solutions. These satisfy the following equation:

$$\psi(k)+\frac{2}{\pi}\int_0^\infty\ln\left(\frac{k^2+kk'+k'^2+\lambda^2}{k^2-kk'+k'^2+\lambda^2}\right)\frac{\psi(k')}{\alpha-\sqrt{3k'^2/4+\lambda^2}}\,dk'=0. \quad (4)$$

Here we have used the notations $z=-\lambda^2$ and

$$\psi(|\mathbf{k}|)=|\mathbf{k}|(\alpha-\sqrt{3\mathbf{k}^2/4+\lambda^2})\,\varphi(\mathbf{k}).$$

Making a change of variables, $k=\lambda(t^2-1)/t\sqrt{3}$ and carrying out a Mellin transformation, we obtain the equation

$$f(s)=\frac{4}{\pi\sqrt{3}}L(s)\times\left\{f(s)+\frac{2\alpha}{\lambda}\int_0^\infty[M(s-s')-M(s+s')]\,f(s')\,ds'\right\};$$

$$L(s)=\frac{2\pi}{s}\frac{\operatorname{sh}(\pi s/6)}{\operatorname{ch}(\pi s/2)},\qquad M(s)=\frac{\operatorname{sh}s(\pi-\arccos(\alpha/\lambda))}{2\sqrt{1-(\alpha/\lambda)^2}\operatorname{sh}\pi s}. \quad (5)^*$$

The solution $\psi(k)$ is related to $f(s)$ by the formula

$$\psi(k)=\int_0^\infty f(s)\sin s\,\ln\left[\frac{\sqrt{3}k}{2\lambda}+\frac{1}{\lambda}\sqrt{3k^2/4+\lambda^2}\right]ds. \quad (6)$$

The term containing the integral in (5) becomes small for large λ. Hence the equation

$$1-\frac{8}{\sqrt{3}}\operatorname{sh}\frac{\pi s}{6}\Big/s\operatorname{ch}\frac{\pi s}{2}=0$$

has a positive root s_0, the solution $f(s)$ exists for all sufficiently small α/λ and has the form

$$f(s)=\delta(s-s_0)+O(1/\lambda). \quad (7)$$

The corresponding function

$$\psi(k)=\sin s_0\ln[\sqrt{3}k/2\lambda+\lambda^{-1}\sqrt{3k^2/4+\lambda^2}]+O(1/\lambda)$$

has the asymptotic form (2) for large k, where

$$A(-\lambda^2)=\cos s_0\ln(\sqrt{3}/\lambda)+O(\lambda^{-1}),$$

$$B(-\lambda^2)=\sin s_0\ln(\sqrt{3}/\lambda)+O(\lambda^{-1}).$$

With these $A(z)$ and $B(z)$, Eq. (3) has an in-

*sh = sinh, ch = cosh.

finite number of roots z_n, no matter what the value of β is. These roots extend to $-\infty$ and have the asymptotic form

$$z_n = -3\exp\left(\frac{2\pi n}{s_0} - \frac{2\,\mathrm{arc\,ctg}\,\beta}{s_0}\right)[1 + O(\lambda^{-1})]. \quad (8)^*$$

We note that a similar situation obtains in the so-called "fall of the particles to the center." [3]

In conclusion we should like to remark that the model of Ter-Martirosyan and Skornyakov is apparently not the only physically acceptable model for the description of a system of three particles with point interactions. A more general scheme is discussed in a mathematical paper of the authors.[4]

*arc ctg = $\cot^{-1}$.

[1] K. A. Ter-Martirosyan and G. V. Skornyakov, JETP **31**, 775 (1956), Soviet Phys. JETP **4**, 648 (1957).

[2] G. S. Danilov, JETP **40**, 498 (1961), Soviet Phys. JETP **13**, 349 (1961).

[3] L. D. Landau and E. M. Lifshitz, Quantum Mechanics, Pergamon Press, London (1958).

[4] R. A. Minlos and L. D. Faddeev, DAN SSSR **141**, No. 6 (1961), Soviet Phys. Doklady **6**, (1962).

Translated by R. Lipperheide
314

SPACING OF NUCLEAR ENERGY SURFACES

V. A. KRAVTSOV

Leningrad Polytechnic Institute

Submitted to JETP editor June 17, 1961

J. Exptl. Theoret. Phys. (U.S.S.R.) 41, 1852-1858 (December, 1961)

A study of the distances between nuclear energy levels derived from experimental data reveals that the mean distances decrease approximately as $A^{-1/2}$. It is confirmed that, on the average, between an even-even surface and the surface of a nucleus with odd mass number A is greater than the distance between an odd-odd surface and the surface of a nucleus with odd A. These mean distances are given by the empirical formula (11). The distances between the surfaces are found to increase for magic numbers and on the boundaries of regions of deformed nuclei.

NUCLEAR energy surfaces are surfaces in a space with coordinates Z, N, and E_b where Z —number of protons, N —number of neutrons, and E_b —binding energy of the given nucleus. The binding energy E_b is the sum of the masses of the nucleons comprising the nucleus minus the mass of the nucleus. We distinguish between four energy surfaces, depending on the parities of Z and N: even-even, even-odd, odd-even, and odd-odd. As is well known, the second and third energy surfaces almost merge into one in the case of nuclei with odd mass number A, whereas the even-even and odd-odd surfaces are located at a considerable distance from the surface for odd A. We consider here only the energy surfaces obtained from experimental data.

The experimental values of the binding energy E_b have been calculated from the best nuclide mass values known on June 1, 1960. The binding energy of light nuclei with $A \leq 70$ are taken from the tables of Everling et al,[1] while those for medium masses are taken from the tables of Wapstra[2] with certain modifications. The binding energies of the nuclei from Xe to Eu were taken from the paper of Johnson and Nier,[3] while the values from Hf to Fr are taken from tables[4] calculated by the author from mass-spectroscopic measurements[5,6] and from the reaction and decay energies. The binding energies of nuclei heavier than Fr are taken from the tables of Foreman and Seaborg. Although listed in Wapstra's tables, the masses of the nuclides in the region from Ru to Xe were insufficiently accurate for use.

Nuclei with different parities have different binding energies because of the presence of pairing energy. The neutron pairing energy (the energy released when the (N + 2)-nd and the (N + 1)-st neutrons form a pair) is defined as

$$P_n(Z, N+2) = B_n(Z, N+2) - B_n(Z, N+1), \quad (1)$$

where Z and N are even and $B_n(Z, N)$ is the binding energy of the last (N-th) neutron or the energy necessary to remove this neutron from a nucleus with Z protons. The neutron pairing energy can be expressed in different fashion, directly in terms of the total binding energies:

$$P_n(Z, N+2) = 2\left\{\tfrac{1}{2}[E_{ee}(Z, N+2) + E_{ee}(Z, N)] - E_{eo}(Z, N+1)\right\} = 2S_n(Z, N+1), \quad (2)$$

where E_{ee} —binding energy of even-even nuclei and E_{eo} —binding energy of even-odd nuclei.

As shown in [7], the neutron pairing energy provides an approximate expression for double the distance S_n between the even-even and even-odd surfaces. Figure 1 shows the intersection between the plane Z = 26 and the even-even and odd-odd surfaces, with reduced slope. The ordinates (in Mev) are

$$E_0 - E_b = 9(Z + N) - E_b(Z, N). \quad (3)$$

It is seen from Fig. 1 that $S_n(Z, N+1) = AL$ is the distance between the even-even and even-odd surfaces in the plane Z = const at the point N+1 = 31, provided we approximate the arc CBF by the line CF.

In the same fashion we introduce the distance

$$S_n(Z, N) = E_{ee}(Z, N) - \tfrac{1}{2}[E_{eo}(Z, N+1) + E_{eo}(Z, N-1)], \quad (4)$$

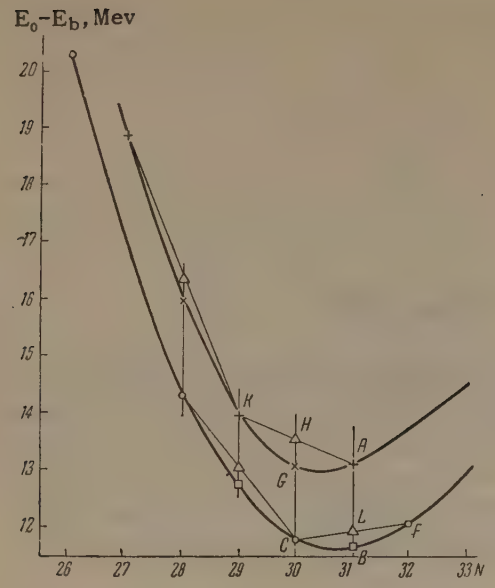

FIG. 1. Traces of the even-even and even-odd energy surfaces with decreasing slope on the plane Z = 26 (Fe): ordinate $E_0 - E_b = 9(Z + N) - E_b(26, N)$[Mev]; the segment $AL = S_n(26, 31) = (1/2) P_n(26, 32)$; the segment $CH = S_n(26, 30)$.

represented in the figure by the segment CH at the point N = 30. It is seen from Fig. 1 that the exact distance between these surfaces in the plane Z = const is greater than $S_n(Z, N+1)$ and smaller than $S_n(Z, N)$. We can therefore assume that the distance between the surfaces along the section Z = const is very close to the arithmetic mean of $S_n(X, N+1)$ and $S_n(Z, N)$:

$$D_n(Z, N) = \tfrac{1}{2}[S_n(Z, N+1) + S_n(Z, N)]$$
$$= \tfrac{1}{4}[3E_{ee}(Z, N) - 3E_{eo}(Z, N+1)$$
$$+ E_{ee}(Z, N+2) - E_{eo}(Z, N-1)]. \quad (5)$$

The existence of the energy gap Δ enabled Bohr, Mottelson, and Pines [8] and Belyaev [9] to apply the theory of superconductivity to nuclear matter. Migdal [10] derived a formula for the energy gap Δ in terms of the nuclear masses, identical to formula (5) for $D_n(Z, N)$. It follows therefore that the distance $D_n(Z, N)$ coincides with the energy gap Δ.

Expanding some of the binding energies E_{ee} and E_{eo} in a Taylor series, we can show that the exact distance between the surfaces, along the section Z = const on the portion from N to N+1, differs from $D_n(Z, N)$ only by the amount

$$\frac{1}{2\cdot 2!}\left\{\frac{\partial^2 E_{ee}(Z, N)}{\partial N^2} - \frac{\partial^2 E_{eo}(Z, N-1)}{\partial N^2}\right\}$$
$$+ \frac{3}{2\cdot 3!}\left\{\frac{\partial^3 E_{ee}(Z, N)}{\partial N^3} - \frac{\partial^3 E_{eo}(Z, N-1)}{\partial N^3}\right\} + \ldots \quad (6)$$

The intersections between the even-even and even-odd surfaces and the plane Z = const are actually at almost equal distance from each other, and therefore expression (6) is approximately equal to zero. Consequently, $D_n(Z, N)$ is a good approximate expression for the distance between the even-even and even-odd surfaces in the plane Z = const in the interval between N and N+1.

We can similarly express the distance between the traces of the even-even and odd-even surfaces on the surface N = const in the interval between Z and Z+1:

$$D_p(Z, N) = \tfrac{1}{2}[S_p(Z+1, N) + S_p(Z, N)]$$
$$= \tfrac{1}{4}[3E_{ee}(Z, N) - 3E_{oe}(Z+1, N)$$
$$+ E_{ee}(Z+2, N) - E_{oe}(Z-1, N)]. \quad (7)$$

The distance between the odd-even and odd-odd surfaces on Z+1 = const in the interval from N to N+1 will be

$$D_n(Z+1, N) = \tfrac{1}{2}[S_n(Z+1, N+1) + S_n(Z+1, N)]$$
$$= \tfrac{1}{4}[3E_{oe}(Z+1, N) - 3E_{oo}(Z+1, N+1)$$
$$+ E_{oe}(Z+1, N+2) - E_{oo}(Z+1, N-1)]. \quad (8)$$

The distance from the even-odd surface to the odd-odd surface on the section N+1 = const in the interval from Z to Z+1 is

$$D_p(Z, N+1) = \tfrac{1}{2}[S_p(Z+1, N+1) + S_p(Z, N+1)]$$
$$= \tfrac{1}{4}[3E_{eo}(Z, N+1) - 3E_{oo}(Z+1, N+1)$$
$$+ E_{eo}(Z+2, N+1) - E_{oo}(Z-1, N+1)]. \quad (9)$$

Figures 2 and 3 show the dependence on the number of neutrons N of the distances $D_n(Z, N)$ and $D_n(Z+1, N)$ between energy surfaces of different parity, at the sections Z = const and Z+1 = const respectively. The distances are calculated from the experimental data by means of formulas (5) and (8). Figures 4 and 5 show the dependence of the distances $D_p(Z, N)$ and $D_p(Z, N+1)$ between energy surfaces of different parity at the sections N = const and N+1 = const on the number of protons Z. The distances were calculated from the experimental data by means of formulas (7) and (9).

A study of Figs. 2—5 shows that the distances between energy surfaces of different parity depend on the number of nucleons in a rather complicated manner. From the well known semi-empirical Weizsäcker-Fermi formula we obtain for this distance

$$D = \delta A^{-3/4}, \quad (10)$$

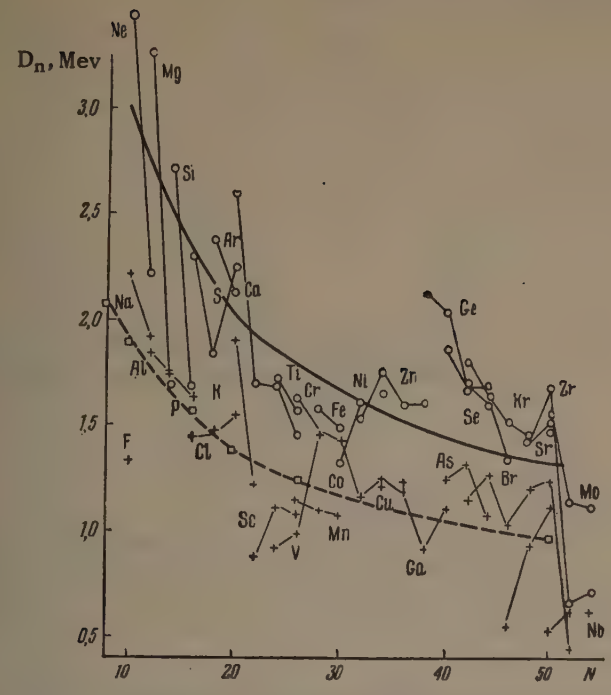

FIG. 2. Distance D_n between traces of energy surfaces of different parity on the surface Z = const as a function of the number of neutrons N, for $N \leq 54$. The points pertaining to identical sections are connected by a broken line, tagged by the element symbol. o – points for distance between even-even surface and even-odd surface; + – points for distance between odd-even and odd-odd surfaces. Solid curve – for average distances D_e dashed curve – for average distances D_o, calculated by formula (11).

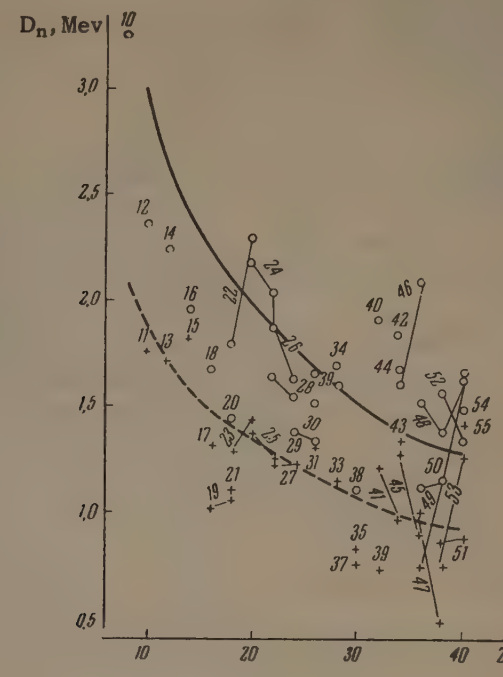

FIG. 4. Distances D_p between energy surfaces of different parity on the sections N = const as a function of the number of protons Z, for $Z \leq 40$. The points pertaining to identical sections are joined by a broken line marked by the number of neutrons N. o – points for distances between even-even and odd-even surfaces; + – points for distances between even-odd and odd-odd surfaces. Continuous curve – for mean values of D_e calculated from formulas (11); dashed curve – the same for D_o.

where A = Z + N – mass number and δ – constant. This formula is suitable both for the distance between the even-even surface and the surface for nuclei with odd A, and for the distance between the surface for nuclei with odd A and the odd-odd surface. Figures 2–5 show that the distance D_e between the even-even surface and the surface for odd A (designated by circles in the figures) are in the mean greater than the distances D_o between the surface for odd A and the odd-odd surface (designated by crosses).

We determined the average empirical values of the distances D_e and D_o, calculated by formulas (5) and (7)–(9). For this purpose we calculated the coefficients of the equation that relates log D with log A. The least-squares calculations were made separately for the distance D_e between the even-even surface and the surface for nuclei with

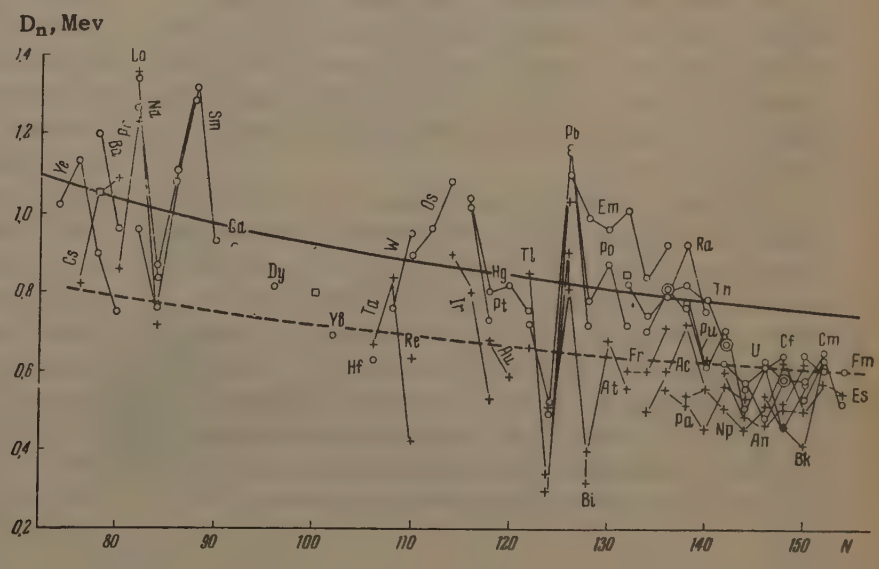

FIG. 3. The same as Fig. 2, but for $74 \leq N \leq 154$; notation the same as in Fig. 2.

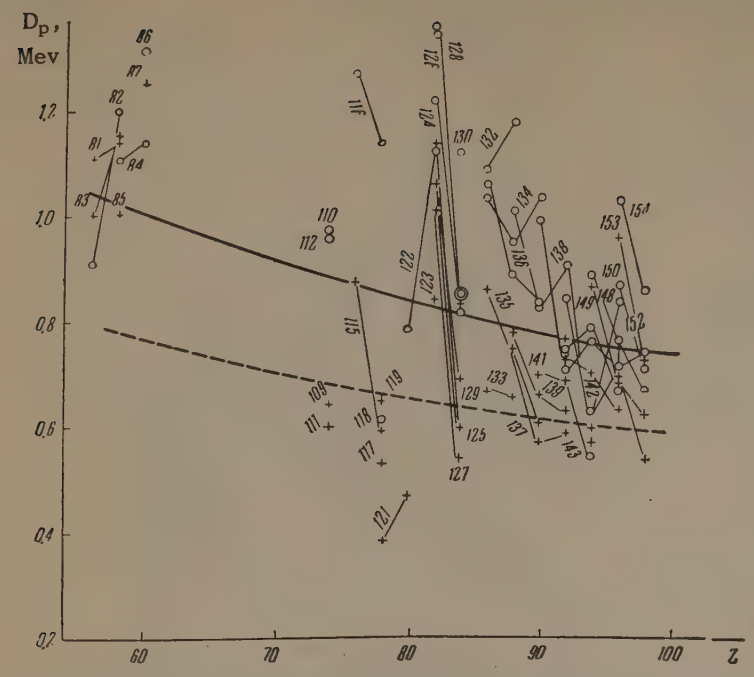

FIG. 5. The same as in Fig. 4, but for $54 \leq Z \leq 98$; notation the same as in Fig. 4.

odd A and for the distances D_o from the surface for nuclei with odd A to the even-even surface. The coefficients for the first distances (D_e) were calculated from 228 experimental values of these distances. The coefficients for the second distance (D_o) were calculated from 198 experimental values. These calculations yield the mean distances as functions of the mass number A:

$$D_e = 14.78 \cdot A^{-0.54} \text{ Mev}. \quad D_o = 7.25 \cdot 10^{-0.45} \text{ Mev}, \quad (11)$$

Comparing these formulas with the eariler expression (10) for D, contained in the Weizsäcker-Fermi formula, we see that the distances D decrease with A more slowly than previously assumed (approximately as $A^{-1/2}$). It is obvious that D depends on A in the same manner as the pairing energy, which, as shown earlier by the author,[7] also apparently decreases as $A^{-1/2}$. By studying the variation of the mean difference of the distances between surfaces $D_e - D_o$ we can see that as A increases this difference decreases uniformly from $D_e - D_o = 1.05$ Mev for light nuclei ($A = 20$) to $D_e - D_o = 0.15$ Mev for the heaviest nuclei ($A = 250$).

The mean values of the distances are shown in Figs. 2—5. The fact that the distance between the even-even surface and the surface for nuclei with odd A is greater than the distance between the surface for nuclei with odd A and the even-even surface was pointed out by Cameron.[11] But the distances between energy surfaces of different parity are excluded from Cameron's new mass formula. These distances, combined by Cameron with the shell effects are given in the form of a table of numerical corrections. Studying the course of the experimental points on Figs. 2—5, we see that at the magic and semi-magic numbers $N = 20$, 38 or 40, 50, 82 and 126 and $Z = 20$, 40 and 82 a certain increase is noted in these distances, owing to the shell effect. This increase occurs for both the even D_e and the odd D_o. Figure 3 shows also for the distances at $N = 88$ and $N = 116$ two maxima, probably connected with the start and the end of the region of deformed nuclei of rare-earth atoms. In the intervals between these two maxima we see an appreciable decrease in the distance, with a minimum in the second half of the region of deformed nuclei.

As indicated earlier, the pairing energies are connected with the distances between energy surfaces of different parity [see, for example, formulas (2) and (5)]. As indicated by Giese and Benson[12] and by the author,[7] the pairing energy has minima, near the magic numbers, while the distance between the energy surfaces increases. This increase in the distances between energy surfaces of different parity is due to the formation of shell grooves on the energy surfaces, the existence of which was pointed out by the author earlier[13] (see Fig. 6). As can be seen from Fig. 6, the formation of the shell groove leads to an increase in the distance between the energy surfaces at a magic number, and at the same time, the segment $S_n(Z, 125)$, equal to twice the pairing energy, decreases sharply when $N = 125$. The increase in the distances between the energy surfaces on both boundaries of the

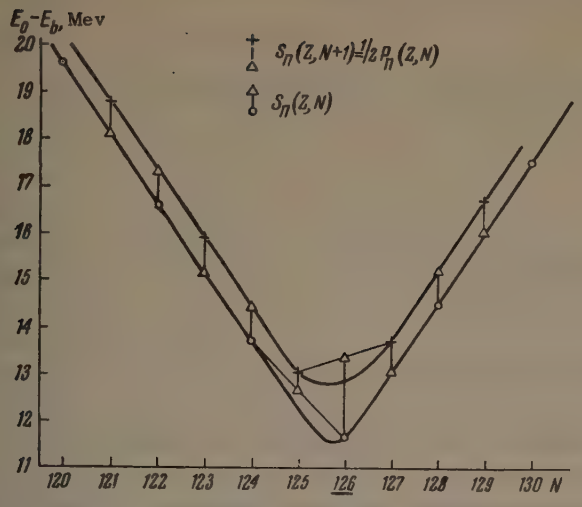

FIG. 6. Intersection of even-even and even-odd energy surfaces of decreasing slope with the plane Z = 82(Pb). Ordinate $E_0 - E_b = 400 + 6(Z + N) - E_b(82, N)$[Mev]; $S_n(Z, N)$ and $S_n(Z, N + 1)$ are determined by formulas (2) and (4).

rare-earth region of deformed nuclei corresponds to an increase in the pairing energy, as was shown in [7].

It can be noted on Figs. 2 and 4 that D_n and D_p increase considerably above their mean values when N and Z are close to 40. This increase is greater and broader than expected for the semi-magic number 40. A similar increase in the pairing energies P in the same region is seen also in the curves of [7]. Unfortunately, the nuclide masses from Ga to Ru have not been measured with sufficient accuracy, and any conclusion concerning this increase in D and P would be premature. It would be interesting to measure the masses of the nuclides in this region with greater accuracy.

[1] Everling, Konig, Mattauch, and Wapstra, Nucl. Phys. **15**, 342 (1960).

[2] A. Wapstra, Physica **21**, 385 (1955).

[3] W. Johnson Jr. and A. Nier, Phys. Rev. **105**, 1014 (1957).

[4] B. Kravtsov, Nucl. Phys., in press.

[5] Demirkhanov, Gutkin, and Dorokhov, JETP **35**, 917 (1958) and **37**, 1217 (1959), Soviet Phys. JETP **8**, 639 (1958) and **10**, 866 (1960); Izv. AN SSSR ser. fiz. **25**, 124 (1961), Columbia Techn. Transl. p. 119.

[6] Benson, Damerow, and Ries, Phys. Rev. **113**, 1105 (1959).

[7] V. A. Kravtsov, JETP **36**, 1224 (1959), Soviet Phys. JETP **9**, 871 (1959).

[8] Bohr, Mottelson, and Pines, Phys. Rev. **110**, 936 (1958).

[9] S. Belyaev, Mat-fys. Medd. Dan. Vid. Selsk. **31**, 11 (1959).

[10] A. Migdal, Nucl. Phys. **3**, 655 (1959).

[11] A. Cameron, Can. J. Phys. **35**, 1021 (1957); Chalk River Report, CRP-690, (1957).

[12] C. Giese and J. Benson, Phys. Rev. **110**, 712 (1958).

[13] V. A. Kravtsov, Izv. AN SSSR, ser. fiz. **18**, 5 (1954).

Translated by J. G. Adashko
315

CONTRIBUTION TO THE THEORY OF ELECTROMAGNETIC FLUCTUATIONS IN A NON-STEADY-STATE PLASMA

F. V. BUNKIN

P. N. Lebedev Physics Institute, Academy of Sciences, U.S.S.R.

Submitted to JETP editor June 20, 1961

J. Exptl. Theoret. Phys. (U.S.S.R.) 41, 1859-1867 (December, 1961)

The components of the tensor $\varphi_{\alpha\beta}(\omega, t)$ of the spectral intensity of an electric current in a non-relativistic magneto-active plasma, located in strong varying electric and magnetic fields, are calculated. From the electrodynamic point of view, such a plasma can be regarded as a medium with time-varying parameters. Some general properties of such a medium are considered.

In a previous paper[1] (cited below as I), the collision-induced fluctuations were considered for a non-relativistic, non-equilibrium plasma. In this case, only the steady state was studied, in which the kinetic parameters of the plasma are unchanging in time.* Such a case is realized, for example, when a strong constant or rapidly varying electric field E acts on the plasma. A work of Silin[3] was also devoted to the study of fluctuations in a non-uniform steady-state plasma, in which a highly rarefied plasma is considered, such that collisions in it can be neglected, and the fluctuations of the electromagnetic field are entirely determined by the Cerenkov radiation of the electrons.

The present paper, which is a direct continuation of paper I, is devoted to the consideration of the electromagnetic fluctuations in a non-relativistic, periodically non-uniform plasma—a case which exists when strong variable (periodic) electric and magnetic fields act on the plasma.

1. STATEMENT OF THE PROBLEM

Let us consider a non-relativistic plasma located in strong variable electric and magnetic fields,† and also in a homogeneous constant magnetic field H_0.

By a strong electric field, we mean a field whose amplitude E_1 satisfies the condition[4,5]

$$E_1 \gtrsim E_p \equiv [3kTm\delta(\Omega^2 + \nu_{\text{eff}}^{02})/e^2]^{1/2}, \qquad (1.1)$$

where e, m are the charge and mass of the electron, k is Boltzmann's constant, T is the absolute temperature of the heavy particles of the plasma, Ω is the frequency of the field, ν_{eff}^0 is the effective collision frequency of the electron with the heavy particle in the absence of the field, δ is the mean relative fraction of the energy lost by the electron in a single collision with a heavy particle: $\delta \ll 1$ (for the precise meaning of ν_{eff} and δ, see [4,5]). We shall regard the variable magnetic field $H_{\text{ext}}(t)$ as strong (and shall accordingly consider its effect on the plasma) in the case in which its amplitude H_1 and frequency Ω satisfy the condition

$$\omega_{H_1} \equiv |e| H_1/mc \gtrsim \Omega, \qquad (1.2)$$

where c is the velocity of light.* It is easy to see that if the field H_{ext} is strong, then the electric field E_{ext} associated with it should generally be strong ($E_1 \gg E_p$). This follows from the fact that the amplitudes of the electric and magnetic fields at each point of space are connected by the linear equation $H_1 = \alpha E_1$, and therefore, by the condition (1.2),

$$E_p \lesssim A\alpha E_1 \qquad (\text{if } \omega_{H_1} \gtrsim \nu_{\text{eff}}^0)$$

or

$$E_p \lesssim A(\nu_{\text{eff}}^0/\omega_{H_1})\alpha E_1 \qquad (\text{if } \omega_{H_1} \ll \nu_{\text{eff}}^0).$$

Here $A \equiv (3kT\delta/mc^2)^{1/2}$. Thus, if special measures are not taken to make the coefficient α suffi-

*The work of Bekefi, Hirshfield and Brown,[2] which is devoted to the same problem, appeared after paper I had gone to press.

†In the problem considered by us, there will always be strong external fields; therefore, we shall omit the word "external," using in certain cases the index "ext" (E_{ext} and H_{ext}).

*We note that in the kinetic theory of electrical conduction in a plasma one usually neglects the effect of the variable magnetic field. This neglect is valid when the condition $u/c \ll 1$ is satisfied (u is the mean ordered velocity of the electron).

ciently large (large relative to A^{-1} or $A^{-1}(\nu^0_{eff}/\omega_{H_1})^{-1}$,* then, in accord with (1.2), the condition $E_p \ll E_1$ is automatically satisfied. In what follows, in speaking of a strong field, we shall always have in mind that the electric field is also strong in this case. It is evident that fulfillment of condition (1.2) no longer follows from satisfaction of the condition (1.1); therefore, the plasma may be situated in a strong electric but weak magnetic field.

The effect on the plasma of strong external variable electric and magnetic fields reduces electrodynamically to the result that the plasma becomes a medium, generally speaking, with properties that are variable in time. The problem of the fluctuating electromagnetic radiation of such a plasma, set up within the framework of macroscopic electrodynamics,[6,7] reduces to the corresponding solution of the following system of macroscopic field equations:

$$\text{rot } \mathbf{H} = \frac{1}{c}\frac{\partial \mathbf{E}}{\partial t} + \frac{4\pi}{c}\int_0^\infty \hat{K}(t,\tau)\,\mathbf{E}(t-\tau)\,d\tau + \frac{4\pi}{c}\mathbf{j},$$

$$\text{rot } \mathbf{E} = -c^{-1}\partial \mathbf{H}/\partial t. \qquad (1.3)\dagger$$

Here $\mathbf{j} = \mathbf{j}(\mathbf{r}, t)$ is the fluctuating current density at the point $\mathbf{r}$, considered as an external current. The integral term in the first equation is the total current density induced by the field $\mathbf{E}(\mathbf{r}, t)$ at the point $\mathbf{r}$,‡ and the coupling is assumed to be space-local (in correspondence with the neglect of spatial dispersion here and everywhere in what follows). The component of the tensor $K_{ik}(t, \tau)$ takes into account the effect of the i-th component of the total current density at the time t on the δ-pulse of the k-th component of the field $\mathbf{E}$, acting at the time $(t - \tau)$; for an inhomogeneous plasma, the components $K_{ik}(t, \tau)$ also depend on $\mathbf{r}$.

Before proceeding to the fluctuation part of the problem, let us consider some electrodynamic properties of a plasma in strong variable fields.

2. SOME ELECTRODYNAMIC PROPERTIES OF A PLASMA IN STRONG ELECTRIC AND MAGNETIC FIELDS

It follows from the definition of the tensor $K_{ik}(t, \tau)$ that $K_{ik}(t, \tau) = 0$ for $\tau < 0$ (principle of causality). Furthermore, if the external influence is periodic with period $2\pi/\Omega$ (and we consider only such interactions) then the components $K_{ik}(t, \tau)$ are periodic in the variable t with period $2\pi/\Omega$:

$$K_{ik}(t, \tau) = K_{ik}(t + 2\pi/\Omega, \tau).$$

The tensor

$$\sigma_{ik}(\omega, t) = \sigma_{ik}(\omega, t + 2\pi/\Omega) = \int_0^\infty K_{ik}(t, \tau)\, e^{i\omega\tau}\, d\tau \qquad (2.1)$$

is obviously a direct generalization of the ordinary conductivity tensor (relative to the total current) to the case under consideration of media with variable parameters: for a harmonic field, $\mathbf{E} = \mathbf{E}_0 e^{-i\omega t}$, the components of the current density are equal to $\sigma_{ik}(\omega, t)E_{0k}e^{-i\omega t}$. Just as for media with constant parameters, the real and imaginary parts of the components

$$\sigma_{ik}(\omega, t) = \sigma'_{ik}(\omega, t) + i\sigma''_{ik}(\omega, t)$$

must satisfy the Kramers-Kronig relations (relative to the variable ω), which follow from the analyticity of the function $\sigma_{ik}(\omega, t)$ in the upper half plane of the complex variable ω (for arbitrary t).[7] It is easy to show that the imaginary and real parts of the coefficients of the expansion

$$\sigma^{(n)}_{ik}(\omega) = \sigma^{(n)'}_{ik} + i\sigma^{(n)''}_{ik}$$

of the function $\sigma_{ik}(\omega, t)$ in the Fourier series

$$\hat{\sigma}(\omega, t) = \sum_n \hat{\sigma}^{(n)}(\omega)\, e^{in\Omega t} \qquad (2.2)$$

must satisfy these relations. The set of the tensors $\hat{\sigma}^{(n)}(\omega)$ completely determines the electrodynamic properties of the medium. It is not difficult to prove that the local absorbing properties of the medium are determined only by the "zero" tensor $\hat{\sigma}^{(0)}(\omega)$, just as they are for media with constant parameters, i.e., for example, for the harmonic field $\mathbf{E}_0 e^{-i\omega t}$, the time average of the power dissipated per unit volume is equal to

$$P = \tfrac{1}{4}[\sigma^{(0)}_{ik}(\omega)\, E_{0k}E^*_{0i} + \text{c.c.}]. \qquad (2.3)$$

Finally, we note the symmetry properties, which follow from (2.1) and (2.2):

$$\sigma_{ik}(\omega, t) = \sigma^*_{ik}(-\omega, t), \qquad (2.4)$$

$$\sigma^{(n)}_{ik}(\omega) = \sigma^{(-n)^*}_{ik}(-\omega). \qquad (2.4')$$

We now turn to the calculation of the tensors $\hat{\sigma}(\omega, t)$ and $\hat{\sigma}^{(n)}(\omega)$ for the cases of interest to us, namely, of a plasma located in strong electric and magnetic fields. On the basis of kinetic theory,[4,5] with accuracy up to the small terms

*An example of such a special case is a system in which a sufficiently small volume of plasma is placed in a resonant cavity in the region of the antinode of the magnetic field and the node of the electric field.

†rot = curl.

‡In the case under consideration, it is useful to divide the total current into the conduction current and the polarization current.

neglected by us,* we have the relation

$$\hat{\sigma}(\omega, t)\,\mathbf{E}_0 e^{-i\omega t} = -\frac{4\pi eN}{3}\int_0^\infty \mathbf{u}v^3\frac{\partial f_0(v, t)}{\partial v}\,dv, \qquad (2.5)$$

where $f_0(v, t)$ is the symmetric part of the electron velocity distribution function (normalized to unity):

$$f(\mathbf{v}, t) = f_0(v, t) + \mathbf{v}\,f_1(v, t)/v,$$

N is the density of electrons, the time dependence of which we shall neglect in what follows;† the vector u is the solution of the linear equation

$$\frac{\partial \mathbf{u}}{\partial t} + \nu(v)\mathbf{u} - \frac{e}{mc}[\mathbf{u}, \mathbf{H}_0 + \mathbf{H}_{ext}(t)] = \frac{e}{m}\mathbf{E}_0 e^{-i\omega t}, \qquad (2.6)‡$$

where $\nu(v) = \nu_m^{el}(v) + \nu_i(v) + \nu_m^{inel}(v)$ is the total number of heavy particle collisions of an electron having a velocity v. We note that the field $\mathbf{E}_{ext}$ does not appear in Eq. (2.6); on the other hand, it does enter into the kinetic equation that determines the function $f_0(v, t)$.[4,5] We shall assume that the variable field $\mathbf{H}_{ext}(t)$ is directed along the constant field $\mathbf{H}_0$, which direction is chosen for the z axis. Substituting $\mathbf{H}_{ext}(t) = \mathbf{H}_1 \cos \Omega t$ in (2.6), and solving the resulting equation, we obtain the following expression for the non-zero components of the tensor $\sigma_{ik}(\omega, t)$ [on the basis of Eq. (2.5)]:

$$\sigma_{zz}(\omega, t) = -\frac{4\pi e^2 N}{3m}\int_0^\infty \frac{v^3}{\nu(v) - i\omega}\frac{\partial f_0(v, t)}{\partial v}\,dv, \qquad (2.7)$$

$$\sigma_{xx}(\omega, t) = \sigma_{yy}(\omega, t)$$

$$= -\frac{2\pi e^2 N}{3m}\sum_{n,m} J_n(\Delta)\,J_m(\Delta)\,e^{i(n-m)\Omega t}$$

$$\times\int_0^\infty v^3\{[\nu(v) - i(\omega - \omega_H + m\Omega)]^{-1}$$

$$+[\nu(v) - i(\omega + \omega_H - n\Omega)]^{-1}\}\frac{\partial f_0(v, t)}{\partial v}\,dv; \qquad (2.7')$$

$$\sigma_{xy}(\omega, t) = -\sigma_{yx}(\omega, t) = -i\frac{2\pi e^2 N}{3m}\sum_{n,m} J_n(\Delta)\,J_m(\Delta)\,e^{i(n-m)\Omega t}$$

$$\times\int_0^\infty v^3\{[\nu(v) - i(\omega - \omega_H + m\Omega)]^{-1}$$

$$-[\nu(v) - i(\omega + \omega_H - n\Omega)]^{-1}\}\frac{\partial f_0(v, t)}{\partial v}\,dv, \qquad (2.7'')$$

where $\omega_H = |e|\,H_0/mc$, $J_n(\Delta)$ is the Bessel function, $\Delta \equiv \omega_{H_1}/\Omega = |e|\,H_1/mc\Omega$. If the field $\mathbf{H}_{ext}$ is absent (more precisely, for $\Delta \ll 1$), only a single term remains of the sums appearing on the right hand sides of (2.7′) and (2.7″), corresponding to $n = m = 0$ ($J_n(0) = \delta_{0n}$). The time dependence of the components of $\sigma_{ik}(\omega, t)$ is determined in this case only by the time dependence of the distribution function $f_0(v, t)$. For a constant or rapidly varying ($\Omega \gg \delta\nu_{eff}$) field $\mathbf{E}_{ext}$, even this source of time dependence vanishes,[4,5] and the electrodynamic properties of the plasma cease to be time dependent. Precisely this case was considered in I.

In the presence of a strong field $\mathbf{H}_{ext}(t)$ ($\Delta \gtrsim 1$), the greatest interest attaches to the case in which $\Omega \gtrsim \nu_{eff}$; under this condition, the distribution function $f_0(v, t)$ does not depend on the time, with accuracy up to small terms, and the effect of the non-stationarity is entirely brought about by a parametric change in the magnetic field. In this case, for the tensor $\sigma_{ik}^{(0)}(\omega)$ which determines the absorption properties of the medium, we obtain the following from (2.7) — (2.7″):

$$\sigma_{xx}^{(0)}(\omega) = \sigma_{yy}^{(0)}(\omega)$$

$$= -\frac{2\pi e^2 N}{3m}\sum_n J_n^2(\Delta)\int_0^\infty v^3\{[\nu(v) - i(\omega - \omega_H + n\Omega)]^{-1}$$

$$+[\nu(v) - i(\omega + \omega_H + n\Omega)]^{-1}\}\frac{\partial f_0(v)}{\partial v}\,dv, \qquad (2.8)$$

$$\sigma_{xy}^{(0)}(\omega) = -\sigma_{yx}^{(0)}(\omega)$$

$$= -i\frac{2\pi e^2 N}{3m}\sum_n J_n^2(\Delta)\int_0^\infty v^3\{[\nu(v) - i(\omega - \omega_H + n\Omega)]^{-1}$$

$$-[\nu(v) - i(\omega + \omega_H + n\Omega)]^{-1}\}\frac{\partial f_0(v)}{\partial v}\,dv. \qquad (2.8')$$

The expression for $\sigma_{zz}^{(0)}(\omega)$ is given by the right side of (2.7) with the replacement of $\partial f_0(v, t)/\partial v$ by $\partial f_0(v)/\partial v$. It follows from these expressions, with account of the condition $\Omega \gtrsim \nu_{eff}$, that, in the case of parametric change of the magnetic field under consideration, the local absorbing properties of the plasma have distinct maxima ("peaks") at the frequencies $\omega = \pm\omega_H + n\Omega$ ($n = 0, \pm 1, \ldots$), the "amplitudes" (heights) of which are deter-

*Let us list the chief small parameters which can appear in our problem. First, we have the quantity δ, which is small in many cases. Next, the small quantity $\delta\nu_{eff}/\Omega$ occurs for rapidly varying fields. In cases of strongly (or conversely, weakly) ionized plasma, there are also small parameters, equal to $\delta\nu/\nu_e$ and $\nu_e/\delta\nu$, respectively (ν_e is the number of interelectronic collisions). In what follows, in speaking of the neglect of small terms, we shall have in mind the neglect (in comparison with unity) of terms of the order of the small parameters enumerated.

†The change in the density $\Delta N(t) = \mathrm{div}\,\mathbf{E}_{ext}(t)/4\pi e$ is also necessarily small if the field $\mathbf{E}_{ext}$ is sufficiently homogeneous.

‡$[\mathbf{u}, \mathbf{H}_0 + \mathbf{H}_{ext}] = \mathbf{u} \times (\mathbf{H}_0 + \mathbf{H}_{ext})$.

mined by the quantity $\Delta = \omega H_1/\Omega$ and the number n. For a particular value of Δ, which coincides with the root of the function $J_n(x)$, the "peaks" of number n vanish. In particular, for $H_1 = x_1 mc\Omega/|e|$ [$x_1 \approx 2.5$ is the first root of the function $J_0(x)$], the zero "peak" vanishes and the plasma becomes practically locally non-absorbing at a gyromagnetic frequency $\omega = \omega_H$.* This effect of the change in the absorption of the plasma was considered briefly by Lugovoĭ[8] in connection with the discussion of the possibility of the use of cyclotron resonance for obtaining negative absorption by means of the parametric change in the external magnetic field.

3. THE SPECTRAL INTENSITY TENSOR FOR THE CURRENT FLUCTUATIONS

Just as in the case of a stationary plasma,[1-3] the spectral intensity of the fluctuation components in the case of a periodically non-stationary plasma is also of prime interest. Set within the framework of macroscopic electrodynamics, the problem reduces, in the first place, to the determination of the spectral intensity tensor of the current fluctuations $\langle j_\alpha(\mathbf{r}, \omega) j^*_\beta(\mathbf{r}', \omega')\rangle$ and in the second place to the corresponding solution of the system (1.3) which, being rewritten for the Fourier amplitudes of the field intensity $\mathbf{E}(\mathbf{r}, \omega)$ and $\mathbf{H}(\mathbf{r}, \omega)$, has the form (the r dependence is not shown)

$$\operatorname{rot}\mathbf{H}(\omega) = -i\frac{\omega}{c}\hat{\varepsilon}(\omega)\mathbf{E}(\omega) + \frac{4\pi}{c}\sum_n{}'\hat{\sigma}^{(n)}(\omega+n\Omega)\mathbf{E}(\omega+n\Omega)+\frac{4\pi}{c}\mathbf{j}(\omega),$$

$$\operatorname{rot}\mathbf{E}(\omega) = i\frac{\omega}{c}\mathbf{H}(\omega), \qquad (3.1)$$

where

$$\varepsilon_{ik}(\omega) = \delta_{ik} + i4\pi\sigma^{(0)}_{ik}(\omega)/\omega,$$

and the prime on the summation sign indicates that the term with n = 0 is omitted.

Inasmuch as spatial dispersion is neglected, the spatial correlation of the current fluctuation j is local (δ correlation)†.[9,10]

Therefore,

$$\langle j_\alpha(\mathbf{r}, \omega) j^*_\beta(\mathbf{r}+\rho, \omega+p)\rangle = D_{\alpha\beta}(\omega, p)\,\delta(\rho), \qquad (3.2)$$

where the tensor $D_{\alpha\beta}(\omega, p)$ can be connected with the correlation function of the fluctuations in the velocity of a single electron in the plasma: $\psi_{\alpha\beta}(\tau, t) = \langle v_\alpha(t) v_\beta(t+\tau)\rangle$. Actually, on the basis of the relation

$$j_\alpha(\mathbf{r}, \omega) = \frac{1}{2\pi}\int_{-\infty}^{\infty} j_\alpha(\mathbf{r}, t)\, e^{i\omega t}dt$$

(see I)

$$\langle j_\alpha(\mathbf{r}, t)\, j_\beta(\mathbf{r}+\rho, t+\tau)\rangle = Ne^2\psi_{\alpha\beta}(\tau, t)\,\delta(\rho),$$

we get*

$$D_{\alpha\beta}(\omega, p) = \frac{Ne^2}{(2\pi)^2}\int_{-\infty}^{\infty}\psi_{\beta\alpha}(\tau, t)\, e^{-ipt}e^{i\omega\tau}dtd\tau = \frac{1}{2\pi}\int_{-\infty}^{\infty}\varphi_{\beta\alpha}(\omega, t)\, e^{-ipt}dt, \qquad (3.3)$$

where

$$\varphi_{\alpha\beta}(\omega, t) = \frac{Ne^2}{2\pi}\int_{-\infty}^{\infty}\psi_{\alpha\beta}(\tau, t)\, e^{i\omega\tau}d\tau. \qquad (3.4)$$

The components of the tensors $\psi_{\alpha\beta}(\tau, t)$ and $\varphi_{\alpha\beta}(\omega, t)$ are periodic functions of t with period $2\pi/\Omega$. It is easy to establish the fact that the components $\varphi_{\alpha\beta}(\omega, t)$ and the coefficients $\varphi^{(n)}_{\alpha\beta}(\omega)$ of their expansions in Fourier series satisfy the same conditions of symmetry as the tensor components $\sigma_{ik}(\omega, t)$ and $\sigma^{(n)}_{ik}(\omega)$. The tensor $\psi_{\alpha\beta}(\tau, t)$ also possesses another obvious symmetry property which follows from its definition: $\psi_{\alpha\beta}(-\tau, t) = \psi_{\beta\alpha}(\tau, t-\tau)$. This property makes it possible to compute the tensor $\varphi_{\alpha\beta}(\omega, t)$ [or $D_{\alpha\beta}(\omega, p)$] from the velocity tensor $\psi_{\alpha\beta}(\tau, t)$, which is given only for $\tau > 0$. For this purpose, it suffices to transform Eq. (3.4) to the following form:

$$\varphi_{\alpha\beta}(\omega, t) = \frac{Ne^2}{2\pi}\left\{\int_0^\infty [\psi_{\alpha\beta}(\tau, t) + \psi_{\beta\alpha}(\tau, t-\tau)]\cos\omega\tau d\tau + i\int_0^\infty [\psi_{\alpha\beta}(\tau, t) - \psi_{\beta\alpha}(\tau, t-\tau)]\sin\omega\tau d\tau\right\}. \qquad (3.5)$$

The components $\psi_{\alpha\beta}(\tau, t)$ can be computed for $\tau > 0$ on the basis of kinetic theory, similar to what was done in I. In the interval between collisions, the electron behaves as if it were free, and

*In another paper, we propose to look into the use of this effect of the local absorption change (by means of a parametric change of the magnetic field) to produce "transparency" at frequencies $\omega = \pm\omega_H + n\Omega$ for a magneto-active plasma with dimensions that are large in comparison with the wavelength.

†We note in passing that neglect of spatial dispersion in the medium itself has no effect on the value of the spectral intensity of the radiation of the medium in the external space.[6,10]

*Some general relations of the correlation theory of periodically non-stationary random processes can be found in [11].

its velocity satisfies the equations*

$$\dot{v}_x + (\omega_H + \omega_{H_1} \cos \Omega t)\, v_y = 0,$$

$$\dot{v}_y - (\omega_H + \omega_{H_1} \cos \Omega t)\, v_x = 0, \quad \dot{v}_z = 0. \qquad (3.6)$$

We introduce the notation: $\Phi(t) \equiv \omega_H t + \Delta \sin \Omega t$. The values of $v_x(t+\tau)$, $v_y(t+\tau)$ and $v_z(t+\tau)$, computed from $v_x(t)$, $v_y(t)$ and $v_z(t)$, under the condition that no collision takes place within the time interval τ, have [on the basis of (3.6)] the form

$$v_x(t+\tau) = [v_x(t)\cos\Phi(t) + v_y(t)\sin\Phi(t)]\cos\Phi(t+\tau) + [v_x(t)\sin\Phi(t) - v_y(t)\cos\Phi(t)]\sin\Phi(t+\tau),$$

$$v_y(t+\tau) = [v_x(t)\cos\Phi(t) + v_y(t)\sin\Phi(t)]\sin\Phi(t+\tau) + [-v_x(t)\sin\Phi(t) + v_y(t)\cos\Phi(t)]\cos\Phi(t+\tau);$$

$$v_z(t+\tau) = v_z(t). \qquad (3.7)$$

Let $w(s, v) \equiv \exp[-s/l(v)]/l(v)$ [$l = v/\nu(v)$] be the distribution function for the length of the mean free path of the electrons for a given velocity v. Then, for non-zero components of $\psi_{\alpha\beta}(\tau, t)$ for $\tau > 0$, and on the basis of Eq. (3.7), we obtain the equation

$$\psi_{zz}(\tau, t) = \int_{-\infty}^{\infty} v_z^2 f_0(v, t)\, d\mathbf{v} \int_0^{\infty} e^{-s/l}\, \theta\left(\frac{s}{v} - \tau\right) \frac{ds}{l},$$

$$\psi_{xx}(\tau, t) = \psi_{yy}(\tau, t) = \cos[\Phi(t+\tau) - \Phi(t)] \times \int_{-\infty}^{\infty} v_x^2 f_0(v, t)\, d\mathbf{v} \int_0^{\infty} e^{-s/l}\, \theta\left(\frac{s}{v} - \tau\right) \frac{ds}{l},$$

$$\psi_{xy}(\tau, t) = -\psi_{yx}(\tau, t) = \sin[\Phi(t+\tau) - \Phi(t)] \times \int_{-\infty}^{\infty} v_x^2 f_0(v, t)\, d\mathbf{v} \int_0^{\infty} e^{-s/l}\, \theta\left(\frac{s}{v} - \tau\right) \frac{ds}{l}, \qquad (3.8)$$

where $\theta(t) = 1$ for $t > 0$ and $\theta(t) = 0$ for $t < 0$.

Further, let us first consider the case when the field $H_{ext}(t)$ is absent ($\Delta \ll 1$); here $\Phi(t+\tau) - \Phi(t) \equiv \omega_H \tau$. Substituting (3.8) in (3.5), and carrying out the integration first over τ and then over s, we get the following expressions for the components of the tensor $\hat{\varphi}^{(n)}(\omega)$:

$$\varphi_{zz}^{(n)}(\omega) = \frac{2}{3} Ne^2 \int_0^{\infty} v^4 \left\{ \frac{\nu(v)/\omega}{\omega^2 + i\nu(v)} + \frac{\nu(v)/(\omega + n\Omega)}{\omega + n\Omega - i\nu(v)} + \frac{in\Omega}{\omega(\omega + n\Omega)} \right\} f_0^{(n)}(v)\, dv,$$

$$\varphi_{xx}^{(n)}(\omega) = \varphi_{yy}^{(n)}(\omega) = \frac{2}{3} Ne^2 \int_0^{\infty} v^4 \left\{ \frac{1}{2} \left[\frac{\nu(v)/(\omega - \omega_H)}{\omega - \omega_H + i\nu(v)} + \frac{\nu(v)/(\omega + \omega_H)}{\omega + \omega_H + i\nu(v)} + \frac{\nu(v)/(\omega + n\Omega - \omega_H)}{\omega + n\Omega - \omega_H - i\nu(v)} + \frac{\nu(v)/(\omega + n\Omega + \omega_H)}{\omega + n\Omega + \omega_H - i\nu(v)} \right] + \frac{i\omega}{\omega^2 - \omega_H^2} - \frac{i(\omega + n\Omega)}{(\omega + n\Omega)^2 - \omega_H^2} \right\} f_0^{(n)}(v)\, dv,$$

$$\varphi_{xy}^{(n)}(\omega) = -\varphi_{yx}^{(n)}(\omega) = i \frac{2}{3} Ne^2 \int_0^{\infty} v^4 \left\{ \frac{1}{2} \left[\frac{\nu(v)/(\omega - \omega_H)}{\omega - \omega_H + i\nu(v)} - \frac{\nu(v)/(\omega + \omega_H)}{\omega + \omega_H + i\nu(v)} + \frac{\nu(v)/(\omega + n\Omega - \omega_H)}{\omega + n\Omega - \omega_H - i\nu(v)} - \frac{\nu(v)/(\omega + n\Omega + \omega_H)}{\omega + n\Omega + \omega_H - i\nu(v)} \right] + \frac{i\omega_H}{\omega^2 - \omega_H^2} - \frac{i\omega_H}{(\omega + n\Omega)^2 - \omega_H^2} \right\} f_0^{(n)}(v)\, dv, \qquad (3.9)$$

where $f_0^{(n)}(v)$ are the expansion coefficients of the distribution function $f_0(v, t)$ in a Fourier series. For a time-independent function $f_0(v)$, we have $f_0^{(n)}(v) = f_0(v)\delta_{0n}$ and Eqs. (3.9) transform into Eq. (6) in I.

In the presence of a strong magnetic field, we again obtain only the case in which $\Omega \gtrsim \nu_{eff}$; here, $\Omega \gg \delta\nu_{eff}$ and the function $f_0(v)$ is time independent (with accuracy up to small terms). Substituting (3.8) in (3.5) for this case, we get

$$\varphi_{zz}^{(n)}(\omega) = \delta_{0n}\varphi_{zz}(\omega) = \frac{4}{3}\delta_{0n} Ne^2 \int_0^{\infty} v^4 \nu(v) [\omega^2 + \nu^2(v)]^{-1} f_0(v)\, dv;$$

$$\varphi_{xx}^{(n)}(\omega) = \varphi_{yy}^{(n)}(\omega) = \frac{2}{3} Ne^2 \sum_k J_k(\Delta) J_{k-n}(\Delta) \times \int_0^{\infty} v^4 \nu(v) \{[(\omega - \omega_H - (k-n)\Omega)^2 + \nu^2(v)]^{-1} + (-1)^n [(\omega + \omega_H - (k-n)\Omega)^2 + \nu^2(v)]^{-1}\} f_0(v)\, dv;$$

$$\varphi_{xy}^{(n)}(\omega) = -\varphi_{yx}^{(n)}(\omega) = i \frac{2}{3} Ne^2 \sum_k J_k(\Delta) J_{k-n}(\Delta) \times \int_0^{\infty} v^4 \nu(v) \{[(\omega - \omega_H - (k-n)\Omega)^2 + \nu^2(v)]^{-1} - (-1)^n [(\omega + \omega_H - (k-n)\Omega)^2 + \nu^2(v)]^{-1}\} f_0(v)\, dv. \qquad (3.10)$$

*The inhomogenous equations, with the right hand sides equal to $(e/m)E_{ext\ i}(t)$ are more accurate equations for the motion of the electron between collisions. However, it can be shown that account of the action of the field $E_{ext}(t)$ results in a contribution of the order δ to the quantity of interest to us; we therefore start out with the homogeneous equation (3.6).

For $\Delta \ll 1$, these expressions transform into the Eqs. (6) of I.

[1] F. V. Bunkin, JETP 41, 288 (1961); Soviet Phys. JETP 14, 206 (1962).

[2] Bekefi, Hirshfield, and Brown, Phys. Fluids 4, 173 (1961).

[3] V. P. Silin, JETP 41, 963 (1961), Soviet Phys. JETP 14, 685 (1962).

[4] V. L. Ginzburg and A. V. Gurevich, Usp. Fiz. Nauk 70, 201, 393 (1960), Soviet Phys. Uspekhi 3, 115 (1960).

[5] V. L. Ginzburg, Rasprostranenie electromagnitnykh voln v plazme (Electromagnetic Wave Propagation in a Plasma) Fizmatgiz, 1960.

[6] S. M. Rytov, Teoriya electricheskikh fluktuatsii i teplovogo izlucheniya (The Theory of Electrical Fluctuations and Thermal Radiation) AN SSSR, 1953, DAN SSSR 110, 371 (1956), Soviet Phys. Doklady 1, 555 (1957).

[7] L. D. Landau and E. M. Lifshitz, Élektrodinamika sploshnykh sred (Electrodynamics of Continuous Media) Gostekhizdat, 1957.

[8] V. N. Lugovoĭ, JETP 41, 1562 (1961), Soviet Phys. JETP 14, 1113 (1962).

[9] Yu. L. Klimontovich, JETP 34, 173 (1958), Soviet Phys. JETP 7, 119 (1958).

[10] V. P. Silin, Izv. vuzov Radiofizika 2, 198 (1959).

[11] L. I. Gudzenko, Radiotekhnika i electronika 4, 1062 (1959).

Translated by R. T. Beyer
316

A POSSIBLE MODEL OF Λ-PARTICLE PRODUCTION IN HIGH ENERGY πN COLLISIONS

WANG JUNG and HU SHIH-KO

Joint Institute for Nuclear Research

Submitted to JETP editor June 22, 1961

J. Exptl. Theoret. Phys. (U.S.S.R.) 41, 1868-1869 (December, 1961)

A possible model of Λ-particle production in high energy πN-collisions, suggested by D. I. Blokhintsev and Wang Jung, is considered. The polarization and the distribution of transverse momentum of the Λ particles, and also the percentage of particles emitted in the forward direction in the center-of-mass system are calculated. It is shown that the model is in agreement with the available experimental data.

SOLOV'EV and Wang Kang-ch'ang et al.[1-3] have recently measured the transverse momentum and angular distribution of Λ particles produced in high-energy πN-collisions (momentum of the incident π meson ≈ 7 Bev/c), and have observed longitudinal polarization of the Λ-particle. In this article we shall show that all characteristic features of Λ-particle production in high-energy πN collisions are in agreement with the model proposed by Blokhintsev and Wang Jung.[4] This model has two essential features: 1) the pole term corresponding to the diagram shown in the accompanying figure gives the dominant contribution; 2) the (ΛNK) vertex part takes the form $1 \pm \gamma_5$ (this model does not assume parity conservation in strong interactions[5]).

Aside from conservation of energy-momentum and strangeness, there are no other restrictions on the multiplicity of particles which may be produced jointly with the Λ. The theoretical results discussed here, as well as the corresponding experimental results, are almost independent of this multiplicity.

The following results were obtained from this model:

1) The optimum transverse momentum of the Λ particle (≈ 400 Mev/c) is almost independent of the energy of the incident π meson.

2) In the center-of-mass system, approximately 13.7% of the Λ particles are emitted in the forward direction.

These are precisely the characteristic kinematical features of Λ-particle production experiments ([2] and also private communication from M. I. Solov'ev). Furthermore, according to this model it is possible to predict the following:

3) The Λ particles are polarized in the laboratory system; the direction of the polarization

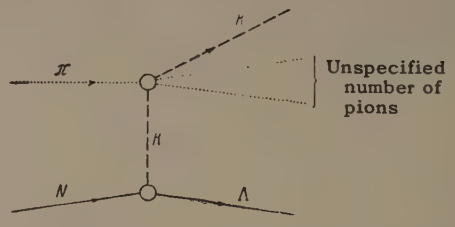

vector coincides with the direction of the momentum of the Λ, i.e., they are longitudinally polarized. Furthermore, the degree of polarization is

$$\overline{P} = \begin{cases} +v/c & \text{for } 1-\gamma_5 \\ -v/c & \text{for } 1-\gamma_5 \end{cases},$$

where v denotes the velocity of the Λ particle in the laboratory system.

For Λ decay the asymmetry parameter is $\alpha \approx -0.85$.[6]

Theoretical values of $\alpha\overline{P}$ are given in the table. We see that this model agrees with the experimental results[3] in so far as the cases with $p_\Lambda \leq 1200$ Mev/c are concerned, if the vertex part takes the form $1 + \gamma_5$.

As far as cases with $p_\Lambda > 1200$ Mev/c are concerned, no experimental data have been obtained because certain difficulties of a kinematical nature arise in connection with the identification of the Λ particle.[3] But momenta in the range $p_\Lambda > 1200$ Mev/c in the laboratory system correspond to larger angles (with respect to the backward direction) and smaller momenta of the Λ particle

p_Λ in Mev/c (lab system)	$\alpha\overline{P}$ (for $1+\gamma_5$)	$\alpha\overline{P}$ (for $1-\gamma_5$)
~200	−0.15	+0.15
~600	−0.40	+0.40
~1000	−0.57	+0.57
~1300	−0.65	+0.65

in the center-of-mass system, and in accordance with the proposed model the relative number of cases in this range is considerably smaller than for $p_\Lambda < 1200$ Mev/c, i.e., it is probable that only a few of the 29 unidentified cases can be Λ particles. Thus the model with vertex part $1 + \gamma_5$ is probably still in agreement with the polarization experiments, even in the region $p_\Lambda > 1200$ Mev/c.

The authors thank D. I. Blokhintsev for his valuable comments, and also thank V. S. Barashenkov, M. I. Solov'ev and Hsien Ting-ch'ang for useful discussions.

[1] M. I. Solov'ev, Proceedings of the 1960 Annual International Conference on High Energy Physics at Rochester (Interscience Publishers, New York, 1960), p. 388.

[2] Wang, Wang, Veksler, Vrana, Ting, Ivanov, Kladnitskaya, Kuznetsov, Nguyen, Nikitin, Solov'ev, and Cheng, JETP 40, 464 (1961), Soviet Phys. JETP 13, 323 (1961).

[3] Wang, Wang, Veksler, Vrana, Ting, Ivanov, Kim, Kladnitskaya, Kuznetsov, Nguyen, Nikitin, Solov'ev, Khofmokl', and Ch'eng, JETP 39, 1854 (1960), Soviet Phys. JETP 12, 1292 (1961).

[4] Blokhintsev and Wang, Nuclear Phys. 22, 410 (1961).

[5] V. G. Solov'ev, JETP 36, 628 (1959), Soviet Phys. JETP 9, 436 (1959).

[6] D. A. Glaser, Proceedings of the 1958 Annual International Conference on High Energy Physics at CERN (CERN, Geneva, 1958), p. 265.

Translated by H. H. Nickle
317

INELASTIC INTERACTION OF 660-*Mev PROTONS WITH CARBON NUCLEI*

A. P. ZHDANOV and P. I. FEDOTOV

Radium Institute, Academy of Sciences, U.S.S.R.

Submitted to JETP editor June 24, 1961

J. Exptl. Theoret. Phys. (U.S.S.R.) **41**, 1870-1878 (December, 1961)

The applicability of the Serber-Goldberger model to the calculation of intranuclear cascades in light nuclei is considered. Some properties of light nuclei that can significantly affect the calculations are discussed. The following factors are taken into account in the calculation of a cascade in a carbon nucleus: 1) collisions of nucleons with α-type substructures, 2) variation of the density of nuclear matter from the center to the periphery of a nucleus, 3) the momentum distribution of nucleons in light nuclei, and 4) processes involving meson production. Satisfactory quantitative agreement is obtained between the calculations and experiment.

EXPERIMENTAL investigations of interactions between nuclei and high-energy particles (of at least a few hundred Mev) show that these interactions can be regarded basically as a succession of collisions between an incoming particle and individual nucleons within a nucleus (the Serber-Goldberger model [1,2]). A comparison between calculations of the intranuclear cascade based on this model and experimental data indicates that the ideas of Serber and of Goldberger are very fruitful for the study of reactions in heavy nuclei ($A \gtrsim 100$). The applicability of these ideas to light nuclei such as C, N, and O is much less certain. This results from a number of specific properties of light nuclei, which we shall consider, as well as from the meagerness and unreliability of experimental data on interactions between high-energy particles and light nuclei.

Calculations that have been attempted [3,4] for light nuclei neglecting the aforementioned properties have not led to satisfactory agreement with experiment. However, it has been noted in [3,5], and especially in [6], that certain particular angular and energy distributions represent correctly the general character of the corresponding experimental distributions. The mean values of some calculated parameters also agree with experiment, thus indicating the possibility, in principle, of applying the Serber-Goldberger ideas to light nuclei.

THE NUCLEAR MODEL

For a more complete understanding of the degree to which the ideas of Serber and Goldberger can be used to calculate the intranuclear cascade in light nuclei a detailed quantitative comparison of the theory and experiment is required. For this purpose we need much reliable experimental data and some modification of the Serber-Goldberger model to take into account more recent information regarding the mechanism of nuclear interactions. The most typical characteristics of inelastic interactions between high-energy particles and light nuclei, differing from similar interactions with heavy nuclei, are the following.

1. The analysis of experimental information regarding the spallation of light nuclei shows that in addition to nucleons more complex structures, mainly α particles, participate in the intranuclear cascade. This has been confirmed by theoretical studies. The strong correlation between nucleons in real nuclei, according to the Brueckner model, [7,8] should result in the formation of a quasi-stable cluster of several nucleons. It is shown in [9-11] that the formation of α groups is most probable. The considerable experimental fraction ($\sim 20\%$) of cascade α particles indicates that α groups must be taken into account in the intranuclear cascade calculation. Details of the calculation of the given collisions will be presented below.

2. In an investigation of 96-Mev proton scattering on carbon and sulfur at 40° Strauch and Titus [12] detected a number of proton energy peaks, which they associate with the excitation of C_6^{12} and S_{16}^{32} levels. Several similar investigations at different proton energies were subsequently published. According to the shell model the peaks result from the excitation of single-particle and, to some extent, collective levels in the given nuclei.

Under our experimental conditions we are interested in the integral cross sections for the ex-

citation of levels above 10 Mev, because at lower excitations U carbon spallation cannot be observed in a nuclear emulsion. The estimated cross section (for U > 10 Mev) does not exceed 1% of the total inelastic scattering cross section. Resonance can therefore be neglected in calculating an intranuclear cascade.

3. Experimental scattering of high-energy electrons on different nuclei has shown that the concept of the nucleus as a sphere with a sharply defined boundary and with uniform density of nuclear matter is unrealistic even for heavy nuclei. These experiments have furnished two parameters characterizing the distribution of nuclear charge, and therefore the distribution of nuclear matter, in light nuclei. These parameters are the radius of an approximately uniform charge distribution within the nucleus and the thickness of the surface layer in which the charge density decreases smoothly. Light nuclei do not appear to contain a central region of uniform density. Therefore, if quantitative comparisons between calculations and experiment are to be made, a nuclear model with nonuniform density is required at least in the case of light nuclei.

Detailed studies of the charge density distribution in C_6^{12} have been presented in [13-15]. Good agreement is obtained between the data on high-energy electron scattering by carbon and the charge density distribution

$$\rho(r) = \rho_0 (1 + \alpha r^2/a_0^2)\, e^{-r^2/a_0^2}, \qquad (1)$$

where $\alpha = 4/3$, and the parameter a_0 is proportional to the rms radius. The best agreement with experiment is obtained at $a_0 = 1.64 \times 10^{-13}$ cm.

When the calculation of the intranuclear cascade is based on a nuclear model with varying density the determination of the nucleon mean free path in the nucleus is complicated considerably. Since the latter calculation is being performed for the first time, we shall first discuss certain factors affecting the determination of the nucleon mean free path within the nucleus.

The "random selection" of the nucleon mean free path in a nucleus is performed using the function

$$F(Y') = 1 - e^{-Y'}, \qquad Y' = \sigma(E) \int_0^x \rho(x')\, dx',$$

where $\rho(x)$ is the nucleon density at the point x, and $\sigma(E)$ is the total nucleon-nucleon interaction cross section. Using the known form of $\rho(r)$, we plot curves $Y_r(x) = \int_0^x \rho(x')\, dx'$ for different values of the impact parameter r_i. When $\rho(r)$ is given by (1), we obtain

$$Y_r(x) = \{(K_1 + K_2')\,\Phi(t') - K_3 t' e^{-t'^2/2}\}\Big|_0^{\frac{\sqrt{2}}{2}\sqrt{R^2 - r_i^2}}$$

$$- \{(K_1 + K_2')\,\Phi(t') - K_3 t' e^{-t'^2/2}\}\Big|_0^{\sqrt{R^2 - r_i^2} - \frac{a_0}{\sqrt{2}} t'},$$

$$t'(x) = \frac{\sqrt{2}}{a_0}\left(\sqrt{R^2 - r_i^2} - x\right),$$

$$K_1 = \frac{\sqrt{\pi}}{2} \rho_0 a_0 e^{-(r_i/a_0)^2} \left(1 + \alpha \frac{r_i^2}{a_0^2}\right),$$

$$K_2' = \frac{\sqrt{\pi}}{2} \rho_0 a_0 \alpha e^{-(r_i/a_0)^2}, \qquad K_3 = \frac{1}{\sqrt{2}} \rho_0 a_0 \alpha e^{-(r_i/a_0)^2},$$

where $\Phi(t')$ is the probability integral. The value $\rho_0 = 0.18$ nucleon/$(10^{-13}\,\text{cm})^3$ is obtained from the relation

$$4\pi\rho_0 \int_0^\infty \left(1 + \alpha \frac{r^2}{a_0^2}\right) e^{-(r/a_0)^2} r^2 dr = A.$$

Figure 1 shows the $Y_r(x)$ curves for several different values of the impact parameter r_i.

From a table of random numbers and functions $F(Y')$ we pick some number Y' and obtain $Y'/\sigma(E) = Y$. The nucleon mean free path in the nucleus is then determined from the curve corresponding to a specific value of r_i.

Although the Fermi gas model for T = 0 has been used quite successfully, the neglect of intranuclear interactions between nucleons must be regarded as a limiting assumption. In actuality, the existence of such processes as capture or the ejection of nucleon groups indicates that interactions between nucleons occur. This means that the momentum distribution of intranuclear nucleons differs from the Fermi distribution for T = 0. Therefore a Fermi gas model for $T \neq 0$ will be a more realistic nuclear model. Information regarding the momentum distribution of nucleons in the nuclear ground state can be obtained from the angular and energy distributions of nuclear interaction products produced by high-energy particles. From investigations of the quasi-elastic scattering of fast protons in light nuclei [16-18] it has been found that the energy spectra of scattered protons agree with a Gaussian momentum distribution of nucleons in Be, C, and O nuclei, with the 1/e value occurring at 13–20 Mev.

For our calculation we used the distribution obtained by the Meshcheryakov group, [17] who had studied the angular and energy distributions of

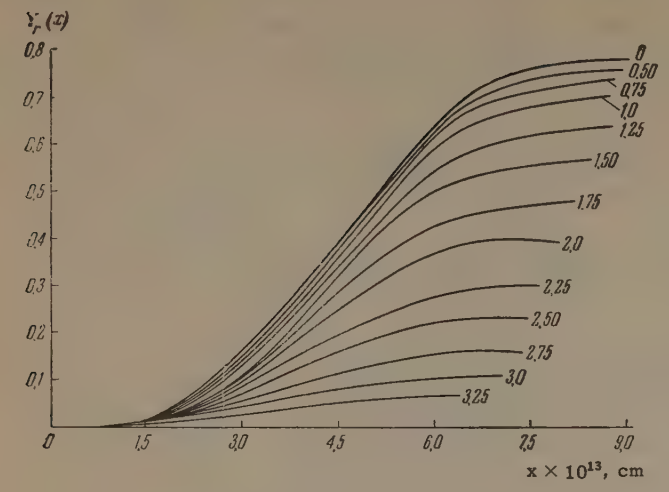

a

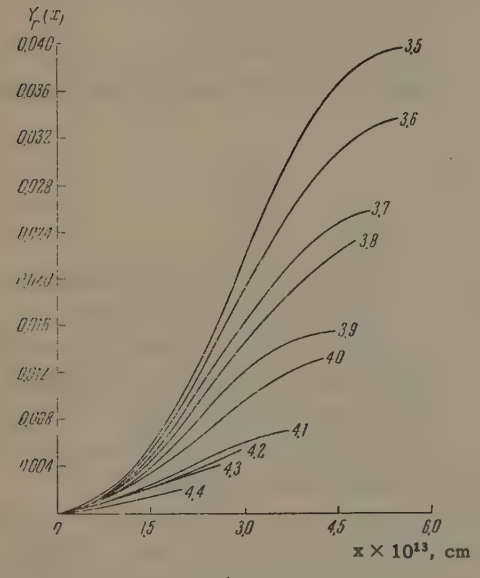

b

FIG. 1. $Y_r(x)$ curves used in determining the nucleon mean free path in the nucleus. Each curve is labeled with the corresponding impact parameter.

secondary protons from p-Be, p-C, p-Cu, and p-U collisions at 660 Mev. The data for Be and C indicate a Gaussian distribution of nucleon momentum with the 1/e value at 20 Mev.

In calculating the intranuclear cascade we also took into account the production, absorption, and scattering of pions on nucleons. For meson production we used the model whereby pions are produced only through an excited $p_{3/2,3/2}$ nucleon resonance state. Satisfactory agreement with experiment was not obtained from a simpler model of pion production. [19]

COMPARISON OF CALCULATIONS AND EXPERIMENT. DISCUSSION

The computed results presented in this section are based on 500 calculated interactions between 660-Mev protons and C_6^{12} nuclei. The intranuclear cascades were calculated by the Monte Carlo method for relativistic three-dimension kinematics with uniform (ρ = const) and varying ($\rho \neq$ const) density of nuclear matter in C_6^{12}.

In order to investigate the aforementioned interaction experimentally we introduced a suspension of diamond dust into a nuclear emulsion registering particles with minimum ionization. The transparency of the diamond particles permits selection of the requisite spallations and guarantees high reliability of the data. We have described this technique in greater detail in [20,21], where we reported results for the low-energy spallation products of C_6^{12}.

a) Absorption cross section. In computing the radius of the C_6^{12} nucleus to be used in our cascade calculations we took $r_0 = 1.36 \times 10^{-13}$ cm. This value of r_0 for the equivalent uniform model of the carbon nucleus was obtained from experiments on charge density distribution in C_6^{12}. The total and diffraction cross sections calculated from the optical model for the interaction between 650-Mev protons and C_6^{12} are in best agreement with experiment for $r_0 = 1.37 \times 10^{-13}$ cm, [22] which practically coincides with our value for r_0.

We computed the following absorption cross sections: σ_a = 220 mb for a nucleus with uniform density, and σ_a = 235 mb for a nucleus with varying density of nuclear matter. We cannot compare these results with a corresponding experimental value from our own work. An experimental cross section cannot be computed with sufficient accuracy for the purpose of comparison, since we did not know the exact magnitude of the proton flux irradiating the nuclear emulsions. However, we can compare our calculations with the experimental results obtained by other investigators under more or less similar conditions. The most suitable data for this purpose are the cross sections for interactions between 650-Mev protons and different nuclei, given in [22]. The cross section σ_a = 227 ± 12 mb for carbon is in very good agreement with our calculation. The absence of any appreciable difference between the calculated absorption cross sections for ρ = const and $\rho \neq$ const is due to the equivalence of both models for the interaction cross section. This determined the selection of r_0 in computing the radius of a uniformly dense carbon nucleus.

b) Cross sections for quasi-elastic p-p and n-p interactions. One of the most serious discrepancies between the calculations and experiment occurred in the case of the cross sections for quasi-elastic nucleon-nucleon scattering. The

experimental cross sections were two to three times larger than the computed cross sections for both heavy and light nuclei. Quasi-elastic proton scattering on carbon has been studied with 660- and 930-Mev protons.[17,18] At 930 Mev[18] the quasi-elastic p-p scattering cross section $\sigma^{q.e.}$ was 46 ± 10 mb. Cross sections of 95—100 mb for combined quasi-elastic p-p and p-n scattering are obtained by angular integration of the proton energy spectra in [17]. When this combined cross section is compared with the ratio σ_{pp}/σ_{np} for elastic scattering on free nucleons we find that at 660 Mev $\sigma_{pp}^{q.e.} \approx 46$ mb and $\sigma_{pn}^{q.e.} \approx 54$ mb. It is suggested in [17] that the disagreement between the computed and experimental cross sections for quasi-elastic scattering is due to failure to take diffuseness of the peripheral region of the nucleus into account in the calculation. This hypothesis is confirmed by our calculations for uniform and nonuniform nuclear density.

Table I shows that considerably improved agreement between the computed and experimental quasi-elastic scattering cross sections results when the nuclear model with varying density is used.

c) Energy and angular distributions of cascade protons. Table II compares the average numbers of cascade protons ($\bar{n}_p$), neutrons ($\bar{n}_n$), and nucleons ($\bar{n}_N$), and the average number of collisions per spallation ($\bar{n}$) derived from both the calculations and experiments.

Since in most instances we cannot determine whether a given emulsion track is produced by a proton or a meson, charged pions are included in the computed value of $\bar{n}_p$ for the purpose of comparison with experiment. The total values including pions are given in parentheses. The fairly high average number of collisions per cascade

Table I

Cross section	$\sigma_{pp}^{q.e.}$, mb	$\sigma_{pn}^{q.e.}$, mb
Experiment	46±10	54±12
Computation (ρ = const)	17±3	19±3
Computation ($\rho \neq$ const)	33±5	33±5

Table II

	$\bar{n}_p$	$\bar{n}_n$	$\bar{n}_N$	$\bar{n}$
Computation (ρ = const)	2.17 (2.56)	1.20	3.37	2.70
Computation ($\rho \neq$ const)	1.87 (2.18)	1.00	2.87	2.20
Experiment	(2.00)	—	—	—

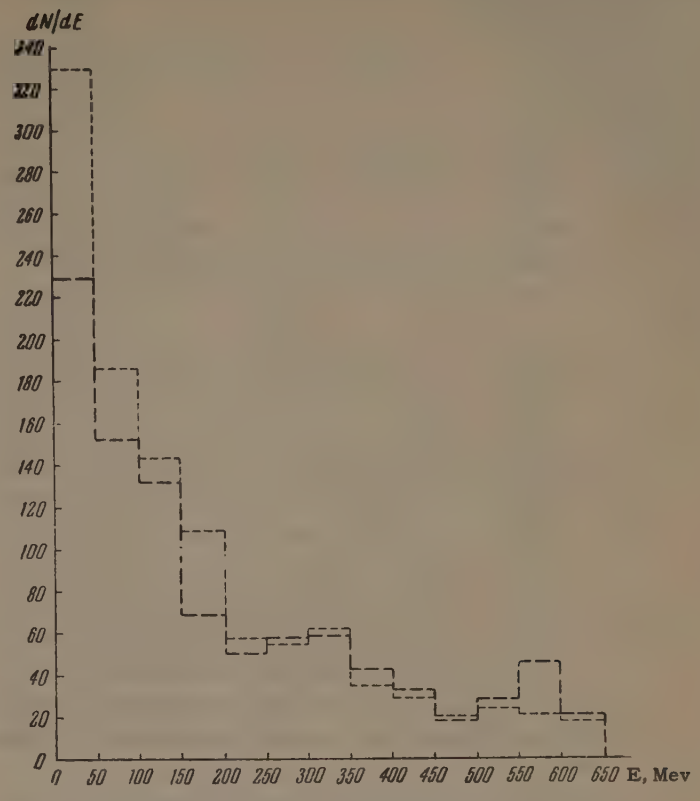

FIG. 2. Computed energy distribution of cascade protons (all U). Long dashes — for $\rho \neq$ const; short dashes — for ρ = const.

even for $\rho \neq$ const results to a considerable extent from the contribution made by pion collisions with intranuclear nucleons. A 100—200 Mev meson has a short mean free path in nuclear matter and sometimes undergoes elastic scattering or scattering with charge transfer before being absorbed or escaping from the nucleus.

Figures 2 and 3 show the computed energy and angular distributions of cascade protons of all energies. It was shown in [17] that the energy spectra of protons from different bombarded nuclei including carbon exhibit a pronounced peak at high energies, corresponding to quasi-elastic single proton-nucleon collisions. The computed spectrum for $\rho \neq$ const in Fig. 2 also has a peak at 500—600 Mev, whereas for ρ = const we observe a continuous decrease of the proton count with increasing energy.

There are no essential differences between the angular distributions computed for C_6^{12} with uniform and varying densities. The angular distribution of protons for ρ = const was, as could be expected, smeared out more toward large angles than for $\rho \neq$ const, since nucleons experience a larger average number of collisions in the nucleus. In a comparison of the computed and experimental spectra the following considerations must be taken into account.

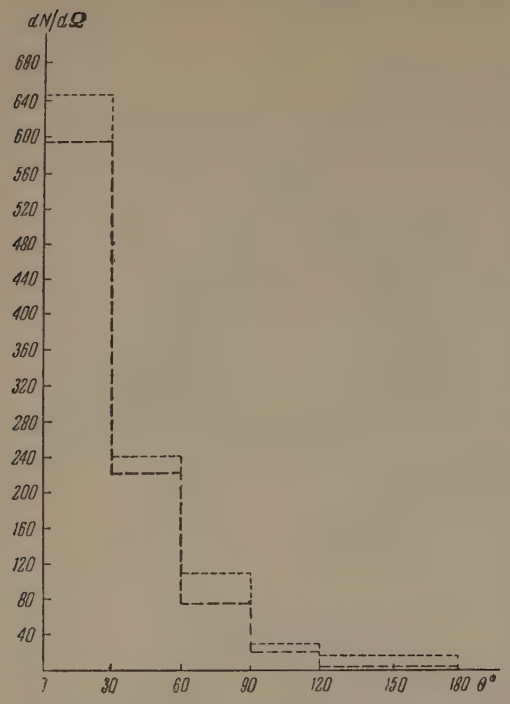

FIG. 3. Computed angular distribution of cascade protons (all U). Long dashes – for $\rho \neq$ const; short dashes – for ρ = const.

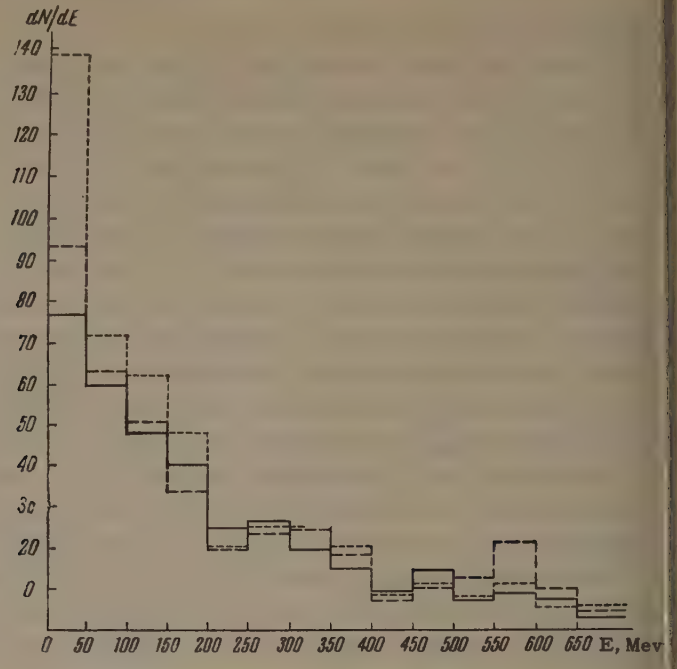

FIG. 4. Energy distribution of cascade protons. Solid line – experimental; long dashes – computed for $\rho \neq$ const; short dashes – computed for ρ = const.

1. The experimental spectra did not take into account one-prong and two-prong stars without a slow-particle track, because the registration of these stars is not sufficiently reliable. In our calculation of the spectra we therefore had to exclude interactions in which, after the emission of one or two cascade protons, the excitation energy U of the residual nucleus is insufficient for the emission of at least one proton or α particle. Our calculations showed that there are no essential differences between proton spectra including all interactions and the spectra including only interactions with $U > U_p$, where U_p is the excitation energy that would permit the residual nucleus to emit at least one proton or α particle. A small difference appears only in the enhanced average number of protons per cascade, due mainly to a larger number of cascade protons in the low-energy portion of the spectrum.

2. The computed spectra had to include charged pions, since singly charged particles were not divided experimentally into protons and pions. Each pion in the computed energy spectra was replaced by a proton having the energy for which the proton would induce the same ionization in the emulsion as the corresponding pion.

In Figs. 4 and 5 the angular and energy spectra computed with the foregoing considerations taken into account are compared with the corresponding experimental distributions. Figure 4 shows that the total experimental number of cascade protons and the overall shape of the experimental spectrum agree satisfactorily with the calculations for $\rho \neq$ const. The discrepancy at high energies is due to insufficient resolution when determining proton energies in this region. The experimental angular distribution of cascade protons is also in better agreement with the calculation for $\rho \neq$ const.

The foregoing comparison of the computed and experimental results shows that the improvements of the nuclear model for the study of the intranuclear cascade in light nuclei lead to satisfactory

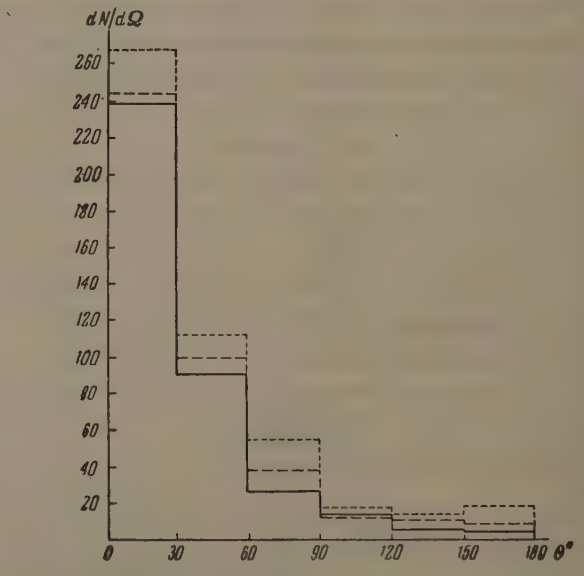

FIG. 5. Angular distribution of cascade protons. Solid line – experimental; long dashes – computed for $\rho \neq$ const; short dashes – computed for ρ = const.

quantitative agreement with experiment. Further confirmation is found in a comparison of the computed and experimental yields of residual nuclei and in the excitation-energy distributions determined by analyzing carbon spallations. A discussion of the pertinent data will be published separately.

The authors wish to thank V. V. Chavchanidze for valuable suggestions regarding the calculating procedure, G. M. Subbotina for assistance with the calculations, L. I. Shur and I. V. Ryzhkova for preparation of the emulsions, and V. N. Kuz'min and I. M. Kuks for useful discussions.

[1] R. Serber, Phys. Rev. **72**, 1114 (1947).

[2] M. Goldberger, Phys. Rev. **74**, 1269 (1948).

[3] J. Combe, Nuovo cimento Supplemento **3**, 182 (1956).

[4] H. Muirhead and W. G. V. Rosser, Phil. Mag. **46**, 652 (1955).

[5] A. P. Zhdanov and F. G. Lepekhin, Trudy Radievogo instituta AN SSSR (Trans. Radium Institute) **9**, 41 (1959).

[6] Petrov, Ivanov, and Rusakov, JETP **37**, 957 (1959), Soviet Phys. JETP **10**, 682 (1960).

[7] Brueckner, Eden, and Francis, Phys. Rev. **98**, 1445 (1955).

[8] H. A. Bethe, Phys. Rev. **103**, 1353 (1956).

[9] A. I. Baz', JETP **31**, 831 (1956), Soviet Phys. JETP **4**, 704 (1957).

[10] M. Rotenberg and L. Wilets, Phys. Rev. **110**, 1126 (1958).

[11] V. G. Solov'ev, DAN SSSR **131**, 286 (1960), Soviet Phys.-Doklady **5**, 298 (1960).

[12] K. Strauch and W. F. Titus, Phys. Rev. **95**, 854 (1954).

[13] J. H. Fregeau and R. Hofstadter, Phys. Rev. **99**, 1503 (1955).

[14] J. H. Fregeau, Phys. Rev. **104**, 225 (1956).

[15] Ehrenberg, Hofstadter, Meyer-Berkhout, Ravenhall, and Sobottka, Phys. Rev. **113**, 666 (1959).

[16] Cladis, Hess, and Moyer, Phys. Rev. **87**, 425 (1952).

[17] Azhgireĭ, Vzorov, Zrelov, Meshcheryakov, Neganov, Ryndin, and Shabudin, JETP **36**, 1631 (1959), Soviet Phys. JETP **9**, 1163 (1959).

[18] Dowell, Frisken, Martelli, and Musgrave, Proc. Phil. Soc. (London) **75**, 24 (1960).

[19] Metropolis, Bivins, Storm, Miller, Friedlander, and Turkevich, Phys. Rev. **110**, 204 (1958).

[20] A. P. Zhdanov and P. I. Fedotov, Pribory i tekhnika éksperimenta (Instruments and Experimental Techniques) No. 3, 133 (1959).

[21] A. P. Zhdanov and P. I. Fedotov, JETP **37**, 392 (1959), Soviet Phys. JETP **10**, 280 (1960).

[22] V. I. Moskalev and B. V. Gavrilovskii, DAN SSSR **110**, 972 (1956), Soviet Phys.-Doklady **1**, 607 (1956).

Translated by I. Emin
318

PRODUCTION OF PIONS IN WEAK INTERACTIONS

Ya. I. AZIMOV

Leningrad Physico-Technical Institute, Academy of Sciences, U.S.S.R.

Submitted to JETP editor June 30, 1961

J. Exptl. Theoret. Phys. (U.S.S.R.) 41, 1879-1884 (December, 1962)

Production of mesons due to the interaction of neutrinos or antineutrinos with nucleons is considered. Numerical estimates of cross sections are derived from electroproduction data.

1. The present paper concerns itself with the interactions of neutrinos or antineutrinos with nucleons resulting in the production of pions. These processes have been considered previously by Lee and Yang[1] in connection with the possibility of experimentally testing the local nature of the leptonic current. The following reactions are possible:

$$\nu + p \to l^- + p + \pi^+, \quad \nu + n \to l^- + n + \pi^+,$$
$$\nu + n \to l^- + p + \pi^0, \qquad (1)$$
$$\bar{\nu} + n \to l^+ + n + \pi^-, \quad \bar{\nu} + p \to l^+ + p + \pi^-,$$
$$\bar{\nu} + p \to l^+ + n + \pi^0, \qquad (2)$$

where $l^\pm$ stands for a charged lepton (electron or μ meson).

In what follows these reactions will be identified by the target and the sign of the meson (p+, n+, n0, etc.).

In Sec. 2 we discuss the structure of the cross sections of processes (1) and (2) assuming the validity of the V,A interaction, and in Sec. 3 we make the connection with electroproduction cross sections.

2. Accurate to first order in the weak interaction the element of the T matrix responsible for processes (1) has the form

$$\langle p_2 q s_2 | T | p_1 s_1 \rangle$$
$$= -\sqrt{2}\, G \bar{u}_l(s_2)\, \gamma^\mu \frac{1+\gamma_5}{2}\, u_\nu(s_1) \cdot \frac{1}{\sqrt{2q_0}}\, \bar{u}_2 H_\mu u_1, \qquad (3)$$

where G is the Feynman-Gell-Mann constant,[2] s_2 and s_1 are the momenta of the final lepton and neutrino respectively, $\bar{u}_l$ and u_ν are their wave functions, q is the momentum of the meson, and p_2 and $\bar{u}_2$, p_1 and u_1 are the momenta and wave functions of the initial and final nucleons. $\bar{u}_2 H_\mu u_1/\sqrt{2q_0}$ represents the matrix element of the baryonic V,A current.

Analogously the amplitude for processes (2) is given by

$$-\sqrt{2}\, G \bar{v}_\nu(-s_1)\, \gamma^\mu \frac{1+\gamma_5}{2}\, v_l(-s_2) \frac{1}{\sqrt{2q_0}}\, \bar{u}_2 \tilde{H}_\mu u_1, \qquad (4)$$

where $\bar{v}_\nu$ and v_l are negative frequency spinors, and $\tilde{H}_\mu$ and H_μ are related to each other like the $\mp$ components of an isotopic vector.

It follows from Eq. (3) that the differential cross section for processes (1) is given by

$$d\sigma = \frac{1}{(4\pi)^4} \frac{G^2}{2} \frac{|s_2|}{s_{10} m} \frac{|q|}{W} \Phi\, ds_{20}\, d\Omega\, d\cos\vartheta, \qquad (5)$$

where s_{10} is the neutrino energy, s_{20} and $\mathbf{s}_2$ are the energy and momentum of the emitted lepton in the laboratory frame, Ω is the solid angle of emission of the lepton; W and q are the total energy and momentum of the final nucleon and meson in their barycentric frame, ϑ is the nucleon scattering angle in the same frame, and m is the nucleon mass.

The quantity Φ is given by the equation

$$\Phi = [S^\mu S^\nu - k^\mu k^\nu - (m_l^2 - k^2)\, g^{\mu\nu}$$
$$- iS_\alpha k_\beta \varepsilon^{\alpha\beta\mu\nu}]\, \mathrm{Sp}(\hat{p}_2 + m)\, H_\mu (\hat{p}_1 + m)\, \bar{H}_\nu, \qquad (6)$$

where $S = s_1 + s_2$, $k = s_1 - s_2$, and $\varepsilon^{\alpha\beta\mu\nu}$ is the completely antisymmetric tensor ($\varepsilon^{0123} = 1$). It is assumed that the incident nucleon is unpolarized.

From a comparison of Eqs. (3) and (4) it follows that the cross section $d\tilde{\sigma}$ for processes (2) is also given by Eq. (5) provided that in the definition (6) for Φ one changes the sign of the last term in the square bracket and replaces H_μ by $\tilde{H}_\mu$.

Instead of H and $\tilde{H}$ (for the sake of brevity we drop the subscript μ on H_μ and $\tilde{H}_\mu$) it is convenient to introduce the amplitudes H^+ and H^- which are simply numbers in isotopic space:

$$H = \pi^m \{H^+ (\delta_{m1} + i\delta_{m2}) + H^- [\tau_m, \tau_+]/\sqrt{2}\},$$
$$\tilde{H} = \pi^m \{H^+ (\delta_{m1} - i\delta_{m2}) + H^- [\tau_m, \tau_-]/\sqrt{2}\}, \qquad (7)$$

π^m stands for the isotopic polarization vector of the pion.

The amplitudes for specific physical processes of the (1) or (2) types are very simply expressed in terms of the H^+ and H^-:

$$H_{p+}=\sqrt{2}(H^+-H^-),\quad H_{n+}=\sqrt{2}(H^++H^-),$$
$$H_{n0}=2H^-; \tag{8}$$
$$\tilde{H}_{n-}=\sqrt{2}(H^+-H^-),\quad \tilde{H}_{p-}=\sqrt{2}(H^++H^-),$$
$$\tilde{H}_{p0}=-2H^-. \tag{9}$$

It is obvious that isotopic invariance makes only two of the three physical amplitudes in each group independent. Consequently there exist relations among the amplitudes

$$H_{p+}-H_{n+}+\sqrt{2}H_{n0}=0,\quad \tilde{H}_{n-}-\tilde{H}_{p-}-\sqrt{2}\tilde{H}_{p0}=0. \tag{10}$$

These relations give rise to inequalities for the cross sections, similar to the inequalities connecting the squares of the sides of a triangle.

The equalities

$$H_{p+}=\tilde{H}_{n-},\quad H_{n+}=\tilde{H}_{p-},\quad H_{n0}=-\tilde{H}_{p0}$$

are a consequence of the fact that the transition from reactions (1) to reactions (2) may be accomplished by means of the charge conjugation operation on the leptons and the charge symmetry transformation on the strongly interacting particles.

If the leptonic current is local then H^+ and H^- depend on the leptonic momenta s_1 and s_2 only through the momentum transfer $k = s_1 - s_2$. At that Eq. (6) shows that the cross section depends on the components of the vector S quadratically. The term linear in S arises from the last term in the square bracket in Eq. (6). This is precisely the term that changes sign on going from reactions (1) to reactions (2). A detailed discussion of the symmetries arising from this property was given by Shekhter.[3]

Consequently the cross sections $d\sigma_{p+}$ and $d\tilde{\sigma}_{n-}$, $d\sigma_{n+}$ and $d\tilde{\sigma}_{p-}$, $d\sigma_{n0}$ and $d\tilde{\sigma}_{p0}$ differ from each other only by the sign of the terms linear in S. This means that if we increase the components of S, at fixed values of k, the corresponding cross sections will tend to the same limit. Such a limit is obtained, for example, if for small angles of emission of the final lepton $s_{10} \gg s_{10} - s_{20}$.

The quantity Φ, Eq. (6), consists of a scalar and pseudoscalar part. The pseudoscalar part describes the correlation between the momenta of the particles partaking in the reaction, of the type $\mathbf{p}_\pi \cdot \mathbf{p}_l \times \mathbf{p}$. Such a correlation is absent if time reversal invariance holds and the interaction in the final state is ignored.

It is easy to see from the definition (6) that the interference of the V,A baryonic currents can enter the scalar part only in the terms linear in S. This means that if we take for each of the above mentioned pairs of cross sections half their sum, then we will get in the scalar part of this half-sum contributions from the V and A currents independently.

3. Additional information may be obtained on the reactions (1) and (2) if use if made of the Feynman-Gell-Mann hypothesis[2] relating the electric current and the vector part of the weak, strangeness-conserving, current. This hypothesis connects reactions (1) and (2) with electroproduction reactions

$$l^\pm+p\to l^\pm+p+\pi^0,\quad l^\pm+n\to l^\pm+n+\pi^0,$$
$$l^\pm+p\to l^\pm+n+\pi^+,\quad l^\pm+n\to l^\pm+p+\pi^-. \tag{11}$$

As is well known (see e.g., [4]) the amplitude for pion electroproduction is given by

$$-e^2\frac{1}{k^2}\bar{u}_l(s_2)\gamma^\mu u_l(s_1)\frac{1}{\sqrt{2q_0}}\bar{u}_2 H^e_\mu u_1, \tag{12}$$

where $e^2/4\pi = \alpha$, u is the wave function of the electron (μ meson) and H^e_μ is related to the matrix element of the electric current.

From this we get for the cross section of this process $d\sigma^e$ the expression

$$d\sigma^e=\frac{1}{(4\pi)^4}\frac{e^4}{4(k^2)^2}\frac{|s_2|}{|s_1|m}\frac{|q|}{W}\Phi^e\,ds_{20}\,d\Omega d\cos\vartheta, \tag{13}$$

where

$$\Phi^e=[S^\mu S^\nu-k^\mu k^\nu+k^2g^{\mu\nu}]\,\mathrm{Sp}\,(\hat{p}_2+m)\,H^e_\mu\,(\hat{p}_1+m)\,\bar{H}^e_\mu. \tag{14}$$

The second term in the bracket contributes nothing as a consequence of gauge invariance.

The isotopic structure is

$$H^e=\pi^m(H^0\tau_m+H^+_V\delta_{m3}+H^-_V[\tau_m,\tau_3]/2), \tag{15}$$

where H^+_V and H^-_V coincide with the vector parts of the corresponding amplitudes H^+ and H^- [Eq. (7)], and H^0 arises from the matrix element of the isoscalar current.

The amplitudes of the reactions (11) are simply expressed in terms of H^0, H^+_V and H^-_V:

$$H^e_{p0}=H^+_V+H^0,\quad H^e_{n0}=H^+_V-H^0,\quad H^e_{p+}=\sqrt{2}(H^0+H^-_V),$$
$$H^e_{n-}=\sqrt{2}(H^0-H^-_V). \tag{16}$$

From here it is easy to express the vector amplitudes (8) and (9) of the reactions (1) and (2) in terms of the amplitudes of the reactions (11):

$$H_{p+V} = \tilde{H}_{n-V} = (H^e_{p0} + H^e_{n0})/\sqrt{2} - \tfrac{1}{2}(H^e_{p+} - H^e_{n-}),$$
$$H_{n+V} = \tilde{H}_{p-V} = (H^e_{p0} + H^e_{n0})/\sqrt{2} + \tfrac{1}{2}(H^e_{p+} - H^e_{n-}),$$
$$H_{n0V} = -\tilde{H}_{p0V} = (H^e_{p+} - H^e_{n-})/\sqrt{2}. \quad (17)$$

Suppose now that the charged lepton involved in these reactions is the electron, and consequently its mass may be ignored. Then the first factor in the scalar part of Φ, Eq. (6), coincides with the factor in Φ^e, Eq. (14). This makes it possible to derive certain relations among the cross sections as well. It is desirable, however, to eliminate the effect of H^0. It is seen from Eq. (16) that half the sum of the cross sections $d\sigma^e_{p0}$ and $d\sigma^e_{n0}$, $d\sigma^e_{p+}$ and $d\sigma^e_{n-}$ does not contain interferences between H^0 and $H^{\pm}_V$. The terms $\sim |H^0|^2$, on the other hand, may be apparently either completely ignored or taken equal to their Born approximation for values of W near to or below the energy of the (3.3) resonance.[4] For simplicity we ignore in what follows the square of H^0 in comparison with the squares of other amplitudes. Then a comparison of Eqs. (5), (6), (8) and (9) with Eqs. (13), (14) and (16) gives rise to the following relations among the cross sections:

$$\tfrac{1}{2}(d\sigma_{n0} + d\tilde{\sigma}_{p0}) > \tfrac{1}{2}(Gk^2/2\pi\alpha)^2 (d\sigma^e_{p+} + d\sigma^e_{n-}), \quad (18)$$

$$\tfrac{1}{2}(d\sigma_{p+} + d\sigma_{n+} + d\tilde{\sigma}_{p-} + d\tilde{\sigma}_{n-}) > (Gk^2/2\pi\alpha)^2 [(d\sigma^e_{p0} + d\sigma^e_{n0}) + \tfrac{1}{2}(d\sigma^e_{p+} + d\sigma^e_{n-})], \quad (19)$$

$$\tfrac{1}{2}(d\sigma_{p+} + d\sigma_{n+} + d\tilde{\sigma}_{p-} + d\tilde{\sigma}_{n-}) - \tfrac{1}{2}(d\sigma_{n0} + d\tilde{\sigma}_{p0}) > (Gk^2/2\pi\alpha)^2 (d\sigma^e_{p0} + d\sigma^e_{n0}). \quad (20)$$

If at least two particles are detected in the final state then from the experimentally obtained cross sections on the left sides of the inequalities one must subtract the terms describing the correlations of the emitted particles so as to be left with the scalar components only.

It was shown earlier that on the left sides there is no interference between the V and A variants, and on the right sides there is no interference between H^0 and $H^{\pm}_V$. The sign > has to do with the fact that the left sides also have a contribution from the axial vector current. In order to make the inequalities more precise one must, of course, subtract from the right sides the contributions due to $|H^0|^2$. Afterwards they may be used to determine the contribution of the axial vector current. The difference of the left and right sides of Eq. (18) gives the contribution $\sim |H^-_A|^2$, and of Eq. (20) the contribution $\sim |H^+_A|^2$.

In connection with these inequalities it is of interest to consider the k^2-dependence of the cross sections. If the electron mass is ignored then $k^2 = -2s_{10}s_{20}(1 - \cos\theta)$, where θ is the angle of emission of the final electron. Since the amplitudes $H^{\pm}$ should not, apparently, have poles as $k^2 \to 0$, it is not hard to see that the quantity $k^{-2}\Phi$ has a finite limit as s_{20} tends to zero at fixed values of θ. It therefore follows from Eq. (5) that for nonzero angles and small k^2 the cross sections $d\sigma$ and $d\tilde{\sigma}$ should go as $(k^2)^2$ or, what is the same, as $(s_{20})^2$.

For small k^2 ($|k^2| \ll 4m_\pi^2$) the electroproduction cross sections on the right sides of the inequalities (18)—(20) may be expressed in terms of photoproduction cross sections according to the equality (see, e.g., [5]).

$$\lim_{k^2\to 0} \frac{\partial^2\sigma^e}{\partial s_{20}\,\partial\Omega} = \frac{\alpha}{(2\pi)^2}\frac{1}{s_{10}(1-\cos\theta)}\sigma^p, \quad (21)$$

where σ^p stands for the photoproduction cross section.

For larger values of $|k^2|$ the inequalities (18)—(20) show that the ratio of the cross sections $d\sigma$ and $d\tilde{\sigma}$ to the electroproduction cross sections grows like $(k^2)^2$. This result is a consequence of the assumption made relating the electric and weak currents, and may be subject to experimental test. If an intermediate vector boson of mass M exists, then for $|k^2| \gg M^2$ the factor $(Gk^2/2\pi\alpha)^2$ in the inequalities (18)—(20) should be replaced by $(GM^2/2\pi\alpha)^2$.

The relations (18)—(20) become simplified when expressed in terms of cross sections for deuteron reactions. The experimental data on electroproduction on deuterons [6] indicate that the cross section is approximately equal to the sum of the cross sections on neutrons and protons. If one makes use of this additivity property of nucleon cross sections one obtains the inequalities

$$\tfrac{1}{2}(d\sigma_{D0} + d\tilde{\sigma}_{D0}) > \tfrac{1}{2}(Gk^2/2\pi\alpha)^2 (d\sigma^e_{D+} + d\sigma^e_{D-}), \quad (18a)$$

$$\tfrac{1}{2}(d\sigma_{D+} + d\tilde{\sigma}_{D-}) > (Gk^2 2\pi\alpha)^2 [d\sigma^e_{D0} + \tfrac{1}{2}(d\sigma^e_{D+} + d\sigma^e_{D-})], \quad (19a)$$

$$\tfrac{1}{2}(d\sigma_{D+} + d\tilde{\sigma}_{D-}) - \tfrac{1}{2}(d\sigma_{D0} + d\tilde{\sigma}_{D0}) > (Gk^2/2\pi\alpha)^2 d\sigma^e_{D0}. \quad (20a)$$

Here $d\sigma_{D+}$, $d\sigma_{D0}$; $d\tilde{\sigma}_{D-}$, $d\tilde{\sigma}_{D0}$; $d\sigma^e_{D0}$, $d\sigma^e_{D+}$, $d\sigma^e_{D-}$ refer to the cross sections for the following reactions

$$\nu + D \to e^- + p + n + \pi^+,\ \nu + D \to e^- + 2p + \pi^0; \quad (1a)$$

$$\bar{\nu} + D \to e^+ + p + n + \pi^-,\ \bar{\nu} + D \to e^+ + 2n + \pi^0; \quad (2a)$$

$$e^{\pm}+D\to e^{\pm}+p+n+\pi^0, \quad e^{\pm}+D\to e^{\pm}+2n+\pi^+, \quad e^{\pm}+D\to e^{\pm}+2p+\pi^-. \tag{11a}$$

From Eqs. (18a)—(20a) one obtains the following relation for the cross sections summed over the charge states of the produced meson:

$$\tfrac{1}{2}(d\sigma_D+d\tilde{\sigma}_D)>(Gk^2/2\pi\alpha)^2\,d\sigma_D^e. \tag{22}$$

The existing experimental data on $\partial^2\sigma_D^e/\partial s_{20}\partial\Omega$[6] permit one to calculate the right side of the inequality (22) for the energy s_{10} in the interval from 460 to 680 Mev at angles $\theta = 90°$ and 135°. One gets in this way the value $\sim(2-6)\times 10^{-43}$ cm^2/Mev·sr.

If one integrated these values over s_{20} one could obtain an estimate for the differential cross section also. A rough numerical calculation using the trapezoidal method gives for the angle $\theta = 90°$ and the energy $s_{10} = 523$ Mev the estimate 4.4×10^{-41} cm^2/sr. By the same method one gets for $\theta = 135°$ the value 3.6×10^{-41} cm^2/sr at $s_{10} = 563$ Mev, and 4.1×10^{-41} cm^2/sr at $s_{10} = 607$ Mev. These numbers should be compared with the contribution of the vector current to the differential cross section for the "elastic" processes $\nu + n \to e^- + p$ and $\bar{\nu} + p \to e^+ + n$ at the same angles and energies. This contribution may be calculated and turns out to be for the above mentioned cases respectively 2.2×10^{-40}, 1.65×10^{-40} and 1.62×10^{-40} cm^2/sr. In this manner we find that the ratio of the differential cross sections for inelastic and "elastic" processes amounts to approximately 0.20—0.25. Unfortunately the experimental data on electroproduction on deuterons are very poor and do not allow more detailed estimates. Neither can we estimate the total cross sections for reactions (1a) and (2a). It is, however, to be expected that the ratio of the total cross sections of "elastic" and inelastic processes will be of the same order of magnitude as the ratio of the differential cross sections.

Beside the processes considered above also processes leading to the production of K mesons and Σ or Λ hyperons are possible. For reactions in which Σ hyperons are produced the inequalities (18)—(20) remain valid if one interprets the signs +, −, 0 as referring to the sign of the produced Σ hyperon.

For the reactions

$$\nu+n\to e^-+\Lambda+K^+, \quad \bar{\nu}+p\to e^+\Lambda+K^0; \tag{23}$$

$$e^{\pm}+p\to e^{\pm}+\Lambda+K^+, \quad e^{\pm}+n\to e^{\pm}+\Lambda+K^0 \tag{24}$$

it is possible to obtain in the same manner as before the relation

$$\tfrac{1}{2}(d\sigma_+ + d\tilde{\sigma}_0)>\tfrac{1}{2}(Gk^2/2\pi\alpha)^2(d\sigma_+^e+d\sigma_0^e), \tag{25}$$

where the subscripts refer to the sign of the produced K meson.

In conclusion the author expresses his gratitude to I. M. Shmushkevich and V. M. Shekhter for suggesting this problem and for useful discussions.

[1] T. D. Lee and C. N. Yang, Phys. Rev. Lett. 4, 307 (1960).

[2] R. P. Feynman and M. Gell-Mann, Phys. Rev. 109, 193 (1958).

[3] V. M. Shekhter, JETP 41, 1953 (1961), this issue, p. 1388.

[4] Fubini, Nambu, and Wataghin, Phys. Rev. 111, 329 (1958).

[5] W. K. H. Panofsky and E. A. Allton, Phys. Rev. 110, 1155 (1958).

[6] G. G. Ohlsen, Phys. Rev. 120, 584 (1960).

Translated by A. M. Bincer
319

ON THE THEORY OF QUANTIZATION OF SPACE-TIME

V. G. KADYSHEVSKII

Moscow State University

Submitted to JETP editor February 7, 1961; resubmitted July 1, 1961

J. Exptl. Theoret. Phys. (U.S.S.R.) 41, 1885-1894 (December, 1961)

The hypothesis is proposed that the geometric structure of x-space "in the small" and correspondingly of p-space "in the large" is closely connected with weak interactions of elementary particles. Furthermore, a scheme is investigated in which momentum space is one of constant curvature [4] and x-space is quantized.[3] It is shown that there are reasons in the new geometry for rejecting the requirement of invariance under space inversion and "strong" time inversion, providing that the CPT theorem is correct.

1. INTRODUCTION

IN this work, as in the previous one,[1] we shall assume that the hypothetical "fundamental length," without whose introduction it is impossible to give a correct description of the physical processes taking place at high energies or, correspondingly, in small space-time scales, is simultaneously a constant which determines the intensity of the weak interaction.* This means that the geometrical structure of x-space "in the small" and of p-space "in the large" must be closely connected with the weak interactions of elementary particles,† and possibly we now have a right to expect an explanation of such unusual "geometric" properties of weak processes as the nonconservation of spatial parity‡ and non-invariance under "strong" time inversion. It is assumed in what follows that the new geometry in x- and p-space should not contradict the basic principles of quantum mechanics and the general theory of relativity, i.e., as before, the states of physical systems can be described by vectors in some Hilbert space, and the observed quantities can be put in correspondence with the operators of this space; also, the invariance under Lorentz transformations is preserved.

In the mathematical methods used, the given research borders on the research of Snyder [3] and Gol'fand,[4] since the constructions carried out below are equivalent to the introduction in p-space of a geometry of space of constant curvature. Our goal is a more detailed exposition of the mathematical problems related thereto.

2. A NEW GEOMETRY OF p-SPACE

As is clear from what was said above, we shall call p-space the four-dimensional momentum space which figures in quantum field theory. In the usual theory, this space is pseudo-Euclidean, and therefore possess a 10-parameter group of motions (L_{10}), consisting of the group of Lorentz transformations (rotations) (L_6), translations (T_4) and reflections. In the new geometry, definite limitations must be placed on the components of these 4-momenta p_m ($m = 0, 1, 2, 3$) when they are near $1/l$.* By analogy with the theory of relativity, we assume that these limitations can be written in the form of some inequalities that connect the components p_m and $1/l$. The simplest relativistically invariant inequalities of the required type (with account of a reasonable limit as $l \to 0$) have the form

$$p^2 \equiv p_0^2 - p_1^2 - p_2^2 - p_3^2 \leqslant 1/l^2, \tag{2.1}$$

$$p^2 \geqslant -1/l^2. \tag{2.2}$$

We now construct the geometry of the 4-space in which all the vectors satisfy either (2.1) or (2.2).† It will be convenient to consider the two cases together if the hypersurfaces $p^2 = l^{-2}$ and $p^2 = -l^{-2}$,

*In[1], l is chosen equal to the "β-decay length" $\sqrt{G/\hbar c} = 6 \times 10^{-17}$ cm (G is the Fermi constant).

†Perhaps in the spirit of the general theory of relativity (see[2]).

‡The possibility of nonconservation of parity in weak interactions on the basis of the new representation of the structure of space in scales of the order of $\sqrt{G/\hbar c}$ was first pointed out by Shapiro.[2]

*The system of units is used in which $\hbar = c = 1$.

†Naturally, it does not then follow that all 4-momenta in the theory (on the basis of which this geometry will be constructed) will obey one of these inequalities. For example, the limitation $v \leq c$ does not extend to the magnitude of the phase velocity in the theory of relativity.

corresponding to (2.1) and (2.2), which limit the admissible values of the squares of the 4-momenta, can be described by the one equation

$$p^2 = \varepsilon/l^2, \qquad (2.3)$$

where $\epsilon = \pm 1$.

In the presence of a limiting hypersurface (2.3), the translation transformations T_4 in the group of motions L_{10} should be replaced by some new transformations $\tilde{T}_4$, which transform this hypersurface into itself; the remaining transformations of the group L_{10} (rotation and reflection) obviously transform without change into the new group of motions ($\tilde{L}_{10}$), since they leave (2.3) invariant.

Thus the new group of motions $\tilde{L}_{10}$ can be defined as the set of transformations which leave the hypersurface (2.3) unmoved. In the usual p-space, this region was infinitely far removed from the region which is fixed relative to the group of motions. Therefore, it is natural to consider the points of the hypersurface (2.3) as infinitely distant points of p-space in the sense of the new geometry. Infinitely distant points in the previous sense of this word [except for those which belong to (2.3)] are now seen to be not at all isolated, and therefore must be regarded in a fashion completely equivalent to the rest. The so-called homogeneous coordinates [5] are most useful for this purpose. In our case, we shall introduce them in the following form:

$$p_m = l^{-1}\eta_m/\eta_4 \qquad (m = 0, 1, 2, 3). \qquad (2.4)$$

To each choice of coordinates (p_0, p_1, p_2, p_3) there corresponds a choice ($\rho\eta_0$, $\rho\eta_1$, $\rho\eta_2$, $\rho\eta_3$, $\rho\eta_4$), where ρ is a non-vanishing factor [and therefore the set of values (0, 0, 0, 0, 0) is excluded]. It is clear that the choice ($\rho\eta_0$, $\rho\eta_1$, $\rho\eta_2$, $\rho\eta_3$, 0) corresponds to an infinitely distant (in the foregoing sense) point in p-space. In homogeneous coordinates, (2.3) takes the form

$$\eta_0^2 - \eta_1^2 - \eta_2^2 - \eta_3^2 - \varepsilon\eta_4^2 = 0 \qquad (2.5)$$

or $g^{\mu\nu}\eta_\mu\eta_\nu = 0$, where $\mu\nu = 0, 1, 2, 3, 4$ and $g^{\mu\nu} = 0$ for $\mu \neq 0$, $g^{00} = -g^{11} = -g^{22} = -g^{33} = 1$, $g^{44} = -\epsilon$. Equation (2.5) remains invariant for all linear orthogonal transformations of the form $\eta'_\mu = a^\nu_\mu\eta_\nu$. These transformations form a group (G_{10}) of the hypersphere of the pseudo-Euclidean 5-space with the variables η_μ. As follows from (2.4), the group $\tilde{L}_{10}$ is isomorphic to the factor-group G_{10} over its subgroup, which consists of two transformations: $\eta_\mu \to \eta_\mu$ and $\eta_\mu \to -\eta_\mu$ ($\mu = 0, 1, 2, 3, 4$). This circumstance makes it possible to consider the five-dimensional hyperspace, whose diametrically opposite points are identical, as a model of our p-space.[5,6] Thus the p-space now represents a space of constant curvature.

The transformation group G_{10} decomposes into four related components, which are distinguished by the following marks:[7]
For $\epsilon = +1$:

$$\begin{aligned} &\text{a)}\ \det a^\nu_\mu = 1, && \partial\eta'_0/\partial\eta_0 > 0;\\ &\text{b)}\ \det a^\nu_\mu = 1, && \partial\eta'_0/\partial\eta_0 < 0;\\ &\text{c)}\ \det a^\nu_\mu = -1, && \partial\eta'_0/\partial\eta_0 > 0;\\ &\text{d)}\ \det a^\nu_\mu = -1, && \partial\eta'_0/\partial\eta_0 < 0. \end{aligned} \qquad (2.6)$$

For $\epsilon = -1$:

$$\begin{aligned} &\text{a)}\ \det a^\nu_\mu = 1, && \partial(\eta'_0, \eta'_4)/\partial(\eta_0, \eta_4) > 0;\\ &\text{b)}\ \det a^\nu_\mu = 1, && \partial(\eta'_0, \eta'_4)/\partial(\eta_0, \eta_4) < 0;\\ &\text{c)}\ \det a^\nu_\mu = -1, && \partial(\eta'_0, \eta'_4)/\partial(\eta_0, \eta_4) > 0;\\ &\text{d)}\ \det a^{\nu}_{\mu} = -1, && \partial(\eta'_0, \eta'_4)/\partial(\eta_0, \eta_4) < 0. \end{aligned} \qquad (2.7)$$

Because of the correspondence between the groups G_{10} and $\tilde{L}_{10}$ pointed out above, one need use only the components a) and b) from (2.6) and (2.7) for the description of $\tilde{L}_{10}$; the components c) and d) need not be considered at all. All the transformations b) can be obtained from the transformations a) if we multiply the latter by special transformations of the form $\eta_0 \to -\eta_0$, $\eta_4 \to -\eta_4$ in the case $\epsilon = 1$, and $\eta\alpha \to -\eta\alpha$, $\eta_4 \to -\eta_4$ in the case $\epsilon = -1$ ($\alpha = 1, 2, 3$). By virtue of (2.4), the first of these two transformations leads to the inversion of 3-space $\mathbf{p} \to -\mathbf{p}$, the second to the inversion of the time axis $p_0 \to -p_0$. The Lorentz rotations are contained in the components a), corresponding to rotations in the planes ($\eta_m\eta_n$) about the η_4 axis, and rotations in the planes ($\eta_4\eta_m$) which should obviously be identified with the transformations $\tilde{T}_4$, wherein m is the index of that axis of p-space in whose direction the "displacement" is carried out.* Rotation in the plane ($\eta_4\eta_0$) will be hyperbolic for $\epsilon = 1$ and elliptic for $\epsilon = -1$; on the other hand, rotations in

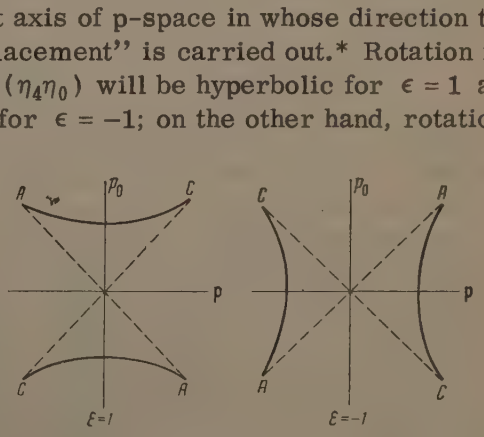

*It then follows that the transformations $\tilde{T}_4$ do not form a group.

the planes (η_4, η_α) will be elliptic for $\epsilon = 1$ and hyperbolic for $\epsilon = -1$. The product of three rotations of angle π in the planes (η_4, η_α) leads, for $\epsilon = 1$, to inversion of the axes η_4, η_α, i.e., in accord with (2.4), to the transformation $p_0 \to -p_0$. Similarly, rotation through π in the plane (η_0, η_4), for $\epsilon - 1$, is a reflection of the axes η_0 and η_4, which is equivalent to $\mathbf{p} \to -\mathbf{p}$.

Thus, with the aid of the translation $\tilde{T}_4$, one can transform (in continuous fashion) a right-hand four-dimensional coordinate system into a left-hand system, and conversely. Inasmuch as rotation in the plane (η_4, η_0) corresponds to a "displacement" along the p_0 axis, then, in the case $\epsilon = -1$, it is necessary to regard the p-space as closed on itself in the direction of the p_0 axis, and topologically equivalent to a four-dimensional Möbius sheet. The p-space has a similar structure for $\epsilon = 1$, only with the obvious difference that here it is closed on itself in the space-like direction (see the drawing; A and C are identical points).

We now find the explicit form of the transformation of the vector p_m by an arbitrary vector k_m. By virtue of (2.4), the desired transformation will be bilinear in the components p_m. Therefore, taking the requirements of relativistic covariance into account, we can write

$$p'_m = \frac{f_1(k^2)\, p_m + f_2(k^2)\,(kp)\, k_m + f_3(k^2)\, k_m}{f_4(k^2)\,(kp) + 1}; \qquad (2.8)$$

$k^2 = (kk)$, $(kp) = k_0 p_0 - \mathbf{k}\cdot\mathbf{p}$. The unknown functions $f_1, \ldots, f_4$ are uniquely determined from the conditions:

1) $p'^2 = \epsilon l^{-2}$ for $p^2 = \epsilon l^{-2}$,
2) $p' = 0$, for $p = -k$,
3) $p' = p$ for $k = 0$.

In sum, Eq. (2.8) takes the form*

$$p'_m = p_m(+)\,k_m = \frac{p_m\sqrt{1-\epsilon k^2 l^2} + k_m\,(1+\epsilon\,(pk)\,l^2/[1+\sqrt{1-\epsilon k^2 l^2}])}{1+\epsilon\,(pk)\,l^2} \qquad (2.9)$$

The symbol $(-)$ is introduced, in accord with [4], in the following natural fashion: $p(-)k = p(+)(-k)$. Here it is shown that $(p(+)k)(-)k = p$. In contrast with the usual translation transformation, the operations $(\pm)$ do not commute. We can establish the fact that

$$\epsilon(p(\pm)k)^2 l^2 = 1 - \frac{(1-\epsilon p^2 l^2)(1-\epsilon k^2 l^2)}{(1\pm\epsilon\,(pk)\,l^2)^2}. \qquad (2.10)$$

The commutability of the operations $(\pm)$ for collinear 4-vectors is evident from (2.10). For example, if $p = p_0$, $k = k_0$, then, for $\epsilon = 1$,

$$p_0(+)\,k_0 = (p_0 + k_0)/(1 + p_0 k_0 l^2). \qquad (2.11)$$

As $l \to 0$, Eqs. (2.9)—(2.11) transform into the corresponding expressions of ordinary geometry.

3. QUANTIZATION OF SPACE-TIME

In accord with the supposition made above on the transfer of the principles of quantum mechanics over into the new geometry, we preserve the previous interpretation of infinitesimal operators of the group of motions. Then the transformation of the wave functions for translation by a small vector k_m in p-space has the form

$$\varphi(p(+)k) = (1 - ix^m k_m)\,\varphi(p), \qquad (3.1)$$

where the x^m are by definition the operators of the coordinates and time (summation is carried out over the index m from 0 to 3. With account of (2.9), we get the following as operators of the scalar wave functions $\varphi(p)$:

$$x^\alpha = i\,(\partial/\partial p_\alpha + \epsilon l^2 p_\alpha p_m \partial/\partial p_m), \qquad \alpha = 1, 2, 3;$$
$$t = i\,(\partial/\partial p_0 - \epsilon l^2 p_0 p_m \partial/\partial p_m). \qquad (3.2)$$

For $\epsilon = 1$, (3.2) are the operators of the coordinates and time, considered in the Snyder theory.[3] We introduce the variables η_μ into (3.2). Since, because of (2.4),

$$\eta_4 \frac{\partial}{\partial \eta_n} = \frac{1}{l}\frac{\partial}{\partial p_n}, \qquad \frac{\partial}{\partial \eta_4} = -\frac{1}{\eta_4} p_m \frac{\partial}{\partial p_m},$$

then

$$x^\alpha = il\left(\eta_4 \frac{\partial}{\partial \eta_\alpha} - \epsilon\eta_\alpha \frac{\partial}{\partial \eta_4}\right), \qquad t = il\left(\eta_4 \frac{\partial}{\partial \eta_0} + \epsilon\eta_0 \frac{\partial}{\partial \eta_4}\right). \qquad (3.3)$$

These operators were first obtained in such a form (for $\epsilon = 1$) by Snyder.*

With the help of (3.3), it is easy to establish that when $\epsilon = 1$ the spatial coordinates have a discrete spectrum of eigenvalues of the form nl, where n is an integer, since the spectrum of the time coordinate remains continuous; for $\epsilon = -1$, the situation is reversed: the time is discrete while the spectrum of the operators x is continuous. The commutation relations between the operators of coordinates, momenta, moments and other features of the Snyder theory are changed in trivial fashion for $\epsilon = -1$, and we shall therefore not consider them. We only note that our formalism is free of the arbitrariness in the determination of the 4-momentum, pointed out by Snyder, for any ϵ, since the quantities $p_m f(\eta_4/\eta)$ are incorrectly transformed in the translations of (2.9).

*We have used the notation of [4] for the operation $\tilde{T}_4$.

*It is obvious that apart from a numerical factor Eqs. (3.3) for x^m can be found immediately from five-dimensional consideration of the translations T_4.

4. SPINOR REPRESENTATION OF THE GROUP OF MOTIONS OF p-SPACE

According to Sec. 2, the group L_{10} is isomorphic to the group of five-dimensional transformations $\eta'_\mu = a^\nu_\mu \eta_\nu$ for which $\det a^\nu_\mu = 1$ [components a) and b) in (2.6) and (2.7)]. Therefore, the spinor representation of this latter group will be the sought representation of the group $\tilde{L}_{10}$. The matrix of the spinor transformation S corresponding to an arbitrary motion $\eta'_\mu = a^\nu_\mu \eta_\nu$ of the components a) and b) can be found from the condition

$$S^{-1}\Gamma^\lambda S = a^\lambda_\mu \Gamma^\mu, \tag{4.1}$$

where Γ^μ are five four-row matrices satisfying the following anticommutation relations:

$$\Gamma^\mu\Gamma^\lambda + \Gamma^\lambda\Gamma^\mu = 2g^{\mu\lambda} \tag{4.2}$$

[$g^{\mu\lambda}$ is the metric tensor from (2.5)].

We choose for Γ^μ the matrices $\gamma^m\gamma^5$, $\sqrt{\epsilon}\gamma^5$ ($m = 0, 1, 2, 3$)* where

$$\gamma^0 = \begin{pmatrix} E & 0 \\ 0 & -E \end{pmatrix}, \qquad \gamma^\alpha = \begin{pmatrix} 0 & \sigma_\alpha \\ -\sigma_\alpha & 0 \end{pmatrix}, \qquad \gamma^5 = -i\begin{pmatrix} 0 & E \\ E & 0 \end{pmatrix}. \tag{4.3}$$

Here $E = \begin{pmatrix} 1 & 0 \\ 0 & 1 \end{pmatrix}$, σ_α are the Pauli matrices ($\alpha = 1, 2, 3$).

Let us introduce the spin tensor of second rank $H(\eta) = \eta_\mu \Gamma^\mu$, which transforms as

$$H' = SHS^{-1}. \tag{4.4}$$

It is easy to establish that $\det H = (\eta^2)^2 = \det H' = (\eta'^2)^2$, i.e., the matrices S actually form a representation of the given group. We can investigate not only linear but also antilinear spinor transformations with the example of the spin tensor H, owing to the simplicity of its structure. Initially, we shall find all the matrices S corresponding to reflections of the η_μ axes. Since $\det a^\nu_\mu = 1$, then the number of reflected axes will always be even.† From the form of H, it is easy to prove [7] that the matrix $S = \lambda\Gamma^{i_1}\Gamma^{i_2}\ldots\Gamma^{i_{2k}}$, where i_m is the number of the coordinate axes and λ is the phase factor, corresponds to the axes $\eta_{i_1}, \eta_{i_2}, \ldots, \eta_{i_{2k}}$.

The matrices obtained in this fashion are shown in Table I. As phase factors in the case of matrices of the time inversion for the case $\epsilon = 1$, and of space inversion for $\epsilon = -1$, imaginary units

Table I

	$\epsilon = 1$	$\epsilon = -1$
$\eta_0 \to -\eta_0$ $\eta_4 \to -\eta_4$	γ^0	$i\gamma^0$
$\eta_\alpha \to -\eta_\alpha$ $\eta_4 \to -\eta_4$	$i\gamma^0\gamma^5$	$\gamma^0\gamma^5$
$\eta_m \to -\eta_m$	$i\gamma^5$	$i\gamma^5$

were chosen so that the square of these transformations are rotations through 2π (see Sec. 2). The remaining phase factors in the first two rows of the table are omitted for simplicity; in the third row, i again appears, since the latter transformation is a product of the first two.

Now let the spinor of first rank ψ be given, transformed according to the law $\psi' = S\psi$ for motions from $\tilde{L}_{10}$. We shall determine how the covariant quadratic forms of the type $\psi^+ O\psi$ can be constructed from ψ and ψ^+ (the "plus" indicates the Hermitian conjugate). We shall first prove that for $\epsilon = 1$,

$$\begin{aligned} &\Gamma^0 S^+ \Gamma^0 = S^{-1} && \text{for the transformations a),} \\ &\Gamma^0 S^+ \Gamma^0 = -S^{-1} && \text{for the transformations b);} \end{aligned} \tag{4.5}$$

and for $\epsilon = -1$,

$$\begin{aligned} &(i\Gamma^0\Gamma^4)\, S^+ (i\Gamma^0\Gamma^4) = S^{-1} && \text{for the transformations a)} \\ &(i\Gamma^0\Gamma^4)\, S^+ (i\Gamma^0\Gamma^4) = -S^{-1} && \text{for the transformations b).} \end{aligned} \tag{4.6}$$

The proofs of the relations (4.5) and (4.6) are entirely similar, and we shall therefore carry out discussions only for the case $\epsilon = -1$. Inasmuch as $H' = SHS^{-1}$, we get $H^+ = (S^{-1})^+ H^+ S^+$. But it follows from (4.3) and Table I that

$$H^+(\eta) = -H(-\eta_0, \eta_\alpha, -\eta_4)$$

$$= -(\Gamma^0\Gamma^4)\, H\, (\Gamma^0\Gamma^4)^{-1} = -(i\Gamma^0\Gamma^4)\, H\, (i\Gamma^0\Gamma^4).$$

Therefore,

$$H'^+ = -(i\Gamma^0\Gamma^4)\, H'\, (i\Gamma^0\Gamma^4) = -(S^{-1})^+ (i\Gamma^0\Gamma^4)\, H\, (i\Gamma^0\Gamma^4)\, S^+,$$

or,

$$H' = (i\Gamma^0\Gamma^4)\, (S^{-1})^+ (i\Gamma^0\Gamma^4)\, H\, (i\Gamma^0\Gamma^4)\, S^+ (i\Gamma^0\Gamma^4).$$

Thus, $(i\Gamma^0\Gamma^4) S^+ (i\Gamma^0\Gamma^4) = \alpha S^{-1}$, where α is a numerical factor. The matrices S, corresponding to the transformations a), can be reduced by a continuous change in the group parameters to the unitary matrix E, as a result of which we find $(i\Gamma^0\Gamma^4) E (i\Gamma^0\Gamma^4) = \alpha E$, i.e., $\alpha = 1$. If now S corresponds to the component b), then such matrices can be reduced to a transformation of time inversion, whence $\alpha = -1$.

*Yu. A. Gol'fand pointed out the necessity of the choice of the basis Γ^μ in such a form. In this case, as $l \to 0$, the five-dimensional spinor representation considered transforms into the usual four-dimensional spinor representation in the basis γ^m.

†The matrix S corresponding to transformations with $\det a^\nu_\mu = -1$, for example, $a^\nu_\mu = -\delta_\mu$, does not generally exist, since it is impossible to find six anticommuting four-row matrices.

Instead of the spinor ψ^+, it is convenient to consider the quantity $\bar{\psi} = \psi^+ L^0$, where $L^0 = \Gamma^0$ for $\epsilon = 1$ and $L^0 = i\Gamma^0\Gamma^4$ for $\epsilon = -1$. Obviously, for transformations of the type a), the law for the transformation of $\bar{\psi}$ will be the following: $\bar{\psi}' = \bar{\psi}S^{-1}$, and for the transformation b): $\bar{\psi}' = -\bar{\psi}S^{-1}$. As can easily be seen, only three independent quadratic forms can be constructed from the quantities ψ and $\bar{\psi}$, which are covariant under the transformations a):

$$1)\ \text{scalar}\ \bar{\psi}\psi, \quad 2)\ \text{vector}\ \bar{\psi}\Gamma^\mu\psi, \quad 3)\ \text{tensor}\ \bar{\psi}\Gamma^\mu\Gamma^\nu\psi. \tag{4.7}$$

If we introduce the usual definition of a conjugate spinor, i.e., if we set $\bar{\psi} = \psi^+\gamma^0$, then the quantities 1)—3) from (4.7) are written (for $\epsilon = 1$) as $\bar{\psi}\gamma^5\psi$, $\bar{\psi}\gamma^5\Gamma^\mu\psi$, $\bar{\psi}\gamma^5\Gamma^\mu\Gamma^\nu\psi$, respectively, and for $\epsilon = -1$, they keep their own form. For Lorentz rotations (rotations about the η_4 axis), five components of the vectors ($\bar{\psi}\psi$ for $\epsilon = 1$ and $\bar{\psi}\gamma^5\psi$ for $\epsilon = -1$) are transformed independently of the first four components ($\bar{\psi}\gamma^m\psi$ for $\epsilon = 1$ and $\bar{\psi}\gamma^m\gamma^5\psi$ for $\epsilon = -1$), i.e., the 5-vector decomposes into an ordinary 4-vector (pseudovector) and a scalar (pseudoscalar). Similarly, the 5-tensor decomposes for Lorentz transformations into an ordinary 4-tensor and a 4-vector for $\epsilon = -1$, or a 4-pseudovector for $\epsilon = 1$.

Concluding the consideration of linear transformations of the spinors of p-space, we shall give (without derivation) the expressions for the operators x^m in the case when the wave function is a spinor:*

$$x^\alpha = i\,(\partial/\partial p_\alpha + \varepsilon l^2 p_\alpha p_m \partial/\partial p_m) + \tfrac{1}{2}\varepsilon\sqrt{-\varepsilon}\, l\gamma^\alpha,$$

$$t = i\,(\partial/\partial p_0 - \varepsilon l^2 p_0 p_m \partial/\partial p_m) - \tfrac{1}{2}\varepsilon\sqrt{-\varepsilon}\, l\gamma^0. \tag{4.8}$$

In order to find all the antilinear spinor transformations, it is necessary to determine such a matrix K that, for an arbitrary transformation $\psi' = S\psi$ the following relation holds:

$$(K\psi^*)' = SK\psi^*. \tag{4.9}$$

It then follows from the equality $\psi'^* = S^*\psi^*$ and (4.9) that

$$K^{-1}SK = S^*. \tag{4.10}$$

With the aid of (4.4), we find

$$H'' = S^* H^* (S^{-1})^*. \tag{4.11}$$

*The reason for the appearance of the matrices γ^m in (4.8) is clear if we take into consideration the obvious circumstance that the infinitesimal operators of the spinor representation group G_{10} are proportional to the expressions $(\Gamma^\mu\Gamma^\nu - \Gamma^\nu\Gamma^\mu)$.

Since the matrices Γ^0, Γ^1, Γ^3, Γ^4 for $\epsilon = 1$ and the matrices Γ^0, Γ^1, Γ^3 for $\epsilon = -1$ are pure imaginaries, the operation of complex conjugation, applied to H, means, in the first case, the reflection of the axes η_0, η_1, η_3, η_4, and, in the second, the reflection of η_0, η_1, . . . , η_3. That is, one can write that for $\epsilon = 1$

$$H^* = (\Gamma^0\Gamma^1\Gamma^3\Gamma^4)\, H\, (\Gamma^0\Gamma^1\Gamma^3\Gamma^4) = \Gamma^{*2} H\, (\Gamma^2)^{-1}, \tag{4.12}$$

and for $\epsilon = -1$

$$H^* = -(\Gamma^2\Gamma^4)\, H\, (\Gamma^2\Gamma^4)^{-1}.$$

Substituting (4.12) in (4.11), we shall have, for $\epsilon = 1$,

$$\Gamma^2 H' (\Gamma^2)^{-1} = S^*\Gamma^2 H (\Gamma^2)^{-1} (S^{-1})^*; \tag{4.13}$$

and for $\epsilon = -1$,

$$(\Gamma^2\Gamma^4)\, H' (\Gamma^2\Gamma^4)^{-1} = S^*\Gamma^2\Gamma^4 H (\Gamma^2\Gamma^4)^{-1} (S^{-1})^*. \tag{4.14}$$

Comparing (4.13) with (4.14), we finally obtain

$$\begin{aligned} K &= (\Gamma^2)^{-1} = \gamma^2\gamma^5 \quad &&\text{for}\ \ \varepsilon = 1, \\ K &= (\Gamma^2\Gamma^4)^{-1} = i\gamma^2 \quad &&\text{for}\ \ \varepsilon = -1. \end{aligned} \tag{4.15}$$

In the case $\epsilon = -1$, the transformation $\psi' = K\psi^*(p) = K\gamma^0\bar{\psi}(p) = -iC\bar{\psi}(p)$, where $C = \gamma^0\gamma^z$, is identical with the ordinary operation of charge conjugation.

For $\epsilon = 1$, we have, correspondingly,

$$\psi' = \gamma^2\gamma^5\gamma^0\bar{\psi} = \gamma^5 C\bar{\psi}\,(p). \tag{4.16}$$

That is, one can show that in this variant the role of charge conjugation should be filled by the new transformation (4.16).

We now write out (see Table II) all the antilinear spinor transformations for reflections of the coordinate axes ($\epsilon = \pm 1$; the phase factors in the operations of charge conjugation are omitted).

To complete consideration in this section of the group of motions of p-space, we shall show on what basis, within the framework of the new geometry, one could remove the requirement of invariance of the theory under space inversion and "strong" time inversion (see Sec. 1). The discussions which we shall give apply fundamentally to transformations of a displacement in p-space. In

Table II

	$\varepsilon = 1$	$\varepsilon = -1$
$\eta_0 \to -\eta_0$, $\eta_4 \to -\eta_4$	$\psi' = \gamma^0\gamma^5 C\bar{\psi}(-\mathbf{p})$	$\psi' = i\gamma^0 C\bar{\psi}(-\mathbf{p})$
$\eta_\alpha \to -\eta_\alpha$, $\eta_4 \to -\eta_4$	$\psi' = -i\gamma^0 C\bar{\psi}(-p_0)$	$\psi' = \gamma^0\gamma^5 C\bar{\psi}(-p_0)$
$\eta_m \to -\eta_m$	$\psi' = -iC\bar{\psi}(-p)$	$\psi' = i\gamma^5 C\bar{\psi}(-p)$

the ordinary theory, these transformations are not connected with any physical symmetry, and therefore their invariance is not required. It is natural to assume that even in the given scheme, there should not be requirements of invariance under displacement in momentum space. Then, in accord with what was pointed out above, the theory will not be invariant relative to the transformations* $\psi' = i\gamma^0\gamma^5\psi(-p_0)$ in the case $\epsilon = 1$ ("strong" time inversion) and $\psi' = i\gamma^0\psi(-p)$ in the case $\epsilon = -1$ (space inversion). If the CPT theorem remains valid, i.e., if invariance under the transformation $\psi' = i\gamma^5\psi(-p)$ is preserved, then in the case $\epsilon = 1$ this will mean the absence of invariance under space inversion and, correspondingly, for $\epsilon = -1$, invariance under "strong" time inversion.

5. TRANSFORMATION OF TRANSLATION IN x-SPACE AND THE ADDITION OF MOMENTA

In the ordinary theory of commuting operators $x^m = i\partial/\partial p_m$, the common eigenfunctions have the form $e^{-i(pa)}$ where a^m are the eigenvalues. If one gives the quantities a^m the meaning of parameters of the translation group, i.e., if we assume that $x'^m = x^m + a^m$, then, as is well known, one can regard the corresponding set of exponentials $e^{-i(pa)}$ as a representation of this group realized by the wave functions $\Psi(p)$:

$$\Psi'(p) = e^{-i(pa)}\Psi(p). \qquad (5.1)$$

Any other arbitrary wave function $\Phi(q)$ will be similarly transformed in a displacement by a^m:

$$\Phi'(q) = e^{-i(qa)}\Phi(q). \qquad (5.2)$$

If the systems described by $\Psi(p)$ and $\Phi(p)$ are regarded as non-interacting, and as a single integral system, then the product $X = \Psi(p)\Phi(q)$ will be the wave function of the compound system that is obtained.† It follows from (5.1) and (5.2) that

$$X' = e^{-i(p+q,\ a)}X, \qquad (5.3)$$

i.e., the four-momentum of the compound system is a vector with components $p_m + q_m$.

The operators x^m from (3.2) do not commute with one another and therefore do not have a common set of eigenfunctions. It then follows that in quantized space-time it is not possible to carry out a translation by an arbitrary 4-vector a^m.[3] But displacements in the direction of any one of the axes are possible, since each of the operators x^m separately has eigenfunctions. For example, for the operator t (at $\epsilon = 1$), the eigenfunction is $\exp(ia\tanh^{-1} p_0 l)$, where a is the characteristic number (see [3]). If $\Psi(p)$ is the wave function, then for $t' = t + a$, we have*

$$\Psi' = \exp(-ia\,\mathrm{Arth}\,p_0 l)\,\Psi(p).$$

Similarly, we can write for (5.2) and (5.3)

$$\Phi' = \exp(-ia\,\mathrm{Arth}\,q_0 l)\,\Phi(q);$$

$$X' = \exp\left[-ia\,\mathrm{Arth}\,\frac{(p_0 + q_0)\,l}{1 + p_0 q_0 l^2}\right]X,$$

where $X = \Psi\Phi$. Thus, in the compound system, $p_0(+)q_0$ appears as an invariant quantity under time translations [see (2.11)]. It can therefore be assumed that the four-dimensional "sum" $p(+)q$ [see (2.9)] is in correspondence with the sum $p + q$ which figures in (5.3), i.e., one can regard $p(+)q$ as the analogue of the total 4-momentum of the system. The noncommutability of the components in this sum and the non-singlevaluedness of its determination (which follows therefrom) correspond to the impossibility of an arbitrary transformation in quantized x-space pointed out above. We shall also show that, although the components of the 4-momentum p_m are not now infinitesimal operators of the displacements in x-space, the permutation relations among them remain as before: $[p_m, p_n] = 0$. Together with the relations of the structure group of Lorentz rotations, they form the usual system of permutation relations of the inhomogeneous Lorentz group (see, for example, [8]).

CONCLUDING REMARKS

As was shown in Sec. 2, after the introduction of the new group of motions L_{10}, p-space can be regarded as a space of constant curvature. In this case, it is shown that the distance between two of its points $(p_0, \mathbf{p})$ and $(q_0, \mathbf{q})$ is determined by the formula [5]

$$\rho(p, q) = l^{-1}\,\mathrm{Arth}\,l\sqrt{\epsilon(p(-)q)^2}. \qquad (6.1)$$

The idea of the replacement of the ordinary pseudo-Euclidean space of momenta by a four dimensional space of constant curvature was recently expressed by Gol'fand.[4] For a description of the processes of interaction, Gol'fand proposed a Feynman diagram technique, generalized in the manner of the new geometry, while for writing down the laws of conservation of energy-momentum, use is made of the addition rule (2.9) (in [4] the case $\epsilon = 1$ was considered). Also, as in the theory of Snyder, invariant integration was introduced in p-space with the volume element $d\Omega = \sqrt{g}\,d_p^4$, where g is the determinant of the metric tensor. For arbitrary ϵ,

*We write out these transformations here in spinor form.

†For simplicity, it is assumed that p and q are the only dynamic variables in the states Ψ and Φ.

*Arth = $\tanh^{-1}$.

$$\sqrt{g} = (1 - \varepsilon p^2 l^2)^{-5/2}. \qquad (6.2)$$

The method of taking integrals in curved p-space [4] leads to a finite result only for $\epsilon = 1$. In connection with going out into the region $p^2 \geq l^{-2}$, which is accomplished in this case, we note the following. The motion group $\tilde{L}_{10}$ which we obtained by starting from the inequalities (2.1) and (2.2), transforms into itself not only the external, but also the internal, region, relative to the hypersurface (2.3).* Therefore, the new geometry also appears in the internal region.[5] All the necessary formulas can easily be obtained from those set down above. It is then clear that going beyond the limit of the inequalities (2.1) and (2.2) has at least a geometric meaning. The physical meaning of this operation can be revealed only in the process of the further development of the theory.

The author is deeply indebted to the participants in the seminars of Acad. N. N. Bogolyubov and Acad. I. E. Tamm, and also to V. I. Grigor'ev, I. S. Shapiro and I. A. Shishmarev for fruitful discussions of the above research. The author also expresses his deep appreciation to Yu. A. Gol'fand for stimulating criticisms and valuable advice.

*A region is called external in relation to the finite cross section if one can draw from it a real tangent plane to this cross section.

[1] V. G. Kadyshevskii, Dokl. Akad. Nauk SSSR **136**, 70 (1961), Soviet Phys. Doklady **6**, 36 (1961).

[2] I. S. Shapiro, Usp. Fiz. Nauk **61**, 313 (1957).

[3] H. Snyder, Phys. Rev. **71**, 38 (1947).

[4] Yu. A. Gol'fand, JETP **37**, 504 (1959), Soviet Phys. JETP **10**, 356 (1960).

[5] F. Klein, Non-Euclidean Geometry (Russian translation), Gostekhizdat, 1936.

[6] B. A. Rozenfel'd, Neevklidovy geometrii (Non-Euclidean Geometries), Gostekhizdat, 1955.

[7] E. Cartan. Lecons sur la Theorie des Spineurs, Hermann, Paris, 1938.

[8] V. Bargmann and E. Wigner, Proc. Nat. Acad. of Sci. **34**, 211 (1948).

Translated by R. T. Beyer
320

DEPOLARIZATION OF μ^- MESONS IN THE FORMATION OF μ-MESIC ATOMS WITH SPIN-$\frac{1}{2}$ NUCLEI

A. P. BUKHVOSTOV and I. M. SHMUSHKEVICH

Leningrad Physico-Technical Institute, Academy of Sciences, U.S.S.R.

Submitted to JETP editor July 6, 1961

J. Exptl. Theoret. Phys. (U.S.S.R.) 41, 1895-1906 (December, 1961)

Besides a fine structure, the levels of μ-mesic atoms formed with nuclei of nonzero spin also have a hyperfine structure. The muon depolarization will be affected if the hyperfine splitting of the weakly excited levels is large in comparison with their width. The magnitude of the effect is estimated for the case in which the nuclear spin is $\frac{1}{2}$. If the hyperfine splitting of the lower excited levels is large in comparison with their width, the polarization of a muon in the K shell should be approximately $\frac{1}{3}$ that of the case with zero nuclear spin. If, on the other hand, the level width considerably exceeds the hyperfine splitting, the hyperfine structure will involve only the K shell and the polarization will decrease to $\frac{1}{2}$ that of the case with zero nuclear spin.

1. INTRODUCTION

THE question of the depolarization of μ^- mesons in the formation of μ-mesic atoms has been considered for spin-zero nuclei by several authors.[1-4] A nonzero spin of the nucleus leads to a hyperfine structure in the mesic-atom levels and to an additional depolarization of the muons. Überall[5] and Lubkin[6] estimated this additional depolarization by taking into account only the hyperfine splitting of the ground-state level 1s. Actually, when the nuclear spin is different from zero, depolarization also occurs in the excited levels, owing to the interaction between the muons and the magnetic moment of the nucleus. This is due to the fact that the hyperfine splitting of weakly excited levels in the μ-mesic atoms is comparable in most cases with the width of the levels and sometimes even considerably exceeds it. We shall therefore consider here the depolarization of the muons with allowance for this effect.

The chief role in the depolarization of the μ^- meson in the formation of μ-mesic atoms is played by the spin-orbit interaction. Of importance here is the ratio between the level width and the fine-structure splitting. The radiative width is always small in comparison with the fine-structure splitting, but in the strongly excited upper levels, the probability of Auger transitions is very large and the total width is greater than the fine-structure splitting. It can be assumed that the depolarization does not occur until the muon reaches the level whose fine-structure splitting is comparable to or larger than the Auger width. For the lower levels we can assume the level width to be small in comparison with the fine structure. This means that the time spent by the muon in the levels is sufficient for the reversal of the spin under the action of the spin-orbit interaction, as a result of which the muon is depolarized.

If the nucleus has a nonzero spin, then below some level the hyperfine-structure interaction begins to have an influence on the muon polarization. This effect becomes appreciable when the level width is comparable to the hyperfine splitting. For nuclei of not very large Z (for example, P^{31}, which was investigated in [7]) the hyperfine splitting is, on the average, of the same order as the radiative width. Consequently, the influence of the hyperfine structure becomes evident in the lower levels, where the probability of Auger transitions is small. Hence there exists an intermediate group of levels for which the total width is much less than the fine-structure, but larger than the hyperfine-structure splitting.

Hence the entire process of a cascade transition to the K shell from highly excited states can be split into three stages: in the first stage the width of the level occupied by the muon, owing to the Auger effect, is larger than the fine-structure splitting; in the second stage the width is smaller than the fine-structure splitting, but greater than the hyperfine splitting; in the third stage it is comparable to the hyperfine splitting. In the first stage

practically no depolarization occurs; in the second stage, depolarization takes place as a result of the spin-orbit interaction; in the third stage it also occurs as a result of the hyperfine interaction between the magnetic moments of the muon and the nucleus. The separation into the second and third stages was introduced here to facilitate a qualitative explanation of the process. Actually, to estimate the depolarization we simultaneously consider the fine and hyperfine structure splitting.

In order to illustrate the relation between the fine-structure splitting and the level width, we have shown in the table the values of the quantities $\omega_f\tau$ and $\omega_h\tau$ (ω_f and ω_h are the values of the fine and hyperfine splitting, and τ is the lifetime of the given level) for different states of the μ-mesic atom P^{31} with a principal quantum number $n = 5$. Also shown are the probability for Auger transitions Γ_a and the total probability for transitions from the given level $\Gamma = 1/\tau$ in units of 10^{15} sec^{-1}. In order to find the probability of radiative transitions we used Table 15 of [8] and calculated the probability for Auger transitions by multiplying the probability for radiative transitions by the conversion coefficient for the corresponding transition in a nucleus of charge $Z - 1 = 14$. It is seen from the table that the conditions $\omega_f\tau \gg 1$ and $\omega_h\tau < 1$, which should hold in the third stage, are already fulfilled for the levels with $n = 5$, except for the s and p levels. We note that the width of the p level has a basically radiative character and the main contribution to the width comes from the probability of a transition to the K shell. But the ratio of the hyperfine splitting to the radiative width depends weakly on the principal quantum number. Hence, for all p levels of a given mesic atom (in any case, for levels that are not very high), $\omega_h\tau$ is approximately constant.

Thus we shall assume that in the initial state the muon is in a level whose fine splitting is small in comparison to the width. The polarization which occurs in this state will be preserved throughout the entire first stage, where the width is larger than the fine-structure splitting.

Initial state	Width, 10^{15} sec^{-1}		$\omega_f\tau$	$\omega_h\tau$	β	$\bar{\beta}$
	Γ_r	$\Gamma = 1/\tau$				
$5s^{1}/_{2}$	0.028	0.16	—	26	0.26	0.26
$5p^{1}/_{2}$	0.43	0.64	73	2.17	—0.20	0.31
$5p^{3}/_{2}$				0.86	0.56	
$5d^{3}/_{2}$	0.15	0.46	34	0,72	—0.23	0.27
$5d^{5}/_{2}$				0.46	0.60	
$5f^{5}/_{2}$	0.076	0.60	13	0.25	—0.31	0.23
$5f^{7}/_{2}$				0.19	0.64	
$5g^{7}/_{2}$	0.045	0.90	5	0,10	—0,33	0.22
$5g^{9}/_{2}$				0,08	0.66	

At the end of the first stage the muon drops to a level whose fine-structure splitting is large in comparison to the width, and this condition is maintained for all subsequent levels occupied by the muon. This second stage has already been considered in detail.[4] For large orbital angular momenta l, which apparently occur most frequently, the probabilities of states with total angular momenta $j = l + 1/2$ and $j = l - 1/2$ are approximately the same, and the muon polarization in each of them is about $1/3$. We assume that l remains large for the entire second stage. Then the muons will undergo a transition, with a probability close to unity, from states with $j = l + 1/2$ to states with $j_1 = l_1 + 1/2$ and from states with $j = l - 1/2$ to states with $j_1 = l_1 - 1/2$, where $l_1 = l - 1$. In transitions of the first type the muon polarization does not change and in transitions of the second type it acquires a factor $(j + 1)j_1/j(j_1 + 1)$; if l is still large at the end of the second stage, we can neglect the difference between this factor and unity. It thus follows that at the end of the second stage the muon polarization in each of the fine-structure states can also be taken equal to $\sim 1/3$.

In the third stage the hyperfine structure will have an appreciable influence on the muon polarization. The following sections of this article will be devoted to an analysis of this influence for the special case of a nuclear spin $I = 1/2$.

A study of the process of muon depolarization in capture by nuclei with spins $I > 1/2$ requires calculations of much greater complexity.

The basic results obtained in the present work reduce to the following.

For nuclei with $I = 1/2$ the 1s level to which the muon drops as a result of all the transitions consists, as is known, of two sublevels of hyperfine structure with a total angular momentum F equal to zero and unity; the separation between the sublevels is much greater than $\hbar/\tau_\mu$, where τ_μ is the muon lifetime. It is natural to expect, and this will also be shown below, that the probability of dropping to one of these sublevels is proportional to the statistical weight. In the state with $F = 0$ the muon polarization is zero, and therefore the average spin of the muon in the K shell is $3/4$ of the average value of the spin in the state with $F = 1$.

We denote by β the ratio of the muon polarization in the K shell to the polarization at the end of the second stage. If the muon is in a state with $j = l + 1/2$ at the end of the second stage, then we have $\beta = 1/2$ in the absence of hyperfine splitting of the excited levels and $\beta \approx 2/3$ for very strong splitting. If the muon was in a state with $j = l - 1/2$ at

the beginning of the third stage, then the influence of the hyperfine splitting of the excited levels will be more important. If there is no hyperfine splitting of the excited levels $\beta \approx 0$, and if the splitting is large $\beta \approx -1/3$, i.e., in this case there is a spin flip. If we take the average over the states $j = l \pm 1/2$ at the beginning of the third stage, we obtain a value of $\sim 1/12$ for the ratio of the final polarization to the initial polarization in the absence of hyperfine splitting in the upper levels and $\sim 1/18$ for strong hyperfine splitting. These results will be discussed in more detail in the following sections. In order to illustrate the results of the calculations, the values of β are given in the table for transitions from different states with a principal quantum number $n = 5$ for the μ-mesic atom P^{31}. The last column of the table gives the quantity

$$\bar{\beta} = \frac{l}{2l+1}\beta_{l-1/2} + \frac{l+1}{2l+1}\beta_{l+1/2}.$$

2. DERIVATION OF BASIC FORMULAS

Since the hyperfine splitting of the μ-mesic atom levels is small, we include these levels in one group. We denote such groups by the letters A, B, C, . . . , M, N and the sublevels of each of these groups by the indices $\alpha, \beta, \gamma, \ldots, \mu, \nu$. Then we readily obtain in the usual way[9] the formula relating the matrix densities $\rho^{(f)}$ and ρ in the final and initial states:

$$\rho^{(f)}_{\nu\nu'} = \exp\{-i\omega_{\nu\nu'}t\}\, S_n \omega_n \rho^{(f_n)}_{\nu\nu'}, \qquad (1)$$

where

$$\rho^{(f_n)} = N_n \sum_{\mu\mu'} \frac{H_{\nu\mu}H^{+}_{\mu'\nu'}}{1 + i(\omega_{\mu\mu'} - \omega_{\nu\nu'})\tau_M} \sum_{\varepsilon\varepsilon'} \frac{H_{\mu\varepsilon}H^{+}_{\varepsilon'\mu'}}{1 + i(\omega_{\varepsilon\varepsilon'} - \omega_{\nu\nu'})\tau_L} \cdots$$

$$\cdots \sum_{\alpha\alpha'} \frac{H_{\beta\alpha}H^{+}_{\alpha'\beta'}}{1 + i(\omega_{\alpha\alpha'} - \omega_{\nu\nu'})\tau_A} \rho_{\alpha\alpha'}. \qquad (2)$$

Here $H_{\alpha\beta}$ is the matrix element for a transition of the system from a state α to a state β with the emission of a quantum or Auger electron; τ_A, τ_B, . . . are the lifetimes of the levels A, B, . . . ; $\omega_{\beta\beta'} = (E_\beta - E_{\beta'})/\hbar$, and E_β and $E_{\beta'}$ are the energies of the sublevels β and β' referring to one group B; the symbol S denotes the summation over different cascades; w_n is the probability for the n-th cascade and N_n is a normalizing factor determined from the condition $\mathrm{Sp}\,\rho^{(f_n)} = 1$. In (2) the summation includes all possible states of the emitted quanta and Auger electrons.

The μ-meson lifetime τ_μ is much greater than $\hbar/\Delta E$, where ΔE is the hyperfine splitting of the ground state level. Hence, in averaging the matrix $\rho^{(f)}$ over the time, the elements for which $\omega_{\nu\nu'} \neq 0$ vanish, owing to the factor $\exp(-i\omega_{\nu\nu'}t)$. Consequently, for the matrix $\rho^{(F)}$ averaged over the time we can write

$$\rho^{(F)} = S_n w_n \rho^{(F_n)}; \qquad (3)$$

$$\rho^{(F_n)} = N_n D\Big(\sum_{\mu\mu'} \frac{H_{\nu\mu}H^{+}_{\mu'\nu'}}{1 + i\omega_{\mu\mu'}\tau_M} \sum_{\varepsilon\varepsilon'} \frac{H_{\mu\varepsilon}H^{+}_{\varepsilon'\mu'}}{1 + i\omega_{\varepsilon\varepsilon'}\tau_L}$$

$$\cdots \sum_{\alpha\alpha'} \frac{H_{\beta\alpha}H^{+}_{\alpha'\beta'}}{1 + i\omega_{\alpha\alpha'}\tau_A} \rho_{\alpha\alpha'}\Big), \qquad (4)$$

where the symbol D means that in the matrix in the parenthesis the elements connecting states with different energies are assumed to vanish (i.e., those for which $\omega_{\nu\nu'} \neq 0$).

The levels A, B, C, . . . occupied by the μ meson are characterized by a principal quantum number n, an orbital angular momentum l, and a quantum number j ($\mathbf{j} = \mathbf{l} + \mathbf{s}$, where $\mathbf{s}$ is the muon spin), and the sublevels $\alpha, \beta, \gamma, \ldots$ differ in the values of the total angular momentum F and its projection M ($\mathbf{F} = \mathbf{j} + \mathbf{I}$, where I is the spin of the nucleus). The symbol D thus signifies the separation of the matrix elements which are diagonal in the F representation.

We limit ourselves to the consideration of the case $I = 1/2$ and write the general expression for the density matrix ρ corresponding to a group of states with given values of n, l, and j. This expression should be linear in $\mathbf{n}$, where $\mathbf{n}$ is a unit vector in the direction of the initial polarization of the muon. Using also the condition that ρ is Hermitian and invariant, we obtain

$$\rho = N\Big(1 + a_1(\mathbf{jI}) + (\mathbf{n})\Big\{a_2\mathbf{j} + a_3\mathbf{I} + a_4[\mathbf{jI}]$$

$$+ a_5\Big(\mathbf{j}(\mathbf{jI}) + (\mathbf{jI})\mathbf{j} - \tfrac{2}{3}j(j+1)\mathbf{I}\Big)\Big\}\Big), \qquad (5)$$

where the coefficients a_i are real. The normalization condition $\mathrm{Sp}\,\rho = 1$ gives $N = (2j+1)^{-1} \times (2I+1)^{-1}$. We shall consider the density matrix ρ given in the form (5) and calculate the matrix $\rho^{(F_n)}$ from formula (4). To do this, we first consider in (4) one of the terms in the sum over n corresponding to a given cascade and we carry out the summation over $\alpha\alpha'$:

$$\rho^{(1)}_{\beta\beta'} = \sum_{\alpha\alpha'} H_{\beta\alpha}H^{+}_{\alpha'\beta'}\rho_{\alpha\alpha'}/(1 + i\omega_{\alpha\alpha'}\tau_A). \qquad (6)$$

It will be convenient to represent the matrix

$$\rho'_{\alpha\alpha'} = \frac{\rho_{\alpha\alpha'}}{1 + i\omega_{\alpha\alpha'}\tau_A} = \rho_{\alpha\alpha'} + \eta_{\alpha\alpha'},$$

$$\eta_{\alpha\alpha'} = -\frac{i\omega_{\alpha\alpha'}\tau_A}{1 + i\omega_{\alpha\alpha'}\tau_A}\rho_{\alpha\alpha'} \qquad (7)$$

in a form similar to (5). For this purpose we provisionally denote states with $F = j + 1/2$ and $F = j - 1/2$ by the subscripts 1 and 2, respectively; then $\omega_{12} = -\omega_{21} = \omega$; omitting the subscript in τ_A, we have

$$\eta_{11} = \eta_{22} = 0;$$

$$\eta_{12} = -\frac{i\omega\tau}{1+i\omega\tau}\rho_{12} = -\frac{\omega^2\tau^2}{1+\omega^2\tau^2}\rho_{12} - \frac{i\omega\tau}{1+\omega^2\tau^2}\rho_{12},$$

$$\eta_{21} = \frac{i\omega\tau}{1-i\omega\tau}\rho_{21} = -\frac{\omega^2\tau^2}{1+\omega^2\tau^2}\rho_{21} + \frac{i\omega\tau}{1+\omega^2\tau^2}\rho_{21},$$

i.e.,

$$\eta = -\frac{\omega^2\tau^2}{1+\omega^2\tau^2}\eta' + \frac{i\omega\tau}{1+\omega^2\tau^2}\eta'';$$

$$\eta' = \rho - D(\rho), \quad \eta'' = \eta' P. \tag{8}$$

Here D denotes the separation of the diagonal parts in the F representation and P is the operator with matrix elements $P_{11} = -P_{22} = 1$, $P_{12} = P_{21} = 0$; it is readily seen that

$$P = (4\mathbf{jI} + 1)/(2j + 1) \tag{9}$$

is such an operator.

In order to separate the diagonal part from (5) we note that the operators $\mathbf{jI}$ and $\mathbf{j} + \mathbf{I} = \mathbf{F}$ are diagonal in the F representation, while $[\mathbf{jI}] = i(\mathbf{j}(\mathbf{jI}) - (\mathbf{jI})\mathbf{j})$ contains no diagonal elements in the F representation. Moreover, we have

$$D(\mathbf{j}) = \frac{j(j+1) + F(F+1) - 3/4}{2F(F+1)}\mathbf{F}$$

$$= \left[\frac{2j}{2j+1}\frac{j+1+2\mathbf{jI}}{2j+1} + \frac{2(j+1)}{2j+1}\frac{j-2\mathbf{jI}}{2j+1}\right]\mathbf{F}$$

$$= \frac{4}{(2j+1)^2}[j(j+1) - \mathbf{jI}](\mathbf{j}+\mathbf{I})$$

$$= \mathbf{j} - \frac{2}{(2j+1)^2}[\mathbf{j}(\mathbf{jI}) + (\mathbf{jI})\mathbf{j} + \mathbf{j} - 2j(j+1)\mathbf{I}],$$

$$D[\mathbf{j}(\mathbf{jI})] = D[(\mathbf{jI})\mathbf{j}]$$

$$= \frac{F(F+1) - j(j+1) - 3/4}{2}\frac{F(F+1) + j(j+1) - 3/4}{2F(F+1)}\mathbf{F}$$

$$= \frac{1}{2}[\mathbf{j}(\mathbf{jI}) + (\mathbf{jI})\mathbf{j}] + \frac{1}{2(2j+1)^2}[\mathbf{j}(\mathbf{jI})$$

$$+ (\mathbf{jI})\mathbf{j} + \mathbf{j} - 2j(j+1)\mathbf{I}]. \tag{10}$$

In these formulas we have used the relations

$$2I_iI_k = \tfrac{1}{2}\delta_{ik} + i\varepsilon_{ikl}I_l; \qquad j_ij_k - j_kj_i = i\varepsilon_{ikl}j_l. \tag{11}$$

With the aid of (5), (8), (9), and (10) we obtain

$$\eta' = a_4\mathbf{n}[\mathbf{jI}] + \frac{2a_0}{(2j+1)^2}\mathbf{n}[\mathbf{j}(\mathbf{jI}) + (\mathbf{jI})\mathbf{j} + \mathbf{j} - 2j(j+1)\mathbf{I}],$$

$$\eta'' = \frac{ia_4}{2j+1}\mathbf{n}[\mathbf{j}(\mathbf{jI}) + (\mathbf{jI})\mathbf{j} + \mathbf{j} - 2j(j+1)\mathbf{I}] - \frac{2ia_0}{2j+1}\mathbf{n}[\mathbf{jI}], \tag{12}$$

where $a_0 = a_2 - a_3 + (1/6)a_5(2j+3)(2j-1)$, and finally, owing to (8) and (7), we have

$$N^{-1}\rho' = 1 + b_1\mathbf{jI} + \mathbf{n}\left\{b_2\mathbf{j} + b_3\mathbf{I} + b_4[\mathbf{jI}]\right.$$

$$\left. + b_5\left[\mathbf{j}(\mathbf{jI}) + (\mathbf{jI})\mathbf{j} - \frac{2}{3}j(j+1)\mathbf{I}\right]\right\}; \tag{13}$$

$$b_1 = a_1, \quad b_2 = a_2 - \frac{1}{2j+1}\frac{\omega\tau}{1+\omega^2\tau^2}\left(a_4 + \frac{2a_0\omega\tau}{2j+1}\right),$$

$$b_4 = \frac{1}{1+\omega^2\tau^2}\left(a_4 + \frac{2a_0\omega\tau}{2j+1}\right),$$

$$b_3 = a_3 + \frac{4}{3}\frac{j(j+1)}{2j+1}\frac{\omega\tau}{1+\omega^2\tau^2}\left(a_4 + \frac{2a_0\omega\tau}{2j+1}\right),$$

$$b_5 = a_5 - \frac{1}{2j+1}\frac{\omega\tau}{1+\omega^2\tau^2}\left(a_4 + \frac{2a_0\omega\tau}{2j+1}\right). \tag{14}$$

For convenience we introduce the notation:

$$A = (j+1)\left(\frac{2a_0}{2j+1} - ia_4\right), \qquad x = \frac{1}{1+i\omega\tau}; \tag{15}$$

then formulas (12) can be rewritten in the form

$$b_1 = a_1, \quad b_2 = a_2 - \frac{\mathrm{Re}\,A(1-x)}{(j+1)(2j+1)}, \quad b_4 = -\frac{\mathrm{Im}\,Ax}{j+1},$$

$$b_3 = a_3 + \frac{4}{3}\frac{j}{2j+1}\mathrm{Re}\,A(1-x),$$

$$b_5 = a_5 - \frac{\mathrm{Re}\,A(1-x)}{(j+1)(2j+1)}. \tag{16}$$

We now carry out the summation in (6). To do this we note that the matrix elements of the different operators occurring in formula (13) between states with different μ and λ (μ and λ are the projections of $\mathbf{j}$ and $\mathbf{I}$) have the following form (the subscripts of the vectors denote the cyclical coordinates −1, 0, 1:

$$\langle\mu\lambda|1|\mu'\lambda'\rangle = \delta_{\mu\mu'}\delta_{\lambda\lambda'}, \quad \langle\mu\lambda|j_l|\mu'\lambda'\rangle = [j(j+1)]^{1/2}\delta_{\lambda\lambda'}C^{j\mu}_{j\mu'1l},$$
$$\langle\mu\lambda|I_l|\mu'\lambda'\rangle = [I(I+1)]^{1/2}\delta_{\mu\mu'}C^{I\lambda}_{I\lambda'1l},$$

$$\langle\mu\lambda|j_ij_k + j_kj_i - \tfrac{2}{3}j(j+1)\delta_{ik}|\mu'\lambda'\rangle$$
$$= \tfrac{1}{3}[10j(j+1)(2j-1)(2j+3)]^{1/2}C^{2l+k}_{1i1k}C^{j\mu}_{j\mu'2l+k}\delta_{\lambda\lambda'}, \tag{17}$$

where C are the Clebsch-Gordan coefficients. Moreover, the matrix elements of the operators H_{LN} and H^+_{LN} (L-th and N-th multipole moment of the transition and its projection) depend on μ and λ in the following way:

$$\langle j_1\mu_1\lambda_1|H_{LN}|j\mu\lambda\rangle = Q\delta_{\lambda\lambda_1}C^{j_1\mu_1}_{j\mu LN},$$

$$\langle j\mu'\lambda'|H^+_{LN}|j_1\mu'_1\lambda'_1\rangle = Q^*\delta_{\lambda'\lambda'_1}C^{j_1\mu'_1}_{j\mu' LN}$$

(j, μ, μ', λ, λ' refer to the level A; j_1, μ_1, μ'_1, λ_1, λ'_1 refer to the level B), where the coefficient Q does not depend on the projection of the angular momenta and can therefore appear only in the

form of an unessential multiplicative factor in front of the entire matrix, owing to the need for normalization. Since the probability of dipole transitions is very large, we can set L equal to unity (apart from the transition 2s – 1s, for which the polarization does not change). We carry out the summation over N in formula (6).

In the calculation of $\rho^{(1)}$ we can carry out the summation over F, replace M by the summation over $\mu\lambda$ and use Racah's method.[10] The matrix $\rho^{(1)}$ will then be represented in the form (5) with the coefficients $a_i^{(1)}$, which are related in the following way to the coefficients b_i appearing in the matrix ρ':

$$\frac{a_1^{(1)}}{b_1}=\frac{a_2^{(1)}}{b_2}=\frac{a_4^{(1)}}{b_4}=\left[\frac{j(j+1)(2j+1)(2j_1+1)}{j_1(j_1+1)}\right]^{1/2}W(jjj_1j_1;1L)(-1)^{-j-j_1+L+1}=\frac{j_1(j_1+1)+j(j+1)-L(L+1)}{2j_1(j_1+1)},$$

$$a_3^{(1)}=b_3,$$

$$a_5^{(1)}=b_5\left[\frac{j(j+1)(2j+1)(2j+3)(2j-1)(2j_1+1)}{j_1(j_1+1)(2j_1+3)(2j_1-1)}\right]^{1/2}W(jjj_1j_1;2L)(-1)^{-j-j_1+L}$$

$$=b_5\left\{\frac{2[j_1(j_1+1)+j(j+1)-L(L+1)]^2+(j_1-j)^2(j_1+j+1)^2-L^2(L+1)^2}{2j_1(j_1+1)(2j_1+3)(2j_1-1)}\right.$$

$$\left.-\frac{(2L^2+2L+3)[j_1(j_1+1)+j(j+1)-L(L+1)]}{2j_1(j_1+1)(2j_1+3)(2j_1-1)}\right\}. \qquad (18)$$

where W are the Racah coefficients.

According to (4), we should find the sum

$$\rho^{(2)}=\sum_{\beta\beta'}H_{\gamma\beta}H^{+}_{\beta'\gamma'}\rho^{(1)}_{\beta\beta'}/(1+i\omega_{\beta\beta'}\tau_B),$$

which will be characterized by the coefficients $a_i^{(2)}$ expressed through $a_i^{(1)}$ in a similar way, etc. After carrying out the last summation, we should separate from the obtained matrix the part diagonal in the F representation, as a result of which we obtain the final density matrix $\rho^{(Fn)}=D(\rho^{(fn)})$. This last operation is not difficult to perform if we note that, according to (7), $\rho'=D(\rho)$ for $\omega\tau=\infty$. Thus representing $\rho^{(fn)}$ in the form (5) with the coefficients $a_i^{(fn)}$, we find from formulas (14) the coefficients $b_i^{(fn)}$; in them we set $\omega\tau=\infty$ and obtain the corresponding coefficients a_i^{Fn} of the matrix $\rho^{(Fn)}$.

We note, moreover, that $j=1/2$ in the lowest level (of the K shell) and therefore some of the five coefficients of the final density matrix prove to be unimportant. As a matter of fact, it is not difficult to show that for $j=1/2$ we have $\mathbf{j}(\mathbf{jI})+(\mathbf{jI})\mathbf{j}+(2/3)\mathbf{j}(\mathbf{j}+1)\mathbf{I}=0$. Since from formula (14) it follows for $\omega\tau=0$ and $j=1/2$ that $b_4=0$, $b_2=b_3=1/2(a_2+a_3)$, then the final density matrix $\rho^{(Fn)}$ will be characterized by two coefficients a_1^{Fn} and $a_2^{Fn}=a_3^{Fn}$. Of course, the same will hold for the matrix $\rho^{(F)}$, for which, according to (3), $a_i^F=\sum_n w_n a_i^{Fn}$. Therefore

$$\rho^{(F)}=\tfrac{1}{4}(1+a_1^F\mathbf{jI}+a_3^F\mathbf{nF})=\tfrac{1}{4}\left[\left(1+\tfrac{1}{4}a_1^F+a_3^F\mathbf{nF}\right)P_+\right.$$

$$\left.+\left(1-\tfrac{3}{4}a_1^F+a_3^F\mathbf{nF}\right)P_-\right]=\tfrac{1}{3}p_+\left(1+\tfrac{3}{2}\lambda^F\mathbf{nF}\right)P_++p_-P_-. \qquad (19)$$

Here $P_+=1/4(3+4\mathbf{jI})$ and $P_-=1/4(1-4\mathbf{jI})$ are the operators of the projection on states with $F=1$ and $F=0$, while P_+ and P_- are the probabilities of the corresponding states:

$$p_+=\tfrac{3}{4}\left(1+\tfrac{1}{4}a_1^F\right),\qquad p_-=\tfrac{1}{4}\left(1-\tfrac{3}{4}a_1^F\right). \qquad (20)$$

The parameter $\lambda^F=(2/3)a_3^F/(1+1/4a_1^F)$ is equal to the polarization of the muon in the triplet state of the K shell.

In a state corresponding to the beginning of the second stage, when the interaction leading to the hyperfine splitting is still very small, the density matrix is equal to the direct product of the muon density matrix in a level with given values of n, l, j[11] and the unpolarized nucleus:

$$\rho=\frac{1}{2(2j+1)}\left(1+\frac{3\lambda}{j+1}\mathbf{jn}\right). \qquad (21)$$

The following values of the coefficients a_i correspond to this state, which we shall call the initial state:

$$a_1=a_3=a_4=a_5=0,\qquad a_2=a_0=3\lambda/(j+1); \qquad (22)$$

the parameter λ is related to the mean value of the spin $\langle\mathbf{s}\rangle$ in this state by the expression

$$\langle\mathbf{s}\rangle=\lambda\mathbf{n}[j(j+1)-l(l+1)+3/4]/2(j+1) \qquad (23)$$

From formulas (16) and (18) it is seen that the coefficient $a_1=b_1$ remains equal to zero in all the subsequent states, too. Consequently, $a_1^F=0$, $p_+=3/4$, and $p_-=1/4$. In this way we arrive at the natural result that the probabilities of the muon dropping to the K-shell levels with $F=1$ and $F=0$ are proportional to their statistical weights. As a result, for the characteristics of the polarized state of the μ-mesic atom in the K shell it

is sufficient to know one coefficient a_3^F, which is connected with the mean value of the muon spin in the K shell $\langle \mathbf{s}_K \rangle$ by the relation

$$\langle \mathbf{s}_K \rangle = \mathrm{Sp}\, \rho^{(F)} \mathbf{s} = \tfrac{1}{4} a_3^F \mathbf{n}. \qquad (24)$$

Taking into account (23), we obtain for the depolarization coefficient $\beta_K = \langle \mathbf{s}_K \mathbf{n} \rangle / \langle \mathbf{s} \mathbf{n} \rangle$:

$$\beta_K = \frac{a_3^F}{2\lambda} \frac{j+1}{j(j+1) - l(l+1) + 3/4} = \frac{a_3^F}{2\lambda} \times \begin{cases} 1, & j = l + 1/2 \\ -(j+1)/j, & j = l - 1/2 \end{cases}. \qquad (25)$$

It is obvious that

$$\beta_K = \sum_n w_n \beta_n, \qquad (26)$$

where β_n is the depolarization coefficient corresponding to a given cascade and the summation is carried out over the entire cascade beginning with the initial level.

3. ESTIMATE OF THE DEPOLARIZATION AND DISCUSSION OF RESULTS

We now determine the change in the polarization in any cascade as the muon goes from the initial state to the K shell. Let the muon be initially in a level with the angular momenta l and $j = l + 1/2$. From such a state a transition is possible to a state with $l_1 = l - 1$ and $j_1 = l - 1/2$ or to a state with $l_1 = l + 1$ and $j_1 = l + 1/2$ or $l + 3/2$. Transitions with an increase in l ($l_1 = l + 1$) are unlikely, as is seen, e.g., from Table 15 in [8], and we shall therefore neglect them (except for transitions from s states).

If we insert $j_1 = j - 1$ into formulas (18), they then take the form

$$a_2^{(1)} = b_2 \frac{j+1}{j}, \quad a_3^{(1)} = b_3, \quad a_4^{(1)} = b_4 \frac{j+1}{j},$$

$$a_5^{(1)} = b_5 \frac{(j+1)(2j+3)}{j(2j+1)}. \qquad (27)$$

Here the quantity

$$A^{(1)} = j\left(\frac{2a_0^{(1)}}{2j-1} - i a_4^{(1)}\right),$$

$$a_0^{(1)} = a_2^{(1)} - a_3^{(1)} + \frac{1}{6} a_5^{(1)} (2j-3)(2j+1)$$

can, after some calculations in which we take (15) and (16) into account, be expressed in terms of A as

$$A^{(1)} = Ax + 2\gamma/(4j^2 - 1),$$

$$\gamma = 2a_2(j+1) - a_3 - \tfrac{2}{3} a_5 (j+1)(2j+3). \qquad (28)$$

Constructing the expression $\gamma^{(1)} = 2a_2^{(1)} j - a_3^{(1)} - \tfrac{2}{3} a_5^{(1)} j(2j+1)$, we can prove with the aid of formulas (16), (15) and (27) that $\gamma^{(1)} = \gamma$. Hence if the transitions occur only with a decrease in j, then it is sufficient to calculate γ once in the initial state, after which we can find the quantity $A^{(i)}$ by applying formula (28) the required number of times.

It is seen from formulas (16) and (18) that in each transition a_3 changes by the quantity $(4/3) j (2j+1)^{-1} \mathrm{Re}\, A (1 - x)$. Hence in the final state

$$a_3^F = a_3 + \frac{4}{3} \sum_{i=0}^{f} \frac{j_i}{2j_i + 1} \mathrm{Re}\, A^{(i)} (1 - x_i),$$

$$A^{(i+1)} = A^{(i)} x_i + \frac{2\gamma}{4j_i^2 - 1}, \qquad (29)$$

where the sum runs over all intermediate levels in the given cascade transition and $i = 0$ corresponds to $j_i = j$. In these formulas referring to a given cascade, we omit for simplicity the subscript that labels the different cascades. In the final state $x_f = 0$, $j_f = 1/2$.

According to formulas (22), (15), and (28), we have in the initial state

$$A = 6\lambda/(2j+1), \quad \gamma = 6\lambda. \qquad (30)$$

Formulas (29) and (30) enable us to determine the coefficient a_3^F for a given cascade transition and, together with this, the depolarization from (25).

We shall consider by way of example the depolarization in two extreme cases: 1) all $x_i = 1$, except for x_f, i.e., the hyperfine splitting is small in comparison to the width of the levels everywhere except for the K shell; 2) $x_i = 0$ for all lower excited levels important for depolarization, i.e., the hyperfine splitting is larger than the level width.

In the first case, formula (28) gives

$$A^{(1)} = \frac{6\lambda}{2j+1} + \frac{12\lambda}{4j^2-1} = \frac{6\lambda}{2j-1}, \quad A^{(2)} = \frac{6\lambda}{2j-3} \text{ etc.}$$

$$A^{(i)} = \frac{6\lambda}{2j_i + 1}, \quad A^{(f)} = 3\lambda, \qquad (31)$$

and formula (29) reduces to $a_3^F = (1/3)\, \mathrm{Re}\, A^{(f)} = \lambda$, since from (25) we have $\beta = 1/2$ (for $j = l + 1/2$). Since this occurs for all important cascades, then, according to (26), $\beta_K = 1/2$. This result should also have been expected, for under these conditions the depolarization occurs only as a result of the hyperfine splitting in the K shell. If x is close to unity, but not exactly equal to it, then, if we neglect products with $(1 - x_i)$, we obtain the following formula:

$$\beta = \frac{1}{2} + \mathrm{Re} \sum_{i=0}^{f-1} \frac{2j_i - 1}{(2j_i + 1)^2} (1 - x_i). \qquad (32)$$

In the second case ($x_i = 0$), we have

$$A^{(i)} = \frac{12\lambda}{4(j_i+1)^2-1},$$

$$a_3^F = 16\lambda \sum_{i=1}^{f} \frac{j_i}{(2j_i+1)^2(2j_i+3)} + \frac{8\lambda j}{(2j+1)^2}$$

$$\approx \lambda\left[3 - \frac{\pi^2}{6} - \frac{2(6j+1)}{3(2j+1)^3}\right]. \qquad (33)$$

Here j corresponds to the highest level occupied in the given cascade for which $x_i = 0$ [the last expression in (33) is valid apart from terms of the order $(2j+1)^{-4}$]. We thus see that $a_3^F > \lambda$. Assuming that j is primarily large, we arrive at the conclusion that $a_3^F \approx 4\lambda/3$. Consequently, according to (25), $\beta \approx 2/3$ and is approximately the same for all cascades; hence $\beta_K \approx 2/3$. Thus, in the second case (strong hyperfine splitting), the depolarization in the transition from states with $j = l + 1/2$ proves to be about 3/4 that of the first case (absence of hyperfine structure everywhere but in the last level).

This result can be explained physically as follows: In the presence of hyperfine structure, the muon polarizes the nucleus during the transitions between excited levels. Hence, the muon is already considerably polarized just before the transition to the K shell, which contributes to the preservation of the muon polarization. When the hyperfine splitting at the upper levels is small the muon polarizes the nucleon only in the K shell, as a result of which it loses half its polarization.

If, assuming the x_i small, we neglect their products we obtain for β the formula

$$\beta = \frac{1}{2}\left[3 - \frac{\pi^2}{6} - \frac{2}{3}\frac{6j+1}{(2j+1)^3} - \mathrm{Re}\left(\frac{8x}{(2j-1)(2j+1)^2} + \sum_{i=1}^{f-1}\frac{16x_i}{(2j_i-1)(2j_i+1)^2(2j_i+3)}\right)\right]. \qquad (34)$$

We now consider transitions from states with $j = l - 1/2$. If we neglect transitions with an increase in l, then the possible transitions here are either $j_1 = j - 1$ or $j_1 = j$, where their relative probabilities are $(j+1)(2j-1)/j(2j+1)$ and $1/j(2j+1)$. For transitions of the first type, formulas (27) are valid, while for transitions of the second type we have the formulas

$$a_2^{(1)} = b_2\frac{j(j+1)-1}{j(j+1)}, \qquad a_3^{(1)} = b_3,$$

$$a_4^{(1)} = b_4\frac{j(j+1)-1}{j(j+1)}, \qquad a_5^{(1)} = b_5\frac{j(j+1)-3}{j(j+1)}. \qquad (35)$$

We now consider all cascades beginning with a given initial state (in which $j = 1 - 1/2$) and involving levels of given n and l. In each transition of these cascades, j decreases by unity until it attains the value j_r at which a transition would occur without a change in j. The relative probability of such a cascade is

$$w_r = \frac{j+1}{2j+1}\frac{1}{j_r(j_r+1)}. \qquad (36)$$

When all x_i are close to unity, we obtain for such a cascade

$$a_3^F = \lambda\,\mathrm{Re}\left\{\frac{j_r(j_r+1)-1}{j_r(j_r+1)}\left[1 - \sum_{i=0}^{r}\frac{2}{(2j_i+1)^2}(1-x_i^{(-)}) + \sum_{i=r+1}^{f-1}\frac{2(2j_i-1)}{(2j_i+1)^2}(1-x_i^{(+)})\right] + \sum_{i=0}^{r}\frac{4j_i}{(2j_i+1)^2}(1-x_i^{(-)})\right\}, \qquad (37)$$

where we have neglected terms containing the factor $(1 - x_i)$. When $x_i \ll 1$ for all x_i we obtain neglecting products of x,

$$a_3^F = \lambda\,\mathrm{Re}\left\{\frac{2}{3}\frac{2j_r(j_r+1)-1}{j_r(j_r+1)} - \left[1 - \frac{4(4j_r+1)}{3(j_r+1)(2j_r+1)^2}\right] \times \sum_{i=0}^{r-1}\frac{16x_i^{(-)}}{(2j_i-1)(2j_i+1)^2(2j_i+3)} - \frac{8(4j_r+1)}{3(j_r+1)(2j_r+1)^4}x_r^{(-)} + \frac{16}{j_r(2j_r-1)(2j_r+1)^4}x_{r+1}^{(+)} - \frac{j_r(j_r+1)-1}{j_r(j_r+1)} \times \sum_{i=r+2}^{f-1}\frac{16x_i^{(+)}}{(2j_i-1)(2j_i+1)^2(2j_i+3)}\right\}. \qquad (38)$$

In formulas (37) and (38) we denote by $x_i^{(+)}$ and $x_i^{(-)}$ the quantities $1/(1 + i\omega\tau)$ for levels with $j_i = l_i + 1/2$ and $j_i = l_i - 1/2$, respectively.

Taking into account (25), (26), and (36), we obtain, after approximate summation over r,

$$\beta_K = -\frac{2(j+1)^2}{j(2j+1)}\mathrm{Re}\left[\frac{10-\pi^2}{4} - \frac{1}{4(j+1)} + \sum_{i=0}^{f-1}\frac{6j_i+1}{6(j_i+1)(2j_i+1)}(1-x_i^{(-)}) + \sum_{i=1}^{f-1}\frac{2j_i-1}{2j_i(2j_i+1)^2}(1-x_i^{(+)})\right], \qquad 1 - x_i \ll 1; \qquad (39)$$

$$\beta_K = -\frac{2(j+1)^2}{j(2j+1)}\mathrm{Re}\left[2 - \frac{\pi^2}{6} - \frac{1}{3(j+1)} - \frac{1}{9}x_{l-1}^{(-)} - \sum_{i=0}^{f-2}\frac{x_i^{(-)}}{j_i(j_i+1)(2j_i+1)(2j_i+3)} - \sum_{i=1}^{f-2}\frac{4x_i^{(+)}}{3(j_i+1)(2j_i-1)(2j_i+1)^2(2j_i+3)}\right], \qquad x_i \ll 1. \qquad (40)$$

From formula (39) it is seen that when $x_i \approx 1$ the depolarization coefficient is $\beta_K \approx 0$, i.e., in this case there is almost complete depolarization. If $x_i \ll 1$, then, as seen from (40), $\beta_K \approx 1/3$ for large

initial j, which indicates a spin flip of the muon. Averaging with equal probabilities expression (39) and the corresponding expression (32) for the case with $j = l + 1/2$, we obtain for $j \gg 1$

$$\overline{\beta_K} = \frac{1}{4}\,\mathrm{Re}\Big[1 - \sum_{i=0}^{j-1} \frac{6j_i+1}{3\,(j_i+1)\,(2j_i+1)}\left(1 - x_i^{(-)}\right) + \sum_{i=0}^{j-1} \frac{(2j_i-1)^2}{j_i\,(2j_i+1)^2}\left(1 - x_i^{(+)}\right)\Big], \qquad 1 - x_i \ll 1. \tag{41}$$

Similar averaging of expressions (40) and (34) for the case $x_i \ll 1$ leads to the following result for $j \gg 1$

$$\overline{\beta_K} = \frac{1}{6}\,\mathrm{Re}\Big[1 + \frac{1}{3}\,x_{j-1}^{(-)} - \frac{1}{8}\,x_{j-1}^{(+)} + \sum_{i=0}^{j-2} \frac{3x_i^{(-)}}{j_i\,(j_i+1)\,(2j_i+1)\,(2j_i+3)} - \sum_{i=0}^{j-2} \frac{8\,(6j_i+5)\,x_i^{(+)}}{(j_i+1)\,(2j_i-1)\,(2j_i+1)^2\,(2j_i+3)}\Big], \qquad x_i \ll 1. \tag{42}$$

In the summations in (42) the coefficients of x_i decrease rapidly with j_i, so that for small x_i we can limit ourselves to the terms with x_{j-1}:

$$\overline{\beta_K} \approx \frac{1}{6}\,\mathrm{Re}\Big[1 + \frac{1}{3}\,x_{j-1}^{(-)} - \frac{1}{8}\,x_{j-1}^{(+)}\Big] \qquad (x_l \ll 1). \tag{43}$$

As regards the case $x_i \sim 1$, we cannot carry out such an operation in formula (41), since the corresponding coefficients in the summations decrease more slowly. We can only note that the limiting value of $\overline{\beta}_K$ for $x_i \to 1$ is $1/4$. Denoting the polarization of the muon in the K shell by λ_K ($\lambda_K = \overline{\beta}_K\lambda$) and taking $\lambda \approx 1/3$, we have

$$\lambda_K = \frac{1}{12} \qquad \text{for } x_l = 1,\ \omega\tau = 0;$$

$$\lambda_K = \frac{1}{18}\left[1 + \frac{1}{3}\,\frac{1}{1+(\omega\tau)^2_{1/2}} - \frac{1}{8}\,\frac{1}{1+(\omega\tau)^2_{3/2}}\right] \qquad \text{for } x_l \ll 1,\ \omega\tau \gg 1. \tag{44}$$

The second formula of (44) contains the quantities $(\omega\tau)_{3/2}$ and $(\omega\tau)_{1/2}$ for the levels $p_{3/2}$ and $p_{1/2}$, for which, as we have already noted, $\omega\tau$ weakly depends on the principal quantum number. For $\omega\tau \gg 1$, we obtain $\lambda_K = 1/18$.

The experimental data for the depolarization of muons on nuclei with spin $I = 1/2$ change only for P^{31}, for which the mean value of the muon polarization in the K shell is $\lambda_K = 3\,(0.025 \pm 0.005)$.[7] For the levels $3p_{1/2}$, $3p_{3/2}$, $3d_{3/2}$, and $3d_{5/2}$ the values of $\omega_h\tau$ are equal to 3.15, 1.26, 2.27, and 1.45, respectively. We therefore have here the intermediate case [$(\omega_h\tau)_{\mathrm{eff}} \sim 1$], and consequently we should expect a value between $1/12$ and $1/18$ for the muon polarization in the K shell λ_K. This is in agreement with the experimental data cited above.

In conclusion, we shall comment on the Z-dependence of the final polarization of the muon λ_K. For hyperfine splitting we have $\omega_h \sim Z^3$, while for the radiative width we have $\Gamma_r \sim Z^4$. Hence for the lower levels of the heavy elements the effective value of $\omega_h\tau$ is small. Consequently (if we disregard the possibility of a very large nuclear magnetic moment), in the formation of μ-mesic atoms with nuclei of spin $1/2$ and Z much larger than for phosphorus, λ_K should be close to $1/12 = 0.083$.

For the lowest levels of the μ-mesic atoms formed with light nuclei with $I = 1/2$, where the main contribution to the width also comes from the radiative transitions, we have $\omega_h\tau \gg 1$. But for such mesic atoms the Auger transitions are already important for weakly excited levels. Hence, although we can also expect λ_K to decrease with decreasing Z, it will apparently not attain the lower limit $1/18 = 0.056$ found here for the lightest nuclei.

[1] V. A. Dzhrbashyan, JETP **36**, 277 (1959), Soviet Phys. JETP 9, 188 (1959).

[2] M. E. Rose, Bull. Am. Phys. Soc. **4**, 80 (1959).

[3] R. A. Mann and M. E. Rose, Phys. Rev. **121**, 293 (1961).

[4] I. M. Shmushkevich, Nuclear Phys. **11**, 419 (1959).

[5] H. Überall, Phys. Rev. **114**, 1640 (1959).

[6] E. Lubkin, Phys. Rev. **119**, 315 (1960).

[7] Egorov, Ignatenko, and Chultém, JETP **37**, 1517 (1959). Soviet Phys. JETP **10**, 1077 (1960).

[8] H. A. Bethe and E. Salpeter, Quantum Mechanics of One- and Two-Electron Atoms, Springer, Berlin, 1957.

[9] G. Goertzel, Phys. Rev. **70**, 897 (1946).

[10] G. Racah, Phys. Rev. **62**, 438 (1942); ibid. **63**, 367 (1943).

[11] I. M. Shmushkevich, JETP **36**, 953 (1959), Soviet Phys. JETP 9, 673 (1959).

Translated by E. Marquit
321

DISPERSION REPRESENTATION OF THE DEUTERON FORM FACTOR

V. V. ANISOVICH

Leningrad Physico-Technical Institute, Academy of Sciences, U.S.S.R.

Submitted to JETP editor July 6, 1961

J. Exptl. Theoret. Phys. (U.S.S.R.) 41, 1907-1914 (December, 1961)

The second anomalous singularity of the deuteron form factor situated at $s \sim 9\mu^2$ is considered. The dispersion representation is given for the simplest graph yielding this singularity. A method is developed which significantly simplifies the calculations of the discontinuities in the absorption parts of the diagrams with three free ends.

1. INTRODUCTION

THE deuteron form factor, the graph for which is shown in Fig. 1a, depends on one invariant—the square of the photon momentum $P^2 = s$. The squares of the momenta of the two deuterons are equal to the squares of their masses $P_1^2 = P_2^2 = D^2$. The deuteron form factor considered as a function of s has in addition to normal singularities also some anomalous ones. The simplest anomalous singularity of the deuteron is given by the graphs shown[1-2] in Fig. 1b. It is situated at $s = 16M\varepsilon$ (M is the nucleon mass, ε is the deuteron binding energy $D = 2M - \varepsilon$). Subsequent singularities of the form factor are situated at $s > 16M\varepsilon$. At $s = 4\mu^2$ (μ is the mass of the π meson) there exists a normal singularity which appears as the result of graphs of the type shown in Fig. 1c. Analogous graphs with three or four π-meson lines lead to normal singularities at $s = 9\mu^2$ and $s = 16\mu^2$. At

$$s = 4\mu^2 + 16\mu\sqrt{\varepsilon(M - \mu^2/4M)}$$

there exists a second anomalous singularity which results from graphs of a different type (cf., Fig. 1d.)

For sufficiently small values of s we can write the dispersion representation for the deuteron form factor by restricting ourselves to the contribution made to the dispersion part by graphs only of the type shown in Fig. 1b. If we want to write the dispersion representation more accurately, or if s is not sufficiently small, then we must include in the absorption part the contribution from the normal singularities and from graphs of Fig. 1d. The dispersion representation of the graphs of Fig. 1d is the most difficult one; it will be carried out in the present paper.

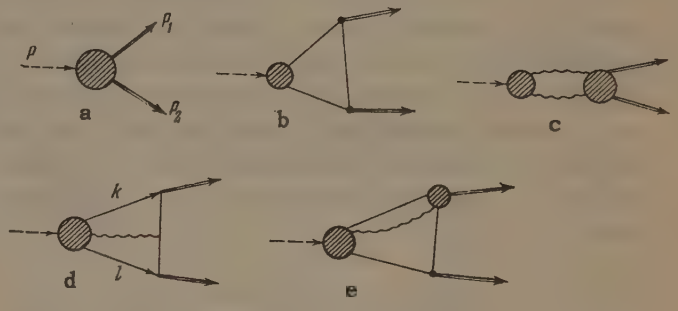

FIG. 1. Dotted line denotes a photon, wavy line denotes a meson, solid line denotes a nucleon, double line denotes a deuteron.

In the absence of anomalous singularities the dispersion representation of the vertex part has the form

$$\frac{1}{\pi}\int_{m^2}^{\infty}\frac{\varphi(s')}{s'-s}\,ds', \qquad (1)$$

where m is the smallest possible sum of the intermediate masses. If we begin to vary any of the masses in the graphs of the vertex part (1), then anomalous singularities can appear in this vertex part. In this case the contour of integration in (1) will not be a simple one: when the masses are varied the singularities in the absorption part of $\varphi(s)$ deform the contour. Such a process of the deformation of the contour of the dispersion integral (1) by graphs of the type shown in Fig. 1b has been discussed in detail by Mandelstam[3].

The graph shown in Fig. 1d will also deform the contour. In order to determine the manner in which the contour of integration is deformed in the latter case we consider the graph of Fig. 1d in which the shaded block is replaced by a dot (we denote this graph by the symbol 1d*). We shall observe with the aid of Landau graphs the behavior of the singularities of interest to us in the absorp-

tion part of such a graph as a function of the variation of the intermediate masses.

The Landau graph for 1d* is shown in Fig. 2a. The double line corresponds to the deuteron mass, the ordinary solid line corresponds to the nucleon mass, the wavy line corresponds to the π-meson mass. The dotted line gives the value of $\sqrt{s_0}$ where s_0 is the position of the singularity of the absorption part of graph 1d* and at the same time is also the position of the singularity of the whole graph 1d. Graphs 2b and 2c give the position of two other singularities of the absorption part. All these singularities of the absorption part are situated approximately at $s \sim \mu^2 - 9\mu^2$. The graph 1d* can in addition also have singularities of the same type as the graphs of Fig. 1e. Corresponding to this the absorption part of 1d* has singularities determined by graphs 2d and 2e. They are situated approximately at $s \sim 4M\mu + \mu^2$. The singularities of the absorption part of graph 1d* determined from Fig. 2 can be not the only possible ones. But these singularities play an essential role in the discussion of the deformation of the contour of integration.

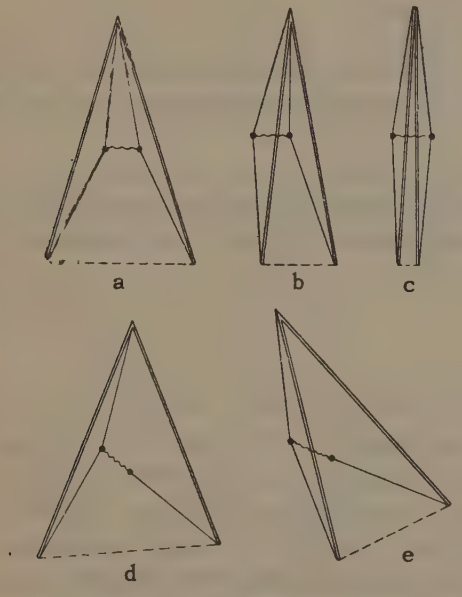

FIG. 2

If we consider the mass μ in graph 1d* to be large, say equal to 2M, then this graph does not have any anomalous singularities and its dispersion representation is given in the form (1), with $m = 2M + \mu$. By means of the graphs of Fig. 2 it can be easily shown that as μ is reduced (μ has a small negative imaginary part) the singularities of the absorption part of 2a and 2d deform the contour of integration, while the singularities of 2b, c and e move without deforming the contour in the direction of smaller values of s. When further decrease in μ causes the singularity of 2a to overtake the singularity of 2e, no further deformations of the contour occur, since μ has a negative imaginary part. The contour of integration in the dispersion representation of graph 1d* is in this case shown in Fig. 3. In the same figure is also shown the position of those singularities of the absorption part of 1d* which are determined by the graphs of Fig. 2. The dotted line shows the position of the cut in the absorption part arising as a result of the singularity a.

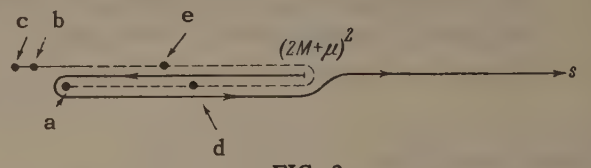

FIG. 3

The dispersion representation of graph 1d* has the form

$$\frac{1}{\pi}\int_{s_0}^{(2M+\mu)^2} ds' \frac{\Delta\varphi(s')}{s'-s} + \frac{1}{\pi}\int_{(2M+\mu)^2}^{\infty} ds' \frac{\varphi(s')}{s'-s},$$

$$s_0 = 4\mu^2 + 16M\mu\sqrt{\frac{\varepsilon}{M}\left(1-\frac{\mu^2}{4M^2}\right)}, \qquad (2)$$

where $\Delta\varphi(s)$ is the discontinuity in the absorption part evaluated on the two edges of the cut coming from the singularity a. If we are interested in the dispersion representation of graph 1d* for small values of s we have to know the discontinuity in the absorption part near the singularity a.

We know the absorption part of graph 1d* for $s > 4D^2$. It is given by (for simplicity we assume the nucleon to be a particle without spin)

$$\varphi(s) = \int dk\, dl\, \delta(k^2 - M^2)\, \delta(l^2 - M^2)\, \delta((P-k-l)^2 - \mu^2) \times [(P_1 - k)^2 - M^2)\,((P_2 - l)^2 - M^2)]^{-1}$$

$$= \frac{\pi^2}{16}\frac{1}{\sqrt{s\left(\frac{s}{4}-D^2\right)}}\int_{(M+\mu)^2}^{(\sqrt{s}-M)^2} d\sigma_1 \int_{\tau_{2-}}^{\tau_{2+}} \frac{d\tau_2}{\tau_2 - M^2} \times \left(\sigma_1\left[\frac{(\sigma_1 - \tau_2 + D^2)^2}{4\sigma_1} - D^2\right]\right)^{-1/2} \ln\frac{\tau_{1+} - M^2}{\tau_{1-} - M^2};$$

$$\tau_{1\pm} = M^2 + D^2 - \frac{1}{2\sigma_1}(\sigma_1 + M^2 - \mu^2)(\sigma_1 - \tau_2 + D^2) \pm 2\left(\left[\frac{(\sigma_1 + M^2 - \mu^2)^2}{4\sigma_1} - M^2\right]\left[\frac{(\sigma_1 - \tau_2 + D^2)^2}{4\sigma_1} - D^2\right]\right)^{1/2},$$

$$\tau_{2\pm} = M^2 + D^2 - \frac{1}{2}(s - \sigma_1 + M^2) \pm 2((s/4 - D^2)\,[(s - \sigma_1 + M^2)^2/4s - M^2])^{1/2}.$$

$$\tau_1 = (P_1 - k)^2, \qquad \tau_2 = (P_2 - l)^2, \qquad \sigma_1 = (P - l)^2. \qquad (3)$$

We can make an analytic continuation of expression (3) towards $s \sim 9\mu^2$ and evaluate the discontinuity in the absorption part. However, such a method of procedure introduces a number of considerable difficulties. We shall proceed in a somewhat different manner. In graph 1d* we shall vary the masses μ and D, ascribing a negative imaginary part to μ, and a positive imaginary part to D. For μ, $D > 2M$ the singularities a, b, c, d, e will go over to the region $s > 16M^2$. In this region we can easily evaluate the discontinuity in the absorption part in the neighborhood of the singularity a. We shall then continue this discontinuity analytically back towards the original values of the masses μ and E. In the next section we shall carry out this procedure.

2. EVALUATION OF THE DISCONTINUITY IN THE ABSORPTION PART OF GRAPH 1d*

The graph 1d* can be analytically continued with respect to the masses μ and D if we ascribe a negative imaginary part to the first mass, and a positive imaginary part to the second mass. As μ is increased the singularities a, b, c, d, e will begin to move towards larger values of s. When μ has almost reached 2M, but we still have $2M - \mu \gg 2M - D$, the position of the singularities will be the same as in Fig. 4a. As μ is increased further the singularities a and d will coincide with the point $(2M + \mu)^2$ (Fig. 4b). Further, the singularity a will move outside the contour of integration (Fig. 4c) and moving in the direction of large values of s will approach the point $s = 4D^2$, will go around it, and will start moving in the direction of smaller values of s (Fig. 4d and e). For $\mu > 2M$ the singularity a will go into the upper half-plane.

If we now increase $D + i\varepsilon$ in such a way that $D > 2M$, then the singularity a will return to the real axis. For $D > 2M$, $\mu > 2M$ and $\mu - 2M \gg D - 2M$ the position of the singularities is shown in Fig. 4f. This follows from the fact that for $|\mu - 2M| \gg |D - 2M|$, $\mu \sim 2M$, $D \sim 2M$ the position of the singularities is a function of the masses of the type

$$A(\mu - 2M) + B\sqrt{(\mu - 2M)(D - 2M)}$$

(this can be seen from the Landau graphs). In going over from D, $\mu < 2M$ to D, $\mu > 2M$ the square root does not change its sign.

Generally speaking, these may not be the only singularities possessed by the absorption part. But from the analytic continuation of (3), which will be carried out below, it can be seen that for $s > (2M + \mu)^2$ the absorption part of graph 1d* has no other singularities. We have to evaluate the discontinuity in the absorption part near the singularity a. This can be done simply if we know the absorption part for values of s situated to the right of the singularity a, and if we then continue it towards smaller values of s.

In the case shown in Fig. 4a, for sufficiently large values of s (for example, for $s \gg 4D^2$) the absorption part is given by expression (3). As μ and D are increased both the region of integration in (3) and the position of the singularities of the integrands will be altered. We begin to vary μ and D in the following order: we first increase $\mu - i\varepsilon$ in such a way that $\mu > 2M$; we then increase $D + i\varepsilon$ in such a way that $D > 2M$, but $\mu - 2M \gg D - 2M$. Then for s lying to the right of the singularity a (cf. Fig. 4b) the region of integration in expression (3) and the position of the singularities in the σ_1, τ_1 plane will be as shown in Fig. 5.

The region of integration is shaded. Singularities I and II come from the logarithm, singularity

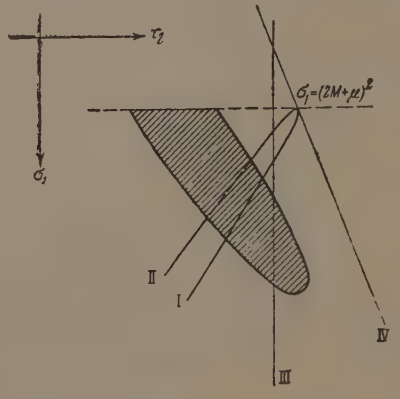

FIG. 5

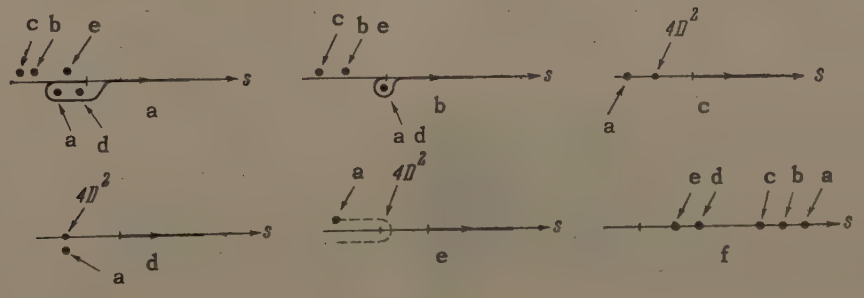

FIG. 4

III comes from the pole, and singularity IV comes from the square root. The fact that the line of singularity is shown by a dotted line signifies that in the complex domain of τ_2 the given singularity lies below the contour of integration.

If we evaluate the integral over τ_2, then the integrand which depends on σ_1 will have singularities which occur at such values of σ_1 at which the line limiting the contour of integration intersects with singularity III (we denote these points of intersection by σ_I, σ_{II}) or with singularity I (σ_{III}, σ_{IV}). Moreover, these singularities occur at σ_1, for which, for example, singularity III intersects with singularities I and II (σ_V and σ_{VI} respectively). The position of the contour of integration with respect to σ_1 and the positions of the singularities $\sigma_I - \sigma_{VI}$ in the case of large s and $\mu > 2M$, $D > 2M$ ($\mu - 2M \gg D - 2M$) are shown in Fig. 6a. If s has a positive imaginary part, then singularities σ_I, σ_{II}, σ_{III} and σ_{IV} are situated in the upper half-plane; therefore, singularities σ_{II} and σ_{IV} displace the contour of integration with respect to σ_1 slightly upwards. If s has a negative imaginary part, σ_I, σ_{II}, σ_{III} and σ_{IV} are displaced into the lower half-plane; singularities σ_I and σ_{III} deform the contour of integration in the direction of their motion.

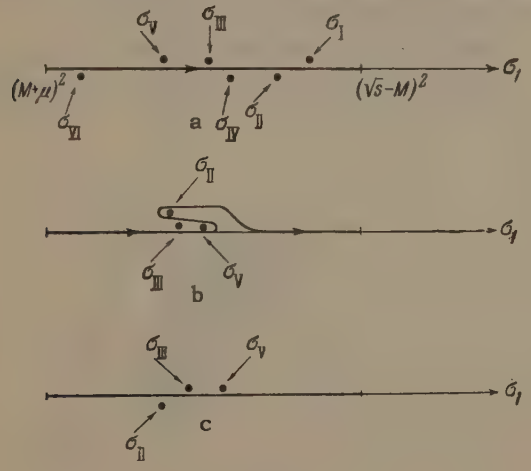

FIG. 6

As s decreases singularities $\sigma_I - \sigma_{IV}$ move in the direction of smaller values of σ_1. When s reaches the singularity a, the singularities σ_{II}, σ_{III} and σ_{IV} will coincide. If s will continue decreasing further retaining a positive imaginary part, then the contour of integration with respect to σ_1 will be deformed (Fig. 6b). If s decreases retaining a negative imaginary part, then there will be no deformation of the contour of integration (Fig. 6c). In this case ($\mathrm{Im}\, s < 0$) the contour of integration with respect to τ_2 for $\sigma_{II} < \sigma_1 < \sigma_V$

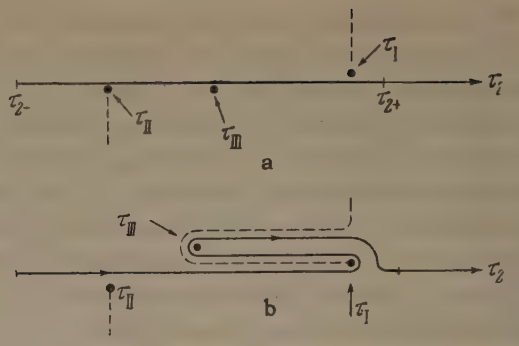

FIG. 7

will be as shown in Fig. 7a; τ_I, τ_{II} denote the positions of the logarithmic singularities, τ_{III} is the position of the pole singularity. Along the contour of integration the logarithm is real to the left of τ_{II} and to the right of τ_I, while in the interval between τ_I and τ_{II} the logarithm has an added imaginary term $i\pi$. For $\mathrm{Im}\, s > 0$ and $\sigma_{II} < \sigma_1 < \sigma_V$ the contour of integration with respect to τ_2 will be deformed. The positions of the singularities and of the contour of integration are shown in Fig. 7b. For $\sigma_1 > \sigma_V$ and $\sigma_1 < \sigma_{II}$ the position of the contour of integration does not depend on the sign of the imaginary part of s.

It can now be easily shown that the discontinuity in the absorption part between the singularity a and b is given by

$$-\Delta\varphi(s) = \varphi(s + i\varepsilon) - \varphi(s - i\varepsilon)$$

$$= \frac{\pi^2}{16}\frac{1}{\sqrt{s(s/4-D^2)}}\int_{\sigma_{II}}^{\sigma_V} d\sigma_1 \frac{(-2\pi i)^2}{\{\sigma_1[(\sigma_1 - M^2 + D^2)^2/4\sigma_1 - D^2]\}^{1/2}};$$

$$\sigma_{II} = s/2 + M^2 - [s(s/4 - D^2)(1 - 4M^2/D^2)]^{1/2},$$

$$\sigma_V = M^2 + D^2\mu^2/2M^2$$

$$+ [4D^2\mu^2(1 - D^2/4M^2)(1 - \mu^2/4M^2)]^{1/2}. \qquad (4)$$

This expression must be analytically continued back towards the physical values of D, μ and towards $s \geq 9\mu^2$, but in reverse order: we first decrease $D + i\varepsilon$ to the physical value of D. The singularity σ_V goes into the upper half plane, and the singularity σ_{II} goes into the lower half plane.

We now decrease $\mu - i\varepsilon$. For $\mu < 2M$ σ_V falls on the real axis, and the upper part of the cut between the singularities of the square root $\sigma_1 = (D - M)^2$, $\sigma_1 = (D + M)^2$. As a result of such continuation the sign in front of the square root in σ_V will not change. Moreover, we must diminish s in order to obtain the value of the discontinuity in the absorption part for $s \geq 9\mu^2$. The values of s must be varied along the path along which the

singularity a moved when we were increasing the masses μ and D from their normal values towards μ, $D > 2M$. This means that we must first take s into the upper half plane, then bring it to the real axis at $s < 4D^2$, increase it to $S = 4D^2$, go around this point clockwise, and then decrease it along the real axis (cf. Fig. 4d, c, e). As a result of this, s reaches the lower edge of the cut from the root $(s/4 - D^2)^{1/2}$; the root in σ_{II} does not change sign.

We obtain the following formula for $\Delta\varphi$ for physical values of μ, D and $4\mu^2 + 16M\mu[\varepsilon(1 - \mu^2/4M^2)/M]^{1/2} < s < 16\mu^2$:

$$\Delta\varphi(s) = \frac{\pi^4}{\sqrt{s(4D^2 - s)}} \int_{\sigma_{II}}^{\sigma_V} d\sigma_1 \{[\sigma_1 - (D - M)^2] \times [-\sigma_1 + (D + M)^2]\}^{-1/2}; \quad (5)$$

σ_{II} and σ_V are given by formula (4). $\Delta\varphi$ vanishes, as it should, for $s = 4\mu^2 + 16M\mu[\varepsilon(1 - \mu^2/4M^2)/M]^{1/2}$.

We have represented the discontinuity in the absorption part in the form of an integral over $\sigma_1 = (P - l)^2$. In addition, we can introduce into formula (5) integration over $\sigma_2 = (P - k)^2$. As long as we are considering only the graph 1d*, generally speaking, this is not worth while doing. But in the more complicated graphs 1d we must carry out the integration both over σ_1 and over σ_2.

In graph 1d* integration over σ_2 can be introduced fairly simply. In the right hand side of (5) we must introduce into the integrand a factor equal to unity:

$$\frac{1}{\pi} \int_{z_-}^{z_+} dz [(z_1^2 - 1)(z_2^2 - 1) - (z - z_1 z_2)^2]^{-1/2};$$

$$z_\pm = z_1 z_2 \pm \sqrt{(z_1^2 - 1)(z_2^2 - 1)}, \quad (6a)$$

where z_1, z_2 and z are defined by the relations

$$\sigma_2 = M^2 + s - \frac{1}{2\sigma_1}(\sigma_1 + M^2 - \mu^2)(\sigma_1 + s - M^2) + 2z\left\{\left[\frac{(\sigma_1 + M^2 - \mu^2)^2}{4\sigma_1} - M^2\right]\left[\frac{(\sigma_1 + s - M^2)^2}{4\sigma_1} - s\right]\right\}^{1/2},$$

$$0 = D^2 - \frac{1}{2\sigma_1}(\sigma_1 + M^2 - \mu^2)(\sigma_1 - M^2 + D^2) + 2z_1\left\{\left[\frac{(\sigma_1 - M^2 + D^2)^2}{4\sigma_1} - D^2\right]\left[\frac{(\sigma_1 + M^2 - \mu^2)^2}{4\sigma_1} - M^2\right]\right\}^{1/2},$$

$$0 = s - \frac{1}{2\sigma_1}(\sigma_1 + s - M^2)(\sigma_1 - M^2 + D^2) + 2z_2\left\{\left[\frac{(\sigma_1 + s - M^2)^2}{4\sigma_1} - s\right]\left[\frac{(\sigma_1 - M^2 + D^2)^2}{4\sigma_1} - D^2\right]\right\}^{1/2}. \quad (6b)$$

Formulas (5) and (6) give the required value of the discontinuity in the absorption part near the singularity a. In the next section we shall formulate a rule which considerably simplifies the evaluation of the discontinuities in the absorption parts of diagrams with three free ends.

3. A SIMPLE RULE FOR THE EVALUATION OF THE DISCONTINUITIES IN THE ABSORPTION PARTS OF DIAGRAMS WITH THREE FREE ENDS

The evaluation of the discontinuity in the absorption part of graph 1d* consisted of three stages. We first increased the masses $\mu + i\varepsilon$, $D + i\varepsilon$ to μ, $D > 2M$, and in doing so we observed the behavior of the absorption part by means of Landau graphs. In the second stage we made an analytic continuation of the absorption part with respect to the masses from the region D, $\mu < 2M$ into the region D, $\mu > 2M$, and we evaluated the discontinuity in this absorption part near the singularity of interest to us. In the third stage we made an analytic continuation in strictly reverse order of the discontinuity which we have obtained back towards the physical values of μ and D and towards $s \gtrsim 4\mu^2 + 16\mu[\varepsilon M(1 - \mu^2/4M^2)]^{1/2}$.

The second stage is considerably more difficult than the first and the third taken together. However, it is specifically for this stage that we can introduce a rule which in practice avoids all these difficult calculations. It has been noted already a long time ago that the discontinuities in the absorption parts are a result of the vanishing of the denominators of the functions Δ_F (private communication from V. N. Gribov and I. T. Dyatlov, cf. also [4]). In the region μ, $D > 2M$ we can attempt to replace in (3) $[(P_1 - k)^2 - M^2]^{-1}[(P_2 - l)^2 - M^2]^{-1}$ by $\alpha\delta[(P_1 - k)^2 - M^2]\delta[(P_2 - l)^2 - M^2]$ and see whether we might not obtain the same result for the discontinuity in the absorption part as we obtain as a result of a direct calculation. It can be seen at once that this can be done if $\alpha = (-2\pi i)^2$. The discontinuity in the absorption part of (2) in the region μ, $D > 2M$ can then be written in the form

$$(-2\pi i)^2 \int dk dl \delta(k^2 - M^2)\delta(l^2 - M^2)\delta((P - k - l)^2 - \mu^2) \times \delta((P_1 - k)^2 - M^2)\delta((P_2 - l)^2 - M^2), \quad (7)$$

In doing this we must remember that expression (7) differs from zero for s lying between the singularities a and c (cf. Fig. 4c). For s lying between the singularities a and b expression (7) gives one function, while for s lying between the singularities c and b it gives another function. We require the value of the discontinuity in the

absorption part near the singularity a, and, therefore, in expression (7) we must keep s between the singularities a and b.

We can also carry out a similar procedure involving analytic continuation with respect to the masses in the case of a simple graph of type 1b. In order that in such a graph all the lines can be real, it must be reduced by varying the masses, for example, to the graph of Fig. 8. If we do this by varying $M_1 - i\varepsilon$, $D_1 + i\varepsilon$ and $D_2 + i\varepsilon$, then we shall see that the discontinuity in the absorption part of such a graph can be correctly evaluated by replacing $[(P_1 - k)^2 - M_1^2]^{-1}$ by $(-2\pi i)\,\delta \times [(P_1 - k)^2 - M_1^2]$.

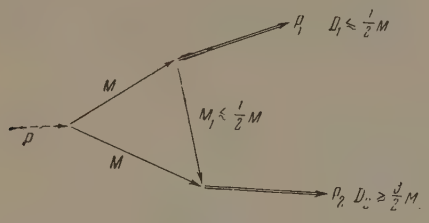

FIG. 8

From these two examples it can be seen that in order to evaluate the discontinuity in the absorption part of any graph corresponding to a diagram with three free ends we must go over to such masses that each vertex of this graph becomes fully decomposable. In the absorption part of this graph we must replace factors of the type $(k^2 - m^2)^{-1}$ by $(-2\pi i)\,\delta\,(k^2 - m^2)$. The discontinuity so obtained must then be continued analytically with respect to the internal masses having a negative imaginary part, and with respect to external masses having a positive imaginary part. The inverse continuation of the discontinuity towards the physical values of the masses is not a very difficult problem. Its solution is aided by an investigation of the behavior of the singularities by means of Landau graphs.

4. CONCLUSION

The introduction of graphs 1c and d into the dispersion representation of the deuteron form factor is of interest since these graphs determine the structure of the deuteron at distances of the order of μ^{-1}. We have presented the dispersion representation only for the graph 1d*. Apparently the representation of other graphs of type 1d is given by the same integrals (5) and (6), but with the integrand containing an additional function $A(s, \sigma_1, \sigma_2)$ corresponding to the shaded block in graph 1d. This is associated with the fact that this shaded block has no anomalous singularities for $s \sim 9\mu^2$ and, therefore, will not likely deform in any manner the contours of the dispersion integrals. It seems to us that by means of the method utilized in the present paper this can be shown more rigorously. Apparently a similar method of evaluating the discontinuities in the absorption parts can be successfully applied to diagrams with four free ends, and this must simplify the evaluation of $\rho(s, t)$ for complicated graphs.

The author is grateful to V. N. Gribov, G. S. Danilov and I. T. Dyatlov for useful discussions.

[1] L. D. Landau, Nuclear Phys. **13**, 181 (1959).
[2] Karplus, Sommerfield, and Wichman, Phys. Rev. **111**, 1187 (1958).
[3] S. Mandelstam, Phys. Rev. Letters **4**, 84 (1960).
[4] R. E. Cutkosky, J. Math. Phys. **1**, 429 (1960).

Translated by G. Volkoff
322

ON THE INTERACTION HAMILTONIAN IN QUANTUM FIELD THEORY

A. D. SUKHANOV

Mathematical Institute, Academy of Sciences, U.S.S.R.

Submitted to JETP editor July 7, 1961

J. Exptl. Theoret. Phys. (U.S.S.R.) 41, 1915-1928 (December, 1961)

The problem of obtaining the interaction Hamiltonian in quantum field theory is considered. An analysis is made of the expression for the Hamiltonian that follows from the Bogolyubov method, in particular for theories with derivative couplings. It is shown that this expression satisfies the condition for integrability of the Tomonaga-Schwinger equation for any renormalized theory. It is also shown how in this method one can accomplish the removal from the S matrix of the nonphysical dependence on the shape of the intermediate surfaces and achieve gauge invariance of the S matrix for scalar electrodynamics in the Klein-Gordon formalism. All of the results are obtained without taking "surface divergences" into account, and the problem of these divergences remains an open one.

1. INTRODUCTION

A step of great importance in the development of quantum field theory was the introduction of the interaction representation and the transition to the covariant Tomonaga-Schwinger equation [1,2]

$$i\delta\Phi(\sigma)/\delta\sigma(x) = H_{int}(x;\sigma)\,\Phi(\sigma), \tag{1}$$

where

$$H_{int}(x;\sigma) = i\frac{\delta S(\sigma)}{\delta\sigma(x)}S^{+}(\sigma) \tag{2}$$

is the interaction Hamiltonian density in the interaction representation, expressed in terms of the matrix $S(\sigma)$, which is the solution of (1) with the initial condition $S(-\infty) = 1$.

Since it is usually the problem of the theory to obtain $S(\sigma)$ for a known $H_{int}(x;\sigma)$, and not conversely, Eq. (2) does not give us a concrete expression for $H_{int}(x;\sigma)$, and we have to determine it from other considerations. Historically, the first way of obtaining $H_{int}(x;\sigma)$ was through various attempts [3,4] based on the use of considerations of correspondence with the Hamiltonian of the ordinary Schrödinger equation. This approach, however, encountered a number of difficulties in theories in which the interaction Lagrangian includes couplings with derivatives (or vector fields), since the $H_{int}(x;\sigma)$ so obtained did not satisfy the condition of integrability of the Tomonaga-Schwinger equation in the form

$$i\frac{\delta H_{int}(x;\sigma)}{\delta\sigma(y)} - i\frac{\delta H_{int}(y;\sigma)}{\delta\sigma(x)} + [H_{int}(x;\sigma), H_{int}(y;\sigma)] = 0$$

$$\text{for } x \sim y \text{ or } x = y. \tag{3}$$

The appearance of these difficulties when correspondence arguments are applied directly is due to the fact that in the ordinary Schrödinger equation the quantity that has physical meaning is only the Hamiltonian

$$H(t) = \int_{-\infty}^{\infty} H(x)\Big|_{x^0=t} dx,$$

and not the Hamiltonian density, which, according to the usual canonical formalism, is written in the form

$$H(x) = \sum_k \frac{\partial L}{\partial(\partial u_k/\partial x^0)}\frac{\partial u_k}{\partial x^0} - L(x). \tag{4}$$

At the same time, what appears in the Tomonaga-Schwinger equation is a Hamiltonian density $H_{int}(x;\sigma)$ which itself has physical meaning, and accordingly must be a covariant function of the field operators and satisfy the condition (3). Naturally when one uses for the $H_{int}(x;\sigma)$ of Eq. (1) the quantity without physical meaning given by Eq. (4) the difficulties we have mentioned arise in cases in which $H_{int}(x;\sigma) \neq -L(x)$.*

Ways of solving the problem were found by Matthews [5] and by Kanesawa and Koba,[6] who proposed two different covariant ways of obtaining $H_{int}(x;\sigma)$ when one has a known Lagrangian.

The idea of the Matthews method is that in going from the ordinary Schrödinger equation to the Tomonaga-Schwinger equation it is not enough merely to go over from state amplitudes $\Phi(t)$ to

*In cases in which the Lagrangian contains a vector field an analogous situation arises in taking the supplementary condition into account.

state amplitudes $\Phi(\sigma)$ and formally go over from the Hamiltonian to the Hamiltonian density; it is necessary to generalize the canonical formalism in a suitable way to the case of arbitrary spacelike surfaces. Then instead of the expression (4) there appears [7] the physically meaningful covariant expression

$$H(x;\sigma)=\sum_k\left(n_\alpha\frac{\partial L}{\partial(\partial u_k/\partial x^\alpha)}\right)\left(n_\beta\frac{\partial u_k}{\partial x^\beta}\right)-L(x), \quad (5)$$

where n_α is the timelike unit vector normal to the arbitrary spacelike surface passing through x, and $(n_\alpha)^2=1$, $n_0>0$.

It must be emphasized that Eq. (5) establishes a connection between the total Lagrangian and the total Hamiltonian, and in general cannot be applied as a connection between the interaction Lagrangian and the interaction Hamiltonian.

Therefore Matthews [5] has proposed the following way of obtaining $H_{int}(x;\sigma)$, starting from Eq. (5). One must first obtain $H_{tot}(x;\sigma)$ in the Heisenberg representation by Eq. (5), then separate off from it $H_{int}(x;\sigma)$, and after this go over to the interaction representation. In this way one gets in any theory an $H_{int}(x;\sigma)$ which satisfies the condition (3). For example, for scalar electrodynamics, for which

$$L_{int}(x)=ie:\left(\varphi^*(x)\frac{\partial\varphi}{\partial x^\alpha}-\frac{\partial\varphi^*}{\partial x^\alpha}\varphi(x)\right)A_\alpha(x):$$
$$+e^2:\varphi^*(x)\varphi(x)A_\alpha^2(x):, \quad (6)$$

one finds that

$$H_{int}(x;\sigma)=-L_{int}(x)+e^2:\varphi^*(x)\varphi(x)[n_\alpha A_\alpha(x)]^2:. \quad (7)$$

As can be seen from Eq. (7), in cases in which the interaction Lagrangian contains a coupling with derivatives (or vector fields) $H_{int}(x;\sigma)$ contains terms which have quadratic dependence on the normal to the spacelike surface σ passing through x, and thus is not only a function of x, but also a functional of the surface σ. The method of Yang and Feldman [8] is also one of the variations on the Matthews method.

A different method for obtaining $H_{int}(x;\sigma)$ directly in the interaction representation has been proposed by Kanesawa and Koba,[6] who took as the starting point $L_{int}(x)$ and proposed to look for $H_{int}(x;\sigma)$ in the form

$$H_{int}(x;\sigma)=-L_{int}(x)+A(x;\sigma), \quad (8)$$

where $A(x;\sigma)$ is a function of the field operators and a functional of the surface σ, and is chosen so that the condition (3) is satisfied for $H_{int}(x;\sigma)$.

If one attentively analyzes the expressions for $H_{int}(x;\sigma)$ obtained by the two methods described above, one can perceive the following connection which holds [as Eq. (5) does not] between the interaction Lagrangian and the interaction Hamiltonian in the interaction representation:

$$H_{int}(x;\sigma)=\frac{1}{2}\sum_k\left(n_\alpha\frac{\partial L_{int}}{\partial(\partial\varphi_k/\partial x^\alpha)}\right)\left(n_\beta\frac{\partial L_{int}}{\partial(\partial\varphi_k/\partial x^\beta)}\right)$$
$$-L_{int}(x). \quad (9)$$

Neither in the Matthews method nor in the Kanesawa-Koba method, however, does this connection appear in a natural way in the course of the calculations. Therefore one would like to have a method for obtaining $H_{int}(x;\sigma)$ [which we shall hereafter call simply $H(x,\sigma)$] in which a connection of the form (9) arises legitimately.

A general feature of the methods expounded here for obtaining $H(x,\sigma)$ is that one starts originally from the bare classical interaction Lagrangian. Therefore in the derivation of the S matrix [9] by the solution of Eq. (1) two problems arise. First, both the expression

$$S(\sigma)=T\exp\left\{-i\int_{-\infty}^{\sigma}H(x;\sigma)\,dx\right\}, \quad (10)$$

and the expression for $S(\infty)$ obtained from it in the limit $\sigma\to\infty$ are divergent expressions and require the use of a regularization procedure. Second, for the case of a coupling with derivatives $H(x,\sigma)$ contains terms quadratically dependent on the normals, which in $S(\sigma)$ are [10] the normals to a family of intermediate surfaces used in the solution of Eq. (1) by the method of successive approximations. Thus $S(\sigma)$ turns out to depend on the particular choice of such a family of surfaces, and this is of course physically meaningless.

As is well known, it has not yet been possible to get an expression for $S(\sigma)$ which is free from divergences. If we reason formally and treat $S(\sigma)$ as an intermediate quantity, this indeed is not a serious trouble, since after going from $S(\sigma)$ to $S(\infty)$ we can remove the divergences by performing a suitable regularization. If, however, we do not remove from $S(\sigma)$ the nonphysical dependence on the shape of the intermediate surfaces, it is still present after the passage to the limit $S(\infty)$. A procedure for the removal of this dependence was also first proposed by Matthews,[5] who showed by extremely cumbersome calculations and far from obvious operations with singular functions that in the calculation of $S(\sigma)$ to second order one can bring to light a term which cancels the terms in the Hamiltonian that contains the normals. Since, however, this calculation is not mathemat-

ically clear, one would like to know a deeper reason for the results Matthews obtained.

In this paper we shall follow the method for obtaining the scattering matrix and the interaction Hamiltonian proposed by Bogolyubov and Shirkov[11]; in this method one starts at the beginning with an effective interaction Lagrangian in the interaction representation

$$L(x; g) = L(x) + \sum_{n=2} \frac{1}{n!} \times \int_{-\infty}^{\infty} \Lambda_n(x, x_1 \ldots x_{n-1})\, g(x_1) \ldots g(x_{n-1})\, dx_1 \ldots dx_{n-1}, \quad (11)$$

which assures the finiteness of the S matrix for the proper choice of the T-product.

We shall consider the possibility of obtaining in the Bogolyubov method an interaction Hamiltonian which will satisfy the condition of integrability of the Tomonaga-Schwinger equation for any renormalizable theory and will have a natural connection of the form (9) with the effective interaction Lagrangian. We shall first examine how to solve in this method the problem of eliminating from the S matrix the nonphysical dependence on the shape of the intermediate surfaces in theories with derivative couplings. At the end we shall consider some features of the structure of the S matrix in scalar electrodynamics.

2. THE INTERACTION HAMILTONIAN IN THE BOGOLYUBOV METHOD

The fundamental quantity in the Bogolyubov method[11] is the matrix S(g), which is a functional of sufficiently smooth functions g(x). The apparatus of the matrix S(g) is, however, insufficient for the solution of all the problems confronting the theory, and it is necessary to introduce the apparatus of the Schrödinger equation. The proposed variational analog of this equation, for sufficiently smooth functions g(x), is

$$i\delta\Phi(g)/\delta g(x) = H(x; g)\,\Phi(g), \quad (12)$$

where

$$H(x; g) = i\frac{\delta S(g)}{\delta g(x)} S^{+}(g) \quad (13)$$

is the generalized interaction Hamiltonian density.

The conditions of relativistic covariance, unitarity, and causality for the matrix S(g) must completely determine an expression for H(x; g) which satisfies the conditions of relativistic covariance, Hermiticity, locality, and integrability. That the first two conditions for H(x; g) are satisfied is obvious. The locality condition of the form

$$\delta H(x; g)/\delta g(y) = 0 \quad \text{for } y \leqslant x \quad (14)$$

also follows directly from the condition of causality for S(g). As for the integrability condition, it is also satisfied, as we shall discuss in more detail in Sec. 4. Thus no new problems arise in connection with the generalized Hamiltonian H(x; g).

The problem arises when we want to go from Eq. (12) to Eq. (1) by going to the limit $g \to \theta_\sigma \to \theta(\tau_\sigma - x^0)$, i.e., when we want to obtain in this way an expression for the Hamiltonian H(x; σ), which, unlike the generalized Hamiltonian H(x; g), has physical meaning and must have local character in the ordinary sense—that is, must depend on the state of the fields only in an infinitely small neighborhood of the point x. As has been shown (cf. [11]), the condition (14) is sufficient to assure the local character of H(x; σ) when we go to the limit $g \to \theta_\sigma$. In practice, however, a number of difficulties arose in carrying out this passage to the limit, in particular the problem of "surface divergences."

First of all it must be emphasized that the expression for H(x; σ) is not equal to the limit of H(x; g), as one might have thought, but must be written in the form

$$H(x; \sigma) = \lim_{g \to \theta_\sigma} \int_{-\infty}^{\infty} H(x; g)\, g'(T_\sigma - x^0)\, dx^0, \quad (15)$$

where the passage to the limit is made after the integration.

Furthermore, in[11] use was made of the formula

$$\int_{-\infty}^{\infty} H_n(x, x_1 \ldots x_n) g(x_1) \ldots g(x_n)\, dx_1 \ldots dx_n = -\int_{-\infty}^{\infty} \Lambda_{n+1}(x, x_1 \ldots x_n)\, g(x_1) \ldots g(x_n)\, dx_1 \ldots dx_n, \quad (16)$$

where Λ_{n+1} are the same quasi-local operators as in Eq. (11). Equation (16) is obtained on the assumption that at first the regularization masses occurring in Λ_{n+1} remain fixed while $g \to \theta_\sigma$. At the same time it must be admitted that a different order in the passages to limits seems more reasonable, namely that of first letting all $M_i^2 \to \infty$, and then $g \to \theta_\sigma$ (private communication from D. A. Slavnov). But even for the terms in H(x; g) that are linear in the contractions, for which the question of the order of the limits does not arise at all, the analysis made in Sec. 4 shows that when there are derivatives in the Lagrangian there must

be some additional terms in the right member of Eq. (16).

The final expression for $H(x; \sigma)$ obtained in [11] by the use of (16) is of the form

$$H(x; \sigma) = \lim_{g \to \theta_\sigma} \left\{ -L(x) - \sum_{n=1} \frac{1}{n!} \int_{-\infty}^{\infty} \Lambda_{n+1}(x, x_1 \ldots x_n) \times g(x_1) \ldots g(x_n)\, dx_1 \ldots dx_n \right\}. \quad (17)$$

Since in the general case the quasi-local operators Λ_{n+1} contain derivatives of δ functions and the differentiations can get transferred to the functions $g(x)$, the limit process $g \to \theta_\sigma$ can lead, as is shown in [11], to the appearance of additional nonintegrable expressions of the type of products of δ functions of equal arguments. A more careful analysis, based on passage to the limit by the formula (15) and proper attention to the symmetry properties of the quasi-local operators, shows that, first, the main term in the expression obtained for $H(x; \sigma)$ is $-L(x; 1)$, and second, the class of diagrams leading to "surface divergences" is much narrower than it seemed at first glance. In particular, there is no such problem in the vacuum diagrams of any theory, and in the linearly divergent diagrams. In this case also, however, there is still a problem of "surface divergences" for the quadratically divergent diagrams,* which is essentially a reflection of the additional difficulties which arise in the construction of a finite $S(\sigma)$ from a finite $S(g)$, and which are due to the fact that in going over from smooth functions $g(x)$ to θ functions it is in general necessary to redefine the coefficient functions of $S(\sigma)$ as integrable generalized functions. It must be noted that the problem of "surface divergences" in $S(\sigma)$ is not a peculiarity of the Bogolyubov method, but is present implicitly also in the Dyson method, as has also been remarked by Stueckelberg.[12]

Thus although the way of constructing $H(x; \sigma)$ in the Bogolyubov method seems to be the most natural one, it cannot be carried through at present because of the problem of "surface divergences." In this connection it must be emphasized that the operator structure of the "surface diverging" terms that appear in the Bogolyubov method has nothing in common with the operator structure of the terms depending quadratically on the normals which appear in the Hamiltonians of theories that contain derivative couplings (cf. e. g., [7]). These terms are in principle of a different nature. Whereas the "surface diverging" terms depend on the form of the passage to the limit $g \to \theta_\sigma$ for arbitrary σ, the ordinary surface terms depend on the shape of the surface σ itself after the passage to the limit.

Accordingly, while leaving to one side the problem of "surface divergences," we wish to examine the question as to whether both $H(x; g)$ and the $H(x; \sigma)$ obtained from it in the limit satisfy the conditions of integrability of the corresponding equations for theories with derivatives in their bare Lagrangians, since it would seem that the formula (17) does not contain the terms necessary for this. Actually the situation is even more serious, since even when there are no derivatives in the bare Lagrangian the counterterms of all effective Lagrangians, except that of Hurst and Thirring, contain terms with derivatives, which according to Eq. (9) must lead to additional terms in the Hamiltonian. For example, for the second-order boson self-energy diagram we in fact have $L'(x) = ae^2 : (\partial\varphi/\partial x_\alpha)^2 :$. Therefore the corresponding $H'(x; \sigma)$ must be of the form

$$H'(x; \sigma) = -L'(x) + \tfrac{1}{2} a^2 e^4 : \left(n_\alpha \frac{\partial \varphi}{\partial x^\alpha} \right)^2 : .$$

Thus the problem of satisfying the integrability conditions of the Tomonaga-Schwinger equation in the Bogolyubov method is exceptionally significant, since it requires the appearance in $H(x; \sigma)$ of a large number of terms with quadratic dependence on the normals. We shall return to this problem in Sec. 4.

3. THE S MATRIX IN THEORIES WITH DERIVATIVE COUPLINGS

Since in the Bogolyubov method the Hamiltonian is found from a known S matrix, we must first elucidate some features of the derivation of the S matrix in theories with derivative couplings. We may ask the question: how is it possible in the methods of Dyson and Bogolyubov to get identical expressions for the S matrix in these theories, although the two methods formally apply the same operation (the T-product) to different original expressions?

As is well known, in deriving the S matrix in such theories by the Dyson method we are forced at first to include in the Hamiltonian terms quadratically dependent on the normals, starting from the condition (3), and then to eliminate these terms from the S matrix by a rather complicated procedure. Naturally this inclusion and subsequent elimination of certain terms is not due to the physics of the problem, but to peculiarities of the mathematical apparatus employed. In fact, in the

*A more detailed communication on this problem will be published later.

Bogolyubov method one is able to avoid these steps and construct the S matrix directly from the Lagrangian, on the basis of a number of general arguments.

A point of primary importance here is that the causality condition in second order (in both its differential [11] and its integral [13] forms) leads to the compatibility condition in the form

$$[L(x),\ L(y)] = 0 \quad \text{for} \quad x \sim y\ (x \neq y), \tag{18}$$

which is valid for any renormalizable theory and in the Bogolyubov method replaces the stronger condition (3).

Next the difference between the actual methods of constructing the S matrix comes into play. In the Bogolyubov method we arrive at once at T-products of Lagrangians. Here, if the Lagrangian contains derivatives, there arises in general the problem of a finite arbitrariness in the definition of the second derivative of $D^c(x-y)$, if the definition of $D^c(x-y)$ for coincident arguments is fixed. In fact, knowing that [11]

$$D^c(x-y) = \theta(x^0-y^0)\,D^-(x-y) - \theta(-x^0+y^0)\,D^+(x-y) = \frac{1}{(2\pi)^4}\int \frac{e^{ik(x-y)}dk}{m^2-k^2-i\varepsilon}, \tag{19}$$

we can define $\partial^2 D^c(x-y)/\partial x^\alpha \partial y^\beta = \tilde{D}^c_{\alpha\beta}(x-y)$ either in the form

$$\tilde{D}^c_{\alpha\beta}(x-y) = \theta(x^0-y^0)\,\tilde{D}^-_{\alpha\beta}(x-y) - \theta(-x^0+y^0)\,\tilde{D}^+_{\alpha\beta}(x-y) - n_\alpha n_\beta \delta(x-y) = \frac{1}{(2\pi)^4}\int \frac{(-k_\alpha k_\beta)\,e^{ik(x-y)}dk}{m^2-k^2-i\varepsilon}, \tag{20}$$

or in the form

$$\tilde{D}^c_{\alpha\beta}(x-y) = \theta(x^0-y^0)\,\tilde{D}^-_{\alpha\beta}(x-y) - \theta(-x^0+y^0)\,\tilde{D}^+_{\alpha\beta}(x-y), \tag{21}$$

or in any other form which differs from the expressions (20) and (21) by a quasi-local covariant operator.

Since, however, the S-matrix apparatus is adapted to the momentum representation, from the point of view of this apparatus the simplest and most physically reasonable definition is Eq. (20), and this is the one adopted in [11]. With this definition of $D^c_{\alpha\beta}(x-y)$ one gets for the S matrix in a theory with derivative coupling the expression

$$S(\infty) = T\exp\left\{i\int_{-\infty}^{\infty} L(x)\,dx\right\}, \tag{22}$$

which is free from any nonphysical dependence on the shapes of the intermediate surfaces.

In Dyson's method, on the other hand, in solving the Tomonaga-Schwinger equation we first arrive at advanced products of repeated commutators of Hamiltonians, and only subsequently, on regrouping them, do we come to the corresponding T-products. In doing so one uses, for example, the formula

$$D^{adv}(x-y) = D^c(x-y) - D^-(x-y), \tag{23}$$

where $D^c(x-y)$ is of the form (19) and

$$D^{adv}(x-y) = -\theta(-x^0+y^0)\,D(x-y). \tag{24}$$

If we now formally differentiate both sides of Eq. (23) twice, we still have equality of the two sides if on both the right side and the left side we simultaneously either do or do not differentiate the θ functions. The actual situation is different, however. In solving the Tomonaga-Schwinger equation we arrive, for example, at an expression $\theta(-x^0+y^0)\,[H(x;\sigma),\ H(y;\sigma)]$, and when we calculate this out in a theory with derivative coupling we get among other quantities a term

$$-\theta(-x^0+y^0)\,\tilde{D}_{\alpha\beta}(x-y), \tag{25}$$

which from the point of view of the apparatus of the Tomonaga-Schwinger equation it is most natural to take as the definition of $\tilde{D}^{adv}_{\alpha\beta}(x-y)$, because in solving this equation the situation in which one would differentiate the θ function in the expression (24) never arises.

Thus for the most reasonable definitions of $\tilde{D}^c_{\alpha\beta}(x-y)$ and $\tilde{D}^{adv}_{\alpha\beta}(x-y)$ the contraction of the type (23) does not occur and is replaced by the formula

$$\tilde{D}^{adv}_{\alpha\beta}(x-y) = \tilde{D}^c_{\alpha\beta}(x-y) - \tilde{D}^-_{\alpha\beta}(x-y) + n_\alpha n_\beta \delta(x-y). \tag{26}$$

This makes understandable a second point of difference of the two methods for constructing the S matrix in the case of a derivative coupling. Solving the Tomonaga-Schwinger equation, we at first arrive at the expression $[\tilde{D}^{adv}_{\alpha\beta}(x-y) + \tilde{D}^-_{\alpha\beta}(x-y)]$; we can call this quantity $\tilde{D}^c_{\alpha\beta}(x-y)$ [in accordance with Eq. (21)], and use for the S matrix the formula

$$S(\infty) = T\exp\left\{-i\int_{-\infty}^{\infty} H(x;\sigma)\,dx\right\}. \tag{27}$$

The expression (21), however, is not the most convenient definition of $\tilde{D}^c_{\alpha\beta}(x-y)$ from the point of view of the S-matrix apparatus. On the other hand, if we wish to use the definition (20), we have to go over from $\tilde{D}^{adv}_{\alpha\beta}(x-y)$ to $\tilde{D}^c_{\alpha\beta}(x-y)$ by Eq. (26),

which automatically brings us from Eq. (27) to Eq. (22).

Thus the possibility in principle which Matthews has indicated for eliminating the nonphysical dependence on the shape of the intermediate surfaces for theories with derivative couplings can be connected with the possibility of giving different definitions* of $\widetilde{D}^c_{\alpha\beta}(x-y)$ and with the fact that the apparatus of the Tomonaga-Schwinger equation leads in the most natural way to the definition (21). Furthermore one can use for the S matrix either a formula of the type (27) or one of the type (22); one need only remember that actually different [in the part with $\widetilde{D}^c_{\alpha\beta}(x-y)$] definitions of the T-product are used in these formulas. We emphasize that with this approach to the problem there is a natural unity between the cases of a Lagrangian with derivatives and a Lagrangian containing a vector field. In both cases one can get an S matrix which has physical meaning by defining the second derivative of $D^c(x-y)$ in a suitable way.

4. THE INTEGRABILITY CONDITION IN THE BOGOLYUBOV METHOD

As is clear from Sec. 3, for the construction of the S matrix by the Bogolyubov method it is not necessary that the condition (3) be satisfied; it suffices for the weaker condition (18) to hold. In this method, however, there exists a Schrödinger equation as well as an S matrix. Here we shall examine in detail what the situation is as to satisfying the integrability condition for this equation and for the Tomonaga-Schwinger equation obtained from it by passage to the limit.

The integrability condition for the variational Schrödinger equation is of the form

$$i\,\delta H(x;g)/\delta g(y) - i\,\delta H(y;g)/\delta g(x) + [H(x;g),\ H(y;g)] = 0 \quad \text{for } x \sim y \text{ or } x = y, \tag{28}$$

and in its form is reminiscent of the condition (3), which, as is well known, is violated at the point $x = y$ for $H(x;\sigma) = -L(x)$ if the Lagrangian contains a coupling involving derivatives.

In our present case, when we use the definition of $H(x;g)$ by Eq. (13) and the fact that $S(g)$ is unitary, the condition (28) takes the form

$$\frac{\delta^2 S(g)}{\delta g(y)\,\delta g(x)} S^+(g) + \frac{\delta^2 S(g)}{\delta g(\ )\,\delta g(y)} S^+(g) - [H(x;g),\ H(y;g)] + [H(x;g),\ H(y;g)] = 0 \quad \text{for } x \sim y \text{ or } x = y. \tag{29}$$

In the expression (29) the commutators cancel and the equality of the second variational derivatives of $S(g)$ at the point $x = y$ does not arouse any doubts.

Thus the integrability condition of the variational Schrödinger equation is satisfied automatically for any theory and does not depend at all on the value of the commutator $[H(x;g),\ H(y;g)]$ (which in second order is $[L(x),\ L(y)]$ at the point $x = y$. There is nothing surprising in this result, since we did not obtain the expression for the generalized Hamiltonian from any sort of collateral arguments, but essentially from the physically meaningful solution of the equation (12).

The question of what happens to the integrability condition for $g \to \theta_\sigma$ calls for closer examination in view of the singular character of the approach to the limit. This is true especially because if we approach Eq. (16) uncritically we would have to admit that for all theories except the Hurst-Thirring field the integrability condition is violated in the limit.

Nevertheless, we are enabled to clear up this question by the analysis of the structure of the S matrix for theories with derivative couplings which we made in Sec. 3. We merely note that every ordinary product or T-product can be represented by an expression of the form

$$T(L(x)\,L(y)) = :L(x)\,L(y): + :\frac{\partial L(x)}{\partial\varphi(x)}\,\frac{\partial L(y)}{\partial\varphi(y)}:\frac{1}{i}D^c(x-y) + \ldots$$

Therefore if the Lagrangian involves a derivative coupling, then according to Eqs. (13) and (15) the Hamiltonian will contain, along with other terms which are linear in the contractions, a term of the type:

$$\Delta H(x;\sigma) = -\lim_{g\to\theta_\sigma}\int_{-\infty}^{\infty} dx^0\,dy g'(T_\sigma - x^0) \times g(T_\sigma - y^0) :\frac{\partial L(x)}{\partial(\partial\varphi/\partial x^\alpha)}\,\frac{\partial L(y)}{\partial(\partial\varphi/\partial y^\beta)}: \{\widetilde{D}^c_{\alpha\beta}(x-y) - \widetilde{D}^-_{\alpha\beta}(x-y)\}. \tag{30}$$

By the arguments which lead to Eq. (16) this term is to be regarded as equal to zero, since it does not depend at all on the order in which the limits are taken. If, however, we recall that in the

*The arbitrariness in the definition of the T-product which we have indicated leads to an additional arbitrariness [14] in the definition of the interpolating field [15] (for a given S matrix); this arbitrariness is of the following character: in the definition of a vector interpolating field there is an additional arbitrariness as compared with the case of a scalar field, owing to the fact that we can have different definitions of $D^c_{\alpha\beta}(x-y)$ with the same S matrix.

Bogolyubov method S(g) depends on the Lagrangian and consequently $\tilde{D}^{c}_{\alpha\beta}(x-y)$ is defined by Eq. (20), then it is clear that to obtain $\Delta H(x;\sigma)$ we must go over to $\tilde{D}^{adv}_{\alpha\beta}(x-y)$ by Eq. (26). We then have

$$\Delta H(x;\sigma) = -\lim_{g\to\theta_\sigma}\int_{-\infty}^{\infty} dx^0\, dy g'(T_\sigma - x^0) \times g(T_\sigma - y^0) : \frac{\partial L(x)}{\partial(\partial\varphi/\partial x^\alpha)} \frac{\partial L(y)}{\partial(\partial\varphi/\partial y^\beta)} : \{\tilde{D}^{adv}_{\alpha\beta}(x-y) - n_\alpha n_\beta \delta(x-y)\}. \quad (31)$$

Here the first term in the curly brackets goes to zero in the limit, and the second term gives the nonvanishing contribution

$$\Delta H(x;\sigma) = \frac{1}{2} : \left[n_\alpha \frac{\partial L(x)}{\partial(\partial\varphi/\partial x^\alpha)}\right]\left[n_\beta \frac{\partial L(x)}{\partial(\partial\varphi/\partial x^\beta)}\right] \quad (32)$$

which assures that the integrability condition of the Tomonaga-Schwinger equation is satisfied both for the bare Lagrangian and for the counter-terms of arbitrary order, since in the Bogolyubov method what one has as L(x) is the effective Lagrangian L(x; 1). In second order in scalar electrodynamics

$$\Delta H(x;\sigma) = e^2 : \varphi^*(x)\varphi(x)[n_\alpha A_\alpha(x)]^2 :,$$

which corresponds to the well known usual expression.

Combining the results of Secs. 2 and 4, we can write (if we drop "surface-diverging" counter-terms) the expression for H(x; σ) which follows from the Bogolyubov method:

$$H(x;\sigma) = -L(x;1) + \frac{1}{2} : \left[n_\alpha \frac{\partial L(x;1)}{\partial(\partial\varphi/\partial x^\alpha)}\right]\left[n_\beta \frac{\partial L(x;1)}{\partial(\partial\varphi/\partial x^\beta)}\right] :. \quad (33)$$

Thus a formula of the type of Eq. (9) arises legitimately in this method.

It is also not hard to understand that with this way of obtaining the Hamiltonian no terms of fourth or higher order in the number of normals can arise, since when there is one derivative in the Lagrangian such terms will correspond to unconnected diagrams, which do not contribute to the Hamiltonian,[11] and when the Lagrangian contains products of derivatives some of the normals that appear will have to be identical, and therefore because $(n_\alpha)^2 = 1$ these terms also will not have more than two normals. Thus in any renormalizable theory a formula of the type of Eq. (33) gives an expression which is exhaustive from this point of view; this is in agreement with the mathematical treatment carried out by Nishijima.[16]

Thus in this method (if we disregard the problem of "surface divergences") both the generalized Hamiltonian H(x; g) and the physical Hamiltonian H(x; σ) obtained from it in the limit $g \to \theta_\sigma$ satisfy the corresponding integrability conditions for any renormalizable theory. This result is all the more attractive because the integrability condition is important not only mathematically but also physically. In particular, for theories with derivative couplings it is only when this condition[16] is satisfied that the energy-momentum conservation law holds.

5. SOME FEATURES OF THE CONSTRUCTION OF THE S MATRIX FOR SCALAR ELECTRODYNAMICS

As is well known,[17,18] the Klein-Gordon and Duffin-Kemmer formalisms can be used with equal success in the construction of the S matrix for scalar electrodynamics by the Dyson method. In particular, the proof of renormalizability has been given in both formalisms. In doing this in the Dyson method one starts from the interaction Hamiltonian, which in one formalism has the form (7) and in the other the form

$$H^{D-K}(x;\sigma) = -ie : \bar{\psi}(x)\Gamma_\alpha\psi(x)A_\alpha(x) : - e^2m^{-1} : \bar{\psi}(x)\Gamma_\alpha\Gamma_\beta\psi(x)A_\alpha(x)A_\beta(x) : + e^2m^{-1} : \bar{\psi}(x)\Gamma_\alpha\Gamma_\beta[n_\delta\Gamma_\delta]^2\psi(x)A_\alpha(x)A_\beta(x) : \quad (34)$$

where Γ_α are the Duffin-Kemmer matrices, and then in obtaining the S matrix one goes over to the Lagrangian, of the form (6) or the form

$$L^{D-K}(x) = ie : \bar{\psi}(x)\Gamma_\alpha\psi(x)A_\alpha(x) :. \quad (35)$$

As can be seen from a comparison of the formulas (7)—(34) and (6)—(35), in going from the Hamiltonian to the Lagrangian in the Dyson method one eliminates not only the terms quadratic in the normals, but also, in the Duffin-Kemmer formalism, all the terms quadratic in the charge, while in the Klein-Gordon formalism the term e^2: $\varphi^*(x)\varphi(x)A^2_\alpha(x)$: remains. As was shown above, the possibility of eliminating from the S matrix the terms that depend quadratically on the normals is due to the fact that there is an extra finite arbitrariness in the definition of the T-product. In all probability the possibility of eliminating the other term of order e^2 in the Duffin-Kemmer formalism is due to this same circumstance.

It is clear from the foregoing that one of the advantages of the construction of the S matrix by the Bogolyubov method is that in this method the situation with the terms quadratically dependent

on the normals is much simpler. Up to this time, however, the S matrix for scalar electrodynamics has been obtained by the Bogolyubov method only in the Duffin-Kemmer formalism [19]; one can ascribe this in particular to the fact that $L^{D-K}(x)$, unlike $L^{K-G}(x)$, contains only a term linear in the charge. In the Bogolyubov method this is of importance in the use of the correspondence arguments, which allow us to have only a first-order term in the bare Lagrangian.

Nevertheless, a careful analysis shows that the S matrix for scalar electrodynamics can also be constructed in the Klein-Gordon formalism by the Bogolyubov method. In fact, following the course of the arguments given in [11], we find from correspondence considerations that

$$S_1(x) = -e : \left(\varphi^*(x)\frac{\partial\varphi}{\partial x^\alpha} - \frac{\partial\varphi^*}{\partial x^\alpha}\varphi(x)\right) A_\alpha(x) :, \qquad (36)$$

because we can include in $S_1(x)$ only terms linear in $g(x)$. If, however, we continue with the construction of the S matrix, we can arrive at the usual formula. Namely, in second order we have

$$S_2(x, y) = e^2 T\left[: \left(\varphi^*(x)\frac{\partial\varphi}{\partial x^\alpha} - \frac{\partial\varphi^*}{\partial x^\alpha}\varphi(x)\right) A_\alpha(x) : \times : \left(\varphi^*(y)\frac{\partial\varphi}{\partial y^\beta} - \frac{\partial\varphi^*}{\partial y^\beta}\varphi(y)\right) A_\beta(y) :\right], \qquad (37)$$

and $S_2(x, y)$ is defined everywhere except at the point $x = y$. This indefiniteness in the T-product enables us not only to make $S_2(x, y)$ an integrable generalized function, but also to secure the gauge invariance of the matrix $S(1)$.

In Sec. 3 we pointed out the existence of a finite arbitrariness in the definition of $\widetilde{D}^c_{\alpha\beta}(x - y)$ with a fixed definition of $D^c(x - y)$. In particular, we can add to the definition (20), which was adopted in [11], a term $g^{\alpha\beta}\delta(x - y)$. This definition of $\widetilde{D}^c_{\alpha\beta}(x - y)$ has the result of bringing out from the diagram that describes the meson Compton effect in second order a term

$$e^2\int_{-\infty}^{\infty} dxdy\, g(x)\, g(y) : \varphi^*(x)\varphi(y) A_\alpha(x) A_\beta(y) : g^{\alpha\beta}\delta(x - y) = e^2\int_{-\infty}^{\infty} dx g^2(x) : \varphi^*(x)\varphi(x) A_\alpha^2(x) :. \qquad (38)$$

We can return to the previous definition of $\widetilde{D}^c_{\alpha\beta}(x - y)$, which is more convenient for the further calculations, and include the term (38) in the effective interaction Lagrangian, which to second order takes the form

$$L(x; g) = ie : \left(\varphi^*\frac{\partial\varphi}{\partial x^\alpha} - \frac{\partial\varphi^*}{\partial x^\alpha}\varphi(x)\right) A_\alpha(x) : + e^2 : \varphi^*(x)\varphi \times (x) A_\alpha^2(x) : g(x) + \frac{1}{2!}\int_{-\infty}^{\infty}\Lambda_2(x, y)\, g(y)\, dy. \qquad (39)$$

A peculiarity of the counterterm $e^2 : \varphi^*(x)\varphi(x) \times A_\alpha^2(x) : g(x)$ is that its appearance is associated not with the problem of securing the finiteness of the S matrix, but with that of securing its gauge invariance. Thus the requirement of gauge invariance [at least for $S(1)$] must be included from the very beginning among the fundamental requirements imposed on the scattering matrix.

At first glance it may seem that there is a great difference between the processes of constructing the S matrix by the Bogolyubov method in the different formalisms of scalar electrodynamics, since in the Klein-Gordon formalism we have to redefine the T-product in order to secure the gauge invariance of the S matrix, whereas in the Duffin-Kemmer formalism it is secured automatically, as it were. The difference, however, is an apparent one. Actually the appearance of the term $e^2 : \varphi^*(x)\varphi(x) A_\alpha^2(x) :$ when we go from the Duffin-Kemmer formalism to the Klein-Gordon formalism is due to the fact that in the definition of the chronological contraction of $\psi(x)$ operators in the momentum representation there is a term $m^{-1}Y$, where Y is a combination of Γ_α matrices. This term is a typically quasi-local one and can be eliminated from the definition of the contraction if we ignore the requirements of gauge invariance.

Thus in the Klein-Gordon formalism we can use for the S matrix, besides formulas of the forms of Eqs. (27) and (22), the expression

$$S = T\exp\left\{i\int_{-\infty}^{\infty} L'(x)\, dx\right\}, \qquad (40)$$

where

$$L'(x) = ie : \left(\varphi^*(x)\frac{\partial\varphi}{\partial x^\alpha} - \frac{\partial\varphi^*}{\partial x^\alpha}\varphi(x)\right) A_\alpha(x) :. \qquad (41)$$

Thus there are no essential differences between the Klein-Gordon and Duffin-Kemmer formalisms in the construction of the S matrix either by the Dyson method or by the Bogolyubov method.

As for the Schrödinger equation, independently of whether we assign the additional term indicated here to the Lagrangian or to the T-product, in the limit $g \to \theta_\sigma$ we get a Hamiltonian which agrees with the usual Hamiltonian of scalar electrodynamics. In the former case this term appears by the same arguments as the usual counterterms. In the latter case it arises in the Hamiltonian in the same way as the terms that depend quadratically on the normals.

Finally, it must be pointed out that the treatment given in Secs. 4 and 5 requires that we make one addition to the apparatus of local dynamical variables introduced by Bogolyubov and Shirkov.[11] One of the important requirements of

this apparatus is that in the limit $g \to 0$ the quantities $B(x; g)$ must become identical with the corresponding expressions $B(x)$ of the free-field theory. If we apply this requirement to $H(x; g)$ for the scalar electrodynamics, then in the limit $g \to 0$ this expression goes over into $L'(x)$ [cf. Eq. (41)], which is neither the Hamiltonian nor even the Lagrangian of the free fields. The same difficulty is found with the corresponding current. A way out of this situation can be found by requiring that in the limit $g \to 0$ a quantity $B(x; g)$ is to agree with only the part of the corresponding free-field quantity that is linear in the charge.

6. CONCLUSION

Thus we have shown that if we leave to one side the problem of "surface divergences" the Bogolyubov method applied to any renormalizable theory gives in a legitimate way an expression for $H(x; \sigma)$ of the form (33) which satisfies the integrability condition for the Tomonaga-Schwinger equation. Since this Hamiltonian includes the usual counterterms, the solution of this equation will give an expression for the S matrix which is free from "ultraviolet" divergences. Thus the derivation of $H(x; \sigma)$ by the Bogolyubov method can be regarded as a third method for obtaining the interaction Hamiltonian in quantum field theory, and the most natural of the existing methods. It is also quite clear how in this method one can eliminate the terms that depend quadratically on the normals from the S matrix obtained by the solution of the Tomonaga-Schwinger equation.

As for the problem of "surface divergences," a consistent treatment of this will in all probability require the use of a more rigorous mathematical apparatus of the type of the new R operation.[11] Only such an approach to the problem will make it possible to decide finally whether it is of mathematical or physical origin, since there also exists the opinion[20] that there is no S matrix which has physical meaning. It is a matter of very great interest to settle this problem, since it arises both in the Bogolyubov method and in the Dyson method.[12] Furthermore, if the problem of "surface divergences" can be positively solved, we shall for the first time have to do with a Hamiltonian which will lead through the solution of the Tomonaga-Schwinger equation to an expression for the matrix $S(\sigma)$ which is free from both ordinary divergences and "surface divergences."

It must be emphasized, however, that even in this case new difficulties of a "surface" character can arise in the construction of the apparatus of local dynamical variables by means of the matrix $S(\sigma)$ (for example, in the construction of the expression for the interpolating field[15]).

Finally, if the Hamiltonian so obtained is used not for the derivation of the S matrix, but in some other apparatus, then the regularizing masses which it contains can lead to expressions which are infinite in the usual sense of the word. Therefore along with the solution to the problem of "surface divergences" one must look for a new and mathematically more rigorous approach to the entire set of questions associated with the Schrödinger equation and the apparatus of local dynamical variables.

In conclusion I express my deep gratitude to B. V. Medvedev for his constant interest in this work and a number of helpful comments. I also express my gratitude to D. V. Shirkov and D. A. Slavnov for a fruitful discussion.

Note added in proof (November 19, 1961). We must emphasize that our use of the notation $\tilde{D}^c_{\alpha\beta}(x-y)$ in Eq. (21) is of a somewhat conditional character, because if taken too literally it could even lead to such an absurd result as $(\Box_x - m^2) \times D^c(x) = 0$. Indeed, in Eqs. (20) and (21) we have written different definitions of the contraction $T\left(\frac{\partial\varphi}{\partial x^\alpha}\frac{\partial\varphi}{\partial y^\beta}\right)$, which are used in the Bogolyubov and Dyson methods, respectively. Furthermore, although the definition (21) follows directly from the intuitive meaning of the T-product for $x \neq y$, the definition (20), for which the equation

$$T\left(\frac{\partial\varphi}{\partial x^\alpha}\frac{\partial\varphi}{\partial y^\beta}\right) = \frac{\partial}{\partial x^\alpha}\frac{\partial}{\partial y^\beta}T(\varphi(x)\varphi(y))$$

holds right down to $x = y$, is more convenient. The same can be said about the notation $\tilde{D}^{adv}_{\alpha\beta}(x-y)$ in Eq. (25).

[1] S. Tomonaga, Progr. Theoret. Phys. 1, 27 (1946).

[2] J. Schwinger, Phys. Rev. 74, 1439 (1948).

[3] Koba, Tati, and Tomonaga, Progr. Theoret. Phys. 2, 101 (1947).

[4] S. Kanesawa and S. Tomonaga, Progr. Theoret. Phys. 3, 1 (1948).

[5] P. T. Matthews, Phys. Rev. 76, 1657 (1949).

[6] S. Kanesawa and Z. Koba, Progr. Theoret. Phys. 4, 297 (1949).

[7] P. Weiss, Proc. Roy. Soc. A169, 102 (1938).

[8] C. N. Yang and D. Feldman, Phys. Rev. 79, 972 (1950).

[9] F. J. Dyson, Phys. Rev. 75, 486 (1949).

[10] Z. Koba. Progr. Theoret. Phys. 5, 139 (1950).

[11] N. N. Bogolyubov and D. V. Shirkov, Vvedenie v teoriyu kvantovannykh polei (Introduction to the Theory of Quantized Fields), Gostekhizdat, 1957.

[12] E. C. G. Stueckelberg, Phys. Rev. 81, 130 (1951).
[13] B. V. Medvedev, JETP 31, 791 (1956), Soviet Phys. JETP 4, 671 (1957).
[14] D. A. Slavnov and A. D. Sukhanov, JETP 41, 1940 (1961), this issue, p. 1379.
[15] Lehmann, Symanzik, and Zimmermann, Nuovo cimento 1, 205 (1955).
[16] K. Nishijima, Progr. Theoret. Phys. 5, 187 (1950).
[17] A. I. Akhiezer and V. B. Berestetskii, Kvantovaya elektrodinamika (Quantum Electrodynamics), 2d ed. Fizmatgiz, 1959.
[18] F. Rohrlich, Phys. Rev. 80, 666 (1950).
[19] V. A. Shakhbazyan, Candidate's Dissertation, Math, Inst. AN SSSR, 1960.
[20] R. Haag, Kgl. Danske Videnskab. Selskab, Mat.-fys. Medd. 29, No. 12 (1955).

Translated by W. H. Furry
323

GIANT RESONANCE IN Pb^{208} PHOTODISINTEGRATION

V. V. BALASHOV, V. G. SHEVCHENKO, and N. P. YUDIN

Nuclear Physics Institute, Moscow State University

Submitted to JETP editor July 12, 1961

J. Exptl. Theoret. Phys. (U.S.S.R.) 41, 1929-1933 (December, 1961)

The cross section for dipole absorption of gamma rays by Pb^{208} nuclei is calculated using the shell model. It is shown that when residual pair interactions between nucleons are taken into account the giant resonance energy is approximately doubled. The calculations agree with experimental results.

It has become clear that the principal shortcoming of the single-particle model of photonuclear reactions [1] lies in the sharply reduced giant resonance energies that are calculated when nucleon-nucleon correlations in the nucleus are neglected.

The calculations for the photodisintegration of O^{16} and Ca^{40} in [2] and [3], with interactions between nucleons taken into account, have shown that the shell model can furnish a comprehensive description of the photodisintegration of light nuclei in the giant resonance region. It was shown that a mixture of states in light nuclei does not essentially shift giant resonance as compared with the "diagonal approximation" (a term used in our earlier work [3]). This is understandable since in light nuclei the average separation between levels of the "zero approximation" considerably exceeds the average value of nondiagonal matrix elements between single-particle dipole states. In heavy nuclei giant resonance represents a large number of single-particle transitions. Therefore, while the initial assumption of the Brown-Bolsterli scheme [4] is a highly idealized procedure for light nuclei, it can be expected that the dipole absorption curve for heavy nuclei will reflect the characteristic features of this scheme.

In the present work the shell model has been used to calculate the dipole cross section for γ-ray absorption by Pb^{208}. With regard to the photodisintegration of Pb^{208} it is noteworthy, first of all, that the diagonal approximation (which takes into account only the diagonal part of the interaction between a particle and a hole) does not yield results essentially different from those obtained with Wilkinson's single-particle model. In this approximation the dipole absorption curve has a broad peak at 5.5—8 Mev (Fig. 1), while the experimental giant resonance energy is 13.5—14 Mev.[5]

The $J = 1^-$ energy levels and the corresponding wave functions were calculated by diagonalizing the interaction matrix based on the single-particle states given in Table I. The single-particle levels were determined from experimental data for neighboring nuclei and from extrapolations based on the single-particle model.[6] The matrix elements for the interaction between a particle and a hole were calculated assuming the following δ in-

Table I. Zero-approximation energies

Single-proton states	E, Mev	Single-proton states	E, Mev	Single-neutron states	E, Mev	Single-neutron states	E, Mev
$1h^{-1}_{11/2}\,1i_{13/2}$	6.4	$2d^{-1}_{5/2}\,2f_{5/2}$	10.0	$1i^{-1}_{13/2}\,1j_{15/2}$	6.7	$2f^{-1}_{7/2}\,3d_{5/2}$	8.5
$3s^{-1}_{1/2}\,3p_{3/2}$	7.5	$2d^{-1}_{5/2}\,2f_{7/2}$	6.6	$3p^{-1}_{1/2}\,3d_{3/2}$	6.6	$2f^{-1}_{5/2}\,2g_{7/2}$	7.3
$3s^{-1}_{1/2}\,3p_{1/2}$	9.0	$1g^{-1}_{7/2}\,2f_{7/2}$	8.3	$3p^{-1}_{3/2}\,3d_{3/2}$	7.5	$2f^{-1}_{7/2}\,2g_{7/2}$	9.6
$2d^{-1}_{3/2}\,3p_{3/2}$	8.0	$1g^{-1}_{7/2}\,2f_{5/2}$	11.8	$3p^{-1}_{3/2}\,3d_{5/2}$	6.3	$2f^{-1}_{7/2}\,2g_{9/2}$	6.6
$2d^{-1}_{3/2}\,3p_{1/2}$	9.5	$1g^{-1}_{9/2}\,2f_{7/2}$	11.7	$3p^{-1}_{1/2}\,4s_{1/2}$	6.0	$1h^{-1}_{9/2}\,1i_{11/2}$	7.9
$2d^{-1}_{5/2}\,3p_{3/2}$	9.8	$1g^{-1}_{9/2}\,1h_{9/2}$	10.8	$3p^{-1}_{3/2}\,4s_{1/2}$	7.9	$1h^{-1}_{9/2}\,2g_{9/2}$	7.1
$2d^{-1}_{3/2}\,2f_{5/2}$	8.2	$1g^{-1}_{7/2}\,1h_{9/2}$	7.5	$2f^{-1}_{5/2}\,3d_{3/2}$	7.4		
				$2f^{-1}_{5/2}\,3d_{5/2}$	6.2	$1h^{-1}_{9/2}\,2g_{7/2}$	10.1

FIG. 1. Histogram of main dipole transitions in Pb^{208} in the diagonal approximation.

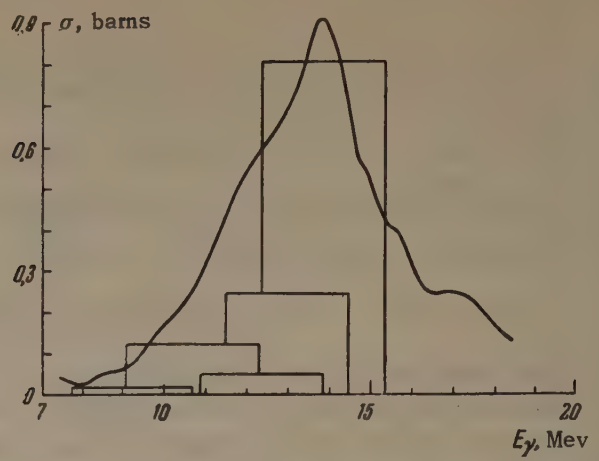

FIG. 2. Experimental and calculated (for Soper forces) integral cross sections for the main dipole transitions in Pb^{208}. The column width is arbitrary.

Table II

E, Mev	σ_{tot}, mb-Mev	E, Mev	σ_{tot}, mb-Mev
9.2	45.2	6.6	24.9
9.3	23.6	7.8	30.7
13.8	2384.2	10.4	24.0
13.0	718.1	12.4	147.8
10.5	361.4	6.6	30.2

teraction between nucleons:

$$V_{12} = -g\,[(1-\alpha) + \alpha\sigma_1\sigma_2]\,\delta(r_1 - r_2);$$

oscillator functions were used in calculating the radial integrals ($r_0 = \sqrt{\hbar/m\omega} = 2.13 \times 10^{-13}$ cm). The interaction amplitude g was taken to be 1220 Mev-f^3 in accordance with calculations of the lowest Pb^{208} levels.[6] Figure 2 and Table II give the calculated cross sections for photoabsorption into 1^- levels, using $\alpha = 0.135$ (for Soper forces).[7]

Unlike the light nuclei O^{16} and Ca^{40}, where the ground and excited dipole states differ in isotopic spin, in heavy nuclei the single-particle dipole excitations contain some admixture of "spurious states" corresponding to the excitation of motion of the nuclear center of gravity. The spurious states were distinguished after diagonalization by calculating the matrix element $|\psi_i|\mathbf{R_A}|\psi_0|$ for each of the derived dipole states ψ_i (ψ_0 is the ground-state function). It was found that ~85% of the spurious states are included in a level corresponding formally to the negative energy E = −4.7 Mev. This level was excluded; thus the remaining states include about 0.5% spurious states for each level.

In order to determine how giant resonance is influenced by the properties of nucleon-nucleon interactions a similar calculation was performed with Wigner forces ($\alpha = 0$). The results are in sharp disagreement with experiment (Fig. 3).

It must be remembered that the foregoing calculations were based on a number of more or less crude assumptions, such as point interactions, oscillator functions etc. Therefore a detailed quantitative comparison with experiment is hardly justified. However, we can draw the following general conclusions.

1. When residual interactions in Pb^{208} are taken into account an isolated "dipole state" is formed, corresponding to the experimental giant resonance energy. The occurrence of this state when the energy matrix is diagonalized results from the high density of single-particle dipole states in the given nucleus. The average separation of single-particle levels (~0.2 Mev) is smaller than the nondiagonal matrix elements (~0.3 Mev).

2. The high density (approximate degeneracy) of single-particle levels is not a sufficient condition for the appearance of an isolated strongly correlated dipole state (the Brown-Bolsterli effect). The character of the configuration mixture depends substantially on the relative magnitudes of the dif-

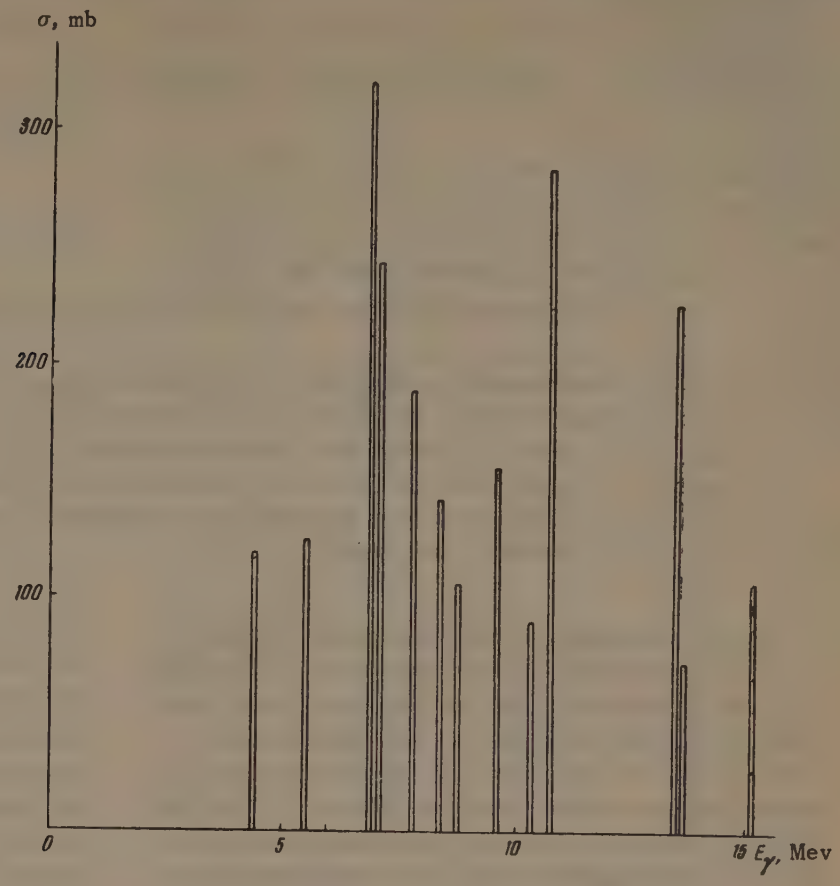

FIG. 3. Histogram of main dipole transitions for Wigner forces in Pb^{208}.

ferent nondiagonal matrix elements for the interaction between a particle and a hole, as determined by the properties of the residual nucleon-nucleon interaction.

Shell-model calculations of photonuclear reactions have by now been performed for all nuclei. The most detailed calculations have been carried out for the magic nuclei O^{16}, Ca^{40}, and Pb^{208}, and show that the principal features of giant resonance in photodisintegration are successfully accounted for by the shell model including configurational mixing. One might expect the principal conclusions derived from these calculations to be applicable to all nuclei. However, technical difficulties arise which make it doubtful that similar calculations can actually be performed for non-magic nuclei, with the exception of some special cases. The problem appears to consist in the construction of a simpler model of nuclear dipole states not requiring the diagonalization procedure and based on a microscopic (shell) interpretation of collective dipole excitation.

[1] D. H. Wilkinson, Physica 22, 1039 (1956).

[2] J. P. Elliott and B. H. Flowers, Proc. Roy. Soc. (London) **A242**, 57 (1957).

[3] Balashov, Shevchenko, and Yudin, Materialy II Vsesoyuznoĭ konferentsii po yadernym reaktsiyam pri malykh i srednikh énergiyakh (Proc. Second All-Union Conference on Nuclear Reactions at Low and Medium Energies); Nuclear Phys. **27**, 323 (1961).

[4] G. E. Brown and M. Bolsterli, Phys. Rev. Letters **3**, 472 (1959).

[5] E. G. Fuller and E. Hayward, International Conference on Nuclear Structure, Kingston, Ontario, Canada, 1960.

[6] True, Pinkston, and Carter, Bull. Am. Phys. Soc. **5**, 243 (1960).

[7] J. M. Soper (to be published); Brown, Castillejo, and Evans, Nuclear Phys. **22**, 1 (1961).

Translated by I. Emin
324

RELATIVISTIC CORRECTIONS TO THE MAGNETIC MOMENTS OF H^3 *AND* He^3

N. S. ZELENSKAYA and Yu. M. SHIROKOV

Moscow State University

Submitted to JETP editor July 12, 1961

J. Exptl. Theoret. Phys. (U.S.S.R.) **41**, 1934-1937 (December, 1961)

A general expression is obtained for the relativistic corrections to the magnetic moment of a nucleus which arise on account of non-Galilean relativistic corrections to the Hamiltonian of the nucleon-nucleon interaction. The corrections to the magnetic moments of the nuclei H^3 and He^3 are calculated numerically. It turns out that the corrections are of the right sign and order of magnitude, but do not explain more than 30 percent of the existing discrepancy between theory and experiment.

1. In nonrelativistic approximation the magnetic moment of a nucleus is determined by the intrinsic magnetic moments of the nucleons and the orbital magnetic moments of the protons. Inclusion of relativistic effects leads to corrections to the nucleon-nucleon interaction Hamiltonian of the order $(p/M)^2$. Because of gauge invariance the appearance in the Hamiltonian of terms that depend on the momentum is necessarily accompanied by the appearance of an additional interaction of the nucleons in the nucleus with the electromagnetic field, which in turn leads to corrections to the magnetic moment of the nucleus. We emphasize that the corrections in question occur only for pairs of nucleons and are absent for isolated nucleons.

The relativistic corrections to the interaction energy of two nucleons can be divided into two groups.

a) Corrections which satisfy the condition of Galilean invariance and consequently do not depend on the total momentum of the nucleons. Corrections to the spin-orbit interaction are corrections of this type.

b) Corrections which do not satisfy the requirement of Galilean invariance and therefore depend on the total momentum of the nucleons. Corrections of this type to the interaction Hamiltonian of two particles of arbitrary masses and spins have been derived by one of the writers.[1]

Both these groups of corrections to the interaction energy lead to corrections to the magnetic moments of nuclei. The relativistic corrections to the magnetic moments of nuclei are on the average of the order of 10^{-3} nuclear magneton. Unfortunately, the wave functions of nuclei of any complexity are known to very small accuracy, and as a rule in the calculation of the nonrelativistic values of the magnetic moments this leads to uncertainties much larger than the relativistic corrections. Therefore at present it makes sense to examine the relativistic corrections only for the simplest nuclei. For the deuteron there are no non-Galilean corrections.[1] Therefore in the present paper we analyze the corrections to the magnetic moments of the nuclei H^3 and He^3.

The values of the magnetic moments of H^3 and He^3 differ considerably from the sum of the magnetic moments of the constituent nucleons (cf. e. g.,[2]). In principle there can be nonrelativistic corrections to the magnetic moments of these nuclei owing to admixtures of states with nonzero orbital angular momenta. The total angular momentum of the ground state of these mirror nuclei is $J = \frac{1}{2}$. Possible states are $^2S_{1/2}$, $^2P_{1/2}$, $^4P_{1/2}$, $^4D_{1/2}$. Mixings of these states, however, cannot completely remove the discrepancy between theory and experiment. In fact, an admixture of P states in amounts which do not disagree with the value of the spin-orbit coupling leaves the magnetic moments practically unchanged,[3] and Sachs and Schwinger[4] have shown that a 4-percent admixture of the $^4D_{1/2}$ state makes it possible to get agreement between theory and experiment only for the sum of the magnetic moments of H^3 and He^3. For the magnetic moments of the individual nuclei there remain discrepancies, which amount to $+0.27$ nuclear magnetons for H^3 and -0.27 nuclear magnetons for He^3.

The Galilean-invariant corrections to the magnetic moments of these nuclei on account of spin-orbit forces have been calculated by Berger.[5] He found that the correction to the difference of the magnetic moments on account of the spin-orbit

interaction is of the order of only 10^{-4} nuclear magnetons, i.e., negligibly small.

In the present paper we calculate the non-Galilean relativistic corrections to the magnetic moments of H^3 and He^3.

2. With relativistic corrections included to order $(p/M)^2$ the Hamiltonian of the nucleon-nucleon interaction is of the form [6]

$$H=\sum_n T_n+\sum_{m>n} H_{mn}+\sum_n T'_n+\sum_{m>n} H'_{mn}+\sum_{m>n} H''_{mn}, \quad (1)$$

where T_n is the kinetic energy of the n-th nucleon, H_{mn} is the interaction energy of the m-th and n-th nucleons, T'_n is the relativistic correction to the kinetic energy of the n-th nucleon, H'_{mn} is the non-Galilean correction to the interaction energy of the m-th and n-th nucleons, and H''_{mn} is the non-Galilean correction associated with spin-orbit forces for this pair of nucleons.

For the nucleon-nucleon interaction the relativistic non-Galilean corrections are of the form [6]

$$\begin{aligned} H_{mn}=\frac{1}{8M^2}\Big\{&-H_{mn}\mathbf{P}^2+i\Big(\mathbf{P}\frac{\partial H_{mn}}{\partial \mathbf{x}}\Big)\Big(\mathbf{P}\frac{\partial}{\partial \mathbf{p}}\Big)\\ &-(\boldsymbol{\sigma}_m-\boldsymbol{\sigma}_n)\Big[\mathbf{P}\frac{\partial H_{mn}}{\partial \mathbf{x}}\Big]-i(\boldsymbol{\sigma}_m-\boldsymbol{\sigma}_n)H_{mn}[\mathbf{pP}]\\ &+iH_{mn}(\boldsymbol{\sigma}_m-\boldsymbol{\sigma}_n)[\mathbf{pP}]\\ &-\Big(\mathbf{P}\frac{\partial H_{mn}}{\partial \mathbf{p}}\Big)(\mathbf{pP})+iP_iP_j\frac{\partial^2 H_{mn}}{\partial x_i\partial p_j}\Big\} \end{aligned} \quad (2)^*$$

Here

$$\mathbf{P}=\mathbf{p}_m+\mathbf{p}_n, \qquad \mathbf{p}=\tfrac{1}{2}(\mathbf{p}_m-\mathbf{p}_n), \qquad \mathbf{x}=\mathbf{x}_m-\mathbf{x}_n$$

By means of the Hamiltonian (2) one can obtain the operator for the non-Galilean relativistic corrections to the magnetic moment of the nucleus. The interaction with the electromagnetic field is introduced in a gauge-invariant way [7] by the replacement:

$$\mathbf{p}_n\to\mathbf{p}_n-e_n\mathbf{A}.$$

For central forces not depending on the velocity the operator for the relativistic non-Galilean corrections to the magnetic-moment vector of the nucleus is obtained from Eq. (2) in the form

$$\begin{aligned} \Delta\boldsymbol{\mu}=\frac{1}{16M^2}\Big\{&2H_{mn}(e_m+e_n)[\mathbf{n}(\mathbf{r}-\mathbf{R})]\mathbf{P}\\ &-(e_m+e_n)(\boldsymbol{\sigma}_m-\boldsymbol{\sigma}_n)\Big[\mathbf{n}\Big((\mathbf{r}-\mathbf{R})\frac{\partial H_{mn}}{\partial \mathbf{r}}\Big)\\ &-(\mathbf{r}-\mathbf{R})\Big(\mathbf{n}\frac{\partial H_{mn}}{\partial \mathbf{r}}\Big)\Big]\Big\} \end{aligned} \quad (3)$$

The corrections (3) have been calculated for the $^2S_{1/2}$ state of the mirror nuclei. Harmonic-oscillator wave functions were used for the calculations. The energy H_{mn} was taken to be of the form

$$H_{mn}=(W+MP_x+BP_\sigma+\mathcal{H}P_xP_\sigma)V(r).$$

The calculations were made for Gaussian and Yukawa forms of the radial factor $V(r)$, with various parameters. Two forms were used for the exchange part of the potential. The results of the calculations are shown in the table.

Form and parameters of V(r) (V_0 in Mev, a in 10^{-13} cm)	$W=M=0.5$, $B=\mathcal{H}=0$		$W=0.222$, $M=0.58$, $B=0.222$, $\mathcal{H}=-0.022$ [9]	
	$\Delta\mu(H^3)$	$\Delta\mu(He^3)$	$\Delta\mu(H^3)$	$\Delta\mu(He^3)$
Gaussian potential				
$V_0=51.9$, $a=1.73$ [8]	0	−0.048	0.014	−0.014
$V_0=45$. $a=1.94$ [9]	0	−0.032	0.009	−0.009
$V_0=68.8$, $a=1.55$ [10]	0	−0.018	0.005	−0.005
Yukawa potential				
$V_0=68$, $a=1.17$ [11]	0	−0.086	0.026	−0.026
$V_0=46.48$, $a=1.184$ [12]	0	−0.056	0.017	−0.017

3. The following conclusions can be drawn from the results.

1) The non-Galilean relativistic corrections to the magnetic moments of the nuclei H^3 and He^3 depend strongly on the choice of the potential. The signs of the corrections are as required, but their size is insufficient for the complete explanation of the discrepancy between theory and experiment. The maximum size of the corrections is 0.086 nuclear magnetons, which is 30 percent of the previously mentioned discrepancy of 0.27 nuclear magnetons.

2) The relativistic non-Galilean correction considerably increases the correction for the spin-orbit interaction.

Thus the relativistic corrections cannot fully explain the discrepancy between the theoretical and experimental values of the magnetic moments of these nuclei. The remaining discrepancy is evidently to be ascribed to the effect of meson-exchange currents. Corrections of this sort are not taken into account in the phenomenological theory developed here. A rough estimate of these corrections has been made by Drell and Walecka [13]; their work shows that inclusion of meson-exchange currents leads to a decrease of the anomalous magnetic moments of the proton and the neutron. Their calculations are made for nuclei in which there is one nucleon outside an even-even core. The even-even core itself is regarded as a Fermi sphere with a definite limiting momentum and energy. Their result gives a change of the spin gyromagnetic ratio by $\Delta g_S = 0.26\,\tau_3$, where τ_3 is the isotopic spin component of the nucleus. Ac-

*$[\mathbf{pP}]=\mathbf{p}\times\mathbf{P}$, $(\mathbf{pP})=\mathbf{p}\cdot\mathbf{P}$.

cording to this the exchange correction is −0.13 magneton for He^3 and +0.13 magneton for tritium. It must be noted that these estimates are very rough. Nevertheless, they give a direct indication that inclusion of the exchange currents will make it possible to explain the differences between the calculated magnetic moments of the mirror nuclei and the experimental values.

In fact, the total correction to the magnetic moment (relativistic correction + correction for exchange currents) is −0.23 magneton for He^3 and +0.23 magneton for H^3, which agrees very well with the observed discrepancy of ± 0.27 magneton.

[1] Yu. M. Shirokov, JETP **36**, 474 (1959), Soviet Phys. JETP 9, 330 (1959).

[2] H. A. Bethe and Philip Morrison, Elementary Nuclear Theory, John Wiley and Sons, Inc., New York, 1956.

[3] R. Avery and R. G. Sachs, Phys. Rev. **74**, 1320 (1948).

[4] R. G. Sachs and J. Schwinger, Phys. Rev. **70**, 41 (1946).

[5] J. M. Berger, Phys. Rev. **115**, 384 (1959).

[6] Zhivopistsev, Perelomov, and Shirokov, JETP **36**, 478 (1959), Soviet Phys. JETP 9, 333 (1959).

[7] R. G. Sachs and N. Austern, Phys. Rev. **81**, 705 (1951).

[8] R. A. Ferrell and W. M. Visscher, Phys. Rev. **102**, 450 (1956).

[9] A. C. Butcher and J. M. McNamee, Proc. Phys. Soc. **74**, 529 (1959).

[10] Pearlstein, Tang, and Wildermuth, Nuclear Phys. **18**, 23 (1960).

[11] J. M. Blatt and V. F. Weisskopf, Theoretical Nuclear Physics, John Wiley and Sons, Inc., New York, 1952, p. 55.

[12] H. Feshbach and J. Schwinger, Phys. Rev. **84**, 194 (1951).

[13] S. D. Drell and J. D. Walecka, Phys. Rev. **120**, 1069 (1960).

Translated by W. H. Furry
325

INTERFERENCE EFFECTS IN THE IONIZATION OF HYDROGEN ATOMS BY ELECTRON IMPACT

R. K. PETERKOP

Physics Institute, Academy of Sciences, Latvian S.S.R.

Submitted to JETP editor July 13, 1961

J. Exptl. Theoret. Phys. (U.S.S.R.) 41, 1938-1939 (December, 1961)

The cross section for ionization of hydrogen atoms by electrons is calculated in the Born approximation, taking interference effects into account.

It has been shown that in the ionization of hydrogen atoms by electrons exchange effects can be considered as an interference between parts of the wave function.[1] This is a purely quantum mechanical effect and can be described by saying that when the wave function is symmetrized in accordance with Pauli's principle, interference occurs between scattering events that differ by an exchange of electrons in the initial or final states. The ionization cross section, taking exchange into account, can be written in the form

$$Q = Q' - Q_{int}, \tag{1}$$

where Q' is the cross section without exchange and Q_{int} is the interference term

$$Q_{int} = \int_0^{E/2} \frac{kc}{q}\, d\varepsilon \iint \mathrm{Re}\,[f(\mathbf{k}, \mathbf{c})\, g^*(\mathbf{k}, \mathbf{c})]\, d\mathbf{k} d\mathbf{c}. \tag{2}$$

In this formula, q is the momentum of the incident electron, $\epsilon = k^2/2$, $E = E_q - \frac{1}{2}$, $E_q = q^2/2$ is the energy of the incident electron, and $f(\mathbf{k}, \mathbf{c})$ is the probability amplitude for the electron being scattered with momentum $\mathbf{c}$ and the atom to have final momentum $\mathbf{k}$; $g(\mathbf{k}, \mathbf{c})$ is the corresponding exchange amplitude. All quantities are measured in atomic units.

We now calculate the interference term in the Born approximation. In this approximation[2]

$$f(\mathbf{k}, \mathbf{c}) = -\frac{2}{x^2}\int \psi_1(\mathbf{r})\, e^{i\mathbf{x}\mathbf{r}}\, \psi_{\mathbf{k}}^*(\mathbf{r})\, d\mathbf{r};$$

$$\mathbf{x} = \mathbf{q} - \mathbf{c},\quad x^2 = q^2 + c^2 - 2qc\cos(\mathbf{q}, \mathbf{c}), \tag{3}$$

where ψ_1 and ψ_2 are atomic wave functions for the initial and final states. The result of the integration is

$$f(\mathbf{k}, \mathbf{c}) = \frac{16\exp(i\delta(k))\,[(1-ik)^2 + x^2]^{n-1}\,[(1-n)\,\mathbf{kx} - x^2]}{\{\pi k\,(1-\exp(-2\pi/k))\}^{1/2} x^2\,[1 + (\mathbf{x}-\mathbf{k})^2]^{n+2}};$$

$$\delta(k) = \arg\Gamma(1 - i/k),\quad n = 1/ik. \tag{4}$$

According to [1], the phase shift η of the wave function of the scattered electron can be chosen so that

$$g(\mathbf{k}, \mathbf{c}) = f(\mathbf{c}, \mathbf{k}). \tag{5}$$

In general, for an arbitrary phase shift $\eta' = \eta - \Delta(\mathbf{k}, \mathbf{c})$, Eq. (5) is to be replaced by

$$g(\mathbf{k}, \mathbf{c}) = f(\mathbf{c}, \mathbf{k})\exp[i\Delta(\mathbf{k}, \mathbf{c}) - i\Delta(\mathbf{c}, \mathbf{k})], \tag{6}$$

and the interference term then becomes

$$Q_{int} = \int_0^{E/2} \frac{kc}{q}\, d\varepsilon \iint \mathrm{Re}\,\{f(\mathbf{k}, \mathbf{c}) f^*(\mathbf{c}, \mathbf{k}) \times \exp[i\Delta(\mathbf{c}, \mathbf{k}) - i\Delta(\mathbf{k}, \mathbf{c})]\}\, d\mathbf{k} d\mathbf{c}. \tag{7}$$

The magnitude of Δ in the Born approximation is not known. However, calculations in the Born-Oppenheimer approximation for incident s-waves[3], and also by Geltman[4], show that near the threshold for ionization the direct and exchange amplitudes do not differ by a rapidly oscillating factor. In the Born approximation this corresponds to the relation $\Delta(\mathbf{k}, \mathbf{c}) = \delta(k)$, and this is the choice which was made in the work being reported upon here. This implies that the factor $\exp\{i\delta(k)\}$ in (4) should be dropped if (5) is used.

The integration over one of the four angles in (7) can be carried out analytically. The remaining integrals were determined with the BÉSM-2 computer. The cross section Q given by formula (1) is then as shown in the figure, with the Born cross section without exchange having been taken from [5].

Since we did not determine Δ rigorously, we also calculated the integral (2) with the amplitudes replaced by moduli, so as to find the maximum possible amount of interference. This corresponds to the choice $\Delta(\mathbf{k}, \mathbf{c}) = \arg f(\mathbf{k}, \mathbf{c})$. The partial cross section for S-wave scattering has also been

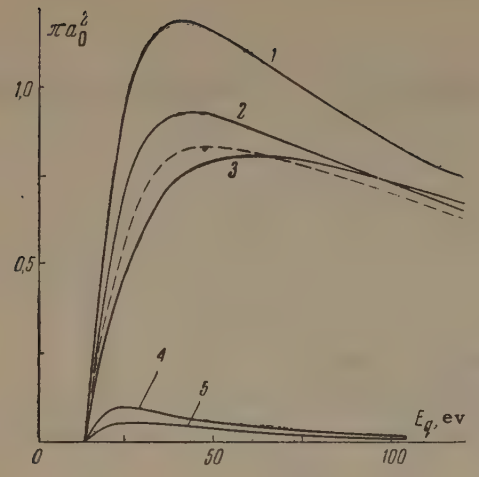

1, 2 – the Born cross section without taking interference into account, and with this effect included; 3 – experimental cross section[6]; dashed line – Born cross section assuming the maximum possible amount of interference; 4, 5 – Born cross sections for S-wave scattering without taking interference into account and with this effect included.

calculated in the Born approximation and the results are shown in the figure. The S-wave partial cross section, which corresponds to both electrons being in s-states after ionization, constitutes only a small part of the total cross section.

The results shown in the figure indicate that by taking interference effects into account the agreement between theory and experiment can be markedly improved.

[1] R. Peterkop, Izv. Akad. Nauk Latv. S.S.R. **12**, 57 (1960); Proc. Phys. Soc. (London) **A77**, 1220 (1961).

[2] N. F. Mott and H. S. W. Massey, Theory of Atomic Collisions, Oxford University Press, London, 1952.

[3] R. Peterkop, Dissertation, Physics Institute, Acad. Sci. Latv. S.S.R., Riga, 1960.

[4] S. Geltman, Phys. Rev. **102**, 171 (1956).

[5] R. McCarroll, Proc. Phys. Soc. (London) **A70**, 460 (1957).

[6] W. Fite and R. Brackman, Phys. Rev. **112**, 1141 (1958).

Translated by R. Krotkov
326

ON THE AMBIGUITY IN THE DEFINITION OF THE INTERPOLATING FIELD

D. A. SLAVNOV and A. D. SUKHANOV

Moscow State University; Mathematical Institute, Academy of Sciences of the U.S.S.R.

Submitted to JETP editor July 14, 1961

J. Exptl. Theoret. Phys. (U.S.S.R.) 41, 1940-1948 (December, 1961)

The question of the ambiguity in the definition of the interpolating field is considered; this ambiguity is shown to be connected with that in the definition of the T-product for a given S matrix, and also with the ambiguity in the determination of the S matrix outside the energy surface. The possibility of going over from one of these interpretations to the other is discussed.

1. INTRODUCTION

ONE type of axiomatic approach to the construction of quantum field theory has been expounded in a series of papers by Lehmann, Symanzik, and Zimmermann.[1] This approach uses as its fundamental quantities two complete sets of field operators* $A_{in}(x)$ and $A_{out}(x)$, which satisfy the conditions

$$(\Box_x - m^2)\, A_{in,\,out}(x) \equiv K_x A_{in,\,out}(x) = 0, \tag{1}$$

$$[A_{in,\,out}(x),\ A_{in,\,out}(y)] = 0 \quad \text{for} \quad x \sim y, \tag{2}$$

$$A_{in,\,out}(x) = A^{+}_{in,\,out}(x). \tag{3}$$

The operators $A_{out}(x)$ and $A_{in}(x)$ are connected with each other by means of a unitary operator S:

$$A_{out}(x) = S^{+} A_{in}(x)\, S, \tag{4}$$

which is identified with the S matrix.[2]

Besides the fields A_{in} and A_{out} one introduces a so-called interpolating field $A(x)$, which is subjected to the following asymptotic condition:

$$\lim_{t \to \pm\infty} (\Phi, A^{f}(t)\, \Psi) = (\Phi, A^{f}_{in,\,out}(t)\, \Psi). \tag{5}$$

Here Ψ and Φ are arbitrary state amplitudes, and

$$A^{f}(t) = i \int\limits_{x^0 = t} dx \left(A(x) \frac{\partial f(x)}{\partial x^0} - f(x) \frac{\partial A(x)}{\partial x^0} \right)$$

$$\equiv i \int\limits_{x^0 = t} \left[A(x) \overset{\leftrightarrow}{\frac{\partial}{\partial x^0}} f(x) \right] dx \tag{6}$$

where $f(x)$ is an arbitrary normalized positive-frequency solution of the Klein-Gordon equation. $A^{f}_{in,\,out}$ is analogously defined and does not depend on t.

It must be noted that an expression very often used as a definition of the interpolating field is

$$A(x) = A_{in,\,out}(x) + \int D^{adv,\,ret}(x - y)\, j(y)\, dy, \tag{7}$$

understood in the sense of weak convergence. It must be emphasized, however, that the field $A(x)$ defined by Eq. (7) satisfies the condition (5) only when definite requirements are imposed on $j(x)$. For example, we can state that a sufficient condition on $j(x)$ is the convergence of an integral of the type

$$\int\limits_{-\infty}^{\infty} dy^0\, (\Phi, \int dy\, f(y)\, j(y)\, \Psi).$$

All treatments ordinarily implicitly make this assumption or an analogous assumption.

Furthermore, it is said that a field $A(x)$ corresponds to a given S matrix if the fields $A_{out}(x)$ and $A_{in}(x)$ which it interpolates are connected by the formula (4).

One of the basic postulates of local field theory is that of microscopic causality. In the approach under consideration[1] this postulate is formulated as follows: an S matrix is called causal if to it there corresponds at least one interpolating field satisfying the locality condition in the form

$$[A(x),\ A(y)] = 0 \qquad \text{for } x \sim y. \tag{8}$$

A paper by Borchers[3] gives proofs of a number of mathematical theorems from which it follows that the local interpolating field is not unambiguously determined by the conditions enumerated above. In particular, if a field $A(x)$ corresponds to a given causal S matrix, then a field of the form

$$B(x) = A(x) + Q(\Box_x)\, j(x), \tag{9}$$

where

$$K\, A(x) = -j(x), \tag{10}$$

and $Q(\Box_x)$ is a polynomial in $\Box_x$ with real con-

*We confine ourselves to the case of a neutral scalar field.

stant coefficients, also corresponds to this S matrix.

The problem of the ambiguity of the various quantities that form the apparatus of present quantum field theory is not encountered here for the first time; in particular, it has been discussed extensively in the book of Bogolyubov and Shirkov.[4] From this mathematical point of view these ambiguities are a result of the fact that in the definitions of the quantities we need we are forced to use expressions containing products of generalized functions, which in the general case are not unambiguously defined. Therefore it is quite clear that the ambiguity that Borchers[3] has pointed out in the determination of the interpolating field must have the same origin.

The purpose of the present paper is to bring out the connections between the arbitrariness in the definition of the interpolating field, on one hand with the ambiguity in the definition of the T-product, and on the other, with the possibilities of different definitions of the S matrix off the energy surface.

2. THE CHRONOLOGICAL PRODUCT

The problem of an arbitrariness in the T-product arises when one constructs the S matrix by going from order to order in perturbation theory, on the basis of a number of general assumptions, as is done in [4]. We are actually concerned there with a T-product of nonlinear operators, of the form $T\ (:\varphi^{k_1}(x_1):\ldots:\varphi^{k_n}(x_n):)$, and there is an arbitrariness in the definition of this quantity when some of its arguments are equal. In order to write out this arbitrariness in explicit form, it is convenient to introduce a T′-product, by which we mean a chronological product which is defined for equal arguments in some arbitary but fixed way, so that the T′-product is an integrable generalized function of all its arguments.

Then the most general form for the T-product is

$$T\ (:\varphi^{k_1}(x_1):\ldots:\varphi^{k_n}(x_n):) = \sum_{m=1}^{n}\frac{1}{m!}P\left((x_1k_1)\ldots(x_{\nu_1}k_{\nu_1})\,|\ldots\ldots(x_nk_n)\right) \times T'\left(\Lambda^{k_1\ldots k_{\nu_1}}(x_1\ldots x_{\nu_1})\ldots\Lambda^{\ldots k_n}(\ldots x_n)\right), \tag{11}$$

where m is the number of factors in the T′-product, and P is the symmetrization operator introduced in [4]. Here

$$\Lambda^{k_1\ldots k_{\nu_1}}(x_1\ldots x_{\nu_1}) = \sum_{l=0}^{k_1+\ldots+k_{\nu_1}} M_l^{k_1\ldots k_{\nu_1}}(x_1,\ldots x_{\nu_1}) :\varphi^l(x_1):,$$
$$\Lambda^{k_l}(x_l) =: \varphi^{k_l}(x_l):, \tag{12}$$

$M_l^{k_1\ldots k_{\nu_1}}$ is a c-number function which differs from zero only for $x_1 = \ldots = x_{\nu_1}$.

It may seem that if the S matrix is prescribed in the entire momentum space, and not merely on the energy surface, then the arbitrariness in the definition of the T product is entirely eliminated. Actually, however, this is not true. All that follows from the general arguments[4] is the formula

$$S = T'\exp\left\{ig\int L^0(x)\,dx\right\}, \tag{13}$$

where

$$L^0(x) = \mathcal{L}(x) + \sum_{n=2}\frac{1}{n!}g^{n-1}\int L_n^0(x, x_1\ldots x_{n-1})\,dx_1\ldots dx_{n-1} \tag{14}$$

Here $\mathcal{L}(x)$ is the bare Lagrangian, and L_n^0 are the quasi-local operators introduced in [4].

It is not hard to verify that without changing the value of the S matrix one can go over in Eq. (13) from the T′-product to the T-product defined by Eq. (11), by changing the effective Lagrangian in a suitable way. In fact, let

$$S = T\exp\left\{ig\int L(x)\,dx\right\}, \tag{15}$$

where L(x) is given by a formula analogous to Eq. (14). To establish the connection between L(x) and $L^0(x)$, let us first consider a T-product of quasi-local operators L_n. Then using Eq. (11) we have

$$T\left(L_{\mu_1}(x_1^1\ldots x_{\mu_1}^1)\ldots L_{\mu_k}\ (\ldots x_n^k)\right) = T'\left(L_{\mu_1}(x_1^1\ldots x_{\mu_1}^1)\ldots L_{\mu_k}(\ldots x_n^k)\right) + \sum_{m=2}^{k-1}\frac{1}{m!}P\left((x^1\mu_1)\ldots(x^{\nu_1}\mu_{\nu_1})\,|\ldots|\ldots(x^k\mu_k)\right)T'\left(R^{\mu_1\ldots\mu_{\nu_1}} \times (x^1\ldots x^{\nu_1})\ldots R^{\ldots\mu_k}(\ldots x^k)\right) + R^{\mu_1\ldots\mu_k}(x^1\ldots x^k), \tag{16}$$

where, for example, x^1 denotes the set $(x_1^1,\ldots,x_{\mu_1}^1)$. In Eq. (16) we have introduced instead of the quasi-local operators $\Lambda(x_1\ldots x_i)$ quasi-local operators $R(x_1\ldots x_i)$ which are more convenient in the present case and which are certain combinations of the $\Lambda(x_1\ldots x_i)$, since in general the operators $L_n(x_1\ldots x_n)$ are sums of expressions of the form $:\varphi^{k_i}(x_i):$ with different values of k_i. The formula (16) can be regarded as a definition of $R(x_1\ldots x_i)$. Expanding Eqs. (13) and (15) in power series in g, equating terms with equal powers of g, and using Eq. (16), we get

$$iL_n(x_1\ldots x_n) = iL_n^0(x_1\ldots x_n) - \sum_{k=2}^{n}\frac{i^k}{k!}P\left(x^1\ldots x^k\right) \times \sum_{u_l}R^{\mu_1\ldots\mu_k}(x^1\ldots x^k), \tag{17}$$

where $P(x^1 \ldots x^k)$ is the operator of complete symmetrization, and the summation goes over values of $\mu_1, \ldots, \mu_k$ that obey the condition $\Sigma \mu_i = n$.

Equation (17) is a recurrence formula which enables us to express the operators L_n in terms of the operators L_k^0 and Λ. If, on the other hand, we use instead of Eq. (16) the transformation from the T′-product to the T-product, we can also get a formula which directly expresses the operators L_n in terms of L_k^0 and Λ.

Thus starting from a number of general propositions we can conclude that there are two possible interpretations of the arbitrariness that arises in the construction of the S matrix by perturbation theory. Namely, this arbitrariness can be regarded as caused either by the ambiguity in the Lagrangian for a fixed definition of the T-product, or by the ambiguity of the T-product itself for a given Lagrangian. Both of these possibilities have been noted already by Bogolyubov and Shirkov.[4] In practice, however, they have used only the first possibility, although the second appears preferable. An example of the use of the second possibility in the construction of the S matrix can be found in the situation[5] that occurs in theories with derivative couplings (or with vector fields), in which the S matrix can be expressed in terms of either the Lagrangian or the Hamiltonian, depending on the use of one or another definition of the T-product. We shall also use this same possibility here to express the indefiniteness in the interpolating field in terms of the ambiguity in the definition of the T-product.

It must only be pointed out that actually one can use for the derivation of a finite S matrix a much narrower definition of the T-product than that of Eq. (11). Namely, since the problem of deriving a finite S matrix reduces essentially to the problem of defining chronological contractions and their products for coinciding arguments, we can simplify the formula (12) by introducing different $M^{\cdots k_i \cdots}$ only for different types of products of chronological contractions in the T′-product. We shall not carry out this simplification for the general case, but shall do so in the next section for the special case we need here.

3. THE INTERPOLATING FIELD AND THE AMBIGUITY IN THE DEFINITION OF THE T-PRODUCT

In order to establish the connection between the arbitrariness in the definition of the interpolating field noted by Borchers[3] and the ambiguity in the definition of the T-product for a given S matrix, we shall use the following expression for the interpolating field:

$$A(x) = S^+ T(A_{in}(x)\, S). \tag{18}$$

Here we can understand the expression $T(A_{in}(x)S)$ if we represent the S matrix in the form

$$S = \sum_{i=0} \int \varphi_i(y_1 \ldots y_i) : A_{in}(y_1) \ldots A_{in}(y_i) : dy_1 \ldots dy_i. \tag{19}$$

Then

$$T(A_{in}(x)\ S) = \sum_{i=0} \int \varphi_i(y_1 \ldots y_i)\, T \times (A_{in}(x) : A_{in}(y_1) \ldots A_{in}(y_i) :)\, dy_1 \ldots dy_i.$$

In order to convince ourselves that the field defined by Eq. (18) satisfies the asymptotic condition (5), let us substitute Eq. (18) in Eq. (5), for example for $t \to -\infty$:

$$\begin{aligned}
&\lim_{t\to-\infty} (\Phi, A^f(t)\Psi) \\
&= \lim_{t\to-\infty} i \int_{x^0=t} dx\, (\Phi, [S^+ T(A_{in}(x)\, S)] \overleftrightarrow{\frac{\partial}{\partial x^0}} f(x)\, \Psi) \\
&= i \lim_{t\to-\infty} \sum_{i=0} \int dy_1 \ldots dy_i \varphi_i(y_1 \ldots y_i) \\
&\times \int_{x^0=t} dx\, (\Phi, [S^+ T(A_{in}(x) : A_{in}(y_1) \ldots A_{in}(y_i):)] \\
&\times \overleftrightarrow{\frac{\partial}{\partial x^0}} f(x)\, \Psi).
\end{aligned} \tag{20}$$

In accordance with the comment made in Sec. 1 we shall assume that the coefficient functions of the S matrix are such that in the right member of Eq. (20) we can take the process $\lim_{t\to-\infty}$ inside the sign of integration over y_k. Then

$$\begin{aligned}
&\lim_{t\to-\infty} (\Phi, A^f(t)\ \Psi) = i \sum_{i=0} \int dy_1 \ldots dy_i \varphi_i(y_1 \ldots y_i) \lim_{t\to-\infty} \\
&\times \int_{x^0=t} dx\, (\Phi, [S^+ : A_{in}(y_1) \ldots A_{in}(y_i) : A_{in}(x)] \\
&\times \overleftrightarrow{\frac{\partial}{\partial x^0}} f(x)\, \Psi) = \lim_{t\to-\infty} i \left(\Phi, S^+ S \int_{x^0=t} dx A_{in}(x) \overleftrightarrow{\frac{\partial}{\partial x^0}} f(x)\, \Psi\right) \\
&= (\Phi, A_{in}^f(t)\Psi).
\end{aligned} \tag{21}$$

We emphasize that these arguments do not make use of the specific properties of the T-product, which in principle can be just as general as in the definition (11). Of course, we have here a special case, with all the k_i equal to 1. Besides this, we are here using the previously indicated possibility of simplifying the T-product defined in Eq. (11), and shall introduce $M^{\cdots k_i \cdots}$ only for different types of products of chronological contractions in

the T′-product. Since in the given case we encounter only one contraction, we have

$$T(\varphi(x):\varphi(y_1)\ldots\varphi(y_n):) = T'(\varphi(x):\varphi(y_1)\ldots\varphi(y_n):) + P(y_1 \mid y_2\ldots y_n)\, M_2(x, y_1):\varphi(y_2)\ldots\varphi(y_n):, \quad (22)$$

where we have introduced a new notation $M_2(x,y) = M^{11}(x,y)$.

Substituting Eq. (22) in Eq. (18) we get the following expression for the interpolating field:

$$A(x) = A_{in}(x) + \frac{1}{i}\int D^{ret}(x-y)\, S^{(1)}(y) + \int M_2(x,y)\, S^{(1)}(y). \quad (23)$$

Here and in what follows we use the abbreviated notation

$$S^{+}\delta S/\delta A_{in}(x) = S^{+}\delta_x S = S^{(1)}(x).$$

Obviously the field $A(x)$ is Hermitian if $M_2(x,y)$ is pure imaginary. The following assertion can be made about the field defined by the formula (23).

If the S matrix satisfies the causality condition[6]

$$\delta_y S^{(1)}(x) = 0 \text{ for } x \lesssim y, \quad (24)$$

then a field $A(x)$ of the form (23) satisfies the locality condition (8).

In fact,

$$[A(x), A(y)] = [A_{in}(x), A_{in}(y)] + \frac{1}{i}\int [D^{ret}(y-z) + iM_2(y,z)]\,[A_{in}(x), S^{(1)}(z)]\,dz + \frac{1}{i}\int [D^{ret}(x-u) + iM_2(x,u)]\,[S^{(1)}(u), A_{in}(y)]\,du - \int [D^{ret}(x-u) + iM_2(x,u)]\,[D^{ret}(y-z) + iM_2(y,z)]\,[S^{(1)}(u), S^{(1)}(z)]\,du\,dz. \quad (25)$$

Let us use the obvious formulas

$$[S^{(1)}(u), S^{(1)}(z)] = \delta_z S^{(1)}(u) - \delta_u S^{(1)}(z), \quad (26)$$

$$[A_{in}(x), S^{(1)}(z)] = \frac{1}{i}\int D(x-u)\,\delta_u S^{(1)}(z)\,du. \quad (27)$$

Then we get

$$[A(x), A(y)] = [A_{in}(x), A_{in}(y)] + \int [D^{ret}(y-z) + iM_2(y,z)]\,[D^{adv}(x-u) + iM_2(x,u)]\,\delta_u S^{(1)}(z)\,du\,dz - \int [D^{ret}(x-u) + iM_2(x,u)]\,[D^{adv}(y-z) + iM_2(y,z)]\,\delta_z S^{(1)}(u)\,du\,dz. \quad (28)$$

It is clear that in virtue of the locality of $A_{in}(x)$, the causality condition (24), and the properties of the functions $D^{ret}(x-y)$, $D^{adv}(x-y)$, and $M_2(x,y)$ each term in Eq. (28) vanishes for $x \sim y$.

We note that, starting from Eqs. (18) and (11), we can also get for the local interpolating field the more general expression

$$A(x) = A_{in}(x) + \frac{1}{i}\int D^{ret}(x-y)\, S^{(1)}(y)\,dy + \sum_{k=1}\frac{1}{k!}\int M_{k+1}(x, y_1, \ldots y_k)\, S^{(k)}(y_1\ldots y_k)\,dy_1\ldots dy_k \quad (29)$$

if we assume that in Eq. (12)

$$\Lambda^{1\ldots 1}(x_1, \ldots x_{\nu_1}) = M_{\nu_1}(x_1\ldots x_{\nu_1}).$$

The local character of this field is proved in an analogous way, but more cumbersome calculations are required.

Let us consider as an example the case in which $M_2(x,y)$ is a polynomial of finite degree in $\partial/\partial x$ applied to δ functions, with constant pure imaginary coefficients. Then when the requirements of relativistic invariance are taken into account $A(x)$ takes the form

$$A(x) = A_{in}(x) + \int D^{ret}(x-y)\, j(y)\,dy + \int Q(\Box_x)\,\delta(x-y)\, j(y)\,dy, \quad (30)$$

or

$$A(x) = \tilde{A}(x) + Q(\Box_x)\, j(x), \quad (31)$$

where

$$\tilde{A}(x) = A_{in}(x) + \int D^{ret}(x-y)\, j(y)\,dy, \quad (32)$$

and[6]

$$j(x) = -iS^{(1)}(x). \quad (33)$$

Equation (31) is identical with Eq. (9). Thus the ambiguity in the definition of the interpolating field pointed out in Borchers' paper[3] has been shown to be capable of being expressed in terms of the ambiguity in the definition of the T-product with a given S matrix.

4. THE INTERPOLATING FIELD AND THE AMBIGUITY IN THE DEFINITION OF THE S MATRIX

In this section we approach our problem from a somewhat more general standpoint and show that any ambiguity in the definition of the interpolating field can be interpreted as an ambiguity in the definition of the S matrix off the energy surface.

First let us give some attention to the problem of the definition of the S matrix off the energy surface. As is well known, the S matrix can be

represented [1] in the form

$$S = \sum_{n=0} \frac{1}{n!} \int dk_1 \ldots dk_n \delta(k_1 + \ldots + k_n) \times h_n(k_1 \ldots k_n)\, \delta(k_1^2 - m^2) \ldots \delta(k_n^2 - m^2) : A_{in}(k_1) \ldots A_{in}(k_n) : . \quad (34)$$

It can be seen from the expression (34) that the S matrix depends only on the values of $h_n(k_1 \ldots k_n)$ on the energy surface, i.e., for $k_1^2 = \ldots = k_n^2 = m^2$.

This, however, is not sufficient for a complete formulation of the theory, and in particular for the formulation of the causality condition. We also need to know the Fourier transforms $h_n(x_1 \ldots x_n)$, and consequently it is necessary to define in some way $h_n(k_1 \ldots k_n)$ off the energy surface. We shall suppose that the S matrix is defined off the energy surface if the $h_n(k_1 \ldots k_n)$ are prescribed in the entire momentum space. In this case we can define the variational derivative of the S matrix in the form

$$\delta_x S = \sum_{n=1} \frac{1}{(n-1)!} \frac{1}{(2\pi)^{n/2}} \times \int e^{ik_1 x} \delta(k_1 + \ldots + k_n)\, \delta(k_2^2 - m^2) \ldots \delta(k_n^2 - m^2) \times h_n(k_1 \ldots k_n) : A_{in}(k_2) \ldots A_{in}(k_n) : dk_1 \ldots dk_n. \quad (35)$$

It can be seen from Eq. (35) that the value of $\delta_x S$ depends in an essential way on the definition of $h_n(k_1 \ldots k_n)$ off the energy surface. It is clear, however, that an expression of the form $\int f(x) \delta_x S\, dx$, where $f(x)$ is an arbitrary solution of the Klein-Gordon equation, depends only on the values of $h_n(k_1 \ldots k_n)$ on the energy surface. It follows from this that the values $(\delta_x S)_1$ and $(\delta_x S)_2$ which correspond to two different definitions of $h_n(k_1 \ldots k_n)$ off the energy surface can differ only by a function $Q(x)$ which satisfies the condition

$$\int f(x)\, Q(x)\, dx = 0. \quad (36)$$

It is also not hard to verify the converse, namely: if $(\delta_x S)_1$ is defined by Eq. (35) with certain fixed functions $h_n^{(1)}(k_1 \ldots k_n)$, and

$$(\delta_x S)_2 = (\delta_x S)_1 + Q(x), \quad (37)$$

where $Q(x)$ satisfies Eq. (36), then $(\delta_x S)_2$ can be represented in the form (35) with certain other functions $h_n^{(2)}(k_1 \ldots k_n)$ which differ from $h_n^{(1)}(k_1 \ldots k_n)$ only off the energy surface.

From these arguments we can conclude that the possibility of different definitions of $h_n(k_1 \ldots k_n)$ off the energy surface reduces to the possibility of an arbitrariness in the current defined by Eq. (33), of the form

$$j(x) = j_0(x) + J(x), \quad (38)$$

where $j(x)$ corresponds to some definite choice of $h_n(k_1 \ldots k_n)$ off the energy surface and $J(x)$ is some operator satisfying the equation

$$\int f(x)\, J(x)\, dx = 0. \quad (39)$$

In order not to make additional complications we shall assume that $J(x)$ satisfies the requirements of Hermiticity and of translational and relativistic invariance, and also, if the theory is causal, the causality condition.

Let us now consider the question to what extent the asymptotic condition (5) fixes the definition of the interpolating field. For this purpose let us write down the difference between the expressions for the asymptotic condition for $t \to +\infty$ and $t \to -\infty$. We have

$$\left(\Phi, \int \frac{\partial}{\partial x^0} \left[A(x) \overleftrightarrow{\frac{\partial}{\partial x^0}} f(x)\right] dx\, \Psi\right) = \left(\Phi, \int [A_{out}(x) - A_{in}(x)] \overleftrightarrow{\frac{\partial}{\partial x^0}} f(x)\, dx\, \Psi\right), \quad (40)$$

It follows from Eq. (4) that

$$A_{out}(x) - A_{in}(x) = \int D(x - y)\, j(y)\, dy. \quad (41)$$

Substituting Eq. (41) in Eq. (40) and making some transformations, we get

$$\int f(x)\, K_x A(x)\, dx = -\int f(x)\, j(x)\, dx. \quad (42)$$

It follows from this that

$$K_x A(x) = -j(x) - J_1(x), \quad (43)$$

where

$$\int f(x)\, J_1(x)\, dx = 0.$$

Using the fact that the definition of $j(x)$ itself contains an arbitrariness [cf. Eq. (38)], we can put Eq. (43) in the form

$$K_x A(x) = -j(x). \quad (44)$$

Thus the asymptotic condition (5), which is fundamental in this approach, [1] leads to a formula (44) for the determination of the interpolating field which shows that all of the ambiguity in the definition of this field is due to the ambiguity in $j(x)$, i.e., to the ambiguity in the definition of the S matrix off the energy surface.

5. DISCUSSION

We now draw some conclusions. It was shown in Sec. 4 that all of the ambiguity in the interpolating field can be regarded as an ambiguity in the definition of the S matrix off the energy surface. On the other hand, in Sec. 3 it was indicated that there is a possible ambiguity in the definition of the interpolating field associated with the ambiguity in the definition of the T-product with a prescribed S matrix. Therefore it is interesting to see whether we can establish a connection between these two approaches to the problem.

In Sec. 3 the ambiguity in the interpolating field was actually determined in terms of the ambiguity of the expression $T(A_{in}(x)S)$, which can be written out explicitly as follows:

$$T(A_{in}(x)S) = \sum_{i=0} \int dy_1 \ldots dy_i P(y_1 | y_2 \ldots y_i) \varphi_i(y_1 \ldots y_i) \times \left(\frac{1}{i} D^c(x - y_1) + M_2(x, y_1)\right) : A_{in}(y_2) \ldots A_{in}(y_i) : . \quad (45)$$

Since $M_2(x, y)$ can be represented in the form $i^{-1}Q(\Box_y)\delta(x-y)$, Eq. (45) can be written in the form

$$T(A_{in}(x)S) = \sum_{i=0} \int dy_1 \ldots dy_i P(y_1 | y_2 \ldots y_i) \varphi_i(y_1 \ldots y_i) \times \frac{1}{i}\left(D^c(x - y_1) - Q(\Box_{y_1}) \times K_{y_1} D^c(x - y_1)\right) : A_{in}(y_2) \ldots A_{in}(y_i) : . \quad (46)$$

Let us integrate Eq. (46) by parts, assuming that when the limits are substituted the expression in question vanishes, in accordance with the remark made in Sec. 1. Then we get

$$T(A_{in}(x)S) = \sum_{i=0} \int dy_1 \ldots dy_i P(y_1 | y_2 \ldots y_i) \frac{1}{i} D^c(x - y_1) \times [\varphi_i(y_1 \ldots y_i) - Q(\Box_{y_1}) K_{y_1} \varphi_i(y_1 \ldots y_i)] : \times A_{in}(y_2) \ldots A_{in}(y_i) : = T'(A_{in}(x)\tilde{S}), \quad (47)$$

where

$$\tilde{S} = \sum_{i=0} \int dy_1 \ldots dy_i [\varphi_i(y_1 \ldots y_i) - Q(\Box_{y_1}) K_{y_1} \varphi_i(y_1 \ldots y_i)] : A_{in}(y_1) \ldots A_{in}(y_i) : . \quad (48)$$

It is clear from the structure of the expression (48) that the matrix $\tilde{S}$ differs from the S matrix only off the energy surface.

Thus we see that the ambiguity in the definition of the interpolating field associated with the ambiguity in the definition of the T-product with a given S matrix can be reformulated in such a way that it turns out to be connected with the ambiguity in the definition of the S matrix off the energy surface with a fixed definition of the T-product.

A very curious situation arises. It turns out that not only is there quite a variety of interpolating fields corresponding to an S matrix defined off the energy surface in a prescribed way, but also conversely there are several expressions for the S matrix off the energy surface corresponding to a single interpolating field. We now recall that the definition of the S matrix off the energy surface is closely connected with the definition of the Dyson matrix $S(\sigma_1, \sigma_2)$ which connects state vectors prescribed on two arbitrary spacelike surfaces. In this connection it becomes very interesting to find out how the ambiguity noted here affects the definition of the Dyson matrix, and we intend to continue with the study of this question.

In conclusion we express our deep gratitude to B. V. Medvedev for suggesting the topic and for his constant interest in the work. We also express our gratitude to M. K. Polivanov for a discussion.

[1] Lehmann, Symanzik, and Zimmermann, Nuovo cimento **1**, 205 (1955), **6**, 319 (1957). Glaser, Lehmann, and Zimmermann, Nuovo cimento **6**, 1122 (1957).

[2] C. N. Yang and D. Feldman, Phys. Rev. **79**, 972 (1950).

[3] H.-J. Borchers, Nuovo cimento **15**, 784 (1960).

[4] N. N. Bogolyubov and D. V. Shirkov, Vvedenie v teoriyu kvantovannykh polei (Introduction to the Theory of Quantized Fields), Gostekhizdat, 1957.

[5] A. D. Sukhanov, JETP **41**, 1915 (1961), this issue, p. 1361.

[6] Bogolyubov, Medvedev, and Polivanov, Voprosy teorii dispersionnykh sootnoshenii (Problems of the Theory of Dispersion Relations) Fizmatgiz, Moscow, 1958.

Translated by W. H. Furry
327

ON THE QUESTION OF THE EXISTENCE OF HEAVY NEUTRAL PSEUDOSCALAR MESONS

I. Yu. KOBZAREV and L. B. OKUN'

Submitted to JETP editor July 17, 1961

J. Exptl. Theoret. Phys. (U.S.S.R.) 41, 1949-1952 (December, 1961)

The arguments in favor of the existence of heavy neutral pseudoscalar mesons with isotopic spin zero are discussed. A number of experiments are proposed by means of which it might be possible to settle the question of the existence of such mesons.

1. As has previously been pointed out,[1,2] in the framework of the Sakata model there can exist besides the known pseudoscalar mesons π and K two further pseudoscalar mesons* σ_1 and σ_2. Out of the nine different charge states of the system baryon + antibaryon three states ($\bar{p}p$, $\bar{n}n$, $\bar{\Lambda}\Lambda$) have identical quantum numbers and can make transitions to each other. From the diagonalization of these states there arise three other states, one with unit isotopic spin,

$$\pi^0 = (p\bar{p} - n\bar{n})/\sqrt{2},$$

and two others with zero isotopic spin,

$$\sigma_1 = \{\alpha(p\bar{p} + n\bar{n})/\sqrt{2} + \beta\Lambda\bar{\Lambda}\},$$
$$\sigma_2 = \{\beta(p\bar{p} + n\bar{n})/\sqrt{2} - \alpha\Lambda\bar{\Lambda}\}.$$

Because of the orthonormality of the states σ_1 and σ_2 the constants α and β satisfy the relation $\alpha^2 + \beta^2 = 1$. These coefficients are determined by the properties of the strong interaction between the three baryons p, n, Λ. As has been shown in a number of papers,[4-8] if the strong interactions of these baryons were identical (as they are, for example, in the model of universal vector interactions[9-11]), the Sakata model would possess an additional symmetry, which bears the name of unitary symmetry. In the framework of unitary symmetry the nine mesons break up into an octet and a singlet, and the mesons occurring in the octet (π, K, σ_1) must have equal masses; the mass of the ninth meson (σ_2) must in general be different, and may be much larger. The values of the coefficients that correspond to unitary symmetry are $\beta = (2/3)^{1/2}$, $\alpha = -(1/3)^{1/2}$. The amount of deviation from unitary symmetry in nature can be characterized by the mass difference of the K and π mesons (~ 350 Mev). This gives us reason to suppose that the mass of the σ_1^0 meson can scarcely exceed 1 Bev. At present we have no definite arguments about the mass of the σ_2^0 meson.

Considerations connected with unitary symmetry make the problem of looking for and discovering the σ meson a matter of great present interest.* In this connection we shall make a number of remarks about the possible properties of this particle.

2. The possible decays of the σ meson have been considered in the greatest detail by Zel'dovich[14] (cf. also [2]). The rapid decay $\sigma \to 2\pi$ is forbidden by parity conservation; the rapid decay $\sigma \to 3\pi$ is forbidden by the conservation of G-parity (the G-parity of σ is positive, and that of π is negative); and the decay $\sigma \to 4\pi$ must be improbable, since the π mesons are produced in states with high orbital angular momenta.

The decays into five and seven π mesons must be forbidden on account of the G-parity. Just like the decay $\sigma \to 4\pi$, the decays into six and eight π mesons will involve high orbital angular momenta, and owing to the smallness of the phase volume these decays cannot compete with $\sigma \to 4\pi$. The high orbital angular momenta in the decay $\sigma \to 4\pi$ are due to the fact that a pseudoscalar configuration of the four π mesons arises. The following 4π decays are possible:

$$\sigma \to 2\pi^+ + 2\pi^-, \qquad \sigma \to 2\pi^0 + \pi^+ + \pi^-, \qquad \sigma \to 4\pi^0.$$

The matrix element for the decay into $2\pi^+ + 2\pi^-$ is of the form

$$M = (L/\mu)^7 \varepsilon_{\alpha\beta\gamma\delta} p_{1\alpha} p_{2\beta} p_{3\gamma} p_{4\delta} (p_1 - p_2)_\mu (p_3 - p_4)_\mu \varphi_1\varphi_2\varphi_3\varphi_4\varphi_\sigma,$$

where μ is the mass of the π meson, L is a dimensionless quantity, p_1 and p_2 are the four-

*In[1,2] these mesons were denoted by ρ_1^0 and ρ_2^0. Recently, however, the letter ρ is used in the literature to denote vector mesons. We do not use the notation π^{00}, since it refers to a hypothetical σ_1^0 meson with a mass equal to that of the π meson.[3]

*Recently, on the basis of ideas about an eightfold symmetry, Gell-Mann[12] has concluded that the σ_1^0 meson may exist; he calls this particle χ^0. The conclusion that such a meson may exist has also been reached by V. M. Shekhter[13] on the basis of an analysis of the symmetries of the strong interactions.

momenta of the π^+ mesons, p_3 and p_4 those of the π^- mesons, and the φ's are wave functions. The expression for M is symmetrical under the interchanges $1 \leftrightarrow 2$ and $3 \leftrightarrow 4$.

In the language of orbital angular momenta the expression for M corresponds to $l' = l'' = 2$, $l = 1$, where l' and l'' are the orbital angular momenta of the π^+ and π^- pairs, and l is the orbital angular momentum of the relative motion of these pairs. For $l = l' = l'' = 0$ the quantity L/μ would be of the order of the effective dimensions of the region of strong interaction, i.e., $L \sim 1$. For $l' = l'' = 2$, $l = 1$, this quantity will be much smaller because of the centrifugal barrier [$L^7 \sim (5!!)^{-2}(3!!)^{-1} \sim 10^{-2}$–$10^{-3}$]. The decay into $2\pi^0 + \pi^+ + \pi^-$ is described by an analogous matrix element. Because of the complete symmetry of the system $4\pi^0$, the decay $\sigma \to 4\pi^0$ contains still higher orbital angular momenta. As V. I. Ogievetskii has shown (private communication), the matrix element for this decay is proportional to

$$\mu^{-11}\varepsilon_{\alpha\beta\gamma\delta}p_{1\alpha}p_{2\beta}p_{3\gamma}p_{4\delta}\,(p_1-p_2)_\mu\,(p_3-p_4)_\mu \times (p_1-p_3)_\nu\,(p_2-p_4)_\nu\,(p_1-p_4)_\rho\,(p_2-p_3)_\rho\,\varphi_1\varphi_2\varphi_3\varphi_4\varphi_\sigma.$$

Therefore the decay to $4\pi^0$ can be neglected in comparison with the other 4π decays. Calculating from M the probability of the decay $\sigma \to 2\pi^+ + 2\pi^-$, one easily gets

$$w \sim 10^{-7}\cdot L^{14}\,(\Delta/\mu)^{17/2}\mu,$$

where $\Delta = m_\sigma - 4\mu$ and the formula holds for values $\Delta \lesssim \mu$. In spite of the rapid rise of the probability with increase of m_σ (for $m_\sigma \gg 4\mu$ we have $w \sim m_\sigma^{15}$), one could think from the smallness of the coefficient in the 4π decay and from the formula for the probability of the decay $\sigma \to 2\pi + \gamma$ (see below) that the decay into 4π could be important only for $m_\sigma \gtrsim 1$ Bev. Beginning at $m_\sigma = 2m_K + \mu$, however, the following fast decays are allowed:

$$\sigma \to K^+ + K^- + \pi^0, \qquad \sigma \to K^0 + \bar{K}^0 + \pi^0,$$
$$\sigma \to K^+ + \bar{K}^0 + \pi^-, \qquad \sigma \to K^- + K^0 + \pi^+.$$

The decay $\sigma \to K^0 + \bar{K}^0 + \pi^0$ is particularly interesting. Because of the conservation of charge parity this decay must go either by the channel $2K_1^0 + \pi^0$ or by the channel $2K_2^0 + \pi^0$, and the channel $K_1^0 + K_2^0 + \pi^0$ must be forbidden. Thus pair production of K_1^0 mesons must occur in the experiment. For small Δ ($\Delta = m_\sigma - 2m_K - \mu$) the probability of this decay is given by

$$w \sim 10^{-3}L^2\Delta^2/m_\sigma \qquad (L \sim 1).$$

3. Let us now turn to decays that involve the electromagnetic interaction. Conservation of charge parity forbids the decay $\sigma \to \pi^0 + \gamma$ (this decay is also forbidden as a 0—0 transition, cf. [14]), and the decays

$$\sigma \to \pi^0 + e^+ + e^-, \qquad \sigma \to \pi^0 + \mu^+ + \mu^-, \qquad \sigma \to 2\pi^0 +$$

are forbidden in second order in the electromagnetic interaction. The decays

$$\sigma \to \pi^+ + \pi^- + \gamma, \qquad \sigma \to 2\gamma$$

are allowed. Because of gauge invariance the probability of the second of these decays must increase as m_σ^3 with increase of the mass of the σ meson. We can take as an approximate formula

$$w_{2\gamma}^{\sigma} = w_{2\gamma}^{\pi^0}(m_\sigma/\mu)^3.$$

Assuming $\tau_{\pi^0} = 10^{-16}$ sec, we see that $w_{2\gamma}^{\sigma} \sim 100$ e for $m_\sigma = 2\mu$. In spite of its small width, however, as Ohnuki has remarked, [4] this decay would be the main one for $m_\sigma \lesssim 2\mu$. For larger values of the mass m_σ, as Zel'dovich has emphasized, [14] the predominant decay is

$$\sigma \to \pi^+ + \pi^- + \gamma.$$

The matrix element of this decay is of the form

$$eL^3\mu^{-3}A_i k_k p_{1l}p_{2m}\varepsilon_{iklm}\varphi_1\varphi_2\varphi_\sigma,$$

where e is the electric charge ($e^2 = \alpha = 1/137$); L is a dimensionless quantity ~ 1; and k, p_1, p_2 are the respective four-momenta of the photon, the π^+ meson, and the π^- meson.

The decay probability calculated with this matrix element is

$$w \sim 10^{-7}\alpha L^6\,(m_\sigma/\mu)^7\,\mu$$

for $m_\sigma \gg 2\mu$. The spectrum of the photons is of the form

$$n(\omega)\,d\omega \sim \omega^3\,(m_\sigma^2 - 2m_\sigma\omega - 4\mu^2)^{3/2}\,(m_\sigma^2 - 2m_\sigma\omega)^{-1/2}\,d\omega.$$

The heavier of the σ mesons (σ_2) can have in addition to these decays the decay $\sigma_2^0 \to \sigma_1^0 + 2\pi$, provided that $m_{\sigma_2^0} > m_{\sigma_1^0} + 2\mu$.

4. Let us now consider possible ways of detecting σ mesons, in the light of the existing experimental data. In the range $0 < m_\sigma < 1.8\,\mu$ a search for σ^0 in the reaction $d + d \to He^4 + \sigma^0$, which was made in Berkeley, [15] gave for the cross section for production of σ_1^0 the value $\sigma < 7 \times 10^{-32}$ cm^2 for $m_\sigma = \mu$, and $\sigma < 0.2 \times 10^{-32}$ cm^2 for $m_\sigma = 1.8\,\mu$. An experiment made with the accelerator in Frascati [16] gave $d\sigma/d\Omega < 6 \times 10^{-32}$ cm^2/sr for the cross section of the reaction $\gamma + p \to \sigma + p$ for a range of σ-meson masses at about $3.5\,\mu$. Experi-

ments in Dubna [17] have not revealed any features associated with the production of σ mesons in the range of masses 270 Mev $\leq m_\sigma \leq$ 400 Mev.

Moreover, there are the following arguments against the existence of a σ meson with a mass much less than that of the K meson. Such a meson would occur in decays $K^+ \to \sigma + \pi^+$ if $m_\sigma < 350$ Mev. The production of σ mesons which decay through the channel $\sigma \to 2\gamma$ would increase the fraction of the energy carried away by neutral particles in the annihilation of antiprotons (in comparison with the experimentally measured value of $\frac{1}{3}$). [18] There are some possible indications against the existence of a σ meson with the decay $\sigma \to 2\gamma$ in the data from the analysis of annihilation stars for "lost mass." [19]

At present there are no experimental data contradicting the existence of a σ meson with mass larger than that of the K meson and with the decay $\sigma^0 \to \pi^+ + \pi^- + \gamma$. A search for this meson can be made either by trying to observe the hard photons arising in its decay or by analyzing reactions for its production (experiments of the types of [16,17,19]). A reaction convenient for kinematical analysis is

$$\begin{array}{ccccc} K^- + p \to \Lambda^0 & + & \sigma^0. \\ \downarrow & & \downarrow \\ p + \pi^- & & \pi^+ + \pi^- + \gamma \end{array}$$

Because of the uncertainty of the theoretical estimates, for a σ-meson mass near 1 Bev we cannot regard the decay $\sigma \to 4\pi$ as excluded. The existence of this decay is, however, improbable. The existence of a σ meson with such a decay could be detected if one were to measure the quantity $M^2 = (E_1 + E_2 + E_3 + E_4)^2 - (p_1 + p_2 + p_3 + p_4)^2$ in reactions in which $2\pi^+ + 2\pi^-$ are produced (the E's and p's are the energies and momenta of these mesons).

For a sufficiently large mass of the σ meson one could look for it in the decay $\sigma \to 2K + \pi$, by studying the kinematical distribution of K mesons (in particular pairs of K_1^0 mesons) in reactions at high energies. For a pair of K mesons produced in the decay of a σ meson the energy of the pair in its center-of-mass system must lie in the range $2m_K < E_{2K} < m_\sigma - \mu$.

In conclusion it must be emphasized that if it should be shown experimentally that σ mesons do not exist, this would mean that in nature unitary symmetry is catastrophically violated.

The authors are grateful to S. M. Bilen'kii, V. N. Gribov, V. I. Ogievetskii, M. I. Podgoretskii, I. Ya. Pomeranchuk, B. M. Pontecorvo, R. M. Ryndin, and K. A. Ter-Martirosyan for interesting discussions.

[1] L. B. Okun', JETP **34**, 469 (1958), Soviet Phys. JETP **7**, 322 (1958).

[2] L. B. Okun', Proc. Ann. Int. Conf. on High Energy Physics at CERN, 1958, p. 223.

[3] A. Baldin, Nuovo cimento **8**, 569 (1958).

[4] S. Ohnuki, Proc. 1960 Ann. Int. Conf. on High Energy Physics at Rochester, Univ. of Rochester, 1960, p. 843.

[5] S. Ogawa, Progr. Theoret. Phys. **21**, 209 (1959).

[6] Ikeda, Ogawa, and Ohnuki, Progr. Theoret. Phys. **22**, 715 (1959).

[7] Y. Yamaguchi, Progr. Theoret. Phys. Suppl. **11**, 1, 37 (1959).

[8] J. E. Wess, Nuovo cimento **15**, 52 (1960).

[9] I. Yu. Kobzarev and L. B. Okun', JETP **41**, 499 (1961), Soviet Phys. JETP **14**, 358 (1962).

[10] I. Yu. Kobzarev and L. B. Okun', JETP **41**, 1205 (1961), Soviet Phys. JETP **14**, 859 (1962).

[11] I. Yu. Kobzarev and L. B. Okun', Nuclear Phys. (in press).

[12] M. Gell-Mann, The Eightfold Way (preprint).

[13] V. M. Shekhter, JETP **36**, 581 (1959), Soviet Phys. JETP **9**, 403 (1959).

[14] Ya. B. Zel'dovich, JETP **34**, 1644 (1958), Soviet Phys. JETP **7**, 1130 (1958).

[15] Booth, Chamberlain, and Rogers, Nuovo cimento **19**, 853 (1961).

[16] Bernardini, Querzoli, Salvini, Silverman, and Stoppini, Nuovo cimento **14**, 268 (1959).

[17] Zinov, Konin, Korenchenko, and Pontecorvo, JETP **38**, 1708 (1960), Soviet Phys. JETP **11**, 1233 (1960).

[18] V. I. Gol'danskii and V. M. Maksimenko, JETP **39**, 841 (1960), Soviet Phys. JETP **12**, 584 (1961).

[19] F. Solmitz, Proc. Ann. Int. Conf. on High Energy Physics at Rochester, Univ. of Rochester, 1960, p. 165.

Translated by W. H. Furry
328

ISOTOPIC STRUCTURE OF WEAK INTERACTIONS AND PROCESSES RESULTING FROM THE ABSORPTION OF A NEUTRINO OR ANTINEUTRINO BY NUCLEONS

V. M. SHEKHTER

Leningrad Physico-Technical Institute, Academy of Sciences, U.S.S.R.

Submitted to JETP editor July 18, 1961

J. Exptl. Theoret. Phys. (U.S.S.R.) **41**, 1953-1961 (December, 1961)

Certain processes of (anti) neutrino absorption by nucleons should give rise to systems of baryons and mesons with total strangeness zero. It is assumed that the weak interaction responsible for these processes is local, CP-invariant, and includes a baryon-meson current which transforms in isotopic spin space like a component of a vector. A relation is established between cross sections of similar reactions, resulting from the absorption of a neutrino or antineutrino respectively, and a method is indicated for qualitatively distinguishing between the V, A and S, P, T variants in the weak interaction. Isotopic equalities between amplitudes for various processes of neutrino or antineutrino absorption by nucleons are also written down.

1. INTRODUCTION

As is known, the processes that occur as a result of absorption by nucleons of high-energy neutrinos or antineutrinos may be divided into two categories. For one class of reactions the total strangeness of the strongly interacting particles in the final state is the same as that of a nucleon (i.e., zero), and for the other class it differs by unity. The following are examples of processes of the first type

$$\nu + n \to p + l^-,\ \nu + p \to p + \pi^+ + l^-,\ \nu + n \to \Lambda + K^+ + l^-,$$
$$\bar{\nu} + p \to n + l^+,\ \bar{\nu} + n \to n + \pi^- + l^+,\ \bar{\nu} + p \to \Lambda + K^0 + l^+$$

etc., whereas the following are examples of the second type

$$\bar{\nu} + p \to \Lambda + l^+, \qquad \bar{\nu} + p \to p + K^- + l^+,$$
$$\nu + p \to p + K^+ + l^-$$

and so forth ($l^\pm$ denotes a charged lepton, i.e., either electron or μ meson). Processes of the first type, proceeding with strangeness conservation, are caused by the same weak interaction that is responsible for nuclear β decay and μ capture, whereas the interaction leading to reactions in which strangeness is not conserved appears only in leptonic decays of K mesons and hyperons.

It is known about the first interaction that for small momentum transfers it consists of the V and A 4-fermion variants, and that the baryon-meson current in it transforms like a component of a vector in isotopic space.[1] This latter circumstance, by the way, cannot be considered as rigorously proven. The reason for this lies in the fact that the decay of $\pi^\pm$ mesons, as well as the β decay of the free neutron and a majority of mirror nuclei (it is precisely these processes that give rise to most of the information on the structure of weak interactions) is due to only the (+) component of an isotopic vector. Even if the weak interaction were to include a current transforming like a component of a second rank tensor in isotopic space (such a current can, for example, be constructed out of the $\bar{\Sigma}$ and Σ operators), it would not contribute to the decays mentioned. An argument against the existence of such a current comes from the observation that it would contribute to the decay of O^{14}, which occurs between different components of an isotopic vector, leading to a disagreement between the vector constants in the decays of $\mu^\pm$ and O^{14}. This last consideration, however, is of a quantitative nature, and furthermore the equality of the constants has lately become subject to doubt.[2] In composite models of elementary particles it turns out, as a rule, to be possible to construct only isovector currents,[3] however these models themselves are greatly in need of experimental verification.

Nothing definite can be said at this time about the interaction of strongly interacting particles in which strangeness is not conserved. According to the Feynman–Gell-Mann scheme[1] the baryon-meson currents are, generally speaking, sums of isospinors of rank $\frac{1}{2}$ and $\frac{3}{2}$. In a number of papers (see, e.g., the review article by Okun'[3]) the hypothesis has been advanced that the isospinor of rank $\frac{3}{2}$ is absent.

A study of reactions resulting from the absorption by nucleons of neutrinos or antineutrinos would give information about the properties of weak interactions for large energies and momentum transfers. A direct calculation of cross sections for specific processes will not, apparently, be very useful, because a large number of unknown form factors appears in the calculations. As a result the calculations, as well as their comparison with experimental data, become difficult or in practice impossible. A different approach seems more reasonable, in which experimental consequences of the general properties of the weak interactions are predicted. It is from this point of view precisely that the neutrino and antineutrino absorption by nucleons was discussed in the article of Lee and Yang.[4]

In this work, as in [4], the consequences of locality, CP invariance, and the proposed isotopic structure of the weak interactions are investigated. From the beginning we include in the considerations all five possible variants of the weak interaction.

In Sec. 2 the strangeness-conserving processes are investigated. The hypothesis that the baryon-meson current transforms like a component of a vector in isotopic space leads to certain relations between the processes of absorption of neutrinos and antineutrinos; these relations turn out to be different for different weak interaction variants. The difference between the V, A and S, P, T variants turns out to be most pronounced for the case when the energy of the neutrino or antineutrino in the laboratory frame is large is comparison with the transferred momenta. In Sec. 3 additional consequences of crossing symmetry for production processes of an arbitrary number of π and K mesons are described. Section 4 is devoted to the establishment of isotopic relations between amplitudes for various reactions.

Questions relating to the identity of electron and μ-meson neutrinos, or to the feasibility of obtaining sufficiently intense beams of these particles, are not discussed in this paper.

2. PROCESSES PROCEEDING WITH NO CHANGE IN STRANGENESS OF THE STRONGLY INTERACTING PARTICLES

Reactions of neutrino or antineutrino absorption by nucleons, resulting in the production of baryons and mesons with zero total strangeness, may be written in general form as

$$\text{a)}\ \nu + N \to B + l^-, \qquad \text{b)}\ \bar{\nu} + N_1 \to B_1 + l^+, \tag{1}$$

where N refers to the nucleon in the initial state, and B to the system of all strongly interacting particles at the end of the reaction. The states N_1 and B_1 may be obtained from N and B by applying the charge symmetry operator. If it is assumed that the latter coincides with rotations by 180° about the first axis in isotopic space, then this operation amounts to the substitutions

$$p \leftrightarrow n,\quad \Lambda \to \Lambda,\quad \Sigma^+ \leftrightarrow \Sigma^-,\quad \Sigma^0 \to -\Sigma^0,\quad \Xi^0 \leftrightarrow \Xi^-,$$
$$\pi^+ \leftrightarrow \pi^-,\quad \pi^0 \to -\pi^0,\quad K^+ \leftrightarrow K^0,\quad K^- \leftrightarrow \overline{K}^0. \tag{2}$$

To each of processes a) there corresponds a definite reaction b), and vice versa. The amplitudes for processses a) and b) are simply related to each other, in the same manner as in ordinary β decay. If the weak interaction is local the matrix element for reaction a) may be written in first order of perturbation theory as

$$M = \sum_i \Gamma_i\, (\bar{u}_l O_i (C_i + C_i' \gamma_5)\, u_\nu), \tag{3}$$

where the sum is over the five variants of the 4-fermion interaction, O_i are the spin matrices for these covariants, and Γ_i are the matrix elements of the corresponding baryon-meson currents taken between the states of N and B; $\gamma_5 = i\gamma_0\gamma_1\gamma_2\gamma_3$; C_i and C_i' are the ordinary β-decay constants.

If CP invariance holds, and if the baryon-meson current transforms like a component of an isovector, then accurate to within the possible appearance of an immaterial common factor of (-1) the matrix element for process b) may be written in the form

$$M_1 = \sum_i \Gamma_i\, (\bar{u}_{\bar{l}} O_i \eta_i (C_i - C_i' \gamma_5)\, u_{\bar{\nu}}), \tag{4}$$

where (after replacing N and B by N_1 and B_1) Γ_i is the same as in Eq. (3) and η_i is determined by (C is the charge-conjugation matrix)

$$C^{-1} O_i C = \eta_i O_i^T,$$
$$\eta_i = \begin{cases} 1 & i = A, S, P, \\ -1 & i = V, T. \end{cases} \tag{5}$$

It follows from a comparison of Eqs. (4) and (5) with (3) that the transition from reaction a) to b) is accomplished by having

$$C_V, C_A', C_S', C_P', C_T \text{ change sign}$$
$$\text{and } C_V', C_A, C_S, C_P, C_T' \text{ do not change sign.} \tag{6}$$

In other words, terms involving interferences of constants appearing in the same line in Eq. (6) are the same in the cross sections for reactions a) and b), whereas interferences between lines contribute to the cross sections terms with opposite signs.

Let us restrict ourselves in this section to the cases where in processes (1) the masses of the

leptons can be ignored. In practice this is permissible whenever the lepton l is an electron. If furthermore the energy of the incident neutrinos and the transferred momenta are much larger than the μ-meson mass, then our conclusions are valid also for the case $l = \mu$. In the case of massless leptons the free Lagrangian is invariant under the γ_5 transformation of the lepton operators, under which in the matrix element (3)

$$\begin{aligned} &C_S, C_P, C_T, C'_S, C'_P, C'_T \quad \text{change sign,} \\ &\text{and } C_V, C_A, C'_V, C'_A \text{ do not change sign.} \end{aligned} \tag{7}$$

Therefore after neglecting m_l the expressions for cross sections for processes (1) cannot contain interferences of constants from the two groups in Eq. (7), i.e., interferences of the V and A variants with the S, P and T variants.

Let us consider now the spinor transformation, used previously in application to leptonic decays:[5]

$$u_\nu(p_\nu) \to v_l^c(-p_l) = C\bar{u}_l(p_l), \quad u_l(p_l) \to v_\nu^c(-p_\nu) = C\bar{u}_\nu(p_\nu) \tag{8}$$

and amounting, in essence, to a crossing transformation of the leptons. The transformation (8) is, apparently, equivalent to the exchange

$$p_\nu \leftrightarrow -p_l \tag{9}$$

(one should also add $m_\nu \leftrightarrow m_l$ except that we have assumed that the leptonic masses may be ignored) in the projection operator or in the density matrix resulting from squaring the matrix element (3). On the other hand, that matrix element remains unchanged if simultaneously with the transformation (8) we require that

$$\begin{aligned} &C'_V, C_A, C_S, C'_S, C_P, C'_P \quad \text{change sign} \\ &\text{and } C_V, C'_A, C_T, C'_T \text{ do not change sign.} \end{aligned} \tag{10}$$

It therefore follows that the expression for the cross section for processes (1) should be left unchanged under the simultaneous transformations (9) and (10). What has been said above is valid provided that the "vertex parts" Γ_i that appear in Eq. (3) are functions of only the four-vector $p_\nu - p_l$, which is invariant under (9), and not the four-vector $p_\nu + p_l$. This is the case for a local weak interaction, as well as in the case when a virtual charged boson exists; we will refer to this latter case as a quasilocal interaction.

A number of conclusions can be derived from the invariance of the cross section under transformation (9)—(10). To this end we observe that, as a consequence of locality or quasilocality of the weak interaction, the cross section for processes (1) may depend on the four-vector $s \equiv (p_\nu + p_l)$ not more than bilinearly. That is to say, the cross section divided by the statistical weight factor may be expressed in the form

$$a(sq_1)(sq_2) + b + d(sq_3), \tag{11}$$

where q_1, q_2 and q_3 are four-vectors made up out of the momenta and polarizations of the strongly interacting particles in the initial and final states, as well as of the four-momentum $p_\nu - p_l$, which is related to the others by the laws of momentum conservation. The coefficients a, b, d are functions of invariants formed out of the same four-vectors. We do not include in Eq. (11) the term proportional to s^2 because

$$s^2 = -(p_\nu - p_l)^2 + 2(m_l^2 + m_\nu^2) \approx -(p_\nu - p_l)^2.$$

Under the transformation (9) the vectors q_i do not, and the vector s does, change sign. It then follows from the invariance under (9), (10) and the circumstance that the coefficients a, b and d depend on C_i and C'_i bilinearly, that the coefficients a and b in Eq. (11) may contain only such interferences of the constants that are even under (10), i.e.,

$$\begin{aligned} &a, b \sim C_V^2 + C_V'^2,\ C_A^2 + C_A'^2,\ C_V C'_A + C'_V C_A, \\ &C_S^2 + C_S'^2,\ C_P^2 + C_P'^2,\ C_S C_P + C'_S C'_P,\ C_T^2 + C_T'^2, \\ &C_S C'_S,\ C_P C'_P,\ C_S C'_P + C'_S C_P,\ C_T C'_T, \end{aligned} \tag{12}$$

whereas the coefficient d should be odd:

$$\begin{aligned} &d \sim C_V C_A + C'_V C'_A,\ C_V C'_V,\ C_A C'_A, \\ &C_S C_T + C'_S C'_T,\ C_P C_T + C'_P C'_T, \\ &C_S C'_T + C'_S C_T,\ C_P C'_T + C'_P C_T. \end{aligned} \tag{13}$$

Comparing now Eqs. (12) and (13) with (6) we find that in the case of a V, A interaction the coefficients a and b are the same for processes a) and b) in Eq. (1), whereas d differs in sign. The sum of the cross sections a) and b) will therefore not contain d, and consequently the interference of the V and A variants may enter only through the combination $C_V C'_A + C'_V C_A$, i.e., only through a pseudoscalar quantity. The scalar part of the sum of the cross sections on the other hand, can contain the V and A variants only in the form of a sum of squares, which is obviously larger than the contribution from a pure V interaction. If the Feynman-Gell-Mann hypothesis relating the β-decay current to the isovector part of the electromagnetic current is valid, then the V contribution may be determined from experiments on electroproduction of the system B or B_1 from nucleons. Such a calculation was carried out by Azimov[6] for the processes $\nu + N \to N + \pi + l$, $\nu + N \to \Lambda + K + l$.

In the presence of the S, P, T variants the situation for the scalar part of the cross section

is the same as in the "pure" V, A case, i.e., a and b are the same for processes a) and b) and d differs in sign. Consequently the experimental comparison of this part of the cross section for processes a) and b) permits one to test independently of what variants might be involved in the fundamental assumptions of the theory, namely locality, CP invariance, and—which is most problematic—the isovector nature of the baryon-meson current. For the pseudoscalar quantities, such as the longitudinal polarization of the produced fermions, the situation is different. Namely for the case of S, P, T, d is the same and a, b differ in sign for processes a) and b), whereas for V, A the opposite is the case. Consequently a comparison of quantities of this type in processes a) and b) would allow, in principle, to establish whether the S, P, T variants contribute at high energies.

Experimentally the coefficients a, b and d can be distinguished by varying the momenta of $\nu(\bar{\nu})$ and l in such a way that only the four-vector $s = p_\nu + p_l$ changes, while $p_\nu - p_l$, as well as the momenta of all the other particles, remain fixed. One can, in particular, in studying any of the processes (1) select only those events for which the neutrino energy in the laboratory system E_ν is large and is almost entirely transferred to the electron (or μ meson). In that case the only large invariants in Eq. (11) are (sq) (with $q \neq p_\nu - p_l$). If, for example, q coincides with the four-momentum of the initial nucleon, then $(sq) = m(E_\nu + E_l) \approx 2mE_\nu$, whereas the invariants not involving the vector s are of the order of either $Q^2 \equiv (p_\nu - p_l)^2$ or $\sim m\sqrt{|Q^2|}$. For $E_\nu \gg \sqrt{|Q^2|}$ only the first term in Eq. (11), i.e., a, is important. Therefore under these conditions the scalar parts of the cross sections for a) and b) should coincide independently of what variants are involved in the weak interaction. (In the case of the V, A interaction the cross section for each of the processes a) and b)—and not only their sum—appears now in the form of a sum of positive contributions from the V and A variants, the first of which may be related to electroprocesses.) The pseudoscalar quantities should have the same signs in the case of the V, A interaction, and opposite signs in the case of S, P, T. Thus again they provide a possibility for determining what variants are involved.

If we consider the cross section integrated over all internal variables of the system B in Eq. (1), then there remain only three independent vectors in the problem: $s = p_\nu + p_l$, $p_\nu - p_l$ and p_N, so that $q = p_N$ and $(sq) = m(E_\nu + E_l)$. At that Eq. (11) means that the cross section depends quadratically on $E_\nu + E_l$ for fixed $E_\nu - E_l$ and the angle of emission of l with, according to what has been said, the terms in the scalar part of the cross section linear in $E_\nu + E_l$ being of opposite sign for processes a) and b), the other terms being of the same sign. This fact has been pointed out previously by Lee and Yang[4] in somewhat different terms.

In conclusion we note that the cross sections for the processes of (anti) neutrino absorption resulting in a change in the strangeness of the strongly interacting particles also have the structure of Eq. (11), with, for $(sq) \gg m\sqrt{|Q^2|}$, the first term dominating. In that case we again have invariance under the transformations (9)—(10), however no analogy of the type (6) between various processes exists.

3. CROSSING SYMMETRY

From among the processes (1) we may select those in which the system B or B_1 consists of one nucleon and an arbitrary number of mesons. In that case besides the relations between the various reactions, that occur as a result of neutrino or antineutrino absorption, described in the previous section it is possible to obtain additional relations due to crossing symmetry. Let us consider the processes

$$\begin{aligned} &\alpha) \quad \nu + N_1 \to N_2 + A + l^-, \\ &\beta) \quad \bar{\nu} + N_1 \to N_2 + \bar{A} + l^+, \end{aligned} \tag{14}$$

where N_1 and N_2 denote nucleons in the initial and final states, and A stands for a system consisting of an arbitrary number of π and K mesons. $\bar{A}$ differs from A in that all particles are replaced by their antiparticles. If the initial nucleon in the reaction α is the same as the final nucleon in the reaction β, in the sense that they are either both protons or both neutrons, and if the same is true of the other pair of nucleons, i.e., if

$$N_{1\alpha} = N_{2\beta}, \qquad N_{2\alpha} = N_{1\beta}, \tag{14a}$$

then the matrix elements of reactions α and β are related by crossing symmetry. Let us denote the momenta of the particles in reaction α by p_ν, p_1, p_2, p_A, p_l, and those in reaction β by q_ν, q_1, q_2, q_A, q_l (p_A and q_A stand for the totality of the momenta of all particles in A or $\bar{A}$) and let us assume in what follows that Eq. (14a) holds. Then the expression for the cross section of process β in Eq. (14) coincides with the expression for the reaction α, provided that we make the following substitutions in the matrix element for the latter, i.e., in Eq. (3):

$$p_1 \to q_2, \quad p_2 \to q_1, \quad p_A \to -q_A,$$
$$p_\nu \to q_l, \quad p_l \to q_\nu, \quad m_\nu \leftrightarrow m_l. \tag{15}$$

If the nucleons are polarized then we must add to Eq. (15): $\zeta_1 \leftrightarrow \eta_2$, $\zeta_2 \leftrightarrow \eta_1$, where ζ_i and η_i are the polarization vectors of the i-th nucleon ($i = 1, 2$) in the reaction α and β. The last relation in Eq. (15) may be omitted if the neglect of the mass of the lepton l is justified. If such is not the case then it becomes convenient to add to Eq. (15) the transformation (9), (10), after which the transition from α to β consists of the replacement (10) together with

$$p_1 \to q_2, \quad p_2 \to q_1, \quad p_A \to -q_A, \quad p_\nu \to -q_\nu,$$
$$p_l \to -q_l \quad (\zeta_1 \to \eta_2, \quad \zeta_2 \to \eta_1). \tag{16}$$

Let us consider in more detail the specific example of "weak" production of a single π meson, i.e., the reactions

$$\alpha_1)\ \nu + p \to p + \pi^+ + l^-, \qquad \beta_1)\ \bar{\nu} + p \to p + \pi^- + l^+,$$
$$\alpha_2)\ \nu + n \to n + \pi^+ + l^-, \qquad \beta_2)\ \bar{\nu} + n \to n + \pi^- + l^+,$$
$$\alpha_3)\ \nu + n \to p + \pi^0 + l^-, \qquad \beta_3)\ \bar{\nu} + p \to n + \pi^0 + l^+. \tag{17}$$

These reactions are related by the transformation (15) or (10), (16). On the other hand, the processes β_1, β_2, β_3 stand in the same relation to α_1, α_2, α_3 as did processes b) to a) in Eq. (1), so that the transition between them is accomplished according to the rule (6), provided that the conditions listed in Sec. 2 are fulfilled. It is easy to see on comparing Eq. (6) with Eqs. (10) and (16) that in the case of the V, A interaction the expression for the cross sections α_3 and β_3 should be even under the exchange $p_1 \leftrightarrow p_2$ and a change of sign of p_ν, p_l and p_π, whereas the cross sections α_1 and α_2, or β_1 and β_2, should under the same transformation go into each other. In the case of S, P, T what has been said above remains true for the scalar part of the cross section, whereas the pseudoscalar part changes sign.

An experimental test of crossing symmetry would require obtaining the dependence of the cross section on the invariants that can be constructed out of the four-vectors entering into Eqs. (15) or (16) which is, apparently, difficult. It may be that selecting events for which N_2 is approximately at rest will somewhat facilitate this task. At that in Eq. (17), as well as in the general case (14), there remain after integration over the internal variables of the system A or $\bar{A}$ only three independent vectors: p_ν, p_l and $p_1 \approx p_2$, out of which one can construct three invariants: $Q^2 \equiv (p_\nu - p_l)^2$, $(p_\nu - p_l)\cdot p_1 = m(E_\nu - E_l)$ and $(sp_1) \equiv (p_\nu + p_l)\cdot p_1 = m(E_\nu + E_l)$. Under the transformation (16) the last two change sign. At large energies E_ν and for $|Q^2| \ll m(E_\nu + E_l)$ the dependence on the last invariant is quadratic so that the transformation (16) amounts to a change in the sign of the one invariant $(p_\nu - p_l)\cdot p_1 = m(E_\nu - E_l)$ only.

4. ISOTOPIC RELATIONS

If the baryon-meson current has definite isotopic structure, i.e., transforms as a component of an isovector or isospinor of a given rank, then the amplitudes for the various processes resulting from absorption of (anti) neutrinos by nucleons are related to each other as a consequence of isotopic invariance. Such relations are given below for reactions with no more than three strongly interacting particles in the final state. In the usual manner there follow from equalities among amplitudes inequalities among cross sections.

Let us consider first processes in which the total strangeness does not change, and let us suppose that the baryon-meson current transforms like a component of an isotopic vector.

1) If the amplitudes for the reactions

$$a)\ \nu + p \to p + \pi^+ + l^-,$$
$$b)\ \nu + n \to n + \pi^+ + l^-,$$
$$c)\ \nu + n \to p + \pi^0 + l^- \tag{18}$$

are denoted respectively by T_a, T_b, T_c, then the relation between them may be written as

$$T_a - T_b - \sqrt{2}\,T_c = 0. \tag{19}$$

The same relation holds also for the processes

$$a)\ \nu + p \to \Sigma^+ + K^+ + l^-,$$
$$b)\ \nu + n \to \Sigma^+ + K^0 + l^-,$$
$$c)\ \nu + n \to \Sigma^0 + K^+ + l^-,$$

or

$$a)\ \nu + p \to \Lambda + K^+ + \pi^+ + l^-,$$
$$b)\ \nu + n \to \Lambda + K^0 + \pi^+ + l^-,$$
$$c)\ \nu + n \to \Lambda + K^+ + \pi^0 + l^-. \tag{20}$$

The inequalities for the cross section arising from Eq. (19) are obvious.

2) In the reactions

$$a)\ \nu + p \to p + \pi^+ + \pi^0 + l^-,$$
$$b)\ \nu + p \to n + \pi^+ + \pi^+ + l^-,$$
$$c)\ \nu + n \to p + \pi^+ + \pi^- + l^-,$$
$$d)\ \nu + n \to p + \pi^0 + \pi^0 + l^-,$$
$$e)\ \nu + n \to n + \pi^+ + \pi^0 + l^- \tag{21}$$

the two pions may be produced in an even or odd orbital state. If the corresponding amplitudes are denoted by T^+ and T^-, and if the Bose nature of

the pions is taken into account, then

$$T_a^+ = T_b^+/\sqrt{8} = -T_e^+ = (T_c^+ - T_d^+)/\sqrt{2},$$
$$T_b^- = T_d^- = 0, \quad T_c^- = (T_a^- - T_e^-)/\sqrt{2}. \qquad (22)$$

In the total cross section the amplitudes T^+ and T^- do not interfere. Consequently one obtains from Eq. (22) inequalities for the total cross sections: $\sigma_a \geq \sigma_b/4$, $\sigma_e \geq \sigma_l/4$, etc. If reaction (21) takes place near threshold then T^- is clearly small in comparison with T^+, so that Eq. (22) gives for the differential cross sections

$$d\sigma_a \approx d\sigma_e \approx d\sigma_b/8 \leqslant (\sqrt{d\sigma_c} + \sqrt{d\sigma_d})^2/2,$$
$$\sqrt{2d\sigma_a} + \sqrt{d\sigma_c} \geqslant \sqrt{d\sigma_d}, \qquad \sqrt{2d\sigma_a} + \sqrt{d\sigma_d} \geqslant \sqrt{d\sigma_c}. \qquad (23)$$

For the total cross sections the relations (23) remain valid provided that

$$d\sigma_a \to \sigma_a, \quad d\sigma_c \to \sigma_c, \quad d\sigma_e \to \sigma_e, \quad d\sigma_b/2 \to \sigma_b, \quad d\sigma_d/2 \to \sigma_d.$$

Since pions obey Bose statistics the amplitudes T^+ and T^- may be interpreted as corresponding to the production of the pion pair in a state with even or odd total isotopic spin. In this sense Eq. (22) is also valid for the processes

$$\begin{aligned}
&a)\ \nu + p \to \Sigma^+ + \pi^0 + K^+ + l^-,\\
&b)\ \nu + p \to \Sigma^+ + \pi^+ + K^0 + l^-,\\
&c)\ \nu + n \to \Sigma^+ + \pi^- + K^+ + l^-,\\
&a')\ \nu + p \to \Sigma^0 + \pi^+ + K^+ + l^-,\\
&c')\ \nu + n \to \Sigma^- + \pi^+ + K^+ + l^-,\\
&e')\ \nu + n \to \Sigma^0 + \pi^+ + K^0 + l^-,\\
&d)\ \nu + n \to \Sigma^0 + \pi^0 + K^+ + l^-,\\
&e)\ \nu + n \to \Sigma^+ + \pi^0 + K^0 + l^-, \qquad (24)
\end{aligned}$$

with $T_a^{\pm\prime} = \pm T_a^{\pm}$, $T_c^{\pm\prime} = \pm T_c^{\pm}$, $T_e^{\pm\prime} = \pm T_e^{\pm}$. The latter equalities are a consequence of isotopic invariance alone. In Eq. (22) the superscripts ± refer now only to the isotopic parity of the $\Sigma\pi$ system and have no relation to the orbital angular momentum. Consequently T^+ and T^- can interfere also in the total cross section.

3) The amplitudes of the reactions

$$\begin{aligned}
&a)\ \nu + p \to \Xi^0 + K^+ + K^+ + l^-,\\
&b)\ \nu + n \to \Xi^0 + K^+ + K^0 + l^-,\\
&c)\ \nu + n \to \Xi^- + K^+ + K^+ + l^- \qquad (25)
\end{aligned}$$

are connected by the equalities (T^+ and T^- now again refer to the amplitudes for production of pions in even or odd states of orbital angular momentum)

$$T_a^+ = T_c^+ = 0, \qquad T_a^- - T_c^- - 2T_b^- = 0. \qquad (26)$$

Since T^+ and T^- do not interfere in the total cross section we get from Eq. (26) the inequalities

$$\sqrt{2\sigma_b} + \sqrt{\sigma_c} \geqslant \sqrt{\sigma_a}, \qquad \sqrt{2\sigma_b} + \sqrt{\sigma_a} \geqslant \sqrt{\sigma_c}. \qquad (27)$$

So far all the relations in this Section have been written for processes involving neutrinos, i.e., reactions of type a) in Eq. (1). The same results are naturally valid for the corresponding reactions of type b) involving antineutrinos.

In conclusion we consider processes in which strangeness changes. As was already remarked, the baryon-meson current is in this case in general a sum of terms of isospin $\frac{1}{2}$ and $\frac{3}{2}$. In the table are given relations between the amplitudes for various processes in the two extreme cases when the current has isospin $\frac{1}{2}$ or $\frac{3}{2}$. Only processes satisfying the $\Delta S = \Delta Q$ rule [1] are considered and only if they result in the production of no more than two strongly interacting particles. The two types of reactions in the last group in the table refer to processes of the type β and α, Eq. (14), and are connected by crossing relations. Relations between cross sections for processes

Reactions	Relations between the amplitudes when the current has isospin	
	$\frac{1}{2}$	$\frac{3}{2}$
$a)\ \bar\nu + p \to \Sigma^0 + l^+$ or $a)\ \bar\nu + p \to \Lambda + \pi^0 + l^+$ $b)\ \bar\nu + n \to \Sigma^- + l^+$ $\quad b)\ \bar\nu + n \to \Lambda + \pi^- + l^+$	$T_a = T_b/\sqrt{2}$	$T_a = -T_b\sqrt{2}$
$a)\ \bar\nu + p \to \Xi^0 + K^0 + l^+$ $b)\ \bar\nu + p \to \Xi^- + K^+ + l^+$ $c)\ \bar\nu + n \to \Xi^- + K^0 + l^+$	$T_a + T_b - T_c = 0$	$T_a = T_b = -T_c$
$a)\ \bar\nu + p \to \Sigma^+ + \pi^- + l^+$ $b)\ \bar\nu + p \to \Sigma^0 + \pi^0 + l^+$ $c)\ \bar\nu + n \to \Sigma^0 + \pi^- + l^+$ $d)\ \bar\nu + p \to \Sigma^- + \pi^+ + l^+$ $e)\ \bar\nu + n \to \Sigma^- + \pi^0 + l^+$	$T_c = -T_e$ $= \sqrt{2}(T_b - T_a)$ $= \sqrt{2}\,(T_d - T_b)$	$T_b = \frac{1}{2}(\sqrt{2}T_c - T_a)$ $= -(T_a + T_d)$ $= T_a + \sqrt{2}T_e$
$a)\ \bar\nu + p \to p + K^- + l^+$ or $a)\ \nu + p \to p + K^+ + l^-$ $b)\ \bar\nu + p \to n + \bar K^0 + l^+$ $\quad b)\ \nu + n \to p + K^0 + l^-$ $c)\ \bar\nu + n \to n + K^- + l^+$ $\quad c)\ \nu + n \to n + K^+ + l^-$	$T_a - T_b - T_c = 0$	$-T_a = T_b = T_c$

$\bar{\nu} + N \to \Sigma + l^+$ were obtained previously by Behrends and Sirlin.[7]

The author is indebted to Ya. I. Azimov for discussions.

[1] R. P. Feynman and M. Gell-Mann, Phys. Rev. **109**, 193 (1958). E. C. G. Sudarshan and R. E. Marshak, Phys. Rev. **109**, 1860 (1958).

[2] R. P. Feynman, Report at the 10-th Rochester Conference on High-Energy Physics, New York (1960).

[3] L. B. Okun', Ann. Rev. Nucl. Sci. **9**, 61 (1959), Usp. Fiz. Nauk **68**, 449 (1959).

[4] T. D. Lee and C. N. Yang, Phys. Rev. Lett. **4**, 307 (1960).

[5] S. Weinberg, Phys. Rev. **112**, 1375 (1958); **115**, 481 (1959). V. M. Shekhter, JETP **38**, 534 (1960), Soviet Phys. JETP **11**, 387 (1960).

[6] Ya. I. Azimov, JETP **14**, 1879 (1961), this issue, p. 1336.

[7] R. E. Behrends and A. Sirlin, Phys. Rev. **121**, 324 (1961).

Translated by A. M. Bincer
329

PARTIAL WAVES WITH COMPLEX ORBITAL ANGULAR MOMENTA AND THE ASYMPTOTIC BEHAVIOR OF THE SCATTERING AMPLITUDE

V. N. GRIBOV

Leningrad Physico-technical Institute, Academy of Sciences, U.S.S.R.

Submitted to JETP editor July 18, 1961

J. Exptl. Theoret. Phys. (U.S.S.R.) 41, 1962-1970 (December, 1961)

It is shown that in relativistic theory the partial wave amplitudes f_l are analytic functions of the angular momentum l. The asymptotic behavior of the scattering amplitude as a function of momentum transfer is determined by the nearest singularities of f_l. An expression is obtained for the scattering amplitude for arbitrary momentum transfer in terms of the f_l, which satisfies the Mandelstam equation relating the spectral functions and absorptive parts. The behavior of the scattering amplitude at high energies is discussed.

1. INTRODUCTION

In a recent paper, Regge,[1] by introducing partial waves with complex orbital angular momenta, obtained an interesting result in nonrelativistic theory concerning the asymptotic behavior of scattering amplitudes and spectral functions in the nonphysical region of large momentum transfers.

In a previous paper of this author[2] the asymptotic behavior was studied under these same conditions in relativistic theory in order to examine the possible types of asymptotic behavior of the scattering amplitude at high energies. In this an important part was played by the Mandelstam equation, obtained by analytic continuation of the usual unitarity condition.

In the present paper we show that partial waves with complex orbital angular momenta l can also be introduced in a relativistic theory. Their analytic properties are to some extent similar to those of the corresponding nonrelativistic quantities. The introduction of complex values of l enables one to find the general solution of the Mandelstam equation and to obtain some information about the possible asymptotic behavior of amplitudes and spectral functions.

2. PARTIAL WAVES WITH COMPLEX ORBITAL ANGULAR MOMENTA

Let us consider the dispersion relation in the momentum transfer in the t channel (region III in Fig. 1):

$$A(s,t) = A(s_0,t) + \frac{1}{\pi}\int_{4\mu^2}^{\infty} ds' A_1(s',t)\left[\frac{1}{s'-s} - \frac{1}{s'-s_0}\right] + \frac{1}{\pi}\int_{4\mu^2}^{\infty} du' A_2(u',t)\left[\frac{1}{u'-u} - \frac{1}{u'-u_0}\right]. \quad (1)$$

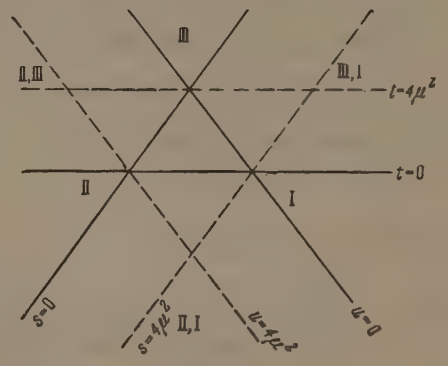

FIG. 1

To be specific, we have written the equation for one subtraction; as will be clear later, the number of subtractions is unimportant.

In addition we shall assume that the Mandelstam representation is valid. Then, assuming for simplicity that the particles all have the same mass μ and are the lightest particles (for example, π mesons), we find, following Mandelstam, that the spectral function $\rho(s,t)$ and the absorptive parts $A_1(s,t)$ and $A_2(u,t)$ must satisfy the equation

$$\rho(s,t) = \sqrt{\frac{t-4\mu^2}{t}}\int \frac{dz_1\,dz_2}{\sqrt{z^2+z_1^2+z_2^2-2zz_1z_2-1}} \times [A_1(s_1,t)\,A_1^*(s_2,t) + A_2(u_1,t)\,A_2^*(u_2,t)];$$

$$s = -\tfrac{1}{2}(t-4\mu^2)(1-z),$$

$$s_{1,2} = -\tfrac{1}{2}(t-4\mu^2)(1-z_{1,2}),$$

$$u_{1,2} = -\tfrac{1}{2}(t-4\mu^2)(1-z_{1,2}),$$

$$z > z_1z_2 + \sqrt{(z_1^2-1)(z_2^2-1)}, \quad (2)$$

for t below the threshold for inelastic processes. (For π mesons, $t < 16\mu^2$).

Using (1), we calculate the amplitude for the wave with angular momentum l:

$$f_l(t) = \frac{1}{2}\int_{-1}^{1} P_l(z)\, A(s,t)\, dz. \qquad (3)$$

For $l \geq 1$

$$f_l(t) = \frac{1}{\pi}\int_{z_0}^{\infty} Q_l(z')\, A_1(s',t)\, dz'$$

$$+ (-1)^l \frac{1}{\pi}\int_{z_0}^{\infty} Q_l(z'')\, A_2(u'',t)\, dz'', \qquad (4)$$

where

$$Q_l(x) = \frac{1}{2}\int_{-1}^{1} \frac{P_l(x')}{x-x'}\, dx',$$

$$z' = 1 + \frac{2s'}{t-4\mu^2} \geqslant z_0 = 1 + \frac{8\mu^2}{t-4\mu^2} > 1,$$

$$z'' = 1 + \frac{2u''}{t-4\mu^2} \geqslant z_0. \qquad (5)$$

If the asymptotic behavior of A for large s required not one but k subtractions, equation (4) would be valid for $l \geq k$. We write (4) in the form

$$f_l(t) = \varphi_l^{(1)}(t) + (-1)^l \varphi_l^{(2)}(t) \qquad (6)$$

and study the properties of, say, $\varphi_l^{(1)}(t)$.

We consider the expression

$$\varphi_l^{(1)}(t) = \frac{1}{\pi}\int_{z_0}^{\infty} Q_l(z')\, A_1(z',t)\, dz' \qquad (7)$$

as the definition of $\varphi_l^{(1)}$ for nonintegral l, where $Q_l(z)$ is the Legendre function of the second kind, and coincides with (5) for integer l. Then under the condition that $|A_1(z,t)| < Cz^a$, it follows from (7) that $\varphi_l^{(1)}$ is an analytic function of l in the half-plane Re $l > a$, since $Q_l(z')$ is an analytic function of l and behaves like $(z')^{-(l+1)}$ for $z' \to \infty$.

For $l \to \infty$,

$$\varphi_l^{(1)}(t) \sim e^{-\alpha l}, \qquad z_0 = \operatorname{ch}\alpha. \qquad (8)^*$$

Using the analytic properties and the asymptotic behavior (8), we can easily invert (7) and express $A_1(z', t)$ in terms of $\varphi_l^{(1)}(t)$. In order to do this, we use the following relation, which is proved in Appendix I:

$$\frac{i}{2\pi}\int_{b-i\infty}^{b+i\infty} dl\,(2l+1)\, P_l(z_1)\, Q_l(z_2) = \delta(z_2 - z_1), \quad b > -1. \qquad (9)$$

Integrating (7) over l for $b \geq a$, we get

$$A_1(z',t) = \frac{i}{2}\int_{b-i\infty}^{b+i\infty} dl\,(2l+1)\,\varphi_l^{(1)}(t)\, P_l(z'). \qquad (10)$$

We note that the right side of (10) is equal to zero for $z < z_0$, since then the asymptotic behavior of $\varphi_l^{(1)}$ and $P_l(z)$ for large l permits us to close the contour to the right for $l \to \infty$. The formula becomes meaningless for $z < 1$.

*ch = cosh.

Formulas (7) and (10) are analogous to the direct and inverse Mellin transformations, but are more convenient than the latter for studying the unitary condition (2).

We can write a similar relation for $A_2(z'', t)$:

$$A_2(z'',t) = \frac{i}{2}\int_{b-i\infty}^{b+i\infty} dl\,(2l+1)\,\varphi_l^{(2)}(t)\, P_l(z''). \qquad (11)$$

Since $\rho(s,t) = \operatorname{Im} A_1(s,t)$,

$$\rho(s,t) = \frac{i}{2}\int_{b-i\infty}^{b+i\infty} dl\,(2l+1)\, P_l(z)\,\frac{i}{2}\left[\varphi_l^{(1)} - (\varphi_{l^*}^{(1)})^*\right]. \qquad (12)$$

Now we can substitute (10), (11) and (12) into (2). As shown in Appendix II, Eq. (2) will be satisfied if

$$\frac{i}{2}\left[\varphi_l^{(1)} - (\varphi_{l^*}^{(1)})^*\right] = \frac{q}{\omega}\left[\varphi_l^{(1)}(\varphi_{l^*}^{(1)})^* + \varphi_l^{(2)}(\varphi_{l^*}^{(2)})^*\right];$$

$$q = \tfrac{1}{2}\sqrt{t-4\mu^2}, \qquad \omega = \tfrac{1}{2}\sqrt{t}. \qquad (13)$$

For real l, (13) goes over into

$$\operatorname{Im}\varphi_l^{(1)} = (q/\omega)\left[|\varphi_l^{(1)}|^2 + |\varphi_l^{(2)}|^2\right]. \qquad (14)$$

If together with Eq. (2), which is obtained by analytic continuation of the unitarity condition in the t channel into the region I, III of Fig. 1 ($s > 4\mu^2$), we also considered the relation between $\rho(u,t)$ and A_1, A_2 which follows from the analytic continuation of the same unitarity condition into the region II, III of Fig. 1 ($u > 4\mu^2$), then as shown by Mandelstam we would get the equation

$$\rho(u,t) = \operatorname{Im} A_2(u,t) = \frac{q}{\omega}\int \frac{dz_1 dz_2}{\sqrt{z^2 + z_1^2 + z_2^2 - 2zz_1z_2 - 1}}$$

$$\times\left[A_1(z_1)\, A_2^*(z_2) + A_1^*(z_1)\, A_2(z_2)\right] \qquad (15)$$

and, analogous to (12),

$$\rho(u,t) = \frac{i}{2}\int_{b-i\infty}^{b+i\infty} dl\,(2l+1)\, P_l(z)\,\frac{i}{2}\left[\varphi_l^{(2)} - (\varphi_{l^*}^{(2)})^*\right]. \qquad (16)$$

Substitution of (10), (11) and (16) in (15) gives

$$\frac{i}{2}\left[\varphi_l^{(2)} - (\varphi_{l^*}^{(2)})^*\right] = \frac{q}{\omega}\left[\varphi_l^{(1)}(\varphi_{l^*}^{(2)})^* + (\varphi_{l^*}^{(1)})^*\varphi_l^{(2)}\right], \qquad (17)$$

where for real l,

$$\operatorname{Im}\varphi_l^{(2)} = (q/\omega)\left[\varphi_l^{(1)}\varphi_l^{(2)*} + \varphi_l^{(1)*}\varphi_l^{(2)}\right]. \qquad (18)$$

If for integer l we multiply (18) by $(-1)^l$ and add to (14), we get the usual unitarity condition:

$$\operatorname{Im} f_l = (q/\omega)|f_l|^2. \qquad (19)$$

Thus formulas (14) and (18) are the generalization of (19) to arbitrary real l, while (13) and (17) generalize it to arbitrary complex l.

For the case of interaction of identical particles, $\varphi_l^{(1)} = \varphi_l^{(2)} = \varphi_l$, but since the integration in the original unitarity condition must be taken only over

half the sphere, the right sides of (1) and (15) contain an additional factor $\frac{1}{2}$, so that instead of (13) and (17) we get

$$\frac{i}{2}[\varphi_l - (\varphi_{l^*})^*] = \frac{q}{\omega}\varphi_l(\varphi_{l^*})^*, \qquad f_l = [1 + (-1)^l]\varphi_l. \quad (20)$$

Thus we have shown that $A_1(s,t)$, $A_2(u,t)$, $\rho(s,t)$ and $\rho(u,t)$ have the form (10), (11), (12) and (16) and satisfy the unitarity condition if $\varphi_l^{(1)}$ and $\varphi_l^{(2)}$ satisfy (13) and (17). The functions $\varphi_l^{(1)}$, $\varphi_l^{(2)}$ are analytic in l, their behavior for large l is given by (8), and for integral $l > a$ they are related simply to the phases for the t channel (Eq. 6).

It is also easy to get the expression for the amplitude $A(z,t)$ in terms of $\varphi_l^{(1)}(t)$ and $\varphi_l^{(2)}(t)$. This can be done either by using the dispersion relation (1) or by analytic continuation of the series

$$A(z,t) = \sum_{l=0}^{\infty} (2l+1) f_l(t) P_l(z),$$

in a way similar to that for the nonrelativistic theory,[1] but including both cuts.

With some simple transformations we get

$$A(z,t) = \sum_{l=0}^{n} (2l+1) f_l(t) P_l(z) + \frac{i}{2}\int_{b-i\infty}^{b+i\infty} \frac{(2l+1)\,dl}{\sin l\pi} \times [\varphi_l^{(1)}(t)\ P_l(-z) + \varphi_l^{(2)}(t) P_l(z)], \quad (21)$$

where $k \le n \le b$.

If we resolve $A(z,t)$ into parts which are symmetric and antisymmetric with respect to the substitution $z \to -z$:

$$A(z,t) = A^+(z,t) + A^-(z,t),$$

then

$$A^{\pm}(z,t) = \frac{1}{2}\sum_{l=0}^{n} (2l+1) f_l(t)\,[1 \pm (-1)^l]\,P_l(z) + \frac{i}{4}\int_{b-i\infty}^{b+i\infty} \frac{(2l+1)\,dl}{\sin l\pi} f_l^{\pm}\,[P_l(-z) \pm P_l(z)], \quad (22)$$

where

$$f_l^{\pm} = \varphi_l^{(1)} \pm \varphi_l^{(2)}$$

satisfy the conditions

$$\frac{i}{2}[f_l^{\pm} - (f_{l^*}^{\pm})^*] = \frac{q}{\omega} f_l^{\pm}(f_{l^*}^{\pm})^*. \quad (23)$$

Contrary to the situation for the nonrelativistic theory, we have not been able to show that $\varphi_l^{(1)}$ and $\varphi_l^{(2)}$ are a) meromorphic functions for $\mathrm{Re}\,l > -\frac{1}{2}$, and b) have singularities only in the upper half-plane. We know of no reasons why the first property (meromorphy) should be retained in the exact theory even when $t - 4\mu^2 \ll 4\mu^2$, i.e., in the nonrelativistic region in the t channel. This is related to the fact that in analyzing the analytic properties of $f_l(t)$ it was necesary to assume that the potential at small distances is not too singular (which was necessary in the nonrelativistic theory, in order for a solution of the form r^l to exist for small r).

It is easy to give examples of potentials for which this property does not hold. For a potential of the type $-\alpha/r^2$, the partial wave has branch points at $l = -\frac{1}{2} + \sqrt{\alpha}$, which for $\alpha > \frac{1}{4}$ represent a collapse into the center. For a δ-function potential, $f_l = 0$ for all $l \neq 0$.

As for the second property (singularities only in the upper half-plane), in nonrelativistic theory it is a consequence of the hermiticity of the Hamiltonian and is closely related to the fact that the singularities of the amplitude as a function of the energy t, which correspond to unstable states, lie only on the second sheet of the t plane.

It may well be that this distinction of the upper half-plane is retained in the relativistic theory, but we have simply been unable to prove it.

In conclusion we consider the analytic properties of $\varphi_l^{(1)}(t)$ as a function of t for arbitrary l where $\mathrm{Re}\,l > \max_t a$. These properties are easily understood, starting from formula (7). Since $A_1(s,t)$ is an analytic function of t, Eq. (7) is conveniently written in the form

$$\varphi_l^{(1)}(t) = \frac{2}{\pi(t-4\mu^2)}\int_{4\mu^2}^{\infty} Q_l\Big(1 + \frac{2s}{t-4\mu^2}\Big) A_1(s,t)\,ds. \quad (24)$$

For $t > 4\mu^2$, the singularities of $\varphi_l^{(1)}(t)$ correspond to singularities of $A_1(s,t)$. For $t \to 4\mu^2$,

$$Q_l\Big(1 + \frac{2s}{t-4\mu^2}\Big) \sim \Big(\frac{t-4\mu^2}{2s}\Big)^{l+1},$$

consequently,

$$\varphi_l^{(1)}(t) \sim q^{2l} \text{ for } q \to 0,$$

which coincides with the usual relation for integer l, with the one difference that $\varphi_l^{(1)}$ for nonintegral l remains complex when $t < 4\mu^2$.

As t decreases, singularities of $\varphi_l^{(1)}(t)$ appear for two reasons: 1) $Q_l(z)$ has a singularity at $z = -1$ and consequently $\varphi_l^{(1)}(t)$ has a singularity at $t = 0$; 2) $A_1(s,t)$ has a singularity for $4\mu^2 - s - t = u = u_0$.

It is also easy to write a dispersion relation for $\varphi_l^{(1)}(t)$. We note that in nonrelativistic theory $A_1(s,t)$ has no singularities for $t < 4\mu^2$, and the left-hand cut for $\varphi_l^{(1)}(t)$ comes only from the singularity of Q_l.

3. ASYMPTOTIC BEHAVIOR OF $A_1(s,t)$ AS $s \to \infty$

To investigate the asymptotic behavior of $A_1(s,t)$ for $s \to \infty$ ($z \to \infty$) it is convenient to use formula (10). Since when $z \to \infty$, $P_l(z) \sim z^l$ (for $\mathrm{Re}\, l > -\frac{1}{2}$), the asymptotic behavior of A_1 as $z \to \infty$ is determined by the position of the nearest singularity on the right for the function $\varphi_l^{(1)}$.

The simplest asymptotic behavior, of the form $sf(t)$, which is discussed in [2], corresponds to the case where $\varphi_l^{(1)}$ has as its nearest singularity for arbitrary t a simple pole at $l = 1$. However, the unitarity condition (18) excludes the possibility that $\varphi_l^{(1)}$ goes to infinity for real l as we approach the first singular point on the right, since it follows from the unitarity condition that $(q/\omega)|\varphi_l^{(1)}| \leq 1$.

In the nonrelativistic theory [1] the only singularities of $\varphi_l^{(1)}$ are poles in the upper half-plane and, consequently, the asymptotic behavior has the form

$$A_1 \sim f(t)\, s^{l_1(t)}, \tag{25}$$

where $l_1(t) = \alpha(t) + i\beta(t)$ is necessarily complex. The same asymptotic behavior was assumed in relativistic theory in the work of Chew and Frautschi.[3] Such behavior is possible, but it is important to understand that it leads to an essentially nondiffractive character of the scattering in the s channel for $s \to \infty$ (cf. [4]). In fact, if we continue (25) into the region $t < 4\mu^2$, then $\beta(t) = 0$ [the pole moves onto the real axis; for $t < 4\mu^2$ we do not have the condition (18)] and we will have

$$A_1 \sim f(t)\, s^{\alpha(t)},$$

where $\alpha(t) \neq \mathrm{const}$ (since the location of the pole of the function $\varphi_l^{(1)}(t)$, which is analytic in t, is a function of t). The assertion of Chew and Frautschi that α is approximately constant in the interval $-20m_\pi^2 < t < 0$ is, to say the least, not understandable.

For $t = 0$, as shown by Froissart,[5] $|A_1| \leq Cs \ln^2 s$, and therefore $\alpha(0) \leq 1$. In order to get a constant total cross section, it is necessary that $\alpha(0) = 1$. Then in the physical region of the s channel (region I in Fig. 1), for small t

$$A_1 \sim sf(t)\, e^{\gamma t \ln s} \tag{26}$$

falls off very rapidly with increasing $-t$ for large s, so that the diffraction cone (the region of values of t for which $d\sigma/dt$ does not tend to zero) is not independent of energy, but has a size $t \sim -1/\ln s$. In particular this has the consequence that the elastic scattering cross section tends to zero at high energies. If with such a behavior for $A_1(s,t)$ we calculated the partial wave amplitudes $a_l(s)$ in the channel s, then in contrast to the case of diffraction, in which $a_l(s) \sim 1$ for $l \lesssim p/\mu$ while the amplitudes drop rapidly for $l > p/\mu$, we would find $a_l(s) \sim 1/\ln s$ for $l \lesssim p\mu^{-1} \ln^{1/2} s$, while the amplitudes would fall off rapidly for $l > p\mu^{-1} \ln^{1/2} s$. This means that as the energy increases the particles "swell" and become more transparent.

The asymptotic behavior $A_1(s,t) = sB(\xi)f(t)$ (where $\xi = \ln s$), which was discussed in [2] and corresponds to a decreasing cross section, occurs if $\varphi_l^{(1)}(t)$ has a branch point for $l = 1$ (for arbitrary t). The fact that by virtue of the unitarity condition $\varphi_l^{(1)}(t)$ remains finite as we approach the branch point, has the consequence that $B(\xi)$ falls off faster than $1/\xi$. The appearance of such a branch point can be pictured classically, for example as follows. Suppose that the interaction in states with l values other than $l = 0$ has the character $-\alpha/r^2$ with $\alpha = \frac{9}{4}$. Then for $l = 1$ the function $\varphi_l^{(1)}(t)$ will have a branch point corresponding to collapse into the center, but $\varphi_l^{(1)}$ will still have a meaning. We note that in nonrelativistic theory among the interactions $1/r^n$ for small r only the interaction $1/r^2$ has a real effect on the analytic properties of $\varphi_l^{(1)}(t)$, since for $n < 2$ the function $\varphi_l^{(1)}$ is meromorphic for $\mathrm{Re}\, l > -\frac{1}{2}$, while for $n > 2$ it does not exist in general. If $\varphi_l^{(1)}$ has a branch point, then $B(\xi) \sim 1/\xi^{3/2}$ for $\xi \to \infty$.

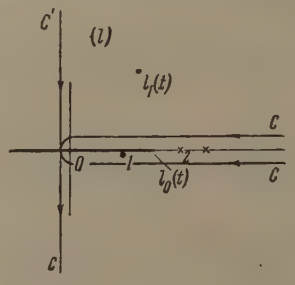

FIG. 2

Let us discuss briefly the possibility of such an asymptotic behavior of $A_1(s,t)$ that, no matter how complicated the asymptotic form for $t > 4\mu^2$ (region I, III in Fig. 1), for $t < 4\mu^2$ it is equal to $sf(t)$. It is clear that if $\varphi_l^{(1)}$ is a meromorphic function, then as we go to $t < 4\mu^2$ a pole cannot develop for $l = 1$ independently of t. But if there is a branch point $l = l_0(t)$ on the real axis (Fig. 2), then it may turn out that $\varphi_l^{(1)}$ has a pole for $l = 1$ which lies on only one side of the cut. The presence of such a pole does not contradict the unitarity condition. If, as t decreased, $l_0(t)$ moved toward the left, and for $t < 4\mu^2$ became less than

unity, leaving a pole on the right, the asymptotic behavior when $t < 4\mu^2$ would be determined by the pole and would have the form $sf(t)$. It is easy to see that in order for the pole to remain at the same place when $t < 4\mu^2$, it is necessary that it be located initially on the lower edge of the cut.

One may also consider a possible behavior like $l_0(t)$ in the region $t > 4\mu^2$. This problem contains several interesting points which we shall not discuss here. We note only that, even though one can make no rigorous assertions, from studies of these possibilities one becomes convinced that a behavior like $sf(t)$ in the region $t > 4\mu^2$ is impossible to obtain if we restrict ourselves to only two-particle states in the unitarity condition for the t channel, and that even the inclusion of any finite number of states may not be enough.

In conclusion I wish to thank I. T. Dyatlov, L. D. Landau, I. Ya. Pomeranchuk and K. A. Ter-Martirosyan for valuable discussions, and Chew, Frautschi and Froissart for sending me their preprints.

APPENDIX I

To prove formula (9), we consider the well-known relation

$$\frac{1}{z_2 - z_1} = \frac{1}{2i} \sum_{l=0}^{\infty} (2l+1)\, P_l(z_1)\, Q_l(z_2), \qquad \text{(AI.1)}$$

which is valid for

$$|z_1 + \sqrt{z_1^2 - 1}| < |z_2 + \sqrt{z_2^2 - 1}|. \qquad \text{(AI.2)}$$

We shall assume that z_2 is real and larger than one, and write an expression for the right side of (AI.1) which is valid for arbitrary complex z_1. To do this we use the Watson transformation:

$$\frac{1}{z_2 - z_1} = -\frac{i}{2} \int_C dl\, (2l+1)\, \frac{P_l(-z_1)}{\sin l\pi}\, Q_l(z_2). \qquad \text{(AI.3)}$$

The contour C is shown in Fig. 2. The integral converges if (AI.2) is satisfied. For $z_1 > 1$, the expression (AI.3) appears at first glance to be undefined, since $P_l(x)$ for integer l has a branch point at $x = -1$. But since

$$\frac{i}{2}\,[P_l(-z - i\varepsilon) - P_l(-z + i\varepsilon)] = \sin l\pi \cdot P_l(z), \qquad \text{(AI.4)}$$

the integral on the right side of (AI.3) vanishes for the difference of the values on the two sides of the cut.

Since for large l and $|z| > 1$

$$P_l(z) \sim (2\pi\, l \operatorname{sh}\xi)^{-1/2} e^{(l+1/2)\xi},\quad Q_l(z) \sim (\pi/2l \operatorname{sh}\xi)^{1/2} e^{-(l+1/2)\xi},$$
$$z = \operatorname{ch}\xi \qquad \text{(AI.5)}^*$$

*sh = sinh.

and are entire functions of l for $\operatorname{Re} l > -1$, for $z_1 < z_2$ the integration contour on the right side of (AI.3) can be deformed into the contour C′. The integral over the contour C′ will converge for all complex z and for real values satisfying $1 < z_1 < z_2$. We may therefore calculate the difference of the values with $z_1 \pm i\epsilon$ for the right and left sides. As a result we get, using (AI.4),

$$\delta(z_2 - z_1) = \frac{i}{2\pi} \int_{a-i\infty}^{a+i\infty} dl\, (2l+1)\, P_l(z_1)\, Q_l(z_2), \qquad \text{(AI.6)}$$

QED.

This formula can also be proved directly. In particular, the fact that the right side is equal to zero for $z_1 < z_2$ follows immediately from the fact that in this case the contour of integration can be closed to the right.

In order to show that the right side of (AI.6) is equal to zero for $z_1 > z_2$, it is convenient to take $a = -1/2$: then using the relations

$$P_{-1/2-\gamma} = P_{-1/2+\gamma},\quad Q_{-1/2-\gamma} = Q_{-1/2+\gamma} + \frac{\pi}{\operatorname{tg}(-1/2+\gamma)\,\pi} P_{1/2+\gamma}, \qquad \text{(AI.7)}$$

it is easy to show that

$$\int_{-i\infty}^{i\infty} \gamma d\gamma P_{-1/2+\gamma}(z_1)\, Q_{-1/2+\gamma}(z_2) = \int_{-i\infty}^{i\infty} \gamma d\gamma P_{-1/2+\gamma}(z_2)\, Q_{-1/2+\gamma}(z_1), \qquad \text{(AI.8)}$$

from which it follows that the right side of (AI.6) is a symmetric function of z_1 and z_2.

APPENDIX II

To prove that the Mandelstam equation (2) is equivalent to Eq. (13), we may use the relation

$$2\pi^2 \frac{\vartheta\left(z - z_1 z_2 - \sqrt{(z_1^2-1)\,(z_2^2-1)}\right)}{\left[\sqrt{z^2 + z_1^2 + z_2^2 - 2z z_1 z_2 - 1}\,\right]^{1/2}}$$
$$= \frac{i}{2} \int_{a-i\infty}^{a+i\infty} (2l+1)\, dl\, Q_l(z_1)\, Q_l(z_2)\, P_l(z),$$
$$a > -1,\ \vartheta(x) = \begin{cases} 1 & x > 0 \\ 0 & x < 0 \end{cases}, \qquad \text{(AII.1)}$$

which can, for example, be proved as follows.

Consider the expression for the absorptive part of the square diagram and carry out the angle integration using (AI.1); we then get

$$\int \frac{dz_1' dz_2'}{\left[1 + 2zz_1'z_2' - z^2 - z_1'^2 - z_2'^2\right]^{1/2}} \frac{1}{z_1 - z_1'} \frac{1}{z_2 - z_2'}$$
$$= \sum_{l=0}^{\infty} Q_l(z_1)\, Q_l(z_2)\, P_l(z)\,(2l+1),$$
$$-1 < z_1',\ z_2' < 1,\quad z_1, z_2 > 1. \qquad \text{(AII.2)}$$

The left side of (AII.2) is easily calculated, and its imaginary part coincides with the left side of

(AII.1). The imaginary part of the right side of (AII.2) is calculated in exactly the same way as we used for obtaining formula (AI.6), and is equal to the right side of (AII.1). Substituting (AII.1) in Eq. (2) and using (10), (11) and (12), we easily obtain Eq. (13).

[1] T. Regge, Nuovo cimento **14**, 951 (1959); **18**, 947 (1960).

[2] V. N. Gribov, Nuclear Phys. **22**, 249 (1961).

[3] G. F. Chew and S. C. Frautschi, Phys. Rev. Letters **5**, 580 (1960).

[4] V. N. Gribov, JETP **41**, 667 (1961), Soviet Phys. JETP **14**, 478 (1962).

[5] M. Froissart, Phys. Rev. **123**, 1053 (1961).

Translated by M. Hamermesh
330

RADIATION OF PLASMA WAVES BY A CHARGE MOVING IN A MAGNETOACTIVE PLASMA

V. Ya. ÉĬDMAN

Radiophysics Institute, Gorkii State University

Submitted to JETP editor July 21, 1961; resubmitted September 9, 1961

J. Exptl. Theoret. Phys. (U.S.S.R.) 41, 1971-1977 (December, 1961)

The spectral distribution and the angle-energy distribution of plasma waves radiated by a charge moving in a magnetoactive plasma are investigated with spatial dispersion taken into account.

THE radiation of electromagnetic waves by a charge moving in a magnetoactive plasma has been considered by a number of authors (cf. [1,2]). As a rule, however, these authors have not taken account of spatial dispersion, that is to say, thermal motion of the electrons has been neglected in these analyses. In many cases, however, spatial dispersion can be extremely important. For instance, there is the possibility of generating new kinds of characteristic waves that do not exist in a cold plasma. Shafranov[3] has obtained an expression for the energy loss of a charge moving in a magnetoactive plasma. However, his expression applies for a cold plasma only ($v_T = 0$, v_T is the mean thermal velocity of the plasma electrons).

In the present paper, using a method different from that used earlier,[2,3] we have obtained an expression for the total energy loss of a charge moving in a magnetoactive plasma with spatial dispersion taken into account. This general expression is used to compute the energy of the plasma wave radiated by the charge. Inasmuch as this energy can be appreciable, the formulas obtained can in certain cases be important in the analysis of radio emission from the radiation belts around the earth,[4] sporadic radio emission from the sun and so on.

Starting with Maxwell's equations for the medium we obtain the following equation for the electric field:

$$-\Delta \mathbf{E} + \mathbf{e}_\alpha \frac{\partial^2 E_\beta}{\partial x_\alpha \partial x_\beta} + \frac{1}{c^2}\mathbf{e}_\alpha \varepsilon_{\alpha\beta}\frac{\partial^2 E_\beta}{\partial t^2} = -\frac{4\pi e}{c^2}\frac{\partial}{\partial t}\mathbf{v}\delta(\mathbf{r}-\mathbf{r}_e), \quad (1)$$

$$\mathbf{D} = \mathbf{e}_\alpha \varepsilon_{\alpha\beta} E_{\alpha\beta}.$$

Here, indices that appear twice indicate summation, $\mathbf{e}_\alpha$ is a unit vector along the coordinate axis denoted by α and $\mathbf{r}_e$ is the radius vector to the charge moving in a magnetic field $\mathbf{H}_0$ parallel to the z axis, i.e.,

$$\mathbf{r}_e\{r_0\cos\Omega t;\ \ r_0\sin\Omega t;\ \ v_0 t\},$$
$$\mathbf{v}\{-v_1\sin\Omega t;\ \ v_1\cos\Omega t;\ \ v_0\},$$
$$v_1 = r_0\Omega, \qquad \Omega = \omega_H\sqrt{1-\beta^2},$$
$$\beta^2 = c^{-2}(v_1^2+v_0^2), \quad \omega_H = eH_0/mc. \quad (2)$$

We expand (1) in a Fourier integral:

$$\mathbf{E}(\mathbf{r}, t) = \int \mathbf{E}_{\omega,\mathbf{k}} e^{i(\mathbf{kr}-\omega t)}\, d\omega\, d\mathbf{k} + \text{c.c.} \quad (3)$$

Substituting (3) in (1) and using (2) and the relations

$$\delta(\mathbf{r}-\mathbf{r}_e) = \frac{1}{(2\pi)^3}\int e^{i(\mathbf{r}-\mathbf{r}_e)\mathbf{k}}\, d\mathbf{k}$$
$$= \frac{1}{(2\pi)^3}\sum_{s=-\infty}^{\infty}\int J_s(\xi)\, e^{i[\mathbf{kr}-t(s\Omega+kv_0\cos\theta)]}\, d\mathbf{k},$$

we obtain the following equations for the Fourier components $\mathbf{E}_{\omega\mathbf{k}\beta}$ (cf. [1]):

$$T_{\alpha\beta}E_{\omega\mathbf{k}\beta} = -\frac{ei}{2\pi^2}\sum_{s=-\infty}^{\infty} j_\alpha \frac{\delta(\omega - kv_0\cos\theta - s\Omega)}{\omega}; \quad (4)$$
$$j_x = -v_1 i J_s'(\xi), \qquad j_y = \xi^{-1}v_1 s J_s(\xi), \qquad j_z = v_0 J_s(\xi),$$

where θ is the angle between $\mathbf{k}$ and $\mathbf{H}_0$, $J_S(\xi)$ is the Bessel function and $\xi = kr_0\sin\theta$. The components of $T_{\alpha\beta}$ are:

$$T_{\alpha\beta} = n^2(\varkappa_\alpha\varkappa_\beta - \delta_{\alpha\beta} + \varepsilon_{\alpha\beta},$$
$$n^2 = k^2c^2/\omega^2, \qquad \varkappa_\alpha = k_\alpha/k. \quad (5)$$

Using the symmetry of the problem we take $\kappa_X = 0$, $\kappa_y = \sin\theta$, $\kappa_Z = \cos\theta$, i.e., the vector $\mathbf{k}$ is assumed to lie in the yz plane.

The solution of (4) is elementary:

$$E_{\omega\mathbf{k}\beta} = -\frac{ei}{2\pi^2\omega}T^{-1}_{\beta\alpha}\, j_\alpha\delta(\omega - kv_0\cos\theta - s\Omega); \quad (6)$$

where $T^{-1}_{\beta\alpha}$ is the reciprocal of $T_{\alpha\beta}$.

The effect of spatial dispersion on the dielectric tensor of a magnetoactive plasma $\epsilon_{\alpha\beta}(\omega, \mathbf{k})$ has been considered by a number of authors (cf. [3,5,6]). Hence we shall not stop here to give the values of

$\epsilon_{\alpha\beta}(\omega, \mathbf{k})$, which are taken from the cited papers,* but immediately write an expression for the components of $T^{-1}_{\alpha\beta}$ [cf. (5)]:

$$T^{-1}_{xx} = \Delta^{-1}\{-n^2(\varepsilon_1 \sin^2\theta + \varepsilon_3\cos^2\theta) + \varepsilon_1\varepsilon_3 - \varepsilon_5^2\},$$
$$T^{-1}_{xy} = \Delta^{-1}\{i\varepsilon_2(-n^2\sin^2\theta + \varepsilon_3) + \varepsilon_4(n^2\sin\theta\cos\theta - i\varepsilon_5)\}$$
$$= T^{-1*}_{yx},$$
$$T^{-1}_{xz} = \Delta^{-1}\{-i\varepsilon_2(n^2\sin\theta\cos\theta + i\varepsilon_5) - \varepsilon_4(-n^2\cos^2\theta + \varepsilon_1)$$
$$= T^{-1*}_{zx}$$
$$T^{-1}_{yy} = \Delta^{-1}\{(-n^2 + \varepsilon_0)(-n^2\sin^2\theta + \varepsilon_3) - \varepsilon_4^2\},$$
$$T^{-1}_{yz} = -\Delta^{-1}\{(-n^2 + \varepsilon_0)(n^2\sin\theta\cos\theta + i\varepsilon_5) - i\varepsilon_4\varepsilon_2\}$$
$$= T^{-1*}_{zy},$$
$$T^{-1}_{zz} = \Delta^{-1}\{(-n^2 + \varepsilon_0)(-n^2\cos^2\theta + \varepsilon_1) - \varepsilon_2^2\}. \quad (7)$$

Here

$$\varepsilon_{xx} = \varepsilon_0, \quad \varepsilon_{yy} = \varepsilon_1, \quad \varepsilon_{xy} = -i\varepsilon_2, \quad \varepsilon_{zz} = \varepsilon_3,$$
$$\varepsilon_{xz} = \varepsilon_4, \quad \varepsilon_{yz} = i\varepsilon_5$$

(cf. [3,5,6]) while $\Delta = |T_{\alpha\beta}|$ is the determinant made up of the components of $T_{\alpha\beta}$. We note that the dispersion relation is obtained from the condition $\Delta(\omega, \mathbf{k}) = 0$.

Now, using (2), (3), and (6) it is easy to compute the energy loss of a charge moving in the plasma ($\tau = 2\pi/\Omega$):

$$A = e\int_0 \mathbf{vE}(\mathbf{r}=\mathbf{r}_e)dt$$
$$= -\frac{e^2\tau i}{2\pi^2}\sum_{s=-\infty}^{\infty}\int\frac{d\omega}{\omega}j_\alpha j^*_\beta T^{-1}_{\beta\alpha}\delta(\omega - kv_0\cos\theta - s\Omega)\,d\mathbf{k} + \text{c.c.} \quad (8)$$

In what follows we shall not be interested in the total energy loss of the moving particle, but only that part associated with the radiation of weakly damped electromagnetic waves, particularly plasma waves. Thus we can limit ourselves to the case $\beta_T^2 \ll 1$, i.e., the case where the velocities of the plasma electrons are small. Then, if the following conditions are satisfied[7]:

$$(v_T k/\omega_H)^2\sin^2\theta \ll 1, \quad (\beta_T n\cos\theta)^2 \ll 1;$$
$$(1 - \omega_H^2/\omega^2)^3 \gg \beta_T^2, \quad 1 - 4\omega_H^2/\omega^2 \gg \beta_T^2, \quad (9)$$

the left-hand side of the dispersion relation can be written in the form† (cf. [7])

$$\Delta = |T_{\alpha\beta}| = \frac{1}{1-u}\{\beta_T^2 VRn^6 - [1 - u - V + uV\cos^2\theta]\,n^4$$
$$+ [2(1-V)^2 + uV\cos^2\theta - u(2-V)]n^2$$
$$+ (1-V)[u - (1-V)^2]\}; \quad (10)$$

where

$$u = \frac{\omega_H^2}{\omega^2}, \quad V = \frac{\omega_0^2}{\omega^2} = \frac{4\pi e^2 N}{m\omega^2},$$

$$R = \frac{3\sin^4\theta}{1-4u} + \left[1 + \frac{5-u}{(1-u)^2}\right]\sin^2\theta\cos^2\theta + 3(1-u)\cos^4\theta$$

(N is the number density of the plasma electrons). We need retain only terms with β_T^0 in the numerators of the expressions in (7) so that

$$\varepsilon_0 = \varepsilon_1 = 1 - V/(1-u), \quad \varepsilon_2 = -V\sqrt{u}/(1-u),$$
$$\varepsilon_3 = 1 - V, \quad \varepsilon_4 = \varepsilon_5 = 0. \quad (11)$$

The equation $\Delta(\omega, \mathbf{k}) = 0$ is cubic in n^2 indicating the possibility that three characteristic waves can be radiated. To calculate the radiated energy associated with each wave, we substitute the values of $T^{-1}_{\alpha\beta}$ [cf. (7)] in (8), taking account of (10) and (11) and carrying out the appropriate integration. The difference between the present case and the case of an electron moving in a cold plasma appears at values of the variables ω and θ for which $n^2 \gg 1$.

A particularly simple result is obtained if the following condition is satisfied[7]:

$$F = 1 - u - V + uV\cos^2\theta \gg \beta_T. \quad (12)$$

Taking account of (9) and (12) we can write (10) in the form

$$\Delta = RV\beta_T^2(n^2 - F/VR\beta_T^2)(n^4 + Bn^2 + C)/(1-u),$$
$$B = -F^{-1}[2(1-V)^2 + uV\cos^2\theta - u(1-V)], \quad (13)$$
$$C = -F^{-1}(1-V)[u - (1-V)^2].$$

The second bracket in (13) corresponds to the radiation of ordinary and extraordinary waves in a cold plasma. The first bracket, however, which is important only when $n^2 \gg 1$, corresponds to the radiation of a longitudinal wave. The electric field of this wave forms a very small angle with the vector $\mathbf{k}$.

Using (7), (11) and (13) we write (8) in the form ($\tilde{T}^{-1}_{\beta\alpha} = T^{-1}_{\beta\alpha}\Delta$):*

$$A = -\frac{e^2\tau i}{2\pi^2\beta_T^2}\sum_{s=-\infty}^{\infty}\int\frac{\delta(\omega - kv_0\cos\theta - s\Omega)\,j_\alpha j^*_\beta\tilde{T}^{-1}_{\beta\alpha}(1-u)\,d\omega d\mathbf{k}}{\omega RV(n^2 - F/RV\beta_T^2)(n^4 + Bn^2 + C)}$$
$$+ \text{c.c.} = A_{1,2} + A_3. \quad (14)$$

Here, the term A_3 is associated with the longitudinal wave

$$n^2 = F/RV\beta_T^2 = n_3^2, \quad (15)$$

while $A_{1,2}$ correspond to ordinary and extraordinary waves ($n^2 = n_{1,2}^2$). For example, the Cerenkov

*Everywhere below it is assumed that the plasma electrons have a Maxwellian distribution in momentum space in the zeroth approximation. Then, for example, $v_T^2 = T/m$ when $\beta_T^2 = v_T^2/c^2 \ll 1$.

†Equation (10) is easily obtained by expanding in powers of $\varepsilon_{\alpha\beta}$ in (7) [5,6] keeping terms of order β_T^2 where necessary (cf. also [8]).

*We note that the integration in (14) extends over values of ω and θ that satisfy (9) and (12).

losses due to radiation of the ordinary and extraordinary waves by a charge moving along the magnetic field $W_{1,2}$ can be obtained from (7), (11) and (13):

$$W_{1,2} = -A_{1,2} = -\frac{e^2\tau v_0^2 i}{2\pi^2}\int \frac{\delta(\omega - kv_0\cos\theta)\,[n^4\cos^2\theta - n^2\varepsilon_1(1+\cos^2\theta) + \varepsilon_1^2 - \varepsilon_2^2]\,d\omega dk}{\omega\,(\varepsilon_1\sin^2\theta + \varepsilon_3\cos^2\theta)\,(n^2 - n_1^2)\,(n^2 - n_2^2)} + \text{c.c.},$$

where ϵ_1, ϵ_2, and ϵ_3 are determined by (11). Our expression for $W_{1,2}$ agrees with the corresponding expression given by Sitenko and Kolomenskiĭ [1].

Nothing new is learned from studying the term $W_{1,2} = -A_{1,2}$ [cf. (14)], which is essentially the radiation in a cold plasma (cf. [2]). For this reason, we discuss below only the plasma radiation (A_3). Because $n_3^2 \gg 1$ the expression for A_3 can be simplified considerably. Keeping only the highest power of n in $\tilde{T}^{-1}_{\alpha\beta}$ we have

$$\tilde{T}^{-1}_{yy} \approx n^4\sin^2\theta, \quad \tilde{T}^{-1}_{yz} \approx n^4\sin\theta\cos\theta, \quad \tilde{T}^{-1}_{zz} \approx n^4\cos^2\theta. \tag{16}$$

The other components of $\tilde{T}^{-1}_{\alpha\beta}$ can be neglected. Thus

$$G = j_\alpha j_\beta^* \tilde{T}^{-1}_{\beta\alpha} = n_3^4\left(\frac{v_{1s}}{\xi}\sin\theta + v_0\cos\theta\right)^2 J_s^2(\xi).$$

Since (14) contains a δ-function of argument $y = \omega - kv_0\cos\theta - s\Omega$, we have $G(y=0) = c^2 n_3^2 J_s^2(\xi)$. Thus, the final expression is ($x = \cos\theta$)

$$A_3 = \sum_{s=-\infty}^{\infty} A_3^{(s)} = -\frac{e^2\tau}{c\beta_T^2}\sum_{s=-\infty}^{\infty}{}'\int \frac{J_s^2(\xi)\,|\,\omega^2 - \omega_H^2\,|\,dx}{Vn_3\,|\,Rd\,[\omega\,(1-\beta_0 n_3 x)]/d\omega\,|}$$

$$= -\frac{e^2\tau}{v_0\omega_0^2\beta_T^2}\sum_{s=-\infty}^{\infty}{}'\int \frac{J_s^2(\xi)\,|\,\omega^2 - \omega_H^2\,|\,\omega\,d\omega}{n_3\,|\,Rd\,(n_3 x)/dx\,|}. \tag{17}$$

In order to go over from (14) to (17) it is necessary to carry out the integration over k, using the pole of the integrand at $n^2 = n_3^2$. The integration over $d\omega$ or dx is carried out with the δ-function $\delta(\omega - kv_0\cos\theta - s\Omega)$, i.e.,

$$\omega\,(1 - \beta_0 n_3\cos\theta) = s\Omega, \qquad \omega > 0, \qquad \beta_0 = v_0/c. \tag{18}$$

In view of the above the limits of integration in (17) are determined from the requirement that the function $x(\omega)$ or $\omega(x)$, given by (18), must be real.

We now consider (17) for a number of particular cases. The Cerenkov radiation corresponds to the s = 0 term in (17):

$$A_3^{(0)} = -\frac{e^2\tau}{v_0\beta_T^2\omega_0^2}\int_{\beta_0 n_3 \geq 1} \frac{|\,\omega^2 - \omega_H^2\,|\,J_0^2(\xi)\,\omega d\omega}{n_3\,|\,Rd\,(n_3 x)/dx\,|}. \tag{19}$$

For Cerenkov radiation of the plasma wave, i.e., for $v_1 = 0$, (19) becomes

$$A_3^{(0)} = -\frac{e^2\tau}{v_0\beta_T^2\omega_0^2}\int_{\beta_0 n_3 \geq 1} \frac{|\,\omega^2 - \omega_H^2\,|\,\omega d\omega}{n_3\,|\,Rd\,(n_3 x)/dx\,|}. \tag{20}$$

The value of $\cos\theta = x$ in the integrals (19) and (20) is determined from the equation $1 - \beta_0 n_3(\omega, x)\,x = 0$. The integration in (2) can be carried out easily if the charge moves in an isotropic medium ($\omega_H = 0$, $n_3^2 = (\omega^2 - \omega_0^2)/3\beta_T^2\omega_0^2$, $R = 3$). Using some simple transformations we have

$$A_3^{(0)} = -\frac{e^2\tau}{v_0}\int_{\omega^2=\bar{\omega}^2}^{\omega_m^2} \frac{d\omega\omega^3}{\omega^2 - \omega_0^2} = -\frac{e^2\tau}{v_0}\left\{\frac{1}{2}\,[\omega_m^2 - \bar{\omega}^2] + \omega_0^2\ln\frac{k_m v_0}{\omega_m}\right\}, \qquad \bar{\omega}^2 = \omega_0^2(1 + 3v_T^2/v_0^2), \tag{21}$$

where, in the usual way, the frequency ω_m is determined from the condition of applicability of macroscopic electrodynamics (cf. [3]), $k_m = \omega_m n_3(\omega_m)/c$. The lower limit of integration in (21) corresponds to the Cerenkov radiation threshold $\beta_0^2 n_3^2 = 1$. In the present case $\beta_T^2 \ll 1$ and $\omega_m - \omega_0 \ll \omega_0$. Hence, the radiated energy associated with Cerenkov excitation of the plasma wave $W_3^{(0)} = -A_3^{(0)}$ is characterized by the quantity

$$W_3^{(0)} \approx \frac{e^2\tau\omega_0^2}{v_0}\ln\frac{k_m v_0}{\omega_0},$$

which, as expected, coincides with the polarization losses in a cold plasma.

When $\xi \ll 1$, i.e., oscillatory motion, the summation in (17) must contain the $s = \pm 1$ terms in addition to (20). As a result we have ($\beta_1 = v_1/c$)

$$A_3^{(\pm 1)} = \frac{-p_0^2\tau}{4v_T^2 v_0\omega_0^2}\int \frac{|\,\omega^2 - \omega_H^2|\,n_3\sin^2\theta\,\omega^3 d\omega}{|\,Rd\,(n_3 x)/dx\,|}, \qquad p_0 = er_0, \tag{22}$$

where $x = \cos\theta$ is determined from the Doppler relations (18) for $s = \pm 1$ respectively.

When the electron moves in a circle ($v_0 = 0$) the radiated energy is given by the expression [cf. (17)]

$$A_3^{(s)} = -\frac{e^2\tau}{cV\beta_T^2}\int \frac{|\,s^2\Omega^2 - \omega_H^2\,|\,J_s^2(\xi)\,dx}{n_3\,|\,R\,|} \qquad (\omega = s\Omega,\ s = 1, 2, 3, \ldots). \tag{23}$$

The applicability of (23) is determined by (9). Strictly speaking it can only be used when the relativistic dependence of Ω on velocity ($\Omega = \omega_H\sqrt{1-\beta^2}$) is taken into account.

If the motion is of oscillatory nature, i.e., $\xi = \beta_1 n_3\sin\theta \ll 1$, the basic contribution to the radiation comes from the s = 1 term [cf. (23)] and we have

$$A_3^{(1)} = -\frac{p_0^2\tau\Omega^2\,|\,\Omega^2 - \omega_H^2\,|}{4\beta_T^2 c^3 V}\int \frac{n_3\sin^2\theta\,dx}{|\,R\,|}, \qquad p_0 = er_0. \tag{24}$$

We may note that the last expression is equal to twice the energy of a plasma wave radiated by an oscillator oscillating perpendicularly to the magnetic field H_0. If the oscillator oscillates at a frequency Ω_0 in an isotropic plasma, i.e.,

$H_0 = 0$, $n_3^2 = (\Omega_0^2 - \omega_0^2)/3\beta_T^2\omega_0^2$, $1 - \omega_0^2/\Omega_0^2 \ll 1$ (cf. [9]), we have from (24)

$$A_3^{(1)} = -p_0^2\tau\Omega_0^4 n_3/9\beta_T^2 c^3. \qquad (25)$$

Proceeding as in the case of radiation in a cold plasma[2], we can obtain from (17) a formula that applies for high harmonic numbers:

$$|s| = \omega\,|\,1 - \beta_0 n_3\cos\theta\,|\,/\,\Omega \gg 1.$$

As a result, for example, when $\beta_1 n_3 \sin\theta\,/|\,1 - \beta_0 n_3\sin\theta\,| \gtrsim 1$, we have

$$A_3^{|s|\gg 1} = -\frac{2^{2/3}e^2\tau}{\pi c\Omega^{1/3}\beta_1^{2/3}\beta_T^2}\int\frac{d\omega\,dx\Phi^2(z)\,|\,\omega^2 - \omega_H^2\,|}{V(\omega n_3\sin\theta)^{2/3}n_3\,|\,R\,|}, \qquad (26)$$

where $\Phi(z)$ is the Airy function [10]:

$$\Phi(z) = \frac{1}{\sqrt{\pi}}\int_0^\infty \cos\left(\frac{t^3}{3} + zt\right)dt,$$

$$z = \left(\frac{2\omega^2}{\Omega^2 n\beta_1\sin\theta}\right)^{1/3}[1 - \beta_0 n_3\cos\theta - \beta_1 n_3\sin\theta].$$

A characteristic feature of all the expressions we have obtained describing energy radiated by plasma waves is the fact that A_3 is proportional to a large quantity $1/\beta_T^2$. For this reason, in certain cases the energy radiated by the plasma wave can be quite appreciable and can even be greater than the energy associated with the transverse waves. Thus, in the case of an oscillator in an isotropic medium the energy ratio for the longitudinal wave [cf. (25)] and the transverse wave ($A_{1,2}^{(1)} = -2p_0^2\Omega_0^4\tau n_1/3c^3$, $n_1^2 = 1 - V$) is $A_3^{(1)}/A_{1,2}^{(1)} = 1/6\beta_T^3 \gg 1$, (cf. [9]). A similar relation will obviously hold for an oscillator in a magnetoactive plasma.

In conclusion we direct attention to the following situation. As we have indicated above, the Cerenkov radiation in a plasma is characterized by the quantity

$$A_3^{(0)} \approx (-e^2\tau\omega_0^2/v_0)\ln(k_m v_0/\omega_0).$$

Thus, when longitudinal waves are excited by an oscillator (with peak velocity v_0) the energy radiated by the plasma wave is appreciably greater than that due to Cerenkov radiation:

$$A_3^{(1)}/A_3^{(0)} \approx \beta^3 n_3/9\beta_T^2 \gg 1.$$

In the final analysis this situation comes about because the frequency spectrum of the excitation current that excites the Cerenkov radiation [$j = v\delta(r - v_0 t)$] is continuous, in contrast with the oscillator, which is a monochromatic source. The Fourier component of the longitudinal field in an isotropic plasma (6) is given by $E_{\omega\mathbf{k}}^{\parallel} \approx 1/\epsilon_{\parallel}(\omega, \mathbf{k})$ [cf. [3], Eq. (6.38)] where $\epsilon_{\parallel}(\omega, \mathbf{k})$ is the dielectric constant for the longitudinal wave; this is a small quantity if the spatial dispersion is small:

$$\varepsilon_{\parallel} = 1 - \omega_0^2/\omega^2 - 3k^2 v_T^2/\omega^2, \qquad \omega - \omega_0 \ll \omega_0.$$

The order of the singularity $1/\epsilon(\omega, \mathbf{k})$ is reduced by integration over frequency. This means that the radiated energy due to the excitation of plasma oscillations by a monochromatic external force $\omega \approx \omega_0$ is greater than that due to excitation by a force with a continuous frequency spectrum.* It will be evident that the above considerations also apply to the excitation of a longitudinal wave in a magnetoactive plasma.

[1] A. G. Sitenko and A. A. Kolomenskiĭ, JETP 30, 511 (1956), Soviet Phys. JETP 3, 410 (1956).

[2] V. Ya. Éĭdman, JETP 34, 131 (1958) and 36, 1335 (1959), Soviet Phys. JETP 7, 91 (1958) and 9, 947 (1959).

[3] V. D. Shafranov, Electromagnitnye volny v plazme, Institut atomnoĭ energii im. I. V. Kurchatova (Electromagnetic Waves in Plasma, I. V. Kurchatov Institute of Atomic Energy), AN SSSR, 1960.

[4] E. A. Benediktov and V. Ya. Éĭdman, Izv. Vuzov, Radiophysics 4, 253 (1961).

[5] B. A. Trubnikov, Fizika plazmy i problema upravlyaemykh termoyadernykh reaktsii (Plasma Physics and the Problem of a Controlled Thermonuclear Reaction) AN SSSR, 1958, Vol. 3, p. 104.

[6] Ibid., Vol. 4, p. 416.

[7] V. L. Ginzburg, Rasprostranenie elektromagnitnykh voln v plazme (Propagation of Electromagnetic Waves in Plasma) Fizmatgiz, 1960.

[8] B. N. Gershman, JETP 24, 453; 659 (1953).

[9] A. A. Andronov and G. V. Gorodinskii, Izv. Vuzov, Radiophysics (1962) (in press).

[10] V. A. Fock, Tablitsy funktsii Éiri (Tables of Airy Functions) M., 1946.

Translated by H. Lashinsky
331

*The situation here is, to some extent, similar to that which obtains when a harmonic oscillator is driven by an external force.

EFFECT OF MUTUAL ENTRAINMENT OF ELECTRONS AND PHONONS ON THE TRANSVERSE ELECTRICAL CONDUCTIVITY IN A STRONG MAGNETIC FIELD

L. É. GUREVICH and A. L. ÉFROS

Leningrad Physico-Technical Institute, Academy of Sciences, U.S.S.R.

Submitted to JETP editor July 21, 1961

J. Exptl. Theoret. Phys. (U.S.S.R.) 41, 1978-1985 (December, 1961)

It is shown that the entrainment of phonons by electrons significantly changes the transverse electrical conductivity in a strong magnetic field at low temperatures ($T \ll \Theta$). The order of magnitude and the temperature dependence change in metals and semimetals. In semiconductors, the dependence on the magnetic field may also change.

1. INTRODUCTION

LET the magnetic field H in a crystal be directed along the z axis. We shall regard this field as strong in the sense that $\omega\tau \gg 1$, where $\omega = eH/mc$ is the Larmor frequency (m is the effective mass of the electron) and τ is the relaxation time of the electrons. We shall be interested in the electric current along the x axis, due to the electric field acting in the same direction. The corresponding component of the electrical conductivity σ_{xx} will therefore be denoted simply σ.

In the displacement of the electron along the x axis, the location of the center of the Landau oscillator x^0 changes. Consequently, the y component of the associated electron momentum also changes ($x^0 = cp_y/eH$). If the electrons are scattered by the phonons, then their displacement along the x axis is associated with the transfer of the y component of the momentum to the phonon, which leads to the formation of a phonon flux along the y axis. If the phonons interacted only with the electrons, then the momentum in the stationary state, obtained by the phonons from the electrons, would be equal to the momentum given up by the electrons in the opposite process. This would produce an electron current along the x axis. In the opposite limiting case, when the phonons give up momentum to defects or to boundaries, or lose momentum as the result of transport processes more rapidly than they obtain it from the electrons, the phonons are virtually in an equilibrium state, and the usual relaxation of electrons takes place relative to the phonons. Here we are interested in the case in which the relaxation time of the phonons relative to electrons, τ_{pe}, is smaller than their nonelectronic relaxation time τ_p.

It is important to bear in mind that the current in the direction of the electric field can be caused by the transfer of the y component of the electronic momentum not only to the phonons, but also to different types of defects in the crystal. Of course, the effect studied by us is of importance only if that part of the electrical conductivity which we tentatively call the defect part (σ_d) is much smaller than the phonon part ($\sigma_d \ll \sigma_p$).

The entrainment effect significantly decreases the transverse electrical conductivity and changes its dependence on the temperature and on the magnetic field. In particular, at sufficiently low temperatures there is a dependence of the electrical conductivity on the dimensions of the specimen in the direction of the Hall current for semiconductors and semimetals. In semiconductors, the electrical conductivity in this temperature region is shown to be inversely proportional to the magnetic field intensity. For somewhat higher temperatures, the electrical conductivity can be shown to be exponentially dependent on the temperature. In Secs. 3 and 4 we consider the effect of entrainment in semimetals (and metals with a closed Fermi surface) and in semiconductors for different phonon relaxation mechanisms.

2. GENERAL THEORY OF THE EFFECT

The quantitative expressions for the case of an arbitrary spectrum of the electrons can be obtained from the equation for the density with the aid of a diagram technique [1]; however, inasmuch as the discussion is of a new physical effect, we shall, for the sake of a better understanding, limit ourselves in the present work to a very simple derivation for the case of an isotropic quadratic spectrum for the electrons.

The kinetic equation for the phonons expresses

the fact that a change in the phonon distribution function per unit time (as a consequence of the emission and absorption of phonons by electrons), which brings about an electric current, is compensated by a change in the distribution function as a result of the relaxation of the phonons relative to the electrons and other scatterers. We shall estimate the relaxation of the phonons in the "relaxation time approximation." As regards the term expressing their entrainment, which is associated with the electrons, it can be easily obtained by starting out from the known formula for the electric current:[1,2]

$$j_1 = \frac{2\pi e}{V\hbar^2 T}\sum_{\alpha\beta q} |J_{\beta\alpha}|^2 |C_q|^2 N_q n_\alpha (1-n_\beta)\,\delta(\omega_{\alpha\beta}+\omega_q)\,X_{\beta\alpha}^2 eE. \tag{1}$$

Here α and β are the aggregates of quantum numbers of the electron in the homogeneous magnetic field (with account of spin), n_α is the equilibrium Fermi function, N_q is the Planck function, ω_q is the phonon function, $J_{\beta\alpha}$ is the matrix element of the operator $e^{i\mathbf{q}\cdot\mathbf{r}/\hbar}$ ($\mathbf{q}$ is the momentum of the phonon), $X_{\beta\alpha} = X_\beta^0 - X_\alpha^0$ is the shift in the center of the oscillator upon transition from the state α to the state β, T is the temperature in energy units, and V is the normalized volume; the quantity C_q characterizes the interaction of the electrons with the phonons; for acoustic phonons, it has the form

$$C_q = E_0\sqrt{qa^3/MsV},$$

where E_0 is the deformation potential, M is the mass of the elementary cell, s is the sound velocity, and a is the lattice constant.

Let g_q be the deviation of the phonon distribution function from its equilibrium value. Then the change in the distribution function as the result of emission and absorption of phonons by electrons is

$$(\partial g_q/\partial t)_e = g_q/\tau_{pe} + g_q/\tau_p. \tag{2}$$

The contribution to the current from the interaction of the electrons with phonons of momentum $\mathbf{q}$ can be treated as the difference between the number of absorbed and emitted phonons per unit time and per unit volume, multiplied by $eX_{\beta\alpha}$ (the latter is independent of the indices β and α, as will be shown below). Then, from (1),

$$\left(\frac{\partial g_q}{\partial t}\right)_e = -\frac{2\pi e}{\hbar^2 T}\sum_{\alpha\beta}|J_{\beta\alpha}|^2|C_q|^2 N_q n_\alpha(1-n_\beta)\,\delta \times(\omega_{\alpha\beta}+\omega_q)\,X_{\beta\alpha}E. \tag{3}$$

The relaxation time of the phonons relative to the equilibrium electrons is determined by the formula

$$\tau_{pe}^{-1} = -\frac{2\pi}{\hbar}\sum_{\alpha\beta}|C_q|^2|J_{\alpha\beta}|^2(n_\alpha - n_\beta)\,\delta(\varepsilon_\alpha - \varepsilon_\beta - \hbar\omega_q) = \frac{2\pi}{\hbar^2}\sum_{\alpha\beta}|C_q|^2|J_{\beta\alpha}|^2 n_\alpha(1-n_\beta)\frac{\delta(\omega_{\alpha\beta}+\omega_q)}{N_q+1}. \tag{4}$$

We now note that $|J_{\beta\alpha}|^2$ preserves the law of conservation of momentum for electron-phonon interactions:

$$|J_{\beta\alpha}|^2 = |J_{nn'}|^2\,\delta_{p_{y\beta},\,p_{y\alpha}+q_y}\delta_{p_{z\beta},\,p_{z\alpha}+q_z} \tag{5}$$

$$J_{nn'} = \int \varphi_n(x - x_\beta^0)\,\varphi_{n'}(x - x_\alpha^0)\,e^{iq_x x/\hbar}\,dx, \tag{6}$$

where $\varphi_n(x - x^0)$ are the normalized wave functions of the oscillator. Then $X_{\beta\alpha}$ does not depend on the indices α and β:

$$X_{\beta\alpha} = cq_y/eH. \tag{7}$$

Substituting (7) and (3) in (2), we get

$$N_q(N_q+1)\frac{E}{H}\frac{cq_y}{T\tau_{pe}} + \frac{g_q}{\tau_{pe}} + \frac{g_q}{\tau_p} = 0, \tag{8}$$

whence

$$g_q = -\frac{\tau_p}{\tau_p+\tau_{pe}}N_q(N_q+1)\frac{E}{H}\frac{cq_y}{T}. \tag{9}$$

We now proceed to the calculation of the transverse electric current. It consists of the component (1), which is not connected with the entrainment, and a second component brought about by the absorption and emission of phonons, which forms (in its nonequilibrium part) a current along the y axis, as has already been pointed out. The change in the momentum p_y of the electron in such an interaction also creates an additional current.

The number of electron transitions from the state α to the state β, due to interaction with phonons of momentum $\mathbf{q}$, is equal to

$$-\frac{2\pi}{\hbar}|C_q|^2|J_{\alpha\beta}|^2\,[n_\alpha(1-n_\beta)(N_q+g_q+1) - n_\beta(1-n_\alpha)(N_q+g_q)]\,\delta(\varepsilon_\alpha - \varepsilon_\beta - \hbar\omega_q). \tag{10}$$

Since the number vanishes for equilibrium of the phonons, we have only terms with g_q left, so that the number of transitions is:

$$-\frac{2\pi}{\hbar}|C_q|^2|J_{\alpha\beta}|^2(n_\alpha - n_\beta)\,\delta(\varepsilon_\alpha - \varepsilon_\beta - \hbar\omega_q)\,g_q.$$

Multiplying by $eX_{\beta\alpha}/V$ and summing over all α, β, and $\mathbf{q}$, we obtain the record part of the current:

$$j_2 = \frac{2\pi e}{\hbar^2 V}\sum_{\alpha\beta q}|C_q|^2|J_{\alpha\beta}|^2 n_\alpha(1-n_\beta)\,\delta(\omega_{\beta\alpha}-\omega_q)\,X_{\beta\alpha}\frac{g_q}{N_q+1}. \tag{11}$$

Combining (11) and (1), we get the total current

$$j = j_1 + j_2 = \frac{2\pi e}{V\hbar^2 T}\sum_{\alpha\beta q} |J_{\beta\alpha}|^2 |C_q|^2 N_q n_\alpha (1 - n_\beta)$$

$$\times \delta(\omega_{\alpha\beta} + \omega_q) X_{\beta\alpha}\left(eEX_{\beta\alpha} + \frac{T}{N_q(N_q+1)} g_q\right), \quad (12)$$

which is identical with the result obtained in [1].

By using (3) and (9), one easily gets

$$\sigma_p = \frac{c^2}{H^2 TV}\sum_q q_y^2 N_q (N_q + 1)/(\tau_p + \tau_{pe}). \quad (13)$$

If the phonons interact only with the electrons, i.e., if $\tau_p \to \infty$, then the transverse current vanishes, in accord with the qualitative considerations given earlier. In the opposite limiting case, when the phonons are in equilibrium ($\tau_p \ll \tau_{pe}$), (13) transforms into (1).

In the classical case ($\hbar\omega \ll \varphi$, where φ is the characteristic energy), Eq. (13) can be obtained by solution of the set of kinetic equations for phonons and electrons, when $\omega\tau \gg 1$.

3. THE ENTRAINMENT EFFECT FOR THE CASE OF DEGENERATE ELECTRONS

We limit ourselves to the case in which $\hbar\omega \ll \zeta$, where ζ is the chemical potential. In this case, the collision integral of electrons with phonons does not depend on the magnetic field, and the classical expression can be used for τ_{pe}:

$$\tau_{pe}^{-1} = -\frac{4\pi |C_q|^2 V}{\hbar (2\pi\hbar)^3}\int d^3p\,\delta(\varepsilon_p - \varepsilon_{p-q} - \hbar\omega_q)(n_p - n_{p-q}). \quad (14)$$

Here, since usually $\omega > \omega_0$, where ω_0 is the frequency of the transitions between states with opposite spin orientations, the sum over the spin indices is replaced by the factor 2. Carrying out the integration over the angles by means of the δ function, we get

$$\tau_{pe}^{-1} = -\frac{1}{\pi}\frac{|C_q|^2 Vm}{\hbar^4 q}\int_{p_{min}}^{\infty} p\,[n(\varepsilon_p) - n(\varepsilon_p - \hbar\omega_q)]\,dp,$$

where $p_{min} = q/2 + ms$. Proceeding to integration over the energy, and replacing $n(\epsilon_p) - n(\epsilon_p - \hbar\omega_q)$ by $(dn/d\epsilon)\hbar\omega_q$, we easily obtain

$$\tau_{pe}^{-1} = \begin{cases} (E_0 ma^2/\hbar^2)^2\, q/\pi Ma & q < 2\sqrt{2m\zeta} \\ 0 & q > 2\sqrt{2m\zeta}. \end{cases} \quad (15)$$

We now consider the case in which the Fermi momentum of the electron is larger than the thermal momentum of the phonon. ($2\sqrt{2m\zeta} > T/s$). Transforming in (13) from a sum over q to an integration, we get

$$\sigma_p = \frac{c^2}{H^2 T(2\pi\hbar)^3}\int d^3q \cdot q_y^2 N_q \frac{N_q + 1}{\tau_p + \tau_{pe}}. \quad (16)$$

Here the principal role in the integral is played by values of q on the order of the thermal momentum of the phonon ($q_T \sim T/s$).

There are three fundamental mechanisms of non-electronic relaxation of the thermal phonons: 1) relaxation on boundaries with the characteristic time $\tau_L \sim L/s$, where L is the dimension of the specimen in the direction of the y axis, 2) relaxation on defects [3]

$$\tau_d^{-1} = \frac{\omega_D}{10}\left(\frac{\hbar\omega_q}{\Theta}\right)^4\left[x + x_i\left(\frac{\Delta M}{M}\right)^2\right], \quad (17)$$

where $\Theta = \hbar\omega_D$ is the Debye temperature and x and x_i are the relative concentrations of the impurity atoms and isotopes, respectively, and 3) relaxation with the help of umklapp processes, with a relaxation time [3]

$$\tau_t \approx \frac{1}{30}\frac{1}{\omega_D}\frac{Ms^2}{\Theta}\frac{T}{\hbar\omega_q} e^{\Theta/\alpha T},\quad T < \Theta,\ \alpha \gtrsim 1. \quad (18)$$

These mechanisms were shown in the order of their importance for an increase in temperature.

In the low temperature region, where the first mechanism dominates the phonon relaxation, the conditions $\tau_p \sim \tau_L \gg \tau_{pe}$ leads to the inequality

$$30\frac{m}{M}\frac{L}{a}\left(\frac{E_0}{\Theta}\right)^2\frac{ms^2}{\Theta}\frac{T}{\Theta} \gg 1,$$

which is practically always satisfied. Substituting $\tau_p = \tau_L$ in Eq. (16) and neglecting τ_{pe}, we get

$$\sigma_p \approx \left(\frac{T}{ms^2}\right)^2\left(\frac{T}{\hbar\omega}\right)^2\frac{e^2}{a\Theta}\frac{s}{L}. \quad (19)$$

Thus the electrical conductivity is shown to be dependent on the dimensions of the specimen in the y direction, perpendicular to the electric and magnetic fields. On the other hand, since

$$\sigma_d \approx \sigma_d^0(\omega\tau)^{-2} = ne^2/m\omega^2\tau \quad (20)$$

(n is the electron concentration, σ_d^0 is the electrical conductivity produced by defects in the absence of a magnetic field, while

$$\tau^{-1} = xa^{-3}v\Delta \sim xv/a, \quad (21)$$

where $\Delta \sim a^2$ is the scattering cross section, v is the Fermi velocity of the electrons), we have the relation

$$\frac{\sigma_p}{\sigma_d} \sim 10\left(\frac{T}{\Theta}\right)^4\frac{1}{(na^3)^{4/3}}\frac{a}{Lx}. \quad (22)$$

In very pure semimetals at the low temperatures which are necessary for the appearance of the effect of phonon scattering on boundaries, the relation (22) can be shown to be larger than unity, so that the entrainment effect can be measured.

A still more important effect is seen in the case in which the phonons relax through the agency of umklapp processes at temperatures below the

Debye temperature. The ratio of the relaxation times is, according to (15) and (18), equal to

$$\frac{\tau_p}{\tau_{pe}} \sim 10^{-2}\ \frac{T}{\Theta}\left(E_0\frac{ma^2}{\hbar^2}\right)^2 e^{\Theta/\alpha T},$$

which can be larger than unity. Here, we get for σ_p:

$$\sigma_p \sim 10^2\,\frac{e^2}{a\hbar}\ \frac{\Theta}{Ms^2}\left(\frac{T}{\hbar\omega}\right)^2\left(\frac{T}{ms^2}\right)^2 e^{-\Theta/\alpha T}, \qquad (23)$$

while, by (20)—(21),

$$\frac{\sigma_p}{\sigma_d} \sim 10^3\ \frac{T}{Ms^2}\left(\frac{T}{\Theta}\right)^3 e^{-\Theta/\alpha T}\frac{1}{(na^3)^{4/3}x}\ .$$

In this case of not very contaminated materials, the latter ratio is also much larger than unity. It is interesting to note that Eq. (23) gives the exponential temperature dependence of the electrical conductivity.

A similar analysis can also be carried out for the case in which the phonons relax on defects of an atomic scale. The ratio of the relaxation times shows that even in this case, the entrainment of the phonons is quite considerable.

However, if the phonons relax on impurities, then the phonon electrical conductivity is shown to be smaller than the impurity conductivity (or commensurate with it). In this case, one falls off along with the other upon decrease in the concentration of impurities. If the phonons relax on isotopes, then, the phonon electrical conductivity can predominate over the impurity conductivity in low contamination materials with a large quantity of isotopes. Here $\sigma_p \sim T^8$, while, without account of entrainment, $\sigma_p \sim T^5$.

Now let us consider the case in which $\sqrt{2m\zeta} < T/s$. In this case, all the phonons that interact with the electrons are subthermal. The most effective relaxation mechanism of the subthermal phonons is the relaxation on normal phonons. In this case, the electrons entrain both the transverse and longitudinal phonons.

For semiconductors and semimetals, the energy of interaction of the electrons with phonons can be written in the form $\Sigma E_{ik}u_{ik}$, where u_{ik} is the tensor of the interaction constant. In the general case of such anisotropic interaction, the coupling of the electrons with transverse and longitudinal phonons is identical in order of magnitude. This is precisely the situation in such crystals as bismuth, germanium, silicon and, perhaps, in most real conductors with which experimenters deal.

A different situation holds for crystals of the type InSb; here the electron spectrum is isotropic and, as a result of the cubic symmetry, the tensor E_{ik} reduces to a scalar. In these crystals, the electrons interact with longitudinal phonons more strongly than with the transverse. However, keeping in mind the very special situation and the estimated character of our entire investigation, we shall regard the coupling of the electrons with transverse and longitudinal phonons as comparable in magnitude, even though we took the isotropic character of the electron spectra into account. For order-of-magnitude estimates, this cannot lead to a contradiction.

Thus, for not too low temperatures, one need take only the transverse phonons into account, inasmuch as they relax on thermal phonons more rapidly and, consequently, they make a larger contribution to the electrical conductivity. The relaxation time of the subthermal transverse phonons is, according to Landau and Rumer,[3,4]

$$\tau_\perp \approx \tfrac{1}{10}(aM/q)(\Theta/T)^4. \qquad (24)$$

According to (15) and (24),

$$\tau_\perp/\tau_{pe} \approx \tfrac{1}{30}(\Theta/T)^4(E_0ma^2/\hbar^2)^2.$$

For $T < \Theta$, this ratio can be large.

Substituting $\tau_\perp$ from (24) in (16), in place of τ_p, and neglecting τ_{pe}, it is easy to calculate the electrical conductivity. In this case, one must replace N_q and $N_q + 1$ by T/sq, and integrate over q up to $q_{max} = 2\sqrt{2m\zeta}$. As a result, we get

$$\sigma_p \approx \frac{e^2}{\hbar a}\left(\frac{\zeta}{\hbar\omega}\right)^2\frac{T}{Ms^2}\left(\frac{T}{\Theta}\right)^4.$$

Thus $\sigma_p \sim T^5$ while, without calculation of the entrainment, $\sigma_p \sim T$. For crystals of a high degree of purity, $\sigma_d < \sigma_p$.

4. THE ENTRAINMENT EFFECT FOR NONDEGENERATE ELECTRONS

We limit ourselves to the quantum case ($\hbar\omega \gg T$) (in the classical case, the effect is clearly absent).

We begin by calculating τ_{pe}. In this case, (3) can be put in the form

$$\tau_{pe}^{-1} = \frac{4\pi}{\hbar^2}\ \frac{|C_q|^2}{N_q+1}$$

$$\times \sum_{\alpha\beta} n_\alpha \delta(\omega_{\beta\alpha} - \omega_q)\,\delta_{p_{y\beta},\,p_{y\alpha}+q_y}\,\delta_{p_{z\beta},\,p_{z\alpha}+q_z}\,|J_{nn'}|^2.$$

Here it is taken into account that $\hbar\omega_0 \ll T$. For $\hbar\omega_0 \gg T$, the factor 4 is replaced by 2.

We transform from summation over p_y and p_z to integration, and set $n = n' = 0$:

$$\tau_{pe}^{-1} = \frac{4\pi}{\hbar^2}\ \frac{|C_q|^2}{N_q+1}\int dp_y dp_z\, n_\alpha \delta\ (\omega_{\beta\alpha} - \omega_q)\,|J_{00}|^2\,\frac{L_yL_z}{(2\pi\hbar)^2}\ .$$

Integration over p_y gives the factor $L_x m\omega$ (L_x, L_y, L_z are the linear dimensions of the normalized volume V):

$$\tau_{pe}^{-1} = \frac{4\pi}{\hbar}\frac{eH}{c}\frac{V|C_q|^2}{(N_q+1)(2\pi\hbar)^2}\int dp_z \exp\left\{\frac{1}{T}\left(\zeta' - \frac{p_z^2}{2m}\right)\right\}|J_{00}|^2$$
$$\times \delta(\varepsilon_{p_z+q_z} - \varepsilon_{p_z} - \hbar\omega_q),$$

where

$$\zeta' = \zeta - \hbar\omega/2 = T\ln[\pi\sqrt{2\pi}n\hbar^2/m^{3/2}T^{1/2}\omega],$$
$$|J_{00}|^2 = \exp(-q_\perp^2/q_H^2), \quad q_\perp^2 = q_x^2 + q_y^2, \quad q_H^2 = 2eH\hbar/c.$$

We shall now assume that

$$q_H^2/q_T^2 = 2(ms^2/T)(\hbar\omega/T) \ll 1,$$

i.e., that the magnetic field is not "superpowerful."[5] Then $N_q + 1 \approx T/sq$ and, after integration over p_z, we get

$$\tau_{pe}^{-1} = \frac{\sqrt{2\pi}}{\hbar}\frac{E_0^2 q^2 m^{1/2} n a^3}{M q_z T^{3/2}} \exp\left(-\frac{q_\perp^2}{q_H^2} - \frac{q_z^2}{8mT}\right). \quad (25)$$

We set $\tau_p = Aq^{-t}$ and substitute this quantity, along with (25), in (16). We introduce cylindrical coordinates with the axis along q_z and integrate over the angles. Moreover, since $q_H > \sqrt{8mT}$, we can assume $q \approx q_\perp$. By introducing the dimensionless variables $\xi = q_z/\sqrt{8mT}$ and $\eta = q_\perp/q_H$, we obtain

$$\sigma_p = \frac{c^2}{s^2}\frac{Tq_H^{t+2}\sqrt{8mT}}{H^2(2\pi\hbar)^3 A}\int \frac{\eta^{t+1}d\xi d\eta}{1 + C\xi\eta^{t-2}\exp(\xi^2+\eta^2)}, \quad (26)$$

where C is the ratio of the coefficient of the exponential term in τ_{pe} to τ_p for $\xi = \eta = 1$. If C is large ($C \gg 1$), then the entrainment effect is absent [the unity term in the denominator of Eq. (26) can be neglected]. If $C \ll 1$, on the other hand, then the factor before the integral in (26) gives an order-of-magnitude estimate of the transverse electrical conductivity, while the integral depends logarithmically on C.

For low temperatures, where the scattering of phonons on the boundary ($A = L/s$ and $t = 0$) plays an important role, we have

$$\sigma_p \approx \frac{1}{100}\frac{e^2}{L\hbar}\frac{T}{\hbar\omega}\left(\frac{T}{ms^2}\right)^{1/2}. \quad (27)$$

For the quantity C,

$$C = \left(\frac{T}{E_0}\right)^2 \frac{s}{\omega L}\frac{M}{m}\frac{1}{na^3}. \quad (28)$$

It is seen from (28) that the entrainment effect increases with increasing electron concentration and with decreasing temperature. In semiconductors, however, the scattering by ionized impurities increases in this case. For estimates of the latter, one can make use of the usual formula[1]

$$\sigma_i = \frac{4\pi eN}{\hbar^2 T}\sum_{\alpha\beta q}|V_{ed}|^2 n_\beta(1-n_\alpha)\delta(\omega_{\alpha\beta})|J_{\beta\alpha}|^2 eX_{\beta\alpha}^2, \quad (29)$$

where

$$|V_{ed}|^2 = 16\pi^2 e^4\hbar^4/V^2\varepsilon^2(q^2+\varkappa^2)^2,$$

N is the concentration of the impurities, $\varkappa$ is the momentum corresponding to the Debye screening radius, and ϵ is the dielectric constant.

Assuming that $q_H \gg \varkappa$, and summing (29) in the same fashion as was done above, one can obtain the following result by neglecting the logarithmic divergence that occurs in the integral:

$$\sigma_i \approx nNe^6/(mT)^{3/2}\omega^2\varepsilon^2. \quad (30)$$

Then the ratio of (30) to (27) takes the form

$$\frac{\sigma_i}{\sigma_p} \approx \frac{100}{\varepsilon^2}(nNa^6)\frac{e^4}{a^2T^2}\frac{L}{a}\left(\frac{q_H a}{\hbar}\right)^2\frac{\Theta}{T}. \quad (31)$$

Equations (28) and (31) show that the entrainment effect can take place in magnetic fields of the order of tens of kilo-oersteds, at temperatures $\sim 10°K$, and in concentrations of electrons and impurities $N \sim n \sim 10^{14}$ cm^{-3}. Here, in accord with (27), $\sigma_p \sim 1/H$, while the transverse magnetoresistance $\rho_{xx} \approx \sigma/\sigma_{xy}^2 \sim H$. The fact that the concurrent mechanism—scattering by ionized impurities—gives a weak (logarithmic) dependence $\rho_{xx}(H)$ should make possible the experimental observation of this effect.

It is an important conclusion of our theory that the ratio of the electrical conductivity, brought about by the ionized impurities, to the phonon electrical conductivity (31) is proportional to the square of the concentration, while in the theory which does not take entrainment into account, the ratio is proportional to the first power of the concentration. This means that for high concentrations (when $C \ll 1$), the transition from the phonon electrical conductivity to the impurity conductivity occurs at much higher temperatures than follows from the theory which does not take the entrainment into account.

[1] L. É. Gurevich and G. M. Nedlin, JETP 40, 809 (1961), Soviet Phys. JETP 13, 568 (1961).

[2] S. Titeica, Ann. d. Phys. 22, 128 (1955); E. Adams and T. Holstein, J. Phys. Chem. Sol. 10, 254 (1959); V. L. Gurevich and Yu. A. Firsov, JETP 40, 198 (1961), Soviet Phys. JETP 13, 137 (1961).

[3] P. Klemens, Solid St. Phys. 7, New York, 1958.

[4] L. Landau and G. Rumer, Phys. Z. Sowjetunion 11, 18 (1937).

[5] L. É. Gurevich and G. M. Nedlin, FTT 3, 2779 (1961), Soviet Phys Solid State 3, 2029 (1962).

Translated by R. T. Beyer
332

ON THE COUPLING CONSTANTS IN μ CAPTURE

L. D. BLOKHINTSEV and É. I. DOLINSKII

Institute of Nuclear Physics, Moscow State University

Submitted to JETP editor July 23, 1961

J. Exptl. Theoret. Phys. (U.S.S.R.) 41, 1986-1995 (December, 1961)

It is shown that within the framework of the theory of the universal Fermi interaction the best agreement with the available experimental data on the interaction of μ mesons with nucleons is obtained with a theory in which there is a conserved vector current and the effective pseudoscalar coupling constant $g_P^{(\mu)}$ is large. The sign of the ratio $g_P^{(\mu)}/g_A^{(\mu)}$ is positive, in agreement with the theory.

1. THE THEORETICAL PREDICTIONS

SINCE all known experimental facts about nuclear β decay and about μ decay are in good agreement with the theory of the universal Fermi interaction (UFI),[1,2] it is natural to compare the experimental data so far accumulated on the interaction of μ mesons with nucleons with the predictions of this theory. In the case of μ decay the theory of the UFI describes the interaction of the four fermions by means of one coupling constant $G = (1.41 \pm 0.01) \times 10^{-49}$ erg cm^3 and the vector (V) and axial vector (A) types of interaction. When, however, weak-interaction processes involve nucleons, which have strong interactions, the effective Lagrangian for the processes $e^- + p \to n + \nu (a \equiv \beta,\ l \equiv e)$ and $\mu^- + p \to n + \nu (a \equiv \mu,\ l \equiv \mu)$ takes the more complicated form[3]:

$$L_{eff}^{(a)} = 2^{-1/2} [g_V^{(a)} (\bar{\psi}_\nu (1 - \gamma_5) \gamma_i \psi_l) (\bar{\psi}_n \gamma_i \psi_p) + g_A^{(a)} (\bar{\psi}_\nu (1 - \gamma_5) \times i\gamma_i\gamma_5 \psi_l) (\bar{\psi}_n i\gamma_i\gamma_5 \psi_p) + (1/2m)\, g_M^{(a)} (\bar{\psi}_\nu (1 - \gamma_5)\, \gamma_i \psi_l) \times (\bar{\psi}_n \sigma_{ik} (p_k - n_k) \psi_p) + g_P^{(a)} (\bar{\psi}_\nu (1 - \gamma_5)\, \gamma_5 \psi_l) (\bar{\psi}_n \gamma_5 \psi_p)]. \quad (1)$$

Here $\sigma_{ik} = (\gamma_i\gamma_k - \gamma_k\gamma_i)/2i$; p_i and n_i are the four-momenta of the proton and the neutron; m is the nucleon mass ($\hbar = c = 1$); and the form-factors $g_V^{(a)}, \ldots, g_P^{(a)}$ are functions of the square of the four-momentum transfer, $(p - n)^2$. When the strong interactions are "turned off" $g_V^{(a)}, g_A^{(a)} \to G$, $g_M^{(a)}, g_P^{(a)} \to 0$, and we get the Lagrangian for μ decay.

Table I summarizes the theoretical predictions regarding the values of the form-factors for μ capture that are given by the theory of the UFI with conserved vector current when strong interactions are taken into account.[3-6] The second column of the table shows the diagrams included in the theoretical estimate of the effects of the strong interactions. One-pion intermediate states lead to the appearance in the effective Lagrangian (1) of a term which imitates a pseudoscalar coupling. The value of the effective pseudoscalar coupling constant $g_P^{(\mu)}$ given in the third column is that calculated in [3,6] by using the renormalized pion-

Table I.

Coupling constants in μ capture	Diagrams taken into account	Expressions in terms of coupling constants for β decay of nucleons
$g_V^{(\mu)}$	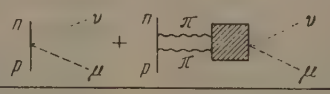	$0.97 \cdot g_V^{(\beta)}$ [6]
$g_A^{(\mu)}$	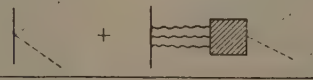	$g_A^{(\beta)}$ [3]
$g_M^{(\mu)}$	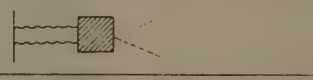	$0.97 \times 3.7\ g_V^{(\beta)}$ [6]
$g_P^{(\mu)}$	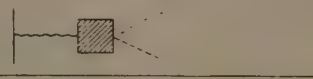	$8 \cdot g_A^{(\beta)}$ [3]

nucleon interaction constant and the experimental probability of the decay $\pi^- \to \mu^- + \bar{\nu}$.

The positive sign of the ratio $g_P^{(\mu)}/g_A^{(\mu)}$ is obtained on the assumption that the main contribution to π decay comes from intermediate states with a nucleon-antinucleon pair. Two-pion intermediate states give the main contribution to the "weak magnetism" constant $g_M^{(\mu)}$ and represent the main dependence on the momentum transfer in $g_V^{(\mu)}$. In the theory of the UFI with conserved vector current the effect of the two-pion intermediate states is easily calculated[1,4,6] and leads to the values of $g_V^{(\mu)}$ and $g_M^{(\mu)}$ shown in the third column of the table. We note, however, that the hypothesis of the conserved vector current has not yet received direct experimental confirmation. The expected dependence on the momentum transfer in $g_A^{(\mu)}$ is extremely small, since its first contribution is from three-pion intermediate states.

Thus experiments to test the predictions of the theory of the UFI regarding the interaction of μ mesons with nucleons include the determination of four coupling constants. In this connection it must be emphasized that the least trivial questions are those of the magnitude and especially the sign of the constant $g_P^{(\mu)}$. The experimental determination of this constant is extremely important both to establish the accuracy of the pole approximation used in calculating it and to test the correctness of our ideas about the mechanism of π decay.

2. ANALYSIS OF THE EXPERIMENTAL DATA

In this paper we do not give a review of all the existing experimental material on μ capture, but consider in detail those experiments that are accurate enough for quantitative comparison with the predictions of the theory.

A. Experiments on the probability of μ capture. Numerous measurements of the total probability of μ capture (cf., e.g., [7,8]) in various nuclei demonstrate convincingly that the coupling constants for the weak interactions of μ mesons and electrons with nucleons are of the same order of magnitude. Furthermore the ratio of the probabilities of μ capture in adjacent nuclei[7,9] evidently indicates that interactions of the Gamow-Teller type predominate to some extent over those of the Fermi type. One cannot, however, get from these experiments any exact information about the numerical values of the coupling constants.

The study of partial μ transitions which obey definite selection rules is more promising. Up to now the only experiments of this type are the measurements of the probability of the reaction[10,11]

$$\mu^- + C^{12} \to B^{12} + \nu \qquad (2)$$

as a fraction of the probability of the β decay

$$B^{12} \to C^{12} + e^- + \bar{\nu} \qquad (2')$$

Since in this reaction about 90 percent of the B^{12} nuclei are produced in the ground state, the transitions (2) and (2') are of the Gamow-Teller type ($\Delta J = 1$, no).

The probability of the reaction (2) with production of the B^{12} nucleus in the ground state is proportional to the square of the effective Gamow-Teller coupling constant[6]:

$$\begin{aligned} (\Gamma_A^{(\mu)})^2 &= (G_A^{(\mu)})^2 + \tfrac{1}{3}\,[(G_P^{(\mu)})^2 - 2G_A^{(\mu)}G_P^{(\mu)}]; \\ G_A^{(\mu)} &= g_A^{(\mu)} - (g_V^{(\mu)} + g_M^{(\mu)})\,(E_\nu/2m), \\ G_P^{(\mu)} &= (g_P^{(\mu)} - g_A^{(\mu)} - g_V^{(\mu)} - g_M^{(\mu)})\,(E_\nu/2m). \end{aligned} \qquad (3)$$

where E_ν is the energy of the neutrino in reaction (2). The most accurate experiment[10] leads to the following estimate for $\Gamma_A^{(\mu)}$:

$$\Gamma_A^{(\mu)} = (1.16 \pm 0.13)\, g_A^{(\beta)}. \qquad (4)$$

The indicated error is mainly due to theoretical inaccuracies which arise in the calculation of the nuclear matrix element for reaction (2).[12]

Let us introduce the notations

$$-g_A^{(\mu)}/g_V^{(\mu)} = \lambda, \quad g_P^{(\mu)}/g_A^{(\mu)} = \varkappa, \quad g_M^{(\mu)}/g_V^{(\mu)} = \mu - 1 \qquad (5)$$

which will be convenient in what follows. If we fix the value of the ratio $g_A^{(\beta)}/g_A^{(\mu)}$, then Eq. (4) gives a connection between the three quantities λ, $\varkappa$, and μ. When we take into account the weak dependence of $g_A^{(\mu)}$ on the four-momentum transfer (see Sec. 1), the latest measurements of the branching ratio $(\pi \to e + \nu)/(\pi \to \mu + \nu)$ of π-meson decay[13] give the result $g_A^{(\mu)} = g_A^{(\beta)}$ to an accuracy of the order of 10 to 15 percent. Furthermore, according to calculations of Goldberger and Treiman,[3] $g_M^{(\mu)}$ is very small in the theory of the UFI without a conserved vector current, so that $\mu \approx 1$. In the theory with conserved vector current, according to Table I, $\mu \approx 4.7$. In comparing theory with experiment we shall consider only these two values of μ.

Figure 1 shows the dependences of $\varkappa$ on λ for $\mu = 4.7$ and for $\mu = 1$. In these diagrams curve 1 corresponds to the values $\Gamma_A^{(\mu)} = (1.16 + 0.13)$, $g_A^{(\beta)} = 1.29\ g_A^{(\beta)}$ and $g_A^{(\mu)} = (1 - 0.15)\, g_A^{(\beta)} = 0.85\, g_A^{(\beta)}$, and curve 2 to the values $\Gamma_A^{(\mu)}$

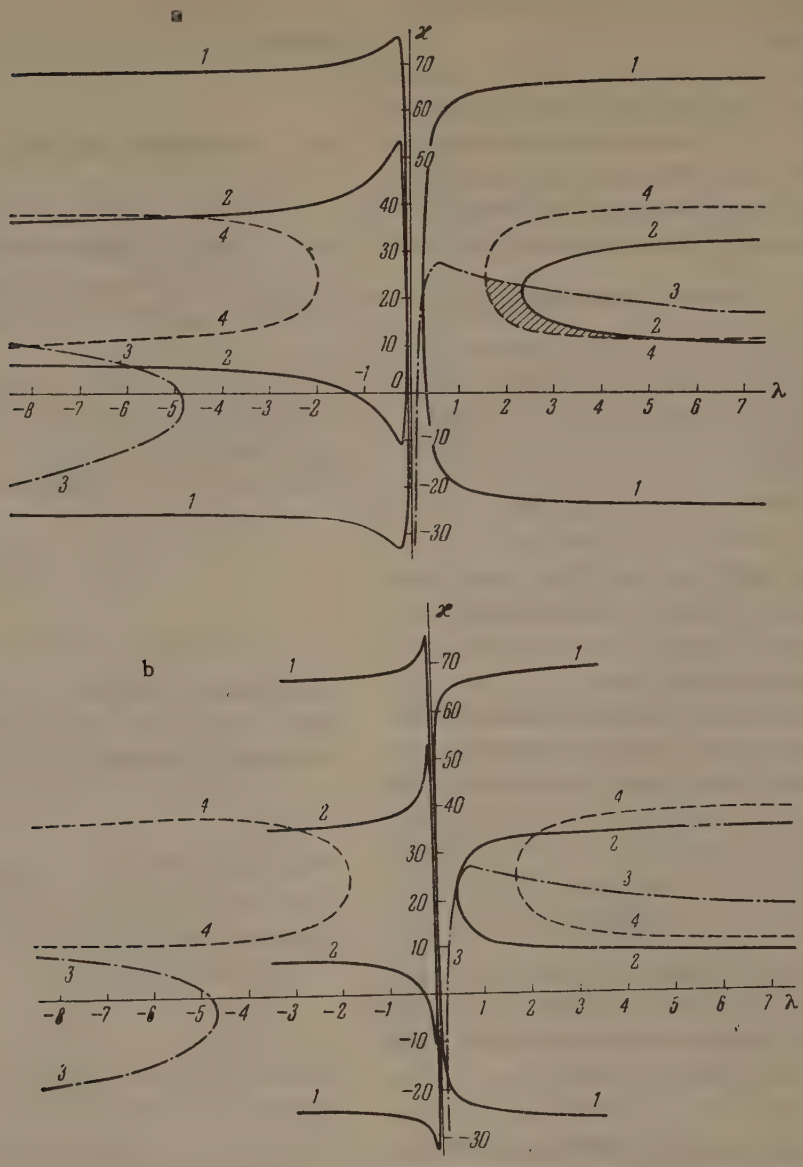

FIG. 1

$= (1.16 - 0.13)$, $g_A^{(\beta)} = 1.03\ g_A^{(\beta)}$ and $g_A^{(\mu)} = (1 + 0.15)\, g_A^{(\beta)} = 1.15\ g_A^{(\beta)}$. The region of allowed values of κ and λ lies between curves 1 and 2. The choice of the values of $\Gamma_A^{(\mu)}$ and $g_A^{(\mu)}$ for curves 1 and 2 has been made so as to obtain the maximum range of admissible values of κ and λ compatible with the existing experimental and theoretical uncertainties in $\Gamma_A^{(\mu)}$ and $g_A^{(\mu)}$. As can be seen from the diagrams of Fig. 1, within the allowed region the values of κ and λ can vary over wide ranges.

Let us now turn to the measurements of the difference of the probabilities of nuclear absorption of μ^- mesons from two states of the hyperfine structure of a mesic atom.[14] So far there have been two experiments of this type.[15,16] Telegdi[15] has studied capture from the states of the hyperfine structure of the mesic atom Al^{27}. The results of this work confirm that terms of the Gamow-Teller type are present in the interaction between μ mesons and nucleons, but a more detailed interpretation of the results is difficult. A paper by Egorov and others[16] describes a measurement of the difference of the probabilities of μ capture from the states of the mesic atom P^{31} with spins $F = 0$ and $F = 1$. The estimate obtained as a lower limit on the quantity

$$\Delta W/W = (W_0 - W_1)/(W_0/4 + 3W_1/4),$$

where W_0 and W_1 are the probabilities of μ capture from the states of the mesic atom with $F = 0$ and $F = 1$, is

$$(\Delta W/W)_{\text{lower}} = 0.29 \pm 0.04 \qquad (6)$$

(the indicated error is the statistical error).

Using the results of the calculation of the value of $\Delta W = W_0 - W_1$ for phosphorus in a paper by Überall[17] and taking into account only the main dependence on the coupling constants in Primakoff's formula for the μ-capture probability W,[18] we get an expression for $\Delta W/W$ as a function of κ, λ, and μ:

$$\Delta W/W = 0.324\,\{\lambda^2(3+2\gamma-2\gamma\varkappa)+\lambda[2\mu\gamma(2+\gamma)+(3+\gamma)(1+\gamma)-(1+\gamma+2\mu\gamma)\gamma\varkappa]+(2+2\gamma+\mu\gamma)\mu\gamma\}\{\lambda^2(3+2\gamma+\gamma^2-2\gamma\varkappa-2\gamma^2\varkappa+\gamma^2\varkappa^2)+4\mu\gamma\lambda+2\mu^2\gamma^2+(1+\gamma)^2\}^{-1}, \quad (7)$$

where $\gamma = \bar{E}_\nu/2m$, and $\bar{E}_\nu$ is the average energy of the neutrinos emitted in μ capture in P^{31}. In Eq. (7) we have adopted the value $\gamma = 0.048$, which corresponds to a mean excitation energy of the P^{31} nucleus of the order of 15 Mev.

The curves 3 in Fig. 1 a and b represent the functions $\kappa = \kappa(\lambda)$ obtained from Eq. (7) for $\mu = 4.7$ and $\mu = 1$, respectively, with $\Delta W/W = +0.25$, which corresponds to subtraction of one standard deviation from the lower limit. The region of allowed values of κ and λ is inside each of the indicated curves. As can be seen from the diagrams, the shape of the curves is not very sensitive to the value of μ. Practically all positive values of λ are allowed, but the allowed negative values begin at large magnitudes $|\lambda| \approx 5$. For positive λ the values of κ are bounded above: $\kappa \leq 27$.

B. Experiments on the angular distribution of the neutrons. When averaged over energy the angular distribution of the neutrons emitted on the absorption of polarized μ^- mesons by nuclei of spin zero is of the form[19,20]

$$1 + a\cos\theta, \quad (8)$$

where θ is the angle between the direction of emission of the neutron and the polarization of the μ^- meson, and the asymmetry coefficient a is given by the formula

$$a = P_\mu P_n \tilde{\beta}\tilde{\alpha}. \quad (9)$$

Here P_μ is the degree of polarization of the μ^- meson in the K shell of the mesic atom at the instant of capture; P_n is a factor that allows for the background of isotropically distributed evaporated neutrons which are products of the decay of the compound nucleus which can be produced by the μ-capture process; $\tilde{\beta}$ is a factor that allows for the decrease of the asymmetry in the angular distribution of the neutrons of the direct process* on account of the motion of the protons in the original nucleus and the interaction of the emerging neutron with the residual nucleus; and $\tilde{\alpha}$ is the "internal" asymmetry coefficient, which depends on the coupling constants of the interaction of μ mesons with nucleons. $\tilde{\alpha}$ differs by only a few percent from the value of the asymmetry coefficient α_H for mesic hydrogen, calculated with neglect of the hyperfine structure of the mesic atom[20] (this difference is due to the smaller value of the mean energy of the neutrinos emitted in μ capture by the nuclei, as compared with that of the neutrinos from μ capture by free protons). The expression for $\tilde{\alpha}$ is given in [20]. Thus to obtain information about the coupling constants from the experimental asymmetry coefficient a it is necessary to get from it the "internal" asymmetry coefficient $\tilde{\alpha}$, i.e., it is necessary to know the values of P_μ, P_n, and $\tilde{\beta}$.

The polarization P_μ of the μ^- mesons is measured directly by an experiment on the amount of asymmetry in the angular distribution of the electrons from μ^- decay, and can be obtained with high accuracy.

The quantity P_n is given by the formula[21]

$$P_n = (gW)/[gW + \tau(\nu W_{exp} - W)], \quad (10)$$

where W is the probability of emission of a direct-process neutron on μ capture; W_{exp} is the total probability of μ capture in the given nucleus; ν is the average multiplicity of neutron emission in a single act of μ capture; g is the fraction of direct-process neutrons with energy E_N above the threshold energy E_0 of the neutron detector; and τ is the fraction of evaporation neutrons with energy $E_N > E_0$. In principle the quantities g, τ, and W can be determined directly from experiment by measuring the spectrum of the neutrons from μ capture and separating out from it the Maxwell spectrum of evaporation neutrons and the spectrum of direct-process neutrons with $E_N > E_0$. Because of great experimental difficulties, however, these measurements have not yet been made, and for the calculation of P_n one uses theoretical values of g, τ, and W and experimental values of the quantities W_{exp} and ν.[21] The result is that the values of P_n shown in Table II and used in going from a to $\tilde{\alpha}$ contain inaccuracies which can arise from the use of the ideas of particular models of nuclear structure in the theoretical calculations. It must be emphasized, however, that if the neutron-registration threshold E_0 is high enough large errors in the theoretical values of the quantities g and W lead to very small errors in P_n.[21]

*Neutrons of the direct process are neutrons emitted from the nucleus immediately after the absorption of the μ^- meson, with omission of the stage of the compound nucleus.

Table II.

Nucleus	Neutron-registration threshold E_0, Mev	$\alpha = P_\mu P_n P_\gamma \tilde{\beta} \tilde{\alpha}$*	P_μ	P_n	$\tilde{\beta}$	$\tilde{\alpha}$
S[27]	3	—(0.045±0.015)	0.126±0.018	(0.7)** 0.28	0.59	(—0.86±0.31) —2.16±0.78
S[25]	5	—(0.019±0.007)	0.084±0.015	0.53	0.62	—0.69±0.28
Mg[26]	5	—(0.020±0.005)	0.066±0.012	0.43	0.62	—1.14±0.36
Ca[21]	7	—(0.066±0.022)	0.135±0.0194	0.96	0.58	—0.93±0.33

*P_γ allows for registration of the isotropic γ-ray background by the neutron detector. In [21] $P_\gamma = 0.96$; in the other cases, in obtaining $\tilde{\alpha}$ it has been assumed that $P_\gamma = 1$.

**The value $P_n = 0.7$ is given in [27].

The factor $\tilde{\beta}$ has been calculated in a number of papers.[19,20,22,23] Calculations made with the Fermi-gas model[22] for an unbounded nucleus, which give a crude correction for the decrease of the asymmetry of the neutrons only on account of the motion of the protons in the original nucleus, give $\tilde{\beta} \approx 0.8$. A modified Fermi-gas model,[23] which takes into account the refraction and reflection of the neutrons at the boundary of the nucleus, gives $\tilde{\beta} \approx 0.7$. More realistic calculations by the use of the shell model and the optical model,[19,20] which have been made for the nuclei C^{12}, O^{16}, Ne^{20}, Si^{28}, S^{32}, and Ca^{40}, lead to values $\tilde{\beta} \approx 0.5 - 0.6$.

In the discussion of the accuracy of the theoretical calculations of the quantity $\tilde{\beta}$ two questions arise at once. The first is the question of the legitimacy of using the ideas of a definite model of nuclear structure in the calculations. An answer to this question can be obtained by an experimental test of the theoretically calculated probabilities and spectra of direct-process neutrons, of the ratios of the asymmetry coefficients a for different nuclei, of the dependence of the amount of asymmetry on the energy of the neutrons, and so on. The second question is that of the degree of accuracy of the calculations when one uses the "method of distorted waves" to take account of the interaction between the emitted neutron and the nucleus. As is shown in a paper by Shapiro,[24] the treatment of the interaction by the method of distorted waves correspond to only the first iteration in the integral equation for the amplitude for μ capture with the emission of a direct-process neutron. The "small parameter" that characterizes the convergence of the iteration procedure is the quantity $\delta = k\sigma_s^{1/2}/8\pi^{5/2}$, where σ_s is the cross section for elastic scattering of neutrons by the given nucleus at the energy $E_N = \hbar^2 k^2/2m$. For light nuclei and neutron energies of the order of 5 — 10 Mev we have $\delta \sim 0.1$; obviously this favors the method of distorted waves, but more exact quantitative conclusions can be reached only through an investigation of the exact solution of the equation for the amplitude for μ capture.

It must be pointed out that in the calculations of $\tilde{\beta}$ in [19,20] the potentials used in the shell and optical models were rectangular wells, which of course is a rather crude approximation. More accurate determination of the quantity $\tilde{\beta}$ within the framework of these models will have to include the making of calculations with better potentials.

We point out that in [19,20] the factor $\tilde{\beta}$ has been calculated for direct-process neutrons that have undergone elastic interaction with the nucleus. Along with these neutrons an experiment will register the direct-process neutrons that have undergone inelastic interactions with the nucleus but have energies above the registration threshold E_0. Since as a rule the angular distribution of the elastically scattered neutrons protrudes forward more than that of the inelastically scattered neutrons,[25] inclusion of the latter can only decrease the value calculated in [19,20]. The relative contributions to β from inelastically and elastically scattered neutrons is determined in first approximation by the ratio of the cross sections for inelastic and elastic scattering ($\sigma_{nn'}$ and σ_s) of neutrons by the given nucleus. Since in the range of energies in which we are interested ($E_N \sim 5 - 20$ Mev) $\sigma_{nn'}/\sigma_s \sim 0.1 - 0.2$,[25] it is to be expected that the contribution to $\tilde{\beta}$ from inelastic processes will be very small.

Let us now consider the experimental data. Table II, which is taken from [21], shows a collection of the experimental data on the asymmetry of the neutrons emitted in μ capture in the nuclei of Mg, S, and Ca.* The values of P_n and $\tilde{\beta}$ are calculated on the basis of the results obtained in [19,20]. Since, as noted above, the quantity P_n can be calculated more reliably for higher values of the reg-

*We note that in the work of Baker and Rubbia [26] no asymmetry was found for Mg. Unfortunately the brevity of the exposition in [26] does not allow us to judge the reasons for the absence of an asymmetry.

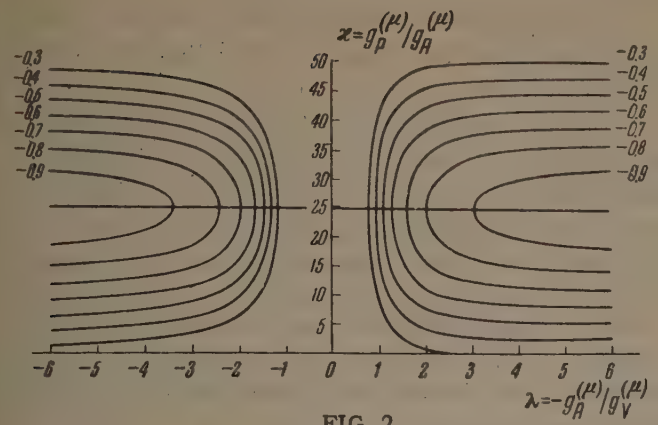

FIG. 2

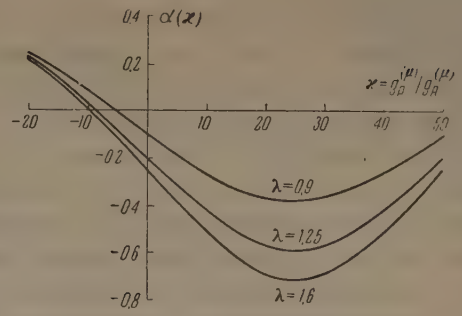

FIG. 3

istration threshold E_0, we shall confine ourselves to a discussion of the asymmetry coefficients for magnesium, sulfur, and calcium obtained in [21,28] and shown in the second, third, and fourth lines of Table II. From these papers we find as the average value of $\tilde{\alpha}$ (treating the experimental errors as standard deviations)

$$\tilde{\alpha}_{av} = -0.92 \pm 0.19. \quad (11)$$

This value differs by more than twice the error from the value $\tilde{\alpha} \approx -0.4$ predicted by the theory of the UFI for the coupling constants of Table I. The curves 4 in Fig. 1, a and b are those obtained for $\mu = 4.7$ and $\mu = 1$, respectively, from Eq. (19) of [20] for $\tilde{\alpha} = -0.7$ (α_{av} plus one standard error).* The allowed region of values of κ and λ is inside the curves 4. As can be seen from the diagrams, the positive values of λ are bounded from below and the negative values from above. The values of κ in the allowed region are positive and lie in the range $10 \leq \kappa \leq 40$.

Figure 2 shows curves $\tilde{\alpha}$ = const in the plane of κ and λ for $\mu = 4.7$ (cf. the last footnote). The curves that correspond to the predictions of the theory of the UFI with the constants of Table I are those for values $\tilde{\alpha} \approx -(0.40 - 0.45)$. Figure 3 shows the dependence of the asymmetry coefficient $\tilde{\alpha}$ on κ for three values of λ with $\mu \sim 4.7$ (cf. the last footnote). For λ = const $\tilde{\alpha}$ has its maximum absolute value at $\kappa \sim 25$. We note that with the value $\lambda = 1.25$ predicted by the theory of the UFI (see Table I) the minimum possible value of $\tilde{\alpha}$ (for $\kappa \sim 25$) differs from the experimental value of $\tilde{\alpha}_{av}$ given by Eq. (11) by one and one-half times the experimental error.

CONCLUSION

Let us summarize the conclusions to be drawn from the preceding section. It follows from Fig. 1 that for negative λ with $\mu = 4.7$ and $\mu = 1$ and for positive λ with $\mu = 1$ there are no values of κ and λ that simultaneously agree with the three types of experiments we have considered—experiments on the capture probabilities in C^{12} and P^{31} and on the angular distributions of the neutrons. For positive λ and $\mu = 4.7$, however, the three regions of allowed values of κ and λ overlap (shaded region in Fig. 1, a); the values of κ and λ consistent with all of the experimental data considered lie in the ranges $10 \lesssim \kappa \lesssim 25$ and $1.6 \lesssim \lambda \leq 6$.

When we compare these results with the predictions of the theory of the UFI, we come to the following conclusions.

1) Within the framework of the theory of the UFI the best agreement with the present experimental data on μ capture is obtained with the type of theory which has a conserved vector current.

2) The vector coupling constant $g_V^{(\mu)}$ and the axial-vector constant $g_A^{(\mu)}$ have opposite signs, which is evidence in favor of the idea of the (V − A) interaction.

3) The axial-vector interaction predominates over the vector interaction:

$$|g_A^{(\mu)}| > |g_V^{(\mu)}|.$$

4) The coupling constant $g_P^{(\mu)}$ of the induced pseudoscalar interaction is large, and the ratio $g_P^{(\mu)}/g_A^{(\mu)}$ is positive, in agreement with the predictions of the theory.

The third and fourth assertions are mainly based on the results of the experiments on the angular distribution of the neutrons.[21,28] The second assertion is based on experiments on the absorption of μ^- mesons from various states of the hyperfine structure of the mesic atom.[15,16] Finally, the first assertion follows from a combined consideration of all three types of experiments analyzed above.

We may also note some tendency toward values of the ratios $|g_A^{(\mu)}/g_V^{(\mu)}|$ and $g_P^{(\mu)}/g_A^{(\mu)}$ that are large in comparison with those predicted by the

*The quantity $\gamma = \bar{E}\gamma/2m$ is assumed to have the value $\gamma = 0.042$.

theory (Table I). It is not excluded, however, that greater accuracy in the experimental data and the theoretical calculations will not confirm this tendency and will lead to agreement with the predictions of the theory. We also emphasize that whereas the experimental data on μ capture in C^{12} and on the branching ratio in π decay indicate the presence of an axial-vector interaction in μ capture, the experiments do not give any direct proof that there is a vector interaction in μ capture.

We express our sincere appreciation to I. S. Shapiro for a discussion of this work and to V. S. Evseev and A. E. Ignatenko for acquainting us with the results of their work before the appearance of their papers.[21,16]

Note added in proof (November 21, 1961). New experimental data have recently appeared. The probability of the process (2) has been found with good accuracy [29] and differs by a factor of one and one-half from the value from [10] used in the present paper. The probability of μ capture in He^3 has been measured.[30] The Liverpool group has obtained [31] for μ capture in sulfur the value $P_n\tilde{\beta}\tilde{\alpha} = -0.22 \pm 0.07$ (for $E_0 = 5$ Mev), which agrees well with the data of [28] (cf. Table II). These new results do not change the conclusions of the present paper.

[1] R. P. Feynman and M. Gell-Mann, Phys. Rev. 109, 193 (1958).

[2] E. C. G. Sudarshan and R. E. Marshak, Phys. Rev. 109, 1860 (1958).

[3] M. L. Goldberger and S. B. Treiman, Phys. Rev. 111, 354 (1958).

[4] M. Gell-Mann, Phys. Rev. 111, 362 (1958).

[5] L. Wolfenstein, Nuovo cimento 8, 882 (1958).

[6] A. Fujii and H. Primakoff, Nuovo cimento 12, 327 (1959).

[7] Sens, Swanson, Telegdi, and Yovanovitch, Phys. Rev. 107, 1464 (1957).

[8] J. C. Sens, Phys. Rev. 113, 679 (1959).

[9] H. A. Tolhoek and J. R. Luyten, Nuclear Phys. 3, 679 (1957).

[10] Burgman, Fischer, Leontic, Lundby, Meunier, Stroot, and Teja, Phys. Rev. Letters 1, 469 (1958).

[11] Argo, Harrison, Kruse, and McGuire, Phys. Rev. 114, 626 (1959). Fetkovich, Fields, and McIlwain, Phys. Rev. 118, 319 (1960). Love, Marder, Nadelhaft, Siegel, and Taylor, Phys. Rev. Letters 2, 107 (1959). T. N. K. Godfrey, Phys. Rev. 92, 512 (1953).

[12] L. Wolfenstein, Nuovo cimento 13, 319 (1959); Proc. 1960 Ann. Int. Conf. on High Energy Phys., Rochester, 1960.

[13] Ashkin, Fazzini, Fidecaro, Merrison, Paul, and Tollestrup, Nuovo cimento 13, 1240 (1959). Anderson, Fujii, Miller, and Tau, Phys. Rev. Letters 2, 53 (1959).

[14] Bernstein, Lee, Yang, and Primakoff, Phys. Rev. 111, 313 (1958).

[15] V. L. Telegdi, Phys. Rev. Letters 3, 59 (1959).

[16] Egorov, Zhuravlev, Ignatenko, Kuptsov, Li, and Petrashku, Preprint, Joint Institute for Nuclear Research, 1961.

[17] H. Überall, Phys. Rev. 121, 1219 (1961).

[18] H. Primakoff, Revs. Modern Phys. 31, 802 (1959).

[19] É. I. Dolinskii and L. D. Blokhintsev, JETP 35, 1488 (1959), Soviet Phys. JETP 8, 1040 (1959); Nuclear Phys. 10, 527 (1959).

[20] Akimova, Blokhintsev, and Dolinskiĭ, JETP 39, 1806 (1960), Soviet Phys. JETP 12, 1260 (1960); Nuclear Phys. 23, 369 (1961).

[21] Evseev, Komarov, Kush, Roganov, Chernogorova, and M. M. Shimchak, Preprint, 1961.

[22] H. Überall, Nuovo cimento 6, 533 (1957).

[23] E. Lubkin, Ann. Phys. 11, 414 (1960).

[24] I. S. Shapiro, Preprint, ITEF (Inst. Theoret. Exper. Phys.) AN SSSR (1961).

[25] E. R. Graves and L. Rosen, Phys. Rev. 89, 343 (1953). Coon, Davis, Felthauser, and Nicodemus, Phys. Rev. 111, 250 (1958).

[26] W. F. Baker and C. Rubbia, Phys. Rev. Letters 3, 179 (1959).

[27] Astbury, Blair, Hussain, Kemp, Muirhead, and Voss, Phys. Rev. Letters 3, 476 (1959).

[28] V. L. Telegdi, Proc. 1960 Ann. Int. Conf. on High Energy Phys., Rochester, 1960, p. 713.

[29] Maier, Bloch, Edelstein, and Siegel, Phys. Rev. Letters 6, 417 (1961).

[30] Zaimidoroga, Kulyukin, Pontecorvo, Sulyaev, Filippov, Tsunko-Sitnikov, and Shcherbakov, Preprint, 1961.

[31] Astbury, Bartley, Blair, Kemp, Muirhead, and Woodhead, Preprint, Liverpool University, 1961.

Translated by W. H. Furry
333

INTERACTION OF γ QUANTA WITH ORIENTED NONSPHERICAL NUCLEI

S. F. SEMENKO and B. A. TULUPOV

P. N. Lebedev Physics Institute, Academy of Sciences, U.S.S.R.

Submitted to JETP editor July 25, 1961

J. Exptl. Theoret. Phys. (U.S.S.R.) 41, 1996-2001 (December, 1961)

The results of an analysis of the possibilities for observing the effects of optical anisotropy by available experimental techniques are presented. The influence of the resolution in the measurement of the energy of the scattered photons and of the degree of the nuclear orientation on these effects is studied. Some consequences of the possible nonaxiality of nuclei are briefly discussed.

1. INTRODUCTION

A number of papers[1-7] have been recently devoted to the discussion of the different effects connected with the optical anisotropy of atomic nuclei. The term "optical anisotropy" signifies that the interaction of photons with the nucleus depends on the orientation of the nuclear spin relative to the wave vector of the photon and that the electric dipole polarizability thus has tensor character.[1] The term "optical anisotropy of nuclei" has been introduced to emphasize the far reaching analogy between the phenomena of the interaction of photons with nuclei and of molecular optics.[5] The investigation of molecular Raman spectra yields considerable amounts of information concerning their structure. One can hope that the investigation of the phenomena associated with the optical anisotropy of nuclei will add to our knowledge of the structure and characteristics of nuclei.

The parameters of the optical anisotropy are nuclear characteristics as basic as, say, the quadrupole or the magnetic moments. These parameters depend very sensitively on the characteristics of the nuclear models. The presently available experimental data on the optical anisotropy of nuclei are very poor. An analysis of the parameters on the basis of a model is thus rather difficult. Besides the experiments by Fuller and Hayward on Ho^{67} and Er^{68} (private communication by A. M. Baldin), where effects associated with the optical anisotropy were indirectly observed, there is no strong experimental proof for the existence of this important property in nuclei. However, the mentioned experiments and the existing theoretical investigations[3] present such strong arguments in favor of the existence of the optical anisotropy in nuclei that we shall be concerned only with the question of the quantitative determination of the relevant parameters.

As has been already pointed out by Baldin[4] a definite experimental proof could be obtained by studying the interaction of γ rays with oriented nuclei. An investigation of the absorption and of elastic and Raman scattering of photons on oriented nuclei can yield information sufficient to determine completely the parameters of the optical anisotropy. However, up to now this question has not been investigated experimentally at all and theoretically only in general terms (see e.g.[3,4], where the elastic scattering on oriented nuclei is treated). Unfortunately, the presently available experimental techniques do not allow the investigation of pure elastic scattering. The energy resolution is such that the elastically scattered photons cannot be separated from those inelastically scattered photons which excite the low lying states. The experiments of Fuller and Hayward are of this kind. However, the questions associated with the influence of the accuracy of the present day experiments and of the degree of the nuclear orientation on the effects of the optical anisotropy have not yet been investigated.

The aim of this paper is the investigation of the capabilities of the present day experiments concerning the observation of the effects of the optical anisotropy. The summary effect of elastic and inelastic photon scattering on oriented nuclei will be studied. From the effective cross section of this process one can deduce the influence of the energy resolution employed in the measurement of the scattered photons and of the degree of orientation on the effects of the optical anisotropy. On the basis of the model of the nonaxial nucleus developed by A. S. Davydov and co-workers, we consider briefly certain effects associated with the possible existence of nonaxial deformation of nuclei.

2. SCATTERING OF γ RAYS ON ORIENTED NUCLEI

It was mentioned above that in the present day experiments on elastic photon scattering on nuclei only an effective cross section can be obtained, with contributions both from purely elastically scattered photons and from those inelastic scattering events that excitate the low lying levels. It is well established experimentally that in highly deformed nuclei the lowest levels are connected with collective excitations which correspond, in particular, to rotations of the nucleus as a whole. It has been shown earlier[6] that the cross section of the inelastic scattering of photons associated with the excitation of rotational levels (the nuclear Raman scattering) can be described in terms of the parameters of the optical anisotropy, namely, the tensor and the vector polarizabilities. The combined effect of elastic and Raman scattering is thus determined by the same parameters (the optical anisotropy parameters) as the pure elastic scattering.

We consider now the combined effect of scattering on oriented axially symmetric nuclei. The scattering matrix for this process can be written in the form[4,6]

$$\langle mJ\lambda | R | m'J'\lambda'\rangle = \Big\{c^0 (-1)^{\nu}\delta_{\mu,-\nu}\delta_{mm'}\delta_{JJ'} + \sqrt{\frac{2J'+1}{2J+1}}\, i(1J'0K|JK) \times (1J'\mu+\nu m'|Jm)\frac{(11\,\mu\nu|1\,\mu+\nu)}{(11{-}11|10)}c^v + \sqrt{\frac{2J'+1}{2J+1}}(2J'0K\ |JK)\,(2J'\mu+\nu m'|Jm) \times \frac{(11\mu\nu|2\mu+\nu)}{(1100|20)}c^t\Big\}(-1)^{\mu+\nu}\lambda'_{-\mu}\lambda_{-\nu}\frac{1}{2\pi}\left(\frac{\omega}{c}\right)^3;$$

$$c^0 = c^s - e^2Z^2/AM\omega^2. \qquad (1)$$

(It is assumed here that the wave function of an axially symmetric nucleus can be written in the form[8]

$$|JmK\rangle = \sqrt{\frac{2J+1}{16\pi^2}}\,(D^J_{mK}(\theta)\,\chi^{\tau}_{K}(q) + (-1)^{J-i}D^J_{m-K}(\theta)\,\chi^{\tau}_{-K}(q)).$$

Furthermore, the condition $\Delta\omega/\omega \ll 1$ was used, where $\Delta\omega$ is the frequency change of the photon on scattering.) In Eq. (1) J and J′ are the nuclear spins and m and m′ their projections on the z axis; λ and λ′ are the photon polarization vectors. The unprimed and primed quantities refer to the state before and after the scattering respectively. (1J′0K|JK) etc are Clebsch-Gordan coefficients. The quantity

$$\frac{1}{2\pi}\left(\frac{\omega}{c}\right)^3\frac{e^2Z^2}{AM\omega^2}$$

is the amplitude of Thomson scattering on a nucleus of charge Z. c^S, c^V, c^t are the scalar, vector and tensor polarizabilities respectively.

The effective cross section for the combined scattering is obtained from (1) by means of the relation

$$d\sigma/d\Omega = (2\pi c/\omega)^2\,\mathrm{Sp}\,R\rho R^+. \qquad (2)$$

Here ρ is the density matrix describing the state of the target nucleus.

Inserting the expression for the R-matrix into (2), averaging over the polarizations of the incoming photons, summing over the polarizations of the scattered photons and over the final-state spins and their projections, we obtain an expression for the effective cross section of the summary process of the scattering of unpolarized photons on oriented nuclei:

$$\left(\frac{d\sigma}{d\Omega} - \frac{d\sigma^{\mathrm{u}}}{d\Omega}\right)2\left(\frac{\omega}{c}\right)^{-4} = \frac{2}{J+1}\mathrm{Re}\left[\left(\frac{1}{5}c^{t*} - c^{0*}\right)c^v\right](\mathbf{k}'\mathbf{k})\,\overline{(\mathbf{J}\,[\mathbf{k}'\mathbf{k}])} + \frac{1}{(J+1)(2J+3)}\Big\{\Big[\mathrm{Re}\,(c^{0*}c^t) + \frac{2}{3}|c^v|^2 - \frac{1}{14}|c^t|^2\Big][3\,\overline{(\mathbf{J}\,[\mathbf{k}'\mathbf{k}])^2} - J(J+1)\,[\mathbf{k}'\mathbf{k}]^2] + \Big[-\mathrm{Re}\,(c^{0*}c^t) + \frac{2}{3}|c^v|^2 - \frac{5}{14}|c^t|^2\Big][3\,\overline{(\mathbf{J}\mathbf{k}')^2} + 3\,\overline{(\mathbf{J}\mathbf{k})^2} - 2J(J+1)]\Big\} - \frac{6}{5}\frac{\mathrm{Re}\,(c^{t*}c^v)}{(J+1)(J+2)(2J+3)} \times \Big\{5S\,\overline{(\mathbf{J}\mathbf{k}')(\mathbf{J}\mathbf{k})(\mathbf{J}\,[\mathbf{k}'\mathbf{k}])} - \Big[J(J+1) - \frac{1}{3}\Big](\mathbf{k}'\mathbf{k})\,\overline{(\mathbf{J}\,[\mathbf{k}'\mathbf{k}])}\Big\} + \frac{18}{35}|c^t|^2\,\frac{1}{2(J+1)(2J+3)(J+2)(2J+5)} \times \Big\{35\,S\,\overline{(\mathbf{J}\mathbf{k}')(\mathbf{J}\mathbf{k}')(\mathbf{J}\mathbf{k})(\mathbf{J}\mathbf{k})} - 5\Big(J^2+J-\frac{5}{6}\Big)[\overline{(\mathbf{J}\mathbf{k}')^2(\mathbf{J}\mathbf{k})^2} + 2\,\overline{(\mathbf{J}\mathbf{k}')(\mathbf{J}\mathbf{k})(\mathbf{k}\mathbf{k}')} + 2\,\overline{(\mathbf{J}\mathbf{k})(\mathbf{J}\mathbf{k}')(\mathbf{k}'\mathbf{k})}] + J(J-1)(J+1)(J+2)[1+2(\mathbf{k}'\mathbf{k})^2]\Big\}. \qquad (3)^*$$

Here k and k′ are unit wave vectors of the photons before and after scattering, respectively, and S means a symmetrized sum [the quantity $S(a_1, a_2, \ldots a_n)$ is the sum of all permutations of the product $a_1, a_2, \ldots a_n$ divided by n!]. Mean values of the type $\overline{(\mathbf{J}\cdot\mathbf{k}\times\mathbf{k}')^2}$ are calculated with the density matrix in the usual way

$$\overline{(\mathbf{J}\,[\mathbf{k}'\mathbf{k}])^2} = \mathrm{Sp}(\mathbf{J}[\mathbf{k}'\mathbf{k}])^2\rho.$$

The quantity

*$(\mathbf{k}'\mathbf{k}) = (\mathbf{k}\cdot\mathbf{k})$, $[\mathbf{k}'\mathbf{k}] = [\mathbf{k}'\times\mathbf{k}]$, $(\mathbf{J}[\mathbf{k}'\mathbf{k}]) \to (\mathbf{J}\cdot\mathbf{k}'\times\mathbf{k})$.

$$\frac{d\sigma^u}{d\Omega} = \frac{1}{2}\left(\frac{\omega}{c}\right)^4 \left\{|c^0|^2(1+(k'k)^2) + \frac{1}{3}|c^v|^2(3-(k'k)^2) + \frac{1}{20}|c^t|^2(13-(k'k)^2)\right\}$$

is the summary cross section for the scattering of unpolarized photons on unoriented nuclei, the quantity which has been measured by Fuller and Hayward.

In order to estimate the effects connected with the optical anisotropy of nuclei we evaluate the quantity α in analogy with [4]:

$$\alpha \frac{d\sigma^u}{d\Omega} \equiv \frac{d\sigma}{d\Omega}(k' = e_x, k = e_y, [k'k] = e_z) - \frac{d\sigma}{d\Omega}(k' = e_z, k = e_y), [k'k] = -e_x). \quad (4)$$

Inserting the values for the cross section from (3) and putting $c^v = 0$ (as has been shown[4] the value of c^v is much smaller than c^0 and c^t) we find for fully polarized nuclei ($\rho_{mm'} = \delta_{mJ}\delta_{m'J}$) the following expression for α:

$$\alpha = \left\{3\left[\mathrm{Re}(c^{0*}c^t) + \frac{1}{7}|c^t|^2\right]\frac{J(2J-1)}{(J+1)(2J+3)} + \frac{9}{28}|c^t|^2 \times \frac{J(2J-1)(J-1)(2J-3)}{(J+1)(2J+3)(J+2)(2J+5)}\right\} \Big/ \left[|c^0|^2 + \frac{13}{20}|c^t|^2\right]. \quad (5)$$

In order to obtain a numerical estimate for α one has to know the optical anisotropy parameters c^0 and c^t. We use the expressions for the tensor and scalar polarizabilities given in [3] and find for the case where the nuclear spin equals $7/2$:

$$\alpha(\omega = \omega_1, c^t \approx 2c^0) = 1.04,$$
$$\alpha(\omega = \omega_2, c^t \approx -c^0) = -0.7.$$

On the other hand, for the case of pure elastic scattering, α has the values

$$\alpha_{el}(\omega = \omega_1, c^t \approx 2c^0) = 1.5,$$
$$\alpha_{el}(\omega = \omega_2, c^t \approx -c^0) = -0.9.$$

One thus can conclude that the observable effects associated with the nuclear optical anisotropy are somewhat smaller if one measures the combined elastic and nuclear Raman scattering, as compared with the measurement of pure elastic scattering. However, experiments of this kind have the advantage that they yield direct evidence on the internal parameters of the optical anisotropy as can be seen from (3) and (5).

The above analysis of the consequences of the impossibility of observing purely elastic scattering from oriented nuclei with present-day techniques was based on (3) under the condition that the nuclei are fully oriented. It is experimentally impossible, however, to achieve full nuclear orientation. This must obviously lead in itself to a decrease in the magnitude of the observed effect. The influence of the degree of nuclear orientation can also be evaluated by (3), which is valid for any kind and degree of nuclear orientation. One just has to specify the density matrix appropriate to the particular case. We shall consider only the frequently applicable case when the density matrix is of the form $\rho_{mm'} = f(m)\delta_{mm'}$ (this case corresponds to a system having z as an axis of symmetry.

With this density matrix one can write (3) for a sufficiently high degree of nuclear orientation in a very simple and convenient way:

$$\left(\frac{d\sigma}{d\Omega} - \frac{d\sigma^u}{d\Omega}\right)2\left(\frac{\omega}{c}\right)^{-4} \approx [-2\mathrm{Re}(c^{0*}c^v) + \frac{2}{5}\mathrm{Re}(c^{t*}c^v)](k'k)[k'k]_z\frac{\bar{m}}{J+1} + [\mathrm{Re}(c^{0*}c^t) + \frac{2}{3}|c^v|^2 - \frac{1}{14}|c^t|^2]\left(\frac{3}{2}[k'k]_z^2 - \frac{[k'k]^2}{2}\right)\frac{3\bar{m}^2 - J(J+1)}{(J+1)(2J+3)} + [-\mathrm{Re}(c^{0*}c^t) + \frac{2}{3}|c^v|^2 - \frac{5}{14}|c^t|^2](\frac{3}{2}k_z'^2 + \frac{3}{2}k_z^2 - 1) \times \frac{3\bar{m}^2 - J(J+1)}{(J+1)(2J+3)}. \quad (6)$$

From (6) one sees immediately that for such a system the effects connected with the vector polarizability are determined by the orientation parameter $f_1 = \bar{m}/(J+1)$, while effects of the tensor polarizability are similarly associated with the orientation parameter $f_2 = [3\bar{m}^2 - J(J+1)]/J(2J-1)$.

The highest value for f_2 which can be achieved experimentally is 0.4 to 0.5. We thus obtain for the observable effects associated with the tensor polarizability at incomplete nuclear orientations ($f_2 = 0.5$) the values

$$\alpha(\omega = \omega_1, c^t \approx 2c^0) = 0.5, \qquad \alpha(\omega = \omega_2, c^t \approx -c^0) = 0.3.$$

The following important circumstances have to be pointed out. As can be seen from (6) one can investigate the effects of the nuclear vector polarizability only with polarized nuclei while the effects of the tensor polarizability can be observed both with polarized and with aligned nuclei. We also note that the effects of the optical anisotropy are largest at a scattering angle of 90°.

It was above assumed that K is a good quantum number with K = J. This is only approximately true.[8,9] Admixture of states with $K \neq J_0$ can, generally speaking, decrease the magnitude of the effects of the optical anisotropy in the described experiment. However, this decrease will be insignificant since direct calculations, analogous to those of Bohr,[8] show that in the ground state K differs from J by at most a few percent. Thus the

most important factors that tend to decrease the magnitude of the observable effects of the optical anisotropy in scattering experiments on oriented nuclei are the incomplete orientation of the nuclei and the poor energy resolution of the photons.

3. INFLUENCE OF THE POSSIBLE NONAXIALITY ON SOME CHARACTERISTICS OF NUCLEAR OPTICAL ANISOTROPY

In conclusion we shall say a few words on the interaction of photons with nonaxial nuclei. Such a model has been developed by Davydov and coworkers.[10] Generally speaking the operator of the tensor polarizability must be characterized by two independent parameters, since it is a symmetric tensor of second rank with zero trace. We consider all the quantities in a system of coordinates fixed with respect to the nucleus (we recall that the low lying nuclear excited states are supposed to be rotational states). We can then choose as the parameters, for example, the quantities $\langle\alpha^t_{zz}\rangle \equiv c^t$ and $\langle\alpha^t_{xx} - \alpha^t_{yy}\rangle$ (α^t_{ik} is the tensor part of the electric dipole polarizability operator). For the above-considered case of a strongly deformed axially symmetric nucleus, $\langle\alpha^t_{xx} - \alpha^t_{yy}\rangle$ equals zero and all effects of the optical anisotropy are given by only one parameter, the tensor polarizability c^t.

This is not true for a nonaxial nucleus, for which the parameter $\langle\alpha^t_{xx} - \alpha^t_{yy}\rangle$ evaluated in the nuclear coordinate system differs from zero. Clearly this parameter will lead to changes in the results obtained above. We consider, for example, the interaction of photons with even-even nonaxial nuclei for which there exist exact wave functions for the rotational states, as given by Davydov and Filippov.[10] In such nuclei the tensor polarizability does not manifest itself in elastic scattering processes. However one can attempt to observe it in the nuclear Raman scattering in which rotational levels are excited.[3 6] Utilizing the wave function of the rotational states of even-even nonaxial nuclei[10] and employing a procedure similar to one used previously,[6] one can show that the effective cross section for inelastic photon scattering under excitation of the states 2^+_1 and 2^+_2 is given by the expression

$$\left(\frac{d\sigma}{d\Omega}\right)_{0^+\to 2^+_i} = \frac{1}{40}\left(\frac{\omega}{c}\right)^4 \left| a_i(\gamma) + \frac{b_i(\gamma)}{\sqrt{3}} \frac{\langle\alpha^t_{xx} - \alpha^t_{yy}\rangle}{c^t}\right|^2 |c^t|^2 (13 + \cos^2\theta). \quad (7)$$

Here i = 1, 2; the quantities c^t and $\langle\alpha^t_{xx} - \alpha^t_{yy}\rangle$ can be calculated by means of the wave functions that describe the internal nuclear state.

We use for estimating $\langle\alpha^t_{xx} - \alpha^t_{yy}\rangle/c^t$ the model of an anisotropic oscillator (according to this model the nucleus is considered to consist of three oscillators with frequencies $\omega_i \sim 1/R$). It can be then shown that up to the order β^2, where β is the axial deformation parameter, we have

$$\langle\alpha^t_{xx} - \alpha^t_{yy}\rangle / c^t = \sqrt{3}\,\mathrm{tg}\,\gamma. \quad (8)^*$$

[In the derivation of (8) it was assumed that the damping constants of all three oscillators are equal. This assumption is obviously true for not too large β.] Inserting (8) into (7) we find for the ratio of the cross sections

$$\left(\frac{d\sigma}{d\Omega}\right)_{0^+\to 2^+_2} \Big/ \left(\frac{d\sigma}{d\Omega}\right)_{0^+\to 2^+_1} = \left(\frac{a_2 + b_2\,\mathrm{tg}\,\gamma}{a_1 + b_1\,\mathrm{tg}\,\gamma}\right)^2. \quad (9)$$

In the region of $\gamma \approx 30°$ (condition for $\Delta\omega/\omega \ll 1$ to be true) this ratio is considerably less than unity. Thus one can conclude that in nonaxial even-even nuclei the cross section for excitation of level 2^+_2 in a scattering process is much smaller than that for the level 2^+_1.

Since the wave functions of nonaxial odd-A nuclei are unknown, it is at present impossible to make any predictions on the influence of the nonaxiality on interactions of photons with oriented nuclei.

The authors express their gratitude to A. M. Baldin for his constant interest in the work and for discussion of the obtained results.

[1] A. M. Baldin, Yadernye reaktsii pri malykh i srednikh energiyakh (Nuclear reactions at small and medium energies), AN SSSR (1958), p. 479.

[2] A. M. Baldin, Nucl. Phys. **9**, 237 (1958).

[3] A. M. Baldin, JETP **37**, 202 (1959), Soviet Phys. JETP 10, 142 (1960).

[4] A. M. Baldin and S. F. Semenko, JETP **39**, 434 (1960), Soviet Phys. JETP **12**, 306 (1961).

[5] A. M. Baldin, Proc II. All-union Conf. Nucl. React. at Small and Med. Energies, Moscow (1960).

[6] B. A. Tulupov, Proc. II All-union Conf. Nucl. React. at Small and Med. Energies, Moscow (1960).

[7] U. Fano, NBS Technical Note **83** (1960).

[8] A. Bohr, Mat.-Fys. Medd. Dansk. Vid. Selsk. **26**, No. 14 (1952).

[9] A. Bohr and B. Mottelson, Mat.-Fys. Medd. Dansk. Vid. Selsk. **27**, No. 16 (1953).

[10] A. S. Davydov and G. F. Filippov, JETP **35**, 440 (1958), Soviet Phys. JETP **8**, 303 (1958); Nucl. Phys. **8**, 237 (1958).

Translated by M. Danos
334

*tg = tan.

POSSIBLE METHOD OF DETECTING HIGH-ENERGY CHARGED PARTICLES

A. I. ALIKHANYAN, F. R. ARUTYUNYAN, K. A. ISPIRYAN, and M. L. TER-MIKAELYAN

Physics Institute, Academy of Sciences, Armenian S.S.R.

Submitted to JETP editor July 25, 1961

J. Exptl. Theoret. Phys. (U.S.S.R.) 41, 2002-2010 (December, 1961)

The characteristics of the radiation produced by fast charged particles moving in a layered medium are investigated. The possibility of detecting this radiation is discussed and experimental methods for observing it are proposed; methods of using this radiation for the detection of charged particles and the measurement of particle energies are considered.

1. CHARACTERISTIC FEATURES OF RADIATION PRODUCED BY THE PASSAGE OF FAST PARTICLES THROUGH A LAYERED MEDIUM. CHOICE OF PARAMETERS.

It has already been pointed out by one of the authors[1-3] that the radiation produced by the passage of fast particles through an arbitrary periodic medium can be of use in high-energy particle physics. As an example we discuss here the theoretical and experimental aspects of the problem of using this radiation (which, for brevity, will be called resonance radiation) for the detection of charged particles and the measurement of particle energy. From the experimental point of view the most convenient periodic medium is one made up of layers. Hence, in what follows we use the example of a one-dimensional layered medium consisting of alternating slabs of two different materials. The thickness of the first slab is denoted by l_1 and the second by l_2. The period of the medium is then

$$l = l_1 + l_2. \tag{1.1}$$

The number of electrons per cubic centimeter in the two materials is denoted by N_1 and N_2 respectively. To be specific we assume that $N_1 > N_2$. The ratio of the thickness of the second slab (less dense) to that of the first is denoted by α:

$$\alpha = l_2/l_1. \tag{1.2}$$

The number of photons radiated in the frequency interval $d\omega$ due to the traversal of one centimeter of the layered medium (transverse to the slabs) is given by the expression

$$dm = \frac{4p^2(1+\alpha)}{137\pi l_1}\sum_{r=1}^{r_{max}}\frac{d\omega}{r^3\omega^3}\frac{\left[1-\frac{1}{4}(E_{1t}/E)^2\omega^2r^{-2}\omega^{-2}\right]}{(1-p/\omega r)^2(1+p\alpha/\omega r)^2}$$
$$\times\sin^2\left[\left(\frac{\alpha}{1+\alpha}\right)\pi r-\frac{\pi}{\omega}\left(\frac{\alpha p}{1+\alpha}\right)\right]. \tag{1.3}$$

The radiated frequency ω is measured in units of

$$\omega_{1min} = l_1 r_e c\,(N_1 + \alpha N_2), \tag{1.4}$$

where r_e is the classical electron radius and c is the velocity of light. The properties of the media appear in this expression through the quantity p, defined by

$$p = (N_1 - N_2)/(N_1 + \alpha N_2). \tag{1.5}$$

The quantity E_{1t} is given by

$$E_{1t} = mc^2 l_1\,[\pi^{-1}r_e\,(1+\alpha)\,(N_1+\alpha N_2)]^{1/2}. \tag{1.6}$$

We note first that the number of radiated photons is made up of radiation corresponding to different orders (or different harmonics); these are enumerated by the letter r. The quantity r can vary from r_e to r_{max}:

$$r_{max} \approx l_1\,[\pi^{-1}r_e\,(1+\alpha)\,(N_1+\alpha N_2)]^{1/2}. \tag{1.7}$$

The basic contribution in the processes considered below is due to harmonics characterized by harmonic numbers appreciably smaller than r_{max}. For these values of r to obtain, the period of the layered medium must be greater than 10^{-5} cm. We now deduce the basic properties of the resonance radiation. Since the expression in the numerator of Eq. (1.3) must be positive, it follows that for each harmonic the radiated frequency interval must lie between ω_{min} and ω_{max}:

$$\omega^{(r)}_{\substack{min\\max}} = (r \mp \sqrt{r^2 - (E_{1t}/E)^2})\,/\,(E_{1t}^2/2E^2). \tag{1.8}$$

This interval can be achieved if the expression under the radical in (1.8) is real, i.e., if $r < E_{1t}/E$

$$\frac{E}{mc^2} \geqslant \frac{E_t}{mc^2}\quad\frac{l_1}{r}\,[\pi^{-1}r_e\,(1+\alpha)\,(N_1+\alpha N_2)]^{1/2}. \tag{1.9}$$

Consequently there is a definite energy threshold

for radiation of a given harmonic. The threshold energy decreases with increasing harmonic number. If the particle energy is appreciably greater than the threshold energy, so that (1.8) can be expanded in the parameter $E_{1t}/2E$, then the interval of radiated frequencies for each harmonic is given by the simple inequality:

$$1/r \approx \omega_{rmin} \leqslant \omega \leqslant \omega_{rmax} \approx 4rE^2/E_t^2. \quad (1.10)$$

The physical meaning of the frequency introduced above ω_{1min} follows from (1.10); it is evident that $r = 1$ gives the lowest possible radiated frequency at the first harmonic $\omega_{1min} = 1$. In what follows the particle energy will be measured in units of E_{1t} ($\alpha = 1$) — the threshold energy for the first harmonic for $\alpha = 1$.

Radiation with the properties described above can be generated only by relativistic particles [(1.7) and (1.9)]. At lower (still relativistic) energies, a particle can only radiate harmonics with high values of r. As the energy of the radiating particle increases radiation will gradually appear at new harmonics. If the particle energy is greater than the threshold energy for the first harmonic, denoted below by $(E/mc^2)_{1t}$ [Eq. (1.9) with $r = 1$], no new harmonics can be produced and the radiation intensity reaches a saturation point. Under these conditions the energy loss due to resonance radiation is approximately 10^4 ev per g/cm^2 for a periodic medium consisting of solid slabs in a gas. It should be noted that the loss given above is a weak function of slab thickness and slab material, and that it falls off slowly with increasing α; at large values of α ($\alpha > 10$) the loss goes as $1/\alpha$. This result can be understood qualitatively if one considers the fact that "harder" photons will be radiated from thicker slabs (1.4).

The differential photon spectrum for a given harmonic is given by a curve that exhibits a maximum at approximately $\omega = 1.5\ \omega_{min}$ and intersects the abscissa axis at ω_{min} and ω_{max}. The number of photons falls off sharply beyond the maximum. For this reason the high-frequency contribution to the radiation intensity can be neglected. The onset frequency ω_{min} does not change as the energy increases, but ω_{max} increases as E^2 [(1.10)].

However, because of the nature of the spectrum indicated above we can neglect the energy dependence of the radiation intensity at each harmonic if the particle energy exceeds the threshold value at a given harmonic. For illustration, in Fig. 1 we show the differential spectrum of resonance radiation for a particular case ($E = 2.2\ E_{1t}$, $\alpha = 1$). The resonance radiation at several harmonics is shown in the figure; the upper curve shows the total differential spectrum for all harmonics with $E = 5\ E_{1t}$ and $\alpha = 1$. The radiation frequency ω (in units of ω_{1min}) is plotted along the abscissa axis while the quantity $l_1 f(\omega)$ is plotted along the ordinate axis. We shall not give the corresponding curves for other values of the parameters here (cf. [3]).

Several parameters characterizing the differential spectrum of the resonance radiation appear in (1.3). It is assumed that $\alpha_2 N_2 \ll N_1$. This condition is satisfied in a periodic medium consisting of solid slabs in a gas. It should be noted that a layered medium consisting of two different kinds of solid slabs would be much easier to use than the one described here; however, to achieve the condition $p \approx 1$ it would be necessary to use solid slabs with markedly different atomic weights (a light material and a dense material). On the other hand, photo-absorption of resonance photons in dense materials could reduce the radiation output

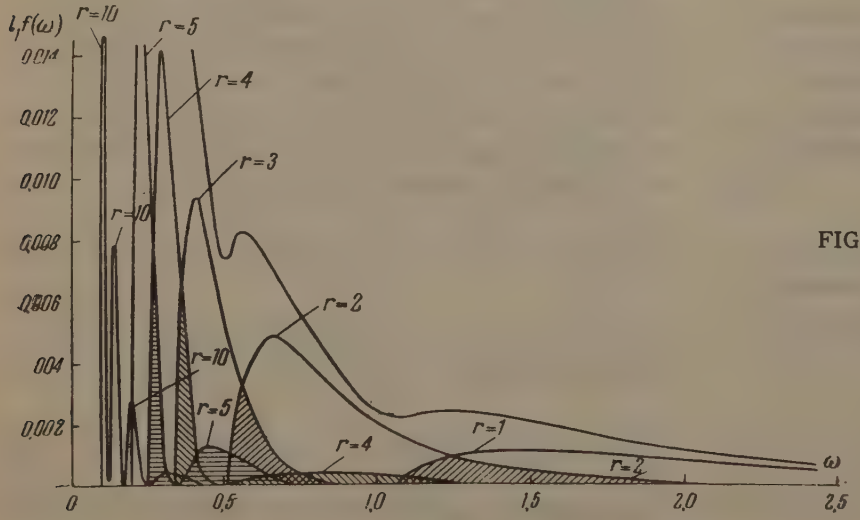

FIG. 1. Differential resonance radiation spectrum ($\alpha = 1$).

severely. With two materials with small atomic weights, however, p is of the order of 0.3 — 0.7 and the radiation intensity (which is proportional to p^2 for small values of p) is smaller than that obtained with slabs in a gas. Inasmuch as intense beams of charged particles are available from accelerators, from the purely experimental point of view it would be preferable to use a layered medium consisting of two different kinds of solid slabs. When cosmic rays are studied, however, it would be necessary to use a medium consisting of slabs located in a gas in order to obtain adequate radiation intensity (we have taken p = 0.99 in these calculations). It follows from Eq. (1.4) that the quantity $\omega_{1\min}$ depends only on slab thickness and electron density when $p \approx 1$.

The values of $\hbar\omega_{1\min}$ for several materials are shown in Table I. We emphasize that slab thickness and slab material determine completely the frequency region in which resonance radiation can be detected. Values of the threshold energy are given in the same table (for $r = 1$ and $\alpha = 1$). We also emphasize that in addition to depending on l_1 and N_1 the threshold energy is also a function of the interslab distance, varying as $(1 + \alpha)^{1/2}$ [(1.9)]. Using (1.4) we can compute $\hbar\omega_{1\min}$ for a given material and thickness. Particles with energies greater than $(E/mc^2)_{1t}$ produce photons with energies greater than $\hbar\omega_{1\min}$, but particles with smaller energies produce softer protons. Thus, an experimental device that detects photons at frequencies (energies) greater than some frequency related to $\omega_{1\min}$ can be used to separate out particles with energies greater than E_{1t}. It will be evident that particles with smaller energies can be detected in precisely the same way if the first harmonic is used instead of the second and so on.

As an example we consider several typical curves (Fig. 2) illustrating the dependence of the number of radiated photons on particle energy. The energy of the initial particle is plotted along the abscissa axis in units of the threshold energy (E/E_{1t}). The ordinates represent the number of radiated photons per centimeter characterized by $\omega > 0.1$, $\omega > 1$, and $\omega > 3$ multiplied by the slab

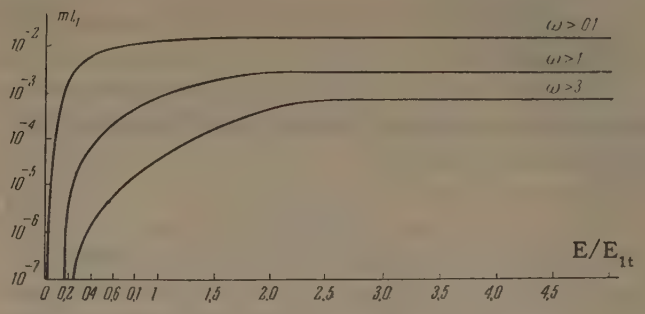

FIG. 2. The total number of photons (ml_1) as a function of particle energy for different ω with $\alpha = 1$.

thickness l_1. These curves show that the number of resonance photons per centimeter of path of layered material is a very sensitive function of particle energy. We do not give corresponding curves here for other values of α or for other values of the minimum frequency. The number of photons radiated per centimeter of path of a layered material increases with α (up to $\alpha \sim 3$) and then falls off approximately as $2/(1 + \alpha)$.

All these results can be easily obtained from (1.3). It is evident that a given experimental device is sensitive to photons in a given energy range. Hence, we start with some initial energy for the photons produced in the layered medium and detected by the device. For instance, the frequency region $\omega \geq 1$ corresponds to photons with energies greater than $\hbar\omega_{1\min}$. We could have chosen the region $\omega \geq 0.1$ or $\omega \geq 10$; however, analysis shows that it is most desirable to operate in the region $\omega = 1.2 - 1.6$. In this region one obtains the maximum number of photons per centimeter with an adequately sensitive dependence of photon number on particle energy. For example, the slab thickness must be reduced by 50 % if the value $\omega = 2$ is taken and the observations are carried out with photons of the same energy. The threshold energies are correspondingly reduced by 50 %. With ω smaller than unity, for example $\omega = 0.1$, we find on comparing with the $\omega = 1$ case that the slab thickness and threshold energies are increased by a factor of ten while the number of photons per centimeter of path is one half as large. Let us assume operation in the region $\omega = 1$, i.e., that the detected photons have energies greater than

Table I

Material	$10^{-22}N_1$, cm^{-3}	$E_\gamma = \hbar\omega_{1min} = 5{,}55 \cdot 10^{-24} N_1 l_1$, Mev	$\frac{10^{-3}}{l_1}\left(\frac{E}{mc^2}\right)_{1t}$, $\alpha = 1$
Paper	2—3	$(1.1—1.7)l_1$	1.6--2.4
Polyethylene	2.8	$1.53l_1$	2.21
Be	4.9	$2.72l_1$	2.95
Al	7.8	$4.33l_1$	3.72

$\hbar\omega_{1min}$. This choice will be used in most of the further analysis.

When absorption in the medium is taken into account the number of photons emitted from the layered material is

$$n = (M/\mu)(1 - e^{-\mu L}), \qquad (1.11)$$

where M is the number of photons produced per centimeter of length of the layered material, μ is the radiation absorption coefficient, and L is the total length of the layered material. When $L \gg 1/\mu$, $n = M/\mu$. The layered material should have the lowest possible value of Z.

The radiation can be detected by several different methods, each of which will be considered individually.

2. METHOD OF ENERGY GENERATION

The particle and the radiation it produces pass through a detector, which registers the amount of generated energy. The detector must be such that the radiation it absorbs can be used to establish the initial radiation from the energy generated by the particle and the initial radiation. It is convenient to use a high-Z absorber. Useful data can be obtained with a proportional gas counter in which a heavy gas is used.

In Fig. 3 we show the quantity I (the ratio of energy generated by the γ photons of the resonance radiation to the energy generated by the particle) as a function of particle energy in Be for different parameters of the layered material. In Table II we give the conversion factor k for other materials. The optimum frequency region for this method is $E_\gamma = 8 - 15$ kev. It is evident from Figs. 2 and 3 that a layered material characterized by high values of α should be used. Making α too large, however, does not increase the value of I appreciably but can make the experimental apparatus, which consists of the layered material and

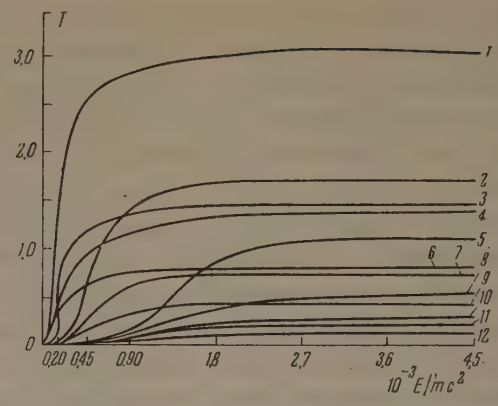

FIG. 3. The ratio of energies generated by resonance radiation and by the particle as a function of energy.

a proportional counter located under it, much more complicated. This method is suitable for the measurement of particle energies in the range $E/mc^2 = 2 \times 10^2 - 2 \times 10^3$ and for the detection of particles with energies greater than this value.

3. CHARACTERISTIC-RADIATION METHOD

The particle and the radiation it produces in the layered material pass through a gas absorber. Gamma photons with energies equal to or greater than the energy of the K level of the given gas produce a photo effect in the K level. The gas then emits characteristic radiation with energy E_K. The absorption coefficient for the characteristic radiation at the K edge is 5 — 7 times smaller than the usual absorption coefficient at the K edge; furthermore, the radiation distribution is isotropic. For these reasons the radiation can be detected in directions other than the direction of motion of the particle. As in the first method the layered material must be one with small Z. In Fig. 4 we show the number of photons emitted from a layered polyethylene material and absorbed in Xe as a function of particle energy for different values of α. The conversion coefficient k for other materials is also given.

Table II

No.	$E_{min} \cdot 10^{-6}$, ev	α	Gas	Slab thickness L, cm	kn_e	k_{Al}	No. of layers
1	1	60	Xe	122	0.3		650
2	1	10	Xe	22		$2.5 \cdot 10^{-2}$	
3	1	60	Ar	122			
4	1.5	60	Xe	235	0.44		840
5	1.5	10	Xe	42		$41 \cdot 10^{-2}$	
6	1.5	60	Ar	235			
7	1	10	Ar	22			
8	1	1	Xe	4			
9	1.5	10	Ar	42			
10	1.5	1	Xe	7.7			
11	1	1	Ar	4			
12	1.5	1	Ar	7.7			

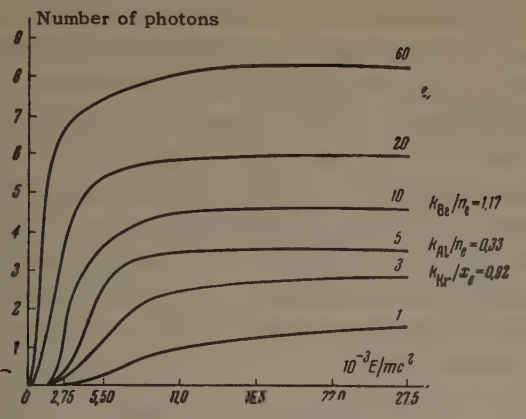

FIG. 4. The number of characteristic-radiation photons as a function of particle energy for various values of α.

The characteristic γ photons with energies E_K = 35 kev (E_K = 14.3 kev for Kr) can be detected transversely by means of scintillators. High-pressure proportional gas counters can be used. The counter walls can be very thin if the pressure in the counters is compensated by a light gas kept at the same pressure as the gas absorber.

Thus, the experimental device consists of the layered material under which there is a gas absorber. The scintillators are located at the sides of the gas absorber. It is desirable to use the scintillator NaI (Tl), in which the detection efficiency for γ photons is almost 100 % in the region 2 — 30 kev. A detection device of the following design can also be used. The γ photons from the gas absorber (Xe) enter another region which is also filled with xenon, but at a pressure such that all the radiation is absorbed. The xenon itself scintillates (the light yield is $^{32}/_{72}$ of the yield from NaI (Tl) [4]). This technique can be used to increase the light yield in a device when it is used for detecting high-energy cosmic-ray particles. We note that the transverse dimensions of the gas absorber must be equal to or less than the longitudinal dimension.

The layered material can also be located directly inside the gas absorber. In this case the characteristic radiation can be detected at the sides of the layered medium. This technique is suitable for measuring particle energies in the range $E/mc^2 = 5 \times 10^2 - 5 \times 10^3$ and for detecting particles with higher energies.

4. COMPTON-SCATTERING METHOD

We assume that the length of the layered material is such that the radiation produced by the particle experiences multiple Compton scattering in the material. The transmission factor T can then be written approximately in the form [5]

$$T = B \exp(-\mu_0 x), \qquad (4.1)$$

where x is the thickness of traversed material and μ_0 is the minimum radiation absorption coefficient while the factor B lies between unity and $(\mu_0 x)^2$.

The remainder of the radiation (1 — T) escapes from the sides of the layered material. This situation holds for "good" geometry. To determine exactly the number and angle-energy distribution of the γ photons escaping from the sides of the layered material in a given geometry would require extremely complicated calculations (for example, a Monte Carlo calculation). We shall use the approximation formula (4.1), which indicates that most of the radiation escapes from the sides of the layered material. These γ photons can be detected most conveniently by means of large liquid scintillators such as those used by Cowan and Reines [6]. In this method the energy of the γ photons must be such that the photoeffect is negligible compared with the Compton effect.

For example, with a layered medium made from Al (l_1 = 0.1 cm, α = 1) we obtain 3×10^{-2} photons with energies greater than 0.5 Mev per centimeter of layered material. For Be, with $l_1 = 3.24 \times 10^{-2}$ and $\alpha = 1$ we find 9.23×10^{-2} photons with energies greater than 0.1 Mev. This method can be used to detect particles over a wide energy range since the detection of the resonance γ photons does not depend on absorption along the particle path.

5. EXPERIMENTAL BACKGROUND

The particle that produces the resonance radiation also produces a background radiation; this background must be taken into account, particularly in cosmic-ray work.

The particle will produce δ electrons in the layered medium and these electrons produce bremsstrahlung in coming to rest in the medium. The number of γ photons produced by the δ electrons per g/cm^2 of the layered medium is

$$N_{\delta\gamma} = \int\int_{\varepsilon E_\gamma} R(\varepsilon)\, N_\delta(E_0, \varepsilon)\, d\varepsilon \cdot N_\gamma(\varepsilon, E_\gamma)\, dE_\gamma;$$

$$N_\delta(E_0, \varepsilon)\, d\varepsilon = 2\pi \frac{N}{A} Z r_e^2 m_e c^2 \frac{1}{\beta^2} \frac{d\varepsilon}{\varepsilon^2},$$

$$N_\gamma(\varepsilon, E_\gamma)\, dE_\gamma = \frac{4}{137} \frac{N}{A} Z^2 r_e^2 \ln(183 Z^{-1/3}) \left(\frac{m_e c^2 + \varepsilon}{\varepsilon}\right) \frac{dE_\gamma}{E_\gamma}. \qquad (5.1)$$

The quantity N_δ is the number of δ electrons with energy ϵ that produce particles with energy E_0 in 1 g/cm^2 of material; $N_\gamma dE_\gamma$ is the number of γ photons with energies E_γ radiated by an electron with energy ϵ per g/cm^2 of material;

$R(\epsilon)$ is the range of an electron with energy ϵ, as given by empirical formulas [7].

In Table III we show the quantity $N_{\delta\gamma} \times 10^2$ for different materials for the case where the energy of the bremsstrahlung γ rays is greater than a given E_γ. The bremsstrahlung produced by the particle itself (not the electron) is negligibly small. Table III can be used to estimate the energy generation in a proportional counter (the first method in Sec. 3) due to bremsstrahlung of the particle and the δ electrons. This background is 0.5 % of the resonance radiation.

The number of background photons in the characteristic-radiation method (Sec. 4) is approximately 4×10^{-2}.

The background radiation is more noticeable in the Compton scattering method. Optimum conditions obtain when $\alpha = 3 - 5$, in which case the number of resonance radiation photons per centimeter of layered material is a maximum. Under these conditions the background radiation is 10 % for Be but as high as 150 % for Al.

The δ electrons produced in the layered medium by the particle can escape and be recorded by the detectors intended for recording the γ radiation. The number of δ electrons escaping from the layered material can be computed from the expression:

$$n_\delta = \int_\varepsilon R(\varepsilon)\, N_\delta(E_0, \varepsilon)\, d\varepsilon. \qquad (5.2)$$

The number of δ electrons with energies greater than ϵ escaping from a layered material with a thickness of 10 g/cm^2 is given below:

E_γ, Mev:	0.01	0.05	0.1	0.25	0.5	0.7	1	2	6	10	20
n_δ:	0.216	0.212	0.200	0.192	0.180	0.170	0.160	0.130	0.094	0.075	0.037

The δ electrons can strike the detectors that are used for recording the γ photons. The geometry of the instrument can be selected to avoid this background. A better way of avoiding effects due to δ electrons is to locate the layered medium in a magnetic field that "ejects" δ electrons.

The energy generated by δ electrons in a proportional counter (Sec. 3) is

$$E_\delta = \int_\varepsilon \left(\frac{d\varepsilon}{dx}\right) [R(\varepsilon)]^2 N_\delta(E_0, \varepsilon)\, d\varepsilon, \qquad (5.3)$$

where $(d\epsilon/dx)$ is the ionization loss of δ electrons with energy ϵ per g/cm^2 of material. The quantity E_γ is 15 — 20 % of the energy generated by the particle in a proportional counter filled with Xe (1.39×10^{-2} g/cm^2).

A particle passing through a gas absorber (characteristic-radiation method) can generate characteristic radiation directly. The number of such characteristic-radiation background photons per g/cm^2 of the gas absorber is

$$n_n = \frac{N}{A} \int_{E_K}^{E_0} \sigma_K(E_\gamma)\, N(E_\gamma)\, dE_\gamma, \text{ where } N(E_\gamma)\, dE_\gamma$$

$$= \frac{2}{137\pi} \ln(E_0/E_\gamma)\, dE_\gamma/E_\gamma \qquad (5.4)$$

is the number of pseudophotons with energies E_γ for a particle with energy E_0 (Weizsäcker-Williams method) and $\sigma_K(E_\gamma)$ is the photo-effect cross section in the K-shell. [5] The quantity $n_n = 5 \times 10^{-2}$ if the amount of gas absorber (Xe) used in the experiment is 5.4×10^{-2} g/cm^2.

Table III

E_γ, Mev	Be	Polyethylene	Al
0.01	3.00	1.66	15.5
0.05	2.24	1.20	11.3
0.10	1.54	0.83	7.7
0.20	1.31	0.71	6.6
0.40	1.06	0.57	5.3
0.70	0.9	0.48	4.5
1.0	0.7	0.42	3.9
2.0	0.6	0.31	1.5

δ electrons with energies of 0.1 Mev or greater also produce background characteristic radiation. The number of such photons is less than 10^{-2}.

6. DETECTION OF COSMIC-RAY PARTICLES

The use of resonance radiation for the detection of charged cosmic-ray particles is made difficult only by the fact that it is necessary to distinguish high-energy particles against a strong background of low-energy particles.

Muons with energies of 10^{11} ev and higher in cosmic rays can be detected by the energy-generation method if two units are connected in coincidence (taking account of ionization fluctuations). When the characteristic radiation method is used it is necessary to detect 3 — 4 characteristic photons simultaneously; thus this technique can be used to detect μ mesons with energies of approximately 5×10^{11} and higher.

[1] M. L. Ter-Mikaelyan, DAN SSSR 134, 318 (1960), Soviet Phys. Doklady 5, 1015 (1961).

[2] M. L. Ter-Mikaelyan and A. D. Gazazyan, JETP **39**, 1693 (1960), Soviet Phys. JETP **12**, 1183 (1961).

[3] M. L. Ter-Mikaelyan, Izv. AN ArmSSR **14**, 103 (1961).

[4] J. A. Northrup and R. Nobles, Nucleonics 14, 36 (1956).

[5] E. Segre, Experimental Nuclear Physics, Wiley, N. Y., 1953.

[6] F. Reines and C. H. Cowan, Phys. Today 10, 12 (1957).

[7] K. Siegbahn, Beta- and Gamma-Ray Spectroscopy, North-Holland, 1955.

Translated by H. Lashinsky
335

PHOTODISINTEGRATION OF THE DEUTERON AT MEDIUM ENERGIES

L. N. SHTARKOV

P. N. Lebedev Physics Institute, Academy of Sciences, U.S.S.R.

Submitted to JETP editor July 31, 1961

J. Exptl. Theoret. Phys. (U.S.S.R.) 41, 2011-2014 (December, 1961)

An analysis is made of earlier experimental data on photodisintegration of the deuteron. Results are obtained for four angular distribution parameters at six values of the γ-quantum mean energy between 50 and 150 Mev. The results are compared with the most recent theoretical calculations. In the greater part of the investigated energy region the agreement is found to be good, the experimental values slightly exceeding the theoretical ones at the highest energies. Some conclusions concerning the theory of photodisintegration of the deuteron are drawn, and some possible reasons why the theoretical values are smaller are discussed. In conclusion it is explained why new and more precise experiments on the photodisintegration of the deuteron at energies below the meson production threshold should be carried out.

MANY recent theoretical papers [1-9] are devoted to photodisintegration of the deuteron at energies below the threshold of pion photoproduction. It is interesting in this connection to analyze the agreement between the results of these papers and the experimental data.

We know that multipole expansion is valid for photodisintegration of deuterons in this energy region. Under these conditions, taking into account only the fundamental dipole transitions and their interference with the quadrupole transitions, one possible angular dependence of the differential cross section is

$$d\sigma/d\Omega = a + b\sin^2\theta + c\cos\theta + d\sin^2\theta\cos\theta. \qquad (1)$$

The theoretical papers [1-9] contain numerical values of the parameters of this distribution, calculated for different γ-quantum energies.

To compare the theoretical and experimental results it is necessary to approximate sufficiently detailed experimental data on the angular distribution of the process by means of a relationship such as (1). Until recently, in spite of the large number of cited experimental data, no such approximation was made and there were no experimental data whatever on the parameters of the distribution (1). In this connection, attempts undertaken in several theoretical papers to compare theory with experiment were unwittingly incorrect and incomplete. For example, Zernik et al [4-9] compared a summary theoretical angular-distribution curve, plotted from (1) with experiment. It is obvious that such a comparison is limited, for it extracts but a fraction of the obtainable information from the available experimental material. Authors of several other papers used for the comparison experimental results obtained by approximating the angular distributions with a formula such as

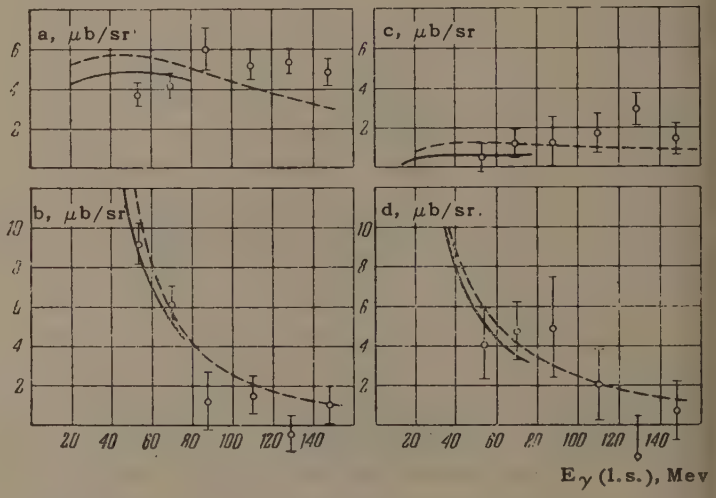

Results of approximation of experimental angular distribution[10] by means of an equation similar to (1) and a comparison with the results of the theoretical calculations of [2] (solid curve) and of [4] (dashed curve).

$$d\sigma/d\Omega = (a^* + b^*\sin^2\theta)(1 + 2\beta\cos\theta), \qquad (2)$$

tacitly assuming thereby that the values of a* and b* should coincide with the values of a and b when the data are approximated by expression (1). Naturally, no comparison is possible in this case for the parameters c and d.

We have approximated, with the aid of expression (1), previously published experimental data on the angular distribution.[10] The results obtained for parameters a and b differ considerably,

although without apparent regularity, from the values of a* and b* obtained earlier in an approximation by means of (2). The experimental results for all four parameters of the distribution (1), obtained for six values of the mean γ-quantum energy in the approximate range from 50 to 150 Mev (see the figure), have made it possible to make in this interesting region a correct and complete comparison of the results of the most recent theoretical calculations with experiment. The direct results of the comparison and the conclusions that can be drawn for the theory of deuteron photodisintegration can be briefly formulated as follows.

1. In the major part of the investigated medium-energy range, at least up to 100 or 120 Mev, the experimental results for all four parameters of the distribution (1) agree, within the limits of experimental accuracy, with the results of the most complete theoretical calculations.[2,4,6,9] This leads to the following conclusions:

a) In the stated energy region, the interaction between the electromagnetic field and a two-nucleon system can be correctly described as an interaction with the current and magnetic moments of the nucleon, without resorting to an explicit account of meson effects.

b) A quantitative agreement with experiment is obtained within the energy region only for those theoretical calculations [2,4,6,9] in which a consistent account is taken of a whole series of circumstances, the role of which was previously neglected, namely: transitions to the $^3F_2$ state, tensor interaction of the nucleons in the final states, and contribution from certain "non-fundamental" multipole terms to the cross section.

c) A quantitative agreement with experiment is obtained only for calculations in which use is made of those sets of phase shifts of nucleon-nucleon interaction in ^3P_J states, which correspond to a positive sign of the tensor potential (see, in particular,[7,8]).

d) The limited accuracy of both the experimental and the theoretical results does not permit at present an unambiguous choice between the two values of the probability D-wave in the deuteron, used in different variants of the calculation.

2. In the region of the highest energies investigated in [10], starting approximately with 100—120 Mev, the experimental results for the isotropic component of the angular distribution and for the component proportional to cos θ exceed noticeably the results of the theoretical calculations (see the figure). This calls for an explanation, which we find by referring, as is usually done, to the virtual meson effects that are possible in this energy region. It seems to us, however, that it is necessary above all to exercise greater care in the usual calculations, in which meson effects are not taken into account, namely:

a) Kramer and Werntz [6] have shown that the interference cross section terms such as $^3E1 \cdot {}^3M2$ and $^1M1 \cdot {}^1E1$ (the superscript denotes the multiplicity of the final state), which are not accounted for in the calculations by other workers, change noticeably the form of the angular distribution even at 50—70 Mev. In the energy region we are considering, they can manifest themselves even stronger, changing the entire pattern of the comparison between theory and experiment.

b) We have made a consistent classification of the multipole cross section terms that can arise in photodisintegration of the deuteron, with an estimate of the relative order of magnitude of the terms. We have established thereby that two other terms of the cross section, namely $^3E1 \cdot {}^3E3$ and $^3E1 \cdot {}^3E1_{s.o.}$, can make a contribution of the same order of magnitude as $^3E1 \cdot {}^3M2$ (the subscript s.o. denotes second order in the expansion of the corresponding amplitude in powers of kr). The former of the foregoing cross-section terms has never appeared in any of the published papers. The contribution of the latter term to the total cross section was essentially calculated by Hsieh [3] but was disregarded in the other papers. According to the foregoing estimates, this term becomes noticeable at energies on the order of 80 Mev and increases rapidly with increasing energy. The classification has disclosed, furthermore, seven other hitherto uncalculated cross-section terms; these may turn out to be of the same order of magnitude as the term $^1M1 \cdot {}^1E1$ which, according to Kramer and Werntz [6] yields an unexpectedly large contribution.

c) Our analysis has shown that the isotropic component of the angular distribution and the component proportional to cos θ are more sensitive to the splitting of the phases of the final states ^3P_J than the other components, while the component proportional to cos θ is furthermore sensitive to the splitting of the ^3D_J phases. A numerical analysis of the isotropic component at energies below 100 Mev was made by Kramer.[7] It is possible that more accurate numerical values of the phase shifts, obtained in the future by further research on the nucleon-nucleon interaction, will change appreciably the foregoing components of the angular distribution.

Summarizing, it appears quite likely that improvements in the theoretical results with account of the foregoing remarks will yield better agree-

ment between theory and experiment over the entire range of energies below the threshold of pion photoproduction, without resorting (in explicit form) to an account of meson effects. The use of two versions of calculations, similar in all respects except for the D-wave probability for the ground state of the deuteron, will probably permit a final choice between the two values, 4 and 7%, which are under discussion at the present time.

In conclusion we note that the accuracy of the experimental results obtained for the parameters c and d is low, although the initial data used for the angular distribution [10] are the most detailed of those published. (The results that can be obtained from the measurements of a recently published paper by Galey [11] are subject to much greater errors, precisely because of the poor investigation of the angular distribution.) In this connection, it seems advisable to set up new, more detailed measurements of the angular distribution of the photodisintegration of the deuteron in the range of energies near the pion photoproduction threshold (for example, 50—200 Mev). In these measurements it is essential to increase the number of investigated angles (at least to 10 or 12) and the range (10 — 170°, and if possible 0 — 180°). When an accuracy on the order of 5% is attained for the parameters c and d, the comparison with the theoretical calculations can be used to verify the results of the phase-shift analysis of nucleon-nucleon interaction not only in the ^3P_J states, but also in the ^3D_J states.

[1] A. F. Nicholson and G. E. Brown, Proc. Phys. Soc. **73**, 221 (1959).

[2] J. J. De Swart and R. E. Marchak, Physica **25**, 1001 (1959).

[3] S. H. Hsieh, Progr. Theor. Phys. **21**, 585 (1959).

[4] Zernik, Rustgi, and Breit, Phys. Rev. **114**, 1358 (1959).

[5] Iwadare, Matsumoto, Otsuki, Tamagaki and Watari, Nuovo cimento **13**, 1263 (1959).

[6] G. Kramer and C. Werntz, Phys. Rev. **119**, 1627 (1960).

[7] G. Kramer, Nucl. Phys. **15**, 60 (1960).

[8] G. Kramer, Phys. Rev. Lett. **5**, 439 (1960).

[9] Rustgi, Zernik, Breit, and Andrews, Phys. Rev. **120**, 1881 (1960).

[10] Aleksandrov, Delone, Sokol, Slovokhotov, and Shtarkov, JETP **33**, 614 (1957), Soviet Phys. JETP **6**, 472 (1958).

[11] J. A. Galey, Phys. Rev. **117**, 763 (1960).

Translated by J. G. Adashko
336

Letters to the Editor

ON N. V. PLESHIVTSEV'S ARTICLE "SPUTTERING OF COPPER BY HYDROGEN IONS WITH ENERGY UP TO 50 kev"

Yu. V. BULGAKOV

Karpov Physico-Chemical Institute

Submitted to JETP editor January 9, 1961; resubmitted July 24, 1961

J. Exptl. Theoret. Phys. (U.S.S.R.) 41, 2015-2016 (December, 1961)

THE cited article by Pleshivtsev[1] contains data on the sputtering of copper by hydrogen ions in a wide energy range (10 kev — 10 Mev). The values obtained for the sputtering coefficient differ greatly both from the results of similar experiments[2-4] and from the theoretical predictions,[5] it being stated that the latter is incorrect from both the qualitative and the quantitative points of view. The principal difference between Pleshivtsev's and other procedures was that the ion beam contained several different components. According to his data, the beam contained the following ions: H^+ (30 — 40%), H_2^+ (40 — 50%), H_3^+ (30 — 10%), O_2^+ and N_2^+ (1 — 3%). We shall show that the sputtering coefficient S_{Obs} observed in that reference could differ greatly from the true coefficient S_{H^+} of sputtering by the hydrogen ion.

If the beam is not too dense we can assume that each ion is sputtered independently of the others. We can then write for the part of S_{Obs} connected with the sputtering by different hydrogen ions

$$S^{H}_{obs} = n_{H^+} S_{H^+}(E) + n_{H_2^+} S_{H_2^+}(E) + n_{H_3^+} S_{H_3^+}(E) \quad (1)$$

(where n_i — fraction of the corresponding ions in the beam). To estimate this quantity we assume that the complex ion exerts approximately the same sputtering action as if all of the particles it contains were separately incident with velocity equal to the velocity of the complex ion (see [2,6]). We can then rewrite (1) in the form

$$\frac{S_{obs}(E)}{S_{H^+}(E)} = n_{H^+} + 2n_{H_2^+}\frac{S_{H^+}(E/2)}{S_{H^+}(E)} + 3n_{H_3^+}\frac{S_{H^+}(E/3)}{S_{H^+}(E)} . \quad (2)$$

If $E_{H^+} \gg 500$ ev, we have according to the theory of Goldman and Simon[5]

$$S(E) \sim \ln(E/E_d)/E,$$

where E_d — binding energy of the atom of the sputtered metal in the lattice (25 ev for copper[7]). Under the least favorable conditions allowed by the author ($n_{H^+} = 20\%$, $n_{H_2^+} = 50\%$, $n_{H_3^+} = 30\%$), we find from these formulas that $S_{Obs} \sim 4S_{H^+}$ at about 50 kev. The error in the determination of the sputtering coefficient can thus reach 400% even in the absence of heavy-ion impurities.

Let us estimate the contribution of heavy impurities to the observed sputtering coefficient. It is known[6] that in the 5 — 25 kev energy range nitrogen ions N^+ sputter copper with a coefficient $S_{H^+} \approx 2$ atoms/ion. In this region the sputtering coefficient vs energy curve for nitrogen passes through a flat maximum and hardly varies with the energy. The observed sputtering coefficient for nitrogen ions is

$$n_{N_2^+} S_{N_2^+}(E) \approx 2n_{N_2^+} S_{N^+}(E/2) \approx 0.12 \text{ atom/ion} .$$

Oxygen ions produce somewhat stronger sputtering than nitrogen ions[2,8]; therefore if we assume that the beam has as many oxygen as nitrogen ions we can expect the given values of the sputtering coefficient to contain a constant component with value close to 0.25 atom/ion, due to the presence of heavy impurities. Under these assumptions, recalculations of Pleshivtsev's data lead to a sputtering coefficient that is in satisfactory agreement with the data given in the literature.

As to the preliminary results of the experiments on the sputtering of copper by high-energy hydrogen ions (up to 10 Mev), we note that the observed increase in the sputtering coefficient with increasing ion energy cannot be reliably ascribed to the action of high-energy protons until the monochromaticity of the sputtering beam is rigorously established. Pleshivtsev's procedure has therefore an important shortcoming, which greatly distorts the results obtained and makes the conclusions concerning the incorrectness of the theory[5] unfounded.

[1] N. V. Pleshivtsev, JETP 37, 1233 (1959), Soviet Phys. JETP 10, 878 (1960).

[2] W. E. Moore, Ann. N. Y. Ac. Sci. 67, 600 (1957); J. Chem. Phys. 32, 1540 (1960).

[3] O. C. Yonst, J. Appl. Phys. 31, 447 (1960).

[4] Gusev, Guseva, Vlasenko, and Elistratov, Izv. AN SSSR ser. fiz. 24, 689 (1960), Columbia Tech. Transl. p.

[5] D. T. Goldman and A. Simon, Phys. Rev. 111, 383 (1958).

[6] Rol, Fluit, and Kistemaker, Physica 26, 1000 (1960).

[7] F. Seitz and D. Turnbull, Solid State Physics 2, (1956).

[8] Rol, Fluit, and Kistemaker, Physica 26, 1009 (1960).

Translated by J. G. Adashko
337

LARGE-ANGLE SCATTERING OF HIGH-ENERGY PIONS

Yu. D. BAYUKOV, G. A. LEKSIN, and Ya. Ya. SHALAMOV

Submitted to JETP editor October 16, 1961

J. Exptl. Theoret. Phys. (U.S.S.R.) 41, 2016-2018 (December, 1961)

RECENTLY there has been discussed in the literature[1,2] the possibility of scattering of high-energy pions at c.m.s. angles close to 180°, in reactions of exchange scattering

$$\pi^- + p \to \pi^0 + n \qquad (1)$$

and elastic scattering

$$\pi^+ + p \to \pi^+ + p \qquad (2)$$

The presence or absence of such scattering indicates the presence or absence of a contribution of Feynman diagrams with virtual nucleons and is connected with the nature of the dependence of the nuclear forces on the distance at high energies. Complete cancellation of the backward scattering signifies, in particular, that the impact parameters involved in the scattering can be made as large as desired, but the amplitudes of the partial waves are very small.

We have previously[3,4] investigated in detail the reaction

$$\pi^- + n \to \pi^- + n, \qquad (3)$$

which is isotopically symmetrical to reaction (2), for an incoming meson with momentum 2.8 Bev/c. It was shown that the cross section for scattering at c.m.s. angles greater than 90° is less than 0.006 mb/sr, and that the probability that the elastic-scattering angles exceed the angle corresponding to the first diffraction minimum is small and decreases sharply with increasing momentum of the incoming pion. Data on exchange scattering at large angles in the energy region above 1 Bev are lacking at the present time.

The total cross section of reaction (1) at 2.8 Bev/c was estimated in a paper by one of the authors and Shebanov[5] using a bubble chamber filled with a propane-xenon mixture; we studied prongless stars accompanied by electron-positron pairs of conversion γ-quanta from the decay of π^0 mesons. In the present note we give the results of a different reduction of the data obtained in the same investigation.

The figure shows the angular distribution of the γ quanta in the πN c.m.s. without account of the chamber γ-quantum counting efficiency. Plot a in this figure corresponds to the case when there are 3 to 6 electron-positron pairs in the direction towards the point of disappearance of the π^- meson,

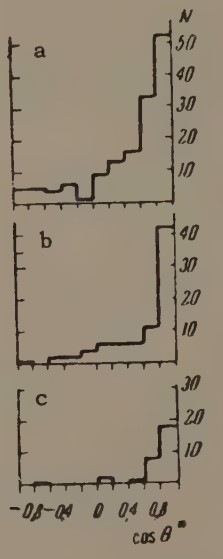

plot b corresponds to two pairs, and plot c to one conversion pair. The high average efficiency for the registration of γ quanta (~ 0.52) enables us to distinguish between process (1) and a reaction in which several π^0 mesons are produced. It is seen from this figure that elastic charge exchange with emission of a π^- meson backward is not observed in practice: one case in the figure (plot b) is connected either with the creation of one more π^0 meson or with the escape of the π^0 meson from the reaction (1) at an angle greater than 1 sr (relative to 180°). The corresponding estimate of the upper limit of the cross section is $\sigma < 0.01$ mb/sr.

The data enable us to estimate the cross section of elastic charge exchange with emission of a π^0 meson at a c.m.s. angle greater than 90°, found to be $\lesssim 0.002$ mb/sr. Similar data are obtained if the bubble chamber is filled with freon.

From the point of view considered here, it is interesting to estimate the cross section of backward scattering of π^- mesons by protons in the process

$$\pi^- + p \to \pi^- + p, \qquad (4)$$

inasmuch as diagrams similar to those responsible for the cancellation of the backward scattering in reactions (1) and (2) may occur in this scattering. Such an estimate was made for a π^- -meson momentum 2.8 Mev/c by a method completely similar to that described in our previous paper.[3] We merely selected the quasi-elastic π^- -p scattering cases, by using additional criteria based on the kinematics of the quasi-elastic process, namely the approximate complanarity (accurate to 15°) and the correspondence between the angles of emission of the charged particles. The cross section of the reaction (4) for l.s. angles greater than 90° (for an interval approximately 1 sr in the c.m.s.) was found to be less than 0.03 mb. This estimate is obtained without subtracting the possible contribution from the background due to creation of π^0 mesons. The cross section for elastic backward scattering, $\sigma < 0.03$ mb, compared with the cross sections for elastic π^- -p scattering given by Wood et al,[6] confirms that the character of the scattering varies with increasing energy.

We are deeply grateful to I. Ya. Pomeranchuk for discussions and continuous interest in the work. We are grateful to V. A. Shebanov for supplying the films and discussing the results.

[1] V. N. Gribov and I. Ya. Pomeranchuk, Preprint 61-15, Inst. Exptl. Theoret. Phys., 1961.

[2] M. Gell-Mann and F. Zachariasen, Preprint, (1961).

[3] Bayukov, Leksin, Suchkov, Shalamov, and Shebanov, JETP 41, 52 (1961), Soviet Phys. JETP 14, 40 (1962).

[4] Bayukov, Leksin, and Shalamov, JETP 41, 1025 (1961), Soviet Phys. JETP 14, 729 (1962).

[5] Ya. Ya. Shalamov and V. A. Shebanov, JETP 39, 1232 (1960), Soviet Phys. JETP 12, 859 (1961).

[6] Wood, Devlin, Helland, Longo, Moyer, and Perez-Mendez, Phys. Rev. Lett. 6, 481 (1961).

Translated by J. G. Adashko
338

MOLECULAR PHOTODISSOCIATION AS A MEANS OF OBTAINING A MEDIUM WITH A NEGATIVE ABSORPTION COEFFICIENT

S. G. RAUTIAN and I. I. SOBEL'MAN

P. N. Lebedev Physics Institute, Academy of Sciences, U.S.S.R.

Submitted to JETP editor October 19, 1961

J. Exptl. Theoret. Phys. (U.S.S.R.) 41, 2018-2020 (December, 1961)

POPULATION inversion in various systems (atoms, molecules, crystals etc.) can be used, as is well known, to obtain a negative absorption coefficient and can be produced by means of optical excitation.[1-7] A new method of obtaining population inversion is discussed below.

We are concerned here with the production of excited atoms as a result of photodissociation of molecules. For simplicity we consider a diatomic molecule XY. In the figure we show a number of typical potential energy curves corresponding to the electron ground and excited states in a molecule (the atomic levels of the X atom are shown in the right side of the figure). Two kinds of curves are possible (these are shown by solid lines and dashed lines in the figure); the following discussion applies to both kinds. The absorption of a photon characterized by a frequency $\omega \gtrsim \omega_0$ causes dissociation of the molecule; as a result one of the atoms (for example, X) can be left in an excited state. Under certain conditions (cf. [1]) an inverted distribution between levels 3 and 2 is obtained in the X atoms, that is to say, the inequality $N_3/g_3 > N_2/g_2$ is satisfied, where N and g are the populations and statistical weights of the corresponding levels shown in the right side of the figure.* This population inversion can be used for

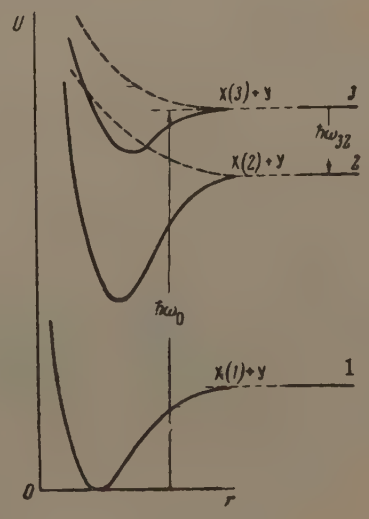

amplification and generation of electromagnetic radiation at the frequency of the atomic transition ω_{32}.

An important feature of the scheme under discussion is the fact that the molecule can, in principle, absorb energy over a relatively wide spectral range ($\sim 10^3$ cm^{-1}) whereas the width of the atomic radiation line is small ($\sim 0.01 - 0.1$ cm^{-1}). This situation favors high gain factors k_ω. The expression for k_ω can be written in the form

$$k_\omega = \frac{\lambda^2}{4}\frac{A_{32}}{\gamma A_3}\frac{Q}{\hbar\omega_0}, \qquad Q = \int\limits_{\omega>\omega_0} E_\omega \varkappa_\omega d\omega. \tag{1}$$

Here, λ, γ and A_{32} are respectively the wavelength, the line width and the Einstein coefficient for the $3 \rightarrow 2$ transition; A_3 is the total decay probability for level 3, E_ω is the spectral power density (w/cm^2 -cycle) of the exciting radiation; $\varkappa_\omega$ is the absorption coefficient associated with the dissociation process $XY \rightarrow X(3) + Y$. The quantity Q is obviously the power absorbed per unit volume as a result of this process. If E_ω varies slowly in the region of effective absorption, then

$$Q = E_\omega \bar{\varkappa}_\omega \Gamma, \quad k_\omega = \frac{\lambda^2}{4}\frac{E_\omega \bar{\varkappa}_\omega}{\hbar\omega_0}\frac{A_{32}}{A_3}\frac{\Gamma}{\gamma}, \tag{2}$$

where $\bar{\kappa}_\omega$ is the mean value of κ_ω, while Γ is the width of the absorption peak. It is easily shown that (1) and (2) are valid for all other versions of optical excitation. It is evident from (2) that, all other conditions being equal, k_ω is determined by the parameter $M = (A_{32}/A_3)\Gamma/\gamma$.† When the atom is excited directly[1,2] $A_{32}/A_3 \lesssim 1$ while the widths Γ and γ are usually determined by the Doppler effect, i.e., $\Gamma/\gamma = \omega_0/\omega_{32} \lesssim 10$. Consequently $M \lesssim 10$ in this case. In crystals $\Gamma \sim 10^3$ cm^{-1}, $\gamma \sim 1 - 10$ cm^{-1} and $A_{32}/A_3 \lesssim 1$[3-6] so that $M \sim 10^2 - 10^3$. In the method proposed here, however, the absorption spectrum is as wide as it is in crystals ($\Gamma \sim 10^3$ cm^{-1}) but γ is appreciably smaller; to be specific, in the visible and near-infrared, $\gamma \sim 0.01 - 0.1$ cm^{-1}. Hence, when $A_{32}/A_3 \sim 1$ we have $M \sim 10^4 - 10^5$. Thus, the advantages of the first two cases—a wide excitation spectrum and a narrow atomic radiation spectrum, can be combined.

An estimate of the absolute magnitude of the absorption coefficient in a typical case ($\gamma = 0.03$ cm^{-1}, $\lambda = 1\,\mu$, $\lambda_0 = 2\pi c/\omega_0 = 2000$ A) gives $k_\omega = 0.3Q\,A_{32}/A_3$ where Q is expressed in units of w/cm^3. Consequently even with relatively low values $Q \sim 1$ w/cm^3 we can obtain $k_\omega = 0.3$ cm^{-1}, which is somewhat greater than the value required to achieve the oscillation.

All the considerations given above for diatomic molecules apply equally to molecules composed of more than two atoms. Hence, in principle there are wide possibilities for the choice of suitable systems. It is obvious that a number of practical considerations must be taken into account. For instance, the term system must be such that the frequency ω_0 lies in the required spectral region and the vapor pressure must be high at reasonable temperatures. The most suitable materials are those which can be produced in the working vessel because the decay products must be easily removed from the vessel and so on. However, the basic problem in choosing a suitable system is the fact that the only well-studied photodissociation processes are those for which one of the atoms is at a resonance level.[8]

*We note that the inequality $N_3/g_3 > N_1/g_1$ cannot be satisfied in practice because the lifetime of the atom in the ground state, which is determined by recombination, attachment at the walls, etc., is much greater than the lifetime of the excited states.

†The quantity $\bar{\kappa}_\omega$ is determined by the need for illuminating the sample and is of order unity in various versions of optical excitation. In practice this is achieved by an appropriate choice of concentration of the absorbing centers.

[1] F. A. Butaeva and V. A. Fabrikant, Issledovaniya po eksperimental'noi i teoreticheskoi fizike, Sb. pamyati akad. G. S. Landsberga (Research in Experimental and Theoretical Physics, Collection in memory of G. S. Landsberg), AN SSSR, 1959, p. 62.

[2] A. L. Schawlow and C. H. Townes, Phys. Rev. 112, 1940 (1958).

[3] T. H. Maiman, Nature 187, 493 (1960).

[4] Collins, Nelson, Schawlow, Bond, Garrett, and Kaiser, Phys. Rev. Letters 5, 303 (1960).

[5] P. P. Sorokin and M. J. Stevenson, Phys. Rev. Letters 5, 557 (1960); I.B.M. J. Research and Develop 5, 56 (1961).

[6] Kaiser, Garrett, and Wood, Phys. Rev. 123, 766 (1961).

[7] S. G. Rautian and I. I. Sobel'man, Optika i spektroskopiya (Optics and Spectroscopy) 10, 134 (1961).

[8] A. N. Terenin, Fotokhimiya parov solei (Photochemistry of Salt Vapors), Gostekhizdat, 1934.

Translated by H. Lashinsky
339

Author Index to Volume 14

References with L are Letters to the Editor

Analytic Subject Index to Volume 14

References with L are Letters to the Editor. Items are listed under the following categories:

Astrophysics

Atoms

Cosmic Radiation

ERRATA

Vol	No	Author	page	col	line	Reads	Should read
13	2	Gofman and Nemets	333	r	Figure	Ordinates of angular distributions for Si, Al, and C should be doubled.	
13	2	Wang et al.	473	r	2nd Eq.	$\sigma_\mu = \frac{e^2 f^2}{4\pi^3}\omega^2 (\ln \frac{2\omega}{m_\mu} - 0.798)$	$\sigma_\mu = \frac{e^2 f^2}{9\pi^3}\omega^2 \left(\ln \frac{2\omega}{m_\mu} - \frac{55}{48}\right)$
			473	r	3rd Eq.	$(e^2 f^2/4\pi^3)\,\omega^2 \geqslant \ldots$	$(e^2 f^2/9\pi^3)\,\omega^2 \geqslant \ldots$
			473	r	17	242 Bev	292 Bev
14	1	Ivanter	178	r	9	1/73	1.58×10^{-6}
14	1	Laperashvili and Matinyan	196	r	4	statistical	static
14	2	Ustinova	418	r	Eq. (10) 4th line	$[-\frac{1}{4}(3\cos^2\theta - 1)\ldots$	$-[\frac{1}{4}(3\cos^2\theta - 1)\ldots$
14	3	Charakhchyan et al.	533		Table II, col. 6 line 1	1.9	0.9
14	3	Malakhov	550		The statement in the first two phrases following Eq. (5) are in error. Equation (5) is meaningful only when s is not too large compared with the threshold for inelastic processes. The last phrase of the abstract is therefore also in error.		
14	3	Kozhushner and Shabalin	677 ff		The right half of Eq. (7) should be multiplied by 2. Consequently, the expressions for the cross sections of processes (1) and (2) should be doubled.		
14	4	Nezlin	725	r	Fig. 6 is upside down, and the description "upward" in its caption should be "downward."		
14	4	Geĭlikman and Kresin	817	r	Eq. (1.5)	$\ldots\left[b^2\sum_{s=1}^{\infty} K_2(bs)\right]^2$	$\ldots\left[b^2\sum_{s=1}^{\infty}(-1)^{s+1}K_2(bs)\right]^2$
			817	r	Eq. (1.6)	$\Phi(T) = \ldots$	$\Phi(T) \approx \ldots$
			818	1	Fig. 6, ordinate axis	$\frac{\varkappa_s(T)}{\varkappa_n(T_c)}$	$\frac{\varkappa_s(T)}{\varkappa_n(T)}$
14	4	Ritus	918	r	4 from bottom	two or three	2.3
14	5	Yurasov and Sirotenko	971	l	Eq. (3)	$1 < d/2 < 2$	$1 < d/r < 2$
14	5	Shapiro	1154	l	Table	2306	23.6

CONTENTS OF COMING ISSUE

SOVIET PHYSICS JETP VOLUME 15, NUMBER 1 JULY, 1962

LETTERS TO THE EDITOR